ADVANCED CELL CULTURE TECHNOLOGIES TO BOOST CELL-BASED THERAPIES

EDITED BY: Dominik Egger, Aldo R. Boccaccini, Diego Correa, Cornelia Kasper and Fergal J. O'Brien

PUBLISHED IN: Frontiers in Bioengineering and Biotechnology

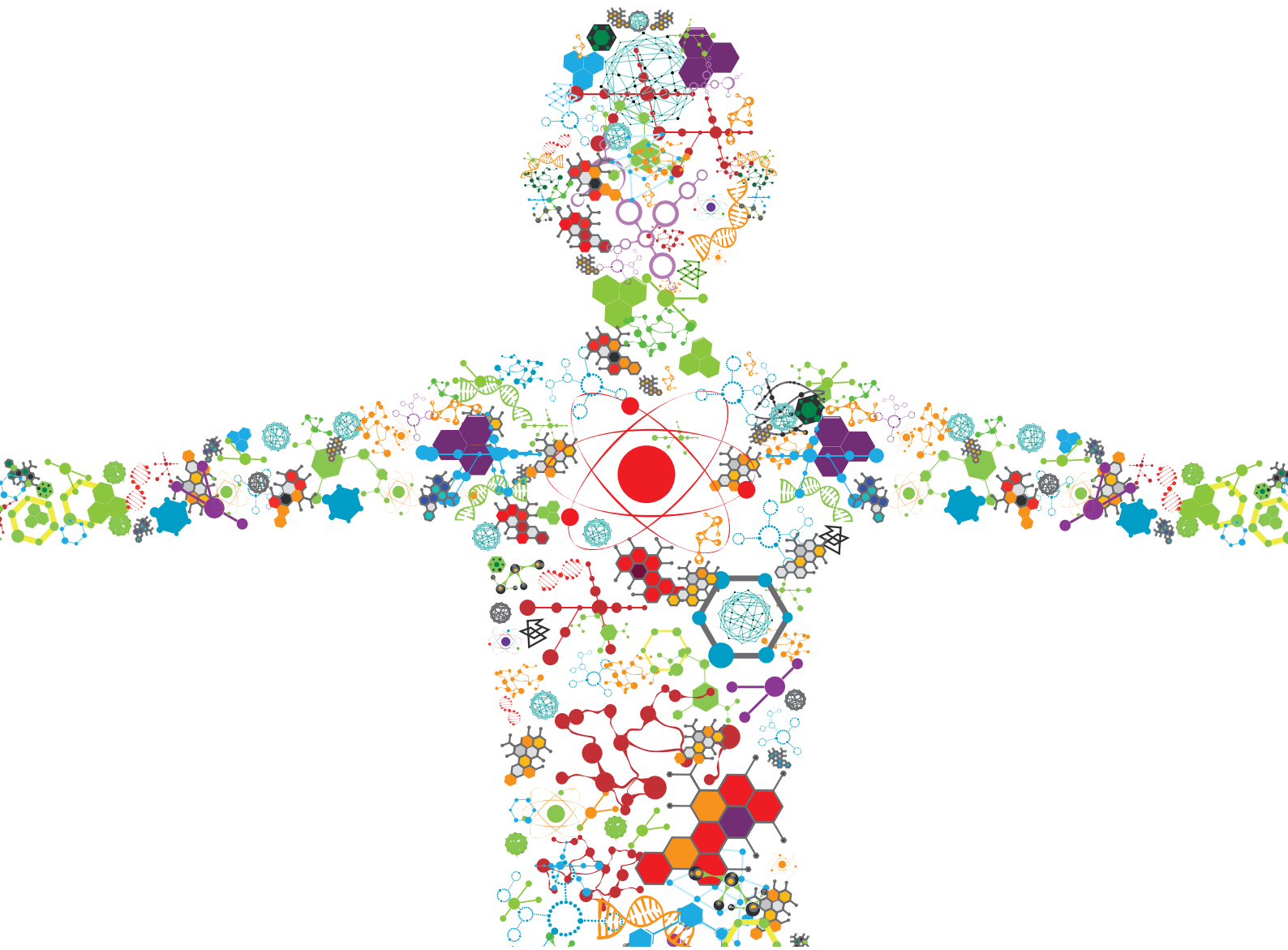

frontiers Research Topics

frontiers

ISSN 1664-8714
ISBN 978-2-88971-330-1
DOI 10.3389/978-2-88971-330-1

About Frontiers

Frontiers is more than just an open-access publisher of scholarly articles: it is a pioneering approach to the world of academia, radically improving the way scholarly research is managed. The grand vision of Frontiers is a world where all people have an equal opportunity to seek, share and generate knowledge. Frontiers provides immediate and permanent online open access to all its publications, but this alone is not enough to realize our grand goals.

Frontiers Journal Series

The Frontiers Journal Series is a multi-tier and interdisciplinary set of open-access, online journals, promising a paradigm shift from the current review, selection and dissemination processes in academic publishing. All Frontiers journals are driven by researchers for researchers; therefore, they constitute a service to the scholarly community. At the same time, the Frontiers Journal Series operates on a revolutionary invention, the tiered publishing system, initially addressing specific communities of scholars, and gradually climbing up to broader public understanding, thus serving the interests of the lay society, too.

Dedication to Quality

Each Frontiers article is a landmark of the highest quality, thanks to genuinely collaborative interactions between authors and review editors, who include some of the world's best academicians. Research must be certified by peers before entering a stream of knowledge that may eventually reach the public - and shape society; therefore, Frontiers only applies the most rigorous and unbiased reviews.
Frontiers revolutionizes research publishing by freely delivering the most outstanding research, evaluated with no bias from both the academic and social point of view. By applying the most advanced information technologies, Frontiers is catapulting scholarly publishing into a new generation.

What are Frontiers Research Topics?

Frontiers Research Topics are very popular trademarks of the Frontiers Journals Series: they are collections of at least ten articles, all centered on a particular subject. With their unique mix of varied contributions from Original Research to Review Articles, Frontiers Research Topics unify the most influential researchers, the latest key findings and historical advances in a hot research area! Find out more on how to host your own Frontiers Research Topic or contribute to one as an author by contacting the Frontiers Editorial Office: frontiersin.org/about/contact

ADVANCED CELL CULTURE TECHNOLOGIES TO BOOST CELL-BASED THERAPIES

Topic Editors:
Dominik Egger, University of Natural Resources and Life Sciences Vienna, Austria
Aldo R. Boccaccini, University of Erlangen Nuremberg, Germany
Diego Correa, University of Miami, United States
Cornelia Kasper, University of Natural Resources and Life Sciences Vienna, Austria
Fergal J. O'Brien, Royal College of Surgeons in Ireland, Ireland

Dr. Correa is the founder of Lumos Biomed Consulting and holds shares in Cryovida Stem Cell Bank (Mexico). Dr O'Brien holds patents related to regeneration technology and was a co-founder of SurgaColl Technologies. All other Topic Editors declare no competing interests with regard to the Research Topic subject.

Citation: Egger, D., Boccaccini, A. R., Correa, D., Kasper, C., O'Brien, F. J., eds. (2021). Advanced Cell Culture Technologies to Boost Cell-Based Therapies. Lausanne: Frontiers Media SA. doi: 10.3389/978-2-88971-330-1

Table of Contents

frontiers in Bioengineering and Biotechnology

EDITORIAL
published: 19 July 2021
doi: 10.3389/fbioe.2021.727298

Editorial: Advanced Cell Culture Technologies to Boost Cell-Based Therapies

Dominik Egger[1], Aldo R. Boccaccini[2], Diego Correa[3], Cornelia Kasper[1] and Fergal J. O'Brien[4]*

[1]Institute of Cell and Tissue Culture Technologies, Department of Biotechnology, University of Natural Resources and Life Sciences, Vienna, Austria, [2]Institute of Biomaterials, Department of Materials Science and Engineering, University of Erlangen Nuremberg, Erlangen, Germany, [3]Diabetes Research Institute & Cell Transplantation Center, University of Miami, Miller School of Medicine, Miami, FL, United States, [4]Tissue Engineering Research Group (TERG) & AMBER Centre Department of Anatomy & Regenerative Medicine, Royal College of Surgeons in Ireland (RCSI), Dublin, Ireland

Keywords: 3D cell culture, physiological conditions, cell-based therapy, therapeutic potential, stem cells

Editorial on the Research Topic

Advanced Cell Culture Technologies to Boost Cell-Based Therapies

Approved cells and cellular products for cell-based therapy (CBT) applications carry a huge promise for the treatment of a broad variety of diseases and several (stem) cell therapies. However, the therapeutic potential of cells is not fully exploited at present. On the one hand, outdated culture conditions are still used during *in vitro* cultivation. On the other hand, technological hurdles block the way to efficient and safe cell-based therapy products. This Research Topic gathered articles about recent advances in cell culture technologies to increase the therapeutic properties of cells or the manufacturing processes for CBT.

Oxygen has an outstanding role as a cell culture parameter as it is involved in numerous cellular processes and the generation of energy. Tse et al. highlighted in their review article the importance of physiological oxygenation in 3D cultures while keeping anoxic regions at a minimum. With finite element modeling the authors demonstrated the degree of anoxic tissue in standard and gas-permeable plates. Further methods such as transwell plates, microfluidic or bioreactor systems to improve oxygenation in 3D cultures are presented. To monitor oxygen gradients occurring inside spheroids, Schmitz et al. reported the development of a modified hypoxia reporter MSC cell line with a genetic sensor for hypoxic conditions. Using this reporter cell line, the authors demonstrated that the method for producing MSC spheroids and cell number per spheroid play a crucial role in the onset of hypoxia in MSC spheroids. The cell line represents a reliable tool for monitoring hypoxic conditions inside spheroids which may be used to increase comparability between different spheroid production systems.

Besides oxygen, also the culture format itself heavily impacts cellular functionalities. Harnessing 3D spheroid culture for MSCs is known to increase therapeutically relevant effects. Kouroupis and Correa summarize in their review article current methods for the generation of MSC spheroids and how spheroid culture increases functionality of MSCs in various therapeutic applications. Thus, recent findings on the anti-inflammatory and therapeutic properties of MSC spheroids in wound healing, osteochondral defects, myocardial infarction, neovascularization/ischemia and liver and kidney diseases are summarized. Findings from this review demonstrate the need to intensify research on and translation of MSC spheroids into clinical applications. Rüger et al. presented an innovative 3D *in vitro* vascular niche model to observe *de novo* vessel formation by vasculogenesis. The model consists of blood-derived progenitor cells, mature immune cells and MSCs, but not

Edited and reviewed by:
Andrea Banfi,
University of Basel, Switzerland

****Correspondence:***
Dominik Egger
dominik.egger@boku.ac.at

Specialty section:
This article was submitted to Preclinical Cell and Gene Therapy, a section of the journal Frontiers in Bioengineering and Biotechnology

Received: *18 June 2021*
Accepted: *06 July 2021*
Published: *19 July 2021*

Citation:
Egger D, Boccaccini AR, Correa D, Kasper C and O'Brien FJ (2021) Editorial: Advanced Cell Culture Technologies to Boost Cell-Based Therapies. Front. Bioeng. Biotechnol. 9:727298. doi: 10.3389/fbioe.2021.727298

mature ECs, providing an environment which led to maturation of ECs through cellular, extracellular and paracrine cross-talk. This model opens up a new possibility for the *in vitro* engineering of autologous blood vessels. Babajani et al. summarized in their review article recent findings in using MSCs as drug delivery system for chemotherapeutic drugs while focusing on possible adverse effects of chemotherapeutics on MSCs and the efficacy of drug loading and releasing.

For applications in cell-based therapies, MSCs and other cell types need to be amplified or expanded to high numbers while keeping their functionality and critical stem cell properties. Thus, advanced methods for the safe expansion of these cells are required. In this context, Nath et al. reviewed the state of the art on technologies for manufacturing of CBTs and point out the current limitations and bottlenecks. They conclude that automated bioreactors are a key technology for providing CBTs in the future. Furthermore, efforts should be made to perform all steps of the production process (genetic modification, expansion, differentiation) in one integrated bioreactor to provide cost-effective solutions. The use of platelet lysate (PL) as serum alternative has become central in manufacturing of CBTs. Kirsch et al. demonstrated that human PL as media supplement is superior to fetal bovine serum (FBS) and human serum for the expansion and differentiation of MSCs, both in 2D and 3D. The cells exhibited enhanced proliferation and differentiation in 2D culture, compared to FBS or human serum. Furthermore, human PL increased cell spreading and proliferation in gelatin-methacryloyl hydrogels. This study underlines the suitability of PL for the culture of MSCs and proof its advantages also for 3D applications. While PL is already available for culture of human cells, there is a lack of standardized processes for the production of equine PL. Hagen et al. presented the production of equine PL for the use as serum alternative in equine MSC culture. If used at the same concentration, equine PL supports MSC expansion as well as adipogenic and osteogenic differentiation comparable to FBS. As cellular therapies experience a notable shift towards the use of small extracellular vesicles (sEVs), there is an urgent need for chemically-defined and xeno-free culture media specialized for the production of EVs. Interestingly, the study of Figueroa-Valdés et al. presented a suitable xeno-free, blood-free and chemically-defined media for the production of MSC-sEVs. An increased MSC-sEV secretion and characteristic expression pattern of sEV markers was observed while retaining the parental cell's stem cell phenotype. Consequently, this medium could enable the large-scale manufacturing of MSC-sEVs under regulatory compliant conditions. To achieve reasonable cell numbers for cell-therapies, advanced processes for the dynamic expansion of MSCs are still required. Van Beylen et al. present an approach to screen for suitable microcarriers for the expansion of MSCs with the later aim for bone formation in an *in vivo* mouse model. They found a microcarrier that supported MSC expansion while keeping potency and functionality regarding *in vivo* bone formation. The microcarrier-based expansion process could be used for the large-scale production of MSCs with subsequent *in vivo* bone formation.

In summary, this article collection provides a comprehensive review of the state of the art in advanced cell culture technologies to boost cell-based therapies which we believe will be of significant interest to the journal readership.

AUTHOR CONTRIBUTIONS

DE wrote the editorial which was proof-read, revised and approved by all other authors.

FUNDING

FO'B is supported by funding from a European Research Council Advanced Grant, ReCaP (agreement no. 788,753).

ACKNOWLEDGMENTS

The editors would like to thank all the authors that contributed to the Research Topic.

Conflict of Interest: The authors declare that the research was conducted in the absence of any commercial or financial relationships that could be construed as a potential conflict of interest.

frontiers in Bioengineering and Biotechnology

REVIEW
published: 23 July 2020
doi: 10.3389/fbioe.2020.00748

Recent Advances on Drug-Loaded Mesenchymal Stem Cells With Anti-neoplastic Agents for Targeted Treatment of Cancer

Amirhesam Babajani[1,2†], Pegah Soltani[2†], Elham Jamshidi[1,3†], Mohammad Hadi Farjoo[1] and Hassan Niknejad[1]*

[1] Department of Pharmacology, School of Medicine, Shahid Beheshti University of Medical Sciences, Tehran, Iran, [2] Student Research Committee, School of Medicine, Shahid Beheshti University of Medical Sciences, Tehran, Iran, [3] Student Research Committee, School of Pharmacy, Shahid Beheshti University of Medical Sciences, Tehran, Iran

Mesenchymal stem cells (MSCs), as an undifferentiated group of adult multipotent cells, have remarkable antitumor features that bring them up as a novel choice to treat cancers. MSCs are capable of altering the behavior of cells in the tumor microenvironment, inducing an anti-inflammatory effect in tumor cells, inhibiting tumor angiogenesis, and preventing metastasis. Besides, MSCs can induce apoptosis and inhibit the proliferation of tumor cells. The ability of MSCs to be loaded with chemotherapeutic drugs and release them in the site of primary and metastatic neoplasms makes them a preferable choice as targeted drug delivery procedure. Targeted drug delivery minimizes unexpected side effects of chemotherapeutic drugs and improves clinical outcomes. This review focuses on recent advances on innate antineoplastic features of MSCs and the effect of chemotherapeutic drugs on viability, proliferation, and the regenerative capacity of various kinds of MSCs. It also discusses the efficacy and mechanisms of drug loading and releasing procedures along with *in vivo* and *in vitro* preclinical outcomes of antineoplastic effects of primed MSCs for clinical prospection.

Keywords: mesenchymal stem cell, cancer, chemotherapeutic drugs, targeted therapy, angiogenesis, metastasis, apoptosis, proliferation

OPEN ACCESS

Edited by:
Cornelia Kasper, University of Natural Resources and Life Sciences, Vienna, Austria

Reviewed by:
Muhammad Nawaz, University of Gothenburg, Sweden
Rodrigo A. Somoza, Case Western Reserve University, United States
Martin Johannes Hoogduijn, Erasmus University Rotterdam, Netherlands

***Correspondence:**
Hassan Niknejad
niknejad@sbmu.ac.ir

†These authors share first authorship

Specialty section:
This article was submitted to Preclinical Cell and Gene Therapy, a section of the journal Frontiers in Bioengineering and Biotechnology

Received: *13 March 2020*
Accepted: *11 June 2020*
Published: *23 July 2020*

Citation:
Babajani A, Soltani P, Jamshidi E, Farjoo MH and Niknejad H (2020) Recent Advances on Drug-Loaded Mesenchymal Stem Cells With Anti-neoplastic Agents for Targeted Treatment of Cancer. Front. Bioeng. Biotechnol. 8:748. doi: 10.3389/fbioe.2020.00748

INTRODUCTION

Cancer is an inflammatory disease that is known as abnormal cell growth with the ability to invade and metastasize to a distance from a primary tumor site. Approximately 1,700,000 new cases of cancer are diagnosed in the United States each year, which is equivalent to more than 4,800 cases per day (Siegel et al., 2019). Establishment of new treatment protocols in recent years can result in a lower mortality rate of cancer patients. There are a variety of methods to treat cancer; all of them aim to whether suppress tumor growth or inhibit metastasis. Chemotherapy is one of the best known therapeutic choices. The effect of chemotherapeutic drugs on tumor tissue depends on

Abbreviations: AM-MSCs, amniotic membrane-derived mesenchymal stem cells; dCDA, deoxycytidine deaminase; GinPa-MSCs, gingival-derived mesenchymal stem cells; hAD-MSCs, human adipose-derived mesenchymal stem cells; hBM-MSCs, human bone marrow-derived mesenchymal stem cells; hD-MSCs, human dental-derived mesenchymal stem cells; Hu-OBNSCs, human olfactory bulb neural stem cells; MMP, matrix metalloproteinases; MMP, mitochondrial membrane potential; MSCs, mesenchymal stem cells.

several factors, especially the route of injection and physiological barriers around the tumor tissue. These drugs can be injected systemically or locally and affect both tumor and normal cells, hence the name collateral toxicity. Therefore, there are many efforts in developing targeted delivery methods with less toxic effects on normal tissues of the body. One of the promising approaches for targeted cancer therapy is using stem cells as both a therapeutic agent and a drug delivery vehicle. Among different types of stem cells, mesenchymal stem cells (MSCs) have characteristic features that facilitate their use in targeted therapy of cancer. MSCs naturally have intrinsic antitumor activities, which include antiproliferative effects, suppressing angiogenesis, decreasing metabolisms, and inducing apoptosis. MSCs are able to modulate immune reactions against themselves and evade the immune system, which makes them capable of being circulated in blood vessels without inducing immune response. They are also able to differentiate into a variety of adult cell types, which makes them capable of reconstructing the damaged tissues after interventions such as surgery (Koç et al., 2000; Uccelli et al., 2006; Rhee et al., 2015; Lee and Hong, 2017).

Mesenchymal stem cells can originate from different human sources. Based on the International Society for Cellular Therapy classification, MSCs include human bone marrow–derived MSCs (hBM-MSCs), human adipose-derived MSCs (hAD-MSCs), human dental-derived MSCs (hD-MSCs), human olfactory bulb neural stem cells (Hu-OBNSCs), and human placenta and umbilical cord–derived MSCs. Approximately 1% of human white adipose tissue consists of hAD-MSCs. There are two main sources of white adipose tissue in human: first, subcutaneous fat in the abdomen, gluteus, and thighs; and second, abdominal fat around gastrointestinal tract, omentum, and perineum (Ong and Sugii, 2013). MSCs can also be isolated from different parts of teeth and gingiva. Human dental-derived MSCs originate from dental pulp, exfoliated deciduous teeth, periodontal ligament, apical papilla, dental follicle, and gingiva (GinPa-MSCs) (Huang et al., 2009; Coccè et al., 2017). MSCs could be isolated from different parts of the placenta and umbilical cord including amniotic membrane (AM-MSCs), chorionic plate, decidua parietalis, and umbilical cord (Wu et al., 2018). MSCs express some common cell markers such as CD73, CD90, and, CD105 but they do not express CD34, CD45, CD14, CD11b, CD79-α, CD19, and HLA-DR (Vidal et al., 2012; Ong and Sugii, 2013; El-Bialy et al., 2014; Gay et al., 2014; El-Sayed et al., 2015; Jin et al., 2015; Yin et al., 2016; Kuci et al., 2019). Although MSCs from different sources display the mentioned common markers, they possess some exclusive characteristics. For example, some types of MSCs possess the capacity to form colonies and differentiate into multilineage cells such as neurons, endothelial cells (Zhang Q. et al., 1950), and myocardial-like cells (Huang et al., 2015). The International Society for Cellular Therapy has considered osteoblastic, adipocytic, and chondrocytic differentiation capacity as minimal criteria to characterize MSCs. As a phenotypic criterion, plastic-adherent capacity in standard culture conditions helps to distinguish MSCs (Dominici et al., 2006).

The important characteristic that makes MSCs superior to the other cells is low immunogenicity. MSCs do not express high levels of major histocompatibility complex (MHC) class II and CD40 (Uccelli et al., 2006; Li et al., 2015). It has been shown that MSCs are immune evasive. This feature makes them a proper candidate for transplantation and migration inside the body when injected intravenously and makes them able to track tumors efficiently without being affected by immune system. Moreover, these cells are able to decrease both initiation and/or progression of tumors through the modulation of immune responses. Several types of cancer tend to occur in the sites of chronic inflammation and tissue damage (Multhoff et al., 2011). This correlation is defined as two main categories: intrinsic and extrinsic pathways. In the intrinsic pathway, genetic factors stimulate activation of protooncogenes and inactivation of tumor suppressor genes, which results in normal cell transformation into abnormal cells and subsequent inflammation. In the extrinsic pathway, the risk of cancer development increases subsequent to a chronic inflammation or infection in the high-risk organs such as prostate and skin. In both pathways, an increase in the production of proinflammatory molecules, cytokines, and interleukins (ILs) stimulates activation and recruitment of different immune cell types (Multhoff et al., 2011). MSCs suppress the early inflammation after exposure to a carcinogen agent. MSCs decrease the infiltration of macrophages to the site of inflammation up to 50% and reprogram these cells to involve in phagocytosis rather than producing proinflammatory cytokines (Francois et al., 2019). MSCs also decrease the expression of both proinflammatory mRNAs and proteins [IL-1α, IL−1β, IL−4, IL-5, IL-6, IL-12, MIP-2, tumor necrosis factor α (TNF−α), and interferon γ (IFN-γ)] and increase the amount of anti-inflammatory mRNAs and proteins [IL-10 and transforming growth factor β (TGF-β)] in the site of inflammation (Tang et al., 2015; Francois et al., 2019). MSCs restore the C-reactive protein concentration in the blood to its basal levels, which is a marker of systemic immune response against carcinogenic agents (Francois et al., 2019). These cells stimulate expression of regulatory T cell (Treg) phenotype, which selectively suppress effector T cells and play an important role in limiting the cell-mediated immune response. MSCs secrete TGF-β, which activates Smad-2. The phosphorylation of the latter factor results in higher amounts of foxp3, which is the transcription factor of Treg cells (Tang et al., 2015). As a result, expression of TGF-β mRNA by MSCs is coherent with higher expression of Treg cells, and their accumulation in lymph nodes suppresses excessive and chronic inflammation before tumor formation and improves patient prognosis (Tang et al., 2015). In addition to inhibition of tumor initiation in sites of chronic inflammation and reducing tumor size, MSCs can limit fibrosis after radiation therapy of tumors and increase survival of the animal models of cancer after irradiation of the tumor site (Francois et al., 2019). MSCs also seem to possess special features, which make them an appropriate choice to be used as drug carrier. They can be loaded with several anticancer molecules such as chemotherapeutic drugs, which can be released in the tumor microenvironment after tumor homing. This type of drug delivery increases the anticancer drug efficacy on tumor cells and decreases collateral toxicity.

In this review, we will summarize recent studies on the inherent anticancer property of MSCs, their resistance against antitumor drugs and involved mechanisms of this resistance, MSCs' capacity of uptaking/releasing the antineoplastic drugs and their related mechanisms, metabolism of anticancer drugs in MSCs, and effectiveness of drug-loaded MSCs in cancer therapy.

ROUTES OF DELIVERY AND TUMOR HOMING OF MSCs

It seems that multiple injections of MSCs directly into the tumor can provide a high number of cells in tumor microenvironment and cause acceptable result (Seo et al., 2011). Single-dose intratumoral injection of MSCs into the pancreatic ductal subcutaneous adenocarcinoma in athymic mice causes approximately 50% reduction in size and weight of the tumor. MSCs were observed around peripheral vasculature and necrotic areas of the tumor (Cousin et al., 2009). Intratumoral administration of MSCs in the subcutaneous induced melanoma model resulted in apoptosis of endothelial cells (Otsu et al., 2009). However, this method of administration requires several invasive interventions, which increases the risk of infection and cannot treat far metastases of the primary tumor site. Besides, repeated intratumoral administration cannot be practical in deep tumors and short-period therapeutic courses. In order to surmount problems of direct injection, application of catheter-based delivery of therapeutic cells can be a choice to deliver MSCs into the deep tumors (Parker Kerrigan et al., 2017). Furthermore, application of drug carriers such as exosomes and nanoparticles is an alternative option to deliver drugs to tumor site. Exosomes are able to cross biological membranes including the blood-brain barrier (BBB), and they show very low unspecific interaction with circulating blood proteins (El Andaloussi et al., 2013; Liao et al., 2019). However, tumor homing inability and providing appropriate sources and amounts of exosomes for clinical application are still main problems (Nawaz et al., 2016; Luan et al., 2017). Nanoparticles are able to carry high amounts of multiple drugs and protect their content from external damage (Jiang and Gao, 2017). Nevertheless, low targeting capacity, toxic effects, and fast clearance from circulation are some bottlenecks of their application (Liao et al., 2019). Considering these concerns, it is critical to find more efficient routes of cell or drug delivery to achieve proper therapeutic goals. The ability of MSCs to migrate to the sites of inflammation and tumor microenvironment makes them suitable to be used by delivery routes other than intratumoral injection.

Systemically injected MSCs can efficiently home to tumor sites. Secretion of different proinflammatory molecules in the tumor sites, including IFN-γ, TNF-α, IL-6, IL-8, TGF-β, hepatocyte growth factor, platelet-derived growth factor (PDGF), vascular endothelial growth factor (VEGF), and CXCL12 and some other chemoattractant molecules (Seo et al., 2011), prompts circulating MSCs to migrate to tumor sites (D'Souza et al., 2013). Precise mechanism of MSC infiltration to the tumor site is not fully understood, but studies have suggested that it is a combination of three main mechanisms. Similar to wounded tissues, several cytokines and chemokines are released in the tumor microenvironment, whose receptors are expressed on the MSC membrane. Monocyte-chemoattractant protein 1 (CCL2), VEGFα, and PDGFαβ are well known to be highly expressed in tumor microenvironment and attract MSCs to the site of tumor (Ball et al., 2007; Dwyer et al., 2007). Expression of chemokine receptors on MSC membrane (e.g., chemokine receptor 4) is influenced by the features of tumor microenvironment (hypoxia and TNF-α), which makes such cytokine/receptor pair reactions more specific for MSC migration to the tumor site (Ponte et al., 2007; Kidd et al., 2009; Otsu et al., 2009). In the second mechanism, it is suggested that metabolic status of tumor microenvironment attracts MSCs. For example, hypoxia increases the expression of MCP-1 through production of nitric oxide and hypoxia-induced transcription factor 1α (Spaeth et al., 2008). Another mechanism involved in MSC migration to tumor site is expression of adhesion molecules on the cell membrane of MSCs. Several adhesion molecules including vascular cell adhesion molecule 1 (VCAM-1), intercellular adhesion molecule 1/3 (ICAM-1/3), activated leukocyte cell adhesion molecule, endoglin, and several subtypes of Toll-like receptors are expressed on the cell membrane of MSCs. These molecules are also expressed by leukocytes, dendritic cells, and monocytes, which suggest a similar mechanism of migration to the site of inflammation for MSCs (Spaeth et al., 2008). These studies have suggested that the highest amount of MSCs migration happened in the presence of the three mechanisms combined.

Based on tumor tracking ability, one of the most appropriate methods for delivery is systemic injection of MSCs in which vascular system delivers cells to tumor and metastasis sites. Different routes of injection have been used to evaluate the efficacy of each of them. It has been reported that intravenous (i.v.) injection resulted in the accumulation of human MSCs (hMSCs) in metastatic melanoma (Tyciakova et al., 2017), glioma (Kosztowski et al., 2009), and colorectal tumor sites (Kucerova et al., 2007). One hour after injection of hMSCs into the femoral vein and the common carotid artery of the rat with established orthotropic glioblastoma, hMSCs appeared in the peripheral zone of glioblastoma where angiogenesis is prominent. By injection of hMSCs into the femoral vein, 0.02% of injected hMSCs accumulated at the glioblastoma site. Common carotid artery and the internal carotid artery injections were 0.1 and 0.5%, respectively. The ipsilateral injection of hMSCs to brain glioblastoma was significantly more efficient than intracardiac injection. It seems, the closer injection sites to a tumor, the better therapeutic outcome.

One of the challenges that should be bypassed to deliver MSCs to brain is BBB. MSCs have the ability to cross this barrier in certain conditions (Akiyama et al., 2002; Chen et al., 2003; Osaka et al., 2010). MSCs express chemokine receptors (e.g., CXCR4, CCR2) and cell adhesion molecules (e.g., CD44, integrins α4 and β1, and CD99) on their surface, which are important during MSC adhesion to BBB endothelial cells in sites of damage and inflammation (Ji et al., 2004). Several *in vitro* studies have been

done to clarify the role of other molecules such as TIMP3 (Menge et al., 2012), VCAM-1, and *P*-selectin during the initial rolling steps of MSC homing (Teo et al., 2012).

Intraperitoneal infusion is another route that can be used to deliver hMSCs to tumor sites. In a metastatic mouse model of ovarian carcinoma, intraperitoneal administration of hMSCs showed localization of these cells in three to four spots by 7 days, and the number of hMSCs remained unchanged for 1 more week (Kidd et al., 2009). Compared with i.v. administration, intraperitoneal injection resulted in better localization of hMSCs in neuroblastoma site, whereas a majority of i.v.-injected hMSCs remained in the lungs for a while (Kimura et al., 2016). Although lung as a filter organ can trap systemically injected hMSCs and postpone cell access to target tumors, hMSCs are able to leave the lungs gradually and appear in tumor sites. There are no mortality or major side effects (e.g., pulmonary embolism) for hMSC injection (Pacioni et al., 2017).

Intranasal delivery is a less invasive method that can increase patient comfort and compliance. Application of hMSCs through nasal cavity shows that these cells can rapidly penetrate nasal cavity wall and enter brain tissues. It seems that quick penetration is related to direct path of hMSCs through the trigeminal and olfactory pathways. In addition, it is reported that irradiation can increase hMSC concentration in tumor sites (Balyasnikova et al., 2014).

Meningeal metastasis is a common problem among neoplasms of central nervous system. Intrathecal administration of MSCs is an appropriate option to eliminate leptomeningeal metastatic glioma. Engineered MSCs can reduce the size of established leptomeningeal glioma up to 80% and prolong the life span of intrathecally injected mice. After injection of MSCs into the cerebellomedullaris cistern, these cells migrated to the peritumoral area and deep parts of established leptomeningeal glioma (Gu et al., 2010).

Different routes of cell/drug delivery and their efficacy are shown in **Figure 1**.

EFFECTS OF MSCs ON TUMORS

In the tumor microenvironment, MSCs interfere with intracellular mechanisms of tumor cells, which control their metabolism and growth. They may reduce tumor cell proliferation (Kuci et al., 2019), angiogenesis, and migration to other tissues and metastases and/or increase their apoptosis. MSCs exert these effects by down-regulating essential signaling pathways for tumor progression such as Wnt, Notch, Shh, and BMP pathways (Imitola et al., 2004; Ponte et al., 2007; Karp and Leng Teo, 2009; Momin et al., 2010; Dai et al., 2013; Naderi-Meshkin et al., 2016; Francois et al., 2019). For example, coculture of MSCs with hepatoma cells results in an increase in tumor cell apoptosis and decrease in proliferation by down-regulating Bcl-2, c-Myc, proliferating cell nuclear antigen (PCNA), and survivin protein levels in hepatoma tumor cells (Lowe et al., 2010); all of them are targets of Wnt signaling (Gordon and Martinez, 2010; Ji et al., 2016). MSCs can inhibit Akt protein kinase in Kaposi sarcoma cells, which is an essential enzyme in multiple cellular processes such as glucose metabolism, apoptosis, cell proliferation, transcription, and cell migration.

Akt promotes Forkhead box O (FoxO) 3a, which regulates transcription of several genes that participate in tumor apoptosis cell cycle progression, DNA repair, oxidative stress resistance, and other cellular functions (Chen J. et al., 2010; Chen Q. et al., 2010; Yang et al., 2010; Lam et al., 2012; Ruvolo, 2012; Shukla et al., 2013, 2014; Wang et al., 2013; Zhang Q. et al., 2020). Understanding the most important mechanisms by which MSCs affect tumors helps us properly manipulate these cells for future translation into the clinic.

Inducing Apoptosis

Mesenchymal stem cells can increase tumor cell apoptosis by suppressing Akt phosphorylation. They increase PTEN (a negative regulator of Akt activation) in tumor cells, which results in higher accumulation of FoxO3 in tumor cells. FoxO3 stimulates the extrinsic pathway of apoptosis by up-regulating death receptor expression including Fas ligand and TNF-related apoptosis-inducing ligand (TRAIL) (Ramasamy et al., 2007). MSCs express Fas ligand on their surface and stimulate the extrinsic pathway of apoptosis in tumor cells through Fas/Fas ligand connection. This connection results in the up-regulation of caspase-3 and caspase-8 enzymes (Di Germanio et al., 2016). Human adipose-derived MSCs when cocultured with T-cell lymphoma model cells *in vitro* down-regulated inactive procaspase-3 and up-regulated poly (ADP-ribose) polymerase (PARP) in tumor cells. PARP (a group of proteins involved in DNA repair) depletes cell ATP while trying to fix DNA damages, and this depletion results in cell death (Ahn et al., 2014). MSCs also induce impairment in mitochondrial function, which is known by an increase in the Bax/Bcl-2 and Bax/Bcl-xL ratio and loss of mitochondrial membrane potential (MMP). These events coinciding with caspase activation stimulate the intrinsic pathway of apoptosis (Willert and Jones, 2006).

Inhibition of Proliferation (Cell Cycle Arrest)

Treatment of tumor cell lines with MSCs has resulted in a decrease in Ki67 expression in tumor cells, which is a marker of cell proliferation (Francois et al., 2019). MSCs affect the expression of several regulators of cell transition between the phases of cell cycle and as a result inhibit cell transition between different phases, which results in lower proliferation levels. MSCs are able to decrease expression of positive regulators of cell cycle including regulators of G1 phase and G1/S transition (CCNE, CCNH, CCND2, CDK2, CDK4, CDK6, CUL1, SKP2, RBL1), S phase and DNA replication (MCM2, MCM3, MCM4, MCM5, PCNA, DDX11), G2 phase and G2/M transition (CCNH, CDK5R1, DDX11)(Magatti et al., 2012; Bu et al., 2016).

Mesenchymal stem cells up-regulate cell cycle inhibitory genes including inhibitors of G1 phase and G1/S transition (CCNG2, CDKN1A, CDKN2B, RB1), G2 phase and G2/M transition [CDKN1A; CCNE1: cyclin E1; CCNH: cyclin H; CCND2: cyclin D2; CDK: cyclin-dependent kinase; CUL1: Cullin 1; SKP2: S-phase kinase-associated protein 2 (p45);

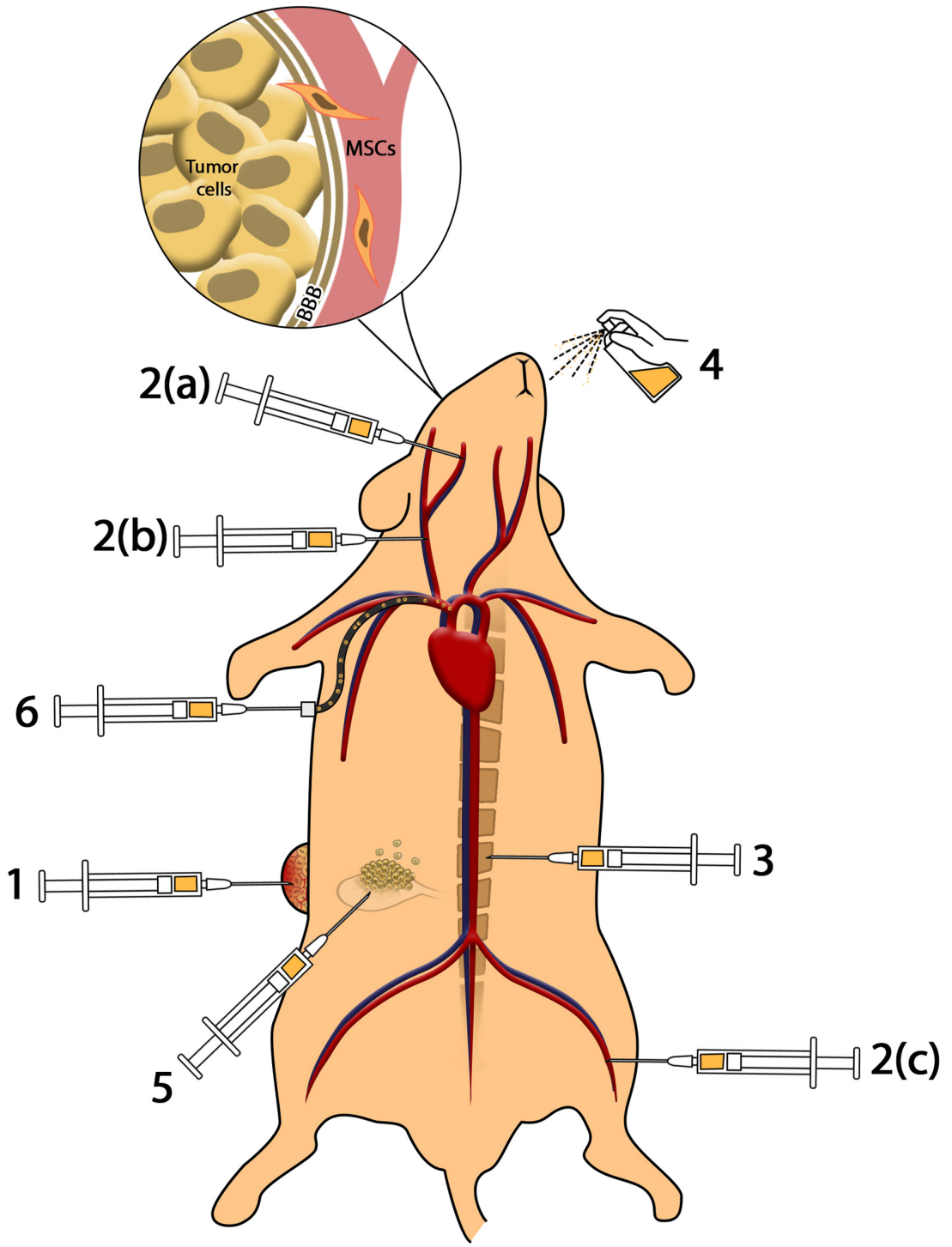

FIGURE 1 | Methods of cell delivery. **(1)** Intratumoral injection provides higher amounts of MSCs in the tumor microenvironment; however, impressive complications including infection, pain, and accessibility to deep tumors reduce the efficacy. **(2)** Intravenous and intra-arterial injection: (a) injection of MSCs to internal carotid artery results in accumulation of MSCs in brain tumors such as glioblastoma; (b) injection of MSCs in common carotid artery reduces the efficacy of cell delivery to glioma in comparison to internal carotid artery; (c) MSCs injected through the femoral vein enter cardiopulmonary circulation that reduces the efficacy of cell administration. Intravenous and intra-arterial injected MSCs cross the BBB to reach brain malignancies. **(3)** Intrathecal administration enables MSCs to access cerebrospinal fluid (CSF) and reach meningeal tumors. **(4)** Intranasal administration of MSCs as a novel method reduces complications of injection and provides MSCs in brain tumors. **(5)** Intraperitoneal injection of MSCs causes distribution in peritoneal cavity and can be used in ovarian malignancies. **(6)** Application of catheter-based cell delivery provides a safe pathway to deliver MSCs to deep organs and reduce the complication of direct injection.

MCM: minichromosome maintenance complex component; PCNA: proliferating cell nuclear antigen; DDX11: DEAD/H (Asp-Glu-Ala- Asp/His box polypeptide 11); CDK5R1: cyclin-dependent kinase 5, regulatory subunit 1 (p35); RBL1: Retinoblastoma-like 1 (p107); CCNG1: cyclin G1; CCNG2: cyclin G2; CDKN1A: cyclin-dependent kinase inhibitor 1A (p21, Cip1); CDKN2B: cyclin-dependent kinase inhibitor 2B (p15, inhibits CDK4); RB1: Retinoblastoma 1] (Magatti et al., 2012; Bu et al., 2016). For example, FoxO3a inhibits cancer cell progression from G1 to S phase by up-regulating cell cycle inhibitory proteins p21 and p27 (Bu et al., 2016), whereas angiostatin and thrombospondin, which are highly expressed in the hAM-MSCs, can increase the number of cancer cells in G1 phase and decrease the number of cells in G2/M phase and S phase and, as a result, inhibit their further proliferation (Ramasamy et al., 2007; Rolfo et al., 2014; Di Germanio et al., 2016; Modaresifar et al., 2017).

Although the lower number of cells is enough for suppressing tumor cell proliferation when MSCs and tumor cells are in direct contact (Bu et al., 2016), a part of cell cycle arrest is related to the secreted molecules from MSCs. The antitumor effects of hAM-MSCs were evident even when MSCs and cancer cells were physically separated using a Transwell membrane (Bu et al., 2016). It is noteworthy that blocking these paracrine signaling pathways, using RNA interference or neutralizing antibodies against antitumor secretions of MSCs, does not suppress the antiproliferative effects of MSC on tumor cells (Zhu et al., 2009), which suggests that the antiproliferative effect of MSCs is through complex paracrine/direct contact-dependent mechanisms.

Inhibition of Angiogenesis

Although MSCs are mostly known for their angiogenesis potential through a variety of secreted molecules, they can efficiently suppress angiogenesis in tumors both *in vivo* and *in vitro* and, as a result, increase focal necrosis in solid tumors (Adelipour et al., 2017). This antiangiogenesis effect may be a result of direct contact between MSC and endothelial cell or may be a result of MSC interaction with cancer cells. Human bone marrow–derived MSCs are able to migrate to capillary walls and intercalate between endothelial cells in capillary network of tumor and connect to endothelial cells through connexin 43. These cells transfer their mitochondria to endothelial cells as a subsequence of the fusion of two cells in order to shape gap junctions through connexin molecules (Otsu et al., 2009). These mitochondria are activated in the target cell and increase the production of reactive oxygen species (Hendrata and Sudiono, 2019) and induce apoptosis in endothelial cells (Otsu et al., 2009). Therefore, it seems that the antiangiogenic effect of MSCs on endothelial cells is dependent on the direct contact between these two types of cells and MSCs/endothelial cells ratio; the higher the number of MSCs, the higher endothelial cells death (Otsu et al., 2009). MSCs also increase the expression of caspase-3 enzyme or activate FasL-dependent pathway in endothelial cells and promote their apoptosis and in turn suppress angiogenesis (Hendrata and Sudiono, 2019).

Cell–cell contact of MSCs with endothelial cells of tumor induces cell cycle arrest in endothelial cells, as mentioned in cancer cells. They decrease the number of cells in S phase, and this effect was dependent on the concentration of MSCs in the culture environment. They also increase the number of cells in G1 phase with no effect on G2/M phase. The cell cycle arrest by MSCs occurs when there is only direct contact between endothelial cells and MSCs (Menge et al., 2013).

Mesenchymal stem cells also resulted in lower expression of IL-1β and cathepsin B in tumor cells. The latter factor is highly expressed in tumor cells, and its down-regulation results in suppression of endothelial progenitor cell mobilization and recruitment to make new vessels in tumor site (Malla et al., 2010). MSCs also reduce the expression of several molecules in tumor such as PDGF, which play an important role in inducing angiogenesis. Platelet-derived growth factor–BB/PDGF receptor β interaction, which is one of the pathways of endothelial progenitor cell mobilization (Gerhardt and Betsholtz, 2003; Bergers and Song, 2005), was suppressed in glioma endothelial cells when cocultured with MSCs, as a result angiogenesis and tumor size reduced in the glioma tumor model (Ho et al., 2013).

Inhibition of Metastasis

Mesenchymal stem cells have the capability to inhibit tumor metastasis. As mentioned before, Akt is an important pathway in tumor progression and metastasis. MSCs up-regulate PTEN, which decreases the amount of phosphorylated Akt. Phosphorylation of Akt is related to tumor metastasis by activating MMP enzymes, which are necessary during extracellular matrix degradation within tumor metastasis (Dasari et al., 2010). MSCs also decrease tumor cell motility (Dasari et al., 2010). This effect may be through increasing expression of intercellular adhesion molecules, for example, *E*-cadherin and vimentin, which play an important role in tumor cell stabilization in its primary site. MSCs also inhibit epithelial-to-mesenchymal transition (EMT), which is an essential mechanism during tumor metastasis. During EMT, tumor cells obtain new mesenchymal-like features including increased motility.

Presence of MSCs when cocultured with glioma cells reduces the number of pericytes in the tumor microenvironment (Ho et al., 2013). Pericytes are groups of cells that play important role in the maintenance of vessel integrity, and their absence is associated with a higher level of permeability of vessels for tumor cells and a subsequent higher level of metastasis (Xian et al., 2006; Gerhardt and Semb, 2008).

Mesenchymal stem cells are able to inhibit secondary tumor cells in sites of metastasis. For example, in Ewing sarcoma model (the most common bone tumor among children), i.v. injection of MSCs inhibited tumor growth in the metastatic site through homing into primary and secondary tumor sites (Hayes-Jordan et al., 2014). We summarized the anticancer effect of MSCs in **Figure 2**.

PROTUMORIGENIC EFFECTS OF MSCs

It has been shown that MSCs sometimes promote tumor progression. Protumorigenic effects of MSCs can be explained in two main categories, direct cell–cell contact and paracrine

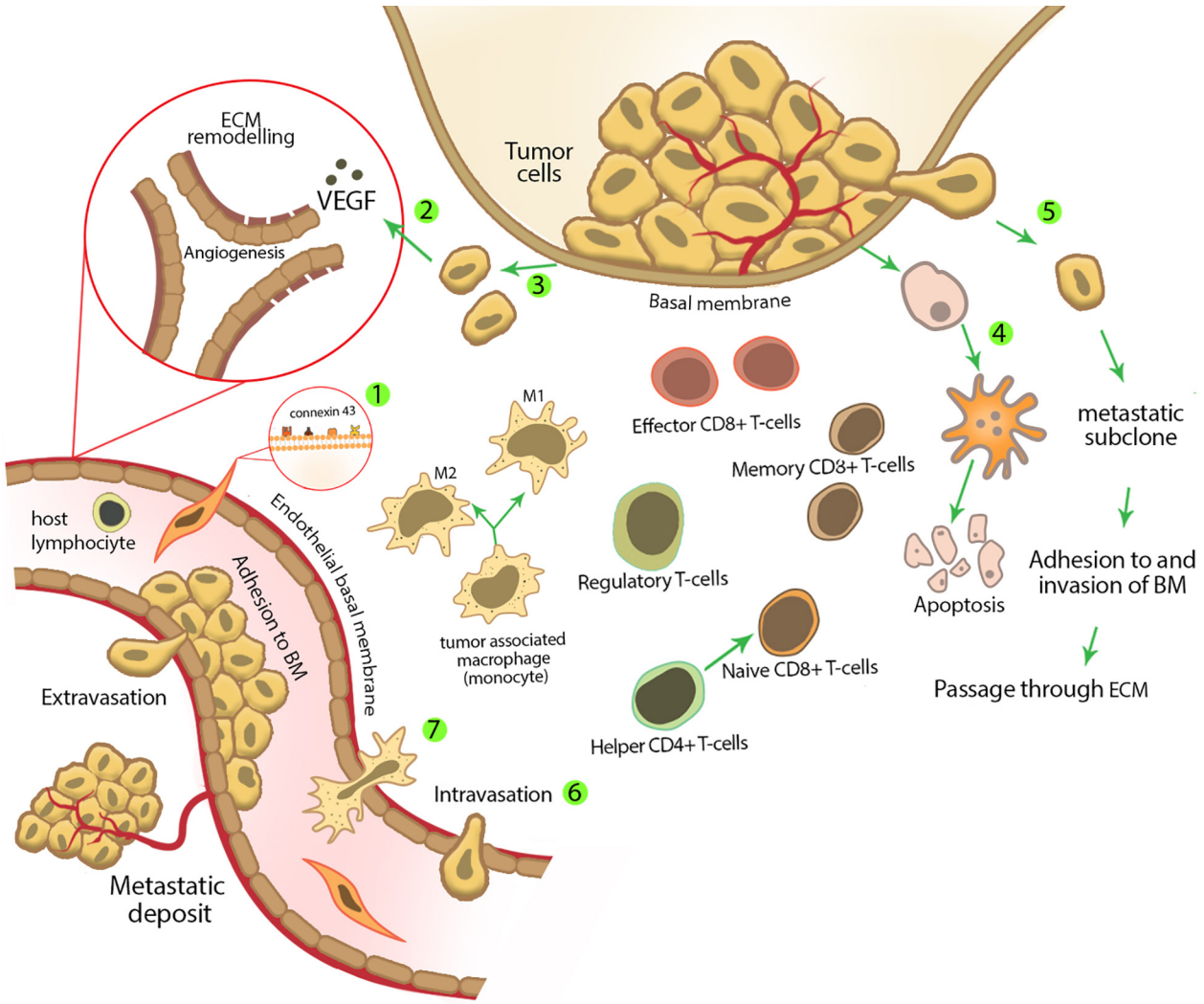

FIGURE 2 | Mesenchymal stem cell characteristics and activities in tumor suppression. **(1)** Mesenchymal stem cells express several surface molecules that have a pivotal role in their homing to tumor sites. These surface molecules are important during MSC adhesion to different cell types; for example, MSCs express connexin 43 on their membrane, which plays an important role in MSC adhesion to endothelial cells. **(2)** Tumor cells are able to produce several growth factors, for example, vascular endothelial growth factor, which stimulates new vessel formation and angiogenesis. Mesenchymal stem cells inhibit tumor angiogenesis by reducing the secretion of these growth factors and inducing apoptosis and/or cell cycle arrest in endothelial cells. **(3)** During and after tumor formation, tumor cells undergo uncontrolled proliferation. Mesenchymal stem cells inhibit tumor cell proliferation by decreasing the expression of positive regulators of cell cycle and/or regulating cell cycle inhibitory genes. **(4)** Mesenchymal stem cells can increase tumor cell apoptosis either by up-regulating death receptors expression (extrinsic pathway of apoptosis) or stimulating intrinsic pathway of apoptosis. **(5)** Mesenchymal stem cells inhibit tumor metastasis by decreasing tumor cell motility in the primary site of a tumor. **(6)** Decreasing permeability of lymphatic or blood vessels for circulating tumor cells. **(7)** Early after carcinogen exposure, the initial inflammatory response is started, which recruits other innate immune cells from nearby capillaries. Mesenchymal stem cells affect different types of immune cells in the site of inflammation and modulate the immune response, which results in tumor inhibition. Mesenchymal stem cells decrease the amount of M2 phenotype macrophages (which promote tumor tolerance and angiogenesis through secretion of VEGF, TGF-β, and other soluble factors) and induce more regulatory T cells (which are produced during the active phase of immune response and limit the strong immune response by $CD4^+$ and $CD8^+$ cells and as a result prevent damage to the host tissue) to enter the inflammatory site.

effects. MSCs can be recruited by tumor and secrete a variety of cytokines and growth factors in the tumor microenvironment, which promote tumor progression through facilitating tumor angiogenesis, modulating antitumor immune responses, and increasing tumor resistance against antitumor drugs. In the other words, the metabolic features of the tumor microenvironment and inflammatory cytokines (which are released from tumor microenvironment resident cells) change MSCs' features and secretory profile, and as a result, they are no more similar to primary MSCs outside the tumor site. For example, tumor microenvironment has a lower tension of oxygen in comparison with normal tissues, called hypoxia. Chronic hypoxia both improves the protective role of MSCs for endothelial progenitors and changes the secretome of MSCs (Liu et al., 2015). The altered

MSCs induce progression in the metastasis, angiogenesis, and macrophage recruitment by tumor cells and also inhibit immune cells infiltration to the tumor site (Rivera-Cruz et al., 2017). It has been shown that expression of indolamine 2,3-dioxygenase was increased in MSCs cocultured with breast cancer cells, which resulted in suppression of immune response by decreasing infiltration of $CD3^+$ and $CD8^+$ T lymphocytes and $CD57^+$ natural killer cells to the tumor site, and also increases the number of regulatory $CD4^+$ T cells (Ino et al., 2008; Bahrami et al., 2017). MSCs have been also shown to improve tumor progression, after injection to the tumor site, through secretion of several growth factors such as TGF-β, epidermal growth factor receptor, periostin, ANG1, PDGF, insulinlike growth factor, and IL-6 (Shangguan et al., 2012; Ye et al., 2012; Akimoto et al., 2013; Lee et al., 2013; Lin et al., 2013; Kansy et al., 2014; Hossain et al., 2015; Wolfe et al., 2016; Wang et al., 2018; Wang Y. et al., 2019). Some studies have suggested that direct contact of MSCs with tumor cells is necessary for exerting their tumor progression roles. For example, MSCs cocultured with breast cancer cells overexpressed CCL5, which stimulates tumor cell motivation and metastasis, whereas this effect was not evident in MSCs separated from tumor cells with a permeable membrane (Karnoub et al., 2007). In addition, MSCs cocultured with cancer cells changed into tumor-associated fibroblasts, which have a pivotal role in tumor stromatogenesis and progression of metastasis (Spaeth et al., 2009).

In order to reduce protumorigenic effects of MSCs and provide more effective therapeutic approaches, some interventional methods have been suggested such as cell engineering, genetic manipulation, and drug loading (Dwyer et al., 2010; Huang et al., 2013). Drug-loaded MSCs inhibit angiogenic factors such as Willebrand factor, CD31 (PECAM1), VEGF-α, Ve-cad, TGF-β1, CD44, and αSMA. Moreover, drug-loaded MSCs are able to inhibit ICAM1, VCAM1, and VEGF, which have a pivotal role in EMT and metastasis (Pessina et al., 2013).

MSCs IN DRUG DELIVERY SYSTEMS

Studies suggested that the application of MSCs as a drug delivery system resulted in a better antineoplastic effect. Gemcitabine-loaded MSCs suppress the proliferation of ductal pancreatic adenocarcinoma more effectively than non-loaded MSCs. In the equal ratio of MSCs and tumor cells, the inhibitory effect of non-loaded MSCs approximately was 15%, whereas that of drug-loaded MSCs was approximately 90% (Bonomi et al., 2017b). An *in vivo* study showed that MSCs loaded with paclitaxel induced strong inhibition of lung metastasis of murine melanoma. Considering the drug content of each cell, this antimetastatic effect was equal to 2,000-fold higher amounts of pure paclitaxel (Nicolay et al., 2016b). Application of MSCs as a drug carrier system provides several advantages in comparison to usual drug administration methods. These advantages include targeted drug delivery to tumor and metastatic cells, reduced side effects of chemotherapeutic drugs, increase in drug half-life, and decrease in administered drug amount. To use MSCs as a drug delivery system, these cells must possess special features besides their innate anticancer capability. Thus, it is essential to evaluate the effects of chemotherapeutic drugs on biological aspects of MSCs such as viability, proliferation, differentiation, and reconstructive ability.

Effects of Chemotherapeutic Drugs on MSCs

Effect of Chemotherapeutic Drugs on Viability of MSCs

As the first influential factor, it is important to evaluate the effect of loaded chemotherapeutic drugs on the viability of MSCs. The type of drug and MSC are two critical factors that affect the sensitivity of MSCs to antineoplastic drugs. Gemcitabine (Bonomi et al., 2015b) and bortezomib (Bonomi et al., 2017b) induce very low cytotoxicity in hBM-MSCs even in concentrations higher than 10,000 ng/mL. These cells showed moderate reduction in viability, in 3,000 ng/mL of cisplatin (Nicolay et al., 2016a) and 10,000 ng/mL of bleomycin (Nicolay et al., 2016b). Human bone marrow–derived MSCs demonstrated low death rate in 10,000 ng/mL of paclitaxel (Pessina et al., 2011, 2013; Bosco et al., 2015; Pascucci et al., 2014; Bonomi et al., 2017b), whereas in concentrations less than half of that (4,000 ng/mL), they showed a moderate cytotoxicity (Münz et al., 2018). Some drugs may be more cytocidal for hBM-MSCs at lower concentrations. Sorafenib causes 40% cell death at 465 ng/mL (Clavreul et al., 2017). Cytarabine, daunorubicin, and vincristine even in very low concentrations significantly induce apoptosis in hBM-MSCs (Nicolay et al., 2016b; Somaiah et al., 2018).

Human AD-MSCs are moderately resistant to cisplatin (Gilazieva et al., 2016; Rimoldi et al., 2018), cationic platinum (II)-complex (Rimoldi et al., 2018), vincristine, and camptothecin (Liang et al., 2011). The viability of hAD-MSCs after exposure to cisplatin and camptothecin for 3 days was more than 70%. Paclitaxel up to 10,000 ng/mL resulted in only 20% cell death in hAD-MSCs (Bonomi et al., 2013). It seems AD-MSCs are more resistant than BM-MSCs to genotoxic damage of anticancer agents.

Human dental-derived MSCs are resistant to paclitaxel, doxorubicin, and gemcitabine (Brini et al., 2016; Coccè et al., 2017; Salehi et al., 2018). Dental pulp stem cells showed higher resistance to paclitaxel than hBM-MSCs (Salehi et al., 2018). Among the three mentioned drugs, GinPa-MSCs are more resistant to gemcitabine than paclitaxel and doxorubicin. However, all three drugs induce only 20% cytotoxic effect on gingival stem cells at concentrations up to 10,000 ng/mL (Coccè et al., 2017, 2019).

Up to 4,000 ng/mL of paclitaxel did not alter the viability of MSCs from olfactory bulbs (Marei et al., 2019). Placenta-derived hAM-MSCs exhibited high resistance to paclitaxel even at concentrations up to 10,000 ng/mL with a viability more than 90% (Bonomi et al., 2015a). These reports show that the type of MSC and type of anticancer drug are two factors that determine the viability of drug-loaded MSCs. Regardless of concentrations

used to evaluate the effect of chemotherapeutic drugs on viability of MSCs, attention to potency and IC_{50} of each chemotherapeutic drug is necessary to load and compare their effects on MSCs, which merits evaluation in the future studies.

Mechanisms of Chemotherapeutic Drugs Resistance of MSCs

A variety of probable mechanisms have been reported for MSCs chemotherapeutic drug resistance. The first mechanism involved in chemotherapeutic drug resistance of MSCs is through augmentation of a specific group of agents called heat shock proteins (HSPs) and their genes. Heat shock proteins appear when cells are exposed to physiological and environmental stress to protect the cell against apoptosis. Heat shock proteins also participate in protein folding, transportation of protein, cell cycle regulation, and intracellular signaling (Jego et al., 2013). Cisplatin–pre-exposed hBM-MSCs showed an increased amount of mRNAs such as HSP90AA1, HSP90AB1 (encoding HSP-90 α and β), HSPA1A (encoding HSP-72), HSPB1 (encoding HSP-27), HSPD1 (encoding HSP-60), and HSPE1 (encoding HSP-10), which pose HSPs as one of the MSCs resistance mechanisms (Nicolay et al., 2016a).

Tubulin proteins are the second mechanism for drug resistance in MSCs. Microtubules are critical structures in cell division, movement, and intracellular trafficking. These structures consist of αβ heterodimers, which are the target of some chemotherapeutic drugs (Borisy et al., 2016). Isotypes of tubulin confer chemotherapeutic drug resistance to MSCs by the difference in their drug-binding capacity and dynamicity. In hBM-MSCs, taxol treatment resulted in higher expression of acetylated tubulins, β-III and β-IV (Polioudaki et al., 2009). Taxol binding to β-III and β-IV is weaker than other isotypes of tubulin (Derry et al., 1997); thus, the higher expression of these two isotypes relative to the other tubulins can be one of the resistance mechanisms to taxol in MSCs. Moreover, β-III tubulin isotype forms more dynamic microtubules during mitosis of MSCs, and its hyperdynamicity inhibits taxol effects on the division process (Stengel et al., 2010).

The inhibition of apoptosis in MSCs is the next resistance mechanism. Suppression of P73-dependent proapoptotic pathway, TRAIL, and overexpression of antiapoptotic factors Bcl2 and Bcl-xL are mechanisms involved in the inhibition of apoptosis (Münz et al., 2018). MSCs of dental pulp treated with paclitaxel showed no translocation of cytochrome C enzyme from mitochondria, which means that these cells did not go through apoptosis after exposure to paclitaxel (Salehi et al., 2018).

As the last mechanism of resistance, paclitaxel treatment resulted in increased expression of macrophage migration inhibitory factor. Migration inhibitory factor as an MSC survival promoter induces doxorubicin resistance in hBM-MSCs through activation of PI3K-Akt survival signaling pathway (Xia and Hou, 2018).

There are two other mechanisms of resistance in non-mesenchymal cells, which are not true about MSCs: drug-inactivating system and ATP-binding cassette transporters (ABC transporters). Lack of these mechanisms shows that MSCs do not deactivate or outpour loaded drugs considerably. This feature makes MSCs capable of delivering chemotherapeutic drugs without reducing their cytotoxic function.

Two enzymes contribute to the metabolism of gemcitabine; deoxycytidine kinase and deoxycytidine deaminase (dCDA) as main activating and inactivating enzymes of gemcitabine, respectively (Pessina et al., 2015). As a prodrug, gemcitabine must be metabolized to its active form in MSCs to inhibit proliferation of cancer cells (Amrutkar and Gladhaug, 2017). Released gemcitabine from drug-loaded hBM-MSCs inhibits the proliferation of squamous cell carcinoma of the tongue and pancreatic carcinoma. Considering this inhibitory effect, not only the drug is not inactivated by dCDA, but it is also activated by deoxycytidine kinase (Bonomi et al., 2015b, 2017b). In hBM-MSCs and Hu-OBNSCs, paclitaxel is metabolized to several metabolites, the most abundant of them is 6-α-hydroxyl paclitaxel; however, these metabolites are so slight, which can be ignored (Pascucci et al., 2014; Marei et al., 2019). This confirms that paclitaxel conserves its cytotoxic effect during uptake and release procedure without being extensively metabolized (Salehi et al., 2018).

ABC is a transporter system superfamily involved in the exchange of a variety of substances such as xenobiotic, antibiotics, and chemotherapeutic drugs across biological membranes. Only prokaryotes benefit from the influx (uptake) function of these proteins, whereas efflux property exists in both prokaryotes and eukaryotes (Nobili et al., 2019). *P*-glycoprotein (P-gp) efflux pump as a member of ABC superfamily can induce chemotherapeutic drug resistance in various cells, but it is not the major method of resistance in normal MSCs (Barbet et al., 2012; Lin et al., 2020; Zhang Y. H. et al., 2020). It is recently suggested that inhibition of efflux pumps by verapamil cannot decrease MSCs' resistance to paclitaxel. In addition, paclitaxel can even down-regulate the expression of P-gp in MSCs (Pessina et al., 2011; Bosco et al., 2015). Other resistance mechanisms cannot be excluded, and further studies should be done to elucidate them.

Effect of Chemotherapeutic Drugs on Proliferation of MSCs

The main reason to investigate the proliferation of MSCs after chemotherapeutic drug loading is that proliferation of primed MSCs results in drug content depletion of each cell and thus insufficient drug concentration in the tumor microenvironment. Moreover, MSCs similar to the other stem cells possess self-renewal ability, which can result in tumorigenesis in the proper microenvironment. Thereby, the antiproliferation effect of chemotherapeutic drugs can reduce tumorigenesis and preserve sufficient drug in each loaded MSC.

So far, almost all studies demonstrated that chemotherapeutic agents significantly reduce the proliferation capacity of MSCs in a dose-dependent manner. Because changes in the proliferation of MSCs has a pivotal role in drug loading, it is necessary to address the effect of chemotherapeutic drugs on cell cycle. It has been shown that treatment with paclitaxel (Pessina et al., 2011; Bonomi et al., 2017b; Petrella et al., 2017; Münz et al., 2018), gemcitabine (Bonomi et al., 2015b), pemetrexed (Petrella et al., 2017), bortezomib (Bonomi et al., 2017b), cytarabine, daunorubicin, and vincristine (Somaiah et al., 2018) inhibits cell

proliferation of hBM-MSCs. Chemotherapeutic drugs decrease the proliferation of hAD-MSCs. As an instance of this inhibitory effect, proliferation of these cells was decreased by 46% after exposure to paclitaxel (Harris et al., 2017). Actually, 2,000 ng/mL of paclitaxel induced complete cell cycle arrest with minimal cytotoxic effect in hAD-MSCs (Bonomi et al., 2013; Choron et al., 2015). Paclitaxel also reduces DNA synthesis of hAD-MSCs by 80% (Choron et al., 2015). Treatment of GinPa-MSCs leads to an increase in the number of cells in G2/M phase (Coccè et al., 2019).

Paclitaxel-treated hAD-MSCs retrieved their cell growth ability after 5 days; however, full recovery of proliferation capacity was never achieved (Harris et al., 2017). Depending on drug type, the accumulation rate is different in each phase of cell cycle. The majority of hBM-MSCs exposed to paclitaxel are arrested in S phase (Pessina et al., 2011). Exposure to gemcitabine causes arrest of 74% of hBM-MSCs in G0/G1 phases (Bonomi et al., 2015b), and cisplatin induces prolonged arrest of hBM-MSCs in G2 phase (Nicolay et al., 2016a).

Several studies have been done to identify the mechanism of antiproliferative effect of chemotherapeutic drugs in MSCs. High expression of P53 as a cell cycle regulator was reported in vincristine-, cisplatin-, and etoposide-treated MSCs (Polioudaki et al., 2009). Furthermore, higher expression of P53 was observed depending on the dose of taxol or nocodazole. Taxol or nocodazole 500 nM increases P53 permanently in hBM-MSCs, whereas 10 nM of the drugs increases P53 expression proportionately with treatment time (Polioudaki et al., 2009). Growth arrest–specific 1 (GAS1) is a critical regulator of the cell cycle and induces quiescence by preventing cells from entering into S phase. It has been shown that treatment of hBM-MSCs with paclitaxel leads to an increase in GAS1 expression and induces quiescent state (Bosco et al., 2015). In addition, a higher amount of senescence-associated β-galactosidase after paclitaxel treatment suggests that premature senescence is a critical mechanism of MSCs to avoid proliferation and preserve metabolic viability (Münz et al., 2018).

Effect of Chemotherapeutic Drugs on Regenerative Capacity of MSCs

Besides the drug delivery ability of MSCs, they play a positive role in chemotherapy-induced tissue damage as a regenerative factor. MSCs are administered to induce postchemotherapeutic tissue regeneration in many organs including kidney (Zoja et al., 2012), hematopoietic system (Koç et al., 2000), lung (Xu et al., 2015), heart (Pinarli et al., 2013), ovary (Badawy et al., 2017), and testis (Sherif et al., 2018). In addition to the ability of MSCs to produce paracrine signals that support progenitors to regenerate chemotherapy-induced tissue damage, they participate in tissue regeneration through other mechanisms such as prevention of inflammation and apoptosis, inducing antioxidative effect, and differentiation to specific cell types in injured organs (Pinarli et al., 2013; Zimmerlin et al., 2013; Sherif et al., 2018). Whether MSCs preserve their initial regenerative characteristics is another important issue that should be evaluated after loading of MSCs with anticancer drugs. A variety of data suggest that the differentiation ability of drug-loaded MSCs as a regenerative mechanism depends on drug and MSC types.

Because BM-MSCs mainly preserve their skeletal differentiation ability after exposure to antineoplastic drugs, they can be preferential to deliver chemotherapeutic agents to skeleton-derived tumors. For example, bleomycin- and paclitaxel-treated hBM-MSCs preserve chondrogenic and osteogenic differentiation capability, respectively (Nicolay et al., 2016b; Münz et al., 2018). On the other hand, some types of MSCs are susceptible to drug-induced differentiation impairment, but they can recover differentiation ability after a drug washing period. These types of MSCs can cause delayed tissue regeneration during the postchemotherapy period. Human adipose-derived MSCs lose their adipogenic and osteogenic differentiation capacity after treatment with paclitaxel. However, partial recovery of differentiation ability was observed after 3 days of drug removal (Harris et al., 2017).

Some chemotherapeutic agents do not influence the differentiation ability of MSCs; thus, these drugs are better choices to provide reconstructive facilities for injured tissues. For example, cisplatin does not influence adipogenic and osteogenic differentiation potential of hBM-MSCs significantly (Nicolay et al., 2016a). In addition, cisplatin- and camptothecin-treated hAD-MSCs did not display any change in osteogenic and adipogenic differentiation capacity (Liang et al., 2011).

Chemotherapeutic Drug Uptake Capacity of MSCs

Mesenchymal stem cells can uptake the majority of anticancer drugs from the culture environment (Kalimuthu et al., 2018; Salehi et al., 2018; Li et al., 2019). Considering this ability, simple methods have been used to prime hBM-MSCs with drugs. Incubation of hBM-MSCs with paclitaxel (Pessina et al., 2011, 2013; Petrella et al., 2017), gemcitabine (Bonomi et al., 2015b), and sorafenib (Clavreul et al., 2017) leads to effective drug uptake. In contrast, hBM-MSCs incubated with pemetrexed were unable to internalize sufficient drug for affecting mesothelioma (Petrella et al., 2017). Through a simple exposure method, hAD-MSCs are able to uptake cisplatin, cationic platinum (II)-complex (Rimoldi et al., 2018), and paclitaxel (Bonomi et al., 2013; Pacioni et al., 2017). Human dental-derived MSCs possess the ability to uptake paclitaxel, doxorubicin, and gemcitabine (Brini et al., 2016; Coccè et al., 2017; Salehi et al., 2018). It seems the amount of loaded drug per cell depends on the type of MSCs. Each hBM-MSC can uptake approximately 2.7 pg of paclitaxel per cell, which is equivalent to 8% of total drug in the culture medium of paclitaxel (Pessina et al., 2011), whereas Hu-OBNSCs were able to internalize 0.19 pg/cell of paclitaxel.

Based on drug type, there are three mechanisms to uptake anticancer drugs into MSCs including transporters, simple diffusion, and endocytosis. Gemcitabine as hydrophilic nucleoside analog enters cells by nucleoside transporters. Human concentrative nucleoside transporter 1 (hCNT1) and human equilibrative nucleoside transporter 1 (hENT1) are the main transporters of gemcitabine (Hung et al., 2015). The high expression level of hCNT1 and hENT1 in MSCs, which

resulted in higher antiproliferative effect of loaded gemcitabine, suggesting that uptake capacity might be attributed to the expression of some transporters (Bonomi et al., 2015b; Coccè et al., 2017). As the next drug internalization mechanism, simple diffusion could be considered according to the lipophilic nature of paclitaxel (Bosco et al., 2015), docetaxel (Wu et al., 2015), camptothecin (Gupta et al., 2000), and etoposide (Patlolla and Vobalaboina, 2008). Endocytosis processes such as pinocytosis, phagocytosis, and receptor-mediated endocytosis are the next mechanisms of drug uptake. The existence of pinocytotic structures in the cytoplasm of GinPa-MSCs implies that the paclitaxel may be internalized by GinPa-MSCs through pinocytosis. CD14 is mainly expressed in the cells, which play a critical role in phagocytosis action (Devitt et al., 1998). Observation of its expression suggests a phagocytic function of GinPa-MSCs for incorporating drugs (Brini et al., 2016). The high expression levels of endocytosis mediator clathrin in hAD-MSCs showed that drugs might internalize through receptor-mediated endocytosis (Wang X. et al., 2019).

Chemotherapeutic Drug Release Capacity of MSCs

It is important to produce a chemotherapeutic drug delivery system that is able to release drugs locally and slowly to provide an efficient concentration in the tumor microenvironment and diminish systemic toxicity of drugs. MSCs can release antineoplastic drugs in a time-dependent manner that makes them a desirable drug delivery system. The efficacy of drug release depends on cell and drug type. For example, drug-loaded hBM-MSCs started releasing 1 pg/cell of paclitaxel after 2 h, which increased to 1.7–2.0 pg/cell at 144 h (Pessina et al., 2011). Approximately 20% of incorporated sorafenib was released during the first 4 h, and 60% of the drug was released in 48 h, which shows a biphasic pattern in hBM-MSCs (Clavreul et al., 2017). Human bone marrow–derived MSCs have more capability than hAD-MSCs to release paclitaxel, but both cells are able to release paclitaxel in a time-dependent manner. It has been demonstrated that during the first 24 h, hAD-MSCs released the majority of contained paclitaxel, and only minor amounts of the drug were released during the next 48 and 144 h (Bonomi et al., 2013). Approximately 52% of internalized paclitaxel is released from Hu-OBNSCs 24 h after priming (Marei et al., 2019). Evaluation of release capacity of paclitaxel loaded hAM-MSCs revealed that 59% of the total internalized drug was released after 48 h; however, drug release was continued for 120 h (Bonomi et al., 2015a). The differences among release capacity may reflect different hydroliposolubility of drugs. For example, GinPa-MSCs release 62.6% of paclitaxel, 91.8% of gemcitabine, and 100% of doxorubicin. Paclitaxel possesses higher lipophilicity, which is released in the lower amount, whereas water solubility resulted in a higher release of gemcitabine and doxorubicin (Wong et al., 2006; Pili et al., 2009; Coccè et al., 2017).

To find the cellular compartments, which are responsible for the storage of drugs, it is necessary to track the anticancer drugs in the MSCs' membrane and cytoplasm. Paclitaxel can be found along with the microtubule networks, in Golgi apparatus and Golgi-derived vesicles of hBM-MSCs. These vesicles were found close to the cell membrane that explains possible drug release capacity (Pessina et al., 2011; Duchi et al., 2014). Evaluation of GinPa-MSCs showed that multivesicular structures originate from cell membrane budding, and the presence of these structures suggests that GinPa-MSCs may produce exosomes (Brini et al., 2016). At 10,000 ng/mL concentration of cisplatin, hAD-MSCs initiate to form exosomes near cellular membranes (Gilazieva et al., 2016). The secreted vesicles from drug-loaded MSCs contain internalized paclitaxel, which significantly induces antineoplastic effect against ductal pancreatic adenocarcinoma cells. There was no plasma membrane interaction such as gap junction or junctional structure between tumor cells and MSCs (Pessina et al., 2013; Bonomi et al., 2017b), but multiple electron-dense vesicles were observed amid paclitaxel-loaded MSCs and tumor cells (Bonomi et al., 2017b). Studies suggest that MSCs and cancer cells communicate through extracellular vehicles (EVs) which can play pivotal roles both as biological vehicles for drugs and/or endogenous particles. It seems that the transportation system recruits EVs for transferring chemotherapeutic drugs between MSCs and tumor cells (Nawaz et al., 2016; Nawaz, 2017; Fatima and Nawaz, 2017). New methods for transferring of chemotherapeutic drugs by loaded MSCs exist, which herald improvement in drug delivery systems such as ultrasound depletion of drugs (Paris et al., 2017), pH-sensitive nanoparticles, which are released in the tumor microenvironment, visible light–dependent drug release (Gisbert-Garzarán et al., 2016; Martínez-Carmona et al., 2017), and thermal energy as a result of applying magnetic field to release drugs (Guisasola et al., 2015). The uptake and release mechanisms of anticancer drugs in MSCs are shown in **Figure 3**.

Antitumor Effect of Drug-Loaded MSCs

Drug-loaded MSCs are applied in two different ways: condition media (CM) and drug carrier cells. Condition media of drug-loaded MSCs contains secretome, which is defined as set of factors secreted to extracellular space. These factors mainly consist of lipids, proteins, free nucleic acids, and EVs. Condition media of drug-loaded MSCs produces more targeted anticancer effect than pure chemotherapeutic drugs. It seems that drug-releasing system of MSCs improve efficacy of loaded drugs through recruiting EVs (Kalimuthu et al., 2018). Application of MSC-sourced CM provides advantages including dosage and potency evaluation, providing storable sources, reduction in invasive cell biopsy procedures, and related safety concerns (Vizoso et al., 2017). Injection of drug-loaded MSCs, which leads to direct cell–cell communication, is another way that causes direct drug transportation between MSCs and cancer cells. Application of the MSCs as a drug carrier is simple and provides a biological sustain release system to deliver chemotherapeutic drugs over a period. Drug-loaded MSCs induce antineoplastic effects through inhibition of proliferation, inducing cytotoxicity against tumor cells, inhibition of angiogenesis and metastasis, and alteration in cytokines secretion of MSCs.

Condition media of drug-loaded hBM-MSCs produces a strong anticancer effect on different cancer cell lines. Condition media of gemcitabine-loaded hBM-MSCs reduced

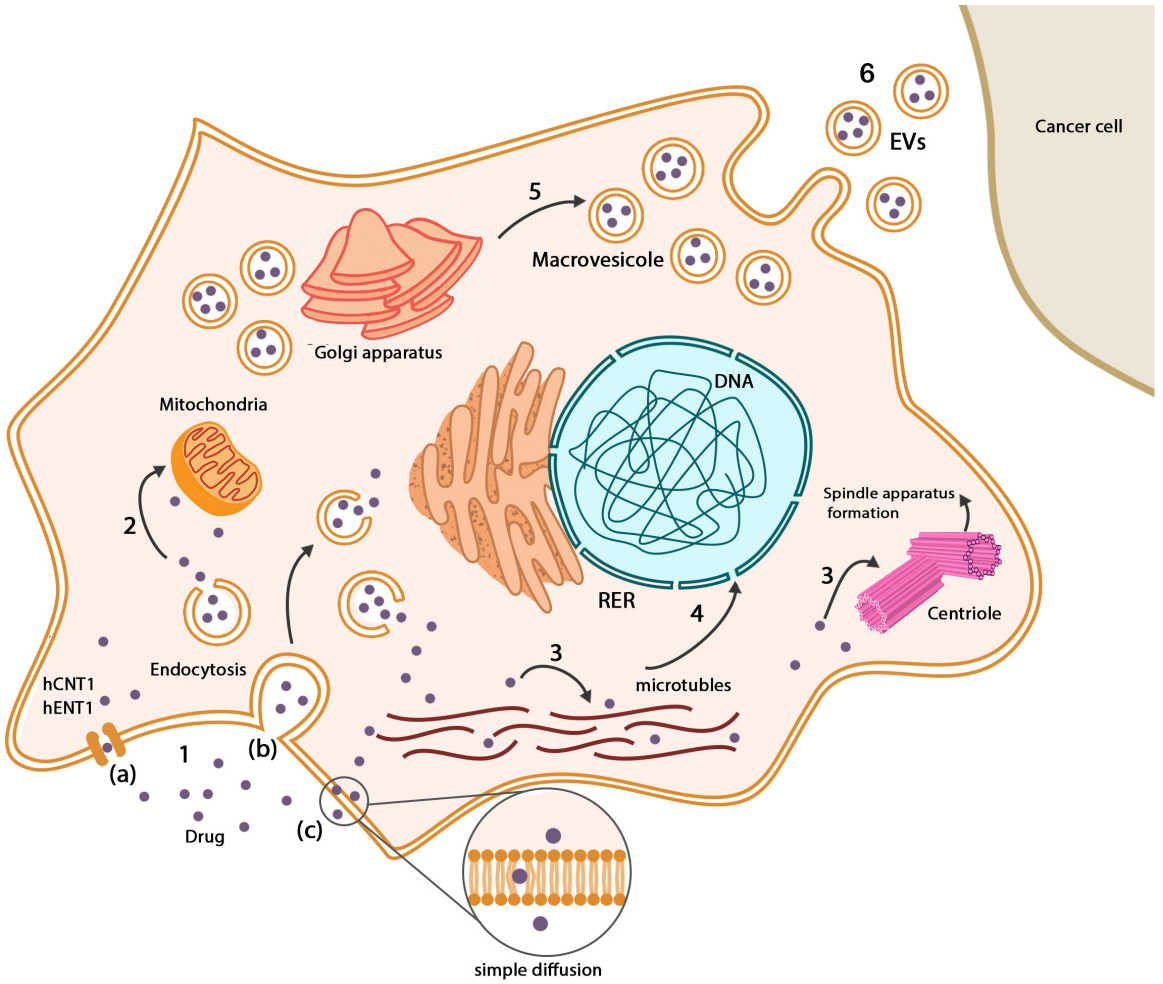

FIGURE 3 | Drugs in MSCs. **(1)** Drugs enter MSCs through a variety of pathways: (a) drug transporters such as hCNT1 and hENT1, (b) endocytosis, (c) simple diffusion based on the chemical nature of chemotherapeutic drugs. **(2)** Some types of drugs such as paclitaxel metabolized in mitochondria, but there is no evidence of impressive inactivation. **(3)** Based on the antineoplastic mechanism of drugs, they are distributed among their place of action such as microtubule networks and centrioles. **(4)** Chemotherapeutic drugs may interfere with the normal gene expression pattern of MSCs, which mainly influence differentiation capacity. **(5)** Mesenchymal stem cells produce vesicles that contain drugs close to the cellular membrane. Drugs can be found in Golgi apparatus and Golgi-derived vesicles. **(6)** Existence of vesicles between MSCs and cancer cells suggests that drugs can be delivered to cancer cells in a vesicular system.

the proliferation of ductal pancreatic adenocarcinoma cells in a concentration-dependent manner (Bonomi et al., 2015b). Condition media of paclitaxel-loaded hBM-MSCs at 1:2 ratio of medium to CM dilution produced 100% growth inhibition in human prostate cancer and glioblastoma cells. This proportion equals 25 ng/mL of pure paclitaxel (Pessina et al., 2011). Condition media of paclitaxel-loaded hBM-MSCs also inhibits proliferation of acute lymphoblastic leukemia, mouse lymphocytic leukemia, malignant pleural mesothelioma, and multiple myeloma cells (Pessina et al., 2013; Bonomi et al., 2017b). Condition media of paclitaxel-treated hAD-MSCs induces a strong dose-dependent antitumor effect on human Ewing sarcoma, human prostate cancer, human blastoma, human neuroblastoma, and acute lymphoblastic leukemia cells. It seems that human Ewing sarcoma cells are more sensitive to paclitaxel in comparison to the other cancer cells (Bonomi et al., 2013). Both CM and lysate of paclitaxel-treated Hu-OBNSCs possess the ability to inhibit glioblastoma and ductal pancreatic adenocarcinoma cells (Marei et al., 2019). Condition media of paclitaxel treated hAM-MSCs can induce dose-dependent antiproliferation effect on ductal pancreatic adenocarcinoma cells (Bonomi et al., 2015a). However, neither CM of pemetrexed- and bortezomib-loaded MSCs, nor lysate of the loaded MSCs, produces antiproliferation activity against malignant pleural mesothelioma, ductal pancreatic adenocarcinoma, or multiple myeloma cells. As mentioned above, hBM-MSCs did not uptake and release pemetrexed and bortezomib sufficiently to produce an antitumor effect (Bonomi et al., 2017b; Petrella et al., 2017). Condition media of GinPa-MSCs exposed to gemcitabine, paclitaxel, and doxorubicin inhibits proliferation of ductal

pancreatic adenocarcinoma and squamous cell carcinoma of the tongue (Brini et al., 2016; Coccè et al., 2017).

The coculture of cancer cells with drug-loaded MSCs is used to evaluate the direct antitumor effect of drug-loaded MSCs. Paclitaxel-loaded hBM-MSCs possess the ability to reduce the proliferation of acute lymphoblastic leukemia, glioblastoma, melanoma, and human prostate cancer cells (Pessina et al., 2011, 2013). Coculture of paclitaxel-loaded GinPa-MSCs resulted in significant inhibition of ductal pancreatic adenocarcinoma and squamous cell carcinoma of the tongue cells, whereas non-loaded GinPa-MSCs did not influence cancer cells growth (Coccè et al., 2019). Drug-loaded MSCs are also able to play an anticancer role in animal models. Cotransplantation of acute lymphoblastic leukemia and paclitaxel-loaded hBM-MSCs completely block the formation of tumors in immunodeficient nude mice. In addition, the administration of pure paclitaxel or non-loaded MSCs did not entirely block subcutaneous tumorigenesis of acute lymphoblastic leukemia, whereas intratumoral injection of paclitaxel-loaded MSCs considerably reduced tumor size and weight. Intraperitoneal injection of paclitaxel-loaded MSCs improved survival of mice with lymphocytic leukemia whereas pure paclitaxel administration did not influence the prognosis (Pessina et al., 2013).

Drug-loaded MSCs can reduce angiogenesis in different ways. The proliferation of human umbilical vein endothelial cells was inhibited by CM of sorafenib-treated MSCs (Clavreul et al., 2017). The CM of paclitaxel-loaded hBM-MSCs inhibits VEGF-α which is the major mediator of tumor angiogenesis (Pessina et al., 2011). Intratumoral injection of paclitaxel loaded MSCs to nude mice with subcutaneous acute lymphoblastic leukemia resulted in a reduction of tumor vascularization, microvascular density, and expression of angiogenic markers such as von Willebrand factor, CD31 (PECAM1), VEGF-α, Ve-cad, TGF-β1, CD44, and αSMA. The tumor vascular density of mice treated by paclitaxel-loaded MSCs was reported four times lower than non-loaded MSCs, which indicates higher efficacy of loaded MSCs (Pessina et al., 2013).

Metastasis of cancer cells is a critical problem in cancer treatment and is associated with recurrence and poor prognosis. It has been discovered that CM of paclitaxel loaded hBM-MSCs considerably down-regulates ICAM1 and VCAM1 on TNF-α–activated human microvascular endothelial cells. This

TABLE 1 | Anticancer mechanisms of drug-loaded MSCs with a variety of chemotherapeutic drugs.

Drug	Source of MSCs	Tumor cells	Antitumor effect (ref)
Doxorubicin	GinPa-MSCs	CFPAC-1 SCC154	Cell cycle arrest (Coccè et al., 2017)
Gemcitabine	hBM-MSCs	CFPAC-1	Cell cycle arrest (Pessina et al., 2015)
	GinPa-MSCs	CFPAC-1 SCC154	Cell cycle arrest (Coccè et al., 2017)
	Pancreas-derived MSCs	CFPAC-1	Cell cycle arrest (Pessina et al., 2015)
Paclitaxel	hBM-MSCs	DU145 T98G MOLT-4 L1210 MPM RPMI8226 B16	Cell cycle arrest, cytokine mediate, cytotoxicity, and antiangiogenesis (Pessina et al., 2011, 2013, 2015; Bonomi et al., 2017b)
	hAD-MSCs	SK-ES-1 DU145 GI-LI-N SH-SY5Y (+) MOLT-4 U87MG	Cell cycle arrest and cytotoxicity (Bonomi et al., 2013; Pacioni et al., 2017)
	GinPa-MSCs	CFPAC-1 SCC154	Cell cycle arrest (Coccè et al., 2017, 2019)
	DPSCs	MCF-7	Cell cycle arrest (Salehi et al., 2018)
	Hu-OBNSCs	U87GM CFPAC-1	Cell cycle arrest (Marei et al., 2019)
	AM-MSCs	CFPAC-1	Cell cycle arrest (Bonomi et al., 2015a)
	SR4987(murine bone marrow-derived MSCs)	MOLT-4 U87MG CFPAC-1 J3T T98G	Cell cycle arrest and antiangiogenesis (Pessina et al., 2011; Pascucci et al., 2014; Pacioni et al., 2015; Bonomi et al., 2017a)
Sorafenib	hBM-MSCs	U87MG	Cytotoxic *in vitro* and antiangiogenesis *in vivo* (Clavreul et al., 2017)

CFPAC-1, ductal pancreatic adenocarcinoma; SCC154, squamous cell carcinoma of the tongue; MPM, malignant pleural mesothelioma; DU145, human prostate cancer; T98G, glioblastoma cell line; MOLT-4, acute lymphoblastic leukemia; L1210, mouse lymphocytic leukemia; B16, murine melanoma; RPMI8226, multiple myeloma; SK-ES-1, human Ewing sarcoma; SH-SY5Y (+), human neuroblastoma; GI-LI-N, human blastoma; MCF-7, breast cancer; J3T, canine glioma; U87MG, glioblastoma.

down-regulation diminishes the ability of leukemic cells to spread through bloodstream and reduces metastasis chance (Pessina et al., 2013).

Recently, novel administration approaches have been developed; for example, intranasal administration of sorafenib-loaded hBM-MSCs impedes angiogenesis and reduces the number of large vessels (Clavreul et al., 2017). The antineoplastic effect of drug-loaded MSCs with different anticancer drugs and the mechanism of actions in cancer cells are categorized in **Table 1**.

CONCLUSION

In recent years, rapid progression in the application of MSCs as a novel treatment for cancer has attracted much interest. MSCs are able to home into the tumor and metastatic sites and change the behavior of cancer and immune cells. They can induce apoptosis and inhibit the proliferation of tumor cells, which are critical points in cancer treatment. In addition, MSCs alter the secretion pattern of cells existing in the tumor microenvironment that can reduce angiogenesis and metastasis. Considering the high resistance of MSCs to a vast majority of antineoplastic agents, MSCs can play a role as a vehicle for targeted drug delivery. Besides this critical characteristic, MSCs can easily uptake chemotherapeutic drugs and release them in a time- and concentration-dependent manner. Both CM and direct contact of primed MSCs induce a considerable antineoplastic effect in a variety of cancer cell lines. Moreover, *in vivo* studies suggest that these drug-loaded cells can reduce the size of tumors and inhibit angiogenesis. Considering promising antineoplastic features of MSCs and drug-loaded ones, MSCs can be a proper candidate to be recruited in the clinic.

AUTHOR CONTRIBUTIONS

AB, PS, EJ, and HN contributed to the conception. AB, PS, and EJ reviewed the manuscript and wrote the original draft. HN and MF contributed to the manuscript revision and editing. All the authors read and approved the submitted version.

FUNDING

This work was supported by Pharmacology Department of School of Medicine, Shahid Beheshti University of Medical Sciences (19261). Research reported in this publication was supported by the National Institutes for Medical Research Development (NIMAD), Tehran, Iran.

ACKNOWLEDGMENTS

The authors would like to express their most sincere words of appreciation to Ms. Tahereh Tayebi for her valuable contribution.

REFERENCES

Adelipour, M., Babaei, F., Mirzababaei, M., and Allameh, A. (2017). Correlation of micro vessel density and c-Myc expression in breast tumor of mice following mesenchymal stem cell therapy. *Tissue Cell* 49(2 Pt B), 315–322. doi: 10.1016/j.tice.2017.01.007

Ahn, J. O., Chae, J. S., Coh, Y. R., Jung, W. S., Lee, H. W., Shin, I. S., et al. (2014). Human adipose tissue-derived mesenchymal stem cells inhibit T-cell lymphoma growth *in vitro* and *in vivo*. *Anticancer Res.* 34, 4839–4847.

Akimoto, K., Kimura, K., Nagano, M., Takano, S., To'a Salazar, G., Yamashita, T., et al. (2013). Umbilical cord blood-derived mesenchymal stem cells inhibit, but adipose tissue-derived mesenchymal stem cells promote, glioblastoma multiforme proliferation. *Stem Cells Dev.* 22, 1370–1386. doi: 10.1089/scd.2012.0486

Akiyama, Y., Radtke, C., Honmou, O., and Kocsis, J. D. (2002). Remyelination of the spinal cord following intravenous delivery of bone marrow cells. *Glia* 39, 229–236. doi: 10.1002/glia.10102

Amrutkar, M., and Gladhaug, I. P. (2017). Pancreatic cancer chemoresistance to gemcitabine. *Cancers* 9:157. doi: 10.3390/cancers9110157

Badawy, A., Sobh, M. A., Ahdy, M., and Abdelhafez, M. S. (2017). Bone marrow mesenchymal stem cell repair of cyclophosphamide-induced ovarian insufficiency in a mouse model. *Int. J. Womens Health* 9, 441–447. doi: 10.2147/ijwh.s134074

Bahrami, B., Hosseini, A., Talei, A. R., Ghaderi, A., and Razmkhah, M. (2017). Adipose derived stem cells exert immunomodulatory effects on natural killer cells in breast cancer. *Cell J.* 19, 137–145.

Ball, S. G., Shuttleworth, C. A., and Kielty, C. M. (2007). Vascular endothelial growth factor can signal through platelet-derived growth factor receptors. *J. Cell Biol.* 177, 489–500. doi: 10.1083/jcb.200608093

Balyasnikova, I. V., Prasol, M. S., Ferguson, S. D., Han, Y., Ahmed, A. U., Gutova, M., et al. (2014). Intranasal delivery of mesenchymal stem cells significantly extends survival of irradiated mice with experimental brain tumors. *Mol. Ther.* 22, 140–148. doi: 10.1038/mt.2013.199

Barbet, R., Peiffer, I., Hutchins, J. R., Hatzfeld, A., Garrido, E., and Hatzfeld, J. A. (2012). Expression of the 49 human ATP binding cassette (ABC) genes in pluripotent embryonic stem cells and in early- and late-stage multipotent mesenchymal stem cells: possible role of ABC plasma membrane transporters in maintaining human stem cell pluripotency. *Cell Cycle* 11, 1611–1620. doi: 10.4161/cc.20023

Bergers, G., and Song, S. (2005). The role of pericytes in blood-vessel formation and maintenance. *Neuro Oncol.* 7, 452–464. doi: 10.1215/s11528517050 00232

Bonomi, A., Coccè, V., Cavicchini, L., Sisto, F., Dossena, M., Balzarini, P., et al. (2013). Adipose tissue-derived stromal cells primed *in vitro* with paclitaxel acquire anti-tumor activity. *Int. J. Immunopathol. Pharmacol.* 26, 33–41. doi: 10.1177/03946320130260s105

Bonomi, A., Ghezzi, E., Pascucci, L., Aralla, M., Ceserani, V., Pettinari, L., et al. (2017a). Effect of canine mesenchymal stromal cells loaded with paclitaxel on growth of canine glioma and human glioblastoma cell lines. *Vet. J.* 223, 41–47. doi: 10.1016/j.tvjl.2017.05.005

Bonomi, A., Silini, A., Vertua, E., Signoroni, P. B., Coccè, V., Cavicchini, L., et al. (2015a). Human amniotic mesenchymal stromal cells (hAMSCs) as potential vehicles for drug delivery in cancer therapy: an *in vitro* study. *Stem Cell Res. Ther.* 6:155.

Bonomi, A., Sordi, V., Dugnani, E., Ceserani, V., Dossena, M., Coccè, V., et al. (2015b). Gemcitabine-releasing mesenchymal stromal cells inhibit *in vitro* proliferation of human pancreatic carcinoma cells. *Cytotherapy* 17, 1687–1695. doi: 10.1016/j.jcyt.2015.09.005

Bonomi, A., Steimberg, N., Benetti, A., Berenzi, A., Alessandri, G., Pascucci, L., et al. (2017b). Paclitaxel-releasing mesenchymal stromal cells inhibit the growth of multiple myeloma cells in a dynamic 3D culture system. *Hematol. Oncol.* 35, 693–702. doi: 10.1002/hon.2306

Borisy, G., Heald, R., Howard, J., Janke, C., Musacchio, A., and Nogales, E. (2016). Microtubules: 50 years on from the discovery of tubulin. *Nat. Rev. Mol. Cell Biol.* 17, 322–328. doi: 10.1038/nrm.2016.45

Bosco, D. B., Kenworthy, R., Zorio, D. A., and Sang, Q.-X. A. (2015). Human mesenchymal stem cells are resistant to Paclitaxel by adopting a non-proliferative fibroblastic state. *PLoS One* 10:e0128511. doi: 10.1371/journal.pone.0128511

Brini, A. T., Coccè, V., Ferreira, L. M. J., Giannasi, C., Cossellu, G., Giannì, A. B., et al. (2016). Cell-mediated drug delivery by gingival interdental papilla mesenchymal stromal cells (GinPa-MSCs) loaded with paclitaxel. *Expert Opin. Drug Deliv.* 13, 789–798. doi: 10.1517/17425247.2016.1167037

Bu, S., Wang, Q., Zhang, Q., Sun, J., He, B., Xiang, C., et al. (2016). Human endometrial mesenchymal stem cells exhibit intrinsic anti-tumor properties on human epithelial ovarian cancer cells. *Sci. Rep.* 6:37019.

Chen, J., Gomes, A. R., Monteiro, L. J., Wong, S. Y., Wu, L. H., Ng, T. T., et al. (2010). Constitutively nuclear FOXO3a localization predicts poor survival and promotes Akt phosphorylation in breast cancer. *PLoS One* 5:0012293. doi: 10.1371/journal.pone.0012293

Chen, J., Zhang, Z. G., Li, Y., Wang, L., Xu, Y. X., Gautam, S. C., et al. (2003). Intravenous administration of human bone marrow stromal cells induces angiogenesis in the ischemic boundary zone after stroke in rats. *Circ. Res.* 92, 692–699. doi: 10.1161/01.res.0000063425.51108.8d

Chen, Q., Ganapathy, S., Singh, K. P., Shankar, S., and Srivastava, R. K. (2010). Resveratrol induces growth arrest and apoptosis through activation of FOXO transcription factors in prostate cancer cells. *PLoS One* 5:0015288. doi: 10.1371/journal.pone.0015288

Choron, R. L., Chang, S., Khan, S., Villalobos, M. A., Zhang, P., Carpenter, J. P., et al. (2015). Paclitaxel impairs adipose stem cell proliferation and differentiation. *J. Surg. Res.* 196, 404–415. doi: 10.1016/j.jss.2015.03.026

Clavreul, A., Pourbaghi-Masouleh, M., Roger, E., Lautram, N., Montero-Menei, C. N., and Menei, P. (2017). Human mesenchymal stromal cells as cellular drug-delivery vectors for glioblastoma therapy: A good deal? *J. Exp. Clin. Cancer Res.* 36:135.

Coccè, V., Farronato, D., Brini, A. T., Masia, C., Giannì, A. B., Piovani, G., et al. (2017). Drug loaded gingival mesenchymal stromal cells (GinPa-MSCs) inhibit *in vitro* proliferation of oral squamous cell carcinoma. *Sci. Rep.* 7: 9376.

Coccè, V., Franzè, S., Brini, A. T., Giannì, A. B., Pascucci, L., Ciusani, E., et al. (2019). *In vitro* anticancer activity of extracellular vesicles (EVs) secreted by gingival mesenchymal stromal cells primed with paclitaxel. *Pharmaceutics* 11:61. doi: 10.3390/pharmaceutics11020061

Cousin, B., Ravet, E., Poglio, S., De Toni, F., Bertuzzi, M., Lulka, H., et al. (2009). Adult stromal cells derived from human adipose tissue provoke pancreatic cancer cell death both *in vitro* and *in vivo*. *PLoS One* 4:e6278. doi: 10.1371/journal.pone.0006278

Dai, T., Yang, E., Sun, Y., Zhang, L., Zhang, L., Shen, N., et al. (2013). Preparation and drug release mechanism of CTS-TAX-NP-MSCs drug delivery system. *Int. J. Pharm.* 456, 186–194. doi: 10.1016/j.ijpharm.2013.07.070

Dasari, V. R., Kaur, K., Velpula, K. K., Gujrati, M., Fassett, D., Klopfenstein, J. D., et al. (2010). Upregulation of PTEN in glioma cells by cord blood mesenchymal stem cells inhibits migration via downregulation of the PI3K/Akt pathway. *PLoS One* 5:e10350. doi: 10.1371/journal.pone.0010350

Derry, W. B., Wilson, L., Khan, I. A., Luduena, R. F., and Jordan, M. A. (1997). Taxol differentially modulates the dynamics of microtubules assembled from unfractionated and purified beta-tubulin isotypes. *Biochemistry* 36, 3554–3562. doi: 10.1021/bi962724m

Devitt, A., Moffatt, O. D., Raykundalia, C., Capra, J. D., Simmons, D. L., and Gregory, C. D. (1998). Human CD14 mediates recognition and phagocytosis of apoptotic cells. *Nature* 392, 505–509. doi: 10.1038/33169

Di Germanio, C., Bernier, M., Petr, M., Mattioli, M., Barboni, B., and de Cabo, R. (2016). Conditioned medium derived from rat amniotic epithelial cells confers protection against inflammation, cancer, and senescence. *Oncotarget* 7, 39051–39064. doi: 10.18632/oncotarget.9694

Dominici, M., Le Blanc, K., Mueller, I., Slaper-Cortenbach, I., Marini, F., Krause, D., et al. (2006). Minimal criteria for defining multipotent mesenchymal stromal cells. The International Society for Cellular Therapy position statement. *Cytotherapy* 8, 315–317. doi: 10.1080/14653240600855905

D'Souza, N., Burns, J. S., Grisendi, G., Candini, O., Veronesi, E., Piccinno, S., et al. (2013). MSC and Tumors: homing, differentiation, and secretion influence therapeutic potential. *Adv. Biochem. Eng. Biotechnol.* 130, 209–266. doi: 10.1007/10_2012_150

Duchi, S., Dambruoso, P., Martella, E., Sotgiu, G., Guerrini, A., Lucarelli, E., et al. (2014). Thiophene-based compounds as fluorescent tags to study mesenchymal stem cell uptake and release of taxanes. *Bioconj. Chem.* 25, 649–655. doi: 10.1021/bc5000498

Dwyer, R. M., Khan, S., Barry, F. P., O'Brien, T., and Kerin, M. J. (2010). Advances in mesenchymal stem cell-mediated gene therapy for cancer. *Stem Cell Res. Ther.* 1:25. doi: 10.1186/scrt25

Dwyer, R. M., Potter-Beirne, S. M., Harrington, K. A., Lowery, A. J., Hennessy, E., Murphy, J. M., et al. (2007). Monocyte chemotactic protein-1 secreted by primary breast tumors stimulates migration of mesenchymal stem cells. *Clin. Cancer Res.* 13, 5020–5027. doi: 10.1158/1078-0432.ccr-07-0731

El Andaloussi, S., Lakhal, S., Mäger, I., and Wood, M. J. (2013). Exosomes for targeted siRNA delivery across biological barriers. *Adv. Drug Deliv. Rev.* 65, 391–397. doi: 10.1016/j.addr.2012.08.008

El-Bialy, T., Alhadlaq, A., Wong, B., and Kucharski, C. (2014). Ultrasound effect on neural differentiation of gingival stem/progenitor cells. *Ann. Biomed. Eng.* 42, 1406–1412. doi: 10.1007/s10439-014-1013-9

El-Sayed, K. M., Paris, S., Graetz, C., Kassem, N., Mekhemar, M., Ungefroren, H., et al. (2015). Isolation and characterisation of human gingival margin-derived STRO-1/MACS(+) and MACS(-) cell populations. *Int. J. Oral Sci.* 7, 80–88. doi: 10.1038/ijos.2014.41

Fatima, F., and Nawaz, M. (2017). Vesiculated long non-coding RNAs: offshore packages deciphering trans-regulation between cells, cancer progression and resistance to therapies. *Noncoding RNA* 3:10. doi: 10.3390/ncrna3010010

Francois, S., Usunier, B., Forgue-Lafitte, M. E., L'Homme, B., Benderitter, M., Douay, L., et al. (2019). Mesenchymal stem cell administration attenuates colon cancer progression by modulating the immune component within the colorectal tumor microenvironment. *Stem Cells Transl. Med.* 8, 285–300. doi: 10.1002/sctm.18-0117

Gay, I., Cavender, A., Peto, D., Sun, Z., Speer, A., Cao, H., et al. (2014). Differentiation of human dental stem cells reveals a role for microRNA-218. *J. Periodontal Res.* 49, 110–120. doi: 10.1111/jre.12086

Gerhardt, H., and Betsholtz, C. (2003). Endothelial-pericyte interactions in angiogenesis. *Cell Tissue Res.* 314, 15–23. doi: 10.1007/s00441-003-0745-x

Gerhardt, H., and Semb, H. (2008). Pericytes: gatekeepers in tumour cell metastasis? *J. Mol. Med.* 86, 135–144. doi: 10.1007/s00109-007-0258-2

Gilazieva, Z., Tazetdinova, L., Arkhipova, S., Solovyeva, V., and Rizvanov, A. (2016). Effect of cisplatin on ultrastructure and viability of adipose-derived mesenchymal stem cells. *BioNanoScience* 6, 534–539. doi: 10.1007/s12668-016-0283-0

Gisbert-Garzarán, M., Lozano, D., Vallet-Regí, M., and Manzano, M. (2016). Self-immolative polymers as novel pH-responsive gate keepers for drug delivery. *RSC Adv.* 7, 132–136. doi: 10.1039/c6ra26771h

Gordon, S., and Martinez, F. O. (2010). Alternative activation of macrophages: mechanism and functions. *Immunity* 32, 593–604. doi: 10.1016/j.immuni.2010.05.007

Gu, C., Li, S., Tokuyama, T., Yokota, N., and Namba, H. (2010). Therapeutic effect of genetically engineered mesenchymal stem cells in rat experimental leptomeningeal glioma model. *Cancer Lett.* 291, 256–262. doi: 10.1016/j.canlet.2009.10.020

Guisasola, E., Baeza, A., Talelli, M., Arcos, D., Moros, M., de la Fuente, J. S. M., et al. (2015). Magnetic-responsive release controlled by hot spot effect. *Langmuir* 31, 12777–12782. doi: 10.1021/acs.langmuir.5b03470

Gupta, E., Luo, F., Lallo, A., Ramanathan, S., Vyas, V., Rubin, E., et al. (2000). The intestinal absorption of camptothecin, a highly lipophilic drug, across Caco-2 cells is mediated by active transporter(s). *Anticancer Res.* 20, 1013–1016.

Harris, W. M., Zhang, P., Plastini, M., Ortiz, T., Kappy, N., Benites, J., et al. (2017). Evaluation of function and recovery of adipose-derived stem cells after exposure to paclitaxel. *Cytotherapy* 19, 211–221. doi: 10.1016/j.jcyt.2016.10.010

Hayes-Jordan, A., Wang, Y. X., Walker, P., and Cox, C. S. (2014). Mesenchymal stromal cell dependent regression of pulmonary metastasis from Ewing's. *Front. Pediatr.* 2:44. doi: 10.3389/fped.2014.00044

Hendrata, M., and Sudiono, J. (2019). A hybrid multiscale model for investigating tumor angiogenesis and its response to cell-based therapy. *In Silico Biol.* 13, 1–20. doi: 10.3233/isb-170469

Ho, I. A., Toh, H. C., Ng, W. H., Teo, Y. L., Guo, C. M., Hui, K. M., et al. (2013). Human bone marrow-derived mesenchymal stem cells suppress human glioma growth through inhibition of angiogenesis. *Stem Cells* 31, 146–155. doi: 10.1002/stem.1247

Hossain, A., Gumin, J., Gao, F., Figueroa, J., Shinojima, N., Takezaki, T., et al. (2015). Mesenchymal stem cells isolated from human gliomas increase proliferation and maintain stemness of glioma stem cells through the IL-6/gp130/STAT3 pathway. *Stem Cells* 33, 2400–2415. doi: 10.1002/stem.2053

Huang, G.-J., Gronthos, S., and Shi, S. (2009). Mesenchymal stem cells derived from dental tissues vs. those from other sources: their biology and role in regenerative medicine. *J. Dent. Res.* 88, 792–806. doi: 10.1177/0022034509340867

Huang, X., Zhang, F., Wang, H., Niu, G., Choi, K. Y., Swierczewska, M., et al. (2013). Mesenchymal stem cell-based cell engineering with multifunctional mesoporous silica nanoparticles for tumor delivery. *Biomaterials* 34, 1772–1780. doi: 10.1016/j.biomaterials.2012.11.032

Huang, Y. S., Li, I. H., Chueh, S. H., Hueng, D. Y., Tai, M. C., Liang, C. M., et al. (2015). Mesenchymal stem cells from rat olfactory bulbs can differentiate into cells with cardiomyocyte characteristics. *J. Tissue Eng. Regen. Med.* 9, E191–E201.

Hung, S. W., Marrache, S., Cummins, S., Bhutia, Y. D., Mody, H., Hooks, S. B., et al. (2015). Defective hCNT1 transport contributes to gemcitabine chemoresistance in ovarian cancer subtypes: overcoming transport defects using a nanoparticle approach. *Cancer Lett.* 359, 233–240. doi: 10.1016/j.canlet.2015.01.017

Imitola, J., Raddassi, K., Park, K. I., Mueller, F. J., Nieto, M., Teng, Y. D., et al. (2004). Directed migration of neural stem cells to sites of CNS injury by the stromal cell-derived factor 1alpha/CXC chemokine receptor 4 pathway. *Proc. Natl. Acad. Sci. U.S.A.* 101, 18117–18122. doi: 10.1073/pnas.0408258102

Ino, K., Yamamoto, E., Shibata, K., Kajiyama, H., Yoshida, N., Terauchi, M., et al. (2008). Inverse correlation between tumoral indoleamine 2,3-dioxygenase expression and tumor-infiltrating lymphocytes in endometrial cancer: its association with disease progression and survival. *Clin. Cancer Res.* 14, 2310–2317. doi: 10.1158/1078-0432.ccr-07-4144

Jego, G., Hazoumé, A., Seigneuric, R., and Garrido, C. (2013). Targeting heat shock proteins in cancer. *Cancer Lett.* 332, 275–285. doi: 10.1016/j.canlet.2010.10.014

Ji, J. F., He, B. P., Dheen, S. T., and Tay, S. S. (2004). Interactions of chemokines and chemokine receptors mediate the migration of mesenchymal stem cells to the impaired site in the brain after hypoglossal nerve injury. *Stem Cells* 22, 415–427. doi: 10.1634/stemcells.22-3-415

Ji, K., Zhang, M., Chu, Q., Gan, Y., Ren, H., Zhang, L., et al. (2016). The role of p-STAT3 as a prognostic and clinicopathological marker in colorectal cancer: a systematic review and meta-analysis. *PLoS One* 11:e0160125. doi: 10.1371/journal.pone.0160125

Jiang, X. C., and Gao, J. Q. (2017). Exosomes as novel bio-carriers for gene and drug delivery. *Int. J. Pharm.* 521, 167–175. doi: 10.1016/j.ijpharm.2017.02.038

Jin, S. H., Lee, J. E., Yun, J. H., Kim, I., Ko, Y., and Park, J. B. (2015). Isolation and characterization of human mesenchymal stem cells from gingival connective tissue. *J. Periodontal Res.* 50, 461–467. doi: 10.1111/jre.12228

Kalimuthu, S., Gangadaran, P., Rajendran, R. L., Zhu, L., Oh, J. M., Lee, H. W., et al. (2018). A new approach for loading anticancer drugs into mesenchymal stem cell-derived exosome mimetics for cancer therapy. *Front. Pharmacol.* 9:1116. doi: 10.3389/fphar.2018.01116

Kansy, B. A., Dißmann, P. A., Hemeda, H., Bruderek, K., Westerkamp, A. M., Jagalski, V., et al. (2014). The bidirectional tumor–mesenchymal stromal cell interaction promotes the progression of head and neck cancer. *Stem Cell Res. Ther.* 5:95. doi: 10.1186/scrt484

Karnoub, A. E., Dash, A. B., Vo, A. P., Sullivan, A., Brooks, M. W., Bell, G. W., et al. (2007). Mesenchymal stem cells within tumour stroma promote breast cancer metastasis. *Nature* 449, 557–563. doi: 10.1038/nature06188

Karp, J. M., and Leng Teo, G. S. (2009). Mesenchymal stem cell homing: the devil is in the details. *Cell Stem Cell* 4, 206–216. doi: 10.1016/j.stem.2009.02.001

Kidd, S., Spaeth, E., Dembinski, J. L., Dietrich, M., Watson, K., Klopp, A., et al. (2009). Direct evidence of mesenchymal stem cell tropism for tumor and wounding microenvironments using *in vivo* bioluminescent imaging. *Stem Cells* 27, 2614–2623. doi: 10.1002/stem.187

Kimura, K., Kishida, T., Wakao, J., Tanaka, T., Higashi, M., Fumino, S., et al. (2016). Tumor-homing effect of human mesenchymal stem cells in a TH-MYCN mouse model of neuroblastoma. *J. Pediatr. Surg.* 51, 2068–2073. doi: 10.1016/j.jpedsurg.2016.09.041

Koç, O. N., Gerson, S. L., Cooper, B. W., Dyhouse, S. M., Haynesworth, S. E., Caplan, A. I., et al. (2000). Rapid hematopoietic recovery after coinfusion of autologous-blood stem cells and culture-expanded marrow mesenchymal stem cells in advanced breast cancer patients receiving high-dose chemotherapy. *J. Clin. Oncol.* 18, 307–316.

Kosztowski, T., Zaidi, H. A., and Quinones-Hinojosa, A. (2009). Applications of neural and mesenchymal stem cells in the treatment of gliomas. *Expert Rev. Anticancer Ther.* 9, 597–612. doi: 10.1586/era.09.22

Kucerova, L., Altanerova, V., Matuskova, M., Tyciakova, S., and Altaner, C. (2007). Adipose tissue-derived human mesenchymal stem cells mediated prodrug cancer gene therapy. *Cancer Res.* 67, 6304–6313. doi: 10.1158/0008-5472.can-06-4024

Kuci, S., Kuci, Z., Schafer, R., Spohn, G., Winter, S., Schwab, M., et al. (2019). Molecular signature of human bone marrow-derived mesenchymal stromal cell subsets. *Sci. Rep.* 9:38517.

Lam, M., Carmichael, A. R., and Griffiths, H. R. (2012). An aqueous extract of *Fagonia cretica* induces DNA damage, cell cycle arrest and apoptosis in breast cancer cells via FOXO3a and p53 expression. *PLoS One* 7:e40152. doi: 10.1371/journal.pone.0040152

Lee, H. Y., and Hong, I. S. (2017). Double-edged sword of mesenchymal stem cells: cancer-promoting versus therapeutic potential. *Cancer Sci.* 108, 1939–1946. doi: 10.1111/cas.13334

Lee, M. J., Heo, S. C., Shin, S. H., Kwon, Y. W., Do, E. K., Suh, D. S., et al. (2013). Oncostatin M promotes mesenchymal stem cell-stimulated tumor growth through a paracrine mechanism involving periostin and TGFBI. *Int. J. Biochem. Cell Biol.* 45, 1869–1877. doi: 10.1016/j.biocel.2013.05.027

Li, L., Wang, D., Zhou, J., Cheng, Y., Liang, T., and Zhang, G. (2015). Characteristics of human amniotic fluid mesenchymal stem cells and their tropism to human ovarian cancer. *PLoS One* 10:e0123350. doi: 10.1371/journal.pone.0123350

Li, M., Sun, S., Dangelmajer, S., Zhang, Q., Wang, J., Hu, F., et al. (2019). Exploiting tumor-intrinsic signals to induce mesenchymal stem cell-mediated suicide gene therapy to fight malignant glioma. *Stem Cell Res. Ther.* 10:88.

Liang, W., Xia, H., Li, J., and Zhao, R. C. (2011). Human adipose tissue derived mesenchymal stem cells are resistant to several chemotherapeutic agents. *Cytotechnology* 63, 523–530. doi: 10.1007/s10616-011-9374-5

Liao, W., Du, Y., Zhang, C., Pan, F., Yao, Y., Zhang, T., et al. (2019). Exosomes: the next generation of endogenous nanomaterials for advanced drug delivery and therapy. *Acta Biomater.* 86, 1–14. doi: 10.1016/j.actbio.2018.12.045

Lin, H., Hu, B., He, X., Mao, J., Wang, Y., Wang, J., et al. (2020). Overcoming Taxol-resistance in A549 cells: a comprehensive strategy of targeting P-gp transporter, AKT/ERK pathways, and cytochrome P450 enzyme CYP1B1 by 4-hydroxyemodin. *Biochem. Pharmacol.* 171:113733. doi: 10.1016/j.bcp.2019.113733

Lin, J. T., Wang, J. Y., Chen, M. K., Chen, H. C., Chang, T. H., Su, B. W., et al. (2013). Colon cancer mesenchymal stem cells modulate the tumorigenicity of colon cancer through interleukin 6. *Exp. Cell Res.* 319, 2216–2229. doi: 10.1016/j.yexcr.2013.06.003

Liu, J., Hao, H., Xia, L., Ti, D., Huang, H., Dong, L., et al. (2015). Hypoxia pretreatment of bone marrow mesenchymal stem cells facilitates angiogenesis

by improving the function of endothelial cells in diabetic rats with lower ischemia. *PLoS One* 10:e0126715. doi: 10.1371/journal.pone.0126715

Lowe, E. L., Crother, T. R., Rabizadeh, S., Hu, B., Wang, H., Chen, S., et al. (2010). Toll-like receptor 2 signaling protects mice from tumor development in a mouse model of colitis-induced cancer. *PLoS One* 5:e13027. doi: 10.1371/journal.pone.0013027

Luan, X., Sansanaphongpricha, K., Myers, I., Chen, H., Yuan, H., and Sun, D. (2017). Engineering exosomes as refined biological nanoplatforms for drug delivery. *Acta Pharmacol. Sin.* 38, 754–763. doi: 10.1038/aps.2017.12

Magatti, M., De Munari, S., Vertua, E., and Parolini, O. (2012). Amniotic membrane-derived cells inhibit proliferation of cancer cell lines by inducing cell cycle arrest. *J. Cell. Mol. Med.* 16, 2208–2218. doi: 10.1111/j.1582-4934.2012.01531.x

Malla, R., Gopinath, S., Alapati, K., Gondi, C. S., Gujrati, M., Dinh, D. H., et al. (2010). Downregulation of uPAR and cathepsin B induces apoptosis via regulation of Bcl-2 and Bax and inhibition of the PI3K/Akt pathway in gliomas. *PLoS One* 5:e13731. doi: 10.1371/journal.pone.0013731

Marei, H. E., Casalbore, P., Althani, A., Cocce, V., Cenciarelli, C., Alessandri, G., et al. (2019). Human olfactory bulb neural stem cells (Hu-OBNSCs) can be loaded with paclitaxel and used to inhibit glioblastoma cell growth. *Pharmaceutics* 11:45. doi: 10.3390/pharmaceutics11010045

Martínez-Carmona, M., Lozano, D., Baeza, A., Colilla, M., and Vallet-Regí, M. (2017). A novel visible light responsive nanosystem for cancer treatment. *Nanoscale* 9, 15967–15973. doi: 10.1039/c7nr05050j

Menge, T., Gerber, M., Wataha, K., Reid, W., Guha, S., Cox, C. S. Jr., et al. (2013). Human mesenchymal stem cells inhibit endothelial proliferation and angiogenesis via cell-cell contact through modulation of the VE-Cadherin/β-catenin signaling pathway. *Stem Cells Dev.* 22, 148–157. doi: 10.1089/scd.2012.0165

Menge, T., Zhao, Y., Zhao, J., Wataha, K., Gerber, M., Zhang, J., et al. (2012). Mesenchymal stem cells regulate blood-brain barrier integrity through TIMP3 release after traumatic brain injury. *Sci. Transl. Med.* 4;3004660.

Modaresifar, K., Azizian, S., Zolghadr, M., Moravvej, H., Ahmadiani, A., and Niknejad, H. (2017). The effect of cryopreservation on anti-cancer activity of human amniotic membrane. *Cryobiology* 74, 61–67. doi: 10.1016/j.cryobiol.2016.12.001

Momin, E. N., Vela, G., Zaidi, H. A., and Quinones-Hinojosa, A. (2010). The oncogenic potential of mesenchymal stem cells in the treatment of cancer: directions for future research. *Curr. Immunol. Rev.* 6, 137–148. doi: 10.2174/157339510791111718

Multhoff, G., Molls, M., and Radons, J. (2011). Chronic inflammation in cancer development. *Front. Immunol.* 2:98. doi: 10.3389/fimmu.2011.00098

Münz, F., Perez, R. L., Trinh, T., Sisombath, S., Weber, K.-J., Wuchter, P., et al. (2018). Human mesenchymal stem cells lose their functional properties after paclitaxel treatment. *Sci. Rep.* 8:312.

Naderi-Meshkin, H., Matin, M. M., Heirani-Tabasi, A., Mirahmadi, M., Irfan-Maqsood, M., Edalatmanesh, M. A., et al. (2016). Injectable hydrogel delivery plus preconditioning of mesenchymal stem cells: exploitation of SDF-1/CXCR4 axis toward enhancing the efficacy of stem cells' homing. *Cell Biol. Int.* 40, 730–741. doi: 10.1002/cbin.10474

Nawaz, M. (2017). Extracellular vesicle-mediated transport of non-coding RNAs between stem cells and cancer cells: implications in tumor progression and therapeutic resistance. *Stem Cell Investig.* 4:83. doi: 10.21037/sci.2017.10.04

Nawaz, M., Fatima, F., Vallabhaneni, K. C., Penfornis, P., Valadi, H., Ekström, K., et al. (2016). Extracellular vesicles: evolving factors in stem cell biology. *Stem Cells Int.* 2016:1073140.

Nicolay, N. H., Perez, R. L., Rühle, A., Trinh, T., Sisombath, S., Weber, K.-J., et al. (2016a). Mesenchymal stem cells maintain their defining stem cell characteristics after treatment with cisplatin. *Sci. Rep.* 6:20035.

Nicolay, N. H., Rühle, A., Perez, R. L., Trinh, T., Sisombath, S., Weber, K.-J., et al. (2016b). Mesenchymal stem cells are sensitive to bleomycin treatment. *Sci. Rep.* 6:26645.

Nobili, S., Lapucci, A., Landini, I., Coronnello, M., Roviello, G., and Mini, E. (2019). Role of ATP-binding cassette transporters in cancer initiation and progression. *Semin. Cancer Biol.* 60, 72–95. doi: 10.1016/j.semcancer.2019.08.006

Ong, W. K., and Sugii, S. (2013). Adipose-derived stem cells: fatty potentials for therapy. *Int. J. Biochem. Cell Biol.* 45, 1083–1086. doi: 10.1016/j.biocel.2013.02.013

Osaka, M., Honmou, O., Murakami, T., Nonaka, T., Houkin, K., Hamada, H., et al. (2010). Intravenous administration of mesenchymal stem cells derived from bone marrow after contusive spinal cord injury improves functional outcome. *Brain Res.* 1343, 226–235. doi: 10.1016/j.brainres.2010.05.011

Otsu, K., Das, S., Houser, S. D., Quadri, S. K., Bhattacharya, S., and Bhattacharya, J. (2009). Concentration-dependent inhibition of angiogenesis by mesenchymal stem cells. *Blood* 113, 4197–4205. doi: 10.1182/blood-2008-09-176198

Pacioni, S., D'Alessandris, Q. G., Giannetti, S., Morgante, L., Coccè, V., Bonomi, A., et al. (2017). Human mesenchymal stromal cells inhibit tumor growth in orthotopic glioblastoma xenografts. *Stem Cell Res. Ther.* 8:53.

Pacioni, S., D'Alessandris, Q. G., Giannetti, S., Morgante, L., De Pascalis, I., Coccè, V., et al. (2015). Mesenchymal stromal cells loaded with paclitaxel induce cytotoxic damage in glioblastoma brain xenografts. *Stem Cell Res. Ther.* 6:194.

Paris, J. L., de la Torre, P., Victoria Cabanas, M., Manzano, M., Grau, M., Flores, A. I., et al. (2017). Vectorization of ultrasound-responsive nanoparticles in placental mesenchymal stem cells for cancer therapy. *Nanoscale* 9, 5528–5537. doi: 10.1039/c7nr01070b

Parker Kerrigan, B. C., Shimizu, Y., Andreeff, M., and Lang, F. F. (2017). Mesenchymal stromal cells for the delivery of oncolytic viruses in gliomas. *Cytotherapy* 19, 445–457. doi: 10.1016/j.jcyt.2017.02.002

Pascucci, L., Coccè, V., Bonomi, A., Ami, D., Ceccarelli, P., Ciusani, E., et al. (2014). Paclitaxel is incorporated by mesenchymal stromal cells and released in exosomes that inhibit *in vitro* tumor growth: a new approach for drug delivery. *J. Control. Release* 192, 262–270. doi: 10.1016/j.jconrel.2014.07.042

Patlolla, R. R., and Vobalaboina, V. (2008). Folate-targeted etoposide-encapsulated lipid nanospheres. *J. Drug Target.* 16, 269–275. doi: 10.1080/10611860801945400

Pessina, A., Bonomi, A., Coccè, V., Invernici, G., Navone, S., Cavicchini, L., et al. (2011). Mesenchymal stromal cells primed with paclitaxel provide a new approach for cancer therapy. *PLoS One* 6:e28321. doi: 10.1371/journal.pone.0028321

Pessina, A., Coccè, V., Pascucci, L., Bonomi, A., Cavicchini, L., Sisto, F., et al. (2013). Mesenchymal stromal cells primed with P aclitaxel attract and kill leukaemia cells, inhibit angiogenesis and improve survival of leukaemia-bearing mice. *Br. J. Haematol.* 160, 766–778. doi: 10.1111/bjh.12196

Pessina, A., Leonetti, C., Artuso, S., Benetti, A., Dessy, E., Pascucci, L., et al. (2015). Drug-releasing mesenchymal cells strongly suppress B16 lung metastasis in a syngeneic murine model. *J. Exp. Clin. Cancer Res.* 34:82.

Petrella, F., Coccè, V., Masia, C., Milani, M., Salè, E. O., Alessandri, G., et al. (2017). Paclitaxel-releasing mesenchymal stromal cells inhibit *in vitro* proliferation of human mesothelioma cells. *Biomed. Pharmacother.* 87, 755–758. doi: 10.1016/j.biopha.2017.01.118

Pili, B., Bourgaux, C., Meneau, F., Couvreur, P., and Ollivon, M. (2009). Interaction of an anticancer drug, gemcitabine, with phospholipid bilayers. *J. Therm. Anal. Calorim.* 98, 19–28. doi: 10.1007/s10973-009-0229-7

Pinarli, F. A., Turan, N. N., Pınarlı, F. G., Okur, A., Sönmez, D., Ulus, T., et al. (2013). Resveratrol and adipose-derived mesenchymal stem cells are effective in the prevention and treatment of doxorubicin cardiotoxicity in rats. *Pediatr. Hematol. Oncol.* 30, 226–238. doi: 10.3109/08880018.2012.762962

Polioudaki, H., Kastrinaki, M. C., Papadaki, H., and Theodoropoulos, P. (2009). Microtubule-interacting drugs induce moderate and reversible damage to human bone marrow mesenchymal stem cells. *Cell Prolifer.* 42, 434–447. doi: 10.1111/j.1365-2184.2009.00607.x

Ponte, A. L., Marais, E., Gallay, N., Langonné, A., Delorme, B., Hérault, O., et al. (2007). The *in vitro* migration capacity of human bone marrow mesenchymal stem cells: comparison of chemokine and growth factor chemotactic activities. *Stem Cells* 25, 1737–1745. doi: 10.1634/stemcells.2007-0054

Ramasamy, R., Lam, E. W., Soeiro, I., Tisato, V., Bonnet, D., and Dazzi, F. (2007). Mesenchymal stem cells inhibit proliferation and apoptosis of tumor cells: impact on *in vivo* tumor growth. *Leukemia* 21, 304–310. doi: 10.1038/sj.leu.2404489

Rhee, K. J., Lee, J. I., and Eom, Y. W. (2015). Mesenchymal stem cell-mediated effects of tumor support or suppression. *Int. J. Mol. Sci.* 16, 30015–30033. doi: 10.3390/ijms161226215

Rimoldi, I., Cocce, V., Facchetti, G., Alessandri, G., Brini, A. T., Sisto, F., et al. (2018). Uptake-release by MSCs of a cationic platinum(II) complex active

in vitro on human malignant cancer cell lines. *Biomed. Pharmacother.* 108, 111–118. doi: 10.1016/j.biopha.2018.09.040

Rivera-Cruz, C. M., Shearer, J. J., Figueiredo Neto, M., and Figueiredo, M. L. (2017). The immunomodulatory effects of mesenchymal stem cell polarization within the tumor microenvironment niche. *Stem Cells Int.* 2017:4015039.

Rolfo, A., Giuffrida, D., Giuffrida, M. C., Todros, T., and Calogero, A. E. (2014). New perspectives for prostate cancer treatment: *in vitro* inhibition of LNCaP and PC3 cell proliferation by amnion-derived mesenchymal stromal cells conditioned media. *Aging Male* 17, 94–101. doi: 10.3109/13685538.2014.896894

Ruvolo, P. P. (2012). The Herculean task of killing cancer cells: suppression of FOXO3A in acute leukemia involves a hydra of multiple survival kinases. *Cell Cycle* 11:2589. doi: 10.4161/cc.21233

Salehi, H., Al-Arag, S., Middendorp, E., Gergely, C., Cuisinier, F., and Orti, V. (2018). Dental pulp stem cells used to deliver the anticancer drug paclitaxel. *Stem Cell Res. Ther.* 9:103.

Seo, S., Kim, K., Park, S., Suh, Y., Kim, S., Jeun, S., et al. (2011). The effects of mesenchymal stem cells injected via different routes on modified IL-12-mediated antitumor activity. *Gene Ther.* 18, 488–495. doi: 10.1038/gt.2010.170

Shangguan, L., Ti, X., Krause, U., Hai, B., Zhao, Y., Yang, Z., et al. (2012). Inhibition of TGF-β/Smad signaling by BAMBI blocks differentiation of human mesenchymal stem cells to carcinoma-associated fibroblasts and abolishes their protumor effects. *Stem Cells* 30, 2810–2819. doi: 10.1002/stem.1251

Sherif, I. O., Sabry, D., Abdel-Aziz, A., and Sarhan, O. M. (2018). The role of mesenchymal stem cells in chemotherapy-induced gonadotoxicity. *Stem Cell Res. Ther.* 9:196.

Shukla, S., Bhaskaran, N., Babcook, M. A., Fu, P., Maclennan, G. T., and Gupta, S. (2014). Apigenin inhibits prostate cancer progression in TRAMP mice via targeting PI3K/Akt/FoxO pathway. *Carcinogenesis* 35, 452–460. doi: 10.1093/carcin/bgt316

Shukla, S., Bhaskaran, N., Maclennan, G. T., and Gupta, S. (2013). Deregulation of FoxO3a accelerates prostate cancer progression in TRAMP mice. *Prostate* 73, 1507–1517. doi: 10.1002/pros.22698

Siegel, R. L., Miller, K. D., and Jemal, A. (2019). Cancer statistics, 2019. *CA Cancer J. Clin.* 69, 7–34.

Somaiah, C., Kumar, A., Sharma, R., Sharma, A., Anand, T., Bhattacharyya, J., et al. (2018). Mesenchymal stem cells show functional defect and decreased anti-cancer effect after exposure to chemotherapeutic drugs. *J. Biomed. Sci.* 25:5.

Spaeth, E., Klopp, A., Dembinski, J., Andreeff, M., and Marini, F. (2008). Inflammation and tumor microenvironments: defining the migratory itinerary of mesenchymal stem cells. *Gene Ther.* 15, 730–738. doi: 10.1038/gt.2008.39

Spaeth, E. L., Dembinski, J. L., Sasser, A. K., Watson, K., Klopp, A., Hall, B., et al. (2009). Mesenchymal stem cell transition to tumor-associated fibroblasts contributes to fibrovascular network expansion and tumor progression. *PLoS One* 4:e4992. doi: 10.1371/journal.pone.0004992

Stengel, C., Newman, S. P., Leese, M. P., Potter, B. V., Reed, M. J., and Purohit, A. (2010). Class III beta-tubulin expression and *in vitro* resistance to microtubule targeting agents. *Br. J. Cancer* 102, 316–324. doi: 10.1038/sj.bjc.6605489

Tang, R. J., Shen, S. N., Zhao, X. Y., Nie, Y. Z., Xu, Y. J., Ren, J., et al. (2015). Mesenchymal stem cells-regulated Treg cells suppress colitis-associated colorectal cancer. *Stem Cell Res. Ther.* 6:71.

Teo, G. S., Ankrum, J. A., Martinelli, R., Boetto, S. E., Simms, K., Sciuto, T. E., et al. (2012). Mesenchymal stem cells transmigrate between and directly through tumor necrosis factor-alpha-activated endothelial cells via both leukocyte-like and novel mechanisms. *Stem Cells* 30, 2472–2486. doi: 10.1002/stem.1198

Tyciakova, S., Matuskova, M., Bohovic, R., and Kucerova, L. (2017). Mesenchymal stromal cells producing TNFα lack inhibitory effect against A375 experimental lung metastases. *Neoplasma* 64, 222–227. doi: 10.4149/neo_2017_208

Uccelli, A., Moretta, L., and Pistoia, V. (2006). Immunoregulatory function of mesenchymal stem cells. *Eur. J. Immunol.* 36, 2566–2573. doi: 10.1002/eji.200636416

Vidal, M. A., Walker, N. J., Napoli, E., and Borjesson, D. L. (2012). Evaluation of senescence in mesenchymal stem cells isolated from equine bone marrow, adipose tissue, and umbilical cord tissue. *Stem Cells Dev.* 21, 273–283. doi: 10.1089/scd.2010.0589

Vizoso, F. J., Eiro, N., Cid, S., Schneider, J., and Perez-Fernandez, R. (2017). Mesenchymal stem cell secretome: toward cell-free therapeutic strategies in regenerative medicine. *Int. J. Mol. Sci.* 18:1852. doi: 10.3390/ijms18091852

Wang, Q., Li, Z., Sun, L., Chen, B., Zhao, Y., Shen, B., et al. (2018). Platelets enhance the ability of bone-marrow mesenchymal stem cells to promote cancer metastasis. *Oncotargets Ther.* 11, 8251–8263. doi: 10.2147/ott.s181673

Wang, W., Li, N. N., Du, Y., Lv, F. F., and Lin, G. Q. (2013). FoxO3a and nilotinib-induced erythroid differentiation of CML-BC cells. *Leuk. Res.* 37, 1309–1314. doi: 10.1016/j.leukres.2013.07.001

Wang, X., Chen, H., Zeng, X., Guo, W., Jin, Y., Wang, S., et al. (2019). Efficient lung cancer-targeted drug delivery via a nanoparticle/MSC system. *Acta Pharm. Sin. B* 9, 167–176. doi: 10.1016/j.apsb.2018.08.006

Wang, Y., Chu, Y., Ren, X., Xiang, H., Xi, Y., Ma, X., et al. (2019). Epidural adipose tissue-derived mesenchymal stem cell activation induced by lung cancer cells promotes malignancy and EMT of lung cancer. *Stem Cell Res. Ther.* 10:168.

Willert, K., and Jones, K. A. (2006). Wnt signaling: is the party in the nucleus? *Genes Dev.* 20, 1394–1404. doi: 10.1101/gad.1424006

Wolfe, A. R., Trenton, N. J., Debeb, B. G., Larson, R., Ruffell, B., Chu, K., et al. (2016). Mesenchymal stem cells and macrophages interact through IL-6 to promote inflammatory breast cancer in pre-clinical models. *Oncotarget* 7, 82482–82492. doi: 10.18632/oncotarget.12694

Wong, H. L., Rauth, A. M., Bendayan, R., Manias, J. L., Ramaswamy, M., Liu, Z., et al. (2006). A new polymer-lipid hybrid nanoparticle system increases cytotoxicity of doxorubicin against multidrug-resistant human breast cancer cells. *Pharm. Res.* 23, 1574–1585. doi: 10.1007/s11095-006-0282-x

Wu, M., Zhang, R., Zou, Q., Chen, Y., Zhou, M., Li, X., et al. (2018). Comparison of the biological characteristics of mesenchymal stem cells derived from the human placenta and umbilical cord. *Sci. Rep.* 8:5014.

Wu, W., Liu, X., Chaftari, P., Cruz Carreras, M. T., Gonzalez, C., Viets-Upchurch, J., et al. (2015). Association of body composition with outcome of docetaxel chemotherapy in metastatic prostate cancer: a retrospective review. *PLoS One* 10:e0122047. doi: 10.1371/journal.pone.0122047

Xia, W., and Hou, M. (2018). Macrophage migration inhibitory factor rescues mesenchymal stem cells from doxorubicin-induced senescence though the PI3K-Akt signaling pathway. *Int. J. Mol. Med.* 41, 1127–1137.

Xian, X., Hakansson, J., Stahlberg, A., Lindblom, P., Betsholtz, C., Gerhardt, H., et al. (2006). Pericytes limit tumor cell metastasis. *J. Clin. Investig.* 116, 642–651. doi: 10.1172/jci25705

Xu, J., Li, L., Xiong, J., Zheng, Y., Ye, Q., and Li, Y. (2015). Cyclophosphamide combined with bone marrow mesenchymal stromal cells protects against bleomycin-induced lung fibrosis in mice. *Ann. Clin. Lab. Sci.* 45, 292–300.

Yang, J. Y., Chang, C. J., Xia, W., Wang, Y., Wong, K. K., Engelman, J. A., et al. (2010). Activation of FOXO3a is sufficient to reverse mitogen-activated protein/extracellular signal-regulated kinase kinase inhibitor chemoresistance in human cancer. *Cancer Res.* 70, 4709–4718. doi: 10.1158/0008-5472.can-09-4524

Ye, H., Cheng, J., Tang, Y., Liu, Z., Xu, C., Liu, Y., et al. (2012). Human bone marrow-derived mesenchymal stem cells produced TGFbeta contributes to progression and metastasis of prostate cancer. *Cancer Investig.* 30, 513–518. doi: 10.3109/07357907.2012.692171

Yin, X., Li, Y., Li, J., Li, P., Liu, Y., Wen, J., et al. (2016). Generation and periodontal differentiation of human gingival fibroblasts-derived integration-free induced pluripotent stem cells. *Biochem. Biophys. Res. Commun.* 473, 726–732. doi: 10.1016/j.bbrc.2015.10.012

Zhang, Q., Li, X., Li, Y., Chen, S., Shen, X., Dong, X., et al. (2020). Expression of the PTEN/FOXO3a/PLZF signalling pathway in pancreatic cancer and its significance in tumourigenesis and progression. *Invest. New Drugs* 38, 321–328. doi: 10.1007/s10637-019-00791-7

Zhang, Q., Shi, S., Liu, Y., Uyanne, J., Shi, Y., Shi, S., et al. (1950). Mesenchymal stem cells derived from human gingiva are capable of immunomodulatory functions and ameliorate inflammation-related tissue destruction in experimental colitis. *J. Immunol.* 183, 7787–7798. doi: 10.4049/jimmunol.0902318

Zhang, Y. H., Gao, Z. F., Dong, G. H., Li, X., Wu, Y., Li, G., et al. (2020). Suppression of alphavbeta6 downregulates P-glycoprotein and sensitizes multidrug-resistant breast cancer cells to anticancer drugs. *Neoplasma* 67, 379–388. doi: 10.4149/neo_2020_190604n486

Zhu, Y., Sun, Z., Han, Q., Liao, L., Wang, J., Bian, C., et al. (2009). Human mesenchymal stem cells inhibit cancer cell proliferation by secreting DKK-1. *Leukemia* 23, 925–933. doi: 10.1038/leu.2008.384

Zimmerlin, L., Park, T. S., Zambidis, E. T., Donnenberg, V. S., and Donnenberg, A. D. (2013). Mesenchymal stem cell secretome and regenerative therapy after cancer. *Biochimie* 95, 2235–2245. doi: 10.1016/j.biochi.2013.05.010

Zoja, C., Garcia, P. B., Rota, C., Conti, S., Gagliardini, E., Corna, D., et al. (2012). Mesenchymal stem cell therapy promotes renal repair by limiting glomerular podocyte and progenitor cell dysfunction in adriamycin-induced nephropathy. *Am. J. Physiol. Renal Physiol.* 303, F1370–F1381.

Conflict of Interest: The authors declare that the research was conducted in the absence of any commercial or financial relationships that could be construed as a potential conflict of interest.

frontiers in Bioengineering and Biotechnology

ORIGINAL RESEARCH
published: 16 November 2020
doi: 10.3389/fbioe.2020.602210

De novo Vessel Formation Through Cross-Talk of Blood-Derived Cells and Mesenchymal Stromal Cells in the Absence of Pre-existing Vascular Structures

Beate M. Rüger[1], Tanja Buchacher[2], Eva-Maria Dauber[1], Markus Pasztorek[3], Pavel Uhrin[4], Michael B. Fischer[1,3], Johannes M. Breuss[4] and Gerda C. Leitner[1]*

[1] Department of Blood Group Serology and Transfusion Medicine, Medical University of Vienna, Vienna, Austria, [2] Turku Bioscience Centre, University of Turku and Åbo Akademi University, Turku, Finland, [3] Department of Health Sciences, Medicine and Research, Faculty of Health and Medicine, Danube University Krems, Krems an der Donau, Austria, [4] Department of Vascular Biology and Thrombosis Research, Center for Physiology and Pharmacology, Medical University of Vienna, Vienna, Austria

OPEN ACCESS

Edited by:
Cornelia Kasper, University of Natural Resources and Life Sciences, Vienna, Austria

Reviewed by:
Richard Schäfer, German Red Cross Blood Donor Service Baden-Württemberg-Hessen gGmbH, Goethe University Hospital Frankfurt am Main, Germany
Pavel Makarevich, Lomonosov Moscow State University, Russia

***Correspondence:**
Beate M. Rüger
beate.rueger@meduniwien.ac.at

Specialty section:
This article was submitted to Preclinical Cell and Gene Therapy, a section of the journal Frontiers in Bioengineering and Biotechnology

Received: *02 September 2020*
Accepted: *26 October 2020*
Published: *16 November 2020*

Citation:
Rüger BM, Buchacher T, Dauber E-M, Pasztorek M, Uhrin P, Fischer MB, Breuss JM and Leitner GC (2020) De novo Vessel Formation Through Cross-Talk of Blood-Derived Cells and Mesenchymal Stromal Cells in the Absence of Pre-existing Vascular Structures. Front. Bioeng. Biotechnol. 8:602210. doi: 10.3389/fbioe.2020.602210

Background: The generation of functional blood vessels remains a key challenge for regenerative medicine. Optimized *in vitro* culture set-ups mimicking the *in vivo* perivascular niche environment during tissue repair may provide information about the biological function and contribution of progenitor cells to postnatal vasculogenesis, thereby enhancing their therapeutic potential.

Aim: We established a fibrin-based xeno-free human 3D *in vitro* vascular niche model to study the interaction of mesenchymal stromal cells (MSC) with peripheral blood mononuclear cells (PBMC) including circulating progenitor cells in the absence of endothelial cells (EC), and to investigate the contribution of this cross-talk to neo-vessel formation.

Materials and Methods: Bone marrow-derived MSC were co-cultured with whole PBMC, enriched monocytes (Mo), enriched T cells, and Mo together with T cells, respectively, obtained from leukocyte reduction chambers generated during the process of single-donor platelet apheresis. Cells were embedded in 3D fibrin matrices, using exclusively human-derived culture components without external growth factors. Cytokine secretion was analyzed in supernatants of 3D cultures by cytokine array, vascular endothelial growth factor (VEGF) secretion was quantified by ELISA. Cellular and structural re-arrangements were characterized by immunofluorescence and confocal laser-scanning microscopy of topographically intact 3D fibrin gels.

Results: 3D co-cultures of MSC with PBMC, and enriched Mo together with enriched T cells, respectively, generated, within 2 weeks, complex $CD31^+/CD34^+$ vascular structures, surrounded by basement membrane collagen type-IV^+ cells and matrix, in association with increased VEGF secretion. PBMC contained $CD31^+CD34^+CD45^{dim}CD14^-$ progenitor-type cells, and EC of neo-vessels were

PBMC-derived. Vascular structures showed intraluminal $CD45^+$ cells that underwent apoptosis thereby creating a lumen. Cross-talk of MSC with enriched Mo provided a pro-angiogenic paracrine environment. MSC co-cultured with enriched T cells formed "cell-in-cell" structures generated through internalization of T cells by $CD31^+CD45^{dim/-}$ cells. No vascular structures were detected in co-cultures of MSC with either Mo or T cells.

Conclusion: Our xeno-free 3D *in vitro* vascular niche model demonstrates that a complex synergistic network of cellular, extracellular and paracrine cross-talk can contribute to *de novo* vascular development through self-organization via co-operation of immune cells with blood-derived progenitor cells and MSC, and thereby may open a new perspective for advanced vascular tissue engineering in regenerative medicine.

Keywords: vascular niche model, 3D fibrin matrix, mesenchymal stromal cells, endothelial progenitor cells, vasculogenesis, self-organization, inflammation, cell-in-cell

INTRODUCTION

The formation of new blood vessels is essential for normal physiological processes, and plays a key role in the repair of injured tissues. Neo-vessels are generated by sprouting of existing vascular structures through angiogenesis supported by incorporation of endothelial progenitor cells (EPC) by vasculogenesis (Asahara et al., 1999; Ribatti et al., 2001). This co-operative process takes place within a tightly controlled inflammatory microenvironment that orchestrates successful regeneration and healing. If not properly coordinated and persisting, a continuous repair process promotes excessive neovascularization and influx of more inflammatory cells eventually causing fibrosis and loss of tissue and organ function. The regenerative vascular niche environment is created via injury-induced increased vascular permeability and perivascular fibrin deposition that attract various types of leukocytes and progenitor cells, providing an ideal platform for complex interactions with resident and recruited mesenchymal stromal cells (MSC). MSC are multipotential cells found in nearly all tissues of the body where they reside close to blood vessels (Crisan et al., 2008). Upon tissue injury, they become activated through inflammatory cytokines such as interleukin (IL)-1β, tumor necrosis factor (TNF)-α, and interferon (IFN)-γ released by inflammatory cells after recruitment to the site of damage (Singer and Caplan, 2011). MSC contribute to repair processes by regulating the local immune response and secreting paracrine factors thereby establishing a regenerative environment and promoting the formation of new blood vessels (Caplan and Correa, 2011). We have recently shown that vascular endothelial growth factor (VEGF) secretion by MSC increases considerably when they encounter and have direct contact with peripheral blood-derived mononuclear cells (PBMC) in a 3D fibrin environment (Rüger et al., 2018).

Macrophages amongst leukocyte subsets, play important roles during all stages of tissue repair. Although they are mainly known as scavenger cells that phagocytize cellular debris, neutrophils, and other apoptotic cells following tissue injury (Peiser et al., 2002), macrophages also exhibit more complex roles in tissue repair (Wynn et al., 2013). They are involved in the initial cellular response following injury by secretion of various cytokines, chemokines, matrix metalloproteinases, as well as other inflammatory mediators (Wynn and Barron, 2010). Similarly, macrophages promote cellular proliferation and blood vessel development in a paracrine fashion through production of numerous growth factors including platelet derived growth factor (PDGF), transforming growth factor (TGF)-β1, insulin-like growth factor (IGF)-1, and VEGF (Shimokado et al., 1985; Rappolee et al., 1988; Berse et al., 1992; Chujo et al., 2009; Willenborg et al., 2012). Macrophages not only regulate the proliferation and expansion of neighboring parenchymal and stromal cells, but can also activate local and recruited progenitor cell populations in the niche that participate in repair. While the contribution of macrophages in tissue repair is well studied, the role of T lymphocytes in this process is not fully understood. Studies in animal models suggest that altered T cell infiltration into the wound site is associated with impaired wound healing (Swift et al., 2001), and there is evidence that $CD4^+$ T cells may play a positive role in wound healing while $CD8^+$ T cells may inhibit the wound healing process (Park and Barbul, 2004). Scarless skin healing has been reported in athymic nude-nu mice that are deficient in both T- and B-cells (Gawronska-Kozak et al., 2006), and a recent study using severe combined immunodeficient (SCID) mice in a wound healing model has shown that the presence of $CD4^+$ T lymphocytes prevents dermal scarring by regulating inflammation and improving neovascularization (Wang et al., 2019). Regulatory T cells (Treg) promote wound healing through attenuating wound-associated inflammation (Nosbaum et al., 2016), and the generation and activation of Treg cells can be induced by MSC (Caplan, 2009; González et al., 2009; Griffin et al., 2010).

Endothelial progenitor cells play an important supportive role in postnatal angiogenesis, and are mobilized as part of the inflammatory response to injured tissues (Kopp et al., 2006). EPC have been shown to improve neovascularization in multiple injury models including wound healing (Crosby Jeffrey et al., 2000; Murohara et al., 2000; Asahara et al., 2011), but also contribute to excessive neo-vessel formation by *in situ* vasculogenesis in inflamed synovial tissues (Ruger et al., 2004). Different subtypes of circulating progenitor cells have been

described and may contribute to neo-vessel formation in different ways. They include culture-derived myeloid angiogenic cells of the hematopoietic lineage, also called early outgrowth EPC, that promote angiogenesis through paracrine mechanisms, but do not give rise to mature endothelial cells (EC) (Asahara et al., 2011; Medina et al., 2011, 2017; Mund et al., 2012), and non-hematopoietic endothelial colony forming cells (ECFC), or late outgrowth EPC, that can differentiate into mature EC (Medina et al., 2017). The origin of these "true" EPC is still elusive, and they appear to be an extremely rare population within circulating blood, as *ex vivo* culture is necessary for their identification (Lin et al., 2000; Ingram et al., 2004). Interestingly, T cells seem to play an important role in the generation of both myeloid angiogenic cells and ECFC. Angiogenic T cells expressing CD3, CD31, and CXCR4 are required for colony formation and differentiation of early EPC (Hur et al., 2007), and the generation of ECFC is also T cell-dependent (Wilde et al., 2016), demonstrating the importance of microenvironmental factors including the presence of differentiated cells in the niche.

Mimicking the cellular and structural complexity of the *in vivo* vascular niche is still a challenge in the field of tissue engineering. The present study aimed to set up an *in vitro* culture environment that combines key cellular players in a biocompatible extracellular matrix simulating *in vivo* tissue repair in order to expand our current knowledge about regenerative processes and advance vascular tissue engineering for therapeutic application. The rationale behind the experimental design was based on the presence of progenitor cells with potent intrinsic angiogenic capacity in peripheral blood that are recruited to sites of injury together with inflammatory cells (e.g., Mo, T cells). Here we addressed the question whether progenitor cells and differentiated mononuclear cells in concert with MSC can form a niche environment promoting tissue repair including the formation of new vascular structures. Fibrin acts as biomimetic scaffold supporting the construction and composition of the niche environment by inducing both differentiation and stem cell marker expression of human EPC (Barsotti et al., 2011). Therefore, we established a fibrin-based xeno-free human 3D *in vitro* model using exclusively human-derived reagents and materials to study the cross-talk of MSC with PBMC obtained from leukocyte reduction system (LRS) chambers generated during the process of single-donor platelet apheresis. It has been reported that PBMC obtained from LRS chambers contain increased numbers of viable $CD34^+$ progenitor cells suitable for culture (Néron et al., 2007). Using this 3D co-culture system, we investigated the vasculogenic potential through self-organization in the absence of externally added growth factors and mature EC, and analyzed the paracrine signaling signature resulting from interaction of enriched Mo and/or enriched T cells with MSC in the 3D fibrin niche environment.

MATERIALS AND METHODS

Ethics Statement

The local Ethics Committee at the Medical University of Vienna approved the use of human bone marrow MSC (EK1193/2015) and human PBMC (EK1168/2015) in order to perform this study. All donors provided written informed consent.

MSC and PBMC

Mesenchymal stromal cells were isolated from human bone marrow (BM) and bone fragments obtained during hip-replacement surgery and expanded in complete αMEM medium (Invitrogen, Carlsbad, CA, United States) containing 10% fetal bovine serum (GE Healthcare Life Sciences, Marlborough, MA, United States), 100 U/ml penicillin, 100 μg/ml streptomycin and 250 ng/ml amphotericin B (Sigma, St. Louis, MO, United States) at 37°C (20% O_2 and 5% CO_2 humidified atmosphere). MSC were characterized by flow cytometry analyses using CD90FITC (Stem Cell Technologies, Cologne, Germany), CD73PE (BD, San Jose, CA, United States), CD105FITC (BD), CD31PE (BioLegend, San Diego, CA, United States), CD34PE (BD), CD45FITC (BD) and CD14PE (BD) antibodies and a FACS Canto II™ instrument (BD). Cells expressed typical MSC markers, CD90, CD73, CD105, lacked expression of CD31, CD34, CD45, and CD14, and could be differentiated into adipocytes, chondrocytes and osteoblasts. For 3D culture, MSC at passage two to five were used showing no apparent functional difference in co-culture experiments.

Peripheral blood mononuclear cells were isolated from LRS chambers (Trima Accel, Version 6.0, CaridianBCT Europe, Garching, Germany), a product generated during the process of single-donor platelet apheresis from healthy donors, by density grade centrifugation. Subpopulations of PBMC, i.e., Mo and T cells, respectively, were enriched by negative selection using RosetteSep Kits (Stem Cell Technologies, Cologne, Germany). RosetteSep Kits were used for obtaining PBMC depleted from Mo and T cells, respectively (Stem Cell Technologies). The percentage of $CD14^+CD45^+$ Mo and $CD3^+CD45^+$ T cells in whole PBMC, monocyte-enriched/depleted and T cell-enriched/depleted cell fractions were determined by flow cytometry analyses using CD14FITC (BD), CD3PE (BD), and CD45APC (BioLegend). Blood-derived progenitor cells were characterized by flow cytometry analyses using combinations of the following antibodies: CD34FITC/PE (BD), CD31FITC/PE (BioLegend), CD14FITC/PE (BD), CD117PE (BioLegend), and CD45APC.

Culture of MSC and Co-culture of MSC With Immune Cells in 3D Fibrin Matrices

Co-culture experiments were set up using MSC obtained from five donors at different passages (n = 10) and PBMC from individual donors (n = 10). Further, MSC at comparable passages, were co-cultured with individual donor-derived enriched Mo (n = 6), individual donor-derived enriched T cells (n = 9), enriched T cells together with enriched Mo obtained from separate donors (n = 4), individual donor-derived PBMC depleted from Mo (n = 6), and individual donor-derived PBMC depleted from T cells (n = 6), respectively. In addition and parallel to co-cultures, the same MSC samples used for co-cultures were cultivated without immune cells. 3D cultures were set up in 24-well plates (Corning, Berlin, Germany). Cells were embedded in fibrin matrices in a ratio 1:100 (for MSC:PBMC

and MSC:Mo + T) and 1:50 (for MSC:Mo and MSC:T), using 5×10^4 MSC/well. Fibrin matrices were prepared as described previously with minor modifications (Ruger et al., 2008; Rüger et al., 2018). In brief, human fibrinogen (2 mg/ml; Calbiochem, Darmstadt, Germany) was dissolved in PBS, human plasma thrombin (0.45 U/ml, Sigma) was added to the fibrinogen solution containing MSC and/or immune cells and gel formation occurred by incubation at 37°C for 30 min. Cells were cultured using complete αMEM medium (Invitrogen) containing 10% human AB serum (GMP grade, PAN-Biotech, Aidenbach, Germany) without externally added growth factors for up to 2 weeks. Control experiments were performed culturing Mo separated from MSC by a 0.4 μm transwell insert (Corning), as well as culturing PBMC, enriched Mo, enriched T cells, and enriched Mo together with enriched T cells, respectively, without MSC. Medium was changed every 3 days. Cellular rearrangement was monitored using a phase contrast microscope (Olympus IMT-2, Tokyo, Japan) and documented using a digital camera (Olympus DP50).

DNA Extraction and Analysis of Polymorphic Marker

In order to determine the origin of EC within the vascular structures that develop in the 3D fibrin gels, we performed gender-mismatched co-cultures using 6-well plates. Male MSC were co-cultured with female PBMC in 3D fibrin matrices for 1 week. Alternatively, female MSC were co-cultured with male PBMC. To obtain single cell suspensions, the fibrin gels were dissolved using nattokinase (NSK-SD; Japan Bio Science Laboratory Co., Ltd., Osaka, Japan) (Carrion et al., 2014), and DNA extracted from FACS-sorted $CD34^+CD45^-$ EC and $CD34^-CD45^+$ leukocytes with the QIAamp DNA Investigator Kit (Qiagen GmbH, Hilden, Germany). An insertion/deletion (indel) polymorphism in the X–Y homologous gene amelogenin was amplified by PCR and subjected to fragment analysis by capillary electrophoresis (CE) according to Steinlechner et al. (2002). In addition, the NGM Detect PCR amplification kit, a 16-locus multiplex PCR of highly polymorphic short tandem repeat (STR) markers was performed and analyzed on an ABI 3130 Genetic Analyzer according to the manufacturer's instructions (Applied Biosystems by Thermo Fisher Scientific, Waltham, MA, United States).

Confocal Laser Scanning Microscopy (CLSM) of Intact 3D Cultures

In order to perform confocal laser scanning microscopy (CLSM) of whole 3D cultures, immunofluorescence analyses of intact 3D fibrin matrices containing the self-organized structures were performed as described previously (Rüger et al., 2018), and stained fibrin gels transferred to ibidi chambers (ibidi GmbH, Martinsried, Germany) for CLSM. Briefly, fibrin matrices were fixed with 4% paraformaldehyde and incubated with a buffer solution containing 0.1% BSA, 0.2% Triton X-100, 0.05% Tween 20 in PBS followed by a blocking step with 20% normal donkey serum (Jackson Immuno Research, West Grove, PA, United States). Fibrin gels were incubated with anti-human CD31 (mouse IgG_1, 8 μg/ml, Dako) or anti-human CD34 (mouse IgG_1, 4 μg/ml, Cell Marque, Rocklin, CA, United States) together with rabbit anti-Col-IV (7.5 μg/ml, Novus Biologicals, Cambridge, United Kingdom) for 6 h at room temperature. The cultures were washed with buffer solution and incubated simultaneously with donkey anti-mouse IgG_1 Alexa Fluor (AF) 488 and donkey anti-rabbit AF555 (2.6 μg/ml, Molecular Probes, Life Technologies, Carlsbad, CA, United States) and cell nuclei stained with DAPI. Omission of primary antibodies and the use of isotype-matched non-immune antibodies served as controls. For triple labeling, the 3D constructs stained with CD31 or CD34 and Col-IV antibodies were blocked with 20% mouse serum (Jackson Immuno Research) and incubated with AF647-mouse anti-CD45 (2.5 μg/ml, BioLegend) or AF647-mouse anti-CD3 (2.5 μg/ml, BioLegend). The cultures were washed with buffer solution, cell nuclei stained with DAPI, and 3D gels kept in PBS at +4°C until CLSM analyses. All 3D cultures were evaluated using a LSM 700 or LSM 780 confocal laser scanning microscope (Carl Zeiss, Jena, Germany) and the acquired images analyzed with the ZEN image processing and analysis software program (Zeiss).

Cytokine Determination

Cell-free supernatants of 3D MSC mono-cultures and MSC co-cultured with enriched Mo or enriched T cells, and enriched Mo together with enriched T cells, respectively, were analyzed 24 h after embedding the cells within fibrin gels, using a cytokine array kit (Proteome Profiler Human XL Cytokine Array Kit, R&D Systems, Minneapolis, MN, United States). For each group, pooled samples of four experiments were used. The intensities of chemiluminescence signals were determined by subtraction of background noise, and the mean gray values of duplicate cytokine spots were determined using Bio-Rad Quantity One software (Bio-Rad, Hercules, CA, United States). VEGF secretion levels in the supernatants of separate samples were quantified utilizing a commercially available ELISA Duoset system (R&D). Supernatants of 3D co-cultures set up as described above, were collected after 24 h, on day 3 and on day 6. VEGF levels were determined in co-cultures of MSC with PBMC ($n = 9$), enriched Mo ($n = 4$), enriched T cells ($n = 4$), enriched Mo together with enriched T cells ($n = 4$), Mo-depleted PBMC ($n = 6$), and T cell-depleted PBMC ($n = 4$), respectively. In addition, supernatants of MSC mono-cultures and supernatants of immune cells cultured without MSC, set up in parallel and corresponding to each co-culture experiment, were collected at the same time points. Experiments were performed with each sample in duplicate, and data are expressed as mean values ± SD. In 3D co-cultures where MSC and Mo were physically separated by a transwell insert, VEGF levels in the supernatants were measured by ELISA (R&D) on day 6. The assays were performed according to the reference manual, and the samples were measured in technical duplicates. Optical density values were measured at 450 nm on an ELISA plate reader (anthos Mikrosysteme, Krefeld, Germany).

Statistics

Statistical analyses were performed using the software package SPSS Statistics for Windows, version 22.0 (SPSS Inc., Chicago, IL, United States). Data were analyzed for statistical significance by

unpaired *t*-test and expressed as means ± SD. Significance was concluded when a probability value (*p* value) was lower than 0.05. (ns: not significant; * $p \leq 0.05$; ** $p \leq 0.01$; *** $p \leq 0.001$).

RESULTS

Vascular Structures Develop *de novo* During Co-culture of MSC and PBMC in 3D Fibrin Matrices

When MSC and PBMC were co-cultured in a xeno-free niche environment, complex vascular structures with several branch points developed within one to 2 weeks in the originally EC-free avascular 3D fibrin gels (**Figures 1A–C**). EC of newly formed vascular structures expressed CD34 (**Figures 1A,E**) and CD31 (**Figure 1I**), and were surrounded by basement-membrane collagen type (Col)-IV expressing MSC and matrix (**Figures 1B,F,J**). $CD45^+$ leukocytes were found in close vicinity and aligned to developing neo-vessels (**Figures 1G,K** and **Supplementary Animated z-stack S1**). PBMC isolated from LRS chambers contained 24.0 ± 7.6% $CD14^+$ Mo, 49.7 ± 11.7% $CD3^+$ T cells and 0.24 ± 0.12% cells with a distinct non-myeloid progenitor phenotype expressing CD34 and CD31, with low CD45 and no CD14 (**Table 1** and **Supplementary Figure S1**). The majority of $CD34^+$ progenitor cells also expressed CD117 (**Supplementary Figure S1**). No vascular structures were detected in fibrin gels with MSC only and in PBMC-mono-cultures, respectively (data not shown), and 3D PBMC cultures without support of MSC showed considerable fibrinolysis in the second week of culture (data not shown). Using a cytokine array kit we found that MSC within 3D fibrin matrices produce a number of pro-inflammatory mediators that are also involved in new vessel formation including interleukin (IL)-6, complement component C5/C5a, CCL2, CXCL8, VEGF, angiogenin, endoglin, PAI-1, thrombospondin, VCAM-1, PDGF-AA, and MMP-9 (**Figure 2**). VEGF release by MSC progressively increased during culture, and in co-culture with PBMC, VEGF secretion was significantly higher compared to MSC mono-cultures after 24 h, at day 3 and 6, respectively, as demonstrated by ELISA (**Figure 1D** and **Table 2**). VEGF secretion levels of PBMC cultured without MSC support were under 100 pg/ml after 24 h fibrin matrix-exposure, and were below detection level on day 6 of culture (data not shown).

EC of Neo-Vascular Structures Are Derived From Cells Present in Peripheral Blood

As both BM-derived EPC contribute to new vessel formation (Asahara et al., 1999), and MSC can differentiate into EC (Oswald et al., 2004; Silva Guilherme et al., 2005; Janeczek Portalska et al., 2012; Wang et al., 2018), we set up experiments to determine the origin of EC forming the neo-vessels in the 3D fibrin gels. In order to avoid problems related to potential cell toxicity and change in cellular behavior induced by labeling cells with cell tracking dyes, we performed gender-mismatched co-cultures using non-manipulated MSC and PBMC. Male MSC were co-cultured with female PBMC, and female MSC were co-cultured with male PBMC, respectively, in 3D fibrin matrices. DNA isolated from FACS-sorted fibrin gel-derived $CD34^+CD45^-$ EC and $CD34^-CD45^+$ leukocytes was subjected to analyses of indel- and STR polymorphisms by PCR and fragment analysis by capillary electrophoresis. The results showed that both the $CD34^-CD45^+$ hematopoietic cells as well as the $CD34^+CD45^-$ cells, i.e., EC of the vascular structures formed in 3D co-cultures, originated from cells circulating in the peripheral blood (**Figure 3**).

Cross-Talk of MSC With Monocytes/Macrophages Creates a Pro-angiogenic Paracrine Microenvironment in 3D Fibrin Gels

Next, we analyzed the contributions of Mo to vascular morphogenesis and paracrine signaling in the *in vitro* vascular niche environment. The Mo-enriched fraction contained 73.5 ± 6.2% cells expressing CD14 with <0.1% $CD3^+$ cells present, and 0.76 ± 0.21% cells with the $CD34^+CD31^+CD45^{dim}CD14^-$ progenitor phenotype as determined by flow cytometry analysis (**Table 1**). Although Mo enrichment significantly increased the number of $CD34^+CD31^+CD45^{dim}CD14^-$ progenitor cells in comparison to whole PBMC (**Supplementary Figure S1F**), no vascular structures were detected when enriched Mo were co-cultured with MSC for 10–14 days in the 3D fibrin environment (**Figures 4A–E**). CLSM analysis of co-cultures in fibrin gels revealed the presence of numerous $CD31^+$ cells (**Figure 4B**) co-expressing CD45 (**Figure 4C**) in close contact to MSC that expressed Col-IV (**Figure 4D**). Analysis of the cytokine secretion profile resulting from interaction of MSC with enriched Mo for 24 h in fibrin matrices revealed that several mediators involved in inflammatory neovascularization were newly detected or up-regulated in the supernatants of co-cultures when compared to MSC mono-cultures, e.g., CXCL1, CXCL5, CXCL8, CXCL10, CCL7, CCL17, CCL20, IL-1ra, and IL-6 (**Figure 2**). In contrast, while MSC monocultures secreted CCL5, the presence of Mo for 24 h decreased CCL5 release in co-cultures (**Figure 2**). Interaction of MSC with enriched Mo for 24 h in the fibrin matrix led to significantly increased VEGF secretion compared to MSC mono-cultures (**Figure 4F** and **Table 2**). VEGF levels in co-cultures progressively increased between day 1 and 6 reaching levels similar to those found in supernatants of MSC co-cultured with whole PBMC (MSC + Mo, day 6: 6820 ± 907, MSC + PBMC, day 6: 8284 ± 2790) (**Figure 4F** and **Table 2**). 3D transwell experiments using 0.4 μm inserts to separate MSC from enriched Mo revealed that the high VEGF levels were dependent on direct contact of MSC with Mo (**Figure 4G**). When PBMC were depleted from $CD3^+$ T cells the percentage of Mo increased around 2-fold compared to whole PBMC samples to 46.9 ± 8.1% (**Table 1**). Accordingly, VEGF levels measured in the supernatants of these co-cultures on day 1 and 3, respectively, were similar to co-cultures containing enriched Mo (**Table 2**). Of note, by day 6, VEGF secretion in co-cultures with T cell-depleted PBMC was even higher in comparison to co-cultures containing enriched Mo (**Table 2** and

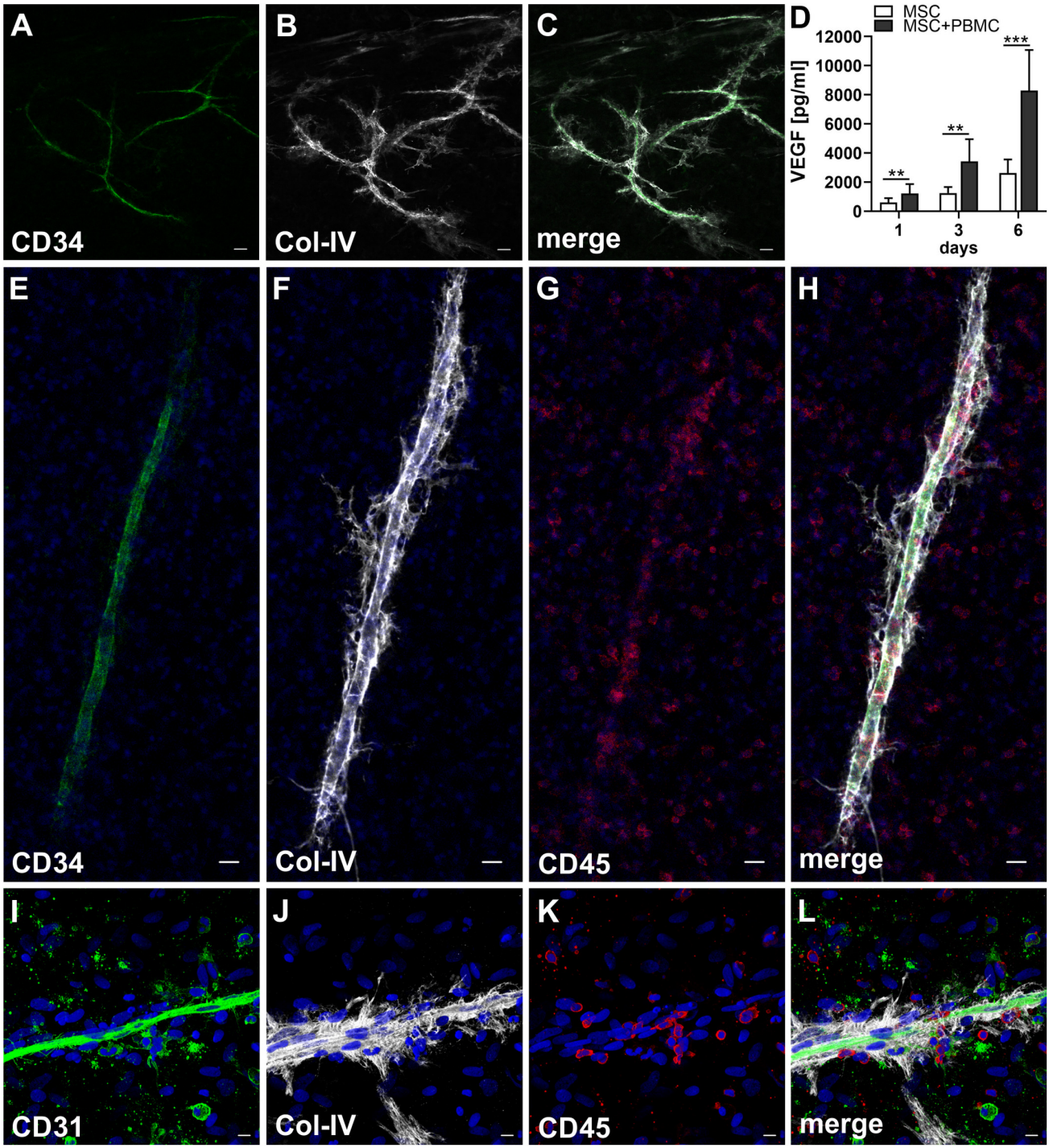

FIGURE 1 | Co-culture of MSC with PBMC in 3D fibrin matrix leads to the development of vascular structures. Representative images from three individual experiments are shown. **(A–C)** Experiment 1. The cells forming vascular structures with several branch points express **(A)** CD34 and are surrounded by **(B)** Col-IV matrix. **(C)** Merge. **(A–C)** CLSM images of an intact fibrin gel on day 10. Scale bars, 50 μm. **(D)** Determination of VEGF by ELISA in cell-free supernatants of 3D MSC monocultures (n = 9) and corresponding MSC-PBMC co-cultures, on day 1, 3, and 6, respectively. The data are expressed as mean values ± SD. $^{**}p$ value ≤ 0.01, $^{***}p$ value ≤ 0.001. **(E–H)** Experiment 2. **(E)** The $CD34^+$ neo-vessel is surrounded by **(F)** Col-IV matrix and develops in close vicinity to **(G)** $CD45^+$ leukocytes. **(H)** Merge. **(E–H)** Nuclei stained with DAPI. CLSM images of an intact fibrin gel on day 10. Scale bars 20 μm. **(I–L)** Experiment 3. Developing vascular strand expresses **(I)** CD31, **(J)** with partial co-expression of Col-IV, and is surrounded by Col-IV^+CD31^- perivascular cells. **(K)** $CD45^+$ leukocytes are distributed around and closely associated with the developing vascular structure. **(L)** Merge. **(I–L)** Nuclei stained with DAPI. CLSM images of an intact fibrin gel on day 10. Collapsed 21.6 μm z-stack consisting of 54 consecutive images. Scale bars 10 μm.

TABLE 1 | Percentage of $CD14^+$ Mo, $CD3^+$ T cells and $CD34^+CD31^+CD45^{dim}CD14^-$ progenitor-type cells in PBMC, Mo-enriched/depleted and T cell-enriched/depleted PBMC used for 3D culture experiments.

Population	%$CD14^+$	%$CD3^+$	%progenitor-type
PBMC	24.0 ± 7.6	49.7 ± 11.7	0.24 ± 0.12
Mo enriched	73.5 + 6.2	<0.1	0.76 ± 0.21
T cells enriched	0	96.4 ± 3.6	0.40 ± 0.36
Mo-depleted	<0.1	69.0 ± 12.2	0.32 ± 0.20
T cell-depleted	46.9 ± 8.1	<0.1	0.45 ± 0.29

The data are expressed as mean values ± SD.

Supplementary Figure S2A). Although the difference was not significant, this suggests that in addition to Mo, other peripheral blood-derived cells may promote the production of VEGF when co-cultured with MSC. However, no vascular structures were detected in co-cultures of MSC with T cell-depleted PBMC (data not shown), even though these co-cultures generated extremely high VEGF levels. VEGF secretion by enriched Mo cultured for 24 h in 3D fibrin gels without MSC support was around 10-fold lower compared to co-cultures with MSC, and after 6 days of culture VEGF release by Mo was below detection level (**Supplementary Figure S2C**).

$CD31^{bright}CD45^-$ Progenitor-Type Cells and T Cells Form Cell-in-Cell Structures in the Presence of MSC Within 3D Fibrin Gels

To assess the contributions of T cells to neo-vessel formation and paracrine signature in the *in vitro* vascular niche environment, T cells were enriched by negative selection. Flow cytometry analyses showed that 96.4 ± 3.6% of cells expressed CD3 (**Table 1**). The enriched T cell fraction completely lacked $CD14^+$ Mo and contained 0.40 ± 0.36% cells with the $CD34^+CD31^+CD45^{dim}CD14^-$ progenitor phenotype (**Table 1**). CLSM analyses of whole fibrin gels containing MSC in co-culture with enriched T cells for one to 2 weeks demonstrated a small number of prominent $CD31^{bright}CD45^-$ cells within the 3D matrix that measured >10 μm and partly contained two or more nuclei (**Figure 5**). Some of these $CD31^+$ cells showed low expression of CD45 (**Supplementary Animated z-stack S2, S3**). $CD31^{bright}CD45^{dim/-}$ cells were associated with a fine Col-IV^+ network, and they were surrounded by $CD31^-$Col-IV^+ MSC and $CD45^+$ leukocytes (**Figures 5A–F** and **Supplementary Animated z-stacks S2, S3**). $CD45^+$ cells, identified as T cells by positive CD3 staining, seemed to "push into" the $CD31^{bright}$ cells (**Figures 5G–L** and **Supplementary Animated z-stacks S4, S5**), and they were also found engulfed and internalized by $CD31^{bright}CD45^-$ cells thereby forming peculiar cell-in-cell structures (**Figures 5M–P** and **Supplementary Animated z-stacks S6, S7**). It appeared that $CD45^+$ leukocytes/T cells were localized inside of vacuoles displaying a $CD31^+CD45^-$ membrane (**Figures 5Q–S**). Interestingly, cell-in-cell structures demonstrating $CD3^+$ T cells engulfed by $CD31^{bright}$ cells were also found in an autologous setting, when whole BM

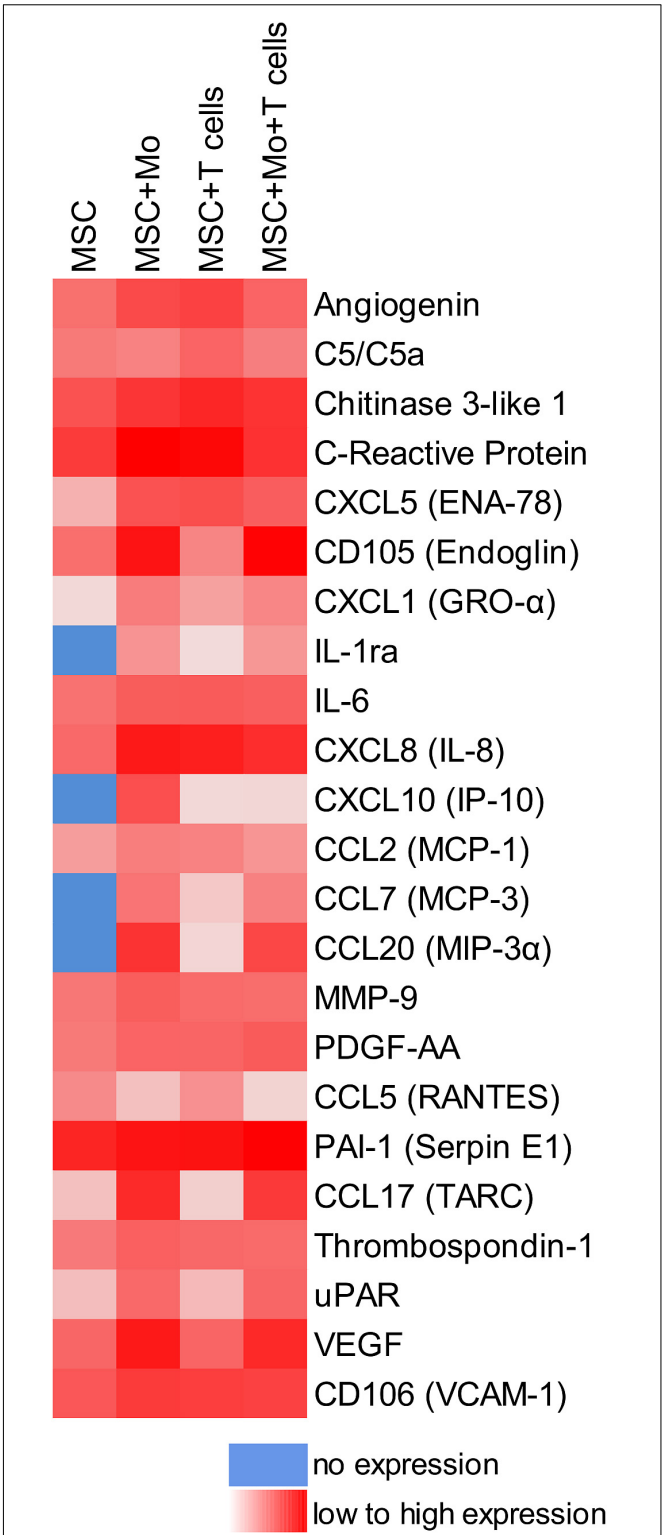

FIGURE 2 | cross-talk of MSC with Mo and/or T cells in 3D fibrin matrix alters the paracrine niche environment. Heat map reflecting the secretion profile by MSC cultured for 24 h in 3D fibrin matrix compared to secretion profile by MSC co-cultured with enriched Mo, enriched T cells, and enriched Mo together with enriched T cells, respectively. Pooled samples from four individual experiments.

TABLE 2 | VEGF secretion levels measured in cell-free supernatants of 3D (co)-cultures on day 1, 3, and 6.

	VEGF [pg/ml]		
	Day 1	**Day 3**	**Day 6**
MSC + PBMC	1212 ± 648	3420 ± 1525	8284 ± 2790
MSC + Mo enriched	1908 ± 587	3492 ± 1299	6820 ± 907
MSC + T cells enriched	321 ± 133	672 ± 130	1589 ± 295
MSC + Mo + T cells	1694 ± 962	3785 ± 1330	6897 ± 2061
MSC + Mo-depleted	259 ± 79	950 ± 80	4444 ± 1153
MSC + T cell-depleted	1430 ± 296	3242 ± 382	8854 ± 1930
MSC only	427 ± 190	1241 ± 424	2620 ± 936

The data are expressed as mean values ± SD.

mononuclear cells were cultured for 2 weeks on fibronectin-coated slides (**Supplementary Figure S3**). As in co-cultures of MSC with enriched Mo, no vascular structures were detected in co-cultures of MSC with enriched T cells. The presence of T cells significantly decreased VEGF secretion by MSC at day 3 (**Figure 5T**). VEGF levels in co-cultures after 24 h and at day 6, respectively, were also lower in comparison to corresponding MSC mono-cultures, however, without reaching significance at these time points (**Figure 5T** and **Table 2**). The cytokine secretion pattern generated within the 3D fibrin environment by co-cultures of enriched T cells and MSC was similar to MSC mono-cultures, with the exception of an increase in CXCL1 and IL-8 levels and a slight decrease in CCL17 levels in MSC-T cell co-cultures (**Figure 2**). In 3D cultures of enriched T cells without MSC support, VEGF levels were below detection level at any time point and no cell-in-cell structures developed (data not shown).

Complex Vascular Structures Develop in 3D Fibrin Matrices When MSC Are Co-cultured With Both Enriched Mo and T Cells

When MSC were co-cultured with enriched Mo and enriched T cells, complex vessel structures developed in the 3D fibrin gels within 1–2 weeks (**Figure 6** and **Supplementary Animated z-stack S8**), suggesting that synergistic interaction effects between T cells, Mo, progenitor cells and MSC were required for neo-vessel formation. Neo-vessels showed several branch points, consisted of $CD31^+$ EC (**Figure 6B**) that co-expressed Col-IV (**Figure 6D**), and were surrounded by $CD31^-$Col-IV^+ MSC and Col-IV^+ matrix (**Figure 6D** and **Supplementary Figure S4B,D**). The vascular tubes contained $CD45^+CD31^-$ hematopoietic cells (**Figure 6H**) localized inside of CD31-lined intracellular spaces adjacent to $CD31^+CD45^-$ EC (**Figures 6F,J** and **Supplementary Animated z-stack S9**). Some of these "intravascular" $CD45^+$ cells showed condensed nuclei (**Figure 6H**) indicating that they underwent apoptosis. EC of newly forming vessels, and in particular, $CD31^+$ cells at the leading edge of neo-vessels showed $CD31^+$ filopodial protrusions (**Figures 6K,L**) that resembled tip cells during angiogenic sprouting. Filopodial protrusions were surrounded by a fine Col-IV^+ network (**Figure 6N** and **Supplementary Animated z-stack S10**), and $CD45^+$ leukocytes were found in their vicinity (**Figure 6M**). In the surrounding of neo-vascular structures, numerous irregular-shaped $CD31^+CD45^+$ cells resembling macrophages were found in close vicinity to Col-IV^+ MSC (**Figures 6A–E** and **Supplementary Animated z-stack S8**). This cellular distribution pattern was reminiscent of a pattern found in 3D synovial explant cultures (Rüger et al., 2018), where vascular outgrowth was also associated with surrounding stromal cells in close contact with $CD31^+CD45^+$ cells (**Supplementary Figure S4E–I** and **Supplementary Animated z-stack S11**). VEGF secretion progressively increased during communication and co-operation of MSC with enriched Mo and T cells, showing significantly higher levels than corresponding cultures of MSC without Mo and T cells from day 3 onward (**Figure 6O** and **Table 2**). VEGF release in co-cultures of Mo and T cells without support of MSC measured on day 6 was below detection level (data not shown). The cytokine secretion profile resulting from interaction of MSC with enriched T cells together with enriched Mo for 24 h showed strong similarities to the secretion profile of MSC co-cultured with enriched Mo (**Figure 2**). However, while CXCL10 - an anti-angiogenic cytokine - was detected at high levels in co-cultures of MSC with enriched Mo, the concomitant presence of enriched T cells in the co-cultures greatly diminished CXCL10 secretion (**Figure 2**).

$CD14^+$ Monocytes Are Not Required for Vascular Morphogenesis

In order to investigate whether Mo are required for the physical assembly of neo-vessels, PBMC were depleted from Mo using a CD36 antibody prior to co-culture with MSC. Flow cytometry analyses revealed that Mo-depleted PBMC contained 0.32 ± 0.20% cells with the progenitor phenotype $CD34^+CD31^+CD45^{dim}CD14^-$ and 69.0 ± 12.2% $CD3^+$ cells (**Table 1**). Despite the absence of $CD14^+$ Mo, Mo-depleted PBMC in co-culture with MSC generated $CD31^+$ vascular structures surrounded by Col-IV^+ matrix in close vicinity to $CD45^+$ leukocytes (**Figure 7**). $CD45^+$ leukocytes were also found inside of developing vascular tubes within CD31-lined intracellular vacuoles (**Figure 7I**, **Supplementary Figure S5** and **Supplementary Animated z-stacks S12, S13**). The morphology of the vascular structures strongly resembled the features of neo-vessels developing in co-cultures of MSC with PBMC and enriched Mo together with enriched T cells, respectively, suggesting that classical Mo do not play a direct role in the assembly of vascular structures. Vascular tubes were found in close contact and perfectly aligned with Col-IV^+ matrix, and collapsed z-stack images demonstrated that Col-IV^+ matrix structures extended beyond the $CD31^+$ vascular structure suggesting that MSC-mediated mechanical signals and guiding cues may promote tube elongation in the 3D fibrin environment (**Figures 7A,B,D** and **Supplementary Animated z-stack S12**). VEGF release in co-cultures of MSC with Mo-depleted PBMC was significantly decreased at day 3, when compared to corresponding MSC monocultures (**Figure 7J** and **Table 2**), showing similarities to co-cultures of MSC with enriched T cells (**Figure 5T**). However, while the presence of T cells decreased

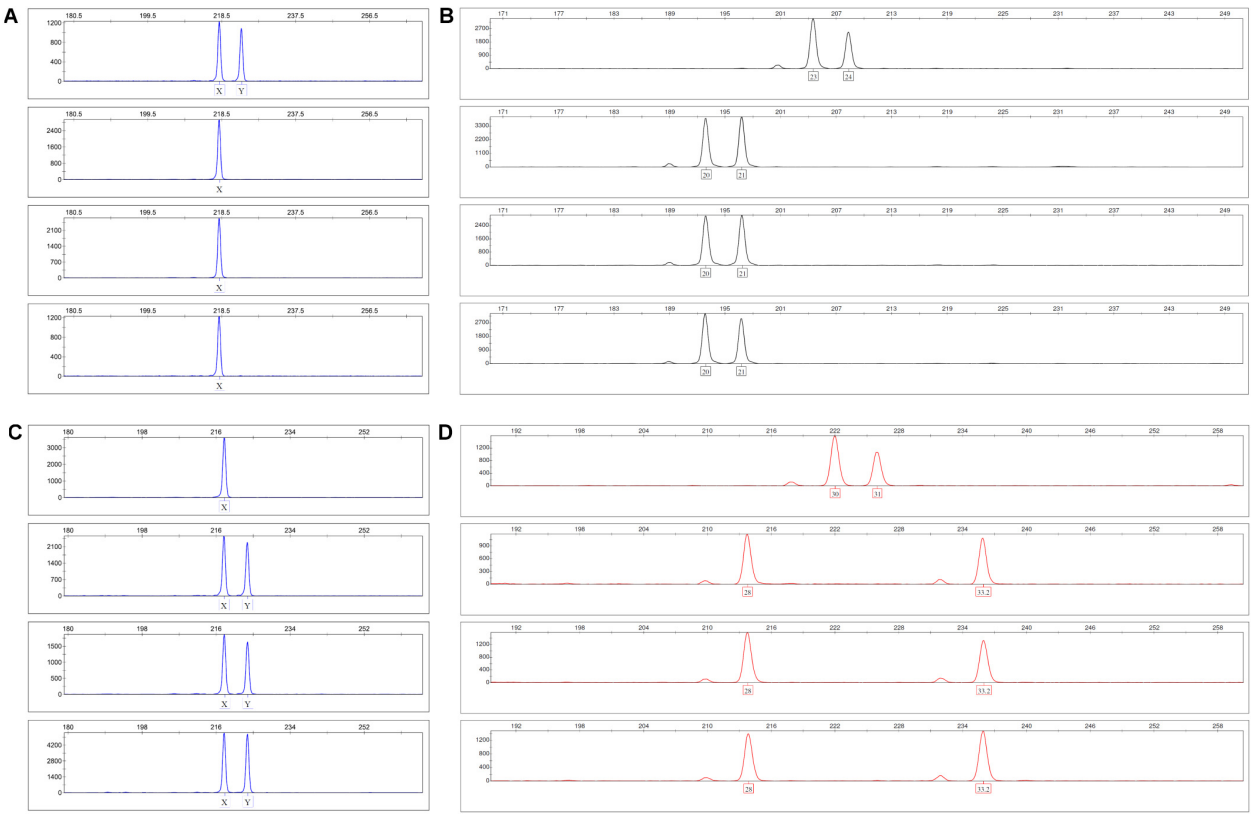

FIGURE 3 | Indel and STR genotypes of post-culture FACS-sorted EC and leukocytes are identical with pre-culture PBMC in fragment analysis. **(A,B)** Male MSC were co-cultured with female PBMC in 3D fibrin matrices for 1 week. Panel **(A)** shows the X-Y homologous indel polymorphism in the amelogenin gene and panel **(B)** the STR polymorphism FGA (4q28) top down: pre-culture MSC, PBMC, post-culture FACS-sorted $CD34^{+}CD45^{-}$ EC and $CD34^{-}CD45^{+}$ leukocytes. **(C,D)** Female MSC were co-cultured with male PBMC in 3D fibrin matrices for 1 week. Panel **(C)** shows the X-Y homologous indel polymorphism in the amelogenin gene and panel **(D)** the STR polymorphism D21S11 (21q21.1) top down: pre-culture MSC, PBMC, post-culture FACS-sorted $CD34^{+}CD45^{-}$ EC and $CD34^{-}CD45^{+}$ leukocytes.

VEGF secretion by MSC at all time points measured, co-cultures of MSC with Mo-depleted PBMC generated significantly higher levels of VEGF by day 6 compared to corresponding MSC monocultures (**Figure 7J**). Furthermore, co-cultures of MSC with Mo-depleted PBMC released significantly higher amounts of VEGF in comparison to MSC-T cell co-cultures from day 3 onward (**Supplementary Figure S2B**) suggesting that other non-myeloid cells contributed to VEGF release in these co-cultures thereby promoting the formation of vascular structures (**Table 2**).

Lumens Appear to Form Through Coalescence of Intracellular Vacuoles and Apoptosis of Leukocytes

In all co-cultures that generated vascular structures, the developing endothelial cords displayed similar characteristic features. They showed large coalescing intracellular vacuoles lined with a membrane expressing CD31 (**Figure 7F**) and CD34 (**Figure 8B**) associated with abluminal Col-IV deposition (**Figure 7G**) as well as intra-vacuolar granular Col-IV deposits (**Figure 8D**). Vacuoles contained $CD45^{+}$ leukocytes, with adjacent parietally located $CD31^{+}/CD34^{+}$ EC (**Figure 7**, **8**). A number of these "intravascular" cells displayed condensed nuclei implying they underwent apoptosis thereby conceivably contributing to the formation of a luminal space (**Figure 8**).

DISCUSSION

Tissue damage is commonly associated with an initial inflammatory reaction. During the repair process immune cells infiltrating the affected area come in contact with tissue-resident cells, and communicate with MSC and EPC co-recruited from the circulation. The perivascular deposition of a fibrin matrix creates the basic scaffold where new blood vessels can form and contribute to the healing process to re-establish homeostasis. In our study, we have established a fibrin-based xeno-free human vascular niche model in which we cultivated, in 3D, MSC with PBMC in order to investigate *de novo* vessel formation in an inflammatory environment closely mimicking the *in vivo* setting. We demonstrated that complex vascular structures can form in a 3D fibrin environment in the absence of pre-existing EC or vascular structures, and that this process is carried out exclusively through complex cell-cell communication and co-operation amongst MSC, mature PBMC and circulation-derived

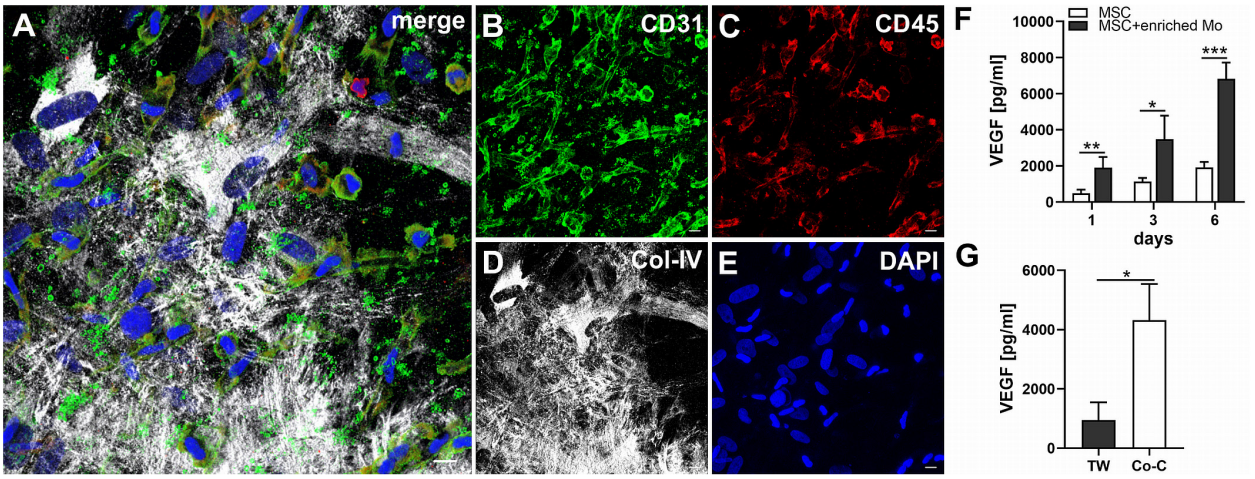

FIGURE 4 | MSC cross-talk with enriched Mo increases VEGF levels in the niche environment. **(A–E)** Representative CLSM images of MSC co-cultured with enriched Mo in 3D fibrin matrix on day 14 showing numerous round and spindle-shaped cells expressing **(B)** CD31 with differential co-expression of **(C)** CD45, embedded in a meshwork of **(D)** Col-IV$^+$ MSC and matrix. **(A)** Merge. **(E)** DAPI stain. Collapsed 21.15 μm z-stack consisting of 47 consecutive images. Scale bars, 10 μm. **(F)** Determination of VEGF by ELISA in cell-free supernatants of 3D MSC monocultures (n = 4) and corresponding co-cultures of MSC with enriched Mo, on day 1, 3, and 6, respectively. The data are expressed as mean values ± SD. *p value ≤ 0.05, **p value ≤ 0.01, ***p value ≤ 0.001. **(G)** VEGF levels in cell-free supernatants of 3D co-cultures where MSC were physically separated from enriched Mo by a transwell insert with 0.4 μm pore size (TW) and corresponding 3D co-cultures allowing for contact of MSC with enriched Mo on day 6 (n = 3). The data are expressed as mean values ± SD. *p value ≤ 0.05.

progenitor cells. Results from gender-mismatched co-cultures demonstrated that EC of vascular structures generated in the 3D fibrin matrices originated from PBMC, suggesting *in situ* differentiation of blood-derived progenitor cells within the fibrin niche environment.

Monocytes and T cells are major players during repair processes, therefore we investigated their specific contributions to neo-vessel formation in the vascular niche model. We observed that neo-vessels formed only in co-cultures of MSC and enriched Mo mixed with enriched T cells, implying a synergistic effect, where Mo and T cell interactions with blood-derived progenitor cells and MSC complemented each other to create conditions allowing for the development of vascular structures in the fibrin environment. Microenvironmental factors, such as the macromolecular concentration of the matrix, as well as cell number influence the phenotype of MSC and play a key role in promoting angiogenesis *in vivo*, as shown e.g., in a hindlimb ischemia model where formation of new blood vessels was accelerated when MSC were delivered at a low cell dose in soft matrix (Thomas et al., 2020). In order to mimic the situation *in vivo*, in our *in vitro* study we set up fibrin scaffolds using a fibrinogen concentration that resembles circulating fibrinogen levels in the blood (2–4 mg/ml) creating malleable and translucent gels, with 3D co-cultures containing 100 times more PBMC (5×10^6) compared to the number of MSC (5×10^4). No vascular tubes developed when MSC were co-cultured exclusively with enriched Mo, even though enriched Mo contained significantly higher numbers of progenitor cells compared to whole PBMC. The contribution of Mo to neo-vessel formation was essentially to create a pro-angiogenic paracrine niche environment via cross-talk with MSC reflected by the secretion of several mediators typically found during inflammatory neo-vessel formation *in vivo* (Szade et al., 2015) including high levels of VEGF (**Figure 2** and **Table 2**). On the other hand, cross-talk of enriched T cells with blood-derived progenitor cells appeared to be crucial for the vascular morphogenesis process *per se*. Although co-cultures of MSC with enriched T cells alone did not generate vascular structures, a small number of conspicuously bright CD31$^+$CD45$^-$ cells, some showing weak CD45 expression, was found in the 3D matrix within 1 week of culture. The phenotype of these cells demonstrated that they were circulation-derived, possibly originating from CD31$^+$CD34$^+$CD45^{dim}CD14$^-$ progenitor cells present in peripheral blood. These CD31$^+$CD45$^-$ cells were closely associated with T cells and partially engulfed them, leading to the formation of cell-in-cell structures. Evidence for a co-operative mechanism involving blood-derived progenitor cells and differentiated immune cells was originally presented in a seminal publication by Asahara et al. (1997), where the concept of circulating EPC was first introduced. The authors showed that cord-like structures and network formation *in vitro* on fibronectin-coated plates occurred only when blood-derived CD34$^+$ progenitor cells were co-cultured with CD34$^-$ cells. Accordingly, we suggest that cross-talk of T cells with progenitor cells could have a functional relationship to differentiation of EPC toward mature EC, and that the process of T cell internalization by progenitor cells might be the initial cue for subsequent EC differentiation in a conducive pro-angiogenic paracrine environment provided by cross-talk of MSC with Mo. Several studies have shown that T cells are the main mature leukocyte subset present in early EPC colonies (Hur et al., 2007; Rohde et al., 2007), and the generation of ECFC requires the presence of T cells (Wilde et al., 2016). Yet, the origin of circulating progenitor cells

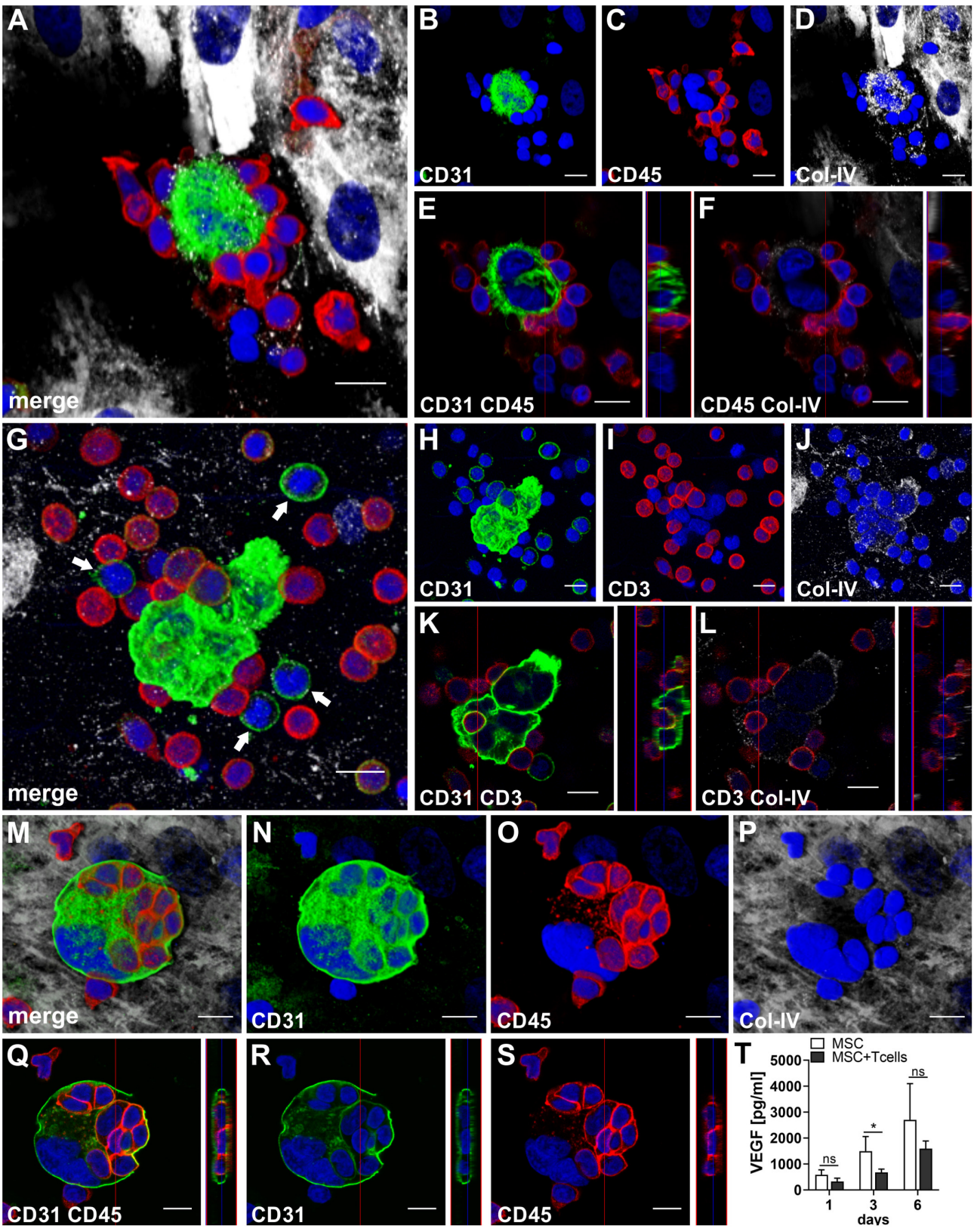

FIGURE 5 | Continued

FIGURE 5 | $CD31^{bright}CD45^{-}$ cells and T cells form cell-in-cell structures in 3D fibrin gels. Representative images from three separate co-culture experiments of MSC with enriched T cells are shown. **(A–F)** Experiment 1. CLSM images of intact fibrin gel on day 14 showing a bi-nucleated cell with **(B)** strong expression of CD31, surrounded by **(C)** $CD45^{+}$ cells. The bi-nucleated cell does not express CD45, and is associated with **(D)** a fine Col-IV^{+} granular network. MSC also express Col-IV, but are $CD31^{-}$. **(A)** Merge. **(A–D)** Nuclei stained with DAPI. Collapsed 11.9 μm-z-stack consisting of 17 consecutive images. Scale bars, 10 μm. **(E,F)** Orthoview CLSM images of collapsed z-stack shown in **(A–D)** demonstrating that **(E)** $CD45^{+}$ cells are closely attached to the $CD31^{bright}$ cell, and showing **(F)** $CD45^{+}$ leukocytes associated with delicate granular Col-IV deposits surrounding the bi-nucleated cell. Scale bars, 10 μm. **(G–L)** Experiment 2. CLSM images of intact fibrin gel on day 6 showing two multi-nucleated cells **(H)** strongly expressing CD31, surrounded by **(I)** $CD3^{+}$ T cells. Some $CD3^{+}$ cells co-express CD31. The multi-nucleated cells are associated with a **(J)** Col-IV^{+} granular network. **(G)** Merge. Note the $CD31^{+}CD3^{-}$ mononuclear cells (arrows) in the surrounding of the multinucleated $CD31^{bright}$ cells. **(G–J)** Nuclei stained with DAPI. Collapsed 17.28 μm-z-stack consisting of 36 consecutive images. Scale bars, 10 μm. **(K,L)** Orthoview CLSM images of collapsed z-stack shown in **(G–J)** demonstrating how **(K)** a $CD3^{+}$ T cell is "pushing into" a multinucleated $CD31^{+}$ cell, and showing **(L)** the fine Col-IV network around the two multi-nucleated cells. Scale bars, 10 μm. **(M–S)** Experiment 3. CLSM images of intact fibrin gel on day 14 showing a multi-nuclear cell with a diameter of 38 μm confined by a **(N)** $CD31^{+}$ membrane and containing **(O)** several $CD45^{+}$ cells. The multi-nuclear cell/structure is surrounded by **(P)** Col-IV^{+} MSC and matrix. **(M)** Merge. **(M–P)** Nuclei stained with DAPI. Collapsed 9.9 μm-z-stack consisting of 22 consecutive images. Scale bars, 10 μm. **(Q–S)** Orthoview CLSM images of collapsed z-stack shown in **(M–P)** demonstrating that **(Q)** $CD45^{+}$ cells are internalized in the $CD31^{+}$ cell building a cell-in-cell structure. **(R)** Internalized cells do not express CD31, and **(S)** the membrane of multicellular $CD31^{+}$ structure is $CD45^{-}$. **(Q–S)** Nuclei stained with DAPI. Scale bars, 10 μm. **(T)** Determination of VEGF by ELISA in cell-free supernatants of 3D MSC monocultures ($n = 4$) and corresponding co-cultures of MSC with enriched T cells, on day 1, 3, and 6, respectively. The data are expressed as mean values ± SD. *p value ≤ 0.05, ns = not significant.

giving rise to ECFC has not been fully clarified. Furthermore, their phenotype is still elusive and might not be the same as the phenotype of ECFC generated by culture of whole PBMC. In contrast to mature EC, ECFC are highly proliferative cells, however, they are phenotypically indistinguishable from mature EC and do not express hematopoietic markers including CD45. A recently published consensus statement concerning EPC criteria discriminates ECFC/'true EPC' ($CD31^{+}CD146^{+}CD45^{-}$) from myeloid angiogenic cells which are of hematopoietic origin (i.e., they express CD45 and CD14) (Medina et al., 2017). In our study, the $CD31^{+}CD34^{+}CD45^{dim}CD14^{-}$ progenitor cells present in LRS chambers showed an expression profile partially related to both endothelial and hematopoietic lineage cells. In addition, we have detected cells with this phenotype also in *ex vivo* samples of human BM (unpublished observation), and a recent study has demonstrated that BM-derived hematopoietic stem cells contribute to vascular network formation *in vitro* when co-cultured with BM-MSC (Sasse et al., 2019). It is tempting to speculate that $CD31^{+}CD34^{+}CD45^{dim}CD14^{-}$ progenitor cells may represent the circulating ECFC progenitors that differentiate *in situ* through cell-in-cell structure formation with T cells once they are recruited to a vascular niche environment where they lose CD45 expression. This line of thought is supported by the presence of $CD31^{+}CD45^{+}$ cells in human BM that can contribute to blood vessel formation by differentiation into mature EC (Kim et al., 2010), and may reconcile conflicting reports about the origin of ECFC in tissue vascular niches (Ingram et al., 2005; Duong et al., 2011; Alphonse et al., 2015) and in the BM (Lin et al., 2000). Moreover, ECFC can be manufactured from steady-state leukapheresis using a program intended for the collection of mononuclear cells including hematopoietic progenitor cells (Siegel et al., 2018), providing additional support for *in situ* development of ECFC from PB-derived progenitor cells that subsequently generate vascular structures in co-operation with MSC as demonstrated in our *in vitro* 3D fibrin model. Interestingly, in our study we could show that human BM harbors $CD31^{+}$ cells that interact with and internalize T cells in culture on fibronectin-coated slides, demonstrating co-operation of progenitor cells and differentiated cells via cell-in-cell structure formation in an autologous setting (**Supplementary Figure S3**). Cell-in-cell structure formation defines a process by which one or more cells penetrate into the cytoplasm of another cell causing cell structure and biological alteration. Although this phenomenon has been revealed nearly 100 years ago under pathological circumstances (Lewis, 1925), only few reports about its biological significance have been published thus far. Yet, cell-in-cell structures definitely represent a specific characteristic feature of several pathological conditions, including Rosai-Dorfman disease, chronic myeloproliferative diseases and some other hematological diseases (Shamoto, 1981; Thiele et al., 1984; Deshpande et al., 2000; Schmitt et al., 2002). In addition, cell-in-cell structure formation occurs during murine T cell development in the thymus, where thymocyte nurse cells internalize immature T cells within cytoplasmatic vacuoles to nurture and educate them into mature T cells (Wekerle et al., 1980), clearly pointing to the specific physiological role of cell-in-cell structures. Similar may also apply to our vascular niche model, where T cell internalization within vacuoles of progenitor-type cells appears to initiate neo-vessel development.

Apart from their role in stabilizing newly formed blood vessels, MSC are known to produce a number of paracrine factors that support new vessel formation (Caplan and Correa, 2011; Watt et al., 2013). Here, we could show that within 24 h, MSC in 3D fibrin matrices produce a considerable number of chemokines, cytokines and growth factors, and several mediators related to inflammatory neo-vessel formation are upregulated when matrix-embedded MSC come in contact with leukocytes, in agreement with previous findings (Szekanecz and Koch, 2001). Amongst the pro-angiogenic mediators, VEGF is one of the most potent inducers of vascular growth, whereby e.g., disruption of a single VEGF allele in mice is embryonically lethal (Carmeliet et al., 1996; Ferrara et al., 1996). In our study, cross-talk of MSC with either Mo or T cells influenced the paracrine secretion pattern including VEGF levels in the niche in distinctive ways. Cross-talk of MSC with Mo increased VEGF secretion in the niche (**Figure 4F**), and as shown by transwell experiment, increased VEGF release was predominantly due to physical interaction (**Figure 4G**).

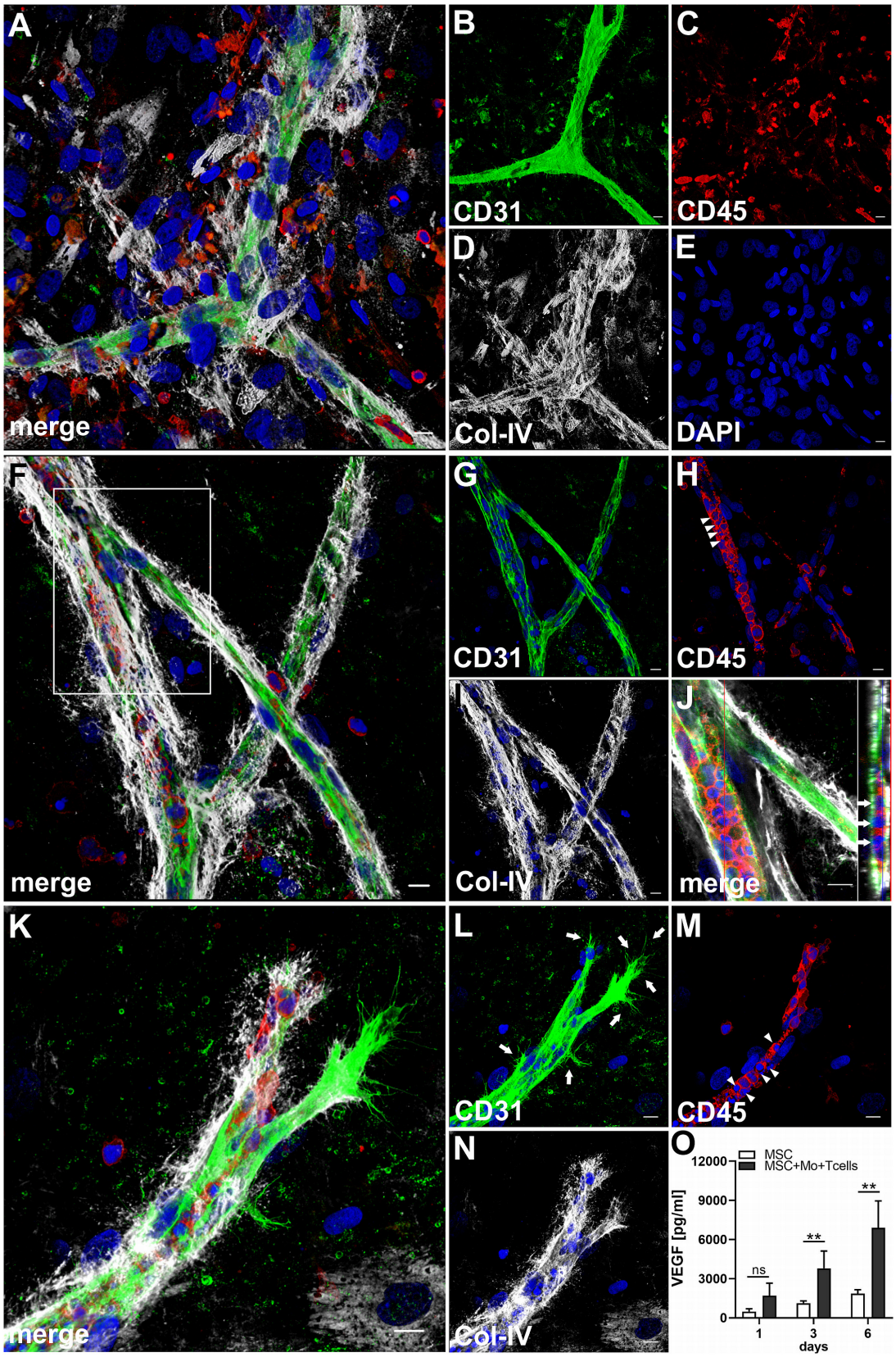

FIGURE 6 | Continued

FIGURE 6 | Co-culture of MSC, enriched Mo and enriched T cells leads to the development of complex vascular structures in 3D fibrin gels. Representative images from two separate co-culture experiments of MSC with both enriched Mo and enriched T cells. **(A–E)** Experiment 1. CLSM images of intact fibrin gel on day 14 showing a **(B)** $CD31^+$ branched vascular structure surrounded by **(D)** Col-IV^+ matrix and cells. $CD31^+$ EC also co-express Col-IV. **(C)** $CD45^+$ leukocytes in the vicinity of the neo-vessel co-express intermediate levels of CD31. **(A)** Merge. **(E)** DAPI nuclear stain. **(A–E)** Collapsed 20.25 μm-z-stack consisting of 45 consecutive images. Scale bars, 10 μm. **(F–N)** Experiment 2. CLSM images of intact fibrin gel on day 14 demonstrating that **(G)** the $CD31^+$ vascular tubes show two branch points, contain **(H)** several $CD45^+$ leukocytes, some of which show condensed nuclei (arrowheads), and is surrounded by **(I)** Col-IV^+ matrix and cells. **(J)** Orthoview CLSM image of collapsed z-stack shown in [**(F)** boxed area] confirming that $CD45^+$ leukocytes are localized inside of the developing neo-vessel (arrows). **(F)** Merge. **(F–J)** DAPI nuclear stain. **(F–I)** Collapsed 16 μm-z-stack consisting of 40 consecutive images. Scale bars, 10 μm. **(K–N)** Leading edge of a neo-vessel demonstrating **(L)** two $CD31^+$ EC at the tip of the vascular structure showing numerous filopodial protrusions (arrows). Proximal EC show fewer filopodia (arrows). **(M)** $CD45^+$ leukocytes are closely associated with one of the "tip cells" of the growing neo-vessel, and they are present inside of the vascular structure, where some of them show condensed nuclei (arrowheads). The vascular tube is surrounded by **(N)** Col-IV^+ matrix building a fine Col-IV^+ network especially toward one of the tip cells of the neo-vessel. **(K)** Merge. **(K–N)** DAPI nuclear stain. Collapsed 9.75 μm-z-stack consisting of 25 consecutive images. Scale bars, 10 μm. **(O)** Determination of VEGF by ELISA in cell-free supernatants of 3D MSC monocultures ($n = 4$) and corresponding co-cultures of MSC with both enriched Mo and enriched T cells, on day 1, 3, and 6, respectively. The data are expressed as mean values ± SD. $^{**}p$ value ≤ 0.01, ns = not significant.

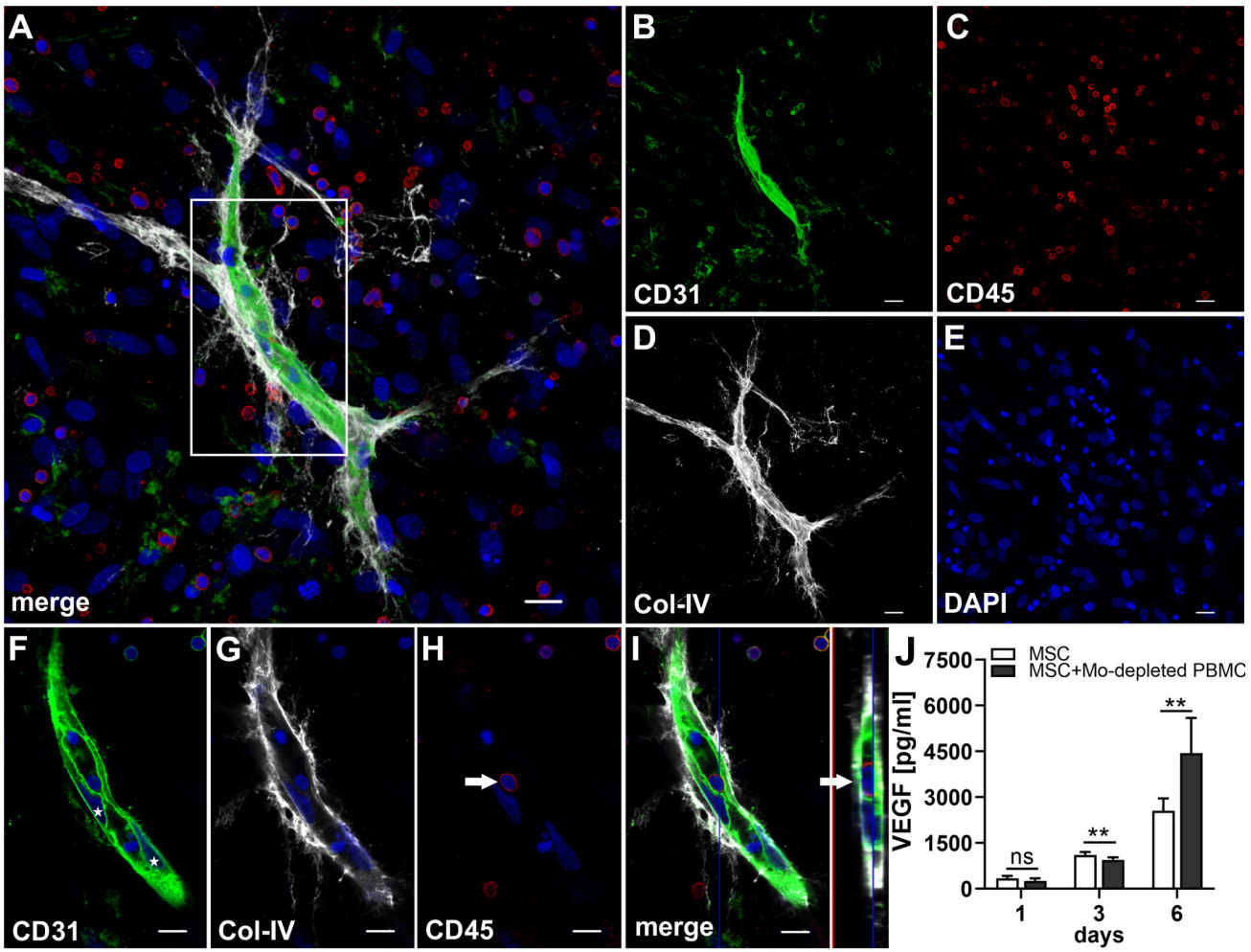

FIGURE 7 | Vascular tubes develop in the absence of $CD14^+$ Mo. Representative CLSM images of MSC co-cultured with Mo-depleted PBMC in 3D fibrin matrix on day 14 showing **(B)** a $CD31^+$ vascular structure amongst **(C)** numerous $CD45^+$ leukocytes. **(D)** Col-IV matrix staining alongside the developing vessel extends beyond the $CD31^+$ vascular structure. **(A)** Merge. **(E)** DAPI nuclear stain. **(A–E)** Collapsed 13.5 μm-z-stack consisting of 27 consecutive images. Scale bars, 20 μm. **(F–H)** 2D cross-section images (frame 10/27) of the boxed area in panel **(A)** showing the core of the vascular structure with **(F)** parietally located $CD31^+$ EC (stars), tightly connected and aligned with **(G)** Col-IV matrix, and associated with **(H)** $CD45^+$ leukocytes. **(I)** Orthoview CLSM image of collapsed z-stack shown in [**(A)**, boxed area] demonstrating that the $CD45^+$ leukocyte [arrow in panel **(H)**] is present inside of a CD31-lined vacuole adjacent to a $CD31^+CD45^-$ EC (arrow). **(F–I)** Nuclei stained with DAPI. Scale bars, 10 μm. **(J)** Determination of VEGF by ELISA in cell-free supernatants of 3D MSC monocultures ($n = 6$) and corresponding co-cultures of MSC with Mo-depleted PBMC, on day 1, 3, and 6, respectively. The data are expressed as mean values ± SD. $^{**}p$ value ≤ 0.01, ns = not significant.

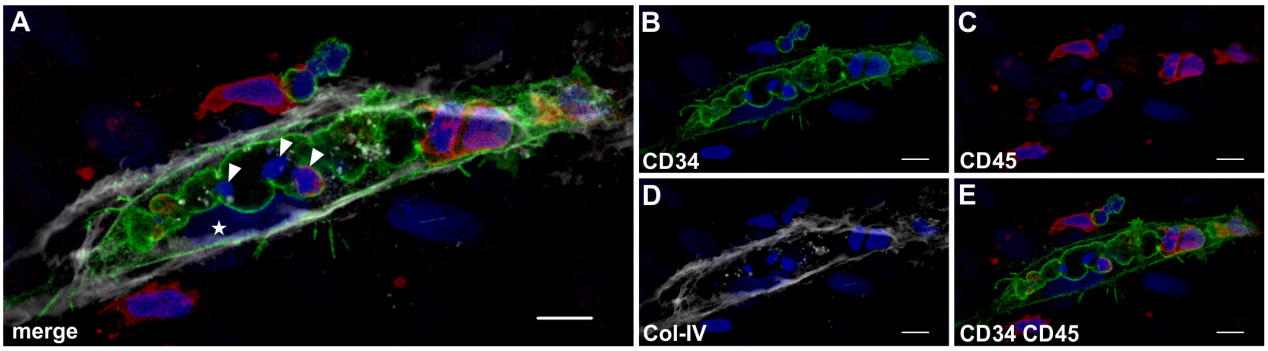

FIGURE 8 | Lumen formation occurs through coalescence of intracellular vacuoles and apoptosis of leukocytes. Representative CLSM images of MSC co-cultured with PBMC in 3D fibrin matrix showing **(A)** a multi-cellular structure confined by a **(B)** $CD34^+$ membrane separating a centrally located space apparently created by coalescing vacuoles that contains **(C)** $CD45^+$ leukocytes. The $CD34^+$ cell [star in panel **(A)**] is part of the parietal EC lining that is closely associated with **(D)** the adjacent Col-IV^+ matrix. **(E)** $CD34^+$ cells do not co-express CD45. **(A)** The merged image demonstrates three cells within the coalescing vacuoles showing condensed nuclei (arrowheads) consistent with apoptosis. Note the elongated cell between vacuole and Col-IV matrix (star) resembling an EC attached to the basement membrane. Scale bars, 10 μm.

On the other hand, cross-talk of MSC with T cells had the opposite effect and cells in the 3D niche secreted lower VEGF levels compared to corresponding MSC mono-cultures (**Figure 5T**). When PBMC were depleted from Mo, VEGF release after 24 h was similar to co-cultures of MSC with enriched T cells (**Table 2**). However, from day 3 onward, VEGF levels were significantly higher (**Supplementary Figure S2B**), suggesting that immune cells, other than Mo, compensated for decreased VEGF levels caused by T cell cross-talk with MSC. In contrast, depletion of T cells from PBMC increased the percentage of Mo (**Table 1**), and co-culture of T cell-depleted PBMC with MSC resulted in even higher VEGF levels on day 6 in comparison with co-cultures containing enriched Mo (**Table 2** and **Supplementary Figure S2A**), consistent with the notion that immune cells other than Mo also contribute to VEGF secretion via cross-talk with MSC. Accordingly, co-cultures of MSC with whole PBMC and T cell-depleted PBMC generated the highest VEGF levels (**Table 2**); however, no vascular structures were formed in co-cultures lacking T cells. In comparison, cross-talk of MSC with Mo-depleted PBMC led to the development of neo-vessels despite lower VEGF levels (**Figure 7**), demonstrating that classical Mo are not mandatory for the formation of neo-vascular structures *per se*, and confirming also the important role of T cells in vascular morphogenesis. These findings further make evident that successful neo-vessel formation requires both a pro-angiogenic paracrine niche environment, e.g., sufficient VEGF levels, as well as key cellular players, e.g., T cells. We have previously shown that VEGF release by BM-derived MSC cultured in 3D fibrin matrices increases significantly under stimulation with inflammatory cytokines, such as TNF-α and IFN-γ, but no vascular structures form in the absence of PBMC (Rüger et al., 2018). This previous study was conducted using medium supplemented with fetal bovine serum, and MSC and PBMC in co-culture formed vasculogenic clusters and cells with endothelial phenotype emerging from them (Rüger et al., 2018). These vascular structures, however, did not reach the complexity of neo-vessels generated under xeno-free conditions as demonstrated in this study.

The assembly of a basement membrane is an essential step in the maturation of new blood vessels as it mediates tissue compartmentalization. The vascular basement membrane interacts directly with the pericytes/MSC on the outside, and the EC that line the inside of the blood vessel. Col-IV, a major constituent of basement membranes, plays a key role in blood vessel morphogenesis and is essential for blood vessel stability (Poschl et al., 2004). Apart from their role as support matrix, recent *in vivo* studies have shown that basement membranes actively shape tissue morphology (Morrissey and Sherwood, 2015). Here we observed association of Col-IV matrix with cell-in-cell structures (**Figure 5** and **Supplementary Animated z-stack S7**), as well as with EC and MSC surrounding the developing vascular structures (**Supplementary Animated z-stacks S1, S8, S9, S12, S13**), supporting the concept that both cellular compartments, i.e., EC and MSC contribute to the assembly of a basement membrane necessary for EC tube formation and vascular development (Stratman and Davis, 2012). Previous work has reported that ECFC deposit matrix proteins including Col-IV organized in a web-like structure (Kusuma et al., 2012), and we have shown recently (Rüger et al., 2018) and also in this study that MSC produce and deposit Col-IV when cultured in fibrin gels. In addition to their contribution to establish a basement membrane, mechanical tension exerted to the 3D matrix by MSC may provide signals promoting elongation of the cell-in-cell structures and thereby physically guide and mediate the formation of vascular tubes, a view consistent with the concept of biomechanical forces regulating tissue vascularization (Ingber, 2002; Kilarski et al., 2009; Mammoto et al., 2009). In this context, $CD31^+$ filopodial protrusions formed by neo-vessel EC (**Figure 6L** and **Supplementary Animated z-stack S10**) may act as points of attachment to the Col-IV matrix, in order to extend the vascular tube and stabilize it as it moves (DeLisser, 2011).

Lumen formation is essential for the generation of a functional vascular system, and in both vasculogenesis and angiogenesis, it takes place in a cord of EC. Different mechanisms of lumen formation have been proposed including cord hollowing and cell hollowing (Iruela-Arispe and Davis, 2009). The current study provides evidence that coalescence of vacuoles generated by $CD31^{bright}$ progenitor cells through engulfment of T cells can contribute to lumen formation in association with apoptosis of engulfed cells (**Figure 8**). The results are consistent with the vacuole coalescence model, where EC form large intracellular vacuoles, which constitute a central vascular lumen inside each EC, thus giving rise to a seamless vascular lumen (Folkman and Haudenschild, 1980; Davis and Camarillo, 1996; Kamei et al., 2006). Two of our previous studies have demonstrated the presence of hematopoietic cells within developing vascular structures. We have shown that BM-derived mononuclear cells can form vascular structures through self-organization in 3D fibrin gels, originating from cell clusters, and that some of these neo-vessels contain $CD45^+$ hematopoietic cells (Ruger et al., 2008). Using a tissue explant model, we have recently demonstrated that vascular outgrowth from synovial tissue samples embedded in fibrin matrices is dependent on the presence of inflammatory cells, and that developing vascular sprouts contain intraluminal $CD45^+$ cells together with apoptotic cells (Rüger et al., 2018), supporting the notion that lumen formation is associated with apoptosis.

Cell-cell interaction and self-organization within physiologically relevant 3D microenvironments have been the focus of a number of recently published co-culture models for vascular tissue engineering. Co-culture of microvascular EC and MSC, both derived from adipose tissue, has been shown to generate complex vascular networks within biodegradable 3D poly-L-lactic acid (PLLA)/poly-lactic-co-glycolic acid (PLGA) constructs (Freiman et al., 2016). Interestingly, we observed that adipose-derived MSC co-cultured with PBMC in 3D fibrin matrices generate neo-vascular structures similar to neo-vessels formed by PB-derived progenitor cells in the presence of BM-derived MSC as shown in this study (unpublished observation). While our 3D model has the limitation of being a static system, microfluidic technology represents a promising platform providing insight into the spatio/temporal dynamics of vascular cell behavior. Using a microfluidic system, Yamamoto et al. have shown that co-culture of human umbilical vein endothelial cells (HUVEC) and human BM-derived MSC forms stable, branching capillary networks in collagen matrices, covered by MSC-derived pericytes and with continuous lumens of <10 μm diameter, comparable to the size of capillaries *in vivo* (Yamamoto et al., 2018). In an innovative blood-brain barrier microvascular network model developed to mimic aspects of the organization and structure of the brain microcirculation observed *in vivo*, stable and perfusable microvascular networks formed through self-assembly of human induced pluripotent stem cell-derived endothelial cells (iPSC-EC), brain pericytes and astrocytes co-cultured together in a 3D fibrin matrix (Campisi et al., 2018). Vascular networks in both studies, generated in microfluidic devices, showed morphological similarities to the neo-vessel structures generated in our 3D model, including branching, formation of lumens of <10 μm diameter and deposition of basement membrane proteins, such as Col-IV. A major difference between our model and the two models using microfluidic devices, is - apart from the methodology - the composition of cell types used for co-culture with MSC. While HUVEC and iPSC-EC, respectively, were included in the two microfluidic models, the initial co-culture set-up in our model did not include EC. The aim of our study was to investigate mechanisms of vasculogenesis by *ex vivo* PB-derived progenitor cells in an inflammatory context, including specific contributions of Mo and T cells in this process. For this reason, we co-cultured MSC with PB-derived cells obtained from LRS chambers that contain increased numbers of viable hematopoietic $CD34^+$ progenitor cells (Néron et al., 2007).

CONCLUSION

In conclusion, in our study, using the xeno-free 3D vascular niche model, we have applied a bottom-up approach that relied on encouraging cells to recapitulate physiological mechanisms of neo-vessel formation, occurring both during development and tissue repair, i.e., *de novo* vessel formation through vasculogenesis. We purposely chose not to include mature EC or culture-derived ECFC in the culture set up. This allowed us, to investigate the potential of peripheral blood-derived progenitor cells obtained *ex vivo* from the circulation, to differentiate into mature EC, when cultured together with mature circulating immune cells and MSC in a 3D fibrin environment. Here, we have demonstrated that vascular structures can form *de novo* through interaction and co-operation of blood-derived progenitor cells with mature immune cells from the circulation, in the presence of MSC, and in the context of a permissive niche environment (3D fibrin matrix). More specifically, the data might indicate that blood-derived progenitors recruited to perivascular niches can change their phenotype, and upon interaction with T cells and supportive MSC, develop into vascular EC *in situ*. Although predominantly descriptive, the niche model used in our study reveals that a complex synergistic network of cellular, extracellular and paracrine cross-talk can contribute to *de novo* vascular development through self-organization. Reproduction in animal models are planned in order to convincingly show that *de novo* formed vascular structures as presented in this *in vitro* model can integrate into a pre-existing vascular system *in vivo*. Altogether, our findings demonstrate an innovative *in vitro* setup enabling *de novo* vessel formation through vasculogenesis, that would be expected to have *in vivo* relevance and that may open up an additional perspective for the successful engineering of autologous blood vessels for therapeutic purposes.

DATA AVAILABILITY STATEMENT

The raw data supporting the conclusions of this article will be made available by the authors, without undue reservation.

ETHICS STATEMENT

The studies involving human participants were reviewed and approved by Ethics Committee of the Medical University of Vienna. The patients/participants provided their written informed consent to participate in this study.

AUTHOR CONTRIBUTIONS

BR conceived the work, designed the study, generated, analyzed, and interpreted the data, and wrote the manuscript. JB and MF contributed to the design of the study. TB generated, analyzed, and interpreted the data. E-MD performed the genetic analyses. MP created the heat map and analyzed the flow cytometry data. TB, PU, MF, JB, and GL revised the work for intellectual content. All authors contributed to the manuscript, read, and approved the submitted version.

ACKNOWLEDGMENTS

The authors thank Andreas Spittler and Günther Hofbauer from the Flow Cytometry Facility of the Medical University Vienna for FACS sorting of cells, and Marion Gröger, Sabine Rauscher, and Christoph Friedl from the Imaging Facility of the Medical University Vienna for their continued support with CLSM. The authors are grateful to the Medical University of Vienna and to Austrian Science Fund FWF (project Nr. P 31743-B30 granted to PU) for financial support.

SUPPLEMENTARY MATERIAL

The Supplementary Material for this article can be found online at: https://www.frontiersin.org/articles/10.3389/fbioe.2020.602210/full#supplementary-material

REFERENCES

Alphonse, R. S., Vadivel, A., Zhong, S., Mcconaghy, S., Ohls, R., Yoder, M. C., et al. (2015). The isolation and culture of endothelial colony-forming cells from human and rat lungs. *Nat. Prot.* 10:1697. doi: 10.1038/nprot.2015.107

Asahara, T., Kawamoto, A., and Masuda, H. (2011). Concise review: circulating endothelial progenitor cells for vascular medicine. *Stem Cells* 29, 1650–1655. doi: 10.1002/stem.745

Asahara, T., Masuda, H., Takahashi, T., Kalka, C., Pastore, C., Silver, M., et al. (1999). Bone marrow origin of endothelial progenitor cells responsible for postnatal vasculogenesis in physiological and pathological neovascularization. *Circ. Res.* 85, 221–228. doi: 10.1161/01.res.85.3.221

Asahara, T., Murohara, T., Sullivan, A., Silver, M., Van Der Zee, R., Li, T., et al. (1997). Isolation of putative progenitor endothelial cells for angiogenesis. *Science* 275:964. doi: 10.1126/science.275.5302.964

Barsotti, M. C., Magera, A., Armani, C., Chiellini, F., Felice, F., Dinucci, D., et al. (2011). Fibrin acts as biomimetic niche inducing both differentiation and stem cell marker expression of early human endothelial progenitor cells. *Cell Prolif.* 44, 33–48. doi: 10.1111/j.1365-2184.2010.00715.x

Berse, B., Brown, L. F., Van De Water, L., Dvorak, H. F., and Senger, D. R. (1992). Vascular permeability factor (vascular endothelial growth factor) gene is expressed differentially in normal tissues, macrophages, and tumors. *Mol. Biol. Cell* 3, 211–220. doi: 10.1091/mbc.3.2.211

Campisi, M., Shin, Y., Osaki, T., Hajal, C., Chiono, V., and Kamm, R. D. (2018). 3D self-organized microvascular model of the human blood-brain barrier with endothelial cells, pericytes and astrocytes. *Biomaterials* 180, 117–129. doi: 10.1016/j.biomaterials.2018.07.014

Caplan, A. I. (2009). Why are MSCs therapeutic? New data: new insight. *J. Pathol.* 217, 318–324. doi: 10.1002/path.2469

Caplan, A. I., and Correa, D. (2011). The MSC: an injury drugstore. *Cell Stem Cell* 9, 11–15. doi: 10.1016/j.stem.2011.06.008

Carmeliet, P., Ferreira, V., Breier, G., Pollefeyt, S., Kieckens, L., Gertsenstein, M., et al. (1996). Abnormal blood vessel development and lethality in embryos lacking a single VEGF allele. *Nature* 380, 435–439. doi: 10.1038/380435a0

Carrion, B., Janson, I. A., Kong, Y. P., and Putnam, A. J. (2014). A safe and efficient method to retrieve mesenchymal stem cells from three-dimensional fibrin gels. *Tissue Eng. Part C Methods* 20, 252–263. doi: 10.1089/ten.tec.2013.0051

Chujo, S., Shirasaki, F., Kondo-Miyazaki, M., Ikawa, Y., and Takehara, K. (2009). Role of connective tissue growth factor and its interaction with basic fibroblast growth factor and macrophage chemoattractant protein-1 in skin fibrosis. *J. Cell. Physiol.* 220, 189–195. doi: 10.1002/jcp.21750

Crisan, M., Yap, S., Casteilla, L., Chen, C. W., Corselli, M., Park, T. S., et al. (2008). A perivascular origin for mesenchymal stem cells in multiple human organs. *Cell Stem Cell* 3, 301–313. doi: 10.1016/j.stem.2008.07.003

Crosby Jeffrey, R., Kaminski Wolfgang, E., Schatteman, G., Martin Paul, J., Raines Elaine, W., Seifert Ron, A., et al. (2000). Endothelial cells of hematopoietic origin make a significant contribution to adult blood vessel formation. *Circ. Res.* 87, 728–730. doi: 10.1161/01.res.87.9.728

Davis, G. E., and Camarillo, C. W. (1996). An alpha 2 beta 1 integrin-dependent pinocytic mechanism involving intracellular vacuole formation and coalescence regulates capillary lumen and tube formation in three-dimensional collagen matrix. *Exp. Cell Res.* 224, 39–51. doi: 10.1006/excr.1996.0109

DeLisser, H. M. (2011). Modulators of endothelial cell filopodia. *Cell Adhes. Migrat.* 5, 37–41. doi: 10.4161/cam.5.1.13575

Deshpande, A. H., Nayak, S., and Munshi, M. M. (2000). Cytology of sinus histiocytosis with massive lymphadenopathy (Rosai-Dorfman disease). *Diagn. Cytopathol.* 22, 181–185. doi: 10.1002/(sici)1097-0339(20000301)22:3<181::aid-dc10>3.0.co;2-6

Duong, H. T., Comhair, S. A., Aldred, M. A., Mavrakis, L., Savasky, B. M., Erzurum, S. C., et al. (2011). Pulmonary artery endothelium resident endothelial colony-forming cells in pulmonary arterial hypertension. *Pulm. Circulat.* 1, 475–486. doi: 10.4103/2045-8932.93547

Ferrara, N., Carver-Moore, K., Chen, H., Dowd, M., Lu, L., O'shea, K. S., et al. (1996). Heterozygous embryonic lethality induced by targeted inactivation of the VEGF gene. *Nature* 380, 439–442. doi: 10.1038/380439a0

Folkman, J., and Haudenschild, C. (1980). Angiogenesis in vitro. *Nature* 288, 551–556.

Freiman, A., Shandalov, Y., Rozenfeld, D., Shor, E., Segal, S., Ben-David, D., et al. (2016). Adipose-derived endothelial and mesenchymal stem cells enhance vascular network formation on three-dimensional constructs in vitro. *Stem Cell Res. Ther.* 7:5.

Gawronska-Kozak, B., Bogacki, M., Rim, J.-S., Monroe, W. T., and Manuel, J. A. (2006). Scarless skin repair in immunodeficient mice. *Wound Repair Regen.* 14, 265–276. doi: 10.1111/j.1743-6109.2006.00121.x

González, M. A., Gonzalez-Rey, E., Rico, L., Büscher, D., and Delgado, M. (2009). Treatment of experimental arthritis by inducing immune tolerance with human adipose-derived mesenchymal stem cells. *Arthrit. Rheumat.* 60, 1006–1019. doi: 10.1002/art.24405

Griffin, M. D., Ritter, T., and Mahon, B. P. (2010). Immunological aspects of allogeneic mesenchymal stem cell therapies. *Hum. Gene Ther.* 21, 1641–1655. doi: 10.1089/hum.2010.156

Hur, J., Yang, H. M., Yoon, C. H., Lee, C. S., Park, K. W., Kim, J. H., et al. (2007). Identification of a novel role of T cells in postnatal vasculogenesis: characterization of endothelial progenitor cell colonies. *Circulation* 116, 1671–1682. doi: 10.1161/circulationaha.107.694778

Ingber, D. E. (2002). Mechanical signaling and the cellular response to extracellular matrix in angiogenesis and cardiovascular physiology. *Circ. Res.* 91, 877–887. doi: 10.1161/01.res.0000039537.73816.e5

Ingram, D. A., Mead, L. E., Moore, D. B., Woodard, W., Fenoglio, A., and Yoder, M. C. (2005). Vessel wall–derived endothelial cells rapidly proliferate because they contain a complete hierarchy of endothelial progenitor cells. *Blood* 105:2783. doi: 10.1182/blood-2004-08-3057

Ingram, D. A., Mead, L. E., Tanaka, H., Meade, V., Fenoglio, A., Mortell, K., et al. (2004). Identification of a novel hierarchy of endothelial progenitor cells using human peripheral and umbilical cord blood. *Blood* 104:2752. doi: 10.1182/blood-2004-04-1396

Iruela-Arispe, M. L., and Davis, G. E. (2009). Cellular and Molecular Mechanisms of Vascular Lumen Formation. *Dev. Cell* 16, 222–231. doi: 10.1016/j.devcel.2009.01.013

Janeczek Portalska, K., Leferink, A., Groen, N., Fernandes, H., Moroni, L., Van Blitterswijk, C., et al. (2012). Endothelial differentiation of mesenchymal stromal cells. *PLoS One* 7:e46842. doi: 10.1371/journal.pone.0046842

Kamei, M., Brian Saunders, W., Bayless, K. J., Dye, L., Davis, G. E., and Weinstein, B. M. (2006). Endothelial tubes assemble from intracellular vacuoles in vivo. *Nature* 442, 453–456. doi: 10.1038/nature04923

Kilarski, W. W., Samolov, B., Petersson, L., Kvanta, A., and Gerwins, P. (2009). Biomechanical regulation of blood vessel growth during tissue vascularization. *Nat. Med.* 15, 657–664. doi: 10.1038/nm.1985

Kim, H., Cho, H. J., Kim, S. W., Liu, B., Choi, Y. J., Lee, J., et al. (2010). CD31+ cells represent highly angiogenic and vasculogenic cells in bone marrow: novel role of nonendothelial CD31+ cells in neovascularization and their therapeutic effects on ischemic vascular disease. *Circ. Res.* 107, 602–614. doi: 10.1161/circresaha.110.218396

Kopp, H.-G., Ramos, C. A., and Rafii, S. (2006). Contribution of endothelial progenitors and proangiogenic hematopoietic cells to vascularization of tumor and ischemic tissue. *Curr. Opin. Hematol.* 13, 175–181. doi: 10.1097/01.moh.0000219664.26528.da

Kusuma, S., Zhao, S., and Gerecht, S. (2012). The extracellular matrix is a novel attribute of endothelial progenitors and of hypoxic mature endothelial cells. *FASEB J.* 26, 4925–4936. doi: 10.1096/fj.12-209296

Lewis, W. H. (1925). The engulfment of living blood cells by others of the same type. *Anat. Rec.* 31, 43–49. doi: 10.1002/ar.1090310106

Lin, Y., Weisdorf, D. J., Solovey, A., and Hebbel, R. P. (2000). Origins of circulating endothelial cells and endothelial outgrowth from blood. *J. Clin. Invest.* 105, 71–77. doi: 10.1172/jci8071

Mammoto, A., Connor, K. M., Mammoto, T., Yung, C. W., Huh, D., Aderman, C. M., et al. (2009). A mechanosensitive transcriptional mechanism that controls angiogenesis. *Nature* 457, 1103–1108. doi: 10.1038/nature07765

Medina, R. J., Barber, C. L., Sabatier, F., Dignat-George, F., Melero-Martin, J. M., Khosrotehrani, K., et al. (2017). Endothelial progenitors: a consensus statement on nomenclature. *Stem Cells Transl. Med.* 6, 1316–1320. doi: 10.1002/sctm.16-0360

Medina, R. J., O'neill, C. L., O'doherty, T. M., Knott, H., Guduric-Fuchs, J., Gardiner, T. A., et al. (2011). Myeloid angiogenic cells act as alternative M2 macrophages and modulate angiogenesis through interleukin-8. *Mol. Med.* 17, 1045–1055. doi: 10.2119/molmed.2011.00129

Morrissey, M. A., and Sherwood, D. R. (2015). An active role for basement membrane assembly and modification in tissue sculpting. *J. Cell Sci.* 128:1661. doi: 10.1242/jcs.168021

Mund, J. A., Estes, M. L., Yoder, M. C., Ingram, D. A. Jr., and Case, J. (2012). Flow cytometric identification and functional characterization of immature and mature circulating endothelial cells. *Arterioscler. Thromb. Vasc. Biol.* 32, 1045–1053. doi: 10.1161/atvbaha.111.244210

Murohara, T., Ikeda, H., Duan, J., Shintani, S., Sasaki, K. I., Eguchi, H., et al. (2000). Transplanted cord blood-derived endothelial precursor cells augment postnatal neovascularization. *J. Clin. Invest.* 105, 1527–1536. doi: 10.1172/jci8296

Néron, S., Thibault, L., Dussault, N., Côté, G., Ducas, É, Pineault, N., et al. (2007). Characterization of mononuclear cells remaining in the leukoreduction system chambers of apheresis instruments after routine platelet collection: a new source of viable human blood cells. *Transfusion* 47, 1042–1049. doi: 10.1111/j.1537-2995.2007.01233.x

Nosbaum, A., Prevel, N., Truong, H. A., Mehta, P., Ettinger, M., Scharschmidt, T. C., et al. (2016). Cutting Edge: regulatory T cells facilitate cutaneous wound healing. *J. Immunol.* 196, 2010–2014. doi: 10.4049/jimmunol.1502139

Oswald, J., Boxberger, S., Jorgensen, B., Feldmann, S., Ehninger, G., Bornhauser, M., et al. (2004). Mesenchymal stem cells can be differentiated into endothelial cells in vitro. *Stem cells* 22, 377–384. doi: 10.1634/stemcells.22-3-377

Park, J. E., and Barbul, A. (2004). Understanding the role of immune regulation in wound healing. *Am. J. Surg.* 187, S11–S16.

Peiser, L., Mukhopadhyay, S., and Gordon, S. (2002). Scavenger receptors in innate immunity. *Curr. Opin. Immunol.* 14, 123–128. doi: 10.1016/s0952-7915(01)00307-7

Poschl, E., Schlotzer-Schrehardt, U., Brachvogel, B., Saito, K., Ninomiya, Y., and Mayer, U. (2004). Collagen IV is essential for basement membrane stability but dispensable for initiation of its assembly during early development. *Development* 131, 1619–1628. doi: 10.1242/dev.01037

Rappolee, D. A., Mark, D., Banda, M. J., and Werb, Z. (1988). Wound macrophages express TGF-alpha and other growth factors in vivo: analysis by mRNA phenotyping. *Science* 241:708. doi: 10.1126/science.3041594

Ribatti, D., Vacca, A., Nico, B., Roncali, L., and Dammacco, F. (2001). Postnatal vasculogenesis. *Mech. Dev.* 100, 157–163. doi: 10.1016/s0925-4773(00)00522-0

Rohde, E., Bartmann, C., Schallmoser, K., Reinisch, A., Lanzer, G., Linkesch, W., et al. (2007). Immune cells mimic the morphology of endothelial progenitor colonies in vitro. *Stem Cells* 25, 1746–1752. doi: 10.1634/stemcells.2006-0833

Ruger, B., Giurea, A., Wanivenhaus, A. H., Zehetgruber, H., Hollemann, D., Yanagida, G., et al. (2004). Endothelial precursor cells in the synovial tissue of patients with rheumatoid arthritis and osteoarthritis. *Arthritis Rheum.* 50, 2157–2166. doi: 10.1002/art.20506

Ruger, B. M., Breuss, J., Hollemann, D., Yanagida, G., Fischer, M. B., Mosberger, I., et al. (2008). Vascular morphogenesis by adult bone marrow progenitor cells in three-dimensional fibrin matrices. *Differ. Res. Biol. Div.* 76, 772–783. doi: 10.1111/j.1432-0436.2007.00259.x

Rüger, B. M., Buchacher, T., Giurea, A., Kubista, B., Fischer, M. B., and Breuss, J. M. (2018). Vascular morphogenesis in the context of inflammation: self-organization in a fibrin-based 3D culture system. *Front. Physiol.* 9:679. doi: 10.3389/fphys.2018.00679

Sasse, S., Skorska, A., Lux, C. A., Steinhoff, G., David, R., and Gaebel, R. (2019). Angiogenic potential of bone marrow derived CD133(+) and CD271(+) intramyocardial stem cell trans- plantation post MI. *Cells* 9, 78. doi: 10.3390/cells9010078

Schmitt, A., Drouin, A., Massé, J. M., Guichard, J., Shagraoui, H., and Cramer, E. M. (2002). Polymorphonuclear neutrophil and megakaryocyte mutual involvement in myelofibrosis pathogenesis. *Leuk. Lymphoma* 43, 719–724. doi: 10.1080/10428190290016809

Shamoto, M. (1981). Emperipolesis of hematopoietic cells in myelocytic leukemia. Electron microscopic and phase contrast microscopic studies. *Virchows Arch. B Cell Pathol. Incl. Mol. Pathol.* 35, 283–290. doi: 10.1007/bf02889168

Shimokado, K., Raines, E. W., Madtes, D. K., Barrett, T. B., Benditt, E. P., and Ross, R. (1985). A significant part of macrophage-derived growth factor consists of at least two forms of PDGF. *Cell* 43, 277–286. doi: 10.1016/0092-8674(85)90033-9

Siegel, G., Fleck, E., Elser, S., Hermanutz-Klein, U., Waidmann, M., Northoff, H., et al. (2018). Manufacture of endothelial colony-forming progenitor cells from steady-state peripheral blood leukapheresis using pooled human platelet lysate. *Transfusion* 58, 1132–1142. doi: 10.1111/trf.14541

Silva Guilherme, V., Litovsky, S., Assad Joao, A. R., Sousa Andre, L. S., Martin Bradley, J., Vela, D., et al. (2005). Mesenchymal stem cells differentiate into an endothelial phenotype, enhance vascular density, and improve heart function in a canine chronic ischemia model. *Circulation* 111, 150–156. doi: 10.1161/01.cir.0000151812.86142.45

Singer, N. G., and Caplan, A. I. (2011). Mesenchymal stem cells: mechanisms of inflammation. *Annu. Rev. Pathol. Mech. Dis.* 6, 457–478. doi: 10.1146/annurev-pathol-011110-130230

Steinlechner, M., Berger, B., Niederstätter, H., and Parson, W. (2002). Rare failures in the amelogenin sex test. *Int. J. Legal Med.* 116, 117–120. doi: 10.1007/s00414-001-0264-9

Stratman, A. N., and Davis, G. E. (2012). Endothelial cell-pericyte interactions stimulate basement membrane matrix assembly: influence on vascular tube remodeling, maturation, and stabilization. *Microsc. Microanal.* 18, 68–80. doi: 10.1017/s1431927611012402

Swift, M. E., Burns, A. L., Gray, K. L., and Dipietro, L. A. (2001). Age-related alterations in the inflammatory response to dermal injury.

J. Invest. Dermatol. 117, 1027–1035. doi: 10.1046/j.0022-202x.2001.01539.x

Szade, A., Grochot-Przeczek, A., Florczyk, U., Jozkowicz, A., and Dulak, J. (2015). Cellular and molecular mechanisms of inflammation-induced angiogenesis. *IUBMB Life* 67, 145–159. doi: 10.1002/iub.1358

Szekanecz, Z., and Koch, A. E. (2001). Chemokines and angiogenesis. *Curr. Opin. Rheumatol* 13, 202–208.

Thiele, J., Krech, R., Choritz, H., and Georgii, A. (1984). Emperipolesis–a peculiar feature of megakaryocytes as evaluated in chronic myeloproliferative diseases by morphometry and ultrastructure. *Virchows Arch. B Cell Pathol. Incl. Mol. Pathol.* 46, 253–263. doi: 10.1007/bf02890314

Thomas, D., Marsico, G., Mohd Isa, I. L., Thirumaran, A., Chen, X., Lukasz, B., et al. (2020). Temporal changes guided by mesenchymal stem cells on a 3D microgel platform enhance angiogenesis in vivo at a low-cell dose. *Proc. Natl. Acad. Sci. U.S.A.* 117:19033. doi: 10.1073/pnas.2008245117

Wang, C., Li, Y., Yang, M., Zou, Y., Liu, H., Liang, Z., et al. (2018). Efficient differentiation of bone marrow mesenchymal stem cells into endothelial cells in vitro. *Eur. J. Vasc. Endovasc. Surg.* 55, 257–265.

Wang, X., Balaji, S., Steen, E. H., Li, H., Rae, M. M., Blum, A. J., et al. (2019). T lymphocytes attenuate dermal scarring by regulating inflammation, neovascularization, and extracellular matrix remodeling. *Adv. Wound Care* 8, 527–537. doi: 10.1089/wound.2019.0981

Watt, S. M., Gullo, F., Van Der Garde, M., Markeson, D., Camicia, R., Khoo, C. P., et al. (2013). The angiogenic properties of mesenchymal stem/stromal cells and their therapeutic potential. *Br. Med. Bull.* 108, 25–53.

Wekerle, H., Ketelsen, U. P., and Ernst, M. (1980). Thymic nurse cells. Lymphoepithelial cell complexes in murine thymuses: morphological and serological characterization. *J. Exp. Med.* 151, 925–944. doi: 10.1084/jem.151.4.925

Wilde, B., Mertens, A. J., Arends, S., Rouhl, R., Bijleveld, R., Huitema, J., et al. (2016). Endothelial progenitor cells are differentially impaired in ANCA-associated vasculitis compared to healthy controls. *Arthrit. Res. Ther.* 18, 147.

Willenborg, S., Lucas, T., Van Loo, G., Knipper, J. A., Krieg, T., Haase, I., et al. (2012). CCR2 recruits an inflammatory macrophage subpopulation critical for angiogenesis in tissue repair. *Blood* 120, 613–625. doi: 10.1182/blood-2012-01-403386

Wynn, T. A., and Barron, L. (2010). Macrophages: master regulators of inflammation and fibrosis. *Semin. Liver Dis.* 30, 245–257. doi: 10.1055/s-0030-1255354

Wynn, T. A., Chawla, A., and Pollard, J. W. (2013). Macrophage biology in development, homeostasis and disease. *Nature* 496, 445–455. doi: 10.1038/nature12034

Yamamoto, K., Tanimura, K., Watanabe, M., Sano, H., Uwamori, H., Mabuchi, Y., et al. (2018). Construction of continuous capillary networks stabilized by pericyte-like perivascular cells. *Tissue Eng. Part A* 25, 499–510. doi: 10.1089/ten.tea.2018.0186

Conflict of Interest: The authors declare that the research was conducted in the absence of any commercial or financial relationships that could be construed as a potential conflict of interest.

frontiers in Bioengineering and Biotechnology

REVIEW
published: 26 November 2020
doi: 10.3389/fbioe.2020.599674

Cell-Based Therapy Manufacturing in Stirred Suspension Bioreactor: Thoughts for cGMP Compliance

Suman C. Nath[1,2], Lane Harper[1]* and Derrick E. Rancourt[1,2]**

[1] *Department of Biochemistry & Molecular Biology, Cumming School of Medicine, University of Calgary, Calgary, AB, Canada,*
[2] *McCaig Institute for Bone and Joint Health, Cumming School of Medicine, University of Calgary, Calgary, AB, Canada*

Cell-based therapy (CBT) is attracting much attention to treat incurable diseases. In recent years, several clinical trials have been conducted using human pluripotent stem cells (hPSCs), and other potential therapeutic cells. Various private- and government-funded organizations are investing in finding permanent cures for diseases that are difficult or expensive to treat over a lifespan, such as age-related macular degeneration, Parkinson's disease, or diabetes, etc. Clinical-grade cell manufacturing requiring current good manufacturing practices (cGMP) has therefore become an important issue to make safe and effective CBT products. Current cell production practices are adopted from conventional antibody or protein production in the pharmaceutical industry, wherein cells are used as a vector to produce the desired products. With CBT, however, the "cells are the final products" and sensitive to physico- chemical parameters and storage conditions anywhere between isolation and patient administration. In addition, the manufacturing of cellular products involves multi-stage processing, including cell isolation, genetic modification, PSC derivation, expansion, differentiation, purification, characterization, cryopreservation, etc. Posing a high risk of product contamination, these can be time- and cost- prohibitive due to maintenance of cGMP. The growing demand of CBT needs integrated manufacturing systems that can provide a more simple and cost-effective platform. Here, we discuss the current methods and limitations of CBT, based upon experience with biologics production. We review current cell manufacturing integration, automation and provide an overview of some important considerations and best cGMP practices. Finally, we propose how multi-stage cell processing can be integrated into a single bioreactor, in order to develop streamlined cGMP-compliant cell processing systems.

Keywords: cell-based therapy, biologics manufacturing, cGMP, genetic engineering, integrated bioprocessing, bioreactor

OPEN ACCESS

Edited by:
Diego Correa,
University of Miami, United States

Reviewed by:
Robert Zweigerdt,
Hannover Medical School, Germany
Rodolfo E. De La Vega,
Mayo Clinic, United States

****Correspondence:***
Derrick E. Rancourt
rancourt@ucalgary.ca
Suman C. Nath
suman.nath1@ucalgary.ca
Lane Harper
lane.harper1@ucalgary.ca

Specialty section:
This article was submitted to Preclinical Cell and Gene Therapy, a section of the journal Frontiers in Bioengineering and Biotechnology

Received: *27 August 2020*
Accepted: *30 October 2020*
Published: *26 November 2020*

Citation:
Nath SC, Harper L and Rancourt DE (2020) Cell-Based Therapy Manufacturing in Stirred Suspension Bioreactor: Thoughts for cGMP Compliance. Front. Bioeng. Biotechnol. 8:599674. doi: 10.3389/fbioe.2020.599674

INTRODUCTION

Human pluripotent stem cells (hPSCs), including embryonic stem cells (ESCs) (Thomson et al., 1998) and induced pluripotent stem cells (iPSCs) (Takahashi et al., 2007) are attractive tools in the field of regenerative medicine because of their ability to self-renew and differentiate into any cell type in the human body. Use of these cells increased exponentially after the discovery of hiPSCs in

2007 (Guhr et al., 2018). Recently, hundreds of biotechnology companies were founded with the mission to treat degenerative diseases using these cells. Age-related macular degeneration (AMD), type I diabetes mellitus, heart failure, Parkinson's disease and spinal cord injury are the most common degenerative diseases being treated with hPSCs (Trounson and McDonald, 2015).

Although hiPSCs are a better source for autologous CBT, they are less preferable for clinical trials because they are less genetically stable than hESCs (Attwood and Edel, 2019). Viral vectors using for iPSC reprogramming integrate into the genome and poses risk of insertional mutagenesis (Baum, 2007). Moreover, genetic modification can cause mutations that associated with cancer (Gore et al., 2011). Evidence of transgene reactivation after iPSC reprogramming also poses risk after transplantation (Galat et al., 2016).

Some clinical studies have already begun using hiPSCs derived from patients. A clinical trial for the treatment of wet AMD has recently been conducted by the Masayo Takahashi group from the Riken Center for Developmental Biology (Reardon and Cyranoski, 2014). Similarly, Jun Takahashi from Kyoto University is also conducting a clinical trial using hiPSCs to treat Parkinson's disease (Cyranoski, 2018). There are also several clinical trials in the United States using hiPSCs for the treatment of various diseases such as β-thalassemia, liver disease, diabetes, etc. and their use is increasing worldwide (Kimbrel and Lanza, 2015).

Since stem CBT trials are proliferating, many clinical studies continue to use both hESCs and hiPSCs. About 8141 CBTs and 1657 stem CBTs were found based upon searches recently performed on clinicaltrials.gov (October, 2020) (ClinicalTrials.gov, 2020). However, as speculated from previous clinical studies, the percentage of success is quiet low. Of the 315 clinical trials carried out, only 0.3% went to Phase 4 (Trounson and McDonald, 2015). The low percentage of clinical trial completion depends on different factors. One of the main factors is the design and implementation of cost-effective, high safety production practices required by regulatory bodies. In addition, multi-dose production costs also hamper the success rate of clinical trials. Since the global revenues from CBT in 2018 were approximately a billion dollars and are forecasted to be in the tens of billions by 2025, a great deal of attention is needed to produce high-quality cells to treat incurable diseases (Davie et al., 2012; PR Newswire, 2019).

The production of stem cell-derived biologics is adapted from the production of conventional pharmaceutical proteins and vaccines. The production of conventional biologics involves the following basic steps: Isolation and identification of raw materials, formulation, filling, packaging and storage, where total processing stops when final products are stored. This provides a very basic model as the production of conventional biologics. Yet CBT products differ in various significant ways. In biologics, cells are used as a platform for the production of desired therapeutic proteins. Cells are discarded after a batch and new cells with the requisite protein expression are used to produce the next batch. Proteins produced in this way are generally stable, uniform, and easily characterized, varying little between batches.

In cell-based therapies, the final products are cells that are sensitive to the physical or chemical attributes of the resident environment and are prone to spontaneous change. Therefore, these considerations must be taken into account when translating from bench to clinic (Roh et al., 2016). The need for CBT products are emerging from various cell lines including chimeric antigen receptor T-cell (CAR-T), retinal pigment epithelial cell, neural cell, hepatic cell, cardiac cell, mesenchymal stem cell (MSCs), ESCs, iPSCs, etc. for treating various degenerative diseases. In this review, we will focus on cell therapy development ranging from unipotent to pluripotent cells, namely, CAR-T cells (unipotent cells), MSCs (multipotent) and iPSCs (pluripotent) (**Figure 1**).

Since CBT needs much consideration for producing large cell numbers, using conventional cell processing systems makes it more complicated and sometimes impossible. Being a multi-step process that can cause batch variability, inefficiency and low quality of transplantable cells in plate culture, there are too many possibilities for human error. CBT needs to be simplified and made more direct. In this context, we will discuss some of the current limitations of cell production strategies. We will propose how to possibly overcome these limitations by integrating the entire process into a single bioreactor system due to advantages over plate culture (**Table 1**). We will also discuss how genetic modification- transfection or transduction, reprogramming, differentiation, purification and development of final products in a single bioreactor can be integrated. In this context, we also discuss some basic, high level cGMP considerations for CBT biomanufacturing.

CONVENTIONAL PRACTICES FOR CBT PRODUCT MANUFACTURING

As stated earlier, cell processing differs widely from pharmaceutical proteins or vaccine production although current manufacturing practices are based on conventional biologics manufacturing that may not be compatible for CBT (Bennett, 2018; Sterlling, 2018). For example, in biologics manufacturing, microorganisms containing genes of interests are expanded and the proteins are isolated and purified for pharmaceutical peptide production (**Figure 1**) (Overton, 2014; Jozala et al., 2016). The purified proteins are screened for both chemical and biological properties for quality assurance. Chemical screening includes the testing of pH, solubility, percentage of active ingredients, whereas biological screening includes sterility test, endotoxin test, etc. Although biologics production from microorganisms is complicated, it is not as complicated as CBT production from living cells. Regardless, having fewer variables that need to be controlled, biologics production from microorganisms results in standardized and homogenous production of both target peptides and stock cells.

Difficulty in bioprocessing is increased when pharmaceutical proteins are produced using human, animal or plant cells. High-quality products in this case depend on the maintenance of high-quality cells and sterile conditions as these cells are generally less robust in culture, and tend to be more difficult to work with. In

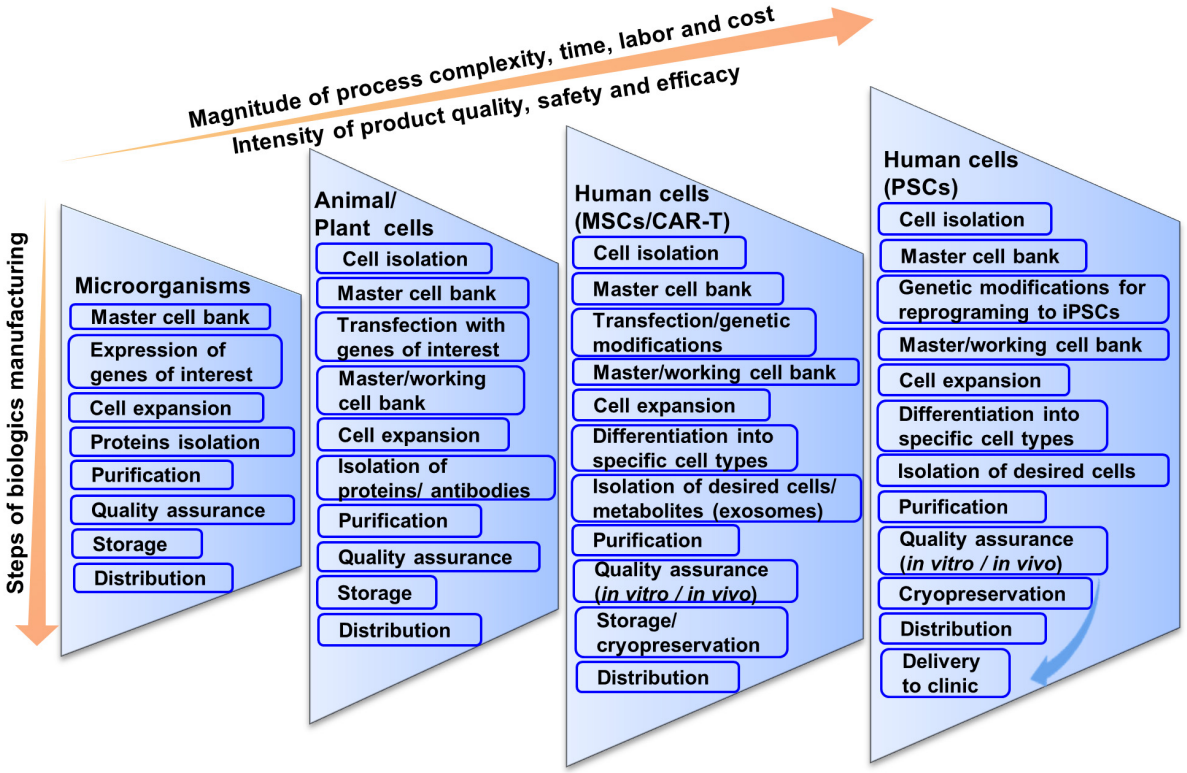

FIGURE 1 | Schematic illustration of current multi-step cell manufacturing strategies in planar culture for cell therapy applications.

this case, cells transfected with the genes of interest are cultivated for a certain period of time after inoculation from a master cell bank (Lai et al., 2013; Tekoah et al., 2015). After expansion, cells are stored for future use or discarded after collecting the supernatant. The desired proteins or antibodies are separated, purified and concentrated. The isolated products are then checked for physical, chemical or biological properties similar to microbial peptide production to meet the regulatory agency's criteria through quality assurance. A considerable benefit is that once the protein is produced, it again tends to be much more stable and characterizable compared to cells for CBT.

TABLE 1 | Comparison of pros and cons of adherent and bioreactor culture.

Cultures	Pros	Cons
Adherent	• Easy to handling • Easy for cell visualization • Easy for genetic manipulation	• Low final cell density • High medium consumption • Limited growth surface area • Large numbers of culture vessels are required • Online sampling is not possible • Labor intensive • Low scalability • Difficulties in cell harvesting (need to detach from culture surface) • Difficult for automation because of cell detachment step
Bioreactor	• High final cell density • Low medium consumption • Unlimited growth surface area • Single vessel is enough • Online sampling • Flexible labor • High scalability • Easy for harvesting (ready to use as aggregate) • Suitable for automation	• Handling requires expertise • Cell visualization requires an extra step • Difficulties in genetic manipulation

Stem cell or blood-derived product manufacturing is not as direct as the production of pharmaceutical proteins or vaccines (**Figure 1**). This is because cells are the product in CBT and they tend to be less robust in the face of perturbations and more vulnerable to changes in cell identity and gene expression. Manufacturing strategies for cell production can vary from source to source and can differ significantly based on autologous or allogeneic transplantation. The main general steps are the acquisition of tissue samples and cell isolation, initial cell purification, selection, activation and transduction, expansion of cells, differentiation, washing, harvesting and formulation, filling and cryopreservation, and finally storage and delivery to clinics (Roh et al., 2016). At every step, quality assurance and consideration for safety and efficacy are important for all CBT products manufactured for clinical application.

CBT products also differ from sources of tissue acquisition and target of diseases treated. For example, in CAR-T therapy, T-cells are isolated from patients' blood, which contain abnormal levels of inhibitory factors and regulatory cells (Bellone et al., 1999;

Gajewski et al., 2013) as patients are commonly also treated with chemo- and radiotherapies. Accordingly, heterogeneity can occur in the final products, which need much attention during the cell isolation step. Then initial cell culture is done for selection, activation or transduction of specific interest, in this case, the CAR gene. The transduced cells are then expanded in plate culture and stored in the master cell bank.

Cells are also screened for quality, safety and efficacy. Product potency is an important criterion to meet before releasing the product. For example, if a CBT product is applied for the CAR-T related cancer therapy, it needs to be examined for the secretion of cytotoxic cytokines (IFN-γ) and killing of target cells (Dudley et al., 2003). After passing all the steps of quality assurance, cells are stored or delivered to the clinic. Often cells need to be delivered in a timelier manner than other biologics and have a much less stable "shelf life", which needs to be taken into serious consideration.

There is a further increase in the magnitude of process complexity, time, labor and cost when moving to CBT production from human hMSCs to hPSCs (**Figure 1**). MSCs are only slightly more complicated than T-cells. For biologics manufacturing from hMSCs, cells are expanded and stored in master cell banks after isolation and purification from patients' bone marrow (Ullah et al., 2015). Then cells are genetically modified or expanded and differentiated into specific types of cells.

An interesting possibility being exploited with MSCs is that sometimes cell-derived bi-products can be used for clinical applications. For example, exosomes secreted from MSCs contain autocrine or paracrine signaling components (cytokines, RNAs, etc.) (Pisitkun et al., 2004; Valadi et al., 2007; NHLBI, 2009; Chen et al., 2010) and show immunological activities (Lai et al., 2011; Zhang et al., 2013; Lou et al., 2017). For this reason, it's possible to consider value-added products, or creation of processes that can utilize such a potential secondary resource. MSC-derived exosomes are currently being studied for treating degenerative diseases (Chang et al., 2018; Yin et al., 2019). MSC-derived exosomes have recently been approved by US FDA for treating burn patients (PRWeb, 2018). For using exosomes in clinical applications, hMSCs are expanded and exosomes are purified by ultracentrifugation or size exclusion chromatography from culture medium. The benefit to this is that if the cell therapy itself is cGMP compliant, then it may be possible to have little added effort to extract a secondary cGMP compliant product in the form of exosomes. However, whether clinical applications use cells or cell-derived products, it needs go through a strict quality screening. Since here the product is cells, it needs to pass the *in vivo* biological tests for quality, efficacy and safety. After confirming the quality assurance, cells are cryopreserved or delivered to clinics.

hPSCs by contrast are very complicated; however, they have many benefits making theme an important cell choice for CBT. Being pluripotent, hPSCs have the ability to be differentiated into any cell type in the body. This provides advantages for therapies involving cells, other than T cells or MSCs that are not accessible via biopsy. Unlike T cells or MSCs, hPSCs do not senesce, making them very conducive to cell bio-banking (Zeng, 2007; Koch et al., 2013).

Biologics manufacturing from hESCs is impractical as isolation from human embryos has been unethical in many jurisdictions (Lo and Parham, 2009). Accordingly hESCs have been superseded by hiPSCs, which avoid such ethical barriers. Compared to hESCs which are subject to immune-rejection due to human leukocyte antigen (HLA) expression after differentiation (Taylor et al., 2005), iPSCs provide a better platform for autologous therapy because terminally-differentiated cells can be reprogrammed to desired cells using the four Yamanaka factors.

iPSCs also provide an alternative option of allogeneic treatment by creating haplotype biobank. HLA-typed biobank can help reduce both the rejection of grafted tissue, and the number of cell lines that are required to meet all populations in a given country (Zimmermann et al., 2012). Nakagawa et al. (2011) reported an integration-free iPSCs generation method that provides HLA-typed biobanking which match 20% of Japanese population.

In the case of biologics production from hiPSCs, the current paradigm is that cells are isolated from patients and reprogrammed into iPSCs using Yamanaka factors in conventional plate culture (Takahashi et al., 2007). As the Yamanaka factors contain the proto-oncogene, c-Myc, there are possibilities of increased genetic abnormalities from viral integration (Nakagawa et al., 2008, 2010). Currently, multiple methods of reprogramming of hiPSCs have been developed due to their unique limitations. Some methods that may be currently considered safer involve using mRNA, proteins, or cytokines although they have their own limitations as well, such as poor transduction efficiency (Kim et al., 2009; Warren et al., 2010). It is well established that these methods are less efficient than viral vectors for reprogramming. However, there are some efficient non-integrative viral vector approaches developed recently for reprogramming that we discuss later part of this study.

Depending on the final product and expected timelines, cell expansion is a very important consideration and area for considerable risk management analysis. After reprogramming, the cells are stored in the master cell bank or expanded for differentiation. Due to generally tighter time considerations in manufacture, application, and shelf-life, large-scale expansion is required in a sterile condition based on demand. This requires intensive consideration because it is a major rate-limiting step in the manufacturing of CBT products. The most important considerations for expansion on a large scale are: operational, economic, quality and safety (**Table 2**).

Before large-scale expansion, it is important to consider operational design (2D or 3D) with manual or automatic operation (Jenkins and Farid, 2015). In order to obtain a large number of cells, bioreactors tend to be far superior to plate culture in total cell production (**Table 1**). Important parameters for operational consideration are online monitoring and control of process parameters (pH, DO, pCO2, etc.), as well as considering the shortest possible cultivation time. Due to the nature of 2D culture, it is often difficult to implement monitoring and control methods and therefore rely on operator know-how and standardization of process methods (such as changing media daily). However, by utilizing 3D vessels it is

TABLE 2 | Considerations for large-scale expansion of hPSCs in bioreactor culture.

Characteristics	What to consider
Operational considerations	• Culture system (2D/3D) • Manual or automatic operation • Process control and monitoring (online/offline) • Culture environment (temperature, pH, DO, pCO_2 etc.) • Scalability (scale-up/scale-out) • Culture time • Culture vessel (single/multi-use) • Target final cell density (cells/mL) • Medium feeding regimen (once/twice in a day) • Prediction model
Economic considerations	• Medium • Resources (devices, labor, etc.) • Cell storage (cryopreservation) • Efficient cell lines • Indirect utilities
Considerations for quality and safety	• Quality control • cGMP compliant • Efficacy (*in vitro* and *in vivo*) • Harvest purity

possible to automate or semi-automate monitoring and process parameters via onboard sensors, with the potential for savings in reagents and removing sources of error. For determining medium feeding regimes, a prediction model for medium consumption (glucose and glutamine) and production of toxic materials (lactic acid and ammonium) can be very useful (Galvanauskas et al., 2019). More data and higher quality data can lead to more effective decisions and use of advanced analytical tools. A single-use vessel is also a major operational consideration that increases expansion cost for cell-based products on a large scale. Although single-use vessel reduces contamination risk by eliminating cleaning procedures and its validation, the cost is not rather dominating here as the priority for the product safety is high. Since cellular products are costly, economic considerations are important for medium, efficient cell lines and other indirect utilities. Above all, product quality and safety are the most important consideration that will provide safe and efficient final product for CBT application.

After expansion, cells are harvested by separating them from the culture substratum of plate or microcarrier using enzymatic treatment or by changing temperature or pH (Yang et al., 2010; Guillaume-Gentil et al., 2011; Dou et al., 2012). For harvesting, aggregate culture in bioreactors may not necessarily require a detachment step (Bartosh et al., 2010; Amit et al., 2011; Larijani et al., 2011; Zweigerdt et al., 2011; Nath et al., 2018), however, microcarrier culture in bioreactor requires detachment step. Purified cells are formulated and checked for quality assurance. Quality assurance is carried out in three different stages: microbial contamination, chemical contamination and quality or potency. Microbial contamination is checked with different methods for bacteria, fungus or virus (Rayment and Williams, 2010; Goldring et al., 2011). A 14-day incubation of cell products for bacterial and fungal contamination is the most commonly used sterility test (Khuu et al., 2006; Hocquet et al., 2014). Chemical testing includes checking molecules that accompany the culture medium or other factors used during isolation, expansion and storage. The LAL test for bacterial endotoxin is a common chemical test. An automated 15-min test to determine endotoxin in CBT products has now been developed in accordance with FDA regulations (Gee et al., 2008). Other chemical testing concerns examine residual proteins of different origins, serum and other harmful cell processing particles.

Quality is the main concern in CBT products, especially when cell growth is a requirement. A cell viability test is therefore performed to determine live or dead cells in the product using a variety of staining methods. It is also useful to determine the biological activity of CBT products (Choi et al., 2011; Schellenberg et al., 2013). Pre-release product potency is an important criterion to meet. For example, the final products for hPSCs are differentiated cells, wherein the potency should be checked through transplantation into disease models.

Strict quality control is imperative for products derived from hPSC before transplantation to patients, as there is a high risk of transferring oncogenes to patients. In Japan, a clinical trial was halted in 2015 when treating AMD with autologous retinal pigmented epithelial cells derived from hiPSC due to genetic abnormality (Garber, 2015). Since genetic abnormalities occur in products derived from hiPSCs from reprogramming to finally differentiated cells (Rohani et al., 2014), cells should be screened strictly for epigenetic signatures, karyotype, telomerase activity, and mitochondrial remodeling, and functional assays including teratoma formation and *in vitro* differentiation (Feng et al., 2010; Kim et al., 2010; Yehezkel et al., 2011; Rohani et al., 2018). Some of the other proposed quality tests include whole- genome sequencing, single- cell genome sequencing, epigenetic analysis, and DNA integrity testing to maximize patient safety.

Cells must be delivered to clinics immediately or stored for future use after the product quality assurance has been passed. If the cells are vitrified, cells are usually shipped to clinics on dry ice (−78°C) or in liquid nitrogen dry shippers (−160°C). The most commonly used cell storage technique is cryopreservation in liquid nitrogen at −196°C, which is adapted from the conventional stem cells banking (Thirumala et al., 2009; Hunt, 2011). For the better recovery of cryopreserved cells, slow-freezing and rapid thawing is generally highly applicable (Kurata et al., 1994; Moon et al., 2008). Recently Celikkan et al. (2019) developed a new media for transporting multipotent stromal cells using Ringer's lactate-based transport media supplemented with human serum albumin that supported more than 90% cell survival after 6 h of transportation. Developing more robust methods and media is also important for long distance cell delivery.

STANDARDIZATION OF BIOLOGICS MANUFACTURING IN BIOREACTORS

Manufacturing of pharmaceutical proteins or other biological products consists of several steps from raw materials to finished

products that may significantly compromise the quality of the product. They also reduce productivity and are prone to human errors. Different pharmaceutical companies have attempted integrated pharmaceutical production to overcome these disadvantages. One of the major attempts to fully integrate the cell processing system is being made by the Novartis-MIT Center for Continuous Production of Pharmaceutical Products (Bisson, 2008; Schaber et al., 2011). Genzyme^{TM} is also attempting to continuously produce pharmaceutical recombinant protein in bioreactors, wherein cell culture is being integrated into a single flow for product isolation and purification (Warikoo, 2011). In order to reduce cumbersome production steps and significantly reduce costs, process integrity is necessary. One such integrated system developed by Johnson and Johnson has recently been approved by the FDA for large-scale production of HIV drugs (FIERCE Pharma, 2016), which have been shown to reduce time and costs by one third compared to conventional batch processing.

The integration of production steps provides high product quality and safety and helps to overcome strict regulatory requirements by easing ability to obtain and retain cGMP compliance. In this context, the next sections will discuss how to integrate certain important basic steps in cell production, in particular genetic modification, cell reprogramming, expansion and differentiation in bioreactors to promote a single step approach for cell-based therapies utilizing T-cells, MSCs, and hPSCs (**Figure 2**).

Standardization of Genetic Modifications in Bioreactors

Genetic modification has been applied for production of antibodies, proteins or other biotechnological drugs production for many years in the pharmaceutical industry. It has also been widely used in recent years to treat multiple incurable genetic diseases. For example, in a neurological disorder called adrenoleukodystrophy (ALD), there is a malfunction of oligodendrocytes and microglia, and genetic modification can directly affect disease outcome. A corrected gene is inserted into the patient-derived hPSCs and transplanted into the patient's brain. The inserted hPSCs differentiate into microglia to promote myelin production in the patient's brain that affects ALD outcomes (Cartier et al., 2009).

Sometimes patients are exposed indirectly to genetic modification. For example, in thalassemia, patient blood cells are extracted from the body are modified and enriched

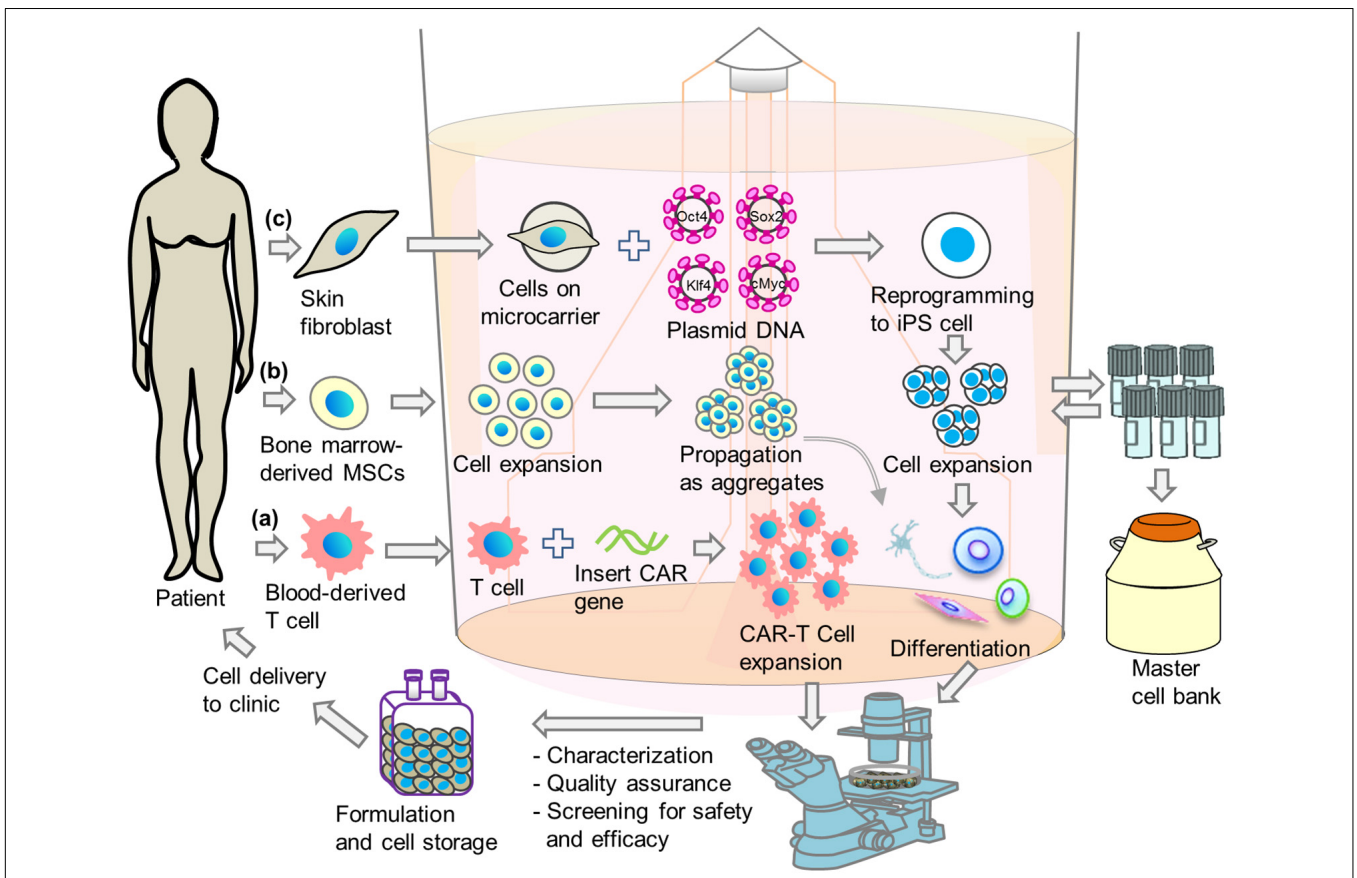

FIGURE 2 | Schematic illustrations of integrated single-step cell manufacturing strategies in bioreactor culture for cell therapy applications. Cells are isolated from patient's (a) blood or (b) bone-marrow, or (c) skin and genetically modified. After expansion, cells are stored in a master cell bank or differentiated directly in bioreactor. After performing characterization, quality assurance and screening for safety and efficacy, cells are delivered to hospital or stored in cell bank for future use.

ex vivo in order to target specific antigens in the body of patients (Naldini, 2011). Other indirect genetic changes include modification of CAR or T cell receptors (TCR) in T- cells (Wang and Riviere, 2015), expression of CD40 ligand in dendritic cells (Kikuchi et al., 2000), etc. Genetically modified CAR-T cells can target antigens specifically and efficiently kill cancer cells (Song, 2013). CARs and TCRs are the most commonly used receptors for the activation of T cells (Kerkar, 2013). Many cell-based CAR-T therapies are now being developed for the treatment of advanced- stage lymphoma (Kochenderfer and Rosenberg, 2013), B-cell lymphoma (Kochenderfer et al., 2010) and other autoimmune diseases (Jethwa et al., 2014).

To transduce cells with desired genes, viral vectors are usually used as genetic cargos. Genetic transduction is a two-step process: preparing viral vectors and transducing cells to express the desired property. For their superior transduction efficiency, lentiviral and gamma-retroviral vectors are widely used. However, these vectors still currently have some issues, such as the ability to integrate into the host genome running the risk of mutation (Sakuma et al., 2012), which raises safety concerns (Yamashita et al., 2016).

Non-integrative viruses, such as, Sendai virus have proven to be useful for transient transfections, including cellular reprogramming. There are other non-viral approaches. DNA vectors can carry large cargo with less immunotoxicity and are easy to scale up (Hsu and Uludag, 2012). However, their use is less efficient than viral transduction. Non-viral cationic reagents have also been reported to successfully transfect cells with high efficiency (Hsu et al., 2018). Effective transduction using mRNA was also reported for reprogramming terminally differentiated cell to hiPSCs (Warren et al., 2010; Rohani et al., 2016). hiPSCs have also been reprogrammed using recombinant protein (Kim et al., 2009).

As viral vectors and/or DNA integration possess high risk of cancer, some methods for removing these vectors have been developed. One method is the piggyBac, a transposon system that was used to remove tandem Yamanaka factors from iPSCs after reprogramming (Woltjen et al., 2009). After CAR was incorporated into T-cells, the removal of transgenes used another transposon system called Sleeping Beauty, which successfully removed genetic scars from the transduced cells (Huls et al., 2013; Singh et al., 2013). Similarly, Cre excision of reprogramming genes via loxP sites has also resulted in transgene-free iPSCs (Sommer et al., 2010). Viral vectors deficient in integration are also good candidates for the production of transgene-free CBT by mutating viral integrase (Yáñez-Muñoz et al., 2006).

Genome engineering technologies are other choices for the addition, deletion or correction of genes in the CBT industry (Lombardo et al., 2007). Zinc-finger nucleases (ZFNs), clustered regulatory interspaced short palindromic repeats (CRISPR)/Cas endonucleases, or transcription-activator nucleases (TALENs) (Provasi et al., 2012) are the most commonly used targeting nucleases. CRISPR/Cas system has recently received much attention due to its broad use in the genome engineering of patient cells (Mullard, 2015). ZFNs are also popular for treating graft-versus-host disease in T-cell therapy (Gaj et al., 2013). In cellular reprogramming, a nuclease dead variant of Cas9 with a transcriptional *trans*-activator was recently used by activating the transcription factors Oct4 and Sox2, which maintained pluripotency and expressed the markers for the three germ layers (Liu et al., 2018).

Genetic modification is considered one of the rate-limiting steps in cell manufacturing industry. Current conventional methods make it more complicated because they are multi-step processes. Genetic modification in planar culture is also expensive, time-consuming and labor-intensive (Hsu et al., 2018). The bioreactor is a better platform for the production of large-scale genetically modified cells for commercial purposes (**Figure 2**). In adherent culture, reprogramming factors are generally transfected in order to generate iPSCs, and cells are then expanded in 2D or 3D, which is a two-step process. By integrating the genetic modification step into the bioreactor, a single-step process can be established that allows the production of cells in an automated and closed bioreactor system (Hsu et al., 2018).

In CAR-T CBT application, genetic modification is also a challenging step. After isolating cells from the blood sample of patients, selection and activation are done followed by expansion (Wang and Rivièrea, 2016). Finally, it is necessary to transduce cells with CAR or any other antigens depending on target diseases (Pampusch et al., 2020). Conventional genetic transduction methods are based on a planar culture wherein each step is carried out in an open culture system posing difficulties in maintaining cGMP.

A few steps have recently been integrated into the bag culture system, wherein selection, activation and expansion can be carried out in a single step using DynaMag^{TM} CTS^{TM} (Hollyman et al., 2009), while the Xuri^{TM} cell expansion system developed by GE Healthcare can expand cells in large numbers (Jin et al., 2012; Somerville et al., 2012). Although washing and concentrating the final product is integrated into the COBE® 2991 system developed by Terumo BCT (Bajgain et al., 2014), the transduction step is not yet integrated into any of the above systems. The integration of the transduction step with the expansion and formulation will make CAR-T CBT straight forward and it is a good platform to carry out these steps in the bioreactor.

Miltenyi Biotech has developed a device called CliniMACS Prodigy^{TM} based on bag culture for CAR-T CBT. In an automated system (Terakura et al., 2012; Casati et al., 2013; Acker et al., 2016), this device integrated major steps in particular cell preparation, selection, activation, transduction, expansion, washing, and formulation. Such integration in the bioreactor will pave the way for the production of closed and automatic cell-based products. This device is also useful for cGMP-compliant production of dendritic cell for cell therapy applications (Erdmann et al., 2018). These systems are now beginning to prove their superiority in implementation of manufacturing protocols and cGMP compliance. Early data also suggests that adoption of such technologies even at an early stage may still be superior to conventional methods and offer returns on investments due to ability to adapt to multiple cell types

and different processes (Terakura et al., 2012; Casati et al., 2013; Acker et al., 2016).

Integration of Expansion and Differentiation in Bioreactors

Current manufacturing practices for cell-based products are multi-step: derivation, expansion, and differentiation. In this process, cells are isolated from any part of patient's body. In case of MSCs, bone marrow-derived stromal cells are mostly used for clinical application. However, only a very limited number of MSCs can be isolated from specific sources, e.g., MSCs represent only approximately 0.01% of the total fraction of mononuclear cells in the bone marrow (Apel et al., 2013; Orozco et al., 2013). The clinical applications of hMSCs require 1–5 million cells per kilogram of body weight of patient (Meirelles and Nardi, 2003; Connick et al., 2012). In addition, it is important that the derived MSCs can differentiate properly. Therefore, bioprocess development for both expansion and differentiation is equally important.

Several clinical trials using MSCs are taking place worldwide and are increasing day by day. More than 200 clinical trials using MSCs were conducted in 2015 and 2016, which require intensified standardization of production practices (Carlsson et al., 2015). Typically, MSCs are expanded in plate culture and transplanted as whole cells or differentiated into lineage-specific cells for clinical application. However, plate culture is disadvantageous when the clinical trial requires large number of cells (**Table 1**). Bioreactor expansion of MSCs is required and can provide a large number of cells to exploit the remarkable potential of MSCs in therapeutic applications. When grown as three-dimensional aggregates or spheroids, MSCs show increased angiogenic, anti-inflammatory and immunomodulatory effects and improved stemness and survival after transplantation (Bunpetch et al., 2019). The dynamic culture of MSCs also increases the survivability, proliferation and paracrine effects.

Different configurations of dynamic bioreactors have been developed for MSC expansion according to specific cell types. Among them stirred suspension bioreactors (SSB), rotating wall vessel bioreactors (RWV), and perfusion bioreactors were widely used for the expansion of MSCs (Chen et al., 2006; Rodrigues et al., 2011; Hanley et al., 2014; Lechanteur et al., 2014; Lawson et al., 2016; Egger et al., 2018). To reduce heterogeneous shear stress, NASA has developed a RWV bioreactor (Somerville et al., 2012) which has been shown to be superior to SSB for MSC expansion and differentiation (Chen et al., 2006). Since MSCs have the capacity for multi-lineage differentiation, integration of expansion and differentiation could help to streamline manufacturing processes. Several researchers have reported the integration of expansion and differentiation in the derivation of osteogenic and adipogenic lineages in bioreactors (Chen et al., 2004; Dominici et al., 2006; Duijvestein et al., 2010; Hoch et al., 2012). MSCs have also been expanded and differentiated on microcarriers (see below) in stirred suspension bioreactors for deriving osteogenic lineages (Field et al., 1994; Mazzini et al., 2003; Goh et al., 2013; Shekaran et al., 2016).

As generation of hPSCs from terminally differentiated patient cells is complicated by several steps, the final products are at high risk of contamination. Therefore, as with any pharmaceutical grade medical product, it is also mandatory to maintain cGMP for CBT products (Sensebe et al., 2011; Heathman et al., 2015; Wuchter et al., 2015), which adds many additional complications in the cell production process. It is therefore necessary to standardize the system that can combine all these steps from derivation to final products. Bioreactors are a platform that has shown capability in filling this role (**Figure 2**).

The bioreactor platform is widely used for the large-scale expansion of hPSC-based CBT production because it is easy to operate and different physicochemical parameters can be regulated in a closed-system. Two groups have shown the bioreactor derivation of PSCs (Fluri et al., 2012; Shafa et al., 2012). Shafa et al. (2012) reported a significantly higher efficiency in bioreactor reprogramming compared to the planar culture. Since mesenchymal-epithelial transition (MET) is an important early step in cellular reprogramming (Samavarchi-Tehrani et al., 2010), transformed fibroblasts moved into the bioreactor form aggregates that are efficiently expanded in the bioreactor. Since fibroblasts are substrate dependent, bioreactor culture can promote the formation of aggregates and therefore cellular reprogramming.

After the bioreactor derivation of hPSCs, expansion and differentiation are the next major steps. A large number of cells are generally required for effective CBT, and can range anywhere from 10^8 to 10^{10} cells per 70 kg patient (Serra et al., 2012). Obtaining such numbers of cells in plate culture is cumbersome because of growth surface limitation. The surface coating with extracellular matrix (ECM) poses a high risk in the production of clinical products because it is usually derived from animal sources. Recently, a discovery of recombinant ECM (laminin E8 fragment) has been developed that can be used efficiently in clinical applications (Miyazaki et al., 2012).

Automated planar culture systems have been established for the production of clinical-grade hPSCs. CompacT Selec^{TM} developed by TAP Biosystems is one of the notable automated systems for cell production. This system is based on T-flask design, which can accommodate ninety T175 flasks for cell expansion on a large scale. This robotic system can automatically perform all cell culture steps, cell counting, seeding, medium change, passage, plating and transient transfection. Such systems are not used for differentiation, however, because differentiation is a complicated process that needs several components to be added to the culture medium. This mainly disintegrates the process of expansion and differentiation in planar culture.

Except for microcarrier culture, cell expansion in bioreactors does not need surface coating. The bioreactor also provides sufficient availability of growth surface. In general, a single bioreactor (100 ml working volume) is sufficient to provide autologous CBT with a clinically relevant number of cells. For the expansion of hPSCs, several types of bioreactors are used (Wang et al., 2014) (**Table 2**).

Microcarriers must be coated with ECM for cell attachment in the bioreactor (Olmer et al., 2012; Lam et al., 2014; Fan et al., 2015; Badenes et al., 2016; Kropp et al., 2017) for

anchorage-dependent expansion of hPSCs. Cells are harvested by removing them from the microcarrier using enzymatic treatment after large-scale expansion. Bioreactor expansion of hPSCs on microcarriers is problematic for clinical use, as separating the microcarrier from the final cell harvest requires an additional step. On the other hand, aggregate cultivation in bioreactors may not necessarily require a detachment step for harvesting (Bartosh et al., 2010; Amit et al., 2011; Larijani et al., 2011; Dou et al., 2012; Nath et al., 2018), and clinically relevant cell numbers has been produced as aggregate in a single bioreactor (Haraguchi et al., 2015; Rungarunlert et al., 2016; Nath et al., 2017, 2018) (**Table 3**).

Size limitation is a major disadvantage in aggregate culture. As the aggregate size increases, the growth potential of the large aggregate decreases due to the limited diffusion of oxygen and nutrients (Nath et al., 2017). Maintenance of aggregate size is therefore an important point in order to maintain a high growth rate and high quality for CBT applications (Dou et al., 2012).

Bioreactor culture is a unique choice for CBT production because differentiation and expansion can be done in the same vessel. Bioreactors have been used to differentiate hPSCs into different cell types, especially for cardiac (Matsuura et al., 2012; Kempf et al., 2015; Rungarunlert et al., 2016), hepatic (Vosough et al., 2013; Park et al., 2014), and neural (Yan et al., 2016) lineages. In order to provide direct methods for clinical applications, it is important to integrate expansion and differentiation, and several reports have recently been published wherein expansion and differentiation have been integrated (Lam et al., 2014; Ting et al., 2014; Fonoudi et al., 2015; Haraguchi et al., 2015). The integration of derivation with expansion and differentiation, however, still faces complications and very few reports are available (Steiner et al., 2010).

Steiner et al. (2010) have reported integrating the derivation, propagation and differentiation of hESCs in the suspension culture where hESCs were isolated from the inner cell mass, and did not involve feeder cells or microcarriers. However, the integration of derivation, expansion and differentiation for personalized medicine, in particular for autologous or allogeneic CBT applications, has still not been achieved. This integration is necessary to overcome multi-step cell processing, which reduces

TABLE 3 | Summary of hPSCs expansion in stirred suspension bioreactor.

Cell types	Seeding density, (cells/mL, 10^5)	Final density, (cells/mL, 10^5)	Culture time (day)	Medium volume, (mL)	Bioreactor types	References
hESC	3.3	7.9	4	100	Bioreactor (DASGIP/Eppendorf)	Kempf et al., 2015
hESC	0.7	7	5	200	Gas permeable single use bag (Nipro)	Otsuji et al., 2014
hiPSC	3	10	6	100	Spinner flask (Cellspin, Integra Biosciences)	Haraguchi et al., 2015
hiPSC	4	16	5	50	Spinner flasks (Cellspin, Integra Bio-sciences)	Wang et al., 2013
hESC	2.5	20	6	60	Spinner flasks (50119114, Thermo Scientific)	Chen et al., 2011
hiPSC	4	15	7	100	Bioreactor (DASGIP/Eppendorf)	Olmer et al., 2012
hiPSC	3	12	7	100	Bioreactor (Cellspin, Integra Biosciences)	Abbasalizadeh et al., 2012
hESC	10	20	7	100	Spinner flask (IBS Integra Biosciences)	Zweigerdt et al., 2011
hESC	1	18	6	50	Spinner flasks (Integra Biosciences)	Amit et al., 2011
hESC	10	20	7	50	Spinner flask (Cellspin, IBS Integra Biosciences)	Singh et al., 2010
hESC	0.2	5	6	100	Bioreactor (NDS Technologies)	Krawetz et al., 2010
hESC	6	360	28	55	Slow-turning lateral vessel (Synthecon)	Gerecht-Nir et al., 2004
hiPSC	5	36	7	125	DASbox mini bioreactor system (Eppendorf AG, Hamburg, Germany)	Kropp et al., 2016
hiPSC	2	12	7	100	Spinner flask (Corning)	Kwok et al., 2018
hESC	6	35	5	100	Spinner flask, Bellco	Oh et al., 2009
hESC	2.5	3	10	125	Spinner flask (Croning)	Silva et al., 2015
hiPSC	5	5	5	100	Bioreactor (NDS Technologies)	Meng et al., 2017
hiPSC	1	45	8	100	Bioreactor (Able)	Nath et al., 2018

the risk of contamination, saves cell processing time and reduces costs for the CBT manufacturing.

REGULATORY CONSTRAINTS IN CBT MANUFACTURING

With the advancement of cell processing facilities, several clinical trials have taken place in recent years using hPSCs (Lebkowski, 2011; Menasché et al., 2015; Schwartz et al., 2015; Trounson and McDonald, 2015; Mandai et al., 2017) which is triggering much attention from regulatory bodies on cGMP implementation in CBT manufacturing (Giancola et al., 2012). Since cell culture media contains various xenogens including source-derived virus and biochemicals (Martin et al., 2005; Cobo et al., 2008), CBT products need to be cultured in the xeno-free condition so that they are free from xeno-mediated infection or immune rejection according to regulatory agencies (Cimino et al., 2017). Currently both hESC and hiPSC lines have been derived following cGMP and deposited into national cell bank from various nations including China, Japan, United States, and United Kingdom, and their efficacy and safety has been tested using standard protocol (Hawkes, 2011; Ilic et al., 2012; Baghbaderani et al., 2015; Wang et al., 2015; Azuma and Yamanaka, 2016; Catapult, 2017). However, their differentiation capability into diverse cell lineages is yet to be tested although a few cell lines have already been tested in cGMP facilities (Kajiwara et al., 2012; Löhle et al., 2012; Heslop et al., 2017; Rao et al., 2018; Blackford et al., 2019; Shafa et al., 2019). Therefore, facilitating cGMP-compliant manufacturing and establishing standard operating procedures (SOP) according to regulatory agencies is a prime concern for CBT products.

cGMP is a regulatory framework overseen at the governmental level meant to establish basic minimum standards in safety, efficacy, and standardization of many types of products. All CBTs must meet regulatory requirements to be approved for sale and marketing. This is the end goal of clinical trials, to make a therapy available for wide scale implementation, and entry into worldwide markets. One of the first considerations is to begin engaging with the national regulatory board as soon as there even a thought about potential commercialization.

Approval from two of the most stringent regulatory organizations: USFDA, and the European Medicines Agency (EMA) that allows for easy entry into virtually every other market in the world (Rehakova et al., 2020). The intended application of human cells, tissues, and cellular and tissue-based products (HCT/P) are regulated by FDA's Center for Biologics Evaluation and Research (CBER). However, FDA is intrinsically concerned about stem cell-related therapeutic products implementation, transplantation and infusion into patient since the cells may change their cellular properties after being expanded outside of body (Reisman and Adams, 2014). The EMA is generally considered the most stringent and well defined regulatory board for CBTs, and usually, if these standards are met, it will lead to the least problems in transferring to other markets, barring other legal issues such as patents and intellectual property rights.

Without engagement with regulatory boards, the CBT products have less chance of avoiding common pitfalls that have led to efficacious products not making it to market, even with good supporting data. This is important because, as mentioned, regulatory standards can differ across national lines. As the field is relatively new and advancing at a fast pace, regulators have been left to working with companies on a case-by-case basis to establish guidelines, and best practices that are in line with the stringency of cGMP standards in other areas (Bedford et al., 2018). This has led to the publishing of various guidance documents rather than overly strict ordinances, which acknowledge the inherent variability in these products, both between types (protein, whole cell, gene, etc.), and even between lots of the same product (European Medicines Agency, 2020; U.S. Food and Drug Administration, 2020).

It is well understood that CBTs inherently carry a higher level of heterogeneity, and difficult to control factors than chemical reactions that can produce extremely homogenous batches of classic pharmaceuticals. As part of this, regulators such as, Health Canada are often eager to work with potential CBT companies and academic institutions to develop guidelines based on the best current science available, and the unique product under review, while also helping to navigate the difficult regulatory terrain to higher phase studies and commercialization.

The second most important consideration is to hire or assign a team member to focus mainly on the navigation of regulation immediately. It is advisable that this be their main task, as the beginning stages are the most important. In CBTs, it is said that "the process is the product" and if the project is taken too far without this consideration it can be virtually impossible or at least economically unlikely to be able to recover after having to go back to earlier stages because details were overlooked. The unavoidable nature of GMP in CBTs is that even sometimes a seemingly simple laboratory procedure must become a multi-page SOP document covering literally every detail of the procedure. These documents then become the trail of documentation, and the very process itself, which is to be adhered to in manufacturing and available for regulatory review.

It is very important to attempt to begin to think about cGMP-like standards as soon as even the idea of a potential commercialization begins to materialize. Often this can be as early as pre-clinical, depending on the data, though perhaps more reasonably around phase 1 trials. For example, Health Canada requires increasing GMP compliance, and increasingly stringent manufacturing controls as trials advance although a manufacturing establishment license is not required while the product is still under any phase of clinical trials (Government of Canada, 2015). The FDA also requires GMP compliance in Investigational New Drug (IND) assessments at phase 1, and stringency increases in manufacturing establishment licensing from phase 2 onwards (US FDA, 2008). Finally, the EMA requires manufacturing authorization and compliance with established GMP regulations for all stages of clinical trial development, with "inspections performed by a competent authority/qualified person (QP) of a member state" (Bedford et al., 2018).

As one can see, in the United States and Canada an early phase can be "boutique" in having each treatment individually created under standard laboratory proper conditions and very carefully controlled, whereas this is not necessarily the case in

Europe. Therefore, with increasing enrolment as trials continue a GMP-like approach should be adopted in every economically and physically feasible manner throughout the process as required. This includes making changes such as using "clinical grade" versus "laboratory grade" reagents, designing a robust manufacturing pipeline, considering quality and assurance guidelines, and creating in-depth documentation to regulatory standards to name merely a few requirements. It should be considered that any change in reagent, manufacturer of said reagents, processes, etc. carries a large weight as there is absolutely a chance of a change in associated outcomes and requirements.

One of the reasons bioreactors and automated processes are extremely useful in meeting GMP standards in CBTs is that, informally, some key aspects can be summarized as: the less manipulations in the process, and the fewer hands that touch to product, the better. Let us recall the phrase "the process is the product," this is essential to remember for CBTs. If the process is not correctly implemented in a GMP-like fashion, it does not matter if the product works as intended. It will be required to go back the drawing board to make the bio-process compliant. This increases the time and cost even further.

It may be the case that for the near-future CBTs will only be successful in smaller-scale manufacturing, and smaller lots due to the challenges with characterization and standardization associated with whole cell populations. This may require smaller, more flexible operations spread across nations rather than mega-manufacturing centers as is currently the case with standard pharmaceuticals. It is prudent to consider de-centralized models of production in order to achieve profitability and market penetration.

CBTs often require more flexibility in production as there are finer windows of effectiveness and therapeutic application, as well as, inherently less ability to control and properly assess safety and efficacy in increasing scale. This may lead to needing to find ways to adapt similar processes across multiple pipelines in order to flexibly meet supply and demand based on various ailments and treatments. The upside of this is that integrated automated processes and bioreactor technologies tend to be far easier to scale up and down as required. Further advances in computing technology, basic biomarker discovery, cell characterization, and onboard or automated monitoring equipment will be essential in decreasing costs and increasing capacity, allowing for CBTs to become more and more ubiquitous in improving human health.

CONCLUDING REMARKS AND FUTURE DIRECTIONS

Application of CBT increases day by day and several clinical studies are continuing to treat incurable diseases. Manufacturing facilities should be compatible with the growing need for cell-based products to meet market demand by providing safe and effective cell-based products. Since current production systems have several disadvantages particularly multi-stage processing, which poses a high risk of contamination, long processing times, and increased production costs, a more straightforward cGMP-compliant system is needed. Bioreactor-based cell production systems can provide cell-based products with single step, easing the practice of cGMP for CBT production. The integration of various steps in bioreactors: derivation, genetic modification, expansion, and differentiation, will pave the way for the future of CBT manufacturing. The integrated production of cell biologics in bioreactor will significantly reduce the risk of contamination, and cell-processing time providing a cost-effective platform for CBTs.

AUTHOR CONTRIBUTIONS

SN and DR perceived the concept and design. SN and LH wrote the manuscript. DR revised and approved the manuscript. All authors contributed to the article and approved the submitted version.

FUNDING

SN is partially supported by a Cumming School of Medicine Postdoctoral Fellowship.

REFERENCES

Abbasalizadeh, S., Larijani, M. R., Samadian, A., and Baharvand, H. (2012). Bioprocess development for mass production of size-controlled human pluripotent stem cell aggregates in stirred suspension bioreactor. *Tissue Eng. Part C Methods* 18, 831–851. doi: 10.1089/ten.tec.2012.0161

Acker, J. P., Marks, D. C., and Sheffield, W. P. (2016). Quality assessment of established and emerging blood components for transfusion. *J. Blood Transfus.* 2016:4860284. doi: 10.1155/2016/4860284

Amit, M., Laevsky, I., Miropolsky, Y., Shariki, K., Peri, M., and Itskovitz-Eldor, J. (2011). Dynamic suspension culture for scalable expansion of undifferentiated human pluripotent stem cells. *Nat. Protoc.* 6, 572–579. doi: 10.1038/nprot.2011.325

Apel, M., Brüning, M., Granzin, M., Essl, M., Stuth, J., Blaschke, J., et al. (2013). Integrated clinical scale manufacturing system for cellular products derived by magnetic cell separation, centrifugation and cell culture. *Chem. Ing. Tech.* 85, 103–110. doi: 10.1002/cite.201200175

Attwood, S. W., and Edel, M. J. (2019). iPS-Cell technology and the problem of genetic instability-can It ever be safe for clinical use? *J. Clin. Med.* 8:288. doi: 10.3390/jcm8030288

Azuma, K., and Yamanaka, S. (2016). Recent policies that support clinical application of induced pluripotent stem cell-based regenerative therapies. *Regen. Ther.* 4, 36–47. doi: 10.1016/j.reth.2016.01.009

Badenes, S. M., Fernandes, T. G., Rodrigues, C. A. V., Diogo, M. M., and Cabral, J. M. S. (2016). Microcarrier-based platforms for in vitro expansion and differentiation of human pluripotent stem cells in bioreactor culture systems. *J. Biotechnol.* 234, 71–82. doi: 10.1016/j.jbiotec.2016.07.02

Baghbaderani, B. A., Tian, X., Neo, B. H., Burkall, A., Dimezzo, T., Sierra, G., et al. (2015). cGMP-Manufactured human induced pluripotent stem cells are available for pre-clinical and clinical applications. *Stem Cell Rep.* 5, 647–659. doi: 10.1016/j.stemcr.2015.08.015

Bajgain, P., Mucharla, R., Wilson, J., Welch, D., Anurathapan, U., Liang, B., et al. (2014). Optimizing the production of suspension cells using the G-Rex 'M' series. *Mol. Ther. Methods Clin. Dev.* 1:14015. doi: 10.1038/mtm.2014.15

Bartosh, T. J., Ylöstalo, J. H., Mohammadipoor, A., Bazhanov, N., Coble, K., Claypool, K., et al. (2010). Aggregation of human mesenchymal stromal cells (MSCs) into 3D spheroids enhances their antiinflammatory properties. *Proc. Natl. Acad. Sci. U.S.A.* 107, 13724–13729. doi: 10.1073/pnas.1008117107

Baum, C. (2007). Insertional mutagenesis in gene therapy and stem cell biology. *Curr. Opin. Hematol.* 14, 337–342. doi: 10.1097/MOH.0b013e3281900f01

Bedford, P., Jy, J., Collins, L., and Keizer, S. (2018). Considering Cell Therapy Product "Good Manufacturing Practice" Status. *Front. Med.* 5:118. doi: 10.3389/fmed.2018.00118

Bellone, G., Turletti, A., Artusio, E., Mareschi, K., Carbone, A., Tibaudi, D., et al. (1999). Tumor-associated transforming growth factor-beta and interleukin-10 contribute to a systemic Th2 immune phenotype in pancreatic carcinoma patients. *Am. J. Pathol.* 155, 537–547. doi: 10.1016/S0002-9440(10)65149-8

Bennett, C. (2018). Available online at: https://www.genengnews.com/insights/cell-therapy-manufacturing-the-supply-chain-challenge/ (accessed April, 2020).

Bisson, W. (2008). "Continuous manufacturing – the ultra-lean way of manufacturing," in *Proceedings of the ISPE Innovations in Process Technology for Manufacture of APIs and BPCs*, Copenhagen.

Blackford, S., Ng, S. S., Segal, J. M., King, A., Austin, A. L., Kent, D., et al. (2019). Validation of current good manufacturing practice compliant human pluripotent stem cell-derived hepatocytes for cell-based therapy. *Stem Cells Transl. Med.* 8, 124–137. doi: 10.1002/sctm.18-0084

Bunpetch, V., Zhang, Z.-Y., Zhang, X., Han, S., Zongyou, P., Wu, H., et al. (2019). Strategies for MSC expansion and MSC-based microtissue for bone regeneration. *Biomaterials* 196, 67–79. doi: 10.1016/j.biomaterials.2017.11.023

Carlsson, P. O., Schwarcz, E., Korsgren, O., and Le Blanc, K. (2015). Preserved β-cell function in type 1 diabetes by mesenchymal stromal cells. *Diabetes* 64, 587–592. doi: 10.2337/db14-0656

Cartier, N., Hacein-Bey-Abina, S., Bartholomae, C. C., Veres, G., Schmidt, M., Kutschera, I., et al. (2009). Hematopoietic stem cell gene therapy with a lentiviral vector in Xlinked adrenoleukodystrophy. *Science* 326, 818–823. doi: 10.1126/science.1171242

Casati, A., Varghaei-Nahvi, A., Feldman, S. A., Assenmacher, M., Rosenberg, S. A., Dudley, M. E., et al. (2013). Clinical-scale selection and viral transduction of human naive and central memory CD8+ T cells for adoptive cell therapy of cancer patients. *Cancer Immunol. Immunother.* 62, 1563–1573. doi: 10.1007/s00262-013-1459-x

Catapult, C. G. T. (2017). *Early Seed Lot and Clinical Grade iPS Cell Line from the Cell and Gene Therapy Catapult*. Available at https://ct.catapult.org.uk/clinical-grade-iPS-cell-line (accessed April 5, 2018).

Celikkan, F. T., Mungan, C., Sucu, M., Ulus, A. T., Cinar, O., Ili, E. G., et al. (2019). Optimizing the transport and storage conditions of current Good Manufacturing Practice -grade human umbilical cord mesenchymal stromal cells for transplantation (HUC-HEART Trial). *Cytotherapy* 21, 64–75. doi: 10.1016/j.jcyt.2018.10.010

Chang, Y. H., Wu, K. C., Harn, H. J., Lin, S. Z., and Ding, D. C. (2018). Exosomes and stem cells in degenerative disease diagnosis and therapy. *Cell Transplant.* 27, 349–363. doi: 10.1177/0963689717723636

Chen, G., Gulbranson, D. R., Hou, Z., Bolin, J. M., Ruotti, V., Probasco, M. D., et al. (2011). Chemically defined conditions for human iPSC derivation and culture. *Nat. Methods* 8, 424–429. doi: 10.1038/nmeth.1593

Chen, S. L., Fang, W. W., Ye, F., Liu, Y. H., Qian, J., and Shan, S. J. (2004). Effect on left ventricular function of intracoronary transplantation of autologous bone marrow mesenchymal stem cell in patients with acute myocardial infarction. *Am. J. Cardiol.* 94, 92–95. doi: 10.1016/j.amjcard.2004.03.034

Chen, T. S., Lai, R. C., Lee, M. M., Choo, A. B., Lee, C. N., and Lim, S. K. (2010). Mesenchymal stem cell secretes microparticles enriched in pre-microRNAs. *Nucleic Acids Res.* 38, 215–224. doi: 10.1093/nar/gkp857

Chen, X., Xu, H., Wan, C., McCaigue, M., and Li, G. (2006). Bioreactor expansion of human adult bone marrow-derived mesenchymal stem cells. *Stem Cells* 24, 2052–2059. doi: 10.1634/stemcells.2005-0591

Choi, W. H., Choi, B. H., Min, B. H., and Park, S. R. (2011). Low-intensity ultrasound increased colony forming unit-fibroblasts of mesenchymal stem cells during primary culture. *Tissue Eng. Part C Methods* 17, 517–526. doi: 10.1089/ten.TEC.2010.0231

Cimino, M., Gonçalves, R. M., Barrias, C. C., and Martins, M. C. L. (2017). Xeno-free strategies for safe human mesenchymal stem/stromal cell expansion: supplements and coatings. *Stem Cells Int.* 2017:6597815. doi: 10.1155/2017/6597815

ClinicalTrials.gov (2020). Available online at: https://clinicaltrials.gov (accessed October 8, 2020).

Cobo, F., Navarro, J. M., Herrera, M. I., Vivo, A., Porcel, D., Hernández, C., et al. (2008). Electron microscopy reveals the presence of viruses in mouse embryonic fibroblasts but neither in human embryonic fibroblasts nor in human mesenchymal cells used for hESC maintenance: toward an implementation of microbiological quality assurance program in stem cell banks. *Cloning Stem Cells* 10, 65–74. doi: 10.1089/clo.2007.0020

Connick, P., Kolappan, M., Crawley, C., Webber, D. J., Patani, R., Michell, A. W., et al. (2012). Autologous mesenchymal stem cells for the treatment of secondary progressive multiple sclerosis: an open-label phase 2a proof-of-concept study. *Lancet Neurol.* 11, 150–156. doi: 10.1016/S1474-4422(11)70305-2

Cyranoski, D. (2018). 'Reprogrammed' stem cells implanted into patient with Parkinson's disease. *Nature* 563, 1–2. doi: 10.1038/d41586-018-07407-9

Davie, N. L., Brindley, D. A., Culme-Seymour, E. J., and Mason, C. (2012). Streaming cell therapy manufacture. *Bioprocess Int.* 10, 24–29.

Dominici, M., Le Blanc, K., Mueller, I., Slaper-Cortenbach, I., Marini, F. C., Krause, D. S., et al. (2006). Minimal criteria for defining multipotent mesenchymal stromal cells. The International Society for Cellular Therapy position statement. *Cytotherapy* 8, 315–317. doi: 10.1080/14653240600855905

Dou, X. Q., Yang, X. M., Li, P., Zhang, Z. G., Schönherr, H., Zhanga, D., et al. (2012). Novel pH responsive hydrogels for controlled cell adhesion and triggered surface detachment. *Soft Matter* 8, 9539–9544. doi: 10.1039/C2SM26442K

Dudley, M. E., Wunderlich, J. R., Shelton, T. E., Even, J., and Rosenberg, S. A. (2003). Generation of tumor-infiltrating lymphocyte cultures for use in adoptive transfer therapy for melanoma patients. *J. Immunother.* 26, 332–342. doi: 10.1097/00002371-200307000-00005

Duijvestein, M., Vos, A. C., Roelofs, H., Wildenberg, M. E., Wendrich, B. B., Verspaget, H. W., et al. (2010). Autologous bone marrow-derived mesenchymal stromal cell treatment for refractory luminal Crohn's disease: results of a phase I study. *Gut* 59, 1662–1669. doi: 10.1136/gut.2010.215152

Egger, D., Tripisciano, C., Weber, V., Dominici, M., and Kasper, C. (2018). Dynamic cultivation of mesenchymal stem cell aggregates. *Bioengineering* 5:48. doi: 10.3390/bioengineering5020048

Erdmann, M., Uslu, U., Wiesinger, M., Brüning, M., Altmann, T., Strasser, E., et al. (2018). Automated closed-system manufacturing of human monocyte-derived dendritic cells for cancer immunotherapy. *J. Immunol. Methods* 463, 89–96. doi: 10.1016/j.jim.2018.09.012

European Medicines Agency (2020). *Multidisciplinary: Cell Therapy and Tissue Engineering*. Available online at: http://www.ema.europa.eu/ema/index.jsp?curl=pages/regulation/general/general_content_000405.jsp&mid=WC0b01ac058002958a (accessed April 5, 2020).

Fan, Y., Wu, J., Ashok, P., Hsiung, M., and Tzanakakis, E. S. (2015). Production of human pluripotent stem cell therapeutics under defined xeno-free conditions: progress and challenges. *Stem Cell Rev.* 11, 96–109. doi: 10.1007/s12015-014-9544-x

Feng, Q., Lu, S. J., Klimanskaya, I., Klimanskaya, I., Gomes, I., Kim, D., et al. (2010). Hemangioblastic derivatives from human induced pluripotent stem cells exhibit limited expansion and early senescence. *Stem Cells* 28, 704–712. doi: 10.1002/stem.321

Field, R. E., Buchanan, J. A., Copplemans, M. G., and Aichroth, P. M. (1994). Bone-marrow transplantation in Hurler's syndrome. Effect on skeletal development. *J. Bone Joint Surg. Br.* 76, 975–981.

FIERCE Pharma (2016). *FDA Urges Companies to Get on Board with Continuous Manufacturing*. Available online at: http://www.fiercepharma.com/manufacturing/fda-urges-companies-to-get-on-board-continuous-manufacturing (accessed April 14, 2016).

Fluri, D. A., Tonge, P. D., Song, H., Baptista, R. P., Shakiba, N., Shukla, S., et al. (2012). Derivation, expansion and differentiation of induced pluripotent stem cells in continuous suspension cultures. *Nat. Methods* 9, 509–516. doi: 10.1038/nmeth.1939

Fonoudi, H., Ansari, H., Abbasalizadeh, S., Larijani, M. R., Kiani, S., Hashemizadeh, S., et al. (2015). A universal and robust integrated platform for the scalable production of human cardiomyocytes from pluripotent stem cells. *Stem Cells Transl. Med.* 4, 1482–1494. doi: 10.5966/sctm.2014-0275

Gaj, T., Gersbach, C. A., and Barbas, C. F. (2013). ZFN, TALEN, and CRISPR/Cas-based methods for genome engineering. *Trends Biotechnol.* 31, 397–405. doi: 10.1016/j.tibtech.2013.04.004

Gajewski, T. F., Schreiber, H., and Fu, Y. X. (2013). Innate and adaptive immune cells in the tumor microenvironment. *Nat. Immunol.* 14, 1014–1022. doi: 10.1038/ni.2703

Galat, V., Galat, Y., Perepitchka, M., Jennings, L. J., Iannaccone, P. M., and Hendrix, M. J. (2016). Transgene reactivation in induced pluripotent stem cell derivatives and reversion to pluripotency of induced pluripotent stem cell-derived mesenchymal stem cells. *Stem Cells Dev.* 25, 1060–1072. doi: 10.1089/scd.2015.0366

Galvanauskas, V., Simutis, R., Nath, S. C., and Kino-Oka, M. (2019). Kinetic modeling of human induced pluripotent stem cell expansion in suspension culture. *Regen. Ther.* 12, 88–93. doi: 10.1016/j.reth.2019.04.007

Garber, K. (2015). RIKEN suspends first clinical trial involving induced pluripotent stem cells. *Nat. Biotechnol.* 33, 890–891. doi: 10.1038/nbt0915-890

Gee, A. P., Sumstad, D., Stanson, J., Watson, P., Proctor, J., Kadidlo, D., et al. (2008). A multicenter comparison study between the Endosafe PTS rapid-release testing system and traditional methods for detecting endotoxin in cell-therapy products. *Cytotherapy* 10, 427–435. doi: 10.1080/14653240802075476

Gerecht-Nir, S., Cohen, S., and Itskovitz-Eldor, J. (2004). Bioreactor cultivation enhances the efficiency of human embryoid body (hEB) formation and differentiation. *Biotechnol. Bioeng.* 86, 493–502. doi: 10.1002/bit.20045

Giancola, R., Bonfini, T., and Iacone, A. (2012). Cell therapy: cGMP facilities and manufacturing. *Muscles Ligaments Tendons J.* 2, 243–247.

Goh, T. K., Zhang, Z. Y., Chen, A. K., Reuveny, S., Choolani, M., Chan, J. K., et al. (2013). Microcarrier culture for efficient expansion and osteogenic differentiation of human fetal mesenchymal stem cells. *Biores. Open Access* 2, 84–97. doi: 10.1089/biores.2013.0001

Goldring, C. E., Duffy, P. A., Benvenisty, N., Andrews, P. W., Ben-David, U., Eakins, R., et al. (2011). Assessing the safety of stem cell therapeutics. *Cell Stem Cell* 8, 618–628. doi: 10.1016/j.stem.2011.05.012

Gore, A., Li, Z., Fung, H. L., Young, J. E., Agarwal, S., Antosiewicz-Bourget, J., et al. (2011). Somatic coding mutations in human induced pluripotent stem cells. *Nature* 471, 63–67.

Government of Canada (2015). *Health Canada Guidance Document: Preparation of Clinical Trial Applications for use of Cell Therapy Products in Humans*. Available online at: https://www.canada.ca/en/health-canada/services/drugs-health-products/drug-products/applications-submissions/guidance-documents/clinical-trials/guidance-document-preparation-clinical-trial-applications-use-cell-therapy-products-humans.html (accessed April 6, 2020).

Guhr, A., Kobold, S., Seltmann, S., Seiler Wulczyn, A. E. M., Kurtz, A., and Löser, P. (2018). Recent trends in research with human pluripotent stem cells: impact of research and use of cell lines in experimental research and clinical trials. *Stem Cell Rep.* 11, 485–496. doi: 10.1016/j.stemcr.2018.06.012

Guillaume-Gentil, O., Semenov, O. V., Zisch, A. H., Zimmermann, R., Voros, J., and Ehrbar, M. (2011). pH-controlled recovery of placenta-derived mesenchymal stem cell sheets. *Biomaterials* 3, 4376–4384. doi: 10.1016/j.biomaterials.2011.02.058

Hanley, P. J., Mei, Z., Durett, A. G., Cabreira-Harrison, M., Klis, M., and Li, W. (2014). Efficient manufacturing of therapeutic mesenchymal stromal cells with the use of the Quantum Cell Expansion System. *Cytotherapy* 16, 1048–1058. doi: 10.1016/j.jcyt.2014.01.417

Haraguchi, Y., Matsuura, K., Shimizu, T., Yamato, M., and Okano, T. (2015). Simple suspension culture system of human iPS cells maintaining their pluripotency for cardiac cell sheet engineering. *J. Tissue Eng. Regen. Med.* 9, 1363–1375. doi: 10.1002/term.1761

Hawkes, N. (2011). Clinical grade stem cells are created by scientists in London. *BMJ* 343:d8001. doi: 10.1136/bmj.d8001

Heathman, T. R. J., Nienow, A. W., McCall, M. J., Coopman, K., Kara, B., and Hewitt, C. J. (2015). The translation of cell-based therapies: clinical landscape and manufacturing challenges. *Regen. Med.* 10, 49–64. doi: 10.2217/rme.14.73

Heslop, J. A., Kia, R., Pridgeon, C. S., Sison-Young, R. L., Liloglou, T., Elmasry, M., et al. (2017). Donor-Dependent and Other Nondefined Factors have Greater Influence on the Hepatic Phenotype than the Starting Cell Type in Induced Pluripotent Stem Cell Derived Hepatocyte-Like Cells. *Stem Cells Transl. Med.* 6, 1321–1331. doi: 10.1002/sctm.16-0029

Hoch, A. I., Binder, B. Y., Genetos, D. C., and Leach, J. K. (2012). Differentiation-dependent secretion of proangiogenic factors by mesenchymal stem cells. *PLoS One* 7:e35579. doi: 10.1371/journal.pone.0035579

Hocquet, D., Sauget, M., Roussel, S., Malugani, C., Pouthier, F., Morel, P., et al. (2014). Validation of an automated blood culture system for sterility testing of cell therapy products. *Cytotherapy* 16, 692–698. doi: 10.1016/j.jcyt.2013.09.005

Hollyman, D., Stefanski, J., Przybylowski, M., Bartido, S., Borquez-Ojeda, O., Taylor, C., et al. (2009). Manufacturing validation of biologically functional T cells targeted to CD19 antigen for autologous adoptive cell therapy. *J. Immunother.* 32, 169–180. doi: 10.1097/CJI.0b013e318194a6e8

Hsu, C. Y. M., and Uludag, H. (2012). Nucleic-acid based gene therapeutics: delivery challenges and modular design of non-viral gene carriers and expression cassettes to overcome intracellular barriers for sustained targeted expression. *J. Drug Target* 20, 301–328. doi: 10.3109/1061186X.2012.655247

Hsu, C. Y. M., Walsh, T., Borys, B., Kallos, M., and Rancourt, D. E. (2018). An integrated approach towards the bio-manufacturing of engineered cell therapy products in a continuous stirred suspension bioreactor. *Mol. Ther. Methods Clin. Dev.* 9, 376–389. doi: 10.1016/j.omtm.2018.04.007

Huls, M. H., Figliola, M. J., Dawson, M. J., Olivares, S., Kebriaei, P., Shpall, E. J., et al. (2013). Clinical application of Sleeping Beauty and artificial antigen presenting cells to genetically modify T cells from peripheral and umbilical cord blood. *J. Vis. Exp.* 72:e50070. doi: 10.3791/50070

Hunt, C. J. (2011). Cryopreservation of human stem cells for clinical application: a review. *Transfus. Med. Hemother.* 38, 107–123. doi: 10.1159/000326623

Ilic, D., Stephenson, E., Wood, V., Jacquet, L., Stevenson, D., Petrova, A., et al. (2012). Derivation and feeder-free propagation of human embryonic stem cells under xeno-free conditions. *Cytotherapy* 14, 122–128. doi: 10.3109/14653249.2011.623692

Jenkins, M. J., and Farid, S. S. (2015). Human pluripotent stem cell-derived products: advances towards robust, scalable and cost-effective manufacturing strategies. *Biotechnol. J.* 10, 83–95. doi: 10.1002/biot.201400348

Jethwa, H., Adami, A. A., and Maher, J. (2014). Use of gene-modified regulatory T-cells to control autoimmune and alloimmune pathology: Is now the right time? *Clin. Immunol.* 150, 51–63. doi: 10.1016/j.clim.2013.11.004

Jin, J., Sabatino, M., Somerville, R., Wilson, J. R., Dudley, M. E., Stroncek, D. F., et al. (2012). Simplified method of the growth of human tumor infiltrating lymphocytes in gas permeable flasks to numbers needed for patient treatment. *J. Immunother.* 35, 283–292. doi: 10.1097/CJI.0b013e31824e801f

Jozala, A. F., Geraldes, D. C., Tundisi, L. L., Feitosa, V. A., Breyer, C. A., Cardoso, S. L., et al. (2016). Biopharmaceuticals from microorganisms: from production to purification. *Braz. J. Microbiol.* 47, 51–63. doi: 10.1016/j.bjm.2016.10.007

Kajiwara, M., Aoi, T., Okita, K., Takahashi, R., Inoue, H., Takayama, N., et al. (2012). Donor-dependent variations in hepatic differentiation from human-induced pluripotent stem cells. *Proc. Natl. Acad. Sci. U.S.A.* 109, 12538–12543. doi: 10.1073/pnas.1209979109

Kempf, H., Kropp, C., Olmer, R., Martin, U., and Zweigerdt, R. (2015). Cardiac differentiation of human pluripotent stem cells in scalable suspension culture. *Nat. Protoc.* 10, 1345–1361. doi: 10.1038/nprot.2015.089

Kerkar, S. P. (2013). Model T" cells: a time-tested vehicle for gene therapy. *Front. Immunol.* 4:304. doi: 10.3389/fimmu.2013.00304

Khuu, H. M., Patel, N., Carter, C. S., Murray, P. R., and Read, E. J. (2006). Sterility testing of cell therapy products: parallel comparison of automated methods with a CFR-compliant method. *Transfusion* 46, 2071–2082. doi: 10.1128/JCM.00302-09

Kikuchi, T., Worgall, S., Singh, R., Moore, M. A., and Crystal, R. G. (2000). Dendritic cells genetically modified to express CD40 ligand and pulsed with antigen can initiate antigen-specific humoral immunity independent of CD4+ T cells. *Nat. Med.* 6, 1154–1159. doi: 10.1038/80498

Kim, D., Kim, C. H., Moon, J. I., Chung, Y. G., Chang, M. Y., Han, B. S., et al. (2009). Generation of human induced pluripotent stem cells by direct delivery of reprogramming proteins. *Cell Stem Cell* 4, 472–476. doi: 10.1016/j.stem.2009.05.005

Kim, K., Doi, A., Wen, B., Ng, K., Zhao, R., Cahan, P., et al. (2010). Epigenetic memory in induced pluripotent stem cells. *Nature* 467, 285–290. doi: 10.1038/nature09342

Kimbrel, E. A., and Lanza, R. (2015). Current status of pluripotent stem cells: moving the first therapies to the clinic. *Nat. Rev. Drug Discov.* 14, 681–692. doi: 10.1038/nrd4738

Koch, C. M., Reck, K., Shao, K., Lin, Q., Joussen, S., Ziegler, P., et al. (2013). Pluripotent stem cells escape from senescence-associated DNA methylation changes. *Genome Res.* 23, 248–259. doi: 10.1101/gr.141945.112

Kochenderfer, J. N., and Rosenberg, S. A. (2013). Treating B-cell cancer with T cells expressing anti-CD19 chimeric antigen receptors. *Nat. Rev. Clin. Oncol.* 10, 267–276. doi: 10.1038/nrclinonc.2013.46

Kochenderfer, J. N., Wilson, W. H., Janik, J. E., Dudley, M. E., Stetler-Stevenson, M., Feldman, S. A., et al. (2010). Eradication of B-lineage cells and regression of lymphoma in a patient treated with autologous T cells genetically engineered to recognize CD19. *Blood* 116, 4099–4102. doi: 10.1182/blood-2010-04-281931

Krawetz, R., Taiani, J. T., Liu, S., Meng, G., Li, X., Kallos, M. S., et al. (2010). Large-scale expansion of pluripotent human embryonic stem cells in stirred-suspension bioreactors. *Tissue Eng. Part C Methods* 16, 573–582. doi: 10.1089/ten.TEC.2009.0228

Kropp, C., Kempf, H., Halloin, C., Robles-Diaz, D., Franke, A., Scheper, T., et al. (2016). Impact of feeding strategies on the scalable expansion of human pluripotent stem cells in single-use stirred tank bioreactors. *Stem Cells Transl. Med.* 5, 1289–1301. doi: 10.5966/sctm.2015-0253

Kropp, C., Massai, D., and Zweigerdt, R. (2017). Progress and challenges in large-scale expansion of human pluripotent stem cells. *Process Biochem.* 59, 244–254. doi: 10.1016/j.procbio.2016.09.032

Kurata, H., Takakuwa, K., and Tanaka, K. (1994). Vitrification of hematopoietic progenitor cells obtained from human cord blood. *Bone Marrow Transplant.* 14, 261–263.

Kwok, C., Ueda, Y., Kadari, A., Günther, K., Ergün, S., Heron, A., et al. (2018). Scalable stirred suspension culture for the generation of billions of human induced pluripotent stem cells using single-use bioreactors. *J. Tissue Eng. Regen. Med.* 12, e1076–e1087. doi: 10.1002/term.2435

Lai, R. C., Chen, T. S., and Lim, S. K. (2011). Mesenchymal stem cell exosome: a novel stem cell-based therapy for cardiovascular disease. *Regen. Med.* 6, 481–492. doi: 10.2217/rme.11.35

Lai, T., Yang, Y., and Ng, S. K. (2013). Advances in mammalian cell line development technologies for recombinant protein production. *Pharmaceuticals* 6, 579–603. doi: 10.3390/ph6050579

Lam, A. T., Chen, A. K., Li, J., Birch, W. R., Reuveny, S., and Oh, S. K. (2014). Conjoint propagation and differentiation of human embryonic stem cells to cardiomyocytes in a defined microcarrier spinner culture. *Stem Cell Res. Ther.* 5:110. doi: 10.1186/scrt498

Larijani, M. R., Seifinejad, A., Pournasr, B., Hajihoseini, V., Hassani, S. N., Totonchi, M., et al. (2011). Long-term maintenance of undifferentiated human embryonic and induced pluripotent stem cells in suspension. *Stem Cells Dev.* 20, 1911–1923. doi: 10.1089/scd.2010.0517

Lawson, T., Kehoe, D. E., Schnitzler, A. C., Rapiejko, P. J., Der, K. A., and Philbrick, K. (2016). Process development for expansion of human mesenchymal stromal cells in a 50L single-use stirred tank bioreactor. *Biochem. Eng. J.* 120, 49–62. doi: 10.1016/j.bej.2016.11.020

Lebkowski, J. (2011). GRNOPC1: the world's first embryonic stem cell-derived therapy. *Regen. Med.* 6, 11–13. doi: 10.2217/rme.11.77

Lechanteur, C., Baila, S., Janssens, M. E., Giet, O., Briquet, A., Baudoux, E., et al. (2014). Large-scale clinical expansion of mesenchymal stem cells in the GMP-compliant, closed automated Quantum® cell expansion system: comparison with expansion in traditional t-flasks. *J. Stem Cell Res. Ther.* 4:1e11. doi: 10.4172/2157-7633.1000222

Liu, P., Chen, M., Liu, Y., Qi, L. S., and Ding, S. (2018). CRISPR-Based Chromatin Remodeling of the Endogenous Oct4 or Sox2 Locus Enables Reprogramming to Pluripotency. *Cell Stem Cell* 22, 252–261. doi: 10.1016/j.stem.2017.12.001

Lo, B., and Parham, L. (2009). Ethical issues in stem cell research. *Endocr. Rev.* 30, 204–213. doi: 10.1210/er.2008-0031

Löhle, M., Hermann, A., Glass, A., Glaß, H., Kempe, A., Schwarz, S. C., et al. (2012). Differentiation efficiency of induced pluripotent stem cells depends on the number of reprogramming factors. *Stem Cells* 30, 570–579. doi: 10.1002/stem.1016

Lombardo, A., Genovese, P., Beausejour, C. M., Colleoni, S., Lee, Y. L., and Kim, K. A. (2007). Gene editing in human stem cells using zinc finger nucleases and integrase-defective lentiviral vector delivery. *Nat. Biotechnol.* 25, 1298–1306. doi: 10.1038/nbt1353

Lou, G., Chen, Z., Zheng, M., and Liu, Y. (2017). Mesenchymal stem cell-derived exosomes as a new therapeutic strategy for liver diseases. *Exp. Mol. Med.* 49, e346. doi: 10.1038/emm.2017.63

Mandai, M., Watanabe, A., Kurimoto, Y., Hirami, Y., Morinaga, C., Daimon, T., et al. (2017). Autologous induced stem-cell-derived retinal cells for macular degeneration. *N. Engl. J. Med.* 376, 1038–1046. doi: 10.1056/NEJMoa1608368

Martin, M. J., Muotri, A., Gage, F., and Varki, A. (2005). Human embryonic stem cells express an immunogenic nonhuman sialic acid. *Nat. Med.* 11:nm1181.

Matsuura, K., Wada, M., Shimizu, T., Haraguchi, Y., Sato, F., Sugiyama, K., et al. (2012). Creation of human cardiac cell sheets using pluripotent stem cells. *Biochem. Biophys. Res. Commun.* 425, 321–327. doi: 10.1016/j.bbrc.2012.07.089

Mazzini, L., Fagioli, F., Boccaletti, R., Mareschi, K., Oliveri, G., Olivieri, C., et al. (2003). Stem cell therapy in amyotrophic lateral sclerosis: a methodological approach in humans. *Amyotroph. Lateral Scler. Other Motor Neuron Disord.* 4, 158–161. doi: 10.1080/14660820310014653

Meirelles, L., and Nardi, N. B. (2003). Murine marrow-derived mesenchymal stem cell: isolation, in vitro expansion, and characterization. *Br. J. Haematol.* 123, 702–711. doi: 10.1046/j.1365-2141.2003.04669.x

Menasché, P., Vanneaux, V., Hagège, A., Bel, A., Cholley, B., Cacciapuoti, I., et al. (2015). Human embryonic stem cell-derived cardiac progenitors for severe heart failure treatment: first clinical case report. *Eur. Heart J.* 36, 2011–2017. doi: 10.1093/eurheartj/ehv189

Meng, G., Liu, S., Poon, A., and Rancourt, D. E. (2017). Optimizing human induced pluripotent stem cell expansion in stirred-suspension culture. *Stem Cells Dev.* 26, 1804–1817. doi: 10.1089/scd.2017.0090

Miyazaki, T., Futaki, S., Suemori, H., Taniguchi, Y., Yamada, M., Kawasaki, M., et al. (2012). Laminin E8 fragments support efficient adhesion and expansion of dissociated human pluripotent stem cells. *Nat. Commun.* 3:1236. doi: 10.1038/ncomms2231

Moon, J. H., Lee, J. R., Jee, B. C., Suh, C. S., Kim, S. H., Lim, H. J., et al. (2008). Successful vitrification of human amnion-derived mesenchymal stem cells. *Hum. Reprod.* 23, 1760–1770. doi: 10.1093/humrep/den202

Mullard, A. (2015). Novartis secures first CRISPR pharma collaborations. *Nat. Rev. Drug Discov.* 14:82. doi: 10.1038/nrd4546

Nakagawa, M., Koyanagi, M., Tanabe, K., Takahashi, K., Ichisaka, T., Aoi, T., et al. (2008). Generation of induced pluripotent stem cells without Myc from mouse and human fibroblasts. *Nat. Biotechnol.* 26, 101–106. doi: 10.1038/nbt1374

Nakagawa, M., Takizawa, N., Narita, M., Ichisaka, T., and Yamanaka, S. (2010). Promotion of direct reprogramming by transformation-deficient Myc. *Proc. Natl. Acad. Sci. U.S.A.* 107, 14152–14157. doi: 10.1073/pnas.1009374107

Nakagawa, M., Tanabe, K., Tezuka, K., Shibata, T., Kunisada, T., Takahashi, M., et al. (2011). A more efficient method to generate integration-free human iPS cells. *Nat. Methods* 8, 409–412. doi: 10.1038/nmeth.1591

Naldini, L. (2011). Ex vivo gene transfer and correction for cell-based therapies. *Nat. Rev. Genet.* 12, 301–315. doi: 10.1038/nrg2985

Nath, S. C., Horie, M., Nagamori, E., and Kino-Oka, M. (2017). Size- and time-dependent growth properties of human induced pluripotent stem cells in the culture of single aggregate. *J. Biosci. Bioeng.* 124, 469–475. doi: 10.1016/j.jbiosc.2017.05.006

Nath, S. C., Tokura, T., Kim, M. H., and Kino-Oka, M. (2018). Botulinum hemagglutinin-mediated in situ break-up of human induced pluripotent stem cell aggregates for high-density suspension culture. *Biotechnol. Bioeng.* 115, 910–920. doi: 10.1002/bit.26526

NHLBI (2009). *Urinary Exosome Protein Database. NHLBI. 2009-05-12. Retrieved 2009-10-11*. Bethesda, MD: NHLBI.

Oh, S. K., Chen, A. K., Mok, Y., Chen, X., Lim, U. M., Chin, A., et al. (2009). Long-term microcarrier suspension cultures of human embryonic stem cells. *Stem Cell Res.* 2, 219–230. doi: 10.1016/j.scr.2009.02.005

Olmer, R., Lange, A., Selzer, S., Kasper, C., Haverich, A., Martin, U., et al. (2012). Suspension culture of human pluripotent stem cells in controlled, stirred bioreactors. *Tissue Eng. Part C* 18, 772–784. doi: 10.1089/ten.TEC.2011.0717

Orozco, L., Munar, A., Soler, R., Alberca, M., Soler, F., Huguet, M., et al. (2013). Treatment of knee osteoarthritis with autologous mesenchymal stem cells: a pilot study. *Transplantation* 95, 1535–1541. doi: 10.1097/TP.0b013e318291a2da

Otsuji, T. G., Bin, J., Yoshimura, A., Tomura, M., Tateyama, D., Minami, I., et al. (2014). A 3D sphere culture system containing functional polymers for

large-scale human pluripotent stem cell production. *Stem Cell Rep*. 2:746. doi: 10.1016/j.stemcr.2014.04.013

Overton, T. W. (2014). Recombinant protein production in bacterial hosts. *Drug Discov. Today* 19, 590–601. doi: 10.1016/j.drudis.2013.11.008

Pampusch, M. S., Haran, K. P., Hart, G. T., Rakasz, E. G., Rendahl, A. K., Berger, E. A., et al. (2020). Rapid transduction and expansion of transduced T cells with maintenance of central memory populations. *Methods Clin. Dev. Protoc.* 16, 1–10. doi: 10.1016/j.omtm.2019.09.007

Park, Y., Chen, Y., Ordovas, L., and Verfaillie, C. M. (2014). Hepatic differentiation of human embryonic stem cells on microcarriers. *J. Biotechnol.* 174, 39–48. doi: 10.1016/j.jbiotec.2014.01.025

Pisitkun, T., Shen, R. F., and Knepper, M. A. (2004). Identification and proteomic profiling of exosomes in human urine. *Proc. Natl. Acad. Sci. U.S.A.* 101, 13368–13373. doi: 10.1073/pnas.0403453101

PR Newswire (2019). *Global Cell and Gene Therapy Market to Reach $11.96 Billion by 2025*. Available online at: https://www.prnewswire.com/news-releases/global-cell-and-gene-therapy-market-to-reach-11-96-billion-by-2025--300896848.html (accessed August 06, 2019).

Provasi, E., Genovese, P., Lombardo, A., Magnani, Z., Liu, P. Q., Reik, A., et al. (2012). Editing T cell specificity towards leukemia by zinc finger nucleases and lentiviral gene transfer. *Nat. Med.* 18, 807–815. doi: 10.1038/nm.2700

PRWeb (2018). Available online at: http://www.prweb.com/releases/2018/05/prweb15476972 (accessed April, 2020).

Rao, M. S., Pei, Y., Garcia, T. Y., Chew, S., Kasai, T., Hisai, T., et al. (2018). Illustrating the potency of current Good Manufacturing Practice-compliant induced pluripotent stem cell lines as a source of multiple cell lineages using standardized protocols. *Cytotherapy* 20, 861–872. doi: 10.1016/j.jcyt.2018.03.037

Rayment, E. A., and Williams, D. J. (2010). Concise review: mind the gap: challenges in characterizing and quantifying cell- and tissue-based therapies for clinical translation. *Stem Cells* 28, 996–1004. doi: 10.1002/stem.416

Reardon, S., and Cyranoski, D. (2014). Japan stem-cell trial stirs envy: researchers elsewhere can't wait to test iPS cells in humans. *Nature* 513, 278–288. doi: 10.1038/513287a

Rehakova, D., Souralova, T., and Koutna, I. (2020). Clinical-grade human pluripotent stem cells for cell therapy: characterization strategy. *Int. J. Mol. Sci.* 21:E2435. doi: 10.3390/ijms21072435

Reisman, M., and Adams, K. T. (2014). Stem cell therapy: a look at current research, regulations, and remaining hurdles. *Pharm. Ther.* 39, 846–847, 854–857.

Rodrigues, C. A. V., Fernandes, T. G., Diogo, M. M., da Silva, C. L., and Cabral, J. M. S. (2011). Stem cell cultivation in bioreactors. *Biotechnol. Adv.* 29, 815–829. doi: 10.1016/j.biotechadv.2011.06.009

Roh, K. H., Nerem, R. M., and Roy, K. (2016). Biomanufacturing of therapeutic cells: state of the art, current challenges, and future perspectives. *Annu. Rev. Chem. Biomol. Eng.* 7, 455–478. doi: 10.1146/annurev-chembioeng-080615-033559

Rohani, L., Fabian, C., Holland, H., Naaldijk, Y., Dressel, R., Löffler-Wirth, H., et al. (2016). Generation of human induced pluripotent stem cells using non-synthetic mRNA. *Stem Cell Res.* 16, 662–672. doi: 10.1016/j.scr.2016.03.008

Rohani, L., Johnson, A. A., Arnold, A., and Stolzing, A. (2014). The aging signature: a hallmark of induced pluripotent stem cells? *Aging Cell* 13, 2–7. doi: 10.1111/acel.12182

Rohani, L., Johnson, A. A., Naghsh, P., Rancourt, D. E., Ulrich, H., and Holland, H. (2018). Concise review: molecular cytogenetics and quality control: clinical guardians for pluripotent stem cells. *Stem Cells Transl. Med.* 7, 867–875. doi: 10.1002/sctm.18-0087

Rungarunlert, S., Ferreira, J. N., and Dinnyes, A. (2016). Novel bioreactor platform for scalable cardiomyogenic differentiation from pluripotent stem cell-derived embryoid bodies. *Methods Mol. Biol.* 1502, 169–179. doi: 10.1007/7651_2016_341

Sakuma, T., Barry, M. A., and Ikeda, Y. (2012). Lentiviral vectors: basic to translational. *Biochem. J.* 443, 603–618. doi: 10.1042/BJ20120146

Samavarchi-Tehrani, P., Golipour, A., David, L., Sung, H. K., Beyer, T. A., Datti, A., et al. (2010). Functional genomics reveals a BMP-driven mesenchymal-to-epithelial transition in the initiation of somatic cell reprogramming. *Cell Stem Cell* 7, 64–77. doi: 10.1016/j.stem.2010.04.01

Schaber, S. D., Gerogiorgis, D. I., Ramachandran, R., Evans, J. M., Barton, P. I., and Trout, B. L. (2011). Economic analysis of integrated continuous and batch pharmaceutical manufacturing: a case study. *I&EC* 50, 10083–10092. doi: 10.1021/ie2006752

Schellenberg, A., Hemeda, H., and Wagner, W. (2013). Tracking of replicative senescence in mesenchymal stem cells by colony-forming unit frequency. *Methods Mol. Biol.* 976, 143–154. doi: 10.1007/978-1-62703-317-6_11

Schwartz, S. D., Regillo, C. D., Lam, B. L., Eliott, D., Rosenfeld, P. J., Gregori, N. Z., et al. (2015). Human embryonic stem cell-derived retinal pigment epithelium in patients with age-related macular degeneration and Stargardt's macular dystrophy: follow-up of two open-label phase 1/2 studies. *Lancet* 385, 509–516. doi: 10.1016/S0140-6736(14)61376-3

Sensebe, L., Bourin, P., and Tarte, K. (2011). Good manufacturing practices production of mesenchymal stem/stromal cells. *Hum. Gene Ther.* 22, 19–26. doi: 10.1089/hum.2010.197

Serra, M., Brito, C., Correia, C., and Alves, P. M. (2012). Process engineering of human pluripotent stem cells for clinical application. *Trends Biotechnol.* 30, 350–359. doi: 10.1016/j.tibtech.2012.03.003

Shafa, M., Day, B., Yamashita, A., Meng, G., Liu, S., Krawetz, R., et al. (2012). Derivation of iPSCs in stirred suspension bioreactors. *Nat. Methods* 9, 465–466. doi: 10.1038/nmeth.1973

Shafa, M., Panchalingam, K. M., Walsh, T., Richardson, T., and Baghbaderani, B. A. (2019). Computational fluid dynamics modeling, a novel, and effective approach for developing scalable cell therapy manufacturing processes. *Biotechnol. Bioeng.* 116, 3228–3241. doi: 10.1002/bit.27159

Shekaran, A., Lam, A., Sim, E., Jialing, L., Jian, L., Wen, J. T. P., et al. (2016). Biodegradable ECM-coated PCL microcarriers support scalable human early MSC expansion and *in vivo* bone formation. *Cytotherapy* 18, 1332–1344. doi: 10.1016/j.jcyt.2016.06.016

Silva, M. M., Rodrigues, A. F., Correia, C., Sousa, M. F. Q., Brito, C., Coroadinha, A. S., et al. (2015). Robust expansion of human pluripotent stem cells: integration of bioprocess design with transcriptomic and metabolomic characterization. *Stem Cells Transl. Med.* 4, 731–742. doi: 10.5966/sctm.2014-0270

Singh, H., Figliola, M. J., Dawson, M. J., Olivares, S., Zhang, L., Yang, G., et al. (2013). Manufacture of clinical-grade CD19-specific T cells stably expressing chimeric antigen receptor using Sleeping Beauty system and artificial antigen presenting cells. *PLoS One* 8:e64138. doi: 10.1371/journal.pone.0064138

Singh, H., Mok, P., Balakrishnan, T., Rahmat, S. N., and Zweigerdt, R. (2010). Upscaling single cell-inoculated suspension culture of human embryonic stem cells. *Stem Cell Res.* 4, 165–179. doi: 10.1016/j.scr.2010.03.001

Somerville, R. P., Devillier, L., Parkhurst, M. R., Rosenberg, S. A., and Dudley, M. E. (2012). Clinical scale rapid expansion of lymphocytes for adoptive cell transfer therapy in the WAVE(R) bioreactor. *J. Transl. Med.* 10:69. doi: 10.1186/1479-5876-10-69

Sommer, C. A., Sommer, A. G., Longmire, T. A., Christodoulou, C., Thomas, D. D., Gostissa, M., et al. (2010). Excision of reprogramming transgenes improves the differentiation potential of iPS cells generated with a single excisable vector. *Stem Cells* 28, 64–74. doi: 10.1002/stem.255

Song, X. T. (2013). Combination of virotherapy and T-cell therapy: arming oncolytic virus with T-cell engagers. *Discov. Med.* 16, 261–266.

Steiner, D., Khaner, H., Cohen, M., Even-Ram, S., Gil, Y., Itsykson, P., et al. (2010). Derivation, propagation and controlled differentiation of human embryonic stem cells in suspension. *Nat. Biotechnol.* 28, 361–364. doi: 10.1038/nbt.1616

Sterlling, J. (2018). Available online at: https://www.genengnews.com/insights/scaling-up-cell-therapy-manufacturing/ (accessed April, 2020).

Takahashi, K., Tanabe, K., Ohnuki, M., Narita, M., Ichisaka, T., Tomoda, K., et al. (2007). Induction of pluripotent stem cells from adult human fibroblasts by defined factors. *Cell* 131, 861–872. doi: 10.1016/j.cell.2007.11.019

Taylor, C. J., Bolton, E. M., Pocock, S., Sharples, L. D., Pedersen, R. A., and Bradley, J. A. (2005). Banking on human embryonic stem cells: estimating the number of donor cell lines needed for HLA matching. *Lancet* 366, 2019–2025. doi: 10.1016/S0140-6736(05)67813-0

Tekoah, Y., Shulman, A., Kizhner, T., Ruderfer, I., Fux, L., Nataf, Y., et al. (2015). Large-scale production of pharmaceutical proteins in plant cell culture-the Protalix experience. *Plant Biotechnol. J.* 13, 1199–1208. doi: 10.1111/pbi.12428

Terakura, S., Yamamoto, T. N., Gardner, R. A., Turtle, C. J., Jensen, M. C., and Riddell, S. R. (2012). Generation of CD19-chimeric antigen receptor modified CD8+ T cells derived from virus-specific central memory T cells. *Blood* 119, 72–82. doi: 10.1182/blood-2011-07-366419

Thirumala, S., Goebel, W. S., and Woods, E. J. (2009). Clinical grade adult stem cell banking. *Organogenesis* 5, 143–154. doi: 10.4161/org.5.3.98113

Thomson, J. A., Itskovitz-Eldor, J., Shapiro, S. S., Waknitz, M. A., Swiergiel, J. J., Marshall, V. S., et al. (1998). Embryonic stem cell lines derived from human blastocysts. *Science* 282, 1145–1147. doi: 10.1126/science.282.5391.1145

Ting, S., Chen, A., Reuveny, S., and Oh, S. K. (2014). An intermittent rocking platform for integrated expansion and differentiation of human pluripotent stem cells to cardiomyocytes in suspended microcarrier cultures. *Stem Cell Res.* 13, 202–213. doi: 10.1016/j.scr.2014.06.002

Trounson, A., and McDonald, C. (2015). Stem cell therapies in clinical trials: progress and challenges. *Cell Stem Cell* 17, 11–22. doi: 10.1016/j.stem.2015.06.007

U.S. Food and Drug Administration (2020). *Cellular & gene therapy guidances*. Available online at: https://www.fda.gov/vaccines-blood-biologics/biologics-guidances/cellular-gene-therapy-guidances (accessed April 5, 2020).

Ullah, I., Subbarao, R. B., and Rho, G. J. (2015). Human mesenchymal stem cells - current trends and future prospective. *Biosci. Rep.* 35:e00191. doi: 10.1042/BSR20150025

US FDA (2008). *US FDA Guidance for Industry: CGMP for Phase 1 Investigational Drugs Regulation (EU) No 536/2014, Article 61(1)*. Available online at: https://www.fda.gov/downloads/drugs/guidances/ucm070273.pdf (accessed April 6, 2020).

Valadi, H., Ekström, K., Bossios, A., Sjöstrand, M., Lee, J. J., and Lötvall, J. O. (2007). Exosome-mediated transfer of mRNAs and microRNAs is a novel mechanism of genetic exchange between cells. *Nat. Cell Biol.* 9, 654–659. doi: 10.1038/ncb1596

Vosough, M., Omidinia, E., Kadivar, M., Shokrgozar, M. A., Pournasr, B., Aghdami, N., et al. (2013). Generation of functional hepatocyte-like cells from human pluripotent stem cells in a scalable suspension culture. *Stem Cells Dev.* 22, 2693–2705. doi: 10.1089/scd.2013.0088

Wang, J., Hao, J., Bai, D., Gu, Q., Han, W., Wang, L., et al. (2015). Generation of clinical-grade human induced pluripotent stem cells in Xeno-free conditions. *Stem Cell Res. Ther.* 6:223. doi: 10.1186/s13287-015-0206-y

Wang, X., and Riviere, I. (2015). Manufacture of tumor- and virus-specific T lymphocytes for adoptive cell therapies. *Cancer Gene Ther.* 22, 85–94. doi: 10.1038/cgt.2014.81

Wang, X., and Rivièrea, I. (2016). Clinical manufacturing of CAR T cells: foundation of a promising therapy. *Mol. Ther. Oncolyt.* 3:16015. doi: 10.1038/mto.2016.15

Wang, Y., Cheng, L., and Gerecht, S. (2014). Efficient and scalable expansion of human pluripotent stem cells under clinically compliant settings: a view in 2013. *Ann. Biomed. Eng.* 42, 1357–1372. doi: 10.1007/s10439-013-0921-4

Wang, Y., Chou, B. K., Dowey, S., He, C., Gerecht, S., and Cheng, L. (2013). Scalable expansion of human induced pluripotent stem cells in the defined xeno-free E8 medium under adherent and suspension culture conditions. *Stem Cell Res.* 11, 1103–1116. doi: 10.1016/j.scr.2013.07.011

Warikoo, V. (2011). *Feasibility Study to Integrate Perfusion Cell Culture Processes to Continuous Downstream Processing*. Anaheim, CA: American Chemical Society.

Warren, L., Manos, P. D., Ahfeldt, T., Loh, Y. H., Li, H., Lau, F., et al. (2010). Highly efficient reprogramming to pluripotency and directed differentiation of human cells with synthetic modified mRNA. *Cell Stem Cell* 7, 618–630. doi: 10.1016/j.stem.2010.08.012

Woltjen, K., Michael, I. P., Mohseni, P., Desai, R., Mileikovsky, M., Hämäläinen, R., et al. (2009). piggyBac transposition reprograms fibroblasts to induced pluripotent stem cells. *Nature* 458, 766–770. doi: 10.1038/nature07863

Wuchter, P., Bieback, K., Schrezenmeier, H., Bornhäuser, M., Müller, L. P., Bönig, H., et al. (2015). Standardization of good manufacturing practice-compliant production of bone marrow-derived human mesenchymal stromal cells for immunotherapeutic applications. *Cytotherapy* 17, 128–139. doi: 10.1016/j.jcyt.2014.04.002

Yamashita, A., Liu, S., Woltjen, K., Thomas, B., Meng, G., Hotta, A., et al. (2016). Cartilage tissue engineering identifies abnormal human induced pluripotent stem cells. *Nat. Sci. Rep.* 3:1978. doi: 10.1038/srep01978

Yan, Y., Song, L., Tsai, A. C., Ma, T., and Li, Y. (2016). Generation of neural progenitor spheres from human pluripotent stem cells in a suspension bioreactor. *Methods Mol. Biol.* 1502, 119–128. doi: 10.1007/7651_2015_310

Yáñez-Muñoz, R. J., Balaggan, K. S., MacNeil, A., Howe, S. J., Schmidt, M., and Smith, A. J. (2006). Effective gene therapy with nonintegrating lentiviral vectors. *Nat. Med.* 12, 348–353. doi: 10.1038/nm1365

Yang, H. S., Jeon, O., Bhang, S. H., Lee, S. H., and Kim, B. S. (2010). Suspension culture of mammalian cells using thermosensitive microcarrier that allows cell detachment without proteolytic enzyme treatment. *Cell Transplant.* 19, 1123–1132. doi: 10.3727/096368910X516664

Yehezkel, S., Rebibo-Sabbah, A., Segev, Y., Tzukerman, M., Shaked, R., Huber, I., et al. (2011). Reprogramming of telomeric regions during the generation of human induced pluripotent stem cells and subsequent differentiation into fibroblast-like derivatives. *Epigenetics* 6, 63–75. doi: 10.4161/epi.6.1.13390

Yin, K., Wang, S., and Zhao, R. C. (2019). Exosomes from mesenchymal stem/stromal cells: a new therapeutic paradigm. *Biomark Res.* 7:8. doi: 10.1186/s40364-019-0159-x

Zeng, X. (2007). Human embryonic stem cells: mechanisms to escape replicative senescence? *Stem Cell Rev.* 3, 270–279. doi: 10.1007/s12015-007-9005-x

Zhang, B., Yin, Y., Lai, R. C., Tan, S. S., Choo, A. B., and Lim, S. K. (2013). Mesenchymal stem cells secrete immunologically active Exosomes. *Stem Cells Dev.* 23, 1233–1244. doi: 10.1089/scd.2013.0479

Zimmermann, A., Preynat-Seauve, O., Tiercy, J. M., Krause, K. H., and Villard, J. (2012). Haplotype-based banking of human pluripotent stem cells for transplantation: potential and limitations. *Stem Cells Dev.* 21, 2364–2373. doi: 10.1089/scd.2012.0088

Zweigerdt, R., Olmer, R., Singh, H., Haverich, A., and Martin, U. (2011). Scalable expansion of human pluripotent stem cells in suspension culture. *Nat. Protoc.* 6, 689–700. doi: 10.1038/nprot.2011.318

Conflict of Interest: The authors declare that the research was conducted in the absence of any commercial or financial relationships that could be construed as a potential conflict of interest.

frontiers in Bioengineering and Biotechnology

ORIGINAL RESEARCH
published: 15 January 2021
doi: 10.3389/fbioe.2020.598389

Comparative Analysis of Mesenchymal Stem Cell Cultivation in Fetal Calf Serum, Human Serum, and Platelet Lysate in 2D and 3D Systems

*Marline Kirsch[1], Jessica Rach[2], Wiebke Handke[3], Axel Seltsam[3], Iliyana Pepelanova[1], Sarah Strauß[4], Peter Vogt[4], Thomas Scheper[1] and Antonina Lavrentieva[1]**

[1] Institute of Technical Chemistry, Leibniz University Hannover, Hanover, Germany, [2] German Red Cross Blood Service NSTOB, Institute Springe, Springe, Germany, [3] Bavarian Red Cross Blood Service, Institute Nuremberg, Nuremberg, Germany, [4] Department of Plastic, Aesthetic, Hand and Reconstructive Surgery, Hannover Medical School, Hanover, Germany

OPEN ACCESS

Edited by:
Cornelia Kasper,
University of Natural Resources and Life Sciences Vienna, Austria

Reviewed by:
Karen Bieback,
Heidelberg University, Germany
Elisabeth Ferreira,
University of Arkansas for Medical Sciences, United States

***Correspondence:**
Antonina Lavrentieva
lavrentieva@iftc.uni-hannover.de

Specialty section:
This article was submitted to Preclinical Cell and Gene Therapy, a section of the journal Frontiers in Bioengineering and Biotechnology

Received: 24 August 2020
Accepted: 08 December 2020
Published: 15 January 2021

Citation:
Kirsch M, Rach J, Handke W, Seltsam A, Pepelanova I, Strauß S, Vogt P, Scheper T and Lavrentieva A (2021) Comparative Analysis of Mesenchymal Stem Cell Cultivation in Fetal Calf Serum, Human Serum, and Platelet Lysate in 2D and 3D Systems. Front. Bioeng. Biotechnol. 8:598389. doi: 10.3389/fbioe.2020.598389

In vitro two-dimensional (2D) and three-dimensional (3D) cultivation of mammalian cells requires supplementation with serum. Mesenchymal stem cells (MSCs) are widely used in clinical trials for bioregenerative medicine and in most cases, *in vitro* expansion and differentiation of these cells are required before application. Optimized expansion and differentiation protocols play a key role in the treatment outcome. 3D cell cultivation systems are more comparable to *in vivo* conditions and can provide both, more physiological MSC expansion and a better understanding of intercellular and cell-matrix interactions. Xeno-free cultivation conditions minimize risks of immune response after implantation. Human platelet lysate (hPL) appears to be a valuable alternative to widely used fetal calf serum (FCS) since no ethical issues are associated with its harvest, it contains a high concentration of growth factors and cytokines and it can be produced from expired platelet concentrate. In this study, we analyzed and compared proliferation, as well as osteogenic and chondrogenic differentiation of human adipose tissue-derived MSCs (hAD-MSC) using three different supplements: FCS, human serum (HS), and hPL in 2D. Furthermore, online monitoring of osteogenic differentiation under the influence of different supplements was performed in 2D. hPL-cultivated MSCs exhibited a higher proliferation and differentiation rate compared to HS- or FCS-cultivated cells. We demonstrated a fast and successful chondrogenic differentiation in the 2D system with the addition of hPL. Additionally, FCS, HS, and hPL were used to formulate Gelatin-methacryloyl (GelMA) hydrogels in order to evaluate the influence of the different supplements on the cell spreading and proliferation of cells growing in 3D culture. In addition, the hydrogel constructs were cultivated in media supplemented with three different supplements. In comparison to FCS and HS, the addition of hPL to GelMA

hydrogels during the encapsulation of hAD-MSCs resulted in enhanced cell spreading and proliferation. This effect was promoted even further by cultivating the hydrogel constructs in hPL-supplemented media.

Keywords: platelet lysate, mesenchymal stem cells, differentiation, medium supplements, fetal calf serum, human serum, gelatin methacryloyl (GelMA), hydrogel

INTRODUCTION

More than half a century has passed since the first isolation and *in vitro* cultivation of mesenchymal stem cells (MSC) described by Friedenstein et al. (1966) and Friedenstein et al. (1970). From that point on, numerous studies about the handling of these cells have been performed. However, the development of an optimal protocol for cultivating MSCs is still in progress (Spees et al., 2016; Lavrentieva et al., 2020). The most common and most widely used cell culture medium supplement is fetal calf serum (FCS). It has been used for the cultivation of several cell types for more than 50 years (Gstraunthaler et al., 2013). To date, most cell isolation or expansion protocols for clinical studies use FCS for supplementation (Schrödel, 2007; Lindroos et al., 2009; Bieback, 2013; Hemeda et al., 2014; Burnouf et al., 2016; Monsanto et al., 2017; Motedayyen et al., 2017; Araújo et al., 2018; Lee et al., 2019; Cherian et al., 2020; Ghamari et al., 2020; Wagner et al., 2020). Even though there are various disadvantages related to FCS such as lot-to-lot variability, ethical concerns about collecting the serum from the heart of unborn calves and the risk of viral, mycoplasm or prion infections or immune responses of the recipients toward foreign factors, there are no widely accepted alternatives for FCS (Lindroos et al., 2009; Bieback, 2013; Jonsdottir-Buch et al., 2013; Hemeda et al., 2014; Burnouf et al., 2016; Monsanto et al., 2017; Motedayyen et al., 2017; Lee et al., 2019; Cherian et al., 2020; Wagner et al., 2020).

A sustained effect on the differentiation capacity and the immunophenotype of cells has been observed in different studies by using xeno-free autologous human serum (HS) as a medium supplement. Due to its promoting effect on cell expansion and its human origin, HS appears to be a potential alternative to FCS (Mannello and Tonti, 2007). However, because of high costs of its manufacture, the production of HS is actually decreasing (Müller et al., 2006; Mannello and Tonti, 2007; Aldahmash et al., 2011; Hemeda et al., 2014). Hence, the goal for the future is a completely chemically defined MSC medium. But to date, there is still no reliable, efficient, comprehensive and fully defined medium available for a broad MSCs cultivation. Moreover, most of the available defined media require additional coatings of the cell culture surface with proteins (Pijuan-Galitó et al., 2016; Salzig et al., 2016; Wu et al., 2016; Cherian et al., 2020). These, in turn are often derived from animal origin, so that in this case no truly xeno-free cultivation with these media is possible.

MSCs have a clinical potential for use in cell therapies and tissue engineering (TE) due to their immunomodulatory potential, stromal functions and their great proliferation as well as differentiation capacities *in vitro* (Dominici et al., 2006). MSCs can be differentiated in different cell types and the potential of controlled chondrogenic and osteogenic differentiation of these cells makes them promising candidates for cartilage and bone TE, as well as for *in vitro* 2D and 3D models for drug screening and disease modeling (Raic et al., 2019). Because of rising ethical, safety and scientific concerns, the World Health Organization and Good Manufacturing Practice (GMP) guidelines recommend the prohibition of the use of animal-derived supplements or supplements containing animal-sourced ingredients for stem cell cultivations or advanced therapy medicinal products (Schrödel, 2007; Lindroos et al., 2009; Bieback, 2013; Gstraunthaler et al., 2013; Hemeda et al., 2014). Hence, until a chemically defined medium is available for MSCs cultivation, it is essential to evaluate existing alternatives to FCS such as human platelet lysate (hPL).

The first attempts to use platelet-rich plasma and platelet lysates as cell culture medium supplement were already made 30 years ago (Gimbrone et al., 1969; Mavrina et al., 1986; Burnouf et al., 2016). Since that time it has been shown that hPL supports *in vitro* growth and osteogenic differentiation of MSCs (Doucet et al., 2005; Lange et al., 2007; Schallmoser et al., 2007; Bieback et al., 2009; Jonsdottir-Buch et al., 2013; Schallmoser and Strunk, 2013; Shih and Burnouf, 2015; Siciliano et al., 2015; Astori et al., 2016; Burnouf et al., 2016; Fernandez-Rebollo et al., 2017), as well as the proliferation of progenitor cells and endothelial colony forming progenitor cells (Schallmoser and Strunk, 2013). hPL appears to be a valuable alternative to FCS and shows several advantages, such as its easy production from human platelet concentrate in conformity with GMP guidelines (Burnouf et al., 2016). Moreover, the use of hPL combines modern social principles of ethics, sustainability, recycling and resources conservation. More than twenty percent of the platelets donated in global blood donation programs expire before they can be used for infusions. Since no difference was determined between using expired or fresh hPL as medium supplements, there is a possibility to recycle expired platelets obtained from blood banks (Jonsdottir-Buch et al., 2013). Furthermore, hPL contains many bioactive factors such as growth factors and cytokines, which act synergistically to support the cell growth, behavior and differentiation of MSCs. Moreover, hPL has demonstrated the ability to enhance the proliferation and differentiation of MSCs in 2D and 3D cultivations in various studies (**Supplementary Table 1**) (Bieback, 2013; Jonsdottir-Buch et al., 2013; Altaie et al., 2016; Burnouf et al., 2016; Kirsch et al., 2019, 2020). However, commercially available hPLs usually contain heparin in order to prevent hPL gelation. Heparin is a product, extracted from porcine small intestine mucosa. Thus, cell cultures grown in the presence of such hPL are no longer xeno-free (Mojica-Henshaw et al., 2013). Furthermore, Hemeda et al. showed that the heparin concentration is critical for 2D MSC cultures in hPL-supplemented medium. This group

demonstrated a concentration-dependent influence of heparin on cell proliferation, the colony-forming unit frequency as well as the *in vitro* differentiation of MSCs (Hemeda et al., 2013). In our study, fibrinogen-depleted hPL was used without addition of heparin to the cell culture medium, in order to maintain true xeno-free cultivation conditions. Providing genuine xeno-free conditions and considering these promising aspects, the challenge is to evaluate and optimize protocols for the production and application of hPL.

Many cell cultivation protocols are still predominantly designed for 2D cultivation. However, compared to 2D-cultured MSCs, 3D cell cultivation seems to be more advantageous, because 3D growing cells reflect the *in vivo* environment of MSCs to a higher extent. Thus, physiological cell-cell and cell-matrix contacts can be simulated and studied only in 3D cell cultures. Moreover, considering angiogenic and immunomodulatory factors, 3D-grown cells have a higher quality (Mark et al., 1977; Cukierman et al., 2001, 2002; Abbott, 2003; Bissell et al., 2003; Schmeichel and Bissell, 2003; Lee et al., 2009; Li and Cui, 2014). Various studies have already investigated the possibility of direct 3D isolation of MSCs from bone and adipogenic tissue to prevent 2D cultivation of the cells (Papadimitropoulos et al., 2014; Egger et al., 2019). Similar to 2D cell cultivation, xeno-free alternatives to FCS are needed for 3D cell cultivation and the influence of medium supplements must be systematically evaluated.

In addition to cellular aggregates and cells growing on scaffolds, hydrogels represent a very promising 3D cultivation system. Hydrogels provide a tunable versatile platform for *in vitro* 3D cultivation, TE and bioprinting (Ruedinger et al., 2015; Pepelanova et al., 2018). Regular semi-synthetic hydrogels are usually stored as lyophilized proteins and are reconstituted with PBS prior cell encapsulation. Thus, they do not normally contain any additional supplements. Regarding 3D hydrogels, the addition of supplements to both, hydrogels and the medium can influence cell behavior. Only a limited number of studies have investigated the influence of direct hPL addition to hydrogels on encapsulated MSCs (Moreira Teixeira et al., 2012; Santos et al., 2018; Jooybar et al., 2019). Most of these studies cultivated the hPL-containing hydrogels in media supplemented with FCS, thus effectively not under true xeno-free conditions (Moreira Teixeira et al., 2012; Santos et al., 2018). So far, no study has shown the influence of different medium supplements on the cell behavior of encapsulated MSCs in comparison. To the best of our knowledge, no study investigating the effect of supplementation of hydrogels and medium on the encapsulated cells has been conducted to date.

In the present study, the influence of hPL (2.5% hPL) on the proliferation, as well as the osteogenic and chondrogenic differentiation of human adipose-derived mesenchymal stem cells (hAD-MSCs) obtained from four different donors was systematically investigated in a 2D cultivation system.

The influence of hPL was compared to FCS (10%) and HS (10%). Online monitoring of osteogenic differentiation in 2D under the influence of different supplements was performed and evaluated.

Recently, we published a study about the influence of formulating GelMA hydrogels with different hPL concentrations (Kirsch et al., 2019). The addition of hPL directly to the hydrogel supported not only the cells but also had a positive impact on the mechanical properties of the GelMA hydrogels. It was demonstrated that the addition of hPL to the hydrogels improves cell growth and cell adhesion. However, this beneficial effect could have been caused by the direct formulation of the hydrogel with a supplement carrying multiple bioactive factors, and must not be directly related to the superior properties of a xeno-free protocol with hPL. In order to investigate this aspect more closely, we expanded the study by formulating GelMA hydrogel with three different media supplements (FCS, HS, and hPL) and studied their influence on cell growth and adhesion. Consequently, the influence of the three supplements as direct additions to the growth media of 3D cultivated cells was also investigated under the aspects of cell spreading, cell morphology, as well as cell viability.

MATERIALS AND METHODS

MSC Cultivation

Human AD-MSCs were isolated from adipose tissue of four donors after abdominoplasty surgery. The use of human tissue from patients (after their informed consent) has been approved by the Institutional Review Board (Hannover Medical School, Ref. Nr.: 3475-2017). As described earlier, we performed surface marker analysis and functional characterization of the isolated cell populations to characterize them as MSCs (Pepelanova et al., 2018). hAD-MSCs were expanded in alpha-MEM medium (Thermo Fisher Scientific, Waltham, MA, USA) and 10% human serum (CC-pro, Oberdorla, Germany) as well as 0.5% gentamicin (Merck Millipore, Darmstadt, Germany), harvested by accutase treatment (Sigma Aldrich, Taufkirchen, Germany), and cryopreserved at passage one or two until the start of the experiment. Experiments were performed with cells of passages two to nine. Following concentrations of cell culture supplements were used for all performed experiments: 10% FCS, 10% HS and 2.5% hPL. hPL concentration of 2.5% was chosen based on preliminary experiments. The tested concentrations in preliminary experiments were 0, 1, 2.5, 5, and 10% of hPL in medium. The highest differentiation capacity and a more even distribution of Alizarin Red staining were observed at a concentration of 2.5% (**Supplementary Figure 1a**). Furthermore, in order to test if lower concentrated FCS or HS could also result in higher osteogenic differentiation, 2.5% of all supplements were used in preliminary experiments. The cell viability and osteogenic differentiation was significantly lower for hAD-MSCs cultivated with 2.5% FCS and 2.5% HS compared to 2.5% hPL (**Supplementary Figure 1b**). Due to those results the standard concentration of 10% FCS and HS was used to supplement the medium in all experiments.

Platelet Lysate Preparation

Human platelet lysates were prepared and provided by the German Red Cross Blood Service NSTOB (Springe, Germany) by freeze-thaw treatments of pooled platelets from surplus buffy

coats. To prevent gelation of hPL and avoid the use of heparin, fribrinogen depletion was performed by the calcium presipitation method, followed by filtration of the platelet lysate.

Cell Proliferation Analysis

For cell proliferation studies, the hAD-MSCs were harvested at 80% of confluency by accutase treatment, counted using a hemocytometer and seeded at a density of 3,000 cells/cm^2 in 25 cm^2 cell culture flasks containing 4 ml medium. Alpha-MEM medium was supplemented with 10% HS, 10% FCS or 2.5% hPL. hAD-MSCs from four different donors were sub-cultivated two times per week with a seeding density of 3,000 cells/cm^2 over five passages; cell number and viability were evaluated by trypan blue exclusion and cumulative cell numbers were calculated.

Osteogenic and Chondrogenic Differentiation

For differentiation experiments, cells were seeded in 24-well plates (growth area 2 cm^2, Sarstedt, Germany) at a density of 10.000 to 15.000 cells/cm^2 in 500 µl alpha-MEM containing 10% HS, 10% FCS or 2.5% hPL and 50 µg/ml gentamicin per well. After seeding, cells were cultivated for 24–48 h (until full confluence was achieved) in a humidified atmosphere containing 5% CO_2 and 21% O_2 at 37°C. Afterwards, the cell culture medium was changed to either the osteogenic or chondrogenic differentiation medium. Osteogenic differentiation medium contained 5 mM β-glycerophosphate, 0.1 µM dexamethasone, 0.2 mM L-ascorbate-2-phosphate, 0.5% gentamicin, as well as 2.5% hPL, 10% HS or 10% FCS. Serum-free chondrogenic differentiation medium was purchased from Gibco (StemPro Chondrogenic differentiation kit, Gibco, Germany) and also supplemented with 2.5% hPL, 10% HS or 10% FCS. The medium was exchanged every 3–4 days. Cells were cultured for the next 7, 14, or 21 days and then washed in PBS and fixed for 15 min at 4°C with 4% paraformaldehyde for staining. Before fixation, indirect cell viability was estimated by CellTiter-Blue® (CTB) assay according to the manufacturer's instructions (Promega, Mannheim, Germany). Briefly, CTB stock solution was diluted in alpha-MEM basal medium (1:10 v/v) and added to the cells. The fluorescence was measured after 2 h of incubation at an extinction wavelength of 544 nm and an emission wavelength of 590 nm with a microplate reader (Fluoroskan Ascent, Thermo Fisher Scientific Inc., Waltham, MA, USA).

Alizarin Red and Alcian Blue Staining

In order to determine the degree of osteogenic differentiation, Alizarin Red staining was used. The fixed cell layers were incubated in Alizarin Red solution, containing 1% Alizarin Red S (Merck KGaA, Darmstadt, Germany) in deionized H_2O, for 15 min at room temperature. After washing with deionized H_2O the red chelates were detected with a microscope. The accumulation of proteoglycans in the extracellular matrix during the chondrogenic differentiation was visualized by using Alcian Blue staining. Fixed cell layers were washed twice with PBS, incubated for 3 min in 3% acetic acid at room temperature, followed by 30 min incubation in Alcian Blue solution (1% Alcian Blue 8GX, Sigma Aldrich, in 3% acetic acid) at room temperature. After incubation, cell layers were washed several times with 3% acetic acid and the presence of bound Alcian Blue stain was detected using a microscope.

Alizarin Red Extraction

To quantify the degree of osteogenic differentiation, Alizarin Red was extracted with 10% hexadecylpyridinium chloride monohydrate (Sigma-Aldrich, St. Louis, WI, USA) in 1× PBS for 20 min at 37°C. The concentration of extracted Alizarin Red was measured at 550 nm (Epoch, BioTek Instruments, Winooski, VT, USA) and calculated using a calibration curve with a regression of 0.997. If required, samples were diluted to bring Alizarin Red concentrations within the linear range of the photometer.

Online Monitoring and Evaluation of Osteogenic Differentiation by Image Analysis

During the differentiation, time-lapse microscopic pictures were taken using an IncuCyte® Live-Cell Imaging System (Sartorius, Göttingen, Germany) placed in the incubator. The osteogenic differentiation of the cells was determined and quantified by training a metric phase object confluence mask for the typical changes in the morphology of the cells toward osteocytes (**Figure 5B**). To add an enhanced coloring mask to the images, the software (IncuCyte® Analysis Software) provides a processing definition step to train the algorithm to highlight the correct markers on a limited representative set of images at different time points and stages of the osteogenic differentiation. This processing step can be visually inspected and adjusted to be valid for all the pictures in the limited training set. After the visual inspection, when the mask highlights the correct parts where the cells are slowly changing their morphology toward osteocytes and increasing the mineralization of the extracellular matrix, the software can automatically analyze the images of the total experiment. When the processing definition is valid for the training image set, this can be used for online monitoring of the experiment.

Alkaline Phosphatase (ALP) Assays

Next to the Alizarin Red staining and quantification, the ALP activity was also measured in the cells as well as in the supernatants (Anh et al., 1998). The fixated cells were incubated with 5-bromo-4-chloro-3-indolyl phosphate (BCIP)/nitro blue tetrazolium (NBT) (SIGMAFAST BCIP®/NBT, B5655, Merck, Darmstadt, Germany) for 30 min at room temperature, washed with PBS and microscopically analyzed with an Olympus IX50 (Olympus Corporation, Tokyo, Japan). For the quantification of the ALP activity in the supernatant 1 day before measurement, the medium was exchanged to proliferation or differentiation medium without supplements, in order to ensure a sensitive measurement of the activity in the medium. As a standard 4-nitrophenol solution (10 mM, Sigma-Aldrich, St. Louis, WI, USA) was used and diluted in ALP buffer (one Trizma® Buffer tablet of SIGMAFAST™ p-Nitrophenyl phosphate dissolved in 20 ml ddH_2O, Merck, Darmstadt, Germany) for a standard series. The five-fold concentrated substrate solution was prepared by dissolving one pNPP tablet and one Trizma® Buffer tablet of

the kit in 4 ml ddH_2O. Each week, the supernatant was removed 5 min centrifuged at 4°C/14.000 rpm and 250 µl were stored at −20°C until further use. At the end of the experiment, all supernatants were thawed, vortexed and 40 µl/well of each sample, control (medium) and the standard series was added in a 96-wellplate. After adding 10 µl of the substrate solution, the plate was shaked for 5 min at 37°C/450 rpm and incubated for 7 h at 37°C. After 7 h, the plate was measured at 405 nm (Epoch, BioTek Instruments, Winooski, VT, USA) and the ALP activity was calculated by using a calibration curve of the standard series with a regression of 0.999.

Quantitative Glycosaminoglycan (GAG) Assay

After 7, 14, and 21 days of culture in chondrogenic differentiation medium, the cells were harvested and digested in 500 µl/well papain solution [500 µl 0.1 M NaH2PO4/0.005 mM EDTA (pH 6), 5 µl β-mercaptoethanol, and 2.5 µl papain (10 mg/ml, Sigma-Aldrich, St. Louis, WI, USA) at 60°C and 800 rpm overnight. The papain digest solution was then used to quantify the deoxyribonucleic acid (DNA) and GAGs. A DNA standard series was prepared with DNA from calf thymus (Sigma-Aldrich, St. Louis, WI, USA). In a 96 well plate, 100 µl preparation buffer and then 100 µl of the respective sample or standard series were added. After 100 µl of bisbenzimide (Sigma-Aldrich, St. Louis, WI, USA) was added to each well, the plate was measured at 360/460 nm with a spectrophotometer (F-7000 FL Spectrophotometer, Hitachi, Tokio, Japan). Chondroitin sulfate (Sigma-Aldrich, St. Louis, WI, USA) was used as a standard and 100 µl of the samples was added to 100 µl/well ddH_2O in a 96 well plate. After adding 150 µl 1,9-dimethyl-methylene blue (DMMB, Sigma-Aldrich, St. Louis, WI, USA) the plate was measured at 530 nm (Epoch, BioTek Instruments, Winooski, VT, USA) and the DNA and GAG concentration was calculated with calibration curves.

GelMA Synthesis and Hydrogel Preparation

As already described in a previous study, GelMA was synthesized according to a previously described protocol (Pepelanova et al., 2018). The degree of functionalization (DoF) of GelMA used in the experiments was of 50%. GelMA solutions were prepared at a concentration of 5% (w/v). The GelMA was dissolved in 50% of PBS and either 50% (v/v) FCS, HS, or hPL (hPL pH value 7.3, manufactured by German Red Cross, Blood Service NSTOB, Springe, Germany) was added (**Figure 1**). After dissolving all GelMA solutions in a water bath at 37°C, they were sterile filtered with 0.45 µm polyethersulfone (PES) filters and 0.1% (w/v) photoinitiator 2-Hydroxy-4′-(2-hydroxyethoxy)-2-methylpropiophenone (Irgacure 2959) was added prior to the encapsulation of cells.

Encapsulation and Cultivation of hAD-MSCs in Hydrogels

The cells were resuspended in the GelMA solutions at a concentration of 1.0×10^6 cells/mL and filled in 50-µL disks (6-mm diameter) *in silicon* molds. With an UV intensity of 1.2 J/cm^2 (polymerization time of ∼5 min) the hAD-MSCs were encapsulated in the hydrogels with the help of a cross linker (BLX-365 Bio-Link, 365 nm, Vilber Lourmat, Germany). The cells encapsulated in GelMA hydrogels formulated with PBS, FCS, HS, and hPL were further cultivated in medium supplemented with 10% FCS, 10% HS, or 2.5% hPL (**Figure 1**).

The preparation of the well-plates and the handling of the hydrogels is described earlier (Kirsch et al., 2019). As described in more detail in our previous study, the indirect cell viability was determined by the CellTiter-Blue® (CTB) (Promega, Mannheim, Germany) assay according to the manufacturer's specifications (Kirsch et al., 2019). For morphological analysis, encapsulated cells were cultivated for one, three or seven days, incubated in basal alpha-MEM with the addition of 4 µM calcein-acetoxymethyl (AM) (Merck, Darmstadt, Germany) for 40 min at 37°C. The hAD-MSCs were analyzed with a Cytation 5-Cell Imaging Multi-Mode Reader (Biotek Instruments, Winooski, VT, USA).

Statistical Analysis

The data are presented as mean value ± standard deviation of the multiple measurements/counts of each sample. A one-way ANOVA (OriginLab) was performed to determine the statistical significance of the measured values, defined as p-value of $^*p < 0.05$, $^{**}p < 0.01$, or $^{***}p < 0.001$.

RESULTS

hAD-MSCs Proliferation in 2D

To evaluate the influence of hPL on hAD-MSCs proliferation, cells isolated from four different donors were cultivated over five passages in alpha-MEM supplemented with 2.5% hPL

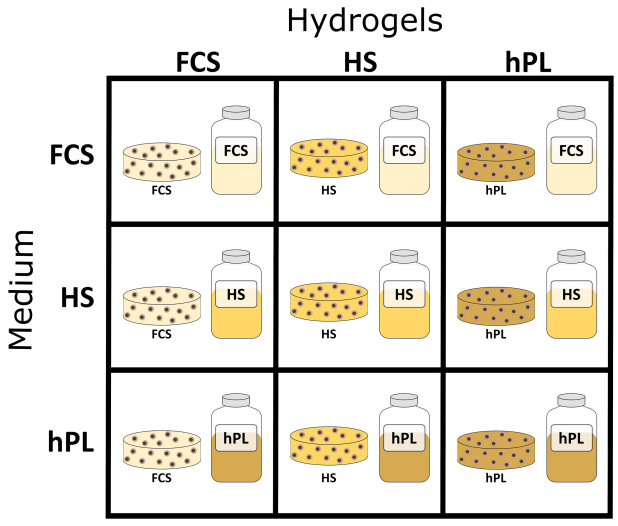

FIGURE 1 | Schematic representation of 3D hydrogel-based cultivation: first GelMA hydrogels were formulated with 50% FCS, 50% HS, or 50% hPL followed by cultivation in medium supplemented with 10% FCS, 10% HS, or 2.5% hPL.

and compared to the cell growth in conventional cell culture conditions: medium with 10% FCS and 10% HS. Differences in the cell growth of the various donors are caused by biological variations. **Figures 2A–D**, that three of the four donor cells cultivated in medium supplemented with hPL show the highest total cell number compared to FCS and HS as supplements. Especially during the first passages, the increase of cell number was highest for cells cultivated in hPL-containing medium. Cells cultivated in medium supplemented with FCS exhibited the lowest cell number and cell division for all donors.

To ensure that hAD-MSCs had not changed their typical immunophenotype during the cultivation with different supplements, a flow cytometry analysis for characteristic MSC-markers was performed and revealed no changes in specific marker expression (**Supplementary Table 2**).

The obtained results demonstrate that medium supplemented with hPL provide a significant higher cell proliferation of hAD-MSCs for three of four donors compared to HS and in all four donors compared to FCS as a supplement. The cumulative cell number after cultivation with hPL was twice to more than five times higher than the cell number after cultivation with FCS. In a short period of time the cell number can be increased significantly, which underlines the potential of hPL-containing medium for rapid MSCs expansion.

Osteogenic Differentiation

The cells were cultivated in differentiation medium supplemented with FCS, HS, or hPL over three weeks. Despite the higher amount of supplements (10% of volume), cells cultivated in medium with conventional supplements (FCS

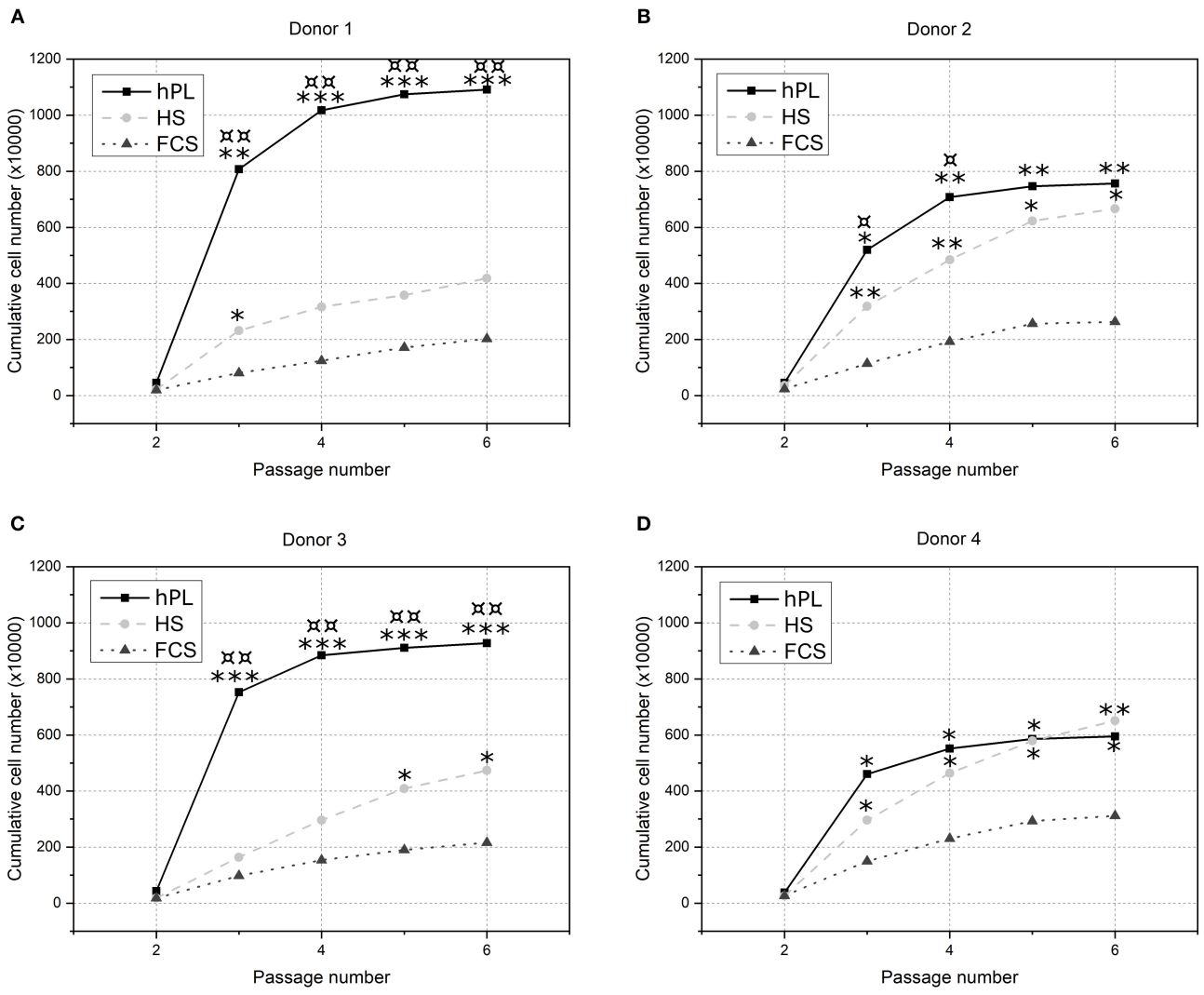

FIGURE 2 | The influence of cell culture supplements on the long-term cultivation of hAD-MSCs. Cells from four donors [**(A)** Donor 1, **(B)** Donor 2, **(C)** Donor 3 and **(D)** Donor 4] were cultivated over five passages in 2.5% hPL (black line), 10% HS (light gray dotted line) or 10% FCS (gray dashed line) and cumulative cell numbers were calculated. $^{*}p < 0.05$, $^{**}p < 0.01$, $^{***}p < 0.001$ (*, **, *** indicates significant difference to FCS); $^{¤}p < 0.05$, $^{¤¤}p < 0.01$ (¤, ¤¤ indicates significant difference to HS).

and HS) only showed an irregular Alizarin red staining after three weeks. As illustrated in **Figure 3**, only MSCs differentiated in medium supplemented with hPL showed an accumulation of calcium already after 1 week of cultivation visualized by Alizarin red staining. The staining was even more intense and homogenously distributed after 3 weeks of cultivation. hAD-MSCs from all donors exhibited an osteogenic differentiation in all used supplements after 3 weeks of stimulation. These results were also confirmed by the quantification of Alizarin red staining during the whole period of differentiation (**Figure 3B**). Only hPL as a supplement was able to induce osteogenic differentiation during the first week of cultivation. As illustrated in **Figure 3C**, the indirectly measured viability of cells remained high and did not change significantly over 3 weeks with all three medium supplements. In addition to the staining and quantification of Alizarin red, the ALP activity was measured in the supernatant and in the cells (**Figure 4**). Only cells differentiated with hPL containing medium showed ALP -positive cells already after 1 week (**Figure 4A**). In comparison, fewer ALP-positive cells were observed in FCS and HS differentiated cells. The quantitative determination of ALP activity in the supernatant showed the lowest activity each week in cells differentiated in FCS (**Figure 4B**). In HS differentiated cells, low ALP activity could be measured after seven days of differentiation. The highest ALP activity was detectable in the supernatant of cells differentiated in hPL-supplemented medium.

Online monitoring and the evaluation of osteogenic differentiation dynamics with the help of a trained metric phase object confluence mask also revealed the superiority of hPL in terms of the onset of calcium deposition (**Figure 5**). However,

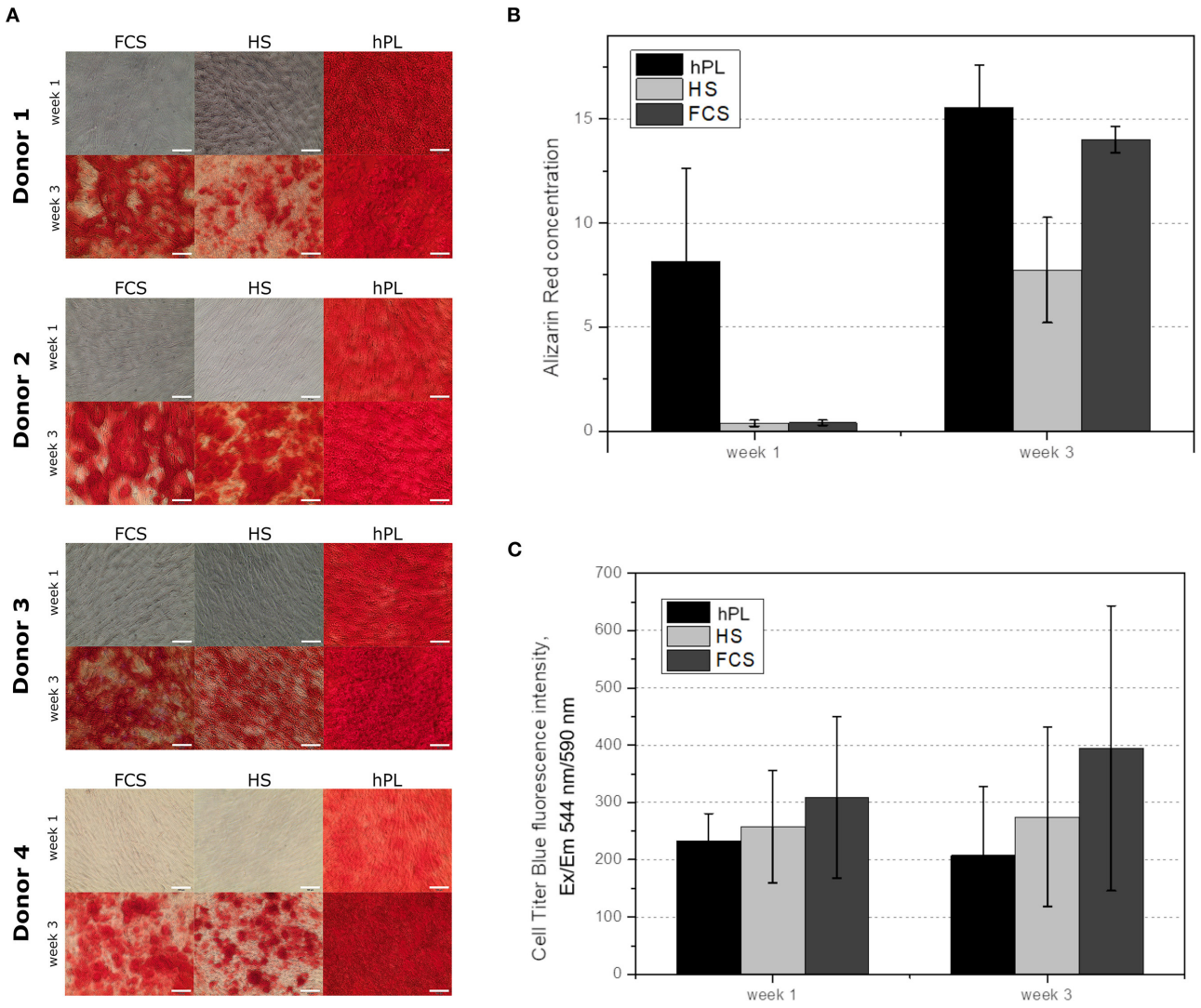

FIGURE 3 | (A) Alizarin red staining of the hAD-MSCs from four donors differentiated in the presence of 2.5% hPL, 10% HS, or 10% FCS. The influence of cell culture supplements on the calcium deposition evaluated by Alizarin red extraction, 10× objective, scale bar 100 µm. **(B)** and on the cell viability during the differentiation **(C)**. Data represent the mean ± SD of a threefold determination for four donors.

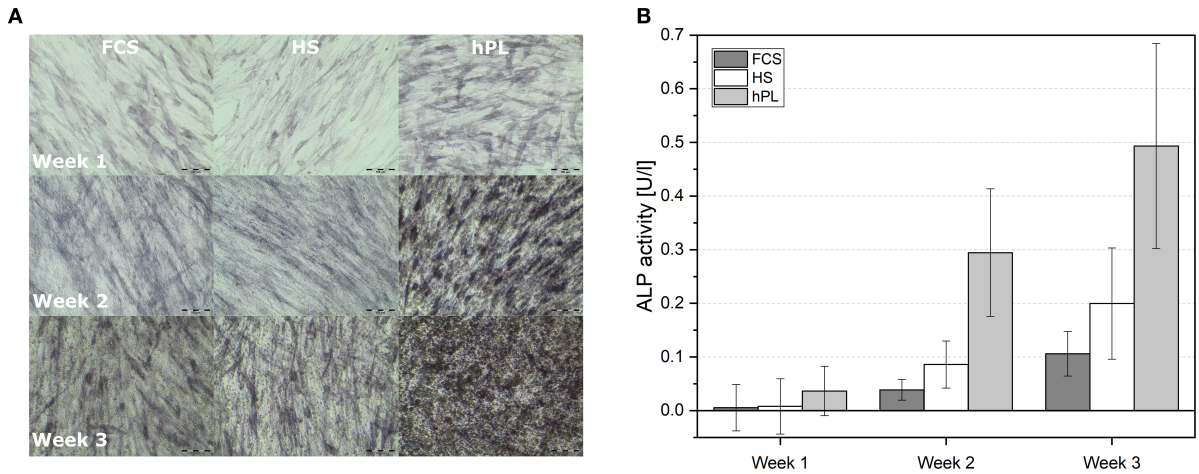

FIGURE 4 | (A) Alkaline phosphatase staining of differentiated hAD-MSCs cultivated for 7, 14, and 21 days and differentiated in medium supplemented with FCS, HS and hPL, 10× objective, scale bar 100 μm. **(B)** Measured ALP activity in the supernatant of hAD-MSCs cultivated with FCS, HS and hPL for 7, 14, and 21 days. Data represent the mean ± SD of a threefold determination for two donors.

in comparison to the Alizarin red staining in the unstained live MSCs culture, the software first recognized the deposition after day seven.

Chondrogenic Differentiation

Traditionally MSCs are only able to differentiate into chondrocytes when cultivated in pellet 3D cultures. In this study, hPL supported chondrogenic differentiation of hAD-MSCs also in 2D cultivations system (**Figure 6**). If media were supplemented with FCS or HS, hAD-MSCs of all tested donors did not show accumulation of proteoglycans after the chondrogenic stimulation (**Figure 6A**). Under FCS and HS cultivation conditions, cells started to detach from the cell culture surface and to agglomerate already after 2 weeks of differentiation. In the presence of hPL, cells from all tested donors started to accumulate proteoglycans already after 2 weeks of stimulation, as demonstrated by the positive Alcian Blue staining. After 2 weeks of stimulation, an increased GAG production was measured in the presence of hPL (**Figure 6B**). hAD-MSCs cultivated with hPL-supplemented differentiation medium showed the highest GAG/DNA ratios during the entire period of differentiation. These data demonstrate that the sole presence of hPL in chondrogenic medium can induce chondrogenic differentiation and accumulation of glycosaminoglycans by hAD-MSCs.

Comparative Analysis of the Influence of Different Medium Supplements in 3D Cultivation

To compare the influence of different supplements on hAD-MSCs cultivated in hydrogels, both addition of supplements directly into hydrogels and addition of supplements to the media were investigated (**Figure 1**). To evaluate the cell growth and behavior, the morphology as well as the metabolic activity of the cells was measured (CTB).

In almost all GelMA hydrogels, increased cell spreading was visible from day three to day seven (**Figure 7**). The lowest amount of spreading after seven days was observed when hAD-MSCs were encapsulated in GelMA prepared in PBS with the addition of 50% FCS. When additionally cultivated with FCS-supplemented medium, spreading cells were rarely seen 7 days (**Figure 7A**) and only a few elongated cells were visible after 7 days in the HS or hPL-supplemented medium (**Figures 7B,C**). In contrast, the addition of HS to the hydrogel had a positive influence on the cell spreading in FCS, HS and hPL-supplemented medium (**Figures 7A–C**). Encapsulating the cells in GelMA with the addition of 50% hPL led to a more distinct cell spreading in all tested culture media. A few elongated cells could be observed already on day one with most cells showing extensive spreading after 7 days. In hPL-supplemented medium, cells were elongated and formed a three dimensional homogenous cell network.

The metabolic activity in all hydrogels increased over the cultivation time (**Figure 7D**). Cells encapsulated in GelMA hydrogels formulated with 50% FCS showed the lowest viability in all media, cells encapsulated in GelMA hydrogels formulated with 50% hPL demonstrated the highest viability. Formulating the hydrogels with 50% hPL instead of FCS led to an almost doubled cell viability when cultivated in FCS-supplemented medium. Regarding the media supplementation, supplementation with HS led to the lowest cell viability compared to the supplementation of FCS and hPL. However, in comparison to FCS-supplemented medium, hAD-MSCs cultivated in hPL-supplemented medium did not show a cell viability increase from day three to day seven. Overall, the cultivation of cells in GelMA hydrogels formulated with 50% FCS, in combination with HS-supplemented medium, represents the worst combination. The best combination, with the highest cell viability, was shown by GelMA hydrogels dissolved in 50% hPL, when cultivated in FCS- or hPL-containing medium.

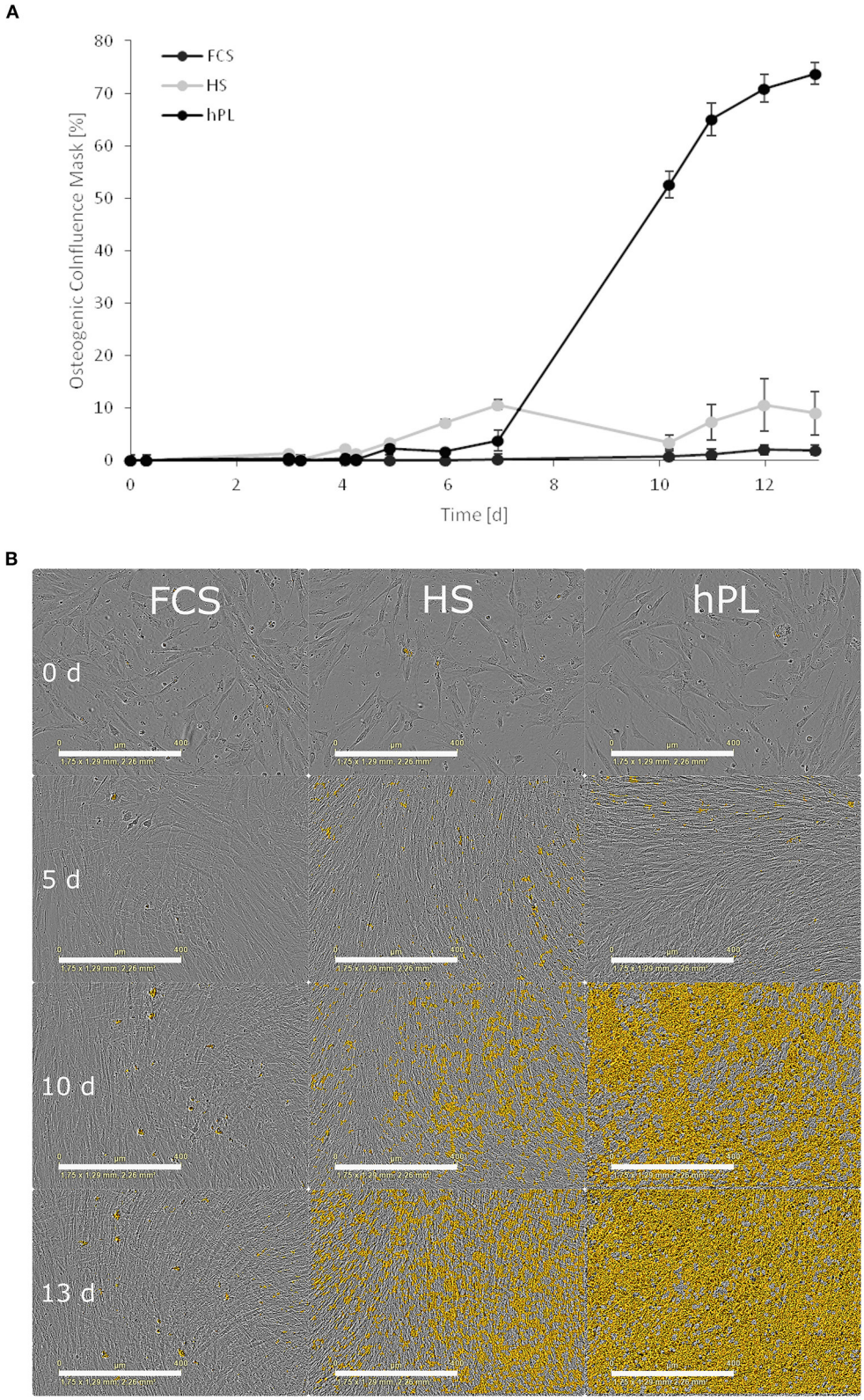

FIGURE 5 | (A) The influence of cell culture supplements on the calcium deposition evaluated by using a trained metric phase object confluence mask for microscopic pictures analyzed by the IncuCyte Live-Cell Imaging System and Software (Essen BioScience, Ann Arbor, MI). Data represent the mean ± SD for a fourfold determination. **(B)** Microscopic pictures taken by an IncuCyte Live-Cell Imaging System and blended with a trained metric phase object confluence mask, which indicates typical osteogenic changes of the cells, scale bar 400 µm.

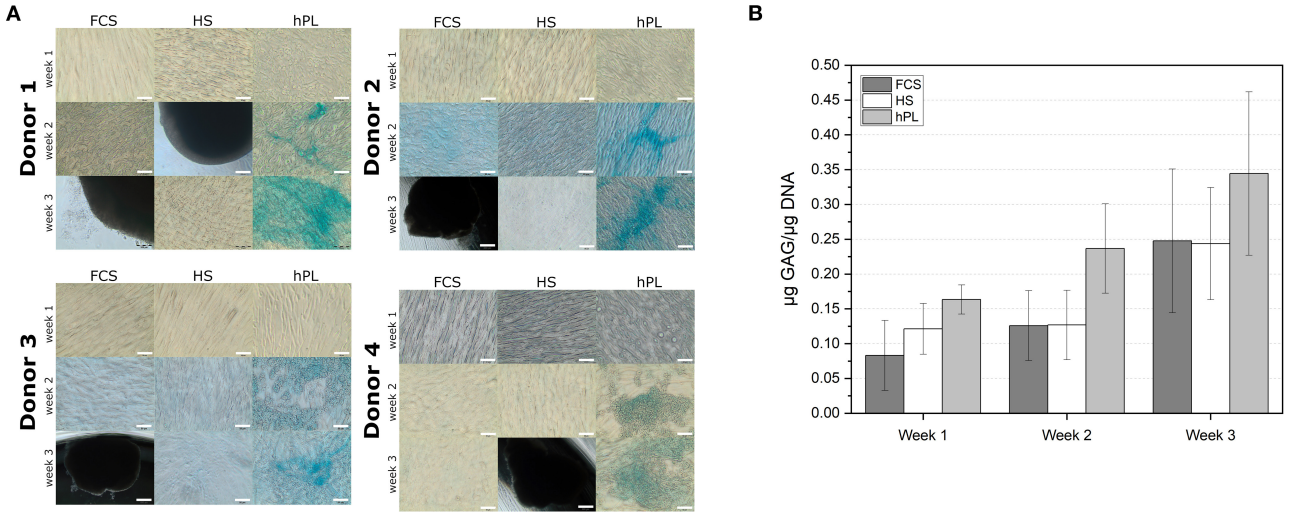

FIGURE 6 | (A) Alcian Blue staining of the hAD-MSCs from four donors differentiated in the presence in 2.5% hPL, 10% HS, or 10% FCS. 10× objective, scale bar 100 µm. **(B)** Determination of the GAG deposition in cells (in µg GAG/µg DNA) differentiated for 7, 14, and 21 days under influence of FCS, HS, and hPL. Data represent the mean ± SD of two independent experiments in threefold determination for two donors.

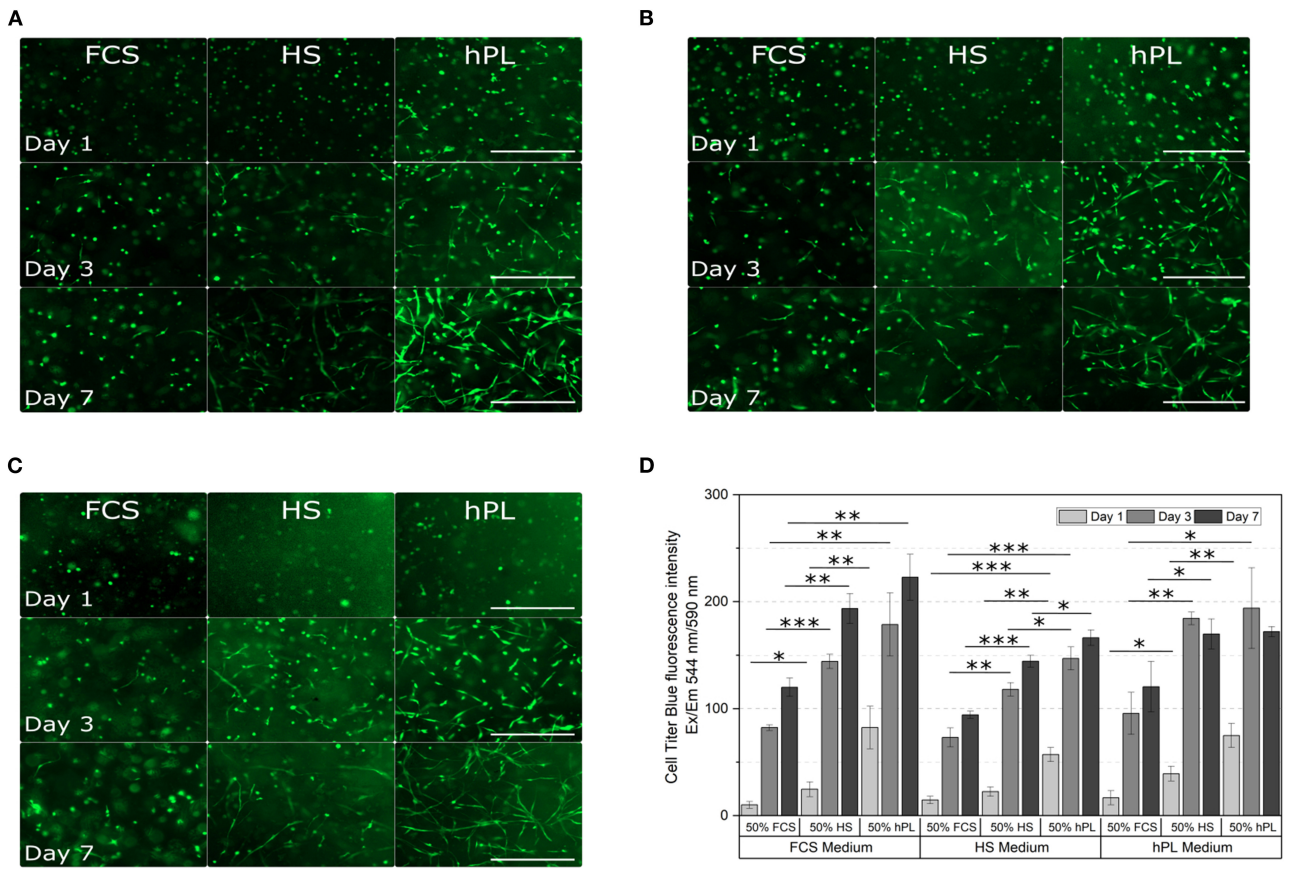

FIGURE 7 | Morphological examination **(A–C)** and cell viability **(D)** of hAD-MSCs encapsulated with a UV dose of 1.2 J/cm^2 in 5% GelMA with 50% degree of functionalization (DoF) formulated with 50% PBS and 50% FCS, 50% HS, or 50% hPL. The hydrogels were cultivated in **(A)** FCS, **(B)** HS, or **(C)** hPL supplemented medium. After cultivating the cells for 1, 3, and 7 days, they were stained with calcein-AM; 4× objective, scale bar 500 µm. **(D)** The CellTiter-Blue (CTB) assay was performed on day 1, day 3, and day 7 of cultivation. Data represent the mean ± SD for a threefold determination. $^*p < 0.05$, $^{**}p < 0.01$, $^{***}p < 0.001$.

DISCUSSION

Cultivation of human cells, including MSCs, in FCS-supplemented media raises concerns since cells cultivated with animal supplements can cause xenogenic immune reactions and transmit prions or other zoonotic infections after transplantation (Bottio et al., 2003; Capelli et al., 2007; Astori et al., 2016). Moreover, the large-scale manufacturing of these cells requires large amounts of clinical grade FCS, which is in limited supply. The use of serum-free media would be the best choice, however, at the moment only few chemically defined, serum-free media are available on the market (e.g., MSCGM-CD™ media from Lonza). The term "serum-free," however, does not always mean that the media does not contain supplements of animal or human origin. Moreover, not every chemically defined medium supports cell growth of all kind of MSCs (MSCs of different origin). For example, it has been demonstrated that Mesencult-XF supports growth of hAD-MSCs, but not of bone marrow-derived mesenchymal stem cells (Al-Saqi et al., 2014). Until efficient "real" serum-free media are developed, it is essential to establish xeno-free systems for *in vitro* expansion of primary human cells, including MSCs. At the moment, more than 1,100 clinical trials are listed where MSCs from different sources are involved (clinicaltrials.gov). Treatment with MSCs often requires an *in vitro* cell expansion step to reach clinically relevant cell numbers. For each treatment, the individual cell dosage is estimated to be 10^5-10^9 cells (Simaria et al., 2014). In addition, the expanded MSCs should retain their biological activity (e.g., immunomodulating properties, differentiation capacity and stromal/rescue function). Thus, it is indispensable to have an efficient xeno-free *in vitro* media to expand these cells for clinical trials and later for therapies.

An additional factor which affects the cell quality is the applied cultivation system. As shown in various studies, the chosen cultivation system influences cell behavior and cell functionality, such as the expression of specific factors (Mark et al., 1977; Cukierman et al., 2001, 2002; Abbott, 2003; Bissell et al., 2003; Schmeichel and Bissell, 2003; Lee et al., 2009; Li and Cui, 2014; Papadimitropoulos et al., 2014; Sart et al., 2014; Egger et al., 2019). Therefore, the application of xeno-free *in vitro* media should be combined with cell cultivation in a 3D cultivation system, in order to obtain the best possible replication of the physiological cell state.

In the present work, the influence of hPL on proliferation and differentiation of hAD-MSCs in 2D cultivation systems was investigated and the obtained results were systematically compared with cells cultivated with HS and FCS. In this study, we revealed that the 2D supplementation of cell culture medium with 2.5% hPL accelerated cell proliferation during the first 2–3 passages. Cells isolated from all four tested donors expanded in 2D faster in the presence of 2.5% hPL than in the presence of 10% HS or 10% FCS. Although differences in proliferation capacities could be observed in each donor, the application of hPL will allow each donor to reach the fastest cell expansion. These results were demonstrated earlier for MSCs isolated from human bone-marrow, umbilical cord blood and adipose tissue (Blande et al., 2009; Shih et al., 2011; Bieback, 2013; Astori et al., 2016). It is important to note that not only supplements (serum) play an essential role in the expansion efficiency, but also the basal media composition. In addition, the right combination of basal media, supplements and seeding strategy is critical to obtain optimal conditions for *in vitro* cell growth (Kasper et al., 2018). In our work, αMEM was used, which is more physiological than the widely used high glucose DMEM or RPMI media.

Human platelets *in vivo* play a major role in homeostasis and represent a rich source of survival and growth factors, which are usually released during wound healing at the site of injury (Shih and Burnouf, 2015). Therefore, hPL could provide an efficient replacement for FCS and HS (Hemeda et al., 2014). Siciliano et al. performed the isolation and successful 2D expansion of human mediastinal hAD-MSCs in virally inactivated GMP-grade hPL (Siciliano et al., 2015). They demonstrated that mediastinal hAD-MSCs cultivated in 10–20% hPL had higher growth rates than the ones cultivated in FCS. In comparison to the above-mentioned study, we could reach the same effect by cultivating the cells with only 2.5% hPL in 2D.

In this work, we also demonstrated that hPL accelerates osteogenic and chondrogenic differentiation in 2D cultures of hAD-MSCs. Cells cultured with hPL remained viable during the entire period of differentiation. The CTB assay is regarded as an indirect measure of viability and proliferation. Since proliferation rate is significantly reduced after induction of differentiation, the low CTB values within hPL supplemented cultures indicate absence of further proliferation and initiation of osteogenic differentiation.

Furthermore, cells from all four donors accumulated calcium in the extracellular matrix already after 1 week of osteogenic stimulation. Concentrations of the extracted Alizarin red were 20 times higher than those measured after cell differentiation in HS and FCS. ALP activity could be detected after the first week, when cultured with hPL-supplemented differentiation medium. In this study, we could monitor the changes in extracellular matrix morphology during osteogenic differentiation online. By training an algorithm with the software of IncuCyte® Live-Cell Imaging and Analysis, the increase of mineralization over time was detected by adding a coloring mask to the images. Using the trained mask, the software first recognized calcium deposition after seven days and evenly distributed early mineralization could be detected after only 10 days. This finding of 2D differentiated cells is in line with the results of previous studies that used hPL for 3D cell culture (Kirsch et al., 2019, 2020; Re et al., 2019). Santo et al. demonstrated that scaffolds loaded with hPL supported accelerated differentiation of hAD-MSCs (Santo et al., 2012). Another group used platelet-functionalized polycaprolactone scaffolds to enhance osteogenic differentiation of MG-63 cells (Rampichová et al., 2017). Altaie et al. reported that osteoconductive scaffolds colonized with hPL-expanded MSCs show a good capability to cure bone deficiencies *in vivo* in pre-clinical studies (Altaie et al., 2016). Since CTB was used, it is not possible to differentiate between the proliferation and metabolic activity directly. In further experiments, the cell proliferation and direct cell viability during differentiation could be measured, in order to distinguish

directly between cell number and the metabolic activity of cells differentiating under the influence of the three different medium supplements.

In the case of chondrogenic differentiation in the 2D cultivation system, only cells cultivated in hPL-containing medium were positively stained with Alcian blue. The production of GAG could be already measured in the second week, if cultivated in the presence of hPL. In addition, hPL cultivated cells demonstrated the highest GAG/DNA ratios during the entire period of differentiation. Moreover, the Alcian blue staining was already positive after 2 weeks of stimulation. It is well-known that for most of the protocols for chondrogenic differentiation, cell pellets or 3D constructs need to be created in order to achieve a successful differentiation. In this work, the addition of hPL was sufficient for chondrogenesis in a 2D system. Merceron et al. were unable to detect any GAG production by hAD-MSCs cultured in 2D (Merceron et al., 2011). Only chondrogenic differentiated cells in 3D pellet cultures showed GAG synthesis and accumulation. In our study, we could show a clear Alcian blue staining, as well as a GAG production of cells differentiated with hPL in 2D. Earlier, Feng et al. demonstrated that 10% hPL could improve chondrogenic differentiation of umbilical cord-derived MSCs in 3D pellets (Feng et al., 2011). It is known that platelets contain numerous growth factors involved in chondrogenesis such as transforming growth factor-β1, vascular endothelial growth factor (VEGF), platelet-derived growth factor (PDGF), insulin-like growth factor 1 (IGF-1), and insulin-like growth factor 2 (IGF-2) (Kabiri et al., 2014). Several groups also demonstrated a positive influence of platelet-rich plasma on chondrogenesis of various MSCs in terms of increased collagen II production as well as upregulation of SOX9 and Aggrecan (Mishra et al., 2009; Xie et al., 2012; Kabiri et al., 2014). Since chondrogenic differentiation of MSCs represents a promising strategy for cartilage regeneration or replacement, application of hPL can provide good conditions for effective *in vitro* induction of chondrogenesis (Boeuf and Richter, 2010). 2D culture applications of osteogenic and chondrogenic differentiated MSCs may be of special interest for high-throughput screening. For instance, they could be used for drug screening in bone and cartilage disease models. Furthermore different studies have shown that osteogenic or chondrogenic pre-differentiated MSCs in 2D can produce cartilage and bone tissue *in vivo* in the same degree as MSCs pre-differentiated in 3D (Merceron et al., 2011).

In addition to the need for xeno-free 2D cell culture protocols, the demand for xeno-free cultivation protocols for 3D cell cultures is also increasing. In the case of hydrogel-based 3D cultivation systems, supplements can be added not only to the medium, but also directly during hydrogel formulation. Although 3D cell cultures with hPL as medium supplement have been studied, there are still certain areas that require further investigation. There are only a limited number of studies which investigated and compared the effect of different supplements on MSCs in general 3D cell culture systems and there are no studies about supplement addition directly to hydrogels (Santos et al., 2018; Kirsch et al., 2019; Re et al., 2019). In a recent study, we have demonstrated that the supplementation of GelMA hydrogels with different hPL concentrations had a positive effect on cell spreading, proliferation and differentiation, as well as on the material properties such as viscosity, storage modulus and swelling ratio (Kirsch et al., 2019).

With this work we have shown that not only the addition of the supplement to hydrogels, but also the supplement origin plays an important role in cell spreading and growth. Due to the direct addition of supplements to the hydrogels, proteins do not have to diffuse into the hydrogels from the media, and growth factors, adhesion factors and other bioactive proteins are directly accessible to encapsulated cells. In this work we could show that especially the addition of hPL to the hydrogel led to better cultivation conditions for the cells.

In situ formulation of hydrogels with hPL increased the cell spreading of hAD-MSCs compared to FCS- and HS-formulated hydrogels. Supporting our previous findings, hPL in hydrogels led to cell attachment and spreading after only 1 day of cultivation in 3D (Kirsch et al., 2019). In contrast, FCS and HS did not show a general positive influence on cell spreading and cell viability in hydrogels. Several studies have previously shown a hPL-dependent or hPL-supported increase of the proliferation rate and cell number of cells growing on the surface or encapsulated in hPL-containing gels (hPL gels/matrix) and hydrogels (Walenda et al., 2012; Babo et al., 2016; Fortunato et al., 2016; Egger et al., 2019; Re et al., 2019). In addition, the hPL enhanced cell spreading of cells encapsulated in hydrogels was previously observed (Fortunato et al., 2016; Santos et al., 2018; Jooybar et al., 2019). MSCs belong to the anchorage-dependent cells. Therefore, increased cell adhesion and enhanced cell spreading have a major impact on migration, proliferation and differentiation of MSCs (Lauffenburger and Horwitz, 1996; Trappmann et al., 2012; Wang et al., 2016; Yang et al., 2019). One reason for the positive effect of hPL on the cell attachment and spreading in the hydrogel could be the α-granules of platelets (Kirsch et al., 2019). The α-granules contain many different adhesion proteins, such as vitronectin, fibronectin, thrombospondin and von Willebrand factor, which are released during the platelet lysis (Sander et al., 1983; Wencel-Drake et al., 1985; Kore-Grodzicki et al., 1988; Heijnen and van der Sluijs, 2015; Burnouf et al., 2016). Another possible reason could be the different stiffness of the matrix material, which was shown to increase with higher hPL concentrations in the hydrogel (Kirsch et al., 2019). Indeed, several studies described the effect of the material stiffness from different matrices on the cell behavior of MSCs, embryonic stem cells and fibroblasts (Engler et al., 2004; Solon et al., 2007; Chowdhury et al., 2010; Park et al., 2011; Sun et al., 2018). For instance, Sun et al. demonstrated that a higher stiffness of fibronectin-coated polyacrylamide hydrogels led to greater spreading and adherence of BM-MSCs, as well as to an increased proliferation rate (Sun et al., 2018). However, the exact reason for the positive influence of hPL on cell adhesion and cell spreading in GelMA hydrogels needs to be investigated in more detail in further studies.

The most promising combinations for enhanced cell spreading and increased cell proliferation were observed by hAD-MSCs encapsulated in hydrogels formulated with 50% hPL

cultivated in medium supplemented with 10% FCS or 2.5% hPL. For clinical studies and applications, however, the use of xeno-free cultivation methods is crucial. Therefore, the more suitable xeno-free 3D cultivation protocol would be the cultivation of MSCs in hydrogels formulated with 50% hPL in medium supplemented with 2.5% hPL. Since allogenic and autologous hPL can be added as a supplement to the hydrogel, but also to the medium, individualized xeno-free off-the-shelf TE constructs can be realized on the long-term using this optimized protocol. In this study, the focus of the 3D experiments was to study and compare cell behavior (morphology, cell spreading and metabolic activity) under all possible combinations of supplements added to the medium or during hydrogel formulation. In further experiments the influence of all possible supplement combinations on the differentiation of the encapsulated cells should be investigated.

The advantages of hPL compared to FCS and HS demonstrated in this work regarding the support of osteogenic and chondrogenic differentiation of MSCs in 2D *in vitro* cultivations must be investigated in further studies for 3D cultivation systems. For example, immunohistological staining of differentiation specific markers can be performed inside the hydrogel, as well as after the preparation of cryosections. Cryosections can be histochemically stained for osteogenic (e.g., calcium or alkaline phosphatase activity) and chondrogenic (e.g., collagen, proteoglycan, or glycosaminoglycan) specific markers. Moreover, the hydrogels can also be enzymatically digested in order to liberate encapsulated cells and allow the performance of cell analysis protocols like gene microarray analysis or flow cytometry.

CONCLUSION

Our work demonstrated that medium supplementation with 2.5% hPL is favorable for cultivation of hAD-MSCs in 2D systems and accelerates proliferation as well as osteogenic and chondrogenic differentiation of these cells. To our knowledge, the progress of osteogenic differentiation under the influence of three different supplements was monitored and evaluated in 2D for the first time. Both, osteogenic and chondrogenic differentiation was already detectable after 1 week of stimulation. In 3D systems, we could show that hAD-MSCs in hPL-supplemented hydrogels cultivated with hPL-supplemented medium adhere and spread faster and in higher numbers when compared to FCS and HS as supplement in hydrogels or medium. This indicates that hPL can be a possible xeno-free alternative to the widely used FCS not only in 2D, but also in hydrogel-based 3D cultivation protocols. Until efficient chemically defined serum-free media are established and approved for the large-scale MSCs production and differentiation, hPL can serve as a suitable supplement for xeno-free cell cultivation in 2D and 3D. Produced under optimal conditions of standardization and safety, hPL can become a key supplement for *ex vivo* production of MSCs and *ex vivo* tissue formation for applications in the field of regenerative medicine. As yet, the precise hPL composition and the reason for fast MSCs differentiation in hPL are unclear.

Further studies including hPL fractionation, protein separation and MS-analysis must be performed in order to elucidate the positive effects of individual components of hPL and for the creation of defined supplements. Taken together, the application of hPL in 2D and 3D *in vitro* cultivation of MSCs appears to be a promising approach for bioregenerative medicine.

DATA AVAILABILITY STATEMENT

The raw data supporting the conclusions of this article will be made available by the authors, without undue reservation.

ETHICS STATEMENT

Human AD-MSCs were isolated from adipose tissue of four donors after abdominoplasty surgery. The use of human tissue from patients (after their informed consent) has been approved by the Institutional Review Board (Hannover Medical School, Ref. Nr.: 3475-2017).

AUTHOR CONTRIBUTIONS

MK performed and planned the experiments and wrote the manuscript. AL and TS planned the experiments and proofread the manuscript. AS, JR, and WH prepared the hPL, participated in the experimental design and in proofreading. IP provided the GelMA and proofread the manuscript. SS and PV provided adipose tissue and cell isolation protocols and proofread the manuscript. All authors contributed to the article and approved the submitted version.

FUNDING

This research was financially supported by the German Research Foundation (DFG Project 398007461 488 3D Dual-Gradient Systems for Functional Cell Screening). The publication of this article was funded by the Open Access fund of Leibniz Universität Hannover.

ACKNOWLEDGMENTS

We would like to acknowledge Ethan Overfelt and Theresa Schulz for the language correction. Furthermore, we want to acknowledge Sandra Miehlke for her help in performing the GelMA experiments and Annabelle-Christin Herder as well as Annalea Brüggemann for their motivation and support.

SUPPLEMENTARY MATERIAL

The Supplementary Material for this article can be found online at: https://www.frontiersin.org/articles/10.3389/fbioe.2020.598389/full#supplementary-material

REFERENCES

Abbott, A. (2003). Cell culture: biology's new dimension. *Nature* 424, 870–872. doi: 10.1038/424870a

Aldahmash, A., Haack-Sørensen, M., Al-Nbaheen, M., Harkness, L., Abdallah, B. M., and Kassem, M. (2011). Human serum is as efficient as fetal bovine serum in supporting proliferation and differentiation of human multipotent stromal (mesenchymal) stem cells *in vitro* and *in vivo*. *Stem Cell Rev.* 7, 860–868. doi: 10.1007/s12015-011-9274-2

Al-Saqi, S. H., Saliem, M., Asikainen, S., Quezada, H. C., Ekblad, A., Hovatta, O., et al. (2014). Defined serum-free media for *in vitro* expansion of adipose-derived mesenchymal stem cells. *Cytotherapy* 16, 915–926. doi: 10.1016/j.jcyt.2014.02.006

Altaie, A., Owston, H., and Jones, E. (2016). Use of platelet lysate for bone regeneration - are we ready for clinical translation? *World J. Stem Cells* 8, 47–55. doi: 10.4252/wjsc.v8.i2.47

Anh, D. J., Dimai, H. P., Hall, S. L., and Farley, J. R. (1998). Skeletal alkaline phosphatase activity is primarily released from human osteoblasts in an insoluble form, and the net release is inhibited by calcium and skeletal growth factors. *Calcif. Tissue Int.* 62, 332–340. doi: 10.1007/s002239900441

Araújo, A. B., Furlan, J. M., Salton, G. D., Schmalfuss, T., Röhsig, L. M., Silla, L. M. R., et al. (2018). Isolation of human mesenchymal stem cells from amnion, chorion, placental decidua and umbilical cord: comparison of four enzymatic protocols. *Biotechnol. Lett.* 40, 989–998. doi: 10.1007/s10529-018-2546-z

Astori, G., Amati, E., Bambi, F., Bernardi, M., Chieregato, K., Schäfer, R., et al. (2016). Platelet lysate as a substitute for animal serum for the *ex-vivo* expansion of mesenchymal stem/stromal cells: present and future. *Stem Cell Res. Ther.* 7:93. doi: 10.1186/s13287-016-0352-x

Babo, P. S., Pires, R. L., Santos, L., Franco, A., Rodrigues, F., Leonor, I., et al. (2016). Platelet lysate-loaded photocrosslinkable hyaluronic acid hydrogels for periodontal endogenous regenerative technology. *ACS Biomater. Sci. Eng.* 3, 1359–1369. doi: 10.1021/acsbiomaterials.6b00508

Bieback, K. (2013). Platelet lysate as replacement for fetal bovine serum in mesenchymal stromal cell cultures. *Transfus. Med. Hemother.* 40, 326–335. doi: 10.1159/000354061

Bieback, K., Hecker, A., Kocaömer, A., Lannert, H., Schallmoser, K., Strunk, D., et al. (2009). Human alternatives to fetal bovine serum for the expansion of mesenchymal stromal cells from bone marrow. *Stem Cells* 27, 2331–2341. doi: 10.1002/stem.139

Bissell, M. J., Rizki, A., and Mian, I. S. (2003). Tissue architecture: the ultimate regulator of breast epithelial function. *Curr. Opin. Cell Biol.* 15, 753–762. doi: 10.1016/j.ceb.2003.10.016

Blande, I. S., Bassaneze, V., Lavini-Ramos, C., Fae, K. C., Kalil, J., Miyakawa, A. A., et al. (2009). Adipose tissue mesenchymal stem cell expansion in animal serum-free medium supplemented with autologous human platelet lysate. *Transfusion* 49, 2680–2685. doi: 10.1111/j.1537-2995.2009.02346.x

Boeuf, S., and Richter, W. (2010). Chondrogenesis of mesenchymal stem cells: role of tissue source and inducing factors. *Stem Cell Res. Ther.* 1:31. doi: 10.1186/scrt31

Bottio, T., Pittarello, G., Bonato, R., Fagiolo, U., and Gerosa, G. (2003). Life-threatening anaphylactic shock caused by porcine heparin intravenous infusion during mitral valve repair. *J. Thorac. Cardiovasc. Surg.* 126, 1194–1195. doi: 10.1016/S0022-5223(03)00813-4

Burnouf, T., Strunk, D., Koh, M. B. C., and Schallmoser, K. (2016). Human platelet lysate: replacing fetal bovine serum as a gold standard for human cell propagation? *Biomaterials* 76, 371–387. doi: 10.1016/j.biomaterials.2015.10.065

Capelli, C., Domenghini, M., Borleri, G., Bellavita, P., Poma, R., Carobbio, A., et al. (2007). Human platelet lysate allows expansion and clinical grade production of mesenchymal stromal cells from small samples of bone marrow aspirates or marrow filter washouts. *Bone Marrow Transplant* 40, 785–791. doi: 10.1038/sj.bmt.1705798

Cherian, D. S., Bhuvan, T., Meagher, L., and Heng, T. S. P. (2020). Biological considerations in scaling up therapeutic cell manufacturing. *Front. Pharmacol.* 11:654. doi: 10.3389/fphar.2020.00654

Chowdhury, F., Na, S., Li, D., Poh, Y.-C., Tanaka, T. S., Wang, F., et al. (2010). Material properties of the cell dictate stress-induced spreading and differentiation in embryonic stem cells. *Nat. Mater.* 9, 82–88. doi: 10.1038/nmat2563

Cukierman, E., Pankov, R., Stevens, D. R., and Yamada, K. M. (2001). Taking cell-matrix adhesions to the third dimension. *Science* 294, 1708–1712. doi: 10.1126/science.1064829

Cukierman, E., Pankov, R., and Yamada, K. M. (2002). Cell interactions with three-dimensional matrices. *Curr. Opin. Cell Biol.* 14, 633–640. doi: 10.1016/S0955-0674(02)00364-2

Dominici, M., Le Blanc, K., Mueller, I., Slaper-Cortenbach, I., Marini, F., Krause, D., et al. (2006). Minimal criteria for defining multipotent mesenchymal stromal cells. *The international society for cellular therapy position statement. Cytotherapy* 8, 315–317. doi: 10.1080/14653240600855905

Doucet, C., Ernou, I., Zhang, Y., Llense, J.-R., Begot, L., Holy, X., et al. (2005). Platelet lysates promote mesenchymal stem cell expansion: a safety substitute for animal serum in cell-based therapy applications. *J. Cell. Physiol.* 205, 228–236. doi: 10.1002/jcp.20391

Egger, D., Oliveira, A. C., Mallinger, B., Hemeda, H., Charwat, V., and Kasper, C. (2019). From 3D to 3D: isolation of mesenchymal stem/stromal cells into a three-dimensional human platelet lysate matrix. *Stem Cell Res. Ther.* 10:248. doi: 10.1186/s13287-019-1346-2

Engler, A. J., Griffin, M. A., Sen, S., Bönnemann, C. G., Sweeney, H. L., and Discher, D. E. (2004). Myotubes differentiate optimally on substrates with tissue-like stiffness: pathological implications for soft or stiff microenvironments. *J. Cell Biol.* 166, 877–887. doi: 10.1083/jcb.200405004

Feng, X., Tian, S., Sun, K., Zhang, J., Zhang, C., Liu, S., et al. (2011). Effect of platelet lysate on chondrogenic differentiation of human umbilical cord derived mesenchymal stem cells *in vitro*. *Zhongguo Xiu Fu Chong Jian Wai Ke Za Zhi* 25, 1250–1255.

Fernandez-Rebollo, E., Mentrup, B., Ebert, R., Franzen, J., Abagnale, G., Sieben, T., et al. (2017). Human platelet lysate versus fetal calf serum: these supplements do not select for different mesenchymal stromal cells. *Sci. Rep.* 7:5132. doi: 10.1038/s41598-017-05207-1

Fortunato, T. M., Beltrami, C., Emanueli, C., de Bank, P. A., and Pula, G. (2016). Platelet lysate gel and endothelial progenitors stimulate microvascular network formation *in vitro*: tissue engineering implications. *Sci. Rep.* 6:25326. doi: 10.1038/srep25326

Friedenstein, A. J., Chailakhjan, R. K., and Lalykina, K. S. (1970). The development of fibroblast colonies in monolayer cultures of guinea-pig bone marrow and spleen cells. *Cell Tissue Kinet* 3, 393–403.

Friedenstein, A. J., Piatetzky-Shapiro, I. I., and Petrakova, K. V. (1966). Osteogenesis in transplants of bone marrow cells. *J. Embryol. Exp. Morphol.* 16, 381–390.

Ghamari, S.-H., Abbasi-Kangevari, M., Tayebi, T., Bahrami, S., and Niknejad, H. (2020). The bottlenecks in translating placenta-derived amniotic epithelial and mesenchymal stromal cells into the clinic: current discrepancies in marker reports. *Front. Bioeng. Biotechnol.* 8:180. doi: 10.3389/fbioe.2020.00180

Gimbrone, M. A., Aster, R. H., Cotran, R. S., Corkery, J., Jandl, J. H., and Folkman, J. (1969). Preservation of vascular integrity in organs perfused *in vitro* with a platelet-rich medium. *Nature* 222, 33–36.

Gstraunthaler, G., Lindl, T., and van der Valk, J. (2013). A plea to reduce or replace fetal bovine serum in cell culture media. *Cytotechnology* 65, 791–793. doi: 10.1007/s10616-013-9633-8

Heijnen, H., and van der Sluijs, P. (2015). Platelet secretory behaviour: as diverse as the granules … or not? *J. Thromb. Haemost.* 13, 2141–2151. doi: 10.1111/jth.13147

Hemeda, H., Giebel, B., and Wagner, W. (2014). Evaluation of human platelet lysate versus fetal bovine serum for culture of mesenchymal stromal cells. *Cytotherapy* 16, 170–180. doi: 10.1016/j.jcyt.2013.11.004

Hemeda, H., Kalz, J., Walenda, G., Lohmann, M., and Wagner, W. (2013). Heparin concentration is critical for cell culture with human platelet lysate. *Cytotherapy* 15, 1174–1181. doi: 10.1016/j.jcyt.2013.05.006

Jonsdottir-Buch, S. M., Lieder, R., and Sigurjonsson, O. E. (2013). Platelet lysates produced from expired platelet concentrates[-108mm]Q22 support growth and osteogenic differentiation of mesenchymal stem cells. *PLoS ONE* 8:e68984. doi: 10.1371/journal.pone.0068984

Jooybar, E., Abdekhodaie, M. J., Alvi, M., Mousavi, A., Karperien, M., and Dijkstra, P. J. (2019). An injectable platelet lysate-hyaluronic acid hydrogel supports cellular activities and induces chondrogenesis of encapsulated mesenchymal stem cells. *Acta Biomater.* 83, 233–244. doi: 10.1016/j.actbio.2018.10.031

Kabiri, A., Esfandiari, E., Esmaeili, A., Hashemibeni, B., Pourazar, A., and Mardani, M. (2014). Platelet-rich plasma application in chondrogenesis. *Adv. Biomed. Res.* 3:138. doi: 10.4103/2277-9175.135156

Kasper, C., Charwat, V., and Lavrentieva, A. (2018). *Cell Culture Technology*. Cham, Switzerland: Springer. doi: 10.1007/978-3-319-74854-2

Kirsch, M., Birnstein, L., Pepelanova, I., Handke, W., Rach, J., Seltsam, A., et al. (2019). Gelatin-methacryloyl (GelMA) formulated with human platelet lysate supports mesenchymal stem cell proliferation and differentiation and enhances the hydrogel's mechanical properties. *Bioengineering* 6:76. doi: 10.3390/bioengineering6030076

Kirsch, M., Herder, A.-C., Boudot, C., Karau, A., Rach, J., Handke, W., et al. (2020). Xeno-free *in vitro* cultivation and osteogenic differentiation of hAD-MSCs on resorbable 3D printed RESOMER®. *Materials* 13:3399. doi: 10.3390/ma13153399

Kore-Grodzicki, B., Tauber-Finkelstein, M., Chain, D., and Shaltiel, S. (1988). Vitronectin is phosphorylated by a cAMP-dependent protein kinase released by activation of human platelets with thrombin. *Biochem. Biophys. Res. Commun.* 157, 1131–1138. doi: 10.1016/S0006-291X(88)80991-4

Lange, C., Cakiroglu, F., Spiess, A.-N., Cappallo-Obermann, H., Dierlamm, J., and Zander, A. R. (2007). Accelerated and safe expansion of human mesenchymal stromal cells in animal serum-free medium for transplantation and regenerative medicine. *J. Cell. Physiol.* 213, 18–26. doi: 10.1002/jcp.21081

Lauffenburger, D. A., and Horwitz, A. F. (1996). Cell migration: a physically integrated molecular process. *Cell* 84, 359–369. doi: 10.1016/s0092-8674(00)81280-5

Lavrentieva, A., Hoffmann, A., and Lee-Thedieck, C. (2020). Limited potential or unfavorable manipulations? *Strategies toward efficient mesenchymal stem/stromal cell applications. Front. Cell Dev. Biol.* 8:316. doi: 10.3389/fcell.2020.00316

Lee, J., Lilly, G. D., Doty, R. C., Podsiadlo, P., and Kotov, N. A. (2009). *In vitro* toxicity testing of nanoparticles in 3D cell culture. *Small* 5, 1213–1221. doi: 10.1002/smll.200801788

Lee, M.-S., Wang, J., Yuan, H., Jiao, H., Tsai, T.-L., Squire, M. W., et al. (2019). Endothelin-1 differentially directs lineage specification of adipose- and bone marrow-derived mesenchymal stem cells. *FASEB J.* 33, 996–1007. doi: 10.1096/fj.201800614R

Li, Z., and Cui, Z. (2014). Three-dimensional perfused cell culture. *Biotechnol. Adv.* 32, 243–254. doi: 10.1016/j.biotechadv.2013.10.006

Lindroos, B., Boucher, S., Chase, L., Kuokkanen, H., Huhtala, H., Haataja, R., et al. (2009). Serum-free, xeno-free culture media maintain the proliferation rate and multipotentiality of adipose stem cells *in vitro*. *Cytotherapy* 11, 958–972. doi: 10.3109/14653240903233081

Mannello, F., and Tonti, G. A. (2007). Concise review: no breakthroughs for human mesenchymal and embryonic stem cell culture: conditioned medium, feeder layer, or feeder-free; medium with fetal calf serum, human serum, or enriched plasma; serum-free, serum replacement nonconditioned medium, or ad hoc formula? *All that glitters is not gold! Stem Cells* 25, 1603–1609. doi: 10.1634/stemcells.2007-0127

Mark, K., von der, Gauss, V., Mark, H., von der, and Müller, P. (1977). Relationship between cell shape and type of collagen synthesised as chondrocytes lose their cartilage phenotype in culture. *Nature* 267, 531–532. doi: 10.1038/267531a0

Mavrina, L., Elstner, E., and Bundschuh, G. (1986). Uber die wirkung von thrombozytenlysat auf das proliferationsverhalten menschlicher knochenmarkzellen. *Biomed. Biochim. Acta* 45, 1007–1014.

Merceron, C., Portron, S., Masson, M., Lesoeur, J., Fellah, B. H., Gauthier, O., et al. (2011). The effect of two- and three-dimensional cell culture on the chondrogenic potential of human adipose-derived mesenchymal stem cells after subcutaneous transplantation with an injectable hydrogel. *Cell Transplant* 20, 1575–1588. doi: 10.3727/096368910X557191

Mishra, A., Tummala, P., King, A., Lee, B., Kraus, M., Tse, V., et al. (2009). Buffered platelet-rich plasma enhances mesenchymal stem cell proliferation and chondrogenic differentiation. *Tissue Eng C Methods* 15, 431–435. doi: 10.1089/ten.tec.2008.0534

Mojica-Henshaw, M. P., Jacobson, P., Morris, J., Kelley, L., Pierce, J., Boyer, M., et al. (2013). Serum-converted platelet lysate can substitute for fetal bovine serum in human mesenchymal stromal cell cultures. *Cytotherapy* 15, 1458–1468. doi: 10.1016/j.jcyt.2013.06.014

Monsanto, M. M., White, K. S., Kim, T., Wang, B. J., Fisher, K., Ilves, K., et al. (2017). Concurrent isolation of 3 distinct cardiac stem cell populations from a single human heart biopsy. *Circ. Res.* 121, 113–124. doi: 10.1161/CIRCRESAHA.116.310494

Moreira Teixeira, L. S., Leijten, J. C. H., Wennink, J. W. H., Chatterjea, A. G., Feijen, J., van Blitterswijk, C. A., et al. (2012). The effect of platelet lysate supplementation of a dextran-based hydrogel on cartilage formation. *Biomaterials* 33, 3651–3661. doi: 10.1016/j.biomaterials.2012.01.051

Motedayyen, H., Esmaeil, N., Tajik, N., Khadem, F., Ghotloo, S., Khani, B., et al. (2017). Method and key points for isolation of human amniotic epithelial cells with high yield, viability and purity. *BMC Res. Notes* 10:552. doi: 10.1186/s13104-017-2880-6

Müller, I., Kordowich, S., Holzwarth, C., Spano, C., Isensee, G., Staiber, A., et al. (2006). Animal serum-free culture conditions for isolation and expansion of multipotent mesenchymal stromal cells from human BM. *Cytotherapy* 8, 437–444. doi: 10.1080/14653240600920782

Papadimitropoulos, A., Piccinini, E., Brachat, S., Braccini, A., Wendt, D., Barbero, A., et al. (2014). Expansion of human mesenchymal stromal cells from fresh bone marrow in a 3D scaffold-based system under direct perfusion. *PLoS ONE* 9:e102359. doi: 10.1371/journal.pone.0102359

Park, J. S., Chu, J. S., Tsou, A. D., Diop, R., Tang, Z., Wang, A., et al. (2011). The effect of matrix stiffness on the differentiation of mesenchymal stem cells in response to TGF-β. *Biomaterials* 32, 3921–3930. doi: 10.1016/j.biomaterials.2011.02.019

Pepelanova, I., Kruppa, K., Scheper, T., and Lavrentieva, A. (2018). Gelatin-methacryloyl (GelMA) hydrogels with defined degree of functionalization as a versatile toolkit for 3D cell culture and extrusion bioprinting. *Bioengineering* 5:55. doi: 10.3390/bioengineering5030055

Pijuan-Galitó, S., Tamm, C., Schuster, J., Sobol, M., Forsberg, L., Merry, C. L. R., et al. (2016). Human serum-derived protein removes the need for coating in defined human pluripotent stem cell culture. *Nat. Commun.* 7:12170. doi: 10.1038/ncomms12170

Raic, A., Naolou, T., Mohra, A., Chatterjee, C., and Lee-Thedieck, C. (2019). 3D models of the bone marrow in health and disease: yesterday, today and tomorrow. *MRS Commun.* 9, 37–52. doi: 10.1557/mrc.2018.203

Rampichová, M., Buzgo, M., Míčková, A., Vocetková, K., Sovková, V., Lukášová, V., et al. (2017). Platelet-functionalized three-dimensional poly-ε-caprolactone fibrous scaffold prepared using centrifugal spinning for delivery of growth factors. *Int. J. Nanomed.* 12, 347–361. doi: 10.2147/IJN.S120206

Re, F., Sartore, L., Moulisova, V., Cantini, M., Almici, C., Bianchetti, A., et al. (2019). 3D gelatin-chitosan hybrid hydrogels combined with human platelet lysate highly support human mesenchymal stem cell proliferation and osteogenic differentiation. *J. Tissue Eng.* 10:2041731419845852. doi: 10.1177/2041731419845852

Ruedinger, F., Lavrentieva, A., Blume, C., Pepelanova, I., and Scheper, T. (2015). Hydrogels for 3D mammalian cell culture: a starting guide for laboratory practice. *Appl. Microbiol. Biotechnol.* 99, 623–636. doi: 10.1007/s00253-014-6253-y

Salzig, D., Leber, J., Merkewitz, K., Lange, M. C., Köster, N., and Czermak, P. (2016). Attachment, growth, and detachment of human mesenchymal stem cells in a chemically defined medium. *Stem Cells Int.* 2016:5246584. doi: 10.1155/2016/5246584

Sander, H. J., Slot, J. W., Bouma, B. N., Bolhuis, P. A., Pepper, D. S., and Sixma, J. J. (1983). Immunocytochemical localization of fibrinogen, platelet factor 4, and beta thromboglobulin in thin frozen sections of human blood platelets. *J. Clin. Invest.* 72, 1277–1287. doi: 10.1172/JCI111084

Santo, V. E., Duarte, A. R. C., Popa, E. G., Gomes, M. E., Mano, J. F., and Reis, R. L. (2012). Enhancement of osteogenic differentiation of human adipose derived stem cells by the controlled release of platelet lysates from hybrid scaffolds produced by supercritical fluid foaming. *J. Control. Release* 162, 19–27. doi: 10.1016/j.jconrel.2012.06.001

Santos, S. C., Custódio, C. A., and Mano, J. F. (2018). Photopolymerizable platelet lysate hydrogels for customizable 3D cell culture platforms. *Adv. Healthc. Mater.* 7:e1800849. doi: 10.1002/adhm.201800849

Sart, S., Tsai, A.-C., Li, Y., and Ma, T. (2014). Three-dimensional aggregates of mesenchymal stem cells: cellular mechanisms, biological properties, and applications. *Tissue Eng. B Rev.* 20, 365–380. doi: 10.1089/ten.TEB.2013.0537

Schallmoser, K., Bartmann, C., Rohde, E., Reinisch, A., Kashofer, K., Stadelmeyer, E., et al. (2007). Human platelet lysate can replace fetal bovine serum for clinical-scale expansion of functional mesenchymal stromal cells. *Transfusion* 47, 1436–1446. doi: 10.1111/j.1537-2995.2007.01220.x

Schallmoser, K., and Strunk, D. (2013). Generation of a pool of human platelet lysate and efficient use in cell culture. *Methods Mol. Biol.* 946, 349–362. doi: 10.1007/978-1-62703-128-8_22

Schmeichel, K. L., and Bissell, M. J. (2003). Modeling tissue-specific signaling and organ function in three dimensions. *J. Cell Sci.* 116, 2377–2388. doi: 10.1242/jcs.00503

Schrödel, A. (2007). Die rolle des fetalen kälberserums in zellkulturmedien. *Biol. Unserer Zeit* 37:289. doi: 10.1002/biuz.200790079

Shih, D. T.-B., and Burnouf, T. (2015). Preparation, quality criteria, and properties of human blood platelet lysate supplements for *ex vivo* stem cell expansion. *N. Biotechnol.* 32, 199–211. doi: 10.1016/j.nbt.2014.06.001

Shih, D. T.-B., Chen, J.-C., Chen, W.-Y., Kuo, Y.-P., Su, C.-Y., and Burnouf, T. (2011). Expansion of adipose tissue mesenchymal stromal progenitors in serum-free medium supplemented with virally inactivated allogeneic human platelet lysate. *Transfusion* 51, 770–778. doi: 10.1111/j.1537-2995.2010.02915.x

Siciliano, C., Ibrahim, M., Scafetta, G., Napoletano, C., Mangino, G., Pierelli, L., et al. (2015). Optimization of the isolation and expansion method of human mediastinal-adipose tissue derived mesenchymal stem cells with virally inactivated GMP-grade platelet lysate. *Cytotechnology* 67, 165–174. doi: 10.1007/s10616-013-9667-y

Simaria, A. S., Hassan, S., Varadaraju, H., Rowley, J., Warren, K., Vanek, P., et al. (2014). Allogeneic cell therapy bioprocess economics and optimization: single-use cell expansion technologies. *Biotechnol. Bioeng.* 111, 69–83. doi: 10.1002/bit.25008

Solon, J., Levental, I., Sengupta, K., Georges, P. C., and Janmey, P. A. (2007). Fibroblast adaptation and stiffness matching to soft elastic substrates. *Biophys. J.* 93, 4453–4461. doi: 10.1529/biophysj.106.101386

Spees, J. L., Lee, R. H., and Gregory, C. A. (2016). Mechanisms of mesenchymal stem/stromal cell function. *Stem Cell Res. Ther.* 7:125. doi: 10.1186/s13287-016-0363-7

Sun, M., Chi, G., Li, P., Lv, S., Xu, J., Xu, Z., et al. (2018). Effects of matrix stiffness on the morphology, adhesion, proliferation and osteogenic differentiation of mesenchymal stem cells. *Int. J. Med. Sci.* 15, 257–268. doi: 10.7150/ijms.21620

Trappmann, B., Gautrot, J. E., Connelly, J. T., Strange, D. G. T., Li, Y., Oyen, M. L., et al. (2012). Extracellular-matrix tethering regulates stem-cell fate. *Nat. Mater.* 11, 642–649. doi: 10.1038/nmat3339

Wagner, M., Yoshihara, M., Douagi, I., Damdimopoulos, A., Panula, S., Petropoulos, S., et al. (2020). Single-cell analysis of human ovarian cortex identifies distinct cell populations but no oogonial stem cells. *Nat. Commun.* 11:1147. doi: 10.1038/s41467-020-14936-3

Walenda, G., Hemeda, H., Schneider, R. K., Merkel, R., Hoffmann, B., and Wagner, W. (2012). Human platelet lysate gel provides a novel three dimensional-matrix for enhanced culture expansion of mesenchymal stromal cells. *Tissue Eng. C Methods* 18, 924–934. doi: 10.1089/ten.tec.2011.0541

Wang, X., Hu, X., Dulińska-Molak, I., Kawazoe, N., Yang, Y., and Chen, G. (2016). Discriminating the independent influence of cell adhesion and spreading area on stem cell fate determination using micropatterned surfaces. *Sci. Rep.* 6:28708. doi: 10.1038/srep28708

Wencel-Drake, J. D., Painter, R. G., Zimmerman, T. S., and Ginsberg, M. H. (1985). Ultrastructural localization of human platelet thrombospondin, fibrinogen, fibronectin, and von willebrand factor in frozen thin section. *Blood* 65, 929–938.

Wu, X., Kang, H., Liu, X., Gao, J., Zhao, K., and Ma, Z. (2016). Serum and xeno-free, chemically defined, no-plate-coating-based culture system for mesenchymal stromal cells from the umbilical cord. *Cell Prolif.* 49, 579–588. doi: 10.1111/cpr.12279

Xie, X., Wang, Y., Zhao, C., Guo, S., Liu, S., Jia, W., et al. (2012). Comparative evaluation of MSCs from bone marrow and adipose tissue seeded in PRP-derived scaffold for cartilage regeneration. *Biomaterials* 33, 7008–7018. doi: 10.1016/j.biomaterials.2012.06.058

Yang, Y., Wang, X., Wang, Y., Hu, X., Kawazoe, N., Yang, Y., et al. (2019). Influence of cell spreading area on the osteogenic commitment and phenotype maintenance of mesenchymal stem cells. *Sci. Rep.* 9:6891. doi: 10.1038/s41598-019-43362-9

Conflict of Interest: The authors declare that the research was conducted in the absence of any commercial or financial relationships that could be construed as a potential conflict of interest.

frontiers in Bioengineering and Biotechnology

ORIGINAL RESEARCH
published: 21 January 2021
doi: 10.3389/fbioe.2020.613621

Scalable Production of Equine Platelet Lysate for Multipotent Mesenchymal Stromal Cell Culture

*A. Hagen[1], H. Lehmann[2], S. Aurich[3], N. Bauer[4], M. Melzer[1], J. Moellerberndt[1], V. Patané[4], C. L. Schnabel[5] and J. Burk[1]**

[1] Equine Clinic (Surgery, Orthopedics), Justus-Liebig-University Giessen, Giessen, Germany, [2] Department of Veterinary Clinical Sciences, Small Animal Clinic, Justus-Liebig-University Giessen, Giessen, Germany, [3] Institute of Hygiene and Infectious Diseases of Animals, Justus-Liebig-University Giessen, Giessen, Germany, [4] Department of Veterinary Clinical Sciences, Clinical Pathology and Clinical Pathophysiology, Justus-Liebig-University Giessen, Giessen, Germany, [5] Faculty of Veterinary Medicine, Institute of Immunology, Leipzig University, Leipzig, Germany

Translation of multipotent mesenchymal stromal cell (MSC)-based therapies is advancing in human and veterinary medicine. One critical issue is the *in vitro* culture of MSC before clinical use. Using fetal bovine serum (FBS) as supplement to the basal medium is still the gold standard for cultivation of many cell types including equine MSC. Alternatives are being explored, with substantial success using platelet lysate-supplemented media for human MSC. However, progress lags behind in the veterinary field. The aim of this study was to establish a scalable protocol for equine platelet lysate (ePL) production and to test the ePL in equine MSC culture. Whole blood was harvested into blood collection bags from 20 healthy horses. After checking sample materials for pathogen contamination, samples from 19 animals were included. Platelet concentrates were prepared using a buffy coat method. Platelets, platelet-derived growth factor BB, and transforming growth factor β1 concentrations were increased in the concentrates compared with whole blood or serum ($p < 0.05$), while white blood cells were reduced ($p < 0.05$). The concentrates were lysed using freeze/thaw cycles, which eliminated the cells while growth factor concentrations were maintained. Donor age negatively correlated with platelet and growth factor concentrations after processing ($p < 0.05$). Finally, all lysates were pooled and the ePL was evaluated as culture medium supplement in comparison with FBS, using adipose-derived MSC from four unrelated donor horses. MSC proliferated well in 10% FBS as well as in 10% ePL. However, using 5 or 2.5% ePL entailed highly inconsistent proliferation or loss of proliferation, with significant differences in generation times and confluencies ($p < 0.05$). MSC expressed the surface antigens CD90, CD44, and CD29, but CD73 and CD105 detection was low in all culture media. Adipogenic and osteogenic differentiation led to similar results in MSC from different culture media. The buffy coat method is useful to produce equine platelet concentrate with increased platelet and reduced white blood cell content in large scales. The ePL obtained supports MSC expansion similar as FBS when used at the same concentration (10%). Further investigations into equine MSC functionality in culture with ePL should follow.

Keywords: mesenchymal stromal cells, platelet concentrate, platelet lysate, fetal bovine serum, equine, cell culture

OPEN ACCESS

Edited by:
Dominik Egger,
University of Natural Resources and Life Sciences Vienna, Austria

Reviewed by:
Thierry Burnouf,
Taipei Medical University, Taiwan
Olafur Eysteinn Sigurjonsson,
Reykjavík University, Iceland

****Correspondence:***
J. Burk
janina.burk@vetmed.uni-giessen.de

Specialty section:
This article was submitted to Preclinical Cell and Gene Therapy, a section of the journal Frontiers in Bioengineering and Biotechnology

Received: *02 October 2020*
Accepted: *16 December 2020*
Published: *21 January 2021*

Citation:
Hagen A, Lehmann H, Aurich S, Bauer N, Melzer M, Moellerberndt J, Patané V, Schnabel CL and Burk J (2021) Scalable Production of Equine Platelet Lysate for Multipotent Mesenchymal Stromal Cell Culture. Front. Bioeng. Biotechnol. 8:613621. doi: 10.3389/fbioe.2020.613621

INTRODUCTION

Cell-based therapies are promising tools for regenerative treatment of human and animal diseases. While some approaches have already been successfully implemented in clinical practice, most are still in developmental stages. In horses, particularly treatment of orthopedic conditions with multipotent mesenchymal stromal cells (MSC) has a well-documented history (Smith, 2003; Pacini et al., 2007; Godwin et al., 2012; Renzi et al., 2013; Schauwer et al., 2013; Ferris et al., 2014; Mariñas-Pardo et al., 2018; Broeckx et al., 2019). One current challenge in the development of successful cell-based products, irrespective of the target species, is the implementation of manufacturing processes that comply with legal regulations and maintain cellular potency. As most research focuses on cell therapies for human patients, it remains particularly challenging to adopt suitable procedures for cells derived from large animal species. However, this is crucial with respect to the treatment of companion animals as well as for the use of large animal species in translational studies. Both, clinical application and translational aspects apply to the equine species.

The cell culture medium is a critical element in cell manufacturing processes and may strongly impact on cell quality and efficacy of therapies. To supply the cells with hormones, nutrients, and growth factors, the supplementation of basal medium with fetal bovine serum (FBS) is still the gold standard for *in vitro* culture of many cell types, including equine MSC (Doucet et al., 2005; van der Valk et al., 2010; Bieback, 2013; Burnouf et al., 2016). However, the use of FBS is afflicted with several problems, including an expected shortage of supply (Jayme et al., 1988; Jochems et al., 2002), the ethically critical harvesting procedures (Hodgson, 1995; Jochems et al., 2002; van der Valk et al., 2004), inconsistent quality (Gstraunthaler, 2003; Zheng et al., 2006; Baker, 2016), and its xenogeneic use with the possibility of recipient immune reactions (Sundin et al., 2007; Bieback, 2013) and transmission of bovine pathogens (Erickson et al., 1991; World Health Organization, 2006; Hawkes, 2015). For these reasons, efforts should be made to reduce or replace the use of FBS. In this line, both the European Medicines Agency (EMA) (European Medicines Agency, London, 2013) and the International Society for Cellular Therapy (ISCT) (Karnieli et al., 2017) have recommended the control of quality and safety of FBS and if possible, its replacement. Several alternatives to using FBS have been explored, with most encouraging results using chemically defined/serum-free or platelet lysate (PL)-supplemented media.

For human MSC, commercially available serum-free culture media were developed. However, when investigating the applicability of such serum-free media in equine adipose-derived MSC, we observed differences in morphology and expression of the surface marker CD90, as well as increased aggregation and spontaneous detachment of these MSC (Schubert et al., 2018). These results underlined that culture condition requirements are species-specific with regard to nutrient and growth factor supplementation. Consequently, the use of commercially available serum-free media for large animal MSC is not a consummate approach.

Production and use of human PL (hPL) for MSC cultivation was first reported in 2005 (Doucet et al., 2005). Platelets (PLT) exhibit an important role not only in primary hemostasis but also in wound healing and tissue regeneration. Their α-granules are rich in chemokines and growth factors, such as platelet-derived growth factor (PDGF), basic fibroblast growth factor (bFGF), insulin-like growth factor (IGF), transforming growth factor-β (TGF-β), vascular endothelial growth factor (VEGF), epidermal growth factor (EGF), adhesion factors, and enzymes (Blair and Flaumenhaft, 2009; Schallmoser et al., 2009; Astori et al., 2016; Burnouf et al., 2016). When released upon PLT activation, these factors support cell proliferation and recruitment (Golebiewska and Poole, 2015). Therefore, PL was considered as a suitable acellular culture media supplement. By now, several studies have shown that hPL is better suited for human MSC expansion than FBS (Blande et al., 2009; Mojica-Henshaw et al., 2013; Mohammadi et al., 2016; Becherucci et al., 2018; Schallmoser et al., 2020), and that the MSC cultured with hPL fulfill the definition criteria recommended by the International Society for Cellular Therapy (ISCT) in 2006 (Dominici et al., 2006; Mojica-Henshaw et al., 2013; Becherucci et al., 2018). Interestingly, it was reported that hPL already replaces FBS in 77% of the good manufacturing practice protocols for MSC production in human medicine (Trento et al., 2018), demonstrating significant progress.

In order to follow this development, first studies have already been carried out with equine PL (ePL) for equine MSC cultivation (Del Bue et al., 2007; Seo et al., 2013; Russell and Koch, 2016; Gilbertie et al., 2018; Naskou et al., 2018; Yaneselli et al., 2019). The equine MSC cultured with ePL showed similar proliferation rates, a fibroblast-like morphology, trilineage differentiation, and improved viability compared with FBS-supplemented cultures (Seo et al., 2013; Naskou et al., 2018) and maintained their immunomodulatory properties (Naskou et al., 2018; Yaneselli et al., 2019). Thus, based on the current state of knowledge, ePL is a promising alternative to FBS for the cultivation of equine MSC. However, in contrast to human blood products, availability of ePL is very limited, entailing the necessity of in-house production. So far, published ePL production procedures mainly include platelet-rich-plasma-based methods in small-scale syringe format (Del Bue et al., 2007; Seo et al., 2013; Russell and Koch, 2016; Gilbertie et al., 2018; Yaneselli et al., 2019) and a plateletpheresis-based method (Naskou et al., 2018), which is scalable but requires specialized equipment. Hence, the procedures used by different laboratories comprise highly distinct approaches, limiting the comparability between studies.

The aim of this study was to provide an ePL production protocol which does not rely on specialized equipment, could easily be adopted by other laboratories, and is scalable to production of large batches. For this purpose, we evaluated a procedure based on the most commonly used techniques in human medicine (Burnouf et al., 2016), a buffy coat-based method to obtain PLT concentrate, followed by repeated freeze/thaw cycles for PLT lysis. In a second step, we tested the obtained ePL in comparison with FBS for its suitability for MSC culture.

MATERIALS AND METHODS

Blood Collection

Whole blood for ePL preparation was collected over a period of 2 months from 20 healthy warmblood horses of similar breeds (5 geldings, 14 mares, and 1 stallion) aged 4–15 years (median: 9 years; interquartile range (IQR): 6) after approval by the local regulatory authority (i.e., regional council Giessen, A14/2019). These donor horses had not received any medication in the last 2 weeks as confirmed by their owners. Furthermore, their health status was evaluated by clinical examination and blood tests comprising complete blood counts with ethylenediaminetetraacetic acid (EDTA) whole blood, blood chemistry with Li-heparin blood and serum, as well as microbiological and virological analyses as specified below.

The whole blood was obtained aseptically from the jugular vein. One milliliter lidocaine hydrochloride 2% was administered subcutaneously at the venipuncture site. A permanent venous catheter (12 G) was inserted in cranial direction and fixed with non-resorbable sutures. First, blood samples were collected into tubes for the blood tests specified above, as well as for an erythrocyte sedimentation rate test.

A total of 2 L whole blood was then collected into four 600 ml commercial blood bags loaded with 70 ml citrate-phosphate-dextrose (CPD; Composelect, Fresenius Kabi, Bad Homburg, Germany) (500 ml whole blood in each), which had been connected via a four-way connector (LS-four-way-connector, B. Braun, Melsungen, Germany) using a sterile tube welder (Compodock, Fresenius Kabi). A blood donation scale (MW5001 electronic, Biotrans GmbH, Dreieich, Germany) was used to standardize the filling volume of the blood bags. After the blood collection was completed, the samples were placed in a CompoCool®Box (Fresenius Kabi) containing butane-1,4-diol cooling plates to cool the whole blood to 20°C within a short time and to improve temperature uniformity. The blood was left there for at least 2 h and a maximum of 3 h until processing in the laboratory. Three of the four blood bag samples per horse were processed as described in the following.

Platelet Concentrate and Lysate Preparation

The blood bags were centrifuged at 711 × *g* for 20 min using a commercial centrifuge designed for blood separation (Hettich Rotanta 460R, Andreas Hettich GmbH & Co.KG, Tuttlingen, Germany) with acceleration settings of 1, deceleration settings of 0, at 22°C, for blood component separation. The buffy coat was recovered by separating the plasma, and the erythrocyte concentrate by a top-bottom method with a blood-separating device (Optipress® II; Fenwal, Baxter S.A., Maurepas, France). The buffy coat was left to rest for 1 h, then 70 ml plasma were added again for resuspension. The resuspended buffy coat was then centrifuged at 159 × *g* for 10 min, acceleration 1, deceleration 0, at 22°C, in the same centrifuge. After that, the resulting supernatant, corresponding to the concentrate, was separated using a manual press (NPBI Holland) (**Figure 1**).

The concentrates from the three separate blood collection bags from each horse were then pooled in transfer bags (R6R2021, Compoflex, Fresenius Kabi) to obtain one bag of concentrate per horse, referred to as "concentrate pooled," and frozen at −80°C. In order to lyse the PLT, three freeze/thaw cycles were performed, in which the PLT concentrate was thawed at 37°C in a dry heating device designed to thaw frozen products intended for infusion under continuous agitation (Plasmatherm, Barkey GmbH &CO.KG, Leopoldshoehe, Germany) for 4 h and then frozen again at −80°C for 20 h. Afterwards, the bags were centrifuged at 4,000 × *g* for 30 min, acceleration 9, deceleration 2, in the same centrifuge described above. The supernatant, corresponding to the lysate, was filtered *via* gravity using Macopharma Plas4 filters (Lot 11290588BM, Macopharma, Langen, Germany) for cell debris removal. The PLT lysate from each donor was stored at −80°C, until the lysate units from all suitable horses ($n = 19$) were pooled under aseptic conditions (**Figure 1**). The lysate from the remaining horse was not included due to a positive herpes virus finding.

Microbiological and Virological Assessment

Absence of pathogens was confirmed in blood samples from the individual animals as well as in the final pooled ePL before its use in cell culture. This comprised a bacteriological analysis with Oxoid signal blood culture system (BC0100M, Oxoid Limited, Hampshire, England), incubated at 37°C for 7 days. On days 1, 2, 4, and 6, the cultured blood was streaked on blood agar (Blood Agar Base, Oxoid, Wesel, Germany) containing 5% defibrinated sheep blood and on water-blue metachrome-yellow lactose agar (Water-blue Metachrome-yellow Lactose Agar acc. to Gassner, sifin diagnostics, Berlin, Germany). The plates were incubated under aerobic conditions at 37°C for 48 h. Additionally, Brain-Heart-Infusion agar (Brain Heart Infusion Agar, Oxoid) was incubated under microaerobic conditions (10% CO_2, 37°C) and analyzed after 24 and 48 h. Schaedler agar (BBL™ Schaedler Agar, Becton Dickinson GmbH, Heidelberg, Germany) and Columbia agar (Columbia Agar (base), E. Merck, Darmstadt, Germany) were incubated at 37°C for 72 h under anaerobic conditions in a jar using AnaeroGen™ gas sachets (AnaeroGen™ 2.5L, Oxoid). For selective culturing of fungi, Kimmig agar (Agar for fungi (base) acc. to Kimmig modified, E. Merck) was incubated for 72 h at 28°C under aerobic conditions. Lastly, a 16S ribosomal RNA gene polymerase chain reaction analysis for mycoplamas (van Kuppeveld et al., 1992) was performed. In addition, a virological examination for equine herpes virus 1 and 4 (virus genome detection), equine arteritis virus (antibody detection by serum neutralization test), equine infectious anemia virus (antibody detection), and virus cultivation in cell culture was commissioned.

Platelet and Leukocyte Counts

Complete blood counts were obtained from samples harvested at different processing stages using an automated flow cytometric hematology analyzer (ADVIA 2120i, Siemens Healthcare GmbH, Erlangen, Germany) with Multispecies software MS 5.9. This included EDTA blood samples, citrated whole blood samples from each blood collection bag before further processing, plasma samples from each collection bag, concentrate samples from each

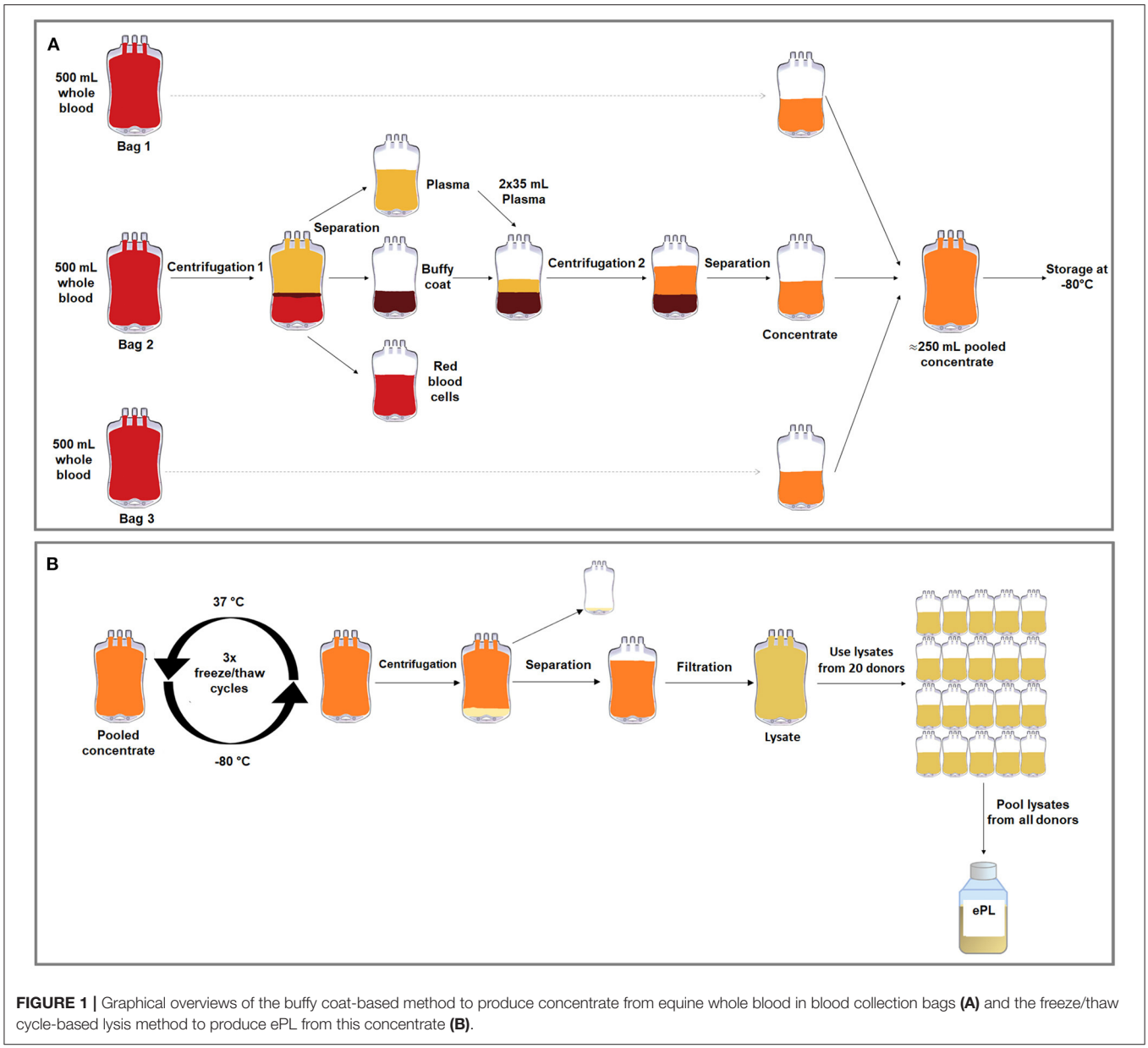

FIGURE 1 | Graphical overviews of the buffy coat-based method to produce concentrate from equine whole blood in blood collection bags **(A)** and the freeze/thaw cycle-based lysis method to produce ePL from this concentrate **(B)**.

collection bag, pooled concentrate from each animal, lysate from each animal, and the final ePL pooled from all horses.

Growth Factor Quantification and Chemical Analyses

Growth factor concentrations were analyzed in serum, plasma, pooled concentrate, and lysate from each horse, as well as in the final pooled ePL. All samples including the concentrates had been stored at −80°C before the growth factors were measured. For comparison, the same growth factors were also measured in the FBS which was used as standard cell culture medium supplement. Specifically, platelet-derived growth factor (PDGF-BB) and transforming growth factor beta 1 (TGF-β1) were quantified using the respective Quantikine ELISA kits (catalog numbers #DBB00 and #DB100B, R&D Systems, Minneapolis, MN, USA), which have been used for equine samples in previous studies (Anderson et al., 1998; Desjardins et al., 2004; Donnelly et al., 2006; Boswell et al., 2014; McClain and McCarrel, 2019). Procedures were performed according to the product manuals, which included TGF-β1 activation with hydrochloric acid, and samples were analyzed using an Infinite F50 (Tecan) plate reader and the corresponding Magellan software (Tecan Ltd., Maennedorf, Switzerland).

Furthermore, in the same samples, according to the chemical quality analysis of FBS, electrolyte and total protein analyses were performed using a blood gas and electrolyte analyzer (Cobas b 123 POC system, Roche Diagnostics GmbH, Mannheim, Germany). The total protein and albumin content

was determined using a clinical chemistry analyzer C400 (Pentra C400 Option I.S.E, HORIBA ABX SAS, Montpellier, France).

MSC Culture With FBS and ePL Media Supplements

The final pooled ePL was evaluated as cell culture supplement for equine adipose-derived MSC, in comparison with FBS. Adipose-derived MSC had been harvested from four healthy standard-bred horses (three geldings, one stallion) aged 5–9 years (median: 8 years; IQR: 1) in the framework of an unrelated previous study as approved by the respective local authority (Landesdirektion Leipzig, TV34/13). MSC had been isolated by collagenase digestion and expanded in FBS-supplemented culture medium until cryopreservation. The cells were thawed and seeded in Dulbecco's modified Eagle's medium (1 g/L glucose; Gibco®, ThermoFisher Scientific, Darmstadt, Germany) supplemented with either 10% FBS (Lot: 2078409, Gibco®, ThermoFisher Scientific) or 10, 5, and 2.5% ePL, 1% penicillin-streptomycin, and 0.1% gentamycin. When using ePL, 1 U/ml heparin-natrium (B. Braun, Melsungen, Germany) was additionally added to the culture medium. MSC were then cultured under standard conditions (humidified atmosphere, 37°C, 5% CO_2) for at least one passage prior to any experiment to allow for possible adaptations to the respective culture media. All experiments were performed using the MSC from all donor horses and except for the flow cytometry experiments, mean values from technical replicates were used for further statistical analyses.

Cell Proliferation and Viability Assays

For estimation of the generation time, population doublings in passages 2 and 3 were evaluated. MSC were seeded at a density of 3,000 cells/cm^2 and incubated for 5 days, with a medium change after 3 days. Phase-contrast photomicrographs were obtained at standardized settings using a Nikon Eclipse Ts2-FL microscope with a DS-Fi3 camera (Nikon GmbH, Duesseldorf, Germany) at day 5 before passaging. Cells were then trypsinized and counted using a hemocytometer and trypan blue for exclusion of dead cells. The generation times were calculated using the following formula:

$$\text{Generation time} = \frac{\text{days in culture}}{\frac{\ln\left(\frac{\text{cell count harvest}}{\text{cell count seeding}}\right)}{\ln 2}}$$

Using Fiji ImageJ software, the images obtained before passaging were uniformly enhanced in contrast, a background subtraction was done and images were binarized, with adapted thresholds for each image, and the confluent area within each image was measured. In addition, MSC metabolic activity was measured at day 1 and 5 using a tetrazolium compound (MTS) assay according to the manufacturer's instructions (CellTiter 96® AQueous One Solution Cell Proliferation Assay, Promega, Mannheim, Germany). The mean absorbance at day 5 was divided by the mean absorbance at day 1 as an indicator for metabolic activity.

Immunophenotyping

Immunophenotypic analyses were performed in passage 3 MSC to assess the presence of inclusion and exclusion marker antigens recommended for MSC characterization, based on procedures established previously for equine MSC (Paebst et al., 2014). Briefly, MSC were analyzed by flow cytometry for CD29, CD44, CD73, CD90, and CD105, as well as for CD14, CD34, CD45, CD79α, and MHC-II. First, MSC were detached in ice-cold 0.01 M EDTA using cell scrapers to prevent loss of surface molecules due to enzymatic detachment. Next, cells were successively incubated with fixable viability dye (1:1,000; eBioscience™ Fixable Viability Dye eFluor™ 780, ThermoFisher Scientific) for 20 min, the respective blocking sera (15% goat serum for CD73 staining and 5% mouse or rat serum for all other stainings, all Sigma-Aldrich, Taufkirchen, Germany), followed by the antibodies detailed in **Table 1**. Incubation steps were performed protected from light for 15 min at 4°C, with interjacent washing steps in staining buffer (phosphate-buffered saline (PBS) supplemented with 0.01% sodium azide and 10% FBS). Finally, all cells were fixed in 2% paraformaldehyde, washed with PBS, and stored in staining buffer overnight at 4°C. For CD79α staining, fixation and permeabilization solutions (BD Cytofix/Cytoperm™, BD Biosciences, Franklin Lakes, NJ) were used according to the manufacturer's instructions. Flow cytometric measurements of a minimum of 20,000 events per sample were performed on an LSR Fortessa II (BD) equipped with FACS Diva 6.2 software (BD). Data was analyzed using FlowJo™ v10.7 software (FlowJo, LLC, BD Biosciences, Ashland, OR, USA). Live MSC were gated as large cells after duplet exclusion and marker expression gates were set based on the corresponding isotype-, secondary antibody- or conjugate controls.

Trilineage Differentiation

The *in vitro* differentiation assays were performed in passage 2 MSC cultured in 10% FBS, 10% ePL, or 2.5% ePL. The MSC differentiation assay was not performed with 5% ePL, as previous approaches had already shown a tendency for a higher ePL concentration to be more potent and therefore the differentiation was only conducted with one low ePL concentration (2.5%).

For adipogenic differentiation, MSCs were seeded at 1,500 cells/cm^2 and incubated for 3 days under standard culture conditions. Then, standard medium was replaced by StemPro™ adipogenic differentiation medium (catalog number A1007001, Gibco®, ThermoFisher Scientific) with 0.1% gentamycin and 5% rabbit serum. After 7 days of incubation, samples were fixed with 50% ethanol for 20 min and stained with Oil Red O and hematoxylin counterstain. The intensity of adipogenic differentiation was assessed by two blinded observers using a scoring system based on the percentage of differentiated cells and the size and arrangement of lipid droplets in these cells, as previously described (Gittel et al., 2013).

For osteogenic differentiation, MSC were seeded at 1,000 cells/cm^2 and incubated for 3 days under standard culture conditions. Then, standard medium was replaced by StemPro™ osteogenic differentiation medium (catalog number A1007201, Gibco®, ThermoFisher Scientific) with 0.1% gentamycin.

TABLE 1 | Antibodies used for immunophenotyping.

Subset	Antibody	Host species, isotype	Clone	Reactivity	Company	References	Dilution
I	CD29-A488	Mouse IgG1	TS2/16	Anti-human	Biolegend, San Diego, CA	Schauwer et al. (2012) and Paebst et al. (2014)	1:20
I	CD44-APC	Rat IgG2b	IM7	Anti-mouse	BD, Franklin Lakes, NJ	Schauwer et al. (2012) and Paebst et al. (2014)	1:100
IV	CD73	Mouse IgG1	10f1	Anti-human	Abcam, Cambridge, UK	Schauwer et al. (2012) and Paebst et al. (2014)	1:5
III	CD90-APC	Mouse IgG1	5E10	Anti-human	BD, Franklin Lakes, NJ	Hillmann et al. (2016)	1:100
II	CD105-PE	Mouse IgG1	SN6	Anti-human	Bio-Rad, Hercules, CA/ Serotec, Kidlington, UK	Schauwer et al. (2012) and Paebst et al. (2014)	1:10
II	CD14-APC	Mouse IgG1	134620	Anti-human	R&D, Minneapolis, MN	Braun et al. (2010) and Paebst et al. (2014)	1:50
V	CD14 biotinylated	Mouse IgG1	105	Anti-equine	Cornell University, Dr. Bettina Wagner	Kabithe et al. (2010)	1:1,500
III	CD34-FITC	Mouse IgG3	43A1	Anti-human	AdipoGen Lifesciences, San Diego, CA	Paebst et al. (2014)	1:25
II	CD45-A488	Mouse IgG2a	F10-89-4	Anti-human	Bio-Rad, Hercules, CA/ Serotec, Kidlington, UK	Schauwer et al. (2012) and Paebst et al. (2014)	1:5
VI	CD79α-PE	Mouse IgG1	HM57	Anti-human	Bio-Rad, Hercules, CA/ Serotec, Kidlington, UK	Schauwer et al. (2012) and Paebst et al. (2014)	1:50
I	MHCII (equine), PE	Mouse IgG1	CVS20	Anti-equine	Bio-Rad, Hercules, CA/ Serotec, Kidlington, UK	Kydd et al. (1994) and Lunn et al. (1998), Schauwer et al. (2012), and Paebst et al. (2014)	1:25
IV	Goat anti-mouse Ig3, FITC	Polyclonal IgG		Anti-mouse	Santa Cruz Biotechnology, Dallas, Texas		1:100
V	SAV-APC	APC streptavidin			Biolegend, San Diego, CA		1:250

Isotyp control	Corresponding antibody	Host species	Company	Dilution
IgG1κ, A488	CD29	Mouse	Biolegend, San Diego, CA	1:20
IgG2bκ, APC	CD44	Rat	Biolegend, San Diego, CA	1:100
IgG2aκ, APC	CD90	Mouse	Biolegend, San Diego, CA	1:100
IgG1κ, PE	CD105	Mouse	Biolegend, San Diego, CA	1:10
IgG1κ, APC	CD14 (Clone:134620)	Mouse	Biolegend, San Diego, CA	1:50
IgG3κ, FITC	CD34	Mouse	Biolegend, San Diego, CA	1:25
IgG2aκ, A488	CD45	Mouse	Biolegend, San Diego, CA	1:5
IgG1κ, PE	CD79α	Mouse	Biolegend, San Diego, CA	1:50
IgG1κ, PE	MHCII	Mouse	Biolegend, San Diego, CA	1:50

This medium was changed twice weekly for 21 days of incubation. Cells were fixed with 4% paraformaldehyde for 10 min and von Kossa staining was performed to detect extracellular mineralization. Bright field photomicrographs were obtained, and mean grayscale values were extracted using Fiji ImageJ software.

Chondrogenic differentiation of MSC was performed in pellet culture with 500,000 cells per pellet. MSC were washed in PBS before StemPro™ chondrogenic differentiation medium (catalog number A1007101, Gibco®, ThermoFisher Scientific), and 0.1% gentamycin were added, and then centrifuged at 280 × *g* at 4°C for 5 min to form a cell pellet. Medium was changed twice a week until day 21. Pellets were fixed with 4% paraformaldehyde for 12 h, paraffin sections prepared and stained with Alcian blue and Masson's Trichrome. Samples were evaluated by two blinded observers, based on the Grogan score (Grogan et al., 2006) adapted to the stainings used in the current study (**Supplementary File 1**). In addition, bright field photomicrographs were analyzed using Fiji ImageJ software (Ruifrok and Johnston, 2001). This included color deconvolution and binarization of the resulting images, followed by the measurement of the percentage areas stained with the respective staining component. Results are presented as ratios of cartilaginous matrix staining and counterstaining (i.e., turquoise to purple staining for Alcian blue and blueish to red staining for Masson's trichrome).

Statistical Analysis

Statistical analyses and graphical presentation of data were performed using IBM SPSS Statistics 26 and GraphPad Prism 8.4.3. Data obtained during blood processing ($n = 19$) are presented as median and 95% confidence interval. These data

were additionally categorized based on donor age [4–9 years ($n = 11$) and 10–15 years ($n = 8$)] and sex [female ($n = 13$) and male ($n = 6$)] for comparisons between these groups. Data from the cell culture experiments ($n = 4$) are presented as scatter plots with median and interquartile range. Correlation between parameters was evaluated based on Spearman's rank correlation, and comparisons between related samples were performed using non-parametric tests for paired samples (Friedman tests with Wilcoxon *post-hoc* tests and Bonferroni correction for multiple testing). For age and sex group comparisons, Mann-Whitney *U*-tests were computed. Differences were considered significant at $p < 0.05$.

RESULTS

Platelet Lysate Preparation

Absence of Pathogen Contamination

No microbiological contamination was evident in the blood samples from the donors or in the final pooled ePL. However, one donor animal tested positive for herpes viridae. Consequently, the ePL obtained from this horse was not included in the final product and data obtained were excluded from all analyses.

Platelet Concentration and WBC Removal

A medium whole blood volume of 504.9 ml (IQR: 25.7) yielded a medium concentrate volume of 86.2 ml (IQR: 7.1) per collected blood bag, with recovery rates of 70.2% (IQR: 19.3) of the total processed PLT and 6.3% (IQR: 2.6) of the total processed WBC. As compared with the whole blood, the obtained PLT concentrates had 4.2-fold increased PLT concentrations and 0.4-fold decreased WBC concentrations ($p < 0.01$ and $p < 0.05$, respectively). The remaining plasma showed low PLT concentrations and very low WBC concentrations ($p < 0.01$ compared with whole blood and concentrate). After lysis of the concentrates, PLT and WBC counts in the lysates were neglectable (**Figure 2**).

Whole blood and concentrate PLT concentrations correlated strongly ($p < 0.001$ and $r = 0.743$). A moderate correlation was also observed between the respective WBC concentrations ($p < 0.05$ and $r = 0.564$). Furthermore, recovery rates of PLT and WBC were correlated ($p < 0.01$ and $r = 0.617$) (**Figure 2**).

Growth Factor Concentration and Chemical Analyses

After storage at −80°C, growth factor concentrations were higher in the PLT concentrates ($p > 0.05$ for PDGF-BB and $p < 0.01$ for TGF-β1) as well as in the lysates ($p < 0.01$ for PDGF-BB and $p < 0.05$ for TGF-β1), as compared with the corresponding serum. The plasma showed very low growth factor concentrations ($p \leq 0.01$ for all comparisons, except for serum vs. plasma TGF-β1) (**Figure 3**), corresponding to its low PLT content.

Platelet concentrations in the concentrates showed moderate to strong correlations with the growth factor concentrations in the concentrates ($p < 0.01$ and $r = 0.599$ for PDGF-BB; $p < 0.001$ and $r = 0.785$ for TGF-β1) as well as in the lysates ($p < 0.05$ and $r = 0.526$ for PDGF-BB; $p < 0.01$ and $r = 0.626$ for TGF-β1). This same trend was observed for PLT concentrations in whole blood which also correlated with the growth factor concentrations in the concentrates ($p < 0.05$ and $r = 0.542$ for PDGF-BB; $p = 0.001$ and $r = 0.687$ for TGF-β1) and in the lysates ($p < 0.05$ and $r = 0.514$ for PDGF-BB; $p < 0.05$ and $r = 0.503$ for TGF-β1) (**Figure 3**).

The chemical analysis of the samples from the different production steps showed a stable pH value. Electrolyte, glucose, total protein, and albumin concentrations differed between serum and the samples from lysate production as anticipated due to binding and/or dilution by the anticoagulant citrate-phosphate-dextrose used in the latter. No major changes were observed throughout blood processing. Compared with FBS, glucose and protein concentrations were higher in serum and all steps of lysate production than in FBS, while potassium and lactate concentrations were lower (**Table 2**).

Donor-Related Parameters Influencing Outcome

Donor age was linked to the outcome of blood processing, despite a lack of correlation between age and whole blood PLT or serum growth factor concentrations ($p > 0.05$). Nevertheless, age was negatively correlated with PLT concentrations in the concentrates ($p < 0.01$ and $r = -0.582$), as well as with PDGF-BB and TGF-β1 concentrations in the concentrates ($p < 0.01$ and $r = -0.627$ for PDGF-BB; $p < 0.05$ and $r = -0.545$ for TGF-β1) and lysates ($p < 0.05$ and $r = -0.483$ for PDGF-BB; $p < 0.05$ and $r = -0.566$ for TGF-β1). When grouping the donors based on their age (4–9 vs. 10–15 years), the younger animals had higher serum PDGF-BB concentrations as well as higher PDGF-BB concentrations in the concentrates and lysates ($p < 0.05$). Fewer differences were found for PLT or TGF-β1 concentrations between age groups (**Figure 4**).

No differences were observed with respect to donor sex ($p > 0.05$ in sex group comparisons for all parameters).

Attempting to identify further attributes of suitable donor animals, parameters typically obtained by routine blood tests were also considered. EDTA whole blood PLT concentrations, similar as the respective values obtained from the blood collection bags, moderately correlated with concentrate PLT concentrations ($p = 00.01$ and $r = 0.573$), but not with the PLT recovery rate. The erythrocyte sedimentation time (median: 37 mm/30 min; IQR: 33.8) appeared to have no predictive effect at all, with no correlation observed for any relevant outcome parameter ($p > 0.05$).

Platelet Lysate in Equine MSC Culture

Growth Factors in Medium Supplements

The pooled ePL used for the cell culture experiments had a PDGF-BB concentration of 3,783 pg/ml, whereas FBS displayed a PDGF-BB concentration near or below the detection level of the assay. The concentration of TGF-β1 was 3,966 pg/ml in ePL and 3,380 pg/ml in FBS.

MSC Morphology, Proliferation, and Viability

MSC displayed the characteristic fibroblast-like morphology in all media, yet their shape tended to be more rounded in ePL-supplemented media and MSC supplemented with 10% ePL appeared to grow in more dense clusters.

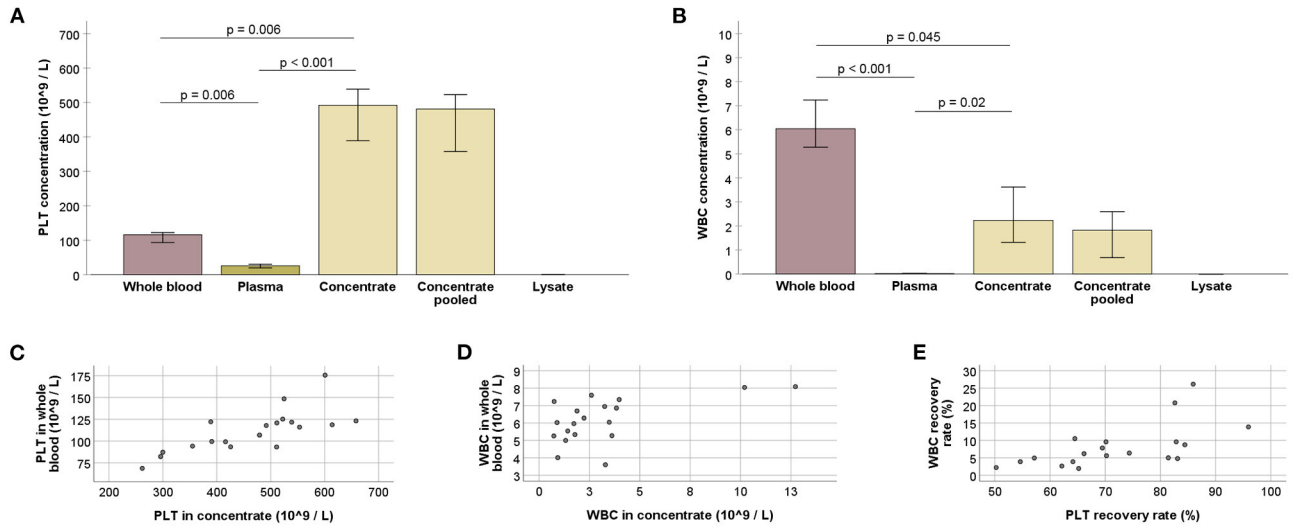

FIGURE 2 | (A,B) Platelet (PLT; **A**) and white blood cell (WBC; **B**) counts at the different stages of blood processing; values for whole blood, plasma, and concentrate were obtained using three technical replicates (blood bags), for each horse; values for concentrate pooled and lysate were obtained after all bags from one animal had been pooled; Friedman and Wilcoxon tests for group comparisons were performed for the former (p-values are indicated); bars represent the median values, error bars the 95% confidence intervals. **(C–E)** PLT **(C)** and WBC **(D)** counts in whole blood vs. concentrate, and WBC vs. PLT recovery rates **(E)** ($p < 0.05$, based on Spearman's rank correlation). All data were obtained from $n = 19$ horses.

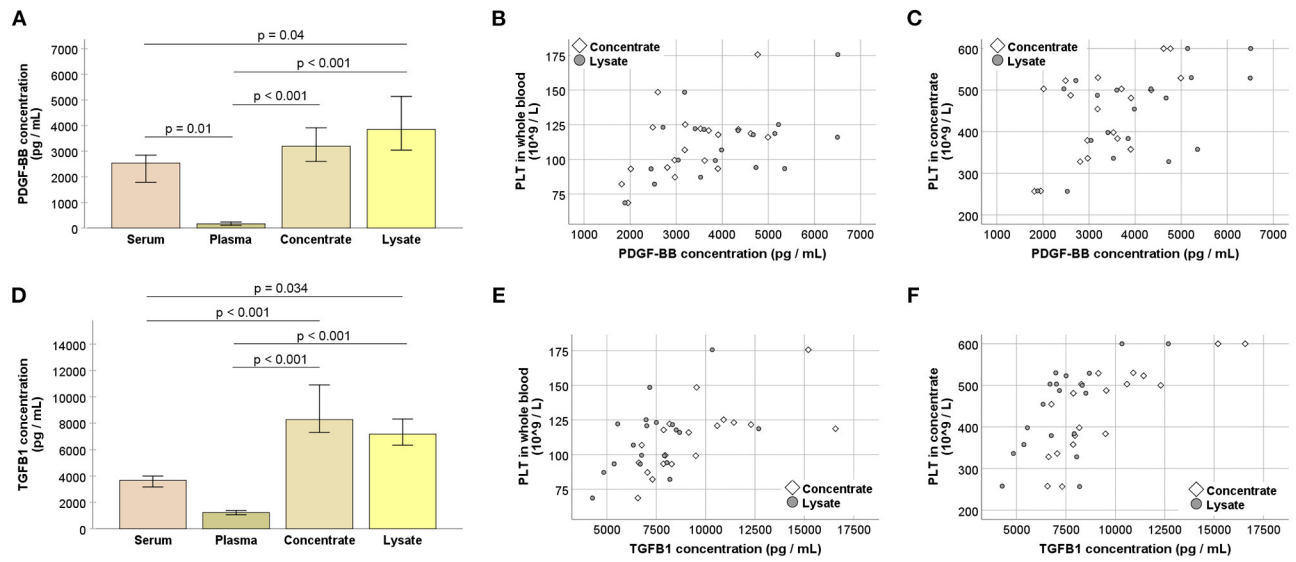

FIGURE 3 | (A,D) Platelet-derived growth factor (PDGF-BB; **A**) and transforming growth factor (TGFB1; **B**) concentrations at the different stages of blood processing; serum samples were directly drawn from each horse and the remaining values were obtained after pooling the replicate samples, i.e., blood bags, for each horse; samples were stored at −80°C before analysis; Friedman and Wilcoxon tests for group comparisons were performed (p-values are indicated); bars represent the median values, error bars the 95% confidence intervals. **(B–F)** Correlations between whole blood **(B,E)** or concentrate **(C,F)** platelet (PLT) counts and PDGF-BB **(B,C)** or TGFB1 **(E,F)** concentrations in concentrates as well as lysates ($p < 0.05$, based on Spearman's rank correlation). All data were obtained from $n = 19$ horses.

The most consistent viability and proliferation was observed in medium supplemented with 10% ePL, but confluency at day 5, generation time, and metabolic activity were similar between 10% ePL MSC and 10% FBS MSC. However, proliferation was highly variable in medium supplemented with 5% ePL and insufficient in medium supplemented with 2.5% ePL. Correspondingly, confluency was lowest in 2.5% ePL medium ($p < 0.05$ compared with 10% ePL in passage 2), and generation time was higher in 5% ePL medium compared with FBS medium ($p < 0.05$ in passage 2) (**Figure 5**). Here, it is of note that in one out of four samples in 5% ePL and in all four samples in 2.5% ePL, generation time calculation generated negative results, thus these values had to

TABLE 2 | pH and electrolyte, glucose, lactate, total protein, and albumin concentrations at the different stages of blood processing; values for serum, plasma, concentrate, and lysate are presented as mean ± SD ($n = 19$).

Sample	pH	Na^+ (mmol/L)	K^+ (mmol/L)	Ca^{2+} (mmol/L)	Cl^- (mmol/L)	HCO_3^- (mmol/L)	Glucose (mmol/L)	Lactate (mmol/L)	Total protein (g/L)	Albumin (g/L)
Serum	7.54 ± 0.03	141.38 ± 2.01	4.26 ± 0.49	1.79 ± 0.07	105.31 ± 2.53	28.06 ± 1.39	4.63 ± 0.49	2.09 ± 0.39	59.69 ± 2.25	32.26 ± 1.44
Plasma	7.53 ± 0.03	148.71 ± 1.79	3.16 ± 0.25	<0.10	84.04 ± 2.64	19.08 ± 1.22	23.92 ± 1.23	1.55 ± 0.24	51.66 ± 1.83	27.33 ± 1.18
Concentrate	7.47 ± 0.04	147.88 ± 1.54	3.62 ± 0.29	<0.10	84.57 ± 1.73	18.44 ± 1.63	22.62 ± 1.37	2.70 ± 0.63	53.39 ± 1.75	28.11 ± 1.10
Lysate	7.50 ± 0.05	148.00 ± 1.46	3.69 ± 0.30	<0.10	84.74 ± 1.68	17.06 ± 1.19	23.01 ± 1.30	2.87 ± 0.66	53.57 ± 2.08	27.99 ± 1.10
Lysate pooled (ePL)	7.52	147.80	3.68	<0.10	84.50	16.7	23.10	2.90	54.10	27.90
Fetal bovine serum	7.45	138.60	11.21	1.27	106.60	12.7	2.20	17.70	36.80	23.00

be excluded from further comparative analyses. Yet interestingly, there were no significant differences between groups with respect to MSC metabolic activity (**Figure 5**).

MSC Immunophenotype

MSC were positive for CD90, with the most consistent expression (≥92% $CD90^+$ cells in all samples) in MSC cultured in 10% ePL. In addition, MSC expressed CD44 and CD29. However, MSC were largely negative for CD73 and CD105 in FBS and ePL media (**Figure 6**).

MSC hardly expressed CD34 (<4% in FBS medium and <2% in all ePL media), CD45 (<2% in all media), and MHC II (<2% in all media). Surprisingly, small subpopulations (up to 26.1% in 10% ePL medium) appeared to be positive for CD79α (**Figure 6**). Furthermore, MSC CD14 staining strongly depended on the antibody used (**Supplementary File 2**). Using the anti-equine CD14 antibody (clone 105), the majority of MSC appeared CD14-positive (≥62% $CD14^+$ cells in 10% FBS medium and ≥87% $CD14^+$ cells in 10% ePL medium) (**Figure 6**).

No statistically significant differences of the marker expressions were found between groups. Yet due to their low yield, MSC cultured in 5 or 2.5% ePL media could not be analyzed by flow cytometry in appropriate cell numbers and with appropriate controls. The attempted analysis suggested a similar but more inconsistent marker expression as in the other media, but this result is of preliminary character (data not shown).

MSC Trilineage Differentiation

Adipogenic differentiation was evident in all samples, with a high percentage of cells containing distinct lipid vacuoles. Similarly, all samples showed extensive extracellular mineral depositions after osteogenic differentiation. Chondrogenic differentiation appeared weaker in MSC expanded in 10% ePL, with the same trend being reflected by Alcian blue and Masson's trichrome stainings, yet these differences were not statistically significant (**Figure 7**).

DISCUSSION

Here, we propose a buffy coat-based protocol for equine PLT concentrate and ePL production, which could provide a basis for improved xeno-free cell culture media for equine MSC expansion. The ePL was prepared without the specific plateletpheresis equipment and with quality controls at different processing steps and can be reproduced in large scales.

PL is produced from PLT concentrate. The shelf life of human PLT concentrates prepared for transfusion medicine is limited to 5–7 days at 22 ± 2°C under permanent agitation to minimize the risk of bacterial growth (Corash, 2011; Burnouf et al., 2014). Even in well-organized blood transfusion services, 10–20% of the platelet concentrates produced have to be discarded because they were not transfused within the specified time (Schallmoser et al., 2020). Those expired PLT concentrates can be allocated for hPL production to avoid an additional donation from blood donors, because several studies showed no differences between fresh and stored PLT concentrates as a source for hPL (Bieback, 2013; Astori et al., 2016; Burnouf et al., 2016), thus a certain amount

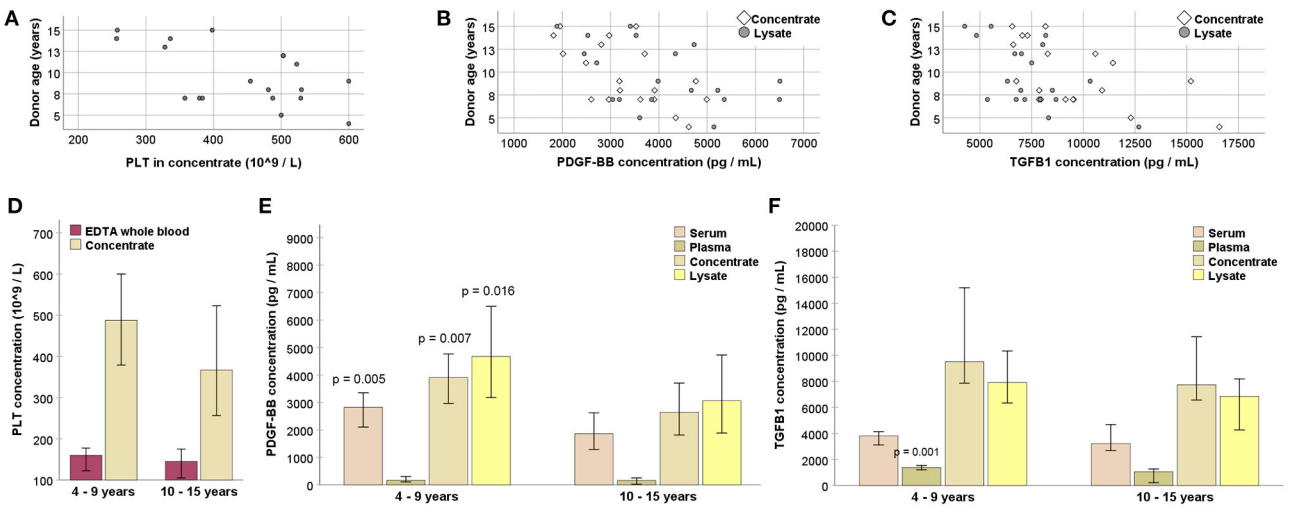

FIGURE 4 | (A–C) Negative correlation of donor age with platelet (PLT; **A**), platelet-derived growth factor (PDGF-BB; **B**) and transforming growth factor (TGFB1; **C**) concentrations ($p < 0.05$ based on Spearman's rank correlation). **(D–F)** PLT **(D)**, PDGF-BB **(E)**, and TGFB1 **(F)** concentrations in EDTA whole blood or serum samples drawn directly from the donor horses, as well as in samples from different processing stages (replicate blood bags pooled for each animal), obtained from younger and older donors; pairwise comparisons between the samples from younger and older animals were performed (Mann-Whitney *U*-test; *p*-values are given for significant differences compared with the respective samples from the older age group). Data were obtained from $n = 11$ younger and $n = 8$ older horses.

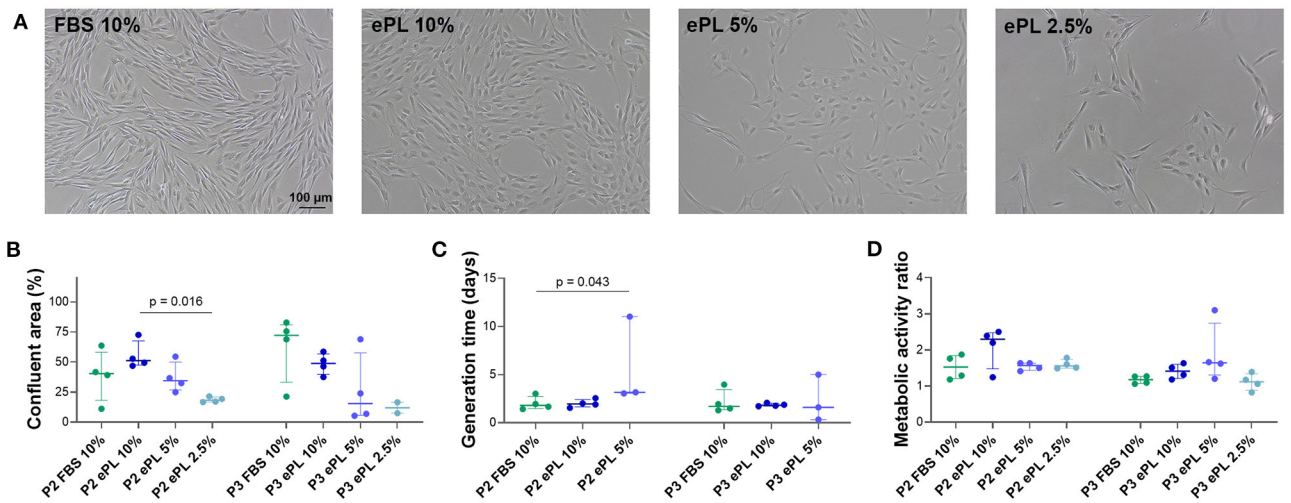

FIGURE 5 | (A) Representative phase-contrast photomicrographs of equine mesenchymal stromal cells (MSC) from one donor at day 5 after seeding for population doubling assays in media supplemented with fetal bovine serum (FBS) or equine platelet lysate (ePL). **(B–D)** Confluent area at day 5, measured using Fiji ImageJ **(B)**, generation times calculated from cell doubling numbers **(C)**, and metabolic activity as determined by MTS tetrazolium-based cell proliferation assay **(D)** for MSC in passage 2 (P2) cultured in the different media; Friedman and Wilcoxon tests for group comparisons were performed (*p*-values are indicated); the plots display the individual values, median, and interquartile ranges. Data were obtained from MSC from $n = 4$ donors. Note that missing generation time data are due to the lack of proliferation in these samples (1 out of 4 in the 5% ePL group, 4 out of 4 in the 2.5% ePL group).

of PLT concentrate is always available for hPL production. However, in contrast to human medicine, PLT concentrates from transfusion services are not available in equine medicine and therefore, PLT concentrates must be prepared directly for ePL production.

Platelet concentrate can be obtained by three distinct procedures: Either from anticoagulated whole blood by the buffy coat-based or the platelet-rich plasma (PRP) method or directly by plateletpheresis. In the buffy coat method, PLT are harvested directly from the buffy coat after a so-called hard spin and subsequently separated from the white blood cells in a second soft spin. In the PRP method, a first soft spin centrifugation is followed by a second hard spin centrifugation, in order to first harvest the PLT together with the plasma

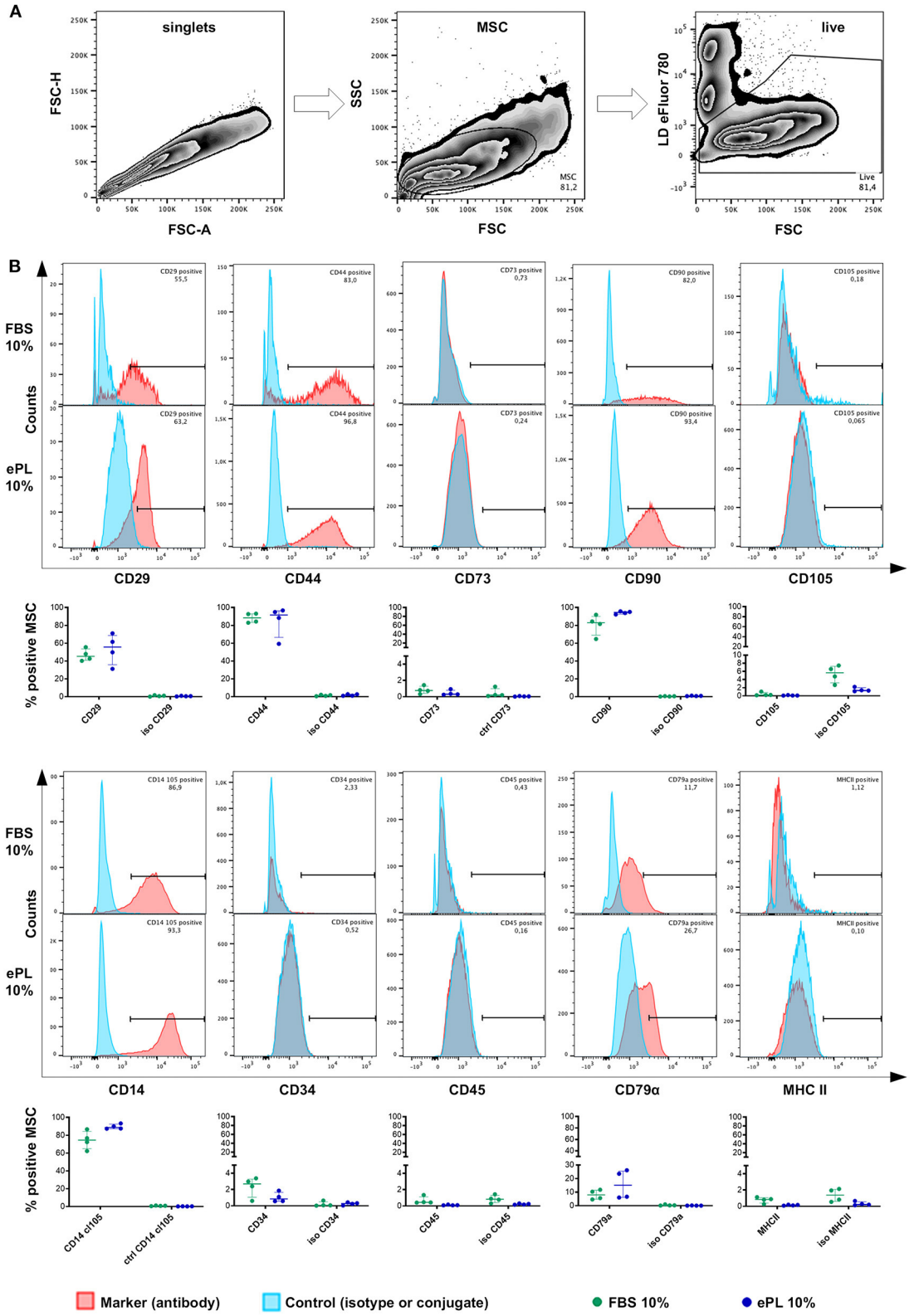

FIGURE 6 | Flow cytometry analysis of equine mesenchymal stromal cells (MSC) cultured with 10% fetal bovine serum (FBS) or 10% equine platelet lysate (ePL) after cells were mechanically detached and stained for 10 different surface markers. **(A)** Gating strategy for live MSC after duplet exclusion. **(B)** Representative examples of overlaid histograms of the surface marker staining and the respective isotype or conjugate control for MSC from one donor, and frequencies of surface marker positive MSC as % of live MSC plotted as individual values; horizontal bars mark the median and interquartile ranges. Data were obtained from MSC from $n = 4$ donors.

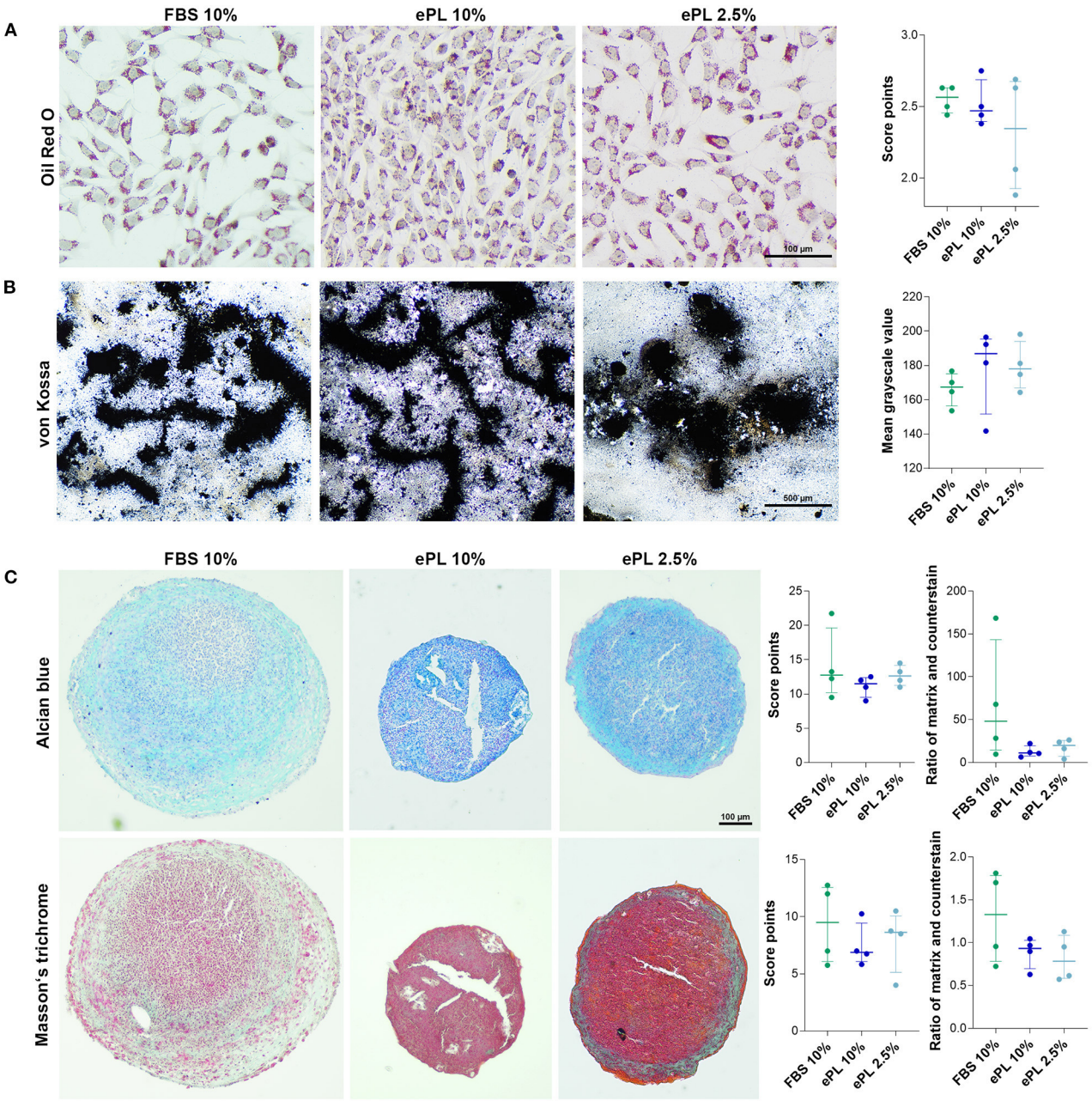

FIGURE 7 | (A) Representative brightfield photomicrographs of equine mesenchymal stromal cells (MSC) after adipogenic **(A)**, osteogenic **(B)**, and chondrogenic **(C)** differentiation and corresponding data obtained by scoring **(A,C)** and image analysis using Fiji ImageJ **(B,C)**. MSC were cultured in the media indicated before differentiation was induced (FBS, fetal bovine serum; ePL, equine platelet lysate). The plots display the individual values, median, and interquartile ranges. Data were obtained from MSC from $n = 4$ donors.

supernatant and then pellet them, at which the second step might lead to reversible PLT aggregation (Gulliksson, 2012). In Europe, the buffy coat method and repeated freeze/thaw cycles represent the most commonly used techniques in human medicine, while the PRP method is not frequently used anymore (Gulliksson, 2012; Burnouf et al., 2016). In contrast, equine PLT concentrates have only been produced by the PRP method or plateletpheresis, with the PRP method performed in most studies, using small sample volumes only. In the present study, we propose the first buffy coat-based method to produce ePL from the donor horses' whole blood collected in commercial blood bags.

For the buffy coat as well as for the PRP method, centrifugation settings are critical for the correct separation of blood components. However, neither in human nor in equine medicine, protocols are standardized. In previous equine studies using the PRP method, the centrifugation settings for the first and second steps varied as detailed in **Table 3**. In human medicine, protocols are available for the buffy coat method, but they differ not only in the centrifugation settings (200–3,200 × *g* for the second centrifugation) but also in the PLT counts yielded in the concentrates (100–10,000 × 10^9/L) (Burnouf et al., 2016).

Using the buffy coat-based method to produce equine PLT concentrate in the present study, we yielded a median PLT count of 484 × 10^9/L. In previous equine studies, PLT counts ranged between 591 × 10^9/L and 1,000–2,000 × 10^9/L using the PRP method with multiple centrifugations (Del Bue et al., 2007; Seo et al., 2013; Russell and Koch, 2016; Gilbertie et al., 2018; Bozorgmanesh et al., 2019; Yaneselli et al., 2019) and 350 ± 106 × 10^9/L to 357 ± 177 × 10^9/L by plateletpheresis (Sumner et al., 2017; Naskou et al., 2018) (**Table 3**). Data regarding the buffy coat method for equine PLT concentrate production are not available for comparison. Nevertheless, the PLT concentration in the current study was in the same order of magnitude as described for the PRP method (Del Bue et al., 2007; Seo et al., 2013; Russell and Koch, 2016; Gilbertie et al., 2018; Bozorgmanesh et al., 2019; Yaneselli et al., 2019) and higher than the PLT concentrations yielded by plateletpheresis (Sumner et al., 2017; Naskou et al., 2018).

Besides PLT counts, WBC removal is a central aspect in PLT concentrate production and near-complete WBC depletion by filtration is recommended by the guidelines for transfusion procedures (Wildt-Eggen et al., 2001; European Committee (Partial Agreement) on Blood Transfusion, 2020; Schallmoser et al., 2020). Leukocytes can enhance PLT aggregation and thromboxane release, and, thus, promote further recruitment of activated PLT, as *in vitro* studies with human PLT have shown (Faraday et al., 2001; Hoareau et al., 2014). However, it should be differentiated between conventional intravenous PLT transfusion and other applications of PLT concentrates, such as local injections in regenerative therapies, where leukocyte removal is controversial (DeLong et al., 2012; Lana et al., 2019). With respect to concentrates for PL production as MSC culture supplement, it is unclear whether a reduction of leukocytes is necessary or whether leukocytes in the concentrate may be even useful in the sense of MSC priming. Yet, as this remains to be investigated, we aimed at a reduction of leukocytes in the present work. In a previous experiment (unpublished data), we had aimed to produce PLT concentrate by sedimentation of whole blood, followed by hard spin centrifugation of the supernatant similar to the PRP method. We had obtained higher PLT counts than with the buffy coat method presented here, but the leukocytes were also concentrated compared with the whole blood (unpublished data), which was in accordance with previous equine studies (Ionita et al., 2014; Bozorgmanesh et al., 2019). Furthermore, we did not succeed to deplete WBC using leukocyte reduction filters for the equine PLT concentrates. The filters were immediately clogged, which could be due to the different characteristics of equine PLT compared with human PLT (Roscher, 2019) or a stronger activation of the PLT in the filter and thus an increased surface activity. Therefore, to avoid increased leukocyte values, we used the buffy coat method for the preparation of ePL. In this line, it needs to be acknowledged that plateletpheresis, while requiring costly and specific equipment, has an even better outcome with respect to leukocyte reduction, with 0.15 × 10^9 WBC/L (Sumner et al., 2017; Naskou et al., 2019).

Lysis of PLT concentrate releases growth factors and chemokines from the PLT. Repeated freeze/thaw cycles are mainly used for this purpose, but direct PLT activation by calcium chloride ($CaCl_2$), sonication, or solvent/detergent treatment is also feasible (Astori et al., 2016; Burnouf et al., 2016; Schallmoser et al., 2020). In contrast to the method presented here, using three freeze/thaw cycles, other equine studies used only one (Del Bue et al., 2007; Seo et al., 2013; Russell and Koch, 2016; Yaneselli et al., 2019) or two freeze/thaw cycles and three centrifugation steps (Sumner et al., 2017; Naskou et al., 2018). During the last centrifugation after lysis, again different centrifugation forces were used (**Table 3**). A systematic analysis determining the optimal number and conditions of the freeze/thaw cycles and centrifugation settings is still pending.

In the present study, the growth factor concentrations in the PLT concentrates were in a similar range as in the ePL, suggesting that PLT lysis is already evident after one freezing step, which was necessary to store the concentrates until the ELISA analyses were performed. However, unexpectedly, we found a discrepancy between the median TGF-β1 concentration in the individual lysates of one horse and its concentration measured in the pooled ePL. This suggests that there is TGF-β1 activation during final processing steps, possibly leading to successively less activatable TGF-β1 over a short time. This issue should be further investigated and procedures or materials used improved. In previous studies, similar (PDGF-BB: 3.5 ng/ml and TGF-β1: 6.1 ng/ml) (Sumner et al., 2017) or higher (PDGF-BB: 5.2 ng/ml and TGF-β: 24.5 ng/ml) (Russell and Koch, 2016) growth factor concentrations were found in ePL prepared from plateletpheresis- or PRP method-derived concentrates, respectively. Furthermore, corresponding to previous data (Russell and Koch, 2016), we could not detect PDGF-BB in FBS. Yet, the concentrations of growth factors measured may not only vary depending on the PL preparation process, but they are also affected by the assay specificity (Doucet et al., 2005; Textor and Tablin, 2012; Sumner et al., 2017), thus direct comparisons between studies or samples from different species are not entirely conclusive.

It was previously reported that breed, sex, and age of the donors can influence the cellular and growth factor profile of equine PLT products. Female horses and horses aged <5 years showed significantly higher concentrations of PDGF-BB and TGF-β1 in blood products. For PDGF, this was also observed in pony breeds (Giraldo et al., 2013). These findings were partially reproduced in our study, in which the PLT and growth factor concentrations in the PLT concentrates and lysates were negatively correlated with the age of the horses. To overcome the individual variations, pooling of the ePL from a large number of animals is beneficial for producing uniform batches.

TABLE 3 | Preparation technique for equine platelet (PLT) concentrate and PLT lysate and resulting PLT counts in the platelet concentrates in previous publications from 2007 to 2019.

References	First centrifugation	Second centrifugation	Final PLT concentration	Lysis
Del Bue et al. (2007)	350 × *g*, 10 min	510 × *g*, 10 min	1,000–2,000 × 10^9/L	Single freeze/thaw cycle + centrifugation (20,000 × *g*, 10 min)
Seo et al. (2013)	230 × *g*, 10 min, 10°C	900 × *g*, 15 min, 10°C	1,000 × 10^9/L	Single freeze/thaw cycle + centrifugation (1,600 × *g*, 30 min, 10°C)
Russell and Koch (2016)	200 × *g*, 15 min	400 × *g*, 15 min	1,000 × 10^9/L	Single freeze/thaw cycle + centrifugation (4,000 × *g*, 15 min)
Yaneselli et al. (2019)	200 × *g*, 10 min	1,500 × *g*, 20 min	591 × 10^9/L	Single freeze/thaw cycle + centrifugation (1,600 × *g*, 30 min)
Bozorgmanesh et al. (2019)	1,000 × *g*, 5 min 45 s	2,000 × *g*, 8 min	713,333 × 10^9/L	
Gilbertie et al. (2018)	250 × *g*, 15 min	1,500 × *g*, 15 min	1,226.38 × 10^9/L	5 freeze/thaw cycles + centrifugation (20,000 × *g*, 20 min)
Sumner et al. (2017) and Naskou et al. (2018)	Plateletpheresis		357 ± 177 × 10^9/L	2 freeze/thaw cycles + 3 centrifugation cycles (4,800 × *g*, 1.60 min and 2./3. 30 min) + centrifugation (3,485 × *g*, 10 min, 4°C)

Nevertheless, it remains recommendable to harvest the blood samples from young donor horses in uniform cohorts in order to obtain PLT concentrate and ePL of high quality.

We further compared the obtained ePL with FBS, in terms of their potential to support equine adipose-derived MSC expansion. PL is an attractive alternative to FBS, which could solve several issues related to FBS. First, it is an allogeneic product, which reduces the possibility of recipient immune reaction, and secondly, harvesting the materials for ePL production is ethically less critical. However, given that the use of MSC and other cell types in large animal models and veterinary medicine will further increase, ePL would be required in large quantities for MSC expansion. Furthermore, producing large batches of ePL according to standardized protocols would support consistent cell culture conditions. In this respect, it is a major advantage that horses tolerate regular blood collection of large amounts up to 8 L (16 ml/kg bodyweight) very well, and there are no adverse effects in the hematological variables (Malikides et al., 2000).

When analyzing the MSC proliferation kinetics, the most consistent viability and proliferation was observed in medium supplemented with 10% ePL. There were no major differences between 10% ePL MSC and 10% FBS MSC with respect to the proliferation parameters assessed. This supports the notion that ePL can be used as a replacement of FBS for equine MSC expansion. Our results are in agreement with the findings of two other studies, one using the PRP method (Seo et al., 2013) and the other using plateletpheresis (Naskou et al., 2018) to produce PLT concentrate and ePL. Furthermore, two other equine studies showed a dose-dependent proliferation of MSC in ePL medium (Del Bue et al., 2007; Russell and Koch, 2016). Yet only in one study, using supplementation with 20% ePL, MSC proliferation was actually increased as compared with FBS (Yaneselli et al., 2019). In comparison with these results, it is well-documented that hPL supplementation increases human bone marrow- and adipose-derived MSC proliferation as compared with FBS (Doucet et al., 2005; Blande et al., 2009; Cholewa et al., 2011; Becherucci et al., 2018). As already suggested earlier (Naskou et al., 2018), we also tested different concentrations of ePL for equine MSC cultivation. However, the proliferation was highly variable in medium supplemented with 5% ePL and insufficient in medium supplemented with 2.5% ePL. This is again in conflict with the findings in human medicine, where basal media supplemented with 5% hPL resulted in a significant increase in the proliferation rates of human MSCs compared with supplementation with FBS (Griffiths et al., 2013). Here, species-specific differences become evident. In contrast to an optimal growth factor content in 5% hPL for improved expansion of human MSC, the growth factor content in a medium supplemented with 5 or 2.5% ePL was not sufficient to support consistent equine MSC expansion. The different PLT concentrations in human and equine whole blood are a probable reason for this. The reference range for PLT counts in humans is 150–450 × 10^9/L (Burnouf et al., 2016), but only 94–232 × 10^9/L in horses (Stokol, 2020). Based on the resulting higher PLT count in the human PLT concentrates, it is not surprising that the growth factor concentrations reported for hPL (Klatte-Schulz et al., 2018) appear higher than in ePL, which may explain that less hPL is needed to support cell growth.

Human MSC characterization, as recommended by the ISCT, includes the evaluation of the positive marker antigens CD73, CD90, and CD105 and the exclusion marker antigens CD14, CD34, CD45, CD79α, and HLA-DR (Dominici et al., 2006). For equine MSC, it was suggested to further include CD29 and CD44 as inclusion markers (Paebst et al., 2014; Hillmann et al., 2016). Until today, the scarcity of reliable commercially available monoclonal antibodies specific for equine cells is a major drawback (Schauwer et al., 2011). The current analysis revealed that the immunophenotype of MSC cultured in media supplemented with FBS or ePL is similar. There were no significant differences in the expression of positive markers CD29, CD44, CD90, CD73, and CD105, while CD73 and CD105 were largely negative in all media. Furthermore, the MSC did not express the exclusion markers CD34, CD45, and MHC II.

These observations are widely comparable with other equine and human studies, where similar expression of surface markers was observed with different media (Doucet et al., 2005; Horn et al., 2010; Mojica-Henshaw et al., 2013; Yaneselli et al., 2019). Lack of CD73 in equine MSC is also in accordance with most previous equine studies (Ranera et al., 2011; Schauwer et al., 2012; Paebst et al., 2014; Hillmann et al., 2016) while CD105 has shown both high (Braun et al., 2010) or minimal or variable expressions in previous studies (Ranera et al., 2011; Schauwer et al., 2012; Paebst et al., 2014). However, in one previous study, a $CD45^+$ population was observed in MSC cultured with FBS as well as with ePL, and CD90 expression was found in a higher percentage of MSC cultured with FBS compared with ePL (Naskou et al., 2018). In contrast, we observed the most consistent expression of CD90 in MSC cultured with 10% ePL media and expression of CD45 was almost undetectable in all media. Furthermore, we made an interesting observation of CD14 detection on the majority of MSC when using an equine-specific antibody for CD14 (Kabithe et al., 2010; Wagner et al., 2013; Bonelli et al., 2017; Schnabel et al., 2019; Larson et al., 2020; Patel et al., 2020). According to the ISCT, CD14 should not be expressed on human MSC (Dominici et al., 2006) as it is a glycolipid anchored membrane glycoprotein expressed on monocytes and macrophages (Tesfaigzi, 2006; Braun et al., 2010) and a leukocyte-secreted molecule in response to LPS stimulation and inflammation, as demonstrated in horses (Wagner et al., 2013). Previously, we described equine MSC as CD14 negative (Paebst et al., 2014). These analyses were based on an anti-human CD14 antibody (clone 134620), which stains putative monocytes in equine peripheral mononuclear blood cells but not equine MSC (Paebst et al., 2014) (**Supplementary File 2**), but its exact specificity for equine CD14 has not been shown. In the current work, we used an equine-specific antibody for the flow cytometric analysis (clone 105, Kabithe et al., 2010), which discriminates the monocyte population in peripheral blood mononuclear cells more clearly (**Supplementary File 2**). While our current finding of equine MSC staining positive for CD14 is in accordance with previous studies (Braun et al., 2010; Hackett et al., 2011), it remains to be clarified if the cells actually express the whole functional CD14 molecule or only part of it, or if the MSC bind soluble CD14 present in FBS and ePL. On human MSC, cross-reactive epitopes have been observed, despite absence of the complete CD14 molecule (Pilz et al., 2011). The details and relevance of our finding of $CD14^+$ equine MSC here will be subject of further research.

We finally verified MSC *in vitro* trilineage differentiation potential. In accordance with previous studies, the MSC expanded in ePL showed no significant differences in osteogenic and adipogenic differentiation (Doucet et al., 2005; Schallmoser et al., 2007; Ben Azouna et al., 2012; Naskou et al., 2018). Interestingly, MSC expanded in medium supplemented with 2.5% ePL differentiated into both adipocytes and osteocytes, although their proliferation had not been satisfying in this medium. In addition, we obtained unexpected results in chondrogenic differentiation, which was weaker in MSC expanded in 10% ePL medium than when expanded in FBS or 2.5% ePL medium. In contrast, others reported that chondrogenic differentiation was improved in equine and human MSC cultured with ePL (Mishra et al., 2009; Shih et al., 2011; Gottipamula et al., 2012; Naskou et al., 2018). It is widely discussed in the literature that MSC express the chondrogenic markers aggrecan and Sox 9 and extracellular cartilage matrix depending on the amount of (platelet-derived) growth factors (Mishra et al., 2009; Prins et al., 2009; Shih et al., 2011; Rubio-Azpeitia and Andia, 2014). In this context, TGF-β appeared to be crucial for chondrogenic differentiation (Grimaud et al., 2002; Chapman et al., 2020). A possible and pragmatic explanation for the discrepancy observed here could be that MSC expanded in 10% ePL medium would have needed more extensive washing steps to remove the ePL completely before being transferred to the chondrogenic differentiation medium.

The current study provides the first evaluation of a buffy coat-based protocol for ePL production. The method presented has several advantages over previously described protocols for equine PLT concentrate and ePL production and complies much better with the current state of the art in human medicine. Therefore, it can serve as a basis to improve the culture of equine MSC and other equine cell types. MSC characterization in the present study was limited in that only four MSC donor horses were investigated, and because so far, we only investigated basic properties of MSC but not their functionality in clinically relevant settings. Based on the herein obtained results, it appears highly promising to continue with the functional characterization of equine MSC in conjunction with their culture in ePL.

DATA AVAILABILITY STATEMENT

The raw data supporting the conclusions of this article will be made available by the authors, without undue reservation.

ETHICS STATEMENT

The animal study was reviewed and approved by Regional council Giessen, Germany. Written informed consent was obtained from the owners for the participation of their animals in this study.

AUTHOR CONTRIBUTIONS

AH: conception of the study and complete experimental design (together with JB), sample acquisition, blood processing, and MSC culture experiments, sample and data analysis, data interpretation and drafting of the manuscript (together with JB). HL: substantial contribution to the experimental design, help with blood processing, analysis, and data interpretation (blood processing). SA: substantial contribution to the experimental design, microbiological analysis, and data interpretation (microbiology). NB: substantial contribution to the experimental design and data interpretation (blood processing). MM: contribution to the experimental design, MSC culture experiments, sample analysis (MSC culture and differentiation). JM: contribution to the experimental

design, help with sample acquisition, histology, sample analysis (blood processing and MSC differentiation). VP: contribution to the experimental design, help with blood processing, and hematological sample analyses (blood processing). CS: substantial contribution to the experimental design, sample and data analysis, data interpretation, and drafting of the manuscript (flow cytometry experiments). JB: conception of the study and complete experimental design (together with AH), help with MSC culture experiments, data analysis, data interpretation and drafting of the manuscript (together with AH). All authors have critically revised the manuscript for important intellectual content and approved the publication of its content.

FUNDING

This work was in part funded by the Akademie fuer Tiergesundheit e.V. (doctoral scholarship, AH).

ACKNOWLEDGMENTS

The authors acknowledge Dr. Hatim Hemeda and Dr. Silke Isenhardt, PL BioScience GmbH, Aachen, Germany, for their scientific input and advice regarding the preparation and quality control of platelet lysate as cell culture supplement. The authors further thank Carla Doll, Equine Clinic (Surgery, Orthopedics) of the JLU Giessen for her help with cell cultures and Dr. Carolin Horstmeier, Department for Horses, Faculty of Veterinary Medicine, University of Leipzig, for primary culture of the cells used in the current experiments.

SUPPLEMENTARY MATERIAL

The Supplementary Material for this article can be found online at: https://www.frontiersin.org/articles/10.3389/fbioe.2020.613621/full#supplementary-material

REFERENCES

Anderson, L. D., Raub, R. H., Grieger, D. M., Morris, J., and Weber, J. D. (1998). Transforming growth factor-β1 concentrations in equine synovial fluid. *J. Equine Vet. Sci*. 18, 109–113. doi: 10.1016/S0737-0806(98)80289-X

Astori, G., Amati, E., Bambi, F., Bernardi, M., Chieregato, K., Schäfer, R., et al. (2016). Platelet lysate as a substitute for animal serum for the ex-vivo expansion of mesenchymal stem/stromal cells: present and future. *Stem Cell Res. Ther*. 7:93. doi: 10.1186/s13287-016-0352-x

Baker, M. (2016). Reproducibility: respect your cells! Numerous variables can torpedo attempts to replicate cell experiments, from the batch of serum to the shape of growth plates. But there are ways to ensure reliability. *Nature* 537, 433–435. doi: 10.1038/537433a

Becherucci, V., Piccini, L., Casamassima, S., Bisin, S., Gori, V., Gentile, F., et al. (2018). Human platelet lysate in mesenchymal stromal cell expansion according to a GMP grade protocol: a cell factory experience. *Stem Cell Res. Ther*. 9:124. doi: 10.1186/s13287-018-0863-8

Ben Azouna, N., Jenhani, F., Regaya, Z., Berraeis, L., Ben Othman, T., Ducrocq, E., et al. (2012). Phenotypical and functional characteristics of mesenchymal stem cells from bone marrow: comparison of culture using different media supplemented with human platelet lysate or fetal bovine serum. *Stem Cell Res. Ther*. 3:6. doi: 10.1186/scrt97

Bieback, K. (2013). Platelet lysate as replacement for fetal bovine serum in mesenchymal stromal cell cultures. *Transfus. Med. Hemother*. 40, 326–335. doi: 10.1159/000354061

Blair, P., and Flaumenhaft, R. (2009). Platelet alpha-granules: basic biology and clinical correlates. *Blood Rev*. 23, 177–189. doi: 10.1016/j.blre.2009.04.001

Blande, I. S., Bassaneze, V., Lavini-Ramos, C., Fae, K. C., Kalil, J., Miyakawa, A. A., et al. (2009). Adipose tissue mesenchymal stem cell expansion in animal serum-free medium supplemented with autologous human platelet lysate. *Transfusion* 49, 2680–2685. doi: 10.1111/j.1537-2995.2009.02346.x

Bonelli, F., Meucci, V., Divers, T. J., Wagner, B., Intorre, L., and Sgorbini, M. (2017). Kinetics of plasma procalcitonin, soluble CD14, CCL2 and IL-10 after a sublethal infusion of lipopolysaccharide in horses. *Vet. Immunol. Immunopathol.* 184, 29–35. doi: 10.1016/j.vetimm.2016.12.010

Boswell, S. G., Schnabel, L. V., Mohammed, H. O., Sundman, E. A., Minas, T., and Fortier, L. A. (2014). Increasing platelet concentrations in leukocyte-reduced platelet-rich plasma decrease collagen gene synthesis in tendons. *Am. J. Sports Med*. 42, 42–49. doi: 10.1177/0363546513507566

Bozorgmanesh, R., Magdesian, K. G., Sutton-Burges, J. W., Owens, S. D., and Tablin, F. (2019). Equine platelet concentrate preparation and validation. *J. Vet. Intern. Med*. 33, 1500–1506. doi: 10.1111/jvim.15472

Braun, J., Hack, A., Weis-Klemm, M., Conrad, S., Treml, S., Kohler, K., et al. (2010). Evaluation of the osteogenic and chondrogenic differentiation capacities of equine adipose tissue-derived mesenchymal stem cells. *Am. J. Vet. Res*. 71, 1228–1236. doi: 10.2460/ajvr.71.10.1228

Broeckx, S. Y., Seys, B., Suls, M., Vandenberghe, A., Mariën, T., Adriaensen, E., et al. (2019). Equine allogeneic chondrogenic induced mesenchymal stem cells are an effective treatment for degenerative joint disease in horses. *Stem Cells Dev*. 28, 410–422. doi: 10.1089/scd.2018.0061

Burnouf, T., Goubran, H. A., and Seghatchian, J. (2014). Multifaceted regenerative lives of expired platelets in the second decade of the 21st century. *Transfus. Apher. Sci*. 51, 107–112. doi: 10.1016/j.transci.2014.08.006

Burnouf, T., Strunk, D., Koh, M. B. C., and Schallmoser, K. (2016). Human platelet lysate: replacing fetal bovine serum as a gold standard for human cell propagation? *Biomaterials* 76, 371–387. doi: 10.1016/j.biomaterials.2015.10.065

Chapman, H.-S., Gale, A. L., Dodson, M. E., Linardi, R. L., and Ortved, K. F. (2020). Autologous Platelet lysate does not enhance chondrogenic differentiation of equine bone marrow-derived mesenchymal stromal cells despite increased TGF-β1 concentration. *Stem Cells Dev*. 29, 144–155. doi: 10.1089/scd.2019.0239

Cholewa, D., Stiehl, T., Schellenberg, A., Bokermann, G., Joussen, S., Koch, C., et al. (2011). Expansion of adipose mesenchymal stromal cells is affected by human platelet lysate and plating density. *Cell Transplant*. 20, 1409–1422. doi: 10.3727/096368910X557218

Corash, L. (2011). Bacterial contamination of platelet components: potential solutions to prevent transfusion-related sepsis. *Expert Rev. Hematol*. 4, 509–525. doi: 10.1586/ehm.11.53

Del Bue, M., Riccò, S., Conti, V., Merli, E., Ramoni, R., and Grolli, S. (2007). Platelet lysate promotes *in vitro* proliferation of equine mesenchymal stem cells and tenocytes. *Vet. Res. Commun.* 31, 289–292. doi: 10.1007/s11259-007-0099-z

DeLong, J. M., Russell, R. P., and Mazzocca, A. D. (2012). Platelet-rich plasma: the PAW classification system. *Arthroscopy* 28, 998–1009. doi: 10.1016/j.arthro.2012.04.148

Desjardins, I., Theoret, C., Joubert, P., Wagner, B., and Lavoie, J.-P. (2004). Comparison of TGF-beta 1 concentrations in bronchoalveolar fluid of horses affected with heaves and of normal controls. *Vet. Immunol. Immunopathol*. 101, 133–141. doi: 10.1016/j.vetimm.2004.03.008

Dominici, M., Le Blanc, K., Mueller, I., Slaper-Cortenbach, I., Marini, F., Krause, D., et al. (2006). Minimal criteria for defining multipotent mesenchymal stromal cells. The International Society for Cellular Therapy position statement. *Cytotherapy* 8, 315–317. doi: 10.1080/14653240600855905

Donnelly, B. P., Nixon, A. J., Haupt, J. L., and Dahlgren, L. A. (2006). Nucleotide structure of equine platelet-derived growth factor-A and -B and expression in horses with induced acute tendinitis. *Am. J. Vet. Res*. 67, 1218–1225. doi: 10.2460/ajvr.67.7.1218

Doucet, C., Ernou, I., Zhang, Y., Llense, J.-R., Begot, L., Holy, X., et al. (2005). Platelet lysates promote mesenchymal stem cell expansion: a safety substitute

for animal serum in cell-based therapy applications. *J. Cell. Physiol.* 205, 228–236. doi: 10.1002/jcp.20391

Erickson, G. A., Bolin, S. R., and Landgraf, J. G. (1991). Viral contamination of fetal bovine serum used for tissue culture: risks and concerns. *Dev. Biol. Stand.* 75, 173–175.

European Committee (Partial Agreement) on Blood Transfusion (2020). *Guide to the Preparation, Use and Quality Assurance of Blood Components*. Technical Report. Council of Europe.

European Medicines Agency, London (2013). *Guideline on the Use of Bovine Serum in the Manufacture of Human Biological Medicinal Products*. Technical Report EMA/CHMP/BWP/457920/2012 rev 1. Committee for Medicinal Products for Human Use (CHMP). European Medicines Agency.

Faraday, N., Scharpf, R. B., Dodd-o, J. M., Martinez, E. A., Rosenfeld, B. A., and Dorman, T. (2001). Leukocytes can enhance platelet-mediated aggregation and thromboxane release via interaction of P-selectin glycoprotein ligand 1 with P-selectin. *Anesthesiology* 94, 145–151. doi: 10.1097/00000542-200101000-00025

Ferris, D. J., Frisbie, D. D., Kisiday, J. D., McIlwraith, C. W., Hague, B. A., Major, M. D., et al. (2014). Clinical outcome after intra-articular administration of bone marrow derived mesenchymal stem cells in 33 horses with stifle injury. *Vet. Surg.* 43, 255–265. doi: 10.1111/j.1532-950X.2014.12100.x,

Gilbertie, J. M., Long, J. M., Schubert, A. G., Berglund, A. K., Schaer, T. P., and Schnabel, L. V. (2018). Pooled platelet-rich plasma lysate therapy increases synoviocyte proliferation and hyaluronic acid production while protecting chondrocytes from synoviocyte-derived inflammatory mediators. *Front. Vet. Sci.* 5:150. doi: 10.3389/fvets.2018.00150

Giraldo, C. E., López, C., Álvarez, M. E., Samudio, I. J., Prades, M., and Carmona, J. U. (2013). Effects of the breed, sex and age on cellular content and growth factor release from equine pure-platelet rich plasma and pure-platelet rich gel. *BMC Vet. Res.* 9:29. doi: 10.1186/1746-6148-9-29

Gittel, C., Brehm, W., Burk, J., Juelke, H., Staszyk, C., and Ribitsch, I. (2013). Isolation of equine multipotent mesenchymal stromal cells by enzymatic tissue digestion or explant technique: comparison of cellular properties. *BMC Vet. Res.* 9, 1–14. doi: 10.1186/1746-6148-9-221

Godwin, E. E., Young, N. J., Dudhia, J., Beamish, I. C., and Smith, R. K. W. (2012). Implantation of bone marrow-derived mesenchymal stem cells demonstrates improved outcome in horses with overstrain injury of the superficial digital flexor tendon. *Equine Vet. J.* 44, 25–32. doi: 10.1111/j.2042-3306.2011.00363.x

Golebiewska, E. M., and Poole, A. W. (2015). Platelet secretion: from haemostasis to wound healing and beyond. *Blood Rev.* 29, 153–162. doi: 10.1016/j.blre.2014.10.003

Gottipamula, S., Sharma, A., Krishnamurthy, S., Majumdar, A. S., and Seetharam, R. N. (2012). Human platelet lysate is an alternative to fetal bovine serum for large-scale expansion of bone marrow-derived mesenchymal stromal cells. *Biotechnol. Lett.* 34, 1367–1374. doi: 10.1007/s10529-012-0893-8

Griffiths, S., Baraniak, P. R., Copland, I. B., Nerem, R. M., and McDevitt, T. C. (2013). Human platelet lysate stimulates high-passage and senescent human multipotent mesenchymal stromal cell growth and rejuvenation *in vitro*. *Cytotherapy* 15, 1469–1483. doi: 10.1016/j.jcyt.2013.05.020

Grimaud, E., Heymann, D., and Rédini, F. (2002). Recent advances in TGF-β effects on chondrocyte metabolism. *Cytokine Growth Factor Rev.* 13, 241–257. doi: 10.1016/S1359-6101(02)00004-7

Grogan, S. P., Barbero, A., Winkelmann, V., Rieser, F., Fitzsimmons, J. S., O'Driscoll, S., et al. (2006). Visual histological grading system for the evaluation of *in vitro*-generated neocartilage. *Tissue Eng.* 12, 2141–2149. doi: 10.1089/ten.2006.12.2141

Gstraunthaler, G. (2003). AltȘes to the use of fetal bovine serum: serum-free cell culture. *ALTEX* 20, 275–281.

Gullikkson, H. (2012). Platelets from platelet-rich-plasma versus buffy-coat-derived platelets: what is the difference? *Rev. Bras. Hematol. Hemoter.* 34, 76–77. doi: 10.5581/1516-8484.20120024

Hackett, C. H., Flaminio, M. J., and La, F. (2011). Analysis of CD14 expression levels in putative mesenchymal progenitor cells isolated from equine bone marrow. *Stem Cells Dev.* 20, 721–735. doi: 10.1089/scd.2010.0175

Hawkes, P. W. (2015). Fetal bovine serum: geographic origin and regulatory relevance of viral contamination. *Bioresour. Bioprocess.* 2:34. doi: 10.1186/s40643-015-0063-7

Hillmann, A., Ahrberg, A. B., Brehm, W., Heller, S., Josten, C., Paebst, F., et al. (2016). Comparative characterization of human and equine mesenchymal stromal cells: a basis for translational studies in the equine model. *Cell Transplant.* 25, 109–124. doi: 10.3727/096368915X687822

Hoareau, G. L., Jandrey, K. E., Burges, J., Bremer, D., and Tablin, F. (2014). Comparison of the platelet-rich plasma and buffy coat protocols for preparation of canine platelet concentrates. *Vet. Clin. Pathol.* 43, 513–518. doi: 10.1111/vcp.12195

Hodgson, J. (1995). To treat or not to treat: that is the question for serum: as regulations on serum importation stagnate the industry moves toward treatment options. *Biotechnology* 13, 333–334; 337–338; 341–343. doi: 10.1038/nbt0495-333

Horn, P., Bokermann, G., Cholewa, D., Bork, S., Walenda, T., Koch, C., et al. (2010). Impact of individual platelet lysates on isolation and growth of human mesenchymal stromal cells. *Cytotherapy* 12, 888–898. doi: 10.3109/14653249.2010.501788

Ionita, J.-C., Kissich, C., Gottschalk, J., Einspanier, A., Köller, G., Winter, K., et al. (2014). Comparison of cellular and growth factor concentrations in equine Autologous Conditioned Plasma® (ACP) and manually prepared Platelet Rich Plasma (mPRP). *PHK* 30, 195–201. doi: 10.21836/PEM20140208

Jayme, D. W., Epstein, D. A., and Conrad, D. R. (1988). Fetal bovine serum alternatives. *Nature* 334, 547–548. doi: 10.1038/334547a0

Jochems, C. E. A., van der Valk, J. B. F., Stafleu, F. R., and Baumans, V. (2002). The use of fetal bovine serum: ethical or scientific problem? *Altern. Lab. Anim.* 30, 219–227. doi: 10.1177/026119290203000208

Kabithe, E., Hillegas, J., Stokol, T., Moore, J., and Wagner, B. (2010). Monoclonal antibodies to equine CD14. *Vet. Immunol. Immunopathol.* 138, 149–153. doi: 10.1016/j.vetimm.2010.07.003

Karnieli, O., Friedner, O. M., Allickson, J. G., Zhang, N., Jung, S., Fiorentini, D., et al. (2017). A consensus introduction to serum replacements and serum-free media for cellular therapies. *Cytotherapy* 19, 155–169. doi: 10.1016/j.jcyt.2016.11.011

Klatte-Schulz, F., Schmidt, T., Uckert, M., Scheffler, S., Kalus, U., Rojewski, M., et al. (2018). Comparative analysis of different platelet lysates and platelet rich preparations to stimulate tendon cell biology: an *in vitro* study. *Int. J. Mol. Sci.* 19:212. doi: 10.3390/ijms19010212

Kydd, J., Antczak, D. F., Allen, W. R., Barbis, D., Butcher, G., Davis, W., et al. (1994). Report of the First International Workshop on Equine Leucocyte Antigens, Cambridge, UK, July 1991. *Vet. Immunol. Immunopathol.* 42, 3–60. doi: 10.1016/0165-2427(94)90088-4

Lana, J. F., Macedo, A., Ingrao, I. L. G., Huber, S. C., Santos, G. S., and Santana, M. H. A. (2019). Leukocyte-rich PRP for knee osteoarthritis: current concepts. *J. Clin. Orthop. Trauma* 10, S179–S182. doi: 10.1016/j.jcot.2019.01.011

Larson, E. M., Babasyan, S., and Wagner, B. (2020). Phenotype and function of IgE-binding monocytes in equine Culicoides hypersensitivity. *PLoS ONE* 15:e0233537. doi: 10.1371/journal.pone.0233537

Lunn, D. P., Holmes, M. A., Antczak, D. F., Agerwal, N., Baker, J., Bendali-Ahcene, S., et al. (1998). Report of the Second Equine Leucocyte Antigen Workshop, Squaw Valley, California, July 1995. *Vet. Immunol. Immunopathol.* 62, 101–143. doi: 10.1016/S0165-2427(97)00160-8

Malikides, N., Mollison, P. J., Reid, S. W., and Murray, M. (2000). Haematological responses of repeated large volume blood collection in the horse. *Res. Vet. Sci.* 68, 275–278. doi: 10.1053/rvsc.2000.0376

Mariñas-Pardo, L., García-Castro, J., Rodríguez-Hurtado, I., Rodríguez-García, M. I., Núñez-Naveira, L., and Hermida-Prieto, M. (2018). Allogeneic adipose-derived mesenchymal stem cells (Horse Allo 20) for the treatment of osteoarthritis-associated lameness in horses: characterization, safety, and efficacy of intra-articular treatment. *Stem Cells Dev.* 27, 1147–1160. doi: 10.1089/scd.2018.0074

McClain, A. K., and McCarrel, T. M. (2019). The effect of four different freezing conditions and time in frozen storage on the concentration of commonly measured growth factors and enzymes in equine platelet-rich plasma over six months. *BMC Vet. Res.* 15:292. doi: 10.1186/s12917-019-2040-4

Mishra, A., Tummala, P., King, A., Lee, B., Kraus, M., Tse, V., et al. (2009). Buffered platelet-rich plasma enhances mesenchymal stem cell proliferation and chondrogenic differentiation. *Tissue Eng. C Methods* 15, 431–435. doi: 10.1089/ten.tec.2008.0534

Mohammadi, S., Nikbakht, M., Malek Mohammadi, A., Zahed Panah, M., Ostadali, M. R., Nasiri, H., et al. (2016). Human platelet lysate as a xeno free alternative of

fetal bovine serum for the *in vitro* expansion of human mesenchymal stromal cells. *Int. J. Hematol. Oncol. Stem Cell Res*. 10, 161–171.

Mojica-Henshaw, M. P., Jacobson, P., Morris, J., Kelley, L., Pierce, J., Boyer, M., et al. (2013). Serum-converted platelet lysate can substitute for fetal bovine serum in human mesenchymal stromal cell cultures. *Cytotherapy* 15, 1458–1468. doi: 10.1016/j.jcyt.2013.06.014

Naskou, M. C., Sumner, S., Berezny, A., Copland, I. B., and Peroni, J. F. (2019). Fibrinogen-depleted equine platelet lysate affects the characteristics and functionality of mesenchymal stem cells. *Stem Cells Dev*. 28, 1572–1580. doi: 10.1089/scd.2019.0070

Naskou, M. C., Sumner, S. M., Chocallo, A., Kemelmakher, H., Thoresen, M., Copland, I., et al. (2018). Platelet lysate as a novel serum-free media supplement for the culture of equine bone marrow-derived mesenchymal stem cells. *Stem Cell Res. Ther*. 9:75. doi: 10.1186/s13287-018-0823-3

Pacini, S., Spinabella, S., Trombi, L., Fazzi, R., Galimberti, S., Dini, F., et al. (2007). Suspension of bone marrow-derived undifferentiated mesenchymal stromal cells for repair of superficial digital flexor tendon in race horses. *Tissue Eng.* 13, 2949–2955. doi: 10.1089/ten.2007.0108

Paebst, F., Piehler, D., Brehm, W., Heller, S., Schroeck, C., Tárnok, A., et al. (2014). Comparative immunophenotyping of equine multipotent mesenchymal stromal cells: an approach toward a standardized definition. *Cytometry A* 85, 678–687. doi: 10.1002/cyto.a.22491

Patel, R. S., Tomlinson, J. E., Divers, T. J., van de Walle, G. R., and Rosenberg, B. R. (2020). *Single cell resolution landscape of equine peripheral blood mononuclear cells reveals diverse immune cell subtypes including T-bet + B cells*. Available online at: https://www.biorxiv.org/content/10.1101/2020.05.05.077362v1 doi: 10.1101/2020.05.05.077362 (accessed October 02, 2020).

Pilz, G. A., Braun, J., Ulrich, C., Felka, T., Warstat, K., Ruh, M., et al. (2011). Human mesenchymal stromal cells express CD14 cross-reactive epitopes. *Cytometry A* 79, 635–645. doi: 10.1002/cyto.a.21073

Prins, H. J., Rozemuller, H., Vonk-Griffioen, S., Verweij, V. G., Dhert, W. J., Slaper-Cortenbach, I. C., et al. (2009). Bone-forming capacity of mesenchymal stromal cells when cultured in the presence of human platelet lysate as substitute for fetal bovine serum. *Tissue Eng. Part A* 15, 3741–3751. doi: 10.1089/ten.tea.2008.0666

Ranera, B., Lyahyai, J., Romero, A., Vázquez, F. J., Remacha, A. R., Bernal, M. L., et al. (2011). Immunophenotype and gene expression profiles of cell surface markers of mesenchymal stem cells derived from equine bone marrow and adipose tissue. *Vet. Immunol. Immunopathol*. 144, 147–154. doi: 10.1016/j.vetimm.2011.06.033

Renzi, S., Riccò, S., Dotti, S., Sesso, L., Grolli, S., Cornali, M., et al. (2013). Autologous bone marrow mesenchymal stromal cells for regeneration of injured equine ligaments and tendons: a clinical report. *Res. Vet. Sci*. 95, 272–277. doi: 10.1016/j.rvsc.2013.01.017

Roscher, K. (2019). *Platelets in equids - an underrated biomarker? DVG Service GmbH*. Available online at: http://geb.uni-giessen.de/geb/volltexte/2019/14904/ (accessed October 01, 2020).

Rubio-Azpeitia, E., and Andia, I. (2014). Partnership between platelet-rich plasma andmesenchymal stem cells: *in vitro* experience. *Muscles Ligaments Tendons J*. 4, 52–62. doi: 10.11138/mltj/2014.4.1.052

Ruifrok, A. C., and Johnston, D. A. (2001). Quantification of histochemical staining by color deconvolution. *Anal. Quant. Cytol. Histol*. 23, 291–299.

Russell, K. A., and Koch, T. G. (2016). Equine platelet lysate as an alternative to fetal bovine serum in equine mesenchymal stromal cell culture - too much of a good thing? *Equine Vet. J*. 48, 261–264. doi: 10.1111/evj.12440

Schallmoser, K., Bartmann, C., Rohde, E., Reinisch, A., Kashofer, K., Stadelmeyer, E., et al. (2007). Human platelet lysate can replace fetal bovine serum for clinical-scale expansion of functional mesenchymal stromal cells. *Transfusion* 47, 1436–1446. doi: 10.1111/j.1537-2995.2007.01220.x

Schallmoser, K., Henschler, R., Gabriel, C., Koh, M. B. C., and Burnouf, T. (2020). Production and quality requirements of human platelet lysate: a position statement from the working party on cellular therapies of the international society of blood transfusion. *Trends Biotechnol*. 38, 13–23. doi: 10.1016/j.tibtech.2019.06.002

Schallmoser, K., Rohde, E., Bartmann, C., Obenauf, A. C., Reinisch, A., and Strunk, D. (2009). Platelet-derived growth factors for GMP-compliant propagation of mesenchymal stromal cells. *Biomed. Mater. Eng*. 19, 271–276. doi: 10.3233/BME-2009-0591

Schauwer, C., de Meyer, E., van de Walle, G. R., and van Soom, A. (2011). Markers of stemness in equine mesenchymal stem cells: a plea for uniformity. *Theriogenology* 75, 1431–1443. doi: 10.1016/j.theriogenology.2010.11.008

Schauwer, C., de Piepers, S., van de Walle, G. R., Demeyere, K., Hoogewijs, M. K., Govaere, J. L. J., et al. (2012). In search for cross-reactivity to immunophenotype equine mesenchymal stromal cells by multicolor flow cytometry. *Cytometry A* 81, 312–323. doi: 10.1002/cyto.a.22026

Schauwer, C., de van de Walle, G. R., van Soom, A., and Meyer, E. (2013). Mesenchymal stem cell therapy in horses: useful beyond orthopedic injuries? *Vet. Q*. 33, 234–241. doi: 10.1080/01652176.2013.800250

Schnabel, C. L., Babasyan, S., Freer, H., and Wagner, B. (2019). CXCL10 production in equine monocytes is stimulated by interferon-gamma. *Vet. Immunol. Immunopathol*. 207, 25–30. doi: 10.1016/j.vetimm.2018.11.016

Schubert, S., Brehm, W., Hillmann, A., and Burk, J. (2018). Serum-free human MSC medium supports consistency in human but not in equine adipose-derived multipotent mesenchymal stromal cell culture. *Cytometry A* 93, 60–72. doi: 10.1002/cyto.a.23240

Seo, J.-p., Tsuzuki, N., Haneda, S., Yamada, K., Furuoka, H., Tabata, Y., et al. (2013). Comparison of allogeneic platelet lysate and fetal bovine serum for in vitro expansion of equine bone marrow-derived mesenchymal stem cells. *Res. Vet. Sci*. 95, 693–698. doi: 10.1016/j.rvsc.2013.04.024

Shih, D. T.-B., Chen, J.-C., Chen, W.-Y., Kuo, Y.-P., Su, C.-Y., and Burnouf, T. (2011). Expansion of adipose tissue mesenchymal stromal progenitors in serum-free medium supplemented with virally inactivated allogeneic human platelet lysate. *Transfusion* 51, 770–778. doi: 10.1111/j.1537-2995.2010.02915.x

Smith, R. K. W. (2003). Isolation and implantation of autologous equine mesenchymal stem cells from bone marrow into the superficial digital flexor tendon as a potentail novel treatment. *Equine Vet. J*. 35, 99–102. doi: 10.2746/042516403775467388

Stokol, T. (2020). Hematology red flags: the value of blood smear examination in horses. *Vet. Clin. North Am. Equine Pract*. 36, 15–33. doi: 10.1016/j.cveq.2019.11.001

Sumner, S. M., Naskou, M. C., Thoresen, M., Copland, I., and Peroni, J. F. (2017). Platelet lysate obtained via plateletpheresis performed in standing and awake equine donors. *Transfusion* 57, 1755–1762. doi: 10.1111/trf.14124

Sundin, M., Ringdén, O., Sundberg, B., Nava, S., Götherström, C., and Le Blanc, K. (2007). No alloantibodies against mesenchymal stromal cells, but presence of anti-fetal calf serum antibodies, after transplantation in allogeneic hematopoietic stem cell recipients. *Haematologica* 92, 1208–1215. doi: 10.3324/haematol.11446

Tesfaigzi, M. D. (2006). *CD14 - an overview | ScienceDirect Topics*. Available online at: https://www.sciencedirect.com/topics/neuroscience/cd14 (accessed October 01, 2020).

Textor, J. A., and Tablin, F. (2012). Activation of equine platelet-rich plasma: comparison of methods and characterization of equine autologous thrombin. *Vet. Surg*. 41, 784–794. doi: 10.1111/j.1532-950X.2012.01016.x

Trento, C., Bernardo, M. E., Nagler, A., Kuçi, S., Bornhäuser, M., Köhl, U., et al. (2018). Manufacturing mesenchymal stromal cells for the treatment of graft-versus-host disease: a survey among centers affiliated with the european society for blood and marrow transplantation. *Biol. Blood Marrow Transplant*. 24, 2365–2370. doi: 10.1016/j.bbmt.2018.07.015

van der Valk, J., Brunner, D., Smet, K., de Fex Svenningsen, A., Honegger, P., Knudsen, L. E., et al. (2010). Optimization of chemically defined cell culture media—replacing fetal bovine serum in mammalian *in vitro* methods. *Toxicol. In Vitro* 24, 1053–1063. doi: 10.1016/j.tiv.2010.03.016

van der Valk, J., Mellor, D., Brands, R., Fischer, R., Gruber, F., Gstraunthaler, G., et al. (2004). The humane collection of fetal bovine serum and possibilities for serum-free cell and tissue culture. *Toxicol. In Vitro* 18, 1–12. doi: 10.1016/j.tiv.2003.08.009

van Kuppeveld, F. J., van der Logt, J. T., Angulo, A. F., van Zoest, M. J., Quint, W. G., Niesters, H. G., et al. (1992). Genus- and species-specific identification of mycoplasmas by 16S rRNA amplification. *Appl. Environ. Microbiol*. 58, 2606–2615. doi: 10.1128/AEM.58.8.2606-2615.1992

Wagner, B., Ainsworth, D. M., and Freer, H. (2013). Analysis of soluble CD14 and its use as a biomarker in neonatal foals with septicemia and horses with recurrent airway obstruction. *Vet. Immunol. Immunopathol.* 155, 124–128. doi: 10.1016/j.vetimm.2013.05.018

Wildt-Eggen, J., de, Schrijver, J. G., and Bins, M. (2001). WBC content of platelet concentrates prepared by the buffy coat method using different processing procedures and storage solutions. *Transfusion* 41, 1378–1383. doi: 10.1046/j.1537-2995.2001.41111378.x

World Health Organization (2006). *WHO Guidelines on Tissue Infectivity Distribution in Transmissible Spongiform Encephalopathies*. Available online at: https://www.who.int/bloodproducts/cs/TSEPUBLISHEDREPORT.pdf?ua=1 (accessed October 02, 2020).

Yaneselli, K., Barrachina, L., Remacha, A. R., Algorta, A., Vitoria, A., Cequier, A., et al. (2019). Effect of allogeneic platelet lysate on equine bone marrow derived mesenchymal stem cell characteristics, including immunogenic and immunomodulatory gene expression profile. *Vet. Immunol. Immunopathol.* 217:109944. doi: 10.1016/j.vetimm.2019.109944

Zheng, X., Baker, H., Hancock, W. S., Fawaz, F., McCaman, M., and Pungor, E. (2006). Proteomic analysis for the assessment of different lots of fetal bovine serum as a raw material for cell culture. Part IV. Application of proteomics to the manufacture of biological drugs. *Biotechnol Prog.* 22, 1294–1300. doi: 10.1021/bp060121o

Conflict of Interest: The authors declare that the research was conducted in the absence of any commercial or financial relationships that could be construed as a potential conflict of interest.

frontiers in Bioengineering and Biotechnology

ORIGINAL RESEARCH
published: 05 February 2021
doi: 10.3389/fbioe.2021.611837

Hypoxia Onset in Mesenchymal Stem Cell Spheroids: Monitoring With Hypoxia Reporter Cells

Carola Schmitz[1], *Ekaterina Potekhina*[2], *Vsevolod V. Belousov*[3,4] *and Antonina Lavrentieva*[1]*

[1] *Institute of Technical Chemistry, Gottfried Wilhelm Leibniz University Hannover, Hanover, Germany,* [2] *Department of Metabolism and Redox Biology, Shemyakin-Ovchinnikov Institute of Bioorganic Chemistry, Moscow, Russia,* [3] *Center for Precision Genome Editing and Genetic Technologies for Biomedicine, Pirogov Russian National Research Medical University, Moscow, Russia,* [4] *Federal Center of Brain Research and Neurotechnologies, Federal Biomedical Agency, Moscow, Russia*

The therapeutic and differentiation potential of human mesenchymal stems cells (hMSCs) makes these cells a promising candidate for cellular therapies and tissue engineering. On the path of a successful medical application of hMSC, the cultivation of cells in a three-dimensional (3D) environment was a landmark for the transition from simple two-dimensional (2D) testing platforms to complex systems that mimic physiological *in vivo* conditions and can improve hMSC curative potential as well as survival after implantation. A 3D arrangement of cells can be mediated by scaffold materials where cells get entrapped in pores, or by the fabrication of spheroids, scaffold-free self-organized cell aggregates that express their own extracellular matrix. Independently from the cultivation method, cells expanded in 3D experience an inhomogeneous microenvironment. Many gradients in nutrient supply, oxygen supply, and waste disposal from one hand mimic *in vivo* microenvironment, but also put every cell in the 3D construct in a different context. Since oxygen concentration in spheroids is compromised in a size-dependent manner, it is crucial to have a closer insight on the thresholds of hypoxic response in such systems. In this work, we want to improve our understanding of oxygen availability and consequensing hypoxia onset in hMSC spheroids. Therefore, we utilized human adipose tissue-derived MSCs (hAD-MSCs) modified with a genetical sensor construct to reveal (I) the influence of spheroid production methods and (II) hMSCs cell number per spheroid to detect the onset of hypoxia in aggregates. We could demonstrate that not only higher cell numbers of MSCs, but also spheroid formation method plays a critical role in onset of hypoxia.

Keywords: hypoxia sensor, cell spheroids, adipose tissue-derived mesenchymal stem cells, hypoxia reporter cells, oxygen concentration measurements

OPEN ACCESS

Edited by:
Diego Correa,
University of Miami, United States

Reviewed by:
Roberta Piva,
University of Ferrara, Italy
Dimitrios Kouroupis,
University of Miami, United States

***Correspondence:**
Antonina Lavrentieva
lavrentieva@iftc.uni-hannover.de

Specialty section:
This article was submitted to Preclinical Cell and Gene Therapy, a section of the journal Frontiers in Bioengineering and Biotechnology

Received: *29 September 2020*
Accepted: *08 January 2021*
Published: *05 February 2021*

Citation:
Schmitz C, Potekhina E, Belousov VV and Lavrentieva A (2021) Hypoxia Onset in Mesenchymal Stem Cell Spheroids: Monitoring With Hypoxia Reporter Cells. Front. Bioeng. Biotechnol. 9:611837. doi: 10.3389/fbioe.2021.611837

INTRODUCTION

Human mesenchymal stem cells (hMSC) are extensively studied in the field of regenerative medicine. Their ability of self-renewal and differentiation makes them a promising tool for biomedical applications (Dominici et al., 2006), additionally hMSCs secrete cytokines and signal hormones which convey angiogenic and anti-apoptotic effects (Teixeira et al., 2013). Another promising bioregenerative potential of hMSCs comes from their ability to produce extracellular

vesicles (EVs), which contain messengerRNAs, microRNAs, enzymes, signal proteins, etc. (Harrell et al., 2019) and support the regeneration and survival of damaged cells and tissues (Ophelders et al., 2016). When cultured on two-dimensional (2D) platforms, cells lack microenvironmental features that are present *in vivo*, like intensive physical and biochemical intercellular interactions, accumulation of signaling molecules or naturally occurring gradients of nutrients, oxygen and metabolic waste products. Researches try to mimic this complex interplay by the use of three-dimensional (3D) cell culture systems, that either require biocompatible or bioactive scaffolds like hydrogels (Caliari and Burdick, 2016; Kirsch et al., 2019) to allow a spatial arrangement of the cells, or through the fabrication of scaffold-free cellular aggregates—spheroids. In comparison to scaffold-based platforms, which contain an exogenic compounds, cells arranged as spheroids build their own extracellular matrix to maintain their 3D organization.

For 3D cell spheroid-based *in vitro* models, drug screenings and spheroid production for biomedical applications, robust and reproducible methods for spheroid fabrication are required. There are many techniques to produce cell spheroids: the traditional and historically the oldest *hanging drop* technique is cheap and easy (Foty, 2011) while *spheroid low attachment microplates* allow a more standardized fabrication procedure and better handling (Howes et al., 2014). In both cases the exact cell number per spheroid can be reproducibly set. Other techniques, including *liquid overlay* technique (Costa et al., 2018) or *spinner flask culture* (Lin and Chang, 2008) produce spheroids in large scale but lack the ability to exactly control spheroid sizes. Microfluidic systems, rotating wall vessel as well as magnetic levitation are more sophisticated, but require special equipment, which is not available to every laboratory (Ryu et al., 2019). One of the newest approaches for the large scale spheroid production are microstructured plates or cultivation chambers. Using these systems, hundreds of spheroids with same size can be generated (Dou et al., 2018).

Spheroid cultures were shown to be advantageous over traditional 2D cultivation since intercellular interactions are enhanced and cells built their own extracellular matrix similar to *in vivo*. During spheroid formation, cadherin and integrin glycoproteins mediate the construction of an adhesive network and take a significant role in cell signaling pathways (Weber et al., 2011). As a result of biochemical and mechanotransducive effects, hMSCs organized in a spheroid show increased angiogenic (Bhang et al., 2012; Cheng et al., 2013), anti-inflammatory (Bartosh et al., 2010; Murphy et al., 2017b) and immunomodulatory potential (Follin et al., 2016; Noronha et al., 2019), as well as increased stemness compared to cells cultivated in 2D (Lee et al., 2017). Moreover, increased cell survival of spheroids applied *in vivo* was observed by several research groups (Liu et al., 2013; Xu et al., 2016). Amos et al. (2010) applied adipose tissue-derived hMSCs spheroids in mouse models for dermal wound treatment and could show, that the injection of suspension cells was less successful than 3D cultivated and applied cells. It is important to note that cultivation in 3D aggregates allows MSC expansion under serum-free conditions (Alimperti et al., 2014). Moreover, even if cells were cultivated in 2D in several passages and then brought to the 3D spheroid cultures, their regenerative potential was significantly improved (Cheng et al., 2013). Application of 3D spheroid culture as priming strategy for enhanced therapeutic potential of MSCs is also described by Kouroupis et al. (2019). Thus, numerous reviews on expansion methods of hMSCs indicate advantages of cultivation in 3D spheroids prior implantation (Egger et al., 2018; Mastrolia et al., 2019; Noronha et al., 2019; Lavrentieva et al., 2020).

Besides MSCs expansion for clinical applications, spheroids created from other cell types provide a suitable platform for studies of tumor growth and behavior, enabling researches to investigate the influence of the microenvironment on 3D arranged cells similar to tumors *in vivo* (Gilkes et al., 2014). Many researchers agreed, that cell metabolism and oxygen consumption in these 3D aggregates lead to the formation of a hypoxic core, which is closely related to altered cell response toward many tumor treatments compared to studies performed in 2D (Däster et al., 2017; Nunes et al., 2019). While application or onset of hypoxia in tumor spheroids is intensively studied, little is known about presence of hypoxia in MSCs aggregates. Tumor spheroids where shown to build a necrotic or hypoxic core (Khaitan et al., 2006; Riffle and Hegde, 2017), in contrast, hMSC spheroids seem to adapt to 3D cultivation by decreasing their packaging density and therefore enable easier oxygen diffusion (Murphy et al., 2017a). Due to different spheroid formation platforms, spheroid sizes and experimental setups, the formation of a hypoxic core and oxygen availability in non-tumor MSCs spheroids remains unclear.

Since cell response to hypoxia is mainly mediated by the stabilization of hypoxia inducible factor 1α (HIF-1α) (Majmundar et al., 2010), this key regulator serves as a great tool to detect and investigate hypoxic conditions *in vitro* and *in vivo*. Under hypoxic conditions, the protein degradation of the constitutively expressed HIF-1α is inhibited (Maxwell et al., 1999) and HIF-1α can enter the cell core, dimerise with HIF-1β and bind to the hypoxia responsive elements (Jiang et al., 1996), triggering oxygen-depended regulation of over 300 genes (Mole et al., 2009). Erapaneedi et al. (2016) utilized HIF-1α stabilization and hypoxia responsive elements to generate a genetic construct which modulates reporter protein expression, when cells are exposed to hypoxia. The system relies on the expression of fluorescent UnaG protein (Kumagai et al., 2013), whose maturation process is independent from presence of molecular oxygen. While this construct provides a great tool for hypoxia research in general, the application of hypoxia reporter cells is invaluable for 3D cell culture applications (Schmitz et al., 2020). Finally, a non-invasive hypoxia monitoring allows the live analysis of the hypoxic state of single cells within complex constructs.

In the present study, we utilized human adipose tissue-derived MSCs (hAD-MSCs) modified with genetical sensor construct to reveal (I) the influence of spheroid production methods and (II) MSCs cell number per spheroid to detect the onset of hypoxia in aggregates. Additionally, we performed oxygen concentration measurements in fabricated spheroids. We could demonstrate that not only higher cell numbers of MSCs, but

also spheroid formation method plays a crucial role in onset of hypoxia.

MATERIALS AND METHODS

Reporter hAD-MSCs

Hypoxia reporter MSCs were created as described earlier (Schmitz et al., 2020). Briefly, hAD-MSC were isolated from adipose tissue after abdominoplasty applying the protocol of Zhu et al. (2008). All patients provided their informed consent, as approved by the Institutional Review Board (Hannover Medical School) with the reference number 3475-2017. The obtained cells were characterized by MSC-typical surface markers and functional properties (Dominici et al., 2006) and the presence of adipogenic, chondrogenic, and ostogenic differentation potential. hAD-MSCs were used for lentiviral transduction, to stably integrate HRE-dUnaG (Erapaneedi et al., 2016) sequence. Efficient transduction with HRE-dUnaG and oxygen-dependend UnaG expression was shown in our previous work (Schmitz et al., 2020). Surface antigen expression of hypoxia reporter modified MSCs was evaluated by flow cytometry. Cells cultivated in 2D were harvested by accutase treatment, washed with cold blocking buffer (2% human serum in PBS) and resuspended in 100 µl of cold washing buffer to a concentration of 10×10^4 cell/100 µl. Each cell solution was incubated for 20 min in the dark at room temperature with respective antibodies. Cells were tested positively for MSC specific antigens as CD73 (ecto-5′-nucleotidase) and CD105 (endoglin). Reporter MSCs were tested negatively for non MSC specific antigens CD34, CD45 and CD31 (**Supplementary Figure 1**). Antibodies with respective reporter dye and isotype controls: PE Mouse IgG1, κ Isotype Control was compared with PE Mouse Anti-Human CD73 and PE Mouse anti-Human CD105. FITC Mouse IgG1, κ Isotype Control was used for APC Mouse Anti-Human CD34 and FITC Mouse Anti-Human CD45 testing. PE-CF594 Mouse Anti-Human CD31 and PE-CF594 Mouse IgG1, κ Isotype were applied (all purchased from BD Bioscience, USA). Cells were cultivated in α-minimum essential medium (MEM; Thermo Fisher Scientific, USA) containing 1 g/L glucose, 2 mM l-glutamine, 10% human serum, and 50 µg/ml gentamicin (Merck KGaA) in a humidified incubator (C16, Labotect, Germany) at 37°C at 5% CO_2.

Spheroid Fabrication, Imaging, and Spheroid Diameter Analysis

Cells (passage 8–10) expanded in 2D were harvested by accutase treatment. Spheroids of different cell numbers (1, 3, 7.5, 15, 30×10^4 cells) were formed using different fabrication methods. In the first technique, cells were seeded into 96-well Corning® Costar® ultra-low attachment plates in 150 µl of αMEM supplemented with 10% human serum and 0.5% gentamycin. For the hanging drop spheroid fabrication, drops of cell suspensions (30 µl) were seeded into Terasaki microassay plate wells (Greiner Bio-One, Austria). For spheroid formation in hanging drop, the plate containing the cell suspensions was turned upside down and placed on the lid. To prevent fluid evaporation 2–3 ml PBS were previously pipetted in the lid. For both methods spheroid formation time was 24 h under similar culturing conditions as mentioned above. After 24 h spheroids were transferred to 24 well lumox multiwell plates (Sarstedt, Germany) and images of at least three spheroids were taken by Cytation®5 multimode imaging reader (BioTek® Instruments, USA). To determine the spheroid diameter, the average of the length of the x-axis and the y-axis of each spheroid was measured in paint.net, using the microscopic scale to translate the length in pixel into decimal system.

Kinetic Imaging of Spheroid Fabrication

The spheroid formation process and onset of hypoxic response during formation were monitored by kinetic imaging via Cytation®5 multimode imaging reader for low attachment plates and with incubator microscope (Lumascope 600, Etaluma Inc., Carlsbad, CA, USA) for Terasaki plates and microstructured plates. For low attachment plates, magnification of 4x was used to take one bright field channel (LED intensity: 5, exposure time: 100, gain: 0.6) and one GFP channel (LED intensity: 6, exposure time: 100, gain: 0) image every 10 min for 24 h. The images were used to create videos by the integrated Gen.2.08 software. For Terasaki plates and microstructured plates, images were taken with the help of Lumaview (Etaluma Inc., Carlsbad, CA, USA) software in bright field and GFP channels every 1 min and videos were created using VideoDub software.

Spheroid Dissociation and Flow Cytometric Analysis

For the flow cytometric analysis, spheroids were washed with PBS, transferred into 2 ml reaction tubes and 200 µl TrypLE Express solution (Thermo fisher, Germany) was added for enzymatic digestion. Cells were incubated at 37°C. Additionally, every 10 min cell separation was stimulated by mechanical disruption through rough pipetting using a glass pipette. After 20 min of incubation, another 200 µl TrypLE Express solution was added to the reaction tube. This process was performed until up to 1 h, or ended earlier, if cells were already singularized. The cells were centrifuged (5 min, 200xg) and the pellet resuspended in PBS for flow cytometric analysis. The flow cytometer BD FACSAria™ Fusion (Becton Dickinson, USA) was used to evaluate single cell fluorescence. The target cell population was excited at 488 nm and fluorescence detected via FL 1 detector (533/30 nm) to analyze the cellular expression of UnaG protein.

Large Scale Spheroid Formation and Imaging in Microstructured Plates

The third studied spheroid fabrication technique was microstructured plates (Sphericalplate 5D, Kugelmeiers Ltd., Switzerland). Here, spheroids with two different cell numbers (∼270 cells and 1,300 cells) were created and studied. Therefore, either 0.2×10^6 or 1×10^6 cells were plated into the microstructured plate in 1 ml cell culture medium accordingly to the manufacturer's instructions. To avoid air bubbles formation, plates were pre-incubated with warm PBS for 2 h prior cell seeding.

In situ Oxygen Measurements

For the measurement of local oxygen concentrations in spheroids OPAL Optical O_2 Measurement System (Colibri Photonics

GmbH, Germany) was used. The OPAL system, integrated into the fluorescent microscope, allows quantitative optical non-invasive oxygen measurements in 2D and 3D cell cultures. During spheroid formation, 0.4 µl CPOx-orange microbeads (50 µm polystyrene beads, 5 mg/ml suspension in PBS) were added in each well of low attachment plate or to each drop of Terasaki plate, resulting in 4–15 beads per spheroid. For the performed oxygen measurements, the analysis was always focused on the center of the 3D aggregate. If several beads were incorporated in the spheroid, the system evaluated an average oxygen tension for all beads in the microscopes focus area. For microstructured plates, microbeads were distributed evenly in the microwells, before cell suspension for spheroid formation was added. After spheroid formation, oxygen measurements were performed at room temperature at Ex530nm/Em600nm using OPAL system. Three spheroids per platform and per cell number were measured to obtain mean values.

Data Analysis

Data is shown as mean value of at least 3 measurements. The error bars show the positive/negative standard deviation. Statistical significance was assessed with the one way ANOVA (Microsoft Exel, Microsoft corporation, USA).

RESULTS

Three different spheroid fabrication platforms (ultra low attachment plate, hanging drop and microstructured plates) were applied to obtain spheroids of different sizes. A direct comparison between ultra low attachment plates und hanging drop method was performed in terms of fluorescent hypoxia reporter protein expression (by fluorescent microscopy and flow cytometry). Additionally, *in situ* oxygen measurements were executed for spheroids of different sizes and fabrication platforms. For microstructured plates, fluorescent microscopy and local oxygen measurements in cell culture medium near spheroids was performed (**Figure 1**).

Spheroid Fabrication in Low Attachment Plates and by Hanging Drop Method

To study (1) the influence of spheroid cell number and (2) spheroid fabrication platform on the onset of hypoxia in 3D cellular aggregates, spheroids of similar cell numbers (1, 3, 7.5, 15 or 30 $\times$ 10^4 cells) were created in ultra low attachment plates or via hanging drop method. To lower the variance of spheroid shape due to different drop geometries, Terasaki plates were used for creation of hanging drops. Spheroids fabricated on both platforms were evaluated after 24 h (**Figures 2A,B**). For both, the ultra low attachment plate and the hanging drop method, expression of UnaG protein as a hypoxia reporter protein could clearly be monitored. For the spheroid formation in well plates, a strong signal was obtained from a spheroids of 3 $\times$ 10^4 cells and larger (**Figure 2A**), for the hanging drop method the reporter protein expression starts at spheroid size from 7.5 $\times$ 10^4 and larger (**Figure 2B**). Moreover, microscopically detected UnaG fluorescence was not only detected in smaller spheroids in the low attachment plates, but this fluorescence was remarkably higher in the spheroids of the same size than in the ones created with hanging drops. Hypoxic core was seen in spheroids with 3 $\times$ 10^4 cells in the low attachment plates and in spheroids

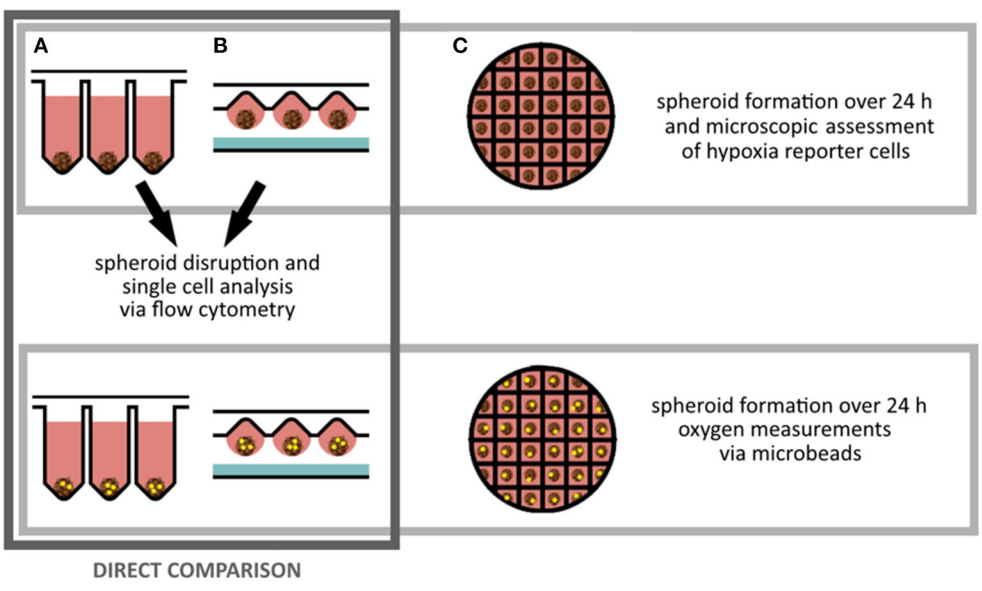

FIGURE 1 | Experimental planning: Spheroids of MSC reporter cells were fabricated for 24 h on three different platforms. **(A)** Ultra low attachment plates, **(B)** by hanging drop method, **(C)** on microstructured plates. Spheroids created on ultra low attachment plates and by hanging drop method were singularized for flow cytometry analysis to investigate the sensor cell output. For all methods oxygen sensitive microbeads were applied to determine local oxygen concentrations inside of the spheroids.

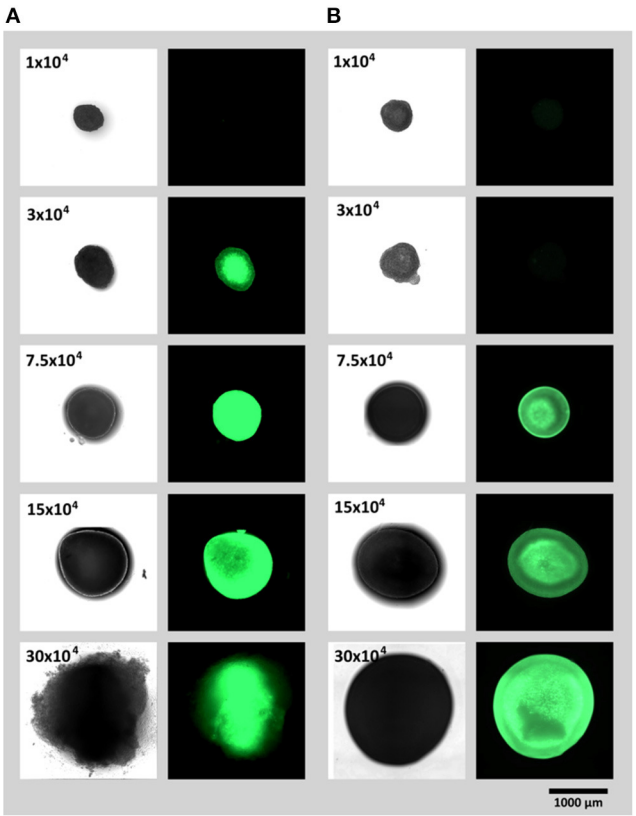

FIGURE 2 | Spheroid formation and resulting reporter hAD-MCSs fluorescence (UnaG expression) after 24 h on **(A)** ultra low attachment plates and **(B)** via hanging drop method.

with 7.5 × 10^4 and 15 × 10^4 cells in hanging drop plates. In low attachment plates, fluoresce of reporter cells was spheroids was even distributed all over the aggregates with 7.5 × 10^4 cells and larger. The largest tested spheroids (30 × 10^4 cells) demonstrated decrease of fluorescence and spheroid dissociation in ultra low attachment plates. Spheroids of the same size in the hanging drop plate demonstrated high fluorescence intensity, but retained integrity.

Kinetic Imaging of Spheroid Formation

The spheroid formation process and onset of sensor fluorescence was also monitored via kinetic imaging. Time-lapse videos are presented in the **Supplementary Videos 1, 2**. For both fabrication platforms, first signals of UnaG expression could be monitored 7 h after start of spheroid formation. Due to the different plate geometries, two different imaging platforms had to be used, which allowed detection of fluorescence but could not be directly compared in terms of fluorescence assessment.

Spheroid Dissociation and Flow Cytometric Analysis

For quantitative analysis of reporter cell fluorescence, flow cytometry was additionally performed. Spheroids were dissociated after 24 h of fabrication to allow access to single cell analysis. The average cell fluorescence for each spheroid size and the respective method is displayed in the **Figure 3A**. With the help of highly sensitive flow cytometry, increase of fluorescence in the low attachment plates (in comparison to hanging drops) was already detected in the smallest studied spheroids (1 × 10^4 cells per spheroid). Supporting the results of fluorescent microscopy significantly increased mean UnaG fluorescence was detected in aggregates formed in ultra low attachment plates if compared to hanging drop plates. For ultra low attachment plates, highest detected fluorescence was in the spheroids with 7.5 × 10^4 cells. For larger spheroids the mean fluorescence was decreasing. In contrast, the mean fluorescence of spheroids created by hanging drop method was much weaker, compared to the ultra low attachment plate. Moreover, a constant increase in mean UnaG fluorescence with increasing spheroid size could be detected.

To additionally study the influence of the different fabrication platforms on spheroid size, which affect oxygen diffusion inside of the 3D construct, the diameters of the undissociated spheroids were evaluated (**Figure 3B**). For most sizes, spheroid diameter appears to be similar for both methods. For 30 × 10^4 cells per spheroid, the average diameter appears to be larger, but when compared to the image in **Figure 2A** and the Video (**Supplementary Video 1**), the actual spheroid seems to dissociate causing the increase in the measured diameter.

In situ Oxygen Measurements in Cell Spheroids With Oxygen Sensitive Microbeads

In addition to the acquired fluorescent hypoxia signal output evaluation, oxygen sensitive microbeads (CpoX orange) were incorporated in spheroids of each size and fabrication platform. Evaluation of the local oxygen concentrations was consistent with fluorescent reporter cell output. With increasing spheroid size, the oxygen content in the 3D cell aggregate drops (**Figure 4A**). Supporting flow cytometry results, spheroids fabricated by hanging drop method show higher local oxygen tensions as spheroids created in ultra low attachment plates. Spheroids of 30 × 10^4 cells reach oxygen concentrations as little as <1% (v/v). Important to note that despite this system allows a local oxygen evaluation also for 3D cellular constructs, the spatial positioning of the microbeads can hardly be controlled (**Figure 4B**).

Application of Hypoxia Reporter Cells in Large Scale Spheroid Formation in Microstructured Plates

According to the manufacturers, microstructured plates allow fast creation of large amounts of spheroids with controlled diameter and identical biological properties. Hypoxia reporter cells were applied in a microstructured plate to control the stabilization of HIF-1α and to confirm the uniformity of large scale spheroid formation. Cells were seeded in 2 different densities: 20 × 10^4 cells per well and 100 × 10^4 cells per well and incubated for 24 h. While no fluorescent signal could be monitored at 20 × 10^4 cell/well (∼267 cells per spheroid,

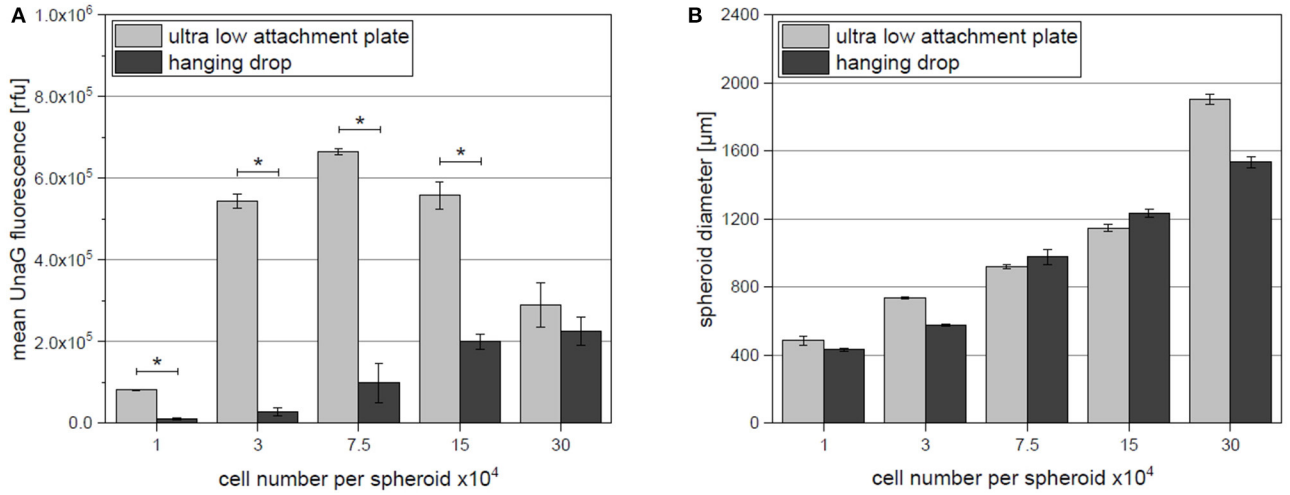

FIGURE 3 | (A) Mean single cell fluorescence determined by flow cytometry. For both fabrication platforms (ultra low attachment plate and hanging drop) hypoxia reporter hAD-MSCs were cultivated as spheroids and dissociated to facilitate single cell analysis. **(B)** Respective spheroid diameters as obtained by both fabrication platforms. Data represent the mean ± SD for a 3-fold determination. *$p < 0.05$.

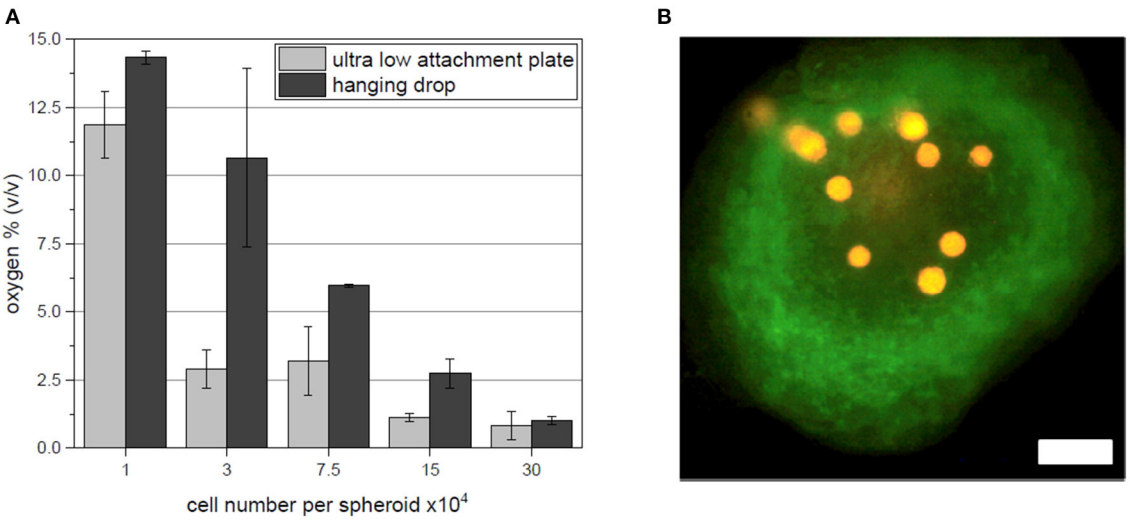

FIGURE 4 | (A) *In situ* oxygen measurements for each spheroids size and fabrication platform. **(B)** Exemplary fluorescent image of microbeads (orange) incorporated in a spheroid of 7.5 × 10^4 hypoxia reporter hAD-MSC (green) fabricated in ultra low attachment plates. Scale bar: 200 µm.

spheroid diameter of 100 µm), 100 × 10^4 cells/ well (∼1,333 cells per spheroid, spheroid diameter of 180 µm) led to the hypoxia reporter signal (expression of UnaG protein) (**Figure 5A**). Interestingly, a gradient of fluorescence could be detected over the microstructured well, when the entire well was accessed. Spheroids at the outer edge of the microstructured well-expressed gradually more UnaG protein as spheroids formed in the center (**Figure 5B**). Big chunks of cells appearing in the image are a result of plate transportation to the imaging system. Due to the agitation, spheroids leave their wells and unwontedly accumulate with other spheroids. Time laps microscopy, however clearly demonstrated the absence of fluorescent spheroids in the middle of the well (**Supplementary Video 3**).

Oxygen Measurement in Medium in Microstructured Wells

Oxygen sensitive microbeads were applied in microstructured plates to measure the local oxygen content of the cell culture medium when spheroids were formed using 100 × 10^4 cells per well. In contrast to previous oxygen measurement experiments, microbeads could not be embedded inside of spheroids since microbead diameter was too large (50 µm) to be incorporated in small (180 µm) spheroids. Here, microbeads were either positioned at the edge of the spheroid, or underneath the 3D cell aggregate in medium (**Figure 6A**). The resulting oxygen concentrations were evaluated with OPAL system, starting in the center of the microstructured well (position 1) to the outer edge

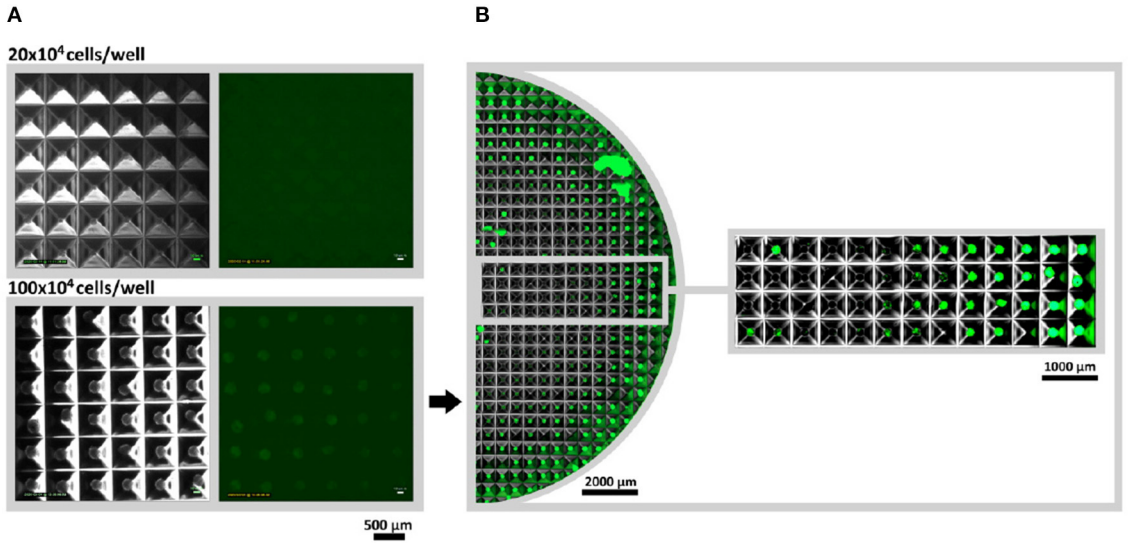

FIGURE 5 | Large scale spheroid formation in microstructured wells. **(A)** Spheroids were monitored via Lumascope for 20 × 10^4 and 100 × 10^4 cells per well after 24 h of formation time. Larger spheroids (100 × 10^4 cells/multiwell) would express the hypoxia reporter protein UnaG, while low numbers (20 × 10^4 cells/multiwell) did not show a signal. For both studied seeded cell numbers images were taken from the outer corner of the well to guarantee comparability. **(B)** For 100 × 10^4 cell/multiwell half the well was accessed via image stitching. Time-laps video of spheroid formation and onset of fluorescence can be seen in **Supplementary Video 3**.

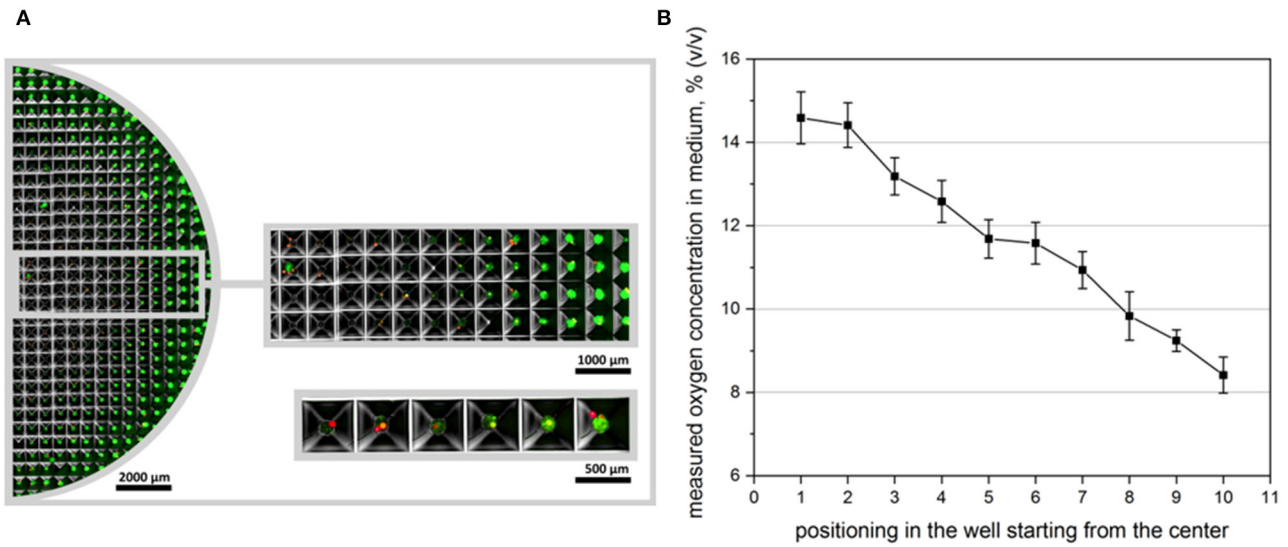

FIGURE 6 | Oxygen measurement in microstructured wells. **(A)** Overview over half the microstructured well with seeded oxygen sensitive microbeads. CpoX beads (red) were placed in the microwells previously to reporter cell seeding. 100 × 10^4 cells/multiwell are displayed 24 h after cell seeding. **(B)** Accordingly oxygen concentrations in different microwells were measured. Position 1 represents microwells mostly in the center, while position 10 represents wells at the outer edge of the well. Measurements were taken in even distances in dependence of the readability of the applied microbeads. A clear gradient in oxygen availability could be monitored as confirmed by reporter cell output.

(position 10). A clear gradient in oxygen tension in medium could be monitored which confirmed reporter cells output (**Figure 6B**).

DISCUSSION

MSCs isolated from different tissues considered to be promising candidates for cell therapies and tissue engineering. In most of the cases, after isolation, MSCs must be expanded *in vitro* prior injection or application in tissue engineered constructs. Cultivation of MSCs in 3D cellular aggregates (spheroids) helps to preserve their biological functions and increase their therapeutic potential (Murphy et al., 2017a; Lavrentieva et al., 2020). Cultivation in spheroids enhances secretion of MSCs angiogenic, immunomodulatory, pro- and anti-inflammatory factors, as well as their differentiation potential (Cesarz and

Tamama, 2016). Even if only shortly cultivated in 3D spheroids, MSCs demonstrate improved biological functions.

The reasons of higher MSCs curative properties after cultivation in 3D spheroids seems to be an increase of pluripotent gene expression via relaxation of cytoskeleton tension (Zhou et al., 2017), lower vascular obstruction via small cell size preservation (Ge et al., 2014) and increased expression and secretion of rescue factors as a sequence of hypoxia (Potapova et al., 2007).

There are several methods for *in vitro* spheroid formation, including centrifugation, low attachment plates, hanging drops and structured microwells (Bartosh et al., 2010; Egger et al., 2018; Lavrentieva et al., 2020). Each method has advantages and disadvantages and is usually chosen according the subsequent application or experimental set-up. With the help of hypoxia reporter cells we for the first time directly detected the onset of hypoxia in spheroids of different diameters and compared the influence on different spheroid fabrication platforms. Two fabrication platforms with different features were directly compared: (1) ultra low attachment microplates, were cells accumulate on the bottom of the wells and oxygen is mostly available through diffusion throughout the medium overlay, and (2) hanging drop in Terasaki plates, where the spheroid accumulates in the drop and the cells are almost directly exposed to the surrounded oxygen-rich atmosphere. Additionally, we applied the hypoxia reporter cells on microstructured wells for large scale spheroid formation and could demonstrate unequal hypoxia reporter protein expression if higher cell numbers were used. In the first part of our study we manufactured spheroids of 1×10^4, 3×10^4, 7.5×10^4, 15×10^4, and 30×10^4 hAD-MSCs in spheroid microplates and via hanging drops in Terasaki plates. For large cell numbers ($>7.5 \times 10^4$ cells per spheroid) strong hypoxia reporter protein expression could be monitored. Interestingly, for 3×10^4 cells per spheroid fluorescent hypoxia signal was present when 3D aggregates were formed in ultra low attachment plates, but no microscopically visible fluorescence was detected for spheroids created via hanging drop method. One possible explanation could be the difference in culture medium volumes used in both methods. A maximal possible medium drop volume for hanging drop method was 30 µl (to avoid the fall of the drop), compared to 150 µl media used for ultra low attachment plates. Additionally, to the larger gas-liquid interface in hanging drops, small drop volume seems to allow a better oxygen supply by decreased oxygen diffusion distances. Disadvantageously, small media volumes can lead to the fast drop of nutrients, so ultra low attachment plates, which facilitate spheroid formation in higher medium volumes, are widely used in scientific community. However, application of hypoxia reporter MSCs demonstrated that in the ultra low attachment plates oxygen transport limitation through cell culture media can cause an earlier onset of hypoxia if compared to hanging drops. These findings were also supported by further flow cytometric analysis.

The spheroids of each fabrication method were dissociated by proteases and fluorescent reporter protein expression was quantified by flow cytometric analysis. We were able to spot a significant increase in fluorescent signal output when ultra low attachment microplates were used. The strongest difference was detected for spheroids of the size of 3×10^4 and 7.5×10^4 cells. Unexpectedly the mean fluorescence of spheroids of 15×10^4 and 30×10^4 cells decreases in ultra low attachment microplates. As shown in **Figure 1A** the spheroid of 30×10^4 cells has loose edges. When watched in the respective formation video (**Supplementary Video 1**), the spheroid fist forms and then cells start to dissociate. This indicates that cells of the two largest spheroids (15×10^4 and 30×10^4) possibly die due to strong oxygen deprivation, which in turn could explain the decrease in fluorescence.

The limitation of the flow cytometric analysis is the breakdown of spatial spheroid organization by dissociation. When the spheroids get dissociated for analysis, cells from the center of the spheroid, where strongest hypoxia is expected, and cells of the outer areas, where oxygen transport limitation are supposed to be weak, get mixed up. As a result, only mean fluorescence of the entire spheroid population can be obtained. As shown in our earlier works, the fluorescent signal of the hypoxia reporter hAD-MSCs at 2.5% O_2 in 2D cultures reached an average signal of $\sim 1.3 \times 10^6$ RFU (Schmitz et al., 2020). The detected average signal in this work is twice weaker (max. mean fluorescence of 6.6×10^5 RFU). In contrast, if looking on the highest fluorescent 1% of the cell population, the fluorescence signal intensity is similar to the highest cell fluorescence detected in 2D by 2.5% O_2 for 24 h (data not shown). This indicates, that some of the cells in the studied spheroid cultures were exposed to oxygen concentrations as low as 2.5% O_2. As confirmed by other researches (Groebe and Mueller-Klieser, 1991; Barisam et al., 2018) a gradient of oxygen is maintained within the spheroid, often causing hypoxia in the spheroid core (hypoxic core), while cells at the spheroid edge are not affected by oxygen diffusion limitations. Consequently, cells at the outer edge of the 3D aggregate experience less or even no oxygen deprivation and weaken the average signal intensity. Dead cells, which do not express UnaG could additionally weaken the average fluorescent signal.

The application of the OPAL system for *in situ* oxygen measurements confirms the findings of the previous results. Increasing spheroid sizes cause lower oxygen concentrations and ultra low attachment plates show fast drop of oxygen tension signals if compared to spheroids fabricated as hanging drops. While the used microbeads based system provides a great tool for oxygen measurements in 3D cell culture applications, the spatial incorporation of the beads could hardly be controlled and Z-axis positioning of beads could not be precisely evaluated. Nevertheless, performed measurements demonstrated the clear trend of stronger oxygen limitations in the ultra low attachment plate.

The application of different spheroid formation methods can influence the spheroid packaging density and consequently spheroid diameters. Evaluation of spheroid size demonstrated no difference between hanging drop and low attachment plate—fabricated spheroids (except for 30×10^4, as discussed before). Thus, only spheroid fabrication platform and medium volume influence the onset of hypoxia. For example, we found that for spheroids of 7.5×10^4 cells the average spheroid diameter

is similar for both fabrication methods (ultra low attachment plate: 920 μm; hanging drop: 979 μm), but the hypoxia signal output is 6.5 times higher when fabrication is performed in ultra low attachment plates. It is widely accepted that spheroid size greatly influences *in situ* conditions and final cellular properties. For years scientists have been trying to estimate the critical sizes of various *in vitro* 3D constructs. Indeed, for cancer cellular aggregates it is believed that constructs with diameter between 200 and 500 μm already demonstrate gradients and exhibit oxygen limitation which leads to the necrosis of the core cells (Hirschhaeuser et al., 2010). Some attempts were earlier made to measure or model hypoxic core in MSCs spheroids, leading to controversial results demonstrating that in some spheroids with 100 μm diameter hypoxia was detected (Zhang et al., 2012), and in other experiments no hypoxia occurred in much larger spheroids up to 500 μm (Murphy et al., 2017a). Interestingly, these findings are subsequent with the outcome of our study, since Zhang et al. (2012) formed their spheroids in low attachment plates, while Murphy et al. (2017a) applied the hanging drop method. Therefore, it is questionable if a direct relation of spheroid diameter and hypoxic response in cell spheroids can be made. As presented, additionally to the cell number and spheroid size, the fabrication platform hugely influences the onset of hypoxia.

At the final step, hypoxia reporter cells were applied on microstructured wells to create high numbers of uniform spheroids as advertised by the manufacturer. By using this platform we could demonstrate that if smaller cell numbers were used to create spheroids, no hypoxia occurred in entire plate (20×10^4 cells/ well, 270 cells per spheroid, spheroid diameter of 100 μm). However, we were able to monitor a gradient in hypoxia signal over the microwells, if higher cell numbers were used (100×10^4 cells/ well, 1,350 cells per spheroid, spheroid diameter of 180 μm). Keeping in mind that over 300 genes are up- or down-regulated by HIF-1α, the resulting spheroids represent biologically heterogenic unequal aggregates, with morphologically similar appearance (spheroid sizes). *In situ* oxygen concentration measurements also confirmed unequal oxygen distribution with decreasing concentrations at the well edge.

Taken together, the results of this study demonstrate the influence of cell number and fabrication platform on the onset of hypoxia in hAD-MSCs spheroids. We demonstrated different thresholds for hypoxia when different fabrication platforms are used. The presence of hypoxia, however, has no necessarily negative effect on the cells. As mentioned above, one of the reasons of improved curative potential of MSCs cultivated in 3D could be the increased stromal function as a result of hypoxia (Potapova et al., 2007). Thus, in further experiments, cytokine expression from the spheroids of the same sizes created by different methods must be studied and influence of onset of hypoxia on expression profile must be evaluated. In the future, various 3D fluorescence monitoring techniques must be also applied to better understand spatial distribution of fluorescent signal inside of spheroids. Additional important platforms, where a possible hypoxic response can be studied with the help of reporter MSCs, are advanced 3D co-culture systems. Indeed, different cell types (e.g., cancer cells, endothelial cells) have different oxygen consumption rates and metabolic activities, which can lead to variations in hypoxia onset in spheroids of the same size/cell number. Since such co-cultures are widely used in basic research and drug screening, direct monitoring of hypoxia in these systems will allow a better understanding of cell behavior. If hypoxia must be avoided, spheroids up to 7.5×10^4 cells and 920 μm diameter can be used if hanging drop technique applied, and up to 3×10^4 cells and 600 μm diameter if low attachment plate is used. Nevertheless, using both platforms, non-hypoxic spheroids can be created at the sizes much higher than it was believed before. In microstructured plates also much attention must be paid to the cell numbers used. Moreover, the reason of the radial oxygen gradient from the center to the well edge must be found. The presence of this gradient can also be used to simultaneously study e.g., the influence of different compounds on 3D aggregates under different oxygen tensions.

CONCLUSION

In this study we for the first time directly demonstrated critical sizes of hAD-MSCs spheroids in terms of onset of hypoxia. We showed that not only cell numbers, but also spheroid fabrication platforms play a crucial role in the onset of hypoxia. Hypoxia-reporter MSCs detected HIF-1α stabilization in spheroids with 3×10^4 cells (600 μm) if ultra low attachment plates are used. By hanging drop technique, hypoxia can be first detected by spheroids with 7.5×10^4 cells (920 μm). In microstructured plates spheroids with 270 cells and 100 μm did not demonstrate hypoxia, but increased cell numbers (1,350 cells per spheroid and diameter of 180 μm) led to a radial oxygen gradient in the wells. This study underlines, that not only cell type, passage or spheroid diameter are crucial parameters for 3D cell aggregate research, but also the actual fabrication platform critically influences the final spheroid state. Uniform cultivation and spheroid formation platforms would help to create comparable data through different research group and increase the amount of utilizable information for 3D cell aggregate applications. Moreover, hypoxia reporter cells proved to be as an easy and reliable tool to monitor hypoxic response in such systems.

DATA AVAILABILITY STATEMENT

The raw data supporting the conclusions of this article will be made available by the authors, without undue reservation.

ETHICS STATEMENT

All patients provided their informed consent, as approved by the Institutional Review Board (Hannover Medical School) with the reference number 3475-2017.

AUTHOR CONTRIBUTIONS

CS performed most of the experiments and drafted the manuscript. EP and VB provided sensor sequence,

introduced sensor sequence into lentiviral vector, helped to analyze and interpretate the results, and proofreaded the manuscript. AL concepted the manuscript, performed oxygen measurements, participated in the data analysis and results interpretation the results, and proofreaded the manuscript. All authors contributed to the article and approved the submitted version.

FUNDING

This study was supported by the German Research Foundation (DFG Project 398007461 488 3D Dual-Gradient Systems for Functional Cell Screening) and Grant # 075-15-2019-1789 from the Ministry of Science and Higher Education of the Russian Federation. The publication of this article was funded by the Open Access Fund of the Leibniz Universität Hannover.

SUPPLEMENTARY MATERIAL

The Supplementary Material for this article can be found online at: https://www.frontiersin.org/articles/10.3389/fbioe.2021.611837/full#supplementary-material

Supplementary Figure 1 | Flow cytometry analysis of surface antigens expressed by reporter MSCs (P9) after cultivation in 2D and prior to spheroid fabrication. Cells were stained with respective antibodies conjugated to fluorescent reporters. MSC typical antigens as CD 73 and CD 105 were expressed and cells were tested negatively for hematopoietic (CD34), leucocytic (CD45), and endothelial (CD31) markers.

REFERENCES

Alimperti, S., Lei, P., Wen, Y., Tian, J., Campbell, A. M., and Andreadis, S. T. (2014). Serum-free spheroid suspension culture maintains mesenchymal stem cell proliferation and differentiation potential. *Biotechnol. Prog.* 30, 974–983. doi: 10.1002/btpr.1904

Amos, P. J., Kapur, S. K., Stapor, P. C., Shang, H., Bekiranov, S., Khurgel, M., et al. (2010). Human adipose-derived stromal cells accelerate diabetic wound healing: impact of cell formulation and delivery. *Tissue Eng. Part A* 16, 1595–1606. doi: 10.1089/ten.tea.2009.0616

Barisam, M., Saidi, M. S., Kashaninejad, N., and Nguyen, N. T. (2018). Prediction of necrotic core and hypoxic zone of multicellular spheroids in a microbioreactor with a U-shaped barrier. *Micromachines* 9, 1–19. doi: 10.3390/mi9030094

Bartosh, T. J., Ylöstalo, J. H., Mohammadipoor, A., Bazhanov, N., Coble, K., Claypool, K., et al. (2010). Aggregation of human mesenchymal stromal cells (MSCs) into 3D spheroids enhances their antiinflammatory properties. *Proc. Natl. Acad. Sci. U.S.A.* 107, 13724–13729. doi: 10.1073/pnas.1008117107

Bhang, S. H., Lee, S., Shin, J.-Y., Lee, T.-J., and Kim, B.-S. (2012). Transplantation of cord blood mesenchymal stem cells as spheroids enhances vascularization. *Tissue Eng. Part A* 18, 2138–2147. doi: 10.1089/ten.tea.2011.0640

Caliari, S. R., and Burdick, J. A. (2016). A practical guide to hydrogels for cell culture. *Nat. Methods* 13, 405–414. doi: 10.1038/nmeth.3839

Cesarz, Z., and Tamama, K. (2016). Spheroid culture of mesenchymal stem cells. *Stem Cells Int.* 2016:9176357. doi: 10.1155/2016/9176357

Cheng, N.-C., Chen, S.-Y., Li, J.-R., and Young, T.-H. (2013). Short-term spheroid formation enhances the regenerative capacity of adipose-derived stem cells by promoting stemness, angiogenesis, and chemotaxis. *Stem Cells Transl. Med.* 2, 584–594. doi: 10.5966/sctm.2013-0007

Costa, E. C., de Melo-Diogo, D., Moreira, A. F., Carvalho, M. P., and Correia, I. J. (2018). Spheroids formation on non-adhesive surfaces by liquid overlay technique: considerations and practical approaches. *Biotechnol. J.* 13, 1–12. doi: 10.1002/biot.201700417

Däster, S., Amatruda, N., Calabrese, D., Ivanek, R., Turrini, E., Droeser, R. A., et al. (2017). Induction of hypoxia and necrosis in multicellular tumor spheroids is associated with resistance to chemotherapy treatment. *Oncotarget* 8, 1725–1736. doi: 10.18632/oncotarget.13857

Dominici, M., Le Blanc, K., Mueller, I., Slaper-Cortenbach, I., Marini, F. C., Krause, D. S., et al. (2006). Minimal criteria for defining multipotent mesenchymal stromal cells. The international society for cellular therapy position statement. *Cytotherapy* 8, 315–317. doi: 10.1080/14653240600855905

Dou, X., Li, P., and Schönherr, H. (2018). Three-dimensional microstructured poly(vinyl alcohol) hydrogel platform for the controlled formation of multicellular cell spheroids. *Biomacromolecules* 19, 158–166. doi: 10.1021/acs.biomac.7b01345

Egger, D., Tripisciano, C., Weber, V., Dominici, M., and Kasper, C. (2018). Dynamic cultivation of mesenchymal stem cell aggregates. *Bioengineering* 5:48. doi: 10.3390/bioengineering5020048

Erapaneedi, R., Belousov, V. V, Schäfers, M., and Kiefer, F. (2016). A novel family of fluorescent hypoxia sensors reveal strong heterogeneity in tumor hypoxia at the cellular level. *EMBO J.* 35, 102–113. doi: 10.15252/embj.201592775

Follin, B., Juhl, M., Cohen, S., Perdersen, A. E., Kastrup, J., and Ekblond, A. (2016). Increased paracrine immunomodulatory potential of mesenchymal stromal cells in three-dimensional culture. *Tissue Eng Part B Rev.* 22, 322–329. doi: 10.1089/ten.teb.2015.0532

Foty, R. (2011). A simple hanging drop cell culture protocol for generation of 3D spheroids. *J. Vis. Exp.* 6:2720. doi: 10.3791/2720

Ge, J., Guo, L., Wang, S., Zhang, Y., Cai, T., Zhao, R. C. H., et al. (2014). The size of mesenchymal stem cells is a significant cause of vascular obstructions and stroke. *Stem Cell Rev. Rep.* 10, 295–303. doi: 10.1007/s12015-013-9492-x

Gilkes, D. M., Semenza, G. L., and Wirtz, D. (2014). Hypoxia and the extracellular matrix: drivers of tumour metastasis. *Nat. Rev. Cancer* 14, 430–439. doi: 10.1038/nrc3726

Groebe, K., and Mueller-Klieser, W. (1991). Distributions of oxygen, nutrient, and metabolic waste concentrations in multicellular spheroids and their dependence on spheroid parameters. *Eur. Biophys. J.* 19, 169–181. doi: 10.1007/BF00196343

Harrell, C. R., Fellabaum, C., Jovicic, N., Djonov, V., Arsenijevic, N., and Volarevic, V. (2019). Molecular mechanisms responsible for therapeutic potential of mesenchymal stem cell-derived secretome. *Cells* 16:467. doi: 10.3390/cells8050467

Hirschhaeuser, F., Menne, H., Dittfeld, C., West, J., Mueller-Klieser, W., and Kunz-Schughart, L. A. (2010). Multicellular tumor spheroids: an underestimated tool is catching up again. *J. Biotechnol.* 148, 3–15. doi: 10.1016/j.jbiotec.2010.01.012

Howes, A. L., Richardson, R. D., Finlay, D., and Vuori, K. (2014). 3-Dimensional culture systems for anti-cancer compound profiling and high-throughput screening reveal increases in EGFR inhibitor-mediated cytotoxicity compared to monolayer culture systems. *PLoS ONE* 9:e108283. doi: 10.1371/journal.pone.0108283

Jiang, B. H., Rue, E., Wang, G. L., Roe, R., and Semenza, G. L. (1996). Dimerization, DNA binding, and transactivation properties of hypoxia- inducible factor 1. *J. Biol. Chem.* 271, 17771–17778. doi: 10.1074/jbc.271.30.17771

Khaitan, D., Chandna, S., Arya, M. B., and Dwarakanath, B. S. (2006). Establishment and characterization of multicellular spheroids from a human glioma cell line; implications for tumor therapy. *J. Transl. Med.* 4:12. doi: 10.1186/1479-5876-4-12

Kirsch, M., Birnstein, L., Pepelanova, I., Handke, W., Rach, J., Seltsam, A., et al. (2019). Gelatin-methacryloyl (GelMA) formulated with human platelet lysate supports mesenchymal stem cell proliferation and differentiation and enhances the hydrogel's mechanical properties. *Bioengineering* 6:76. doi: 10.3390/bioengineering6030076

Kouroupis, D., Sanjurjo-Rodriguez, C., Jones, E., and Correa, D. (2019). Mesenchymal stem cell functionalization for enhanced therapeutic applications. *Tissue Eng Part B Rev.* 25, 55–77. doi: 10.1089/ten.teb.2018.0118

Kumagai, A., Ando, R., Miyatake, H., Greimel, P., Kobayashi, T., Hirabayashi, Y., et al. (2013). A bilirubin-inducible fluorescent protein from eel muscle. *Cell* 153, 1602–1611. doi: 10.1016/j.cell.2013.05.038

Lavrentieva, A., Hoffmann, A., and Lee-Thedieck, C. (2020). Limited potential or unfavorable manipulations? Strategies toward efficient mesenchymal stem/stromal cell applications. *Front. Cell Dev. Biol.* 8:316. doi: 10.3389/fcell.2020.00316

Lee, S., Il, Ko, Y., and Park, J. B. (2017). Evaluation of the shape, viability, stemness and osteogenic differentiation of cell spheroids formed from human gingiva-derived stem cells and osteoprecursor cells. *Exp. Ther. Med.* 13, 3467–3473. doi: 10.3892/etm.2017.4388

Lin, R. Z., and Chang, H. Y. (2008). Recent advances in three-dimensional multicellular spheroid culture for biomedical research. *Biotechnol. J.* 3:1285. doi: 10.1002/biot.1285

Liu, B. H., Yeh, H. Y., Lin, Y. C., Wang, M. H., Chen, D. C., Lee, B. H., et al. (2013). Spheroid formation and enhanced cardiomyogenic potential of adipose-derived stem cells grown on chitosan. *BioRes. Open Access* 2, 28–39. doi: 10.1089/biores.2012.0285

Majmundar, A. J., Wong, W. J., and Simon, M. C. (2010). Hypoxia-Inducible factors and the response to hypoxic stress. *Mol. Cell* 40, 294–309. doi: 10.1016/j.molcel.2010.09.022

Mastrolia, I., Foppiani, E. M., Murgia, A., Candini, O., Samarelli, A. V., Grisendi, G., et al. (2019). Challenges in clinical development of mesenchymal stromal/stem cells: concise review. *Stem Cells Transl. Med.* 8, 1135–1148. doi: 10.1002/sctm.19-0044

Maxwell, P. H., Wlesener, M. S., Chang, G. W., Clifford, S. C., Vaux, E. C., Cockman, M. E., et al. (1999). The tumour suppressor protein VHL targets hypoxia-inducible factors for oxygen-dependent proteolysis. *Nature* 399, 271–275. doi: 10.1038/20459

Mole, D. R., Blancher, C., Copley, R. R., Pollard, P. J., Gleadle, J. M., Ragousis, J., et al. (2009). Genome-wide association of hypoxia-inducible factor (HIF)-1α and HIF-2α DNA binding with expression profiling of hypoxia-inducible transcripts. *J. Biol. Chem.* 284, 16767–16775. doi: 10.1074/jbc.M901790200

Murphy, K. C., Hung, B. P., Browne-Bourne, S., Zhou, D., Yeung, J., Genetos, D. C., et al. (2017a). Measurement of oxygen tension within mesenchymal stem cell spheroids. *J. R. Soc. Interf.* 14:20160851. doi: 10.1098/rsif.2016.0851

Murphy, K. C., Whitehead, J., Falahee, P. C., Zhou, D., Simon, S. I., and Leach, J. K. (2017b). Multifactorial experimental design to optimize the anti-inflammatory and proangiogenic potential of mesenchymal stem cell spheroids. *Stem Cells* 35, 1493–1504. doi: 10.1002/stem.2606

Noronha, N. D. C., Mizukami, A., Caliári-Oliveira, C., Cominal, J. G., Rocha, J. L. M., Covas, D. T., et al. (2019). Priming approaches to improve the efficacy of mesenchymal stromal cell-based therapies. *Stem Cell Res. Ther.* 10:131. doi: 10.1186/s13287-019-1259-0

Nunes, A. S., Barros, A. S., Costa, E. C., Moreira, A. F., and Correia, I. J. (2019). 3D tumor spheroids as *in vitro* models to mimic *in vivo* human solid tumors resistance to therapeutic drugs. *Biotechnol. Bioeng.* 116, 206–226. doi: 10.1002/bit.26845

Ophelders, D. R. M. G., Wolfs, T. G. A. M., Jellema, R. K., Zwanenburg, A., Andriessen, P., Delhaas, T., et al. (2016). Mesenchymal stromal cell-derived extracellular vesicles protect the fetal brain after hypoxia-ischemia. *Stem Cells Transl. Med.* 5, 754–763. doi: 10.5966/sctm.2015-0197

Potapova, I. A., Gaudette, G. R., Brink, P. R., Robinson, R. B., Rosen, M. R., Cohen, I. S., et al. (2007). Mesenchymal stem cells support migration, extracellular matrix invasion, proliferation, and survival of endothelial cells *in vitro*. *Stem Cells* 25, 1761–1768. doi: 10.1634/stemcells.2007-0022

Riffle, S., and Hegde, R. S. (2017). Modeling tumor cell adaptations to hypoxia in multicellular tumor spheroids. *J. Exp. Clin. Cancer Res.* 36:102. doi: 10.1186/s13046-017-0570-9

Ryu, N.-E., Lee, S.-H., and Park, H. (2019). Spheroid culture system methods and applications for mesenchymal stem cells. *Cells* 8:1620. doi: 10.3390/cells8121620

Schmitz, C., Pepelanova, I., Seliktar, D., Potekhina, E., Belousov, V. V., Scheper, T., et al. (2020). Live reporting for hypoxia: hypoxia sensor–modified mesenchymal stem cells as *in vitro* reporters. *Biotechnol. Bioeng.* 117, 3265–3276. doi: 10.1002/bit.27503

Teixeira, F. G., Carvalho, M. M., Sousa, N., and Salgado, A. J. (2013). Mesenchymal stem cells secretome: a new paradigm for central nervous system regeneration? *Cell. Mol. Life Sci.* 70, 3871–3882. doi: 10.1007/s00018-013-1290-8

Weber, G. F., Bjerke, M. A., and DeSimone, D. W. (2011). Integrins and cadherins join forces to form adhesive networks. *J. Cell Sci.* 124, 1183–1193. doi: 10.1242/jcs.064618

Xu, Y., Shi, T., Xu, A., and Zhang, L. (2016). 3D spheroid culture enhances survival and therapeutic capacities of MSCs injected into ischemic kidney. *J. Cell. Mol. Med.* 20, 1203–1213. doi: 10.1111/jcmm.12651

Zhang, Q., Nguyen, A. L., Shi, S., Hill, C., Wilder-smith, P., Krasieva, T. B., et al. (2012). Three-dimensional spheroid culture of human gingiva-derived mesenchymal stem cells enhances mitigation of chemotherapy-induced oral mucositis. *Stem Cells Dev.* 21, 937–947. doi: 10.1089/scd.2011.0252

Zhou, Y., Chen, H., Li, H., and Wu, Y. (2017). 3D culture increases pluripotent gene expression in mesenchymal stem cells through relaxation of cytoskeleton tension. *J. Cell. Mol. Med.* 21, 1073–1084. doi: 10.1111/jcmm.12946

Zhu, Y., Liu, T., Song, K., Fan, X., Ma, X., and Cui, Z. (2008). Adipose-derived stem cell: a better stem cell than BMSC. *Cell Biochem. Funct.* 26, 664–675. doi: 10.1002/cbf.1488

Conflict of Interest: The authors declare that the research was conducted in the absence of any commercial or financial relationships that could be construed as a potential conflict of interest.

frontiers in Bioengineering and Biotechnology

REVIEW
published: 12 February 2021
doi: 10.3389/fbioe.2021.621748

Increased Mesenchymal Stem Cell Functionalization in Three-Dimensional Manufacturing Settings for Enhanced Therapeutic Applications

Dimitrios Kouroupis[1,2]* *and Diego Correa*[1,2]

[1] Department of Orthopedics, UHealth Sports Medicine Institute, University of Miami, Miller School of Medicine, Miami, FL, United States, [2] Diabetes Research Institute & Cell Transplantation Center, University of Miami, Miller School of Medicine, Miami, FL, United States

OPEN ACCESS

Edited by:
Elizabeth R. Balmayor, MERLN Institute for Technology-Inspired Regenerative Medicine, Maastricht University, Netherlands

Reviewed by:
Vanessa L. S. LaPointe, Maastricht University, Netherlands
Patrina Su Ping Poh, Charité – Universitätsmedizin Berlin, Germany

***Correspondence:**
Dimitrios Kouroupis
dxk504@med.miami.edu

Specialty section:
This article was submitted to Preclinical Cell and Gene Therapy, a section of the journal Frontiers in Bioengineering and Biotechnology

Received: 26 October 2020
Accepted: 07 January 2021
Published: 12 February 2021

Citation:
Kouroupis D and Correa D (2021) Increased Mesenchymal Stem Cell Functionalization in Three-Dimensional Manufacturing Settings for Enhanced Therapeutic Applications. Front. Bioeng. Biotechnol. 9:621748. doi: 10.3389/fbioe.2021.621748

Mesenchymal stem/stromal cell (MSC) exist within their *in vivo* niches as part of heterogeneous cell populations, exhibiting variable stemness potential and supportive functionalities. Conventional extensive 2D *in vitro* MSC expansion, aimed at obtaining clinically relevant therapeutic cell numbers, results in detrimental effects on both cellular characteristics (e.g., phenotypic changes and senescence) and functions (e.g., differentiation capacity and immunomodulatory effects). These deleterious effects, added to the inherent inter-donor variability, negatively affect the standardization and reproducibility of MSC therapeutic potential. The resulting manufacturing challenges that drive the qualitative variability of MSC-based products is evident in various clinical trials where MSC therapeutic efficacy is moderate or, in some cases, totally insufficient. To circumvent these limitations, various *in vitro/ex vivo* techniques have been applied to manufacturing protocols to induce specific features, attributes, and functions in expanding cells. Exposure to inflammatory cues (cell priming) is one of them, however, with untoward effects such as transient expression of HLA-DR preventing allogeneic therapeutic schemes. MSC functionalization can be also achieved by *in vitro* 3D culturing techniques, in an effort to more closely recapitulate the *in vivo* MSC niche. The resulting spheroid structures provide spatial cell organization with increased cell–cell interactions, stable, or even enhanced phenotypic profiles, and increased trophic and immunomodulatory functionalities. In that context, MSC 3D spheroids have shown enhanced "medicinal signaling" activities and increased homing and survival capacities upon transplantation *in vivo*. Importantly, MSC spheroids have been applied in various preclinical animal models including wound healing, bone and osteochondral defects, and cardiovascular diseases showing safety and efficacy *in vivo*. Therefore, the incorporation of 3D MSC culturing approach into cell-based therapy would significantly

impact the field, as more reproducible clinical outcomes may be achieved without requiring *ex vivo* stimulatory regimes. In the present review, we discuss the MSC functionalization in 3D settings and how this strategy can contribute to an improved MSC-based product for safer and more effective therapeutic applications.

Keywords: MSC functionalization, MSC spheroids, MSC therapeutic properties, MSC anti-inflammatory properties, mesenchymal stem cell manufacturing

MSC THERAPEUTIC PROPERTIES IN CONVENTIONAL 2D CULTURES

Mesenchymal stem/stromal cells (MSC) are non-hematopoietic cells first isolated from the bone marrow tissue by Friedenstein et al. (1974), and thereafter from various other connective tissues and biological fluids including fat pad (Dragoo et al., 2003), adipose (Zuk et al., 2002), synovium (De Bari et al., 2001), synovial fluid (Jones et al., 2008), and umbilical cord (Weiss and Troyer, 2006). The perceived advantage of MSC as cell therapy is associated with their ease of isolation and high proliferative capacity while retaining their stemness *in vitro*, but most importantly their paracrine immunomodulatory and trophic (i.e., angiogenic, anti-fibrotic, anti-apoptotic, and mitogenic) actions *in vivo*. On this basis, MSC "medicinal signaling" activities (Caplan, 2017) exploit their environmental sensory capacity and by secretion of modulatory mediators induce the restoration of the distorted local homeostasis of the target tissue. The immunomodulatory effects of MSC are mediated by secreted bioactive molecules (i.e., IDO, PGE2, TGFβ, IGF, and IL-10), and by cell–cell contact affecting both innate and adaptive immunity (Waterman et al., 2010; Caplan and Correa, 2011; Singer and Caplan, 2011; Bernardo and Fibbe, 2013; Krampera et al., 2013; Uccelli and Rosbo, 2015; Kouroupis et al., 2017, 2018). The trophic effects are mediated by several bioactive molecules resulting in anti-apoptotic [VEGF, HGF, IGF-I, stanniocalcin-1 (STC-1), TGF-β, and GM-CSF] and mitotic (SCF, LIF, M-CSF, SDF-1, and angiopoietin-1) effects on tissue-intrinsic progenitors (da Silva Meirelles et al., 2009). Most importantly, MSC support the new vessel formation not only by functioning as pericytes and stabilizing newly formed vasculature (Sorrell et al., 2009) but also by secreting ECM molecules and angiogenic factors (VEGF, IGF-1, PIGF, MCP-1, bFGF, and IL-6) (da Silva Meirelles et al., 2009).

As reviewed in Kouroupis et al. (2017), MSC therapeutic usage *in vivo* in both autologous and allogeneic settings is safe due to their immunoevasive characteristics, and therefore, even multiple infusions of allogeneic MSC do not elicit a strong immune response that can lead to rejection progression (Koç et al., 2002; Aggarwal and Pittenger, 2005; Ringden et al., 2006; Le Blanc et al., 2008; Pittenger et al., 2019). Over the past 30 years, the safety profile of MSC has been clearly demonstrated in clinical trials to treat multiple clinical indications, with efficacy starting to produce encouraging results in some of them. To date, more than 10,000 patients have been treated as part of clinical trials, with 188 phase 1 or phase 2 trials completed and 10 trials advanced to phase 3.[1] However, to obtain clinically relevant cell numbers, therapeutic protocols usually require MSC extensive *in vitro* 2D expansion resulting in MSC products with limited stem cell potency and, as a result in some cases, only moderate or inconsistent effectiveness to treat various clinical indications. Also, according to previous studies, MSC isolated from different tissue sources demonstrate similar, but not identical, functional capacity (Guilak et al., 2010; Moretti et al., 2010; Hass et al., 2011). Efficacy and reproducibility of MSC therapies are not only affected by the composition of the cell preparation but also by the functionality of the infused MSC to consistently home and engraft within dysregulated tissues, and subsequently to predictably exert their therapeutic effects by inducing and/or modifying specific host responses. To circumvent these limitations, various *in vitro/ex vivo* techniques have been applied to manufacturing protocols to induce specific features, attributes, and functions in expanding cells. On this basis, MSC functionalization can be achieved by *in vitro* 3D culturing techniques, in an effort to more closely recapitulate the *in vivo* 3D MSC niche and therefore preserve or enhance cellular phenotypes that result in improved *in vivo* therapeutics.

MSC SPHEROID FORMATION AND STRUCTURE

Adult MSC possesses a remarkable ability to coalesce and assemble in tri-dimensional (3D) structures, reminiscent of their innate aggregation as limb cell precursors in the mesenchymal condensation during early skeletogenesis. In that context, 3D organoid formation *in vitro* closely recapitulates the *in vivo* MSC niche by providing spatial cell organization with increased cell–cell interactions.

According to the differential adhesion hypothesis that was first introduced in the 1960s, the cell movement and cell aggregation phenomena present in self-assembly processes are driven by differential cadherin expression levels and guided by the reduction of adhesive-free energy as cells tend to maximize their mutual binding (Foty and Steinberg, 2005). In general, cell aggregation and subsequent multicellular spheroid formation processes involve three phases (**Figure 1A**). Initially, cells form loose aggregates via the tight binding of extracellular matrix arginine–glycine–aspartate (RGD) motifs with membrane-bound integrin. As a result of the increased cell–cell interactions, *cadherin* gene expression levels are upregulated, whereas cadherin protein is accumulated on the cell membrane. During the later phase, homophilic cadherin-to-cadherin binding induce the formation of compact cell spheroids from cell aggregates. The extracellular matrix proteins and cadherin type

[1] www.clinicaltrials.gov

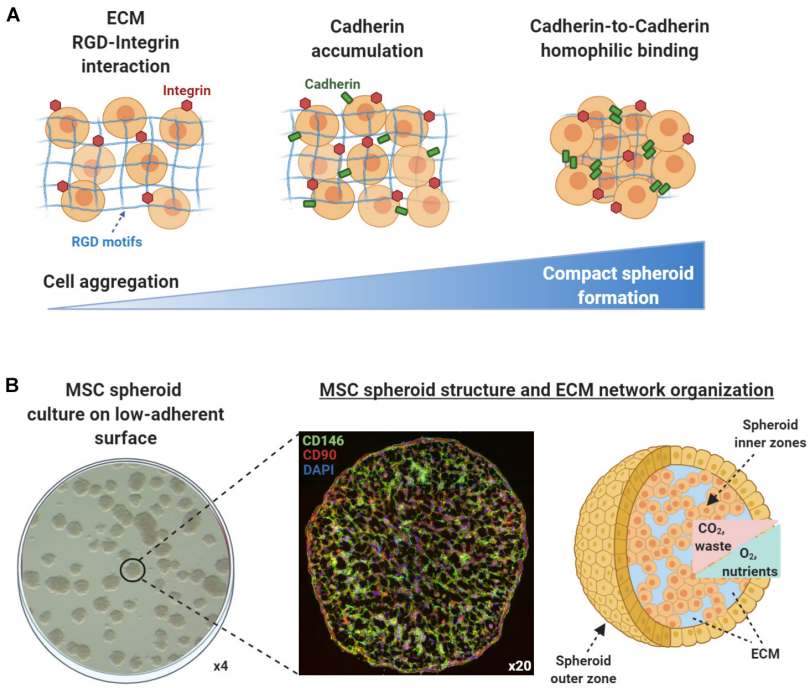

FIGURE 1 | Mesenchymal stem/stromal cell (MSC) spheroids formation process and structure. **(A)** Cell aggregation and spheroid formation involving three phases. Initially, cells form loose aggregates via the tight binding of extracellular matrix arginine–glycine–aspartate (RGD) motifs with membrane-bound integrin. Due to increased cell–cell interactions, *cadherin* gene expression levels are upregulated and cadherin protein is accumulated on the cell membrane. In the later phase, homophilic cadherin-to-cadherin binding induce the formation of compact cell spheroids from cell aggregates. **(B)** Methylcellulose-based technique can be used to generate viable MSC spheroids on low-attachment gas-permeable plates (left panel). Generated MSC spheroids show stable immunophenotypic profile by expressing high levels of the pericytic marker CD146 (green) and MSC-related marker CD90 (red) (middle panel) (unpublished data). Structurally, based on their size and abundance of nutrients and oxygen *in vitro*, MSC spheroids can be divided into zones (outer and inner). The nutrients, oxygen, and waste concentration gradients within the spheroids should be always taken into consideration when selecting the optimal technique to generate spheroids *in vitro* in order to achieve increased spheroid functionality in *in vivo* settings (right panel).

and concentration are variable between different cell types, whereas other intercellular proteins such as connexin, pannexins, and actin cytoskeleton filaments play crucial roles in cell–cell interactions and subsequent multicellular cell spheroid formation (reviewed in Cui et al., 2017). Structurally, based on their size and abundance of nutrients and oxygen *in vitro*, most multicellular spheroids can be divided into three zones (Mueller-Klieser, 1984; Alvarez-Pérez et al., 2005; Curcio et al., 2007; **Figure 1B**). The outer asynchronously proliferative zone contains cells with intact nuclei that are proliferative with active metabolism. The intermediate zone contains cells with shrunk nuclei that are in quiescent state possessing minimum metabolic activities. Usually depending on the spheroid size, the inner necrotic zone contains cells with disintegrated nuclei that are senescent/apoptotic due to limited nutrients and oxygen influx (hypoxia) in the spheroid core. The inner necrotic zone is formed as the diffusion limitation of most molecules in spheroids is 150–200 μm, and as a result, metabolic wastes are gradually accumulating within the spheroid core. Additionally, Curcio et al. (2007) indicated that aggregates of 200-μm diameter or greater show severe oxygen limitation in the most part of their dimensions, and Alvarez-Pérez et al. (2005) related drastic intra-spheroidal pH alterations to spheroid size, with spheroids of 600-μm diameter or greater showing acidic necrotic core. Based on these findings, a three-part spheroid zonation is highly dependent on cell aggregation size and microenvironment conditions, whereas a 200-μm diameter can be putatively considered a reliable size threshold for limited/diminished inner necrotic core zone formation. Therefore, the nutrients, oxygen, and waste concentration gradients within the spheroids should be always taken into consideration when selecting the optimal technique to generate spheroids *in vitro* in order to achieve increased spheroid functionality in *in vivo* settings.

The organization of MSC in 3D spheroids result in altered cell morphology, cytoskeleton rearrangement, and polarization due to the cell–cell and cell–extracellular matrix interactions within the spheroid structure. Additionally, 3D cultures account for the established reduction in size of individual MSC (about 0.25–0.5 the volume of an average 2D cultured cell) (Bartosh et al., 2010). Specifically, studies showed that individual MSC strain is increased within the spheroid structure and equally dispersed in all cell dimensions (a Young's Modulus of approximately 60 Pascal), whereas overall MSC tension is greater in the outer zone compared with the inner zone of spheroids. These tension differences affect MSC morphology and polarization resulting in a more flattened morphology and high integrin expression

for outer zone MSC and a more irregular morphology with high cadherin expression for the inner zone MSC (Baraniak et al., 2012; Sart et al., 2014). On this basis, Lee et al. (2012) indicated E-cadherin as the main calcium-dependent adhesion molecule that plays a crucial role in MSC spheroid formation *in vitro*. During spheroid formation, E-cadherin activation and cell–cell interactions regulate the proliferative and paracrine activity of MSC via the ERK/AKT signaling pathway (Lee et al., 2012). Importantly, studies showed that cadherins, and especially N-cadherin and OB-cadherin, are both affecting the proliferation, migration, and differentiation potential of 2D MSC cultures (Theisen et al., 2007; Xu et al., 2013). Of note, cadherin levels may be important in mediating MSC anti-inflammatory actions as reports indicated that they are crucial in the response of synovial fibroblasts to inflammation (Agarwal and Brenner, 2006; Chang et al., 2011). To this end, engineered cadherin surfaces and engineered surface microtopology have been generated to control differentiation, and cell-to-cell adhesion and signaling of 2D cultured MSC *in vitro* (reviewed in Alimperti and Andreadis, 2015). However, the inherent increased cadherin levels upon MSC spheroid formation can be directly related to increased MSC spheroid functionality *in vitro* and *in vivo*, offering an advantage over 2D MSC cultures.

Interestingly, studies showed that mild hypoxia present within the inner zones of MSC spheroids positively affect MSC survival and secretory capacity. Moreover, spheroid hypoxic microenvironment upregulate the expression of hypoxia-adaptive molecules (such as *CXCL12* and *HIF-1α*), inhibit MSC apoptosis, and increase the secretion of angiogenic and anti-apoptotic molecules including HGF, VEGF, and FGF-2 compared to 2D MSC cultures (Bhang et al., 2011). Specifically, studies showed that MSC spheroids embedded in fibrin gel secrete up to 100-fold more VEGF compared with dissociated MSC in fibrin gel (Murphy et al., 2014). Except these molecules, the angiogenic trophic enhancement is produced via the upregulation of other key angiogenic factors such as angiogenin (ANG) and angiopoietin 2 (ANGPT-2; Potapova et al., 2007; Potapova et al., 2008; Yeh et al., 2014). However, Murphy et al. (2017) reported that even though cellular metabolism decreased significantly with higher cell numbers and resultant spheroid sizes, oxygen tension show a gradient that vary less than 10% from the outer zone to the inner core even for spheroids with diameters up to 353 ± 18 μm. This indicates that increased MSC functionality within the spheroid is not oxygen gradient driven but due to increased ECM production and autocrine signaling. Overall, the advantages and disadvantages of MSC functionalization in 3D spheroids are described in **Table 1**.

TABLE 1 | Advantages and disadvantages of MSC functionalization in 3D spheroids.

Advantages	Disadvantages
• Increased stability of MSC immunophenotypic and molecular profiles • Enhanced stemness features and differentiation potential • Upon infusion, enhanced survival and homing *in vivo* • Enhanced secretory profile exerting mitogenic, anti-apoptotic, angiogenic, anti-fibrotic and anti-inflammatory properties	• Size variability depending on the technique used to generate spheroids • Depending on spheroid size, nutrients, oxygen, and waste concentration gradients within the spheroids • Depending on spheroid size, necrotic spheroid core formation • Depending on the clinical needs, development of reproducible, simple and cost-effective techniques are needed for large-scale production of MSC spheroids

METHODS AND BIOMATERIALS USED TO GENERATE MSC SPHEROIDS *EX VIVO*

Lately, standardization of MSC manufacturing has been extensively evaluated in order to translate *in vitro* and *in vivo* preclinical research into safe and effective therapeutic products. Toward this goal, the large-scale clinical-grade generation of MSC spheroids possessing enhanced functionality *in vivo* is an imminent need for various therapeutic applications. To date, various methods have been used to generate MSC spheroids including the "classic" hanging drop technique and other improved methods such as the application of low-adhesive substrates, the membrane-based aggregation, and the forced aggregation techniques (reviewed in Petrenko et al., 2017).

SCAFFOLD-FREE MESENCHYMAL STEM/STROMAL CELL SPHEROID CULTURE PLATFORMS

Mesenchymal stem/stromal cell spheroid culture platforms are usually trivial, rapid, and low-cost methods to generate spheroids in a non- or low-adherent environment that allows the self-organization of cells into suspended spheroids (**Figures 2A–D**). In the hanging drop technique, MSCs are aggregated by gravitational force but due to the absence of direct contact with solid surfaces, the composition of ECM proteins is the main factor for the regulation of spheroid microenvironment (Foty, 2011). Therefore, the hanging drop technique can generate MSC spheroids of controlled size and number; however, its main limitation is the laborious preparation of the 3D cultures that significantly limits the large-scale production of spheroids for *in vivo* applications. Using the hanging drop technique, Bartosh et al. indicated a 100-fold upregulation of anti-inflammatory (*TSG-6*) and anti-tumorigenic (*IL-24* and *TRAIL*) genes compared to 2D MSC cultures (Bartosh et al., 2010). In addition, the hanging drop technique results in higher expression of stemness markers *Oct4*, *Sox2*, and *Nanog* in MSC spheroids compared to 2D MSC cultures (Lou et al., 2016). Forced aggregation technique (or pellet culture) is also used to generate scaffold-free MSC aggregates by gravitational force that are further induced toward 3D differentiation protocols such as high-density MSC chondrogenic pellet culture (Mackay et al., 1998). A less laborious and more standardized technique is the use of low-attachment surfaces. Similar to the hanging drop technique, spontaneously secreted ECM proteins are regulating the spheroid microenvironment, however, generated spheroids show increased variability in size and morphology

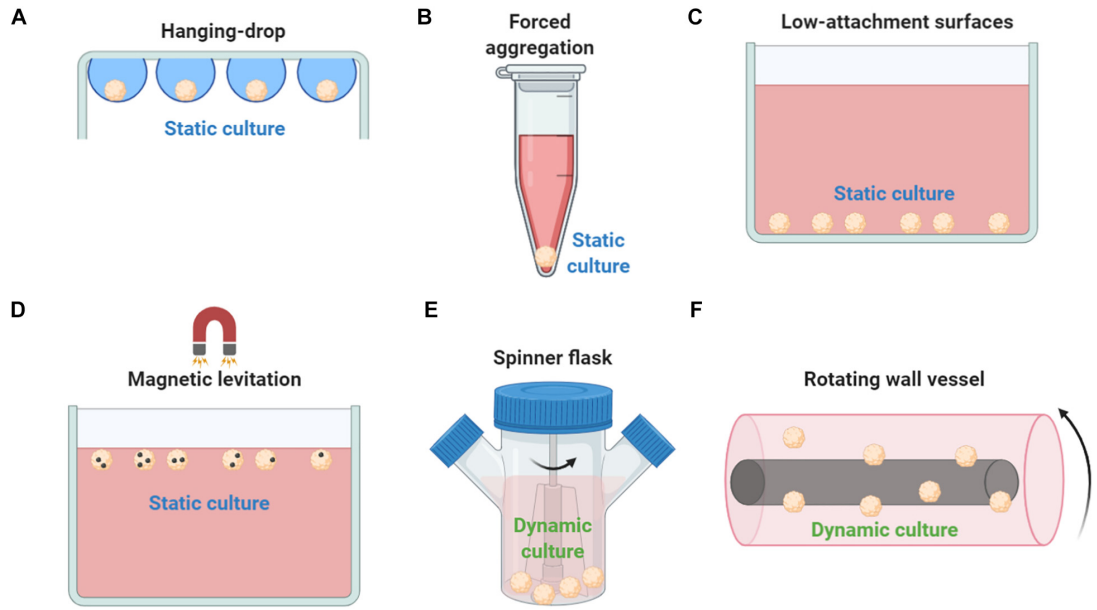

FIGURE 2 | Methods used to generate MSC spheroids *ex vivo*. **(A)** In hanging drop technique, MSCs are aggregated by gravitational force. **(B)** Forced aggregation technique (or pellet culture) is used to generate MSC aggregates by gravitational force that are further induced toward 3D differentiation protocols. **(C)** Low-attachment surfaces allow the self-organization of cells into suspended spheroids. **(D)** Magnetic levitation diminish gravitational force, promotes cell–cell contact and induces cell aggregation *in vitro*. **(E)** In a spinner flask bioreactor system, cells are continuously mixed by stirring. **(F)** Rotating wall vessel technique simulates microgravity by constant circular rotation and, therefore, cells are continuously in suspension. Both dynamic culturing techniques (spinner flask and rotating wall vessel) form viable compact MSC spheroids but with altered cell size, altered phenotypic and molecular profiles, and enhanced differentiation potential compared to 2D conventional MSC cultures.

(Redondo-Castro et al., 2018b). Interestingly, studies showed that MSC spheroids generated on low-attachment surfaces secreted more hypoxia-induced angiogenic cytokines including VEGF, SDF, and HGF, whereas phosphorylation of Akt cell survival signaling was higher and the expression of pro-apoptotic molecules lower in MSC spheroids compared with 2D MSC cultures (Lee et al., 2016). Magnetic levitation can be used to generate MSC spheroids as by diminishing gravitational force, it promotes cell–cell contact and induces cell aggregation *in vitro*. In detail, cells are mixed with magnetic particles in culture, and cells incorporated with them can levitate due to exogenously applied magnetic field. Although preliminary studies show spheroid formation reproducibility and stable MSC spheroid phenotype, others have reported that abnormal gravity induces classic apoptotic alterations such as cell size reduction and cell membrane blebbing, reduced cell viability, nuclear chromatin condensation and margination, and increased caspase-3/7 activity (Meng et al., 2011).

Except the static techniques, various dynamic approaches have been investigated to generate MSC spheroids including spinner flask culture and rotating wall vessel techniques (**Figures 2E,F**). Spinner culture technique is based on a spinner flask bioreactor system where cells are continuously mixed by stirring, whereas rotating wall vessel technique simulates microgravity by constant circular rotation where cells are continuously in suspension. In a comparative study between dynamic and 2D MSC cultures, Frith et al. indicated that both spinner and rotating wall vessel dynamic cultures can form viable compact MSC spheroids showing altered cell size, altered phenotypic and molecular profiles, and enhanced osteogenic and adipogenic differentiation potential (Frith et al., 2010). Further studies showed that rotating wall vessel microgravity dramatically affect the molecular profile of MSC spheroids by upregulating genes related to adipogenic and downregulating genes related to osteogenic and chondrogenic differentiation potentials (Sheyn et al., 2010). MSC spheroid culturing in microgravity conditions results in reduced osteogenic differentiation due to decreased Collagen I gene expression and subsequent Collagen I/integrin signaling pathway activation (Meyers et al., 2004). Also, microgravity disrupts F-actin stress fibers, increase intracellular lipid accumulation, and significantly reduces RhoA activity (Meyers et al., 2005). Interestingly, others indicated that microgravity has a synergistic effect with chemical induction in stimulation of chondrogenesis mediated by p38 MAPK activation (Yu et al., 2011).

The abovementioned advantages of MSC spheroids over 2D MSC cultures make them a great candidate as building blocks for 3D bioprinting. For the large-scale manufacturing of spheroid-based tissue complexes *in vitro*, various 3D bioprinting techniques have been reported including extrusion-based bioprinting (Jakab et al., 2008; Mironov et al., 2009; Bulanova et al., 2017; Mekhileri et al., 2018), droplet-based bioprinting (Gutzweiler et al., 2017), Kenzan (Moldovan et al., 2017), and biogripper (Blakely et al., 2015; Ip et al., 2016) approaches. Studies showed that homogeneous MSC-derived

cartilage spheroids with a mean diameter of 116 ± 2.8 μm can be assembled using extrusion-based bioprinting into viable cartilage constructs with stable phenotype (De Moor et al., 2020). Also, MSC-derived adipose spheroids bioprinted into a microtissue showed multilocular microvacuoles and successful differentiation toward mature adipocytes (Colle et al., 2020). However, existing 3D bioprinting techniques involve several limitations related to substantial damage to biological, structural, and mechanical spheroid properties. Recently, Ayan et al. (2020) proposed aspiration-assisted bioprinting as a novel approach for MSC spheroid assembly that causes minimal cellular damage and precisely bioprint a wide range of spheroid dimensions (ranging from 80 to 800 μm). On this basis, authors demonstrated the patterning of angiogenic sprouting spheroids and self-assembly of osteogenic spheroids. Further advancements into bioprinting field would benefit the generation of various types of MSC spheroid-derived microtissues *in vitro*.

SCAFFOLD-BASED MESENCHYMAL STEM/STROMAL CELL SPHEROID CULTURE PLATFORMS

In addition to the scaffold-free culture platforms, various scaffold-based MSC spheroid generation approaches have been proposed using both natural and synthetic biomaterials. As mentioned before, MSC spheroids can benefit the *in vivo* microenvironment primarily by their immunomodulatory and trophic actions, and secondarily (if any) by their direct differentiation toward specialized cells. The latter supports the notion that MSC spheroids should maintain their integrity in order to achieve effective cell replacement *in vivo* as biodegradation is a key factor in tissue engineering. Therefore, depending on the therapeutic application mode, biomaterial selection except from biological factors (cell adhesion, biocompatibility, etc.) should take into consideration physic-chemical (porosity to support nutrients/oxygen influx, biodegradation, etc.) parameters (Nikolova and Chavali, 2019). On this basis, even though scaffold's topography allows seeded MSC to form a microstructured matrix within the 3D spheroid microenvironment, depending on the treated tissue's nature, scaffold biodegradation rate should be controlled accordingly by the incorporation of chemical components that trigger gradual hydroytic degradation. However, to date, no specific studies have been performed to define if long-term maintenance of MSC spheroid structure is crucial for its therapeutic use.

Scaffold-based culture platforms using natural polymers such as agar/agarose, chitosan, and collagen can promote spheroid formation. Agar/agarose non-adherent surfaces have been used to promote MSC aggregation and spheroid formation *in vitro* (Vorwald et al., 2018). Specifically, chitosan-based substrates result in a more complex spheroid microenvironment compared to scaffold-free methods as the carbohydrate structure of chitosan is similar to the glycosaminoglycans in the ECM (Cui et al., 2017). Chitosan is a polycationic natural biocompatible polysaccharide, whereas the degree of its deacetylation can modulate the cell adhesion and spheroid formation capacity *in vitro*. On this basis, highly deacetylated chitosan substrate supports strongly the attachment and proliferation of fibroblasts (Seda Tığlı et al., 2007). Interestingly, Yeh et al. showed that MSC spheroid culturing on chitosan membranes results in increased intracellular calcium levels, whereas the calcium binding capacity of chitosan affect the cell–substrate and cell–cell interactions within the MSC spheroid. As a result, the chitosan-cultured MSC spheroids show significantly upregulated expression of calcium-, cell adhesion/ migration-, and anti-inflammatory-associated genes compared to 2D MSC on tissue culture polystyrene plates (Yeh et al., 2012, 2014). Hsu and Huang showed that Wnt signaling is not only distinct in MSC spheroids compared to 2D MSC cultures but also substrate dependent. MSC spheroids derived on chitosan-activated Wnt3α-mediated canonical Wnt signaling is prone to osteogenesis, whereas MSC spheroids derived on hyaluronan-grafted chitosan activated Wnt5α-mediated non-canonical Wnt signaling that is prone to chondrogenesis (Hsu and Huang, 2013). On this basis, Huang et al. (2011) showed that MSC spheroids generated on chitosan and chitosan–hyaluronan substrates preserve the expression of stemness markers *Oct4*, *Sox2*, and *Nanog*, and increase their chondrogenic differentiation capacity. As autophagy is an important mechanism promoting cell survival, a study showed that MSC spheroids derived on chitosan respond to environmental stress (H_2O_2 treatment) by upregulating autophagy-related markers in a calcium-dependent manner (Yang et al., 2015). This effect is important as it may increase the MSC spheroid survival and therapeutic efficacy in *in vivo* settings. Interestingly, nanomagnetically levitated MSCs cultured as spheroids within type I collagen gels preserve their quiescent phenotype indicated by the expression of *STRO-1* and *Nestin*, whereas in response to co-culture wounding, they are capable of migrating to the wound site and differentiate accordingly (Lewis et al., 2016).

Polymers and chemically modified polymers have been extensively investigated for the development of novel biomaterials with good physic-chemical properties and biocompatibility. On this basis, MSC spheroid generation has been performed on various synthesized polymer substrates such as polycaprolactone, micropatterned poly(ethylene glycol), poly(L-glutamic acid)/chitosan, and methylcellulose. In one study, Messina et al. (2017) showed that fibroblast, myoblast, and neural cell spheroids on polymeric membranes possess high biological activity in terms of oxygen uptake, whereas they undergo faster fusion and maturation on polycaprolactone than on agarose substrates. Also, Wang W. et al. (2009) showed improved adipogenic and osteogenic differentiation capacity of MSC spheroids generated on micropatterned poly(ethylene glycol) substrates. Microarray analysis indicated not only the upregulation of genes related to adipogenesis and osteogenesis but also the downregulation of genes related to MSC stemness such as the mesoderm–specific transcript (*MEST*) and the mesenchymal stem cell specific marker (*THY1*) (Wang W. et al., 2009). Similarly, Zhang et al. (2015) indicated that MSC spheroids generated on poly(L-glutamic acid)/chitosan substrate show increased chondrogenic differentiation capacity by increased GAGs and COLII, and decreased COLI deposition during *in vitro* chondrogenic induction.

Methylcellulose, an ether derivative of cellulose, which is synthesized by the replacement of hydrogen atoms from hydroxy groups with methyl groups, has been recently used to generate successfully MSC spheroids *in vitro*. Deynoux et al. (2020) showed that methylcellulose allows MSC spheroid formation within 24 h, which tends to shrink in size partially due to the balance between proliferation and cell death triggered by hypoxia and oxidative stress up to 3 weeks *in vitro*. Similar to methylcellulose-based technique published by Markou et al. (2020), we have generated successfully viable MSC spheroids in a gas-permeable plate system that possess stable phenotypic and molecular profiles, and increased functionality both *in vitro* and *in vivo* (Kouroupis et al., 2021). The usage of this system is aimed to ensure uniform oxygenation throughout the MSC spheroid culture, as it is based on previous reports demonstrating that in gas-permeable plates 3D cell structures efficiently receive air from both the top (after diffusion through the medium) and the bottom (after diffusion across permeable membrane) of the culture (Fraker et al., 2007, 2013; Cechin et al., 2014). These reports show that MSC spheroid generation on synthesized substrates can dramatically affect their stemness and multipotential differentiation capacities *in vitro*.

CULTURE MEDIUM EFFECTS ON MESENCHYMAL STEM/STROMAL CELL SPHEROIDS

With the exception of the scaffold-free or scaffold-based culture platforms, reports showed that culture medium composition strongly affect the spheroid formation progression and MSC spheroid functionality *in vitro*. To date, most studies use fetal bovine serum (FBS)-based media to generate spheroids *in vitro*. However, safety concerns have been raised regarding FBS usage for the manufacturing of MSC products for clinical applications, most of them related to prion exposure risk, toxicological risk, and immunological risk (Mendicino et al., 2014; Karnieli et al., 2017). Regulatory-complaint xeno-free media such as chemically defined formulations and human platelet lysate (hPL) are promising alternatives to generate clinically relevant cell numbers and to preserve or even enhance the MSC functionality *in vitro* prior to their *in vivo* application (Doucet et al., 2005; Centeno et al., 2008; Jung et al., 2010; Kouroupis et al., 2020a,b). On this basis, Ylostalo et al. (2014) showed that MSCs cannot condense into tight spheroids when cultured in several commercial stem cell media and only chemically defined formulation supplemented with human serum albumin (HSA) can result in compact MSC spheroids with high viability and enhanced anti-inflammatory secretory profile. Importantly, MSC spheroids generated with HAS supplementation show increased anti-inflammatory capacity when co-cultured with lipopolysaccharide-stimulated macrophages *in vitro* (Ylostalo et al., 2014). In contrast, another study indicated that MSC spheroids generated in FBS-based medium show low or no proliferation but increased paracrine secretory profile (PGE2 and IDO), whereas MSC spheroids generated in xeno-free medium show significant proliferative capacity but low paracrine secretory profile (Zimmermann and McDevitt, 2014).

Overall, further investigations have to be performed in order to optimize the *in vitro* culturing conditions for the standardization and reproducibility of MSC spheroid therapeutic potential. Most importantly, challenges still exist related to the generation of clinically relevant cell numbers in 3D cultures and the qualitative assessment of the generated MSC spheroids using conventional methods. Specifically, the less laborious dynamic approaches, such as the spinner flask culture and the rotating wall vessel techniques, offer a viable solution to generate large MSC spheroid numbers; however, novel bioreactor systems are needed to additionally monitor and control all culture environmental variables (temperature, gas exchange, pH, and metabolite levels) (de Bournonville et al., 2019). Similar to 2D MSC cultures, qualitative evaluation of MSC spheroids requires their phenotypic protein profiling using fluorescent microscopy and flow cytometry methods. Fluorescent imaging is often laborious for xyz images and represent only a fraction of MSC spheroid cultures, whereas flow cytometry requires the enzymatic/mechanical dissociation of the spheroids to a single cell, usually disrupting important sensitive phenotypic attributes (CD146 immunomodulation-related marker). Furthermore, comparative preclinical studies are needed to evaluate how different MSC spheroid generation platforms *in vitro* are affecting the therapeutic outcomes upon their implantation or infusion *in vivo*.

ANTI-INFLAMMATORY PROPERTIES OF MESENCHYMAL STEM/STROMAL CELL SPHEROIDS

In MSC spheroid settings, their enhanced anti-inflammatory effects have been mainly attributed to high expression of TGF-β1, IL-6, TSG-6, stanniocalcin (STC-1), and PGE-2 anti-inflammatory molecules (Bartosh et al., 2010; Ylöstalo et al., 2012; Zimmermann and McDevitt, 2014; **Figure 3**). Specifically, Bartosh et al. showed that BM-derived MSC spheroid increased secretion of anti-inflammatory TSG-6 and STC-1 results in reduced TNFα expression and secretion by LPS-stimulated macrophages in MSC spheroid/macrophages co-cultures *in vitro*. In a mouse zymosan-induced peritonitis model, intraperitoneal injection of 1.5×10^6 BM-derived MSC spheroids for a 6-h time-frame resulted in decreased protein content and volume of the lavage fluid, neutrophil activity, and decreased levels of TNFα, IL-1β, CXCL2/MIP-2, and PGE2. Also, MSC spheroid injection significantly decreased the serum levels of plasmin activity, an inflammation-related protease that is inhibited by secreted TSG-6 (Bartosh et al., 2010). Importantly, *in vitro* studies showed that BM-derived MSC spheroid conditioned medium affect LPS-stimulated macrophages not only by inhibiting the secretion of pro-inflammatory cytokines TNFα, CXCL2, IL-6, IL12-p40, and IL-23 but also by increasing the secretion of anti-inflammatory cytokines IL-10 and IL1-Ra and the expression of M2-polarization CD206 marker. The main anti-inflammatory molecule secreted in the conditioned medium was PGE2, whereas

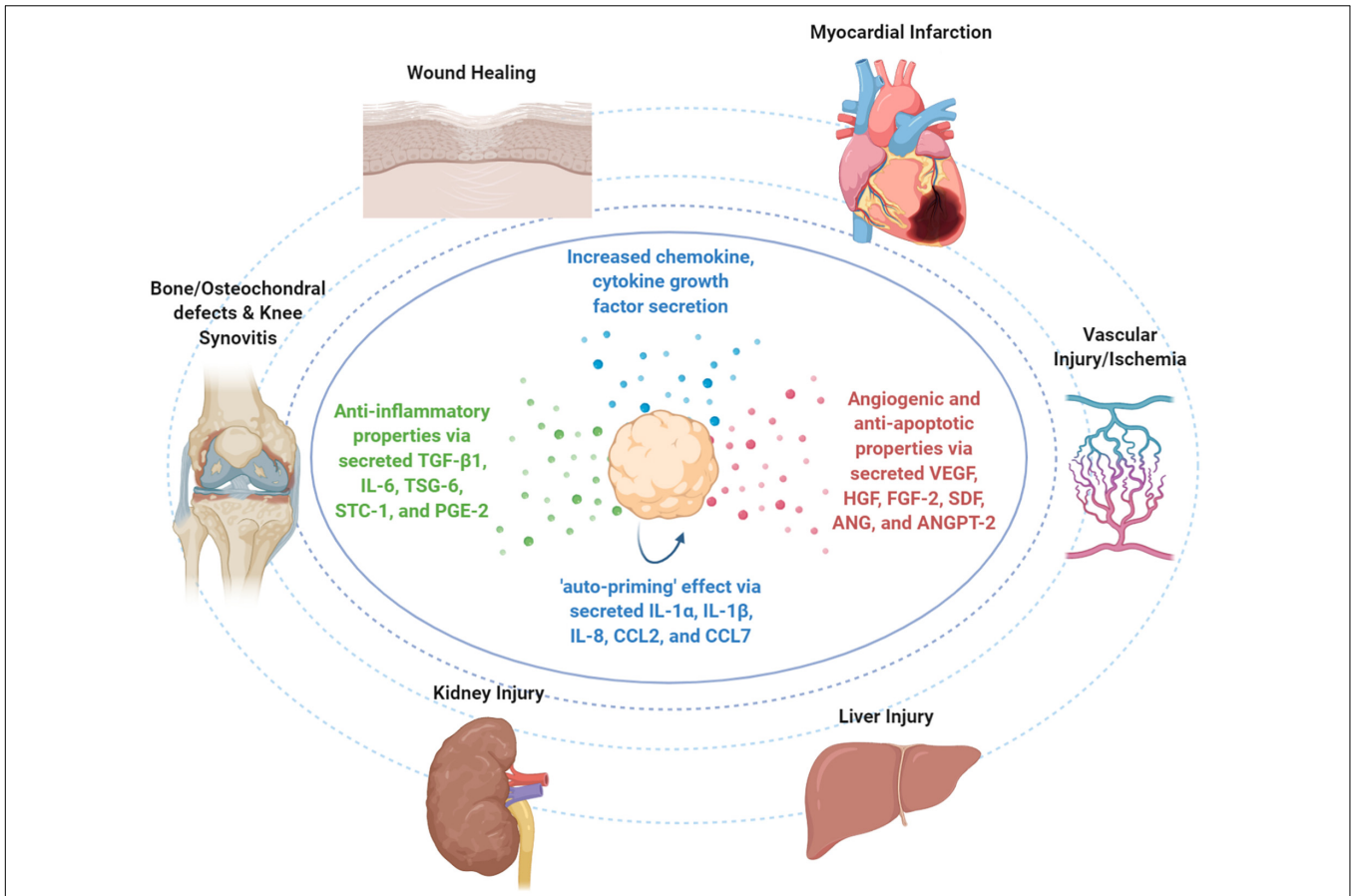

FIGURE 3 | Therapeutic properties of MSC spheroids *in vivo*. Upon infusion *in vivo*, MSC spheroid "medicinal signaling" activities are exerted by the paracrine secretion of modulatory mediators that possess immunomodulatory and trophic (i.e., angiogenic, anti-fibrotic, anti-apoptotic, and mitogenic) actions. MSC spheroids have been safely and effectively applied in various preclinical animal models for the treatment of skin wounds, myocardial infarction, vascular injury/ischemia, liver injury, kidney injury, bone and osteochondral defects, and knee synovitis.

its production is dependent on caspase activity and NFkB activation in MSC spheroids (Ylöstalo et al., 2012).

Upon MSC homing to the target site and depending on the molecular composition of the local microenvironment, they exhibit a therapeutic responsive polarization into either anti-inflammatory (MSC-2) or pro-inflammatory (MSC-1) phenotypes. Interestingly, studies showed that except for the abovementioned secreted molecules with anti-inflammatory effects, MSC spheroids increase the secretion of pro-inflammatory cytokines (including IL-1α, IL-1β, and IL-8) and chemokines (including CCL2 and CCL7) (Potapova et al., 2007; Bartosh et al., 2010, 2013; Yeh et al., 2014) that contribute in the inflammatory cell recruitment locally and putatively in the overall inflammatory response of the host. However, Bartosh et al. showed that BM-derived MSC assembly into MSC spheroids triggers the caspase-dependent IL-1 signaling and activates the expression of IL-1 in an autocrine secretion manner, resulting in an "auto-priming" effect (**Figure 3**). In MSC spheroids, the increased PGE2 secretion was related to activation of both caspase-dependent IL-1 and Notch signaling pathways, whereas TSG-6 and STC-1 secretion was related only to caspase-dependent IL-1 signaling activation (Bartosh et al., 2010). Collectively, MSC priming by paracrine and/or autocrine pro-inflammatory modes is a prerequisite in order to acquire their anti-inflammatory MSC2 phenotype and exert strong anti-inflammatory effects *in vivo*.

As reviewed in Kouroupis et al. (2018), several studies indicate that activation of specific Toll-like receptors (TLRs) in MSC *in vitro* prior to infusion *in vivo* has a profound effect on MSC functionalization toward immunomodulatory phenotype. However, Redondo-Castro et al. (2018a) reported that IL-1 stimulation of BM-derived MSC spheroids resulted in significantly increased expression of IL1-Ra, VEGF, and G-CSF molecules without anti-inflammatory effects on LPS-treated microglial cells in co-cultures. These discrepancies of the data underline the necessity for optimization of the priming methods and culture conditions. Previous studies showed that MSC immunomodulatory factor secretion is strongly affected by the composition of the culture medium (Zimmermann and McDevitt, 2014). In 2D culture settings, BM-derived and adipose-derived MSC cultured with FBS or hPL showed differences in expression of immunomodulatory

and adhesion molecules, with adipose-derived MSC being more potent functionally in inhibiting T-cell proliferation (Menard et al., 2013). Similarly, in two studies, Kouroupis et al. (2020a; 2020b) indicated that fat pad-derived (IFP) MSCs when cultured in regulatory-compliant conditions *in vitro* are superior functionally in Substance P degradation and T-cell proliferation inhibition compared to FBS-grown MSC. In an acute synovitis rat model, IFP-MSC intra-articular injection *in vivo* reversed more effectively signs of synovitis and IFP fibrosis when they were cultured under regulatory-compliant conditions (Kouroupis et al., 2020a,b). In 3-D settings, MSC spheroids cultured in serum and animal component-free chemically defined medium had less secretion of IDO, PGE2, TGF-β1, and IL-6 immunomodulatory factors compared to the typical MSC cultures supplemented with FBS (Zimmermann and McDevitt, 2014). In order to overcome these hurdles, Ylostalo et al. proposed specific protocols to efficiently prime MSCs in 3-D settings and preserve their robust anti-inflammatory properties under chemically defined xeno-free conditions (Ylostalo et al., 2017).

Overall, further studies are required to address the effects of pro-inflammatory cytokines and culturing conditions on anti-inflammatory properties of MSC spheroids *in vitro* and *in vivo*.

THERAPEUTIC PROPERTIES OF MESENCHYMAL STEM/STROMAL CELL SPHEROIDS IN PRECLINICAL ANIMAL MODELS

With exception to the therapeutic safety that most MSC clinical trials are investigating for various clinical disorders,[2] crucial factors that affect the therapeutic efficiency are MSC homing to target tissues and subsequent MSC survival *in vivo*. It cannot be overlooked that initial outcomes from many of such studies revealed that MSC therapies show a significant degree of variability with cases of non-reproducible clinical data. The inconsistent evidence potentially relates not only to intrinsic differences in the cell-based products used but importantly related with their *in vivo* fate upon implantation or infusion [parameters affecting MSC functionalization *in vitro* and *in vivo* are reviewed in Kouroupis et al. (2018)]. On this basis, a pioneering study showed that 5.0×10^5 BM-MSC injected into the left ventricle of uninjured mouse heart can effectively engraft the myocardium; however, only 0.44% of the MSCs could be identified after 4 days of injection (Toma et al., 2002). In addition, Toma et al. showed that 92 ± 7% of intraarterially injected MSC in rats are entrapped in the microvasculature (Toma et al., 2009). Collectively, even though long-term engraftment seems not to be a prerequisite for MSC reparative effects *in vivo*, their initial homing and survival is a crucial factor affecting the therapeutic outcomes. In that context, 3D spheroid formation *in vitro* closely recapitulates the *in vivo* MSC niche by providing spatial cell organization with increased cell–cell interactions that protect MSC viability and intrinsic properties. For example, in a mouse model of hind limb ischemia, MSC spheroid transplantation improved its survival compared to MSC suspension, by suppressing a key apoptotic signaling molecule (Bax), while activating anti-apoptotic signaling (BCL-2; Bhang et al., 2012). These positive effects can also be attributed to improved resistance to oxidative stress-induced apoptosis exerted by hypoxia-induced genes (e.g., VEGF-A, HIF-1^{α}, and MnSOD), elevated by the hypoxic conditions at the spheroid core (Potapova et al., 2007; Zhang et al., 2012).

Mesenchymal stem/stromal cell-based spheroids have been applied in various preclinical models including wound healing (Amos et al., 2009; Zhang et al., 2012; Hsu and Hsieh, 2015), bone and osteochondral defects (Ma et al., 2011; Suzuki et al., 2012; Suenaga et al., 2015), knee synovitis (Kouroupis et al., 2021), and cardiovascular diseases (Wang C.-C. et al., 2009; Emmert et al., 2013a) (**Figure 3**).

WOUND HEALING

To date, three separate studies applied MSC spheroids for wound healing in a model of diabetic healing impaired (leptin receptor-deficient) mice (Amos et al., 2009), in chemotherapy-induced oral mucositis (Zhang et al., 2012), and in a rat skin repair model (Hsu and Hsieh, 2015). In a pioneering study, Amos et al. investigated the applicability of MSC spheroids to treat chronic wounds such as diabetic ulcers, which remain a significant health burden for diabetic patients. In detail, full-thickness dermal wounds (approximately 78.5 mm^2 area) were generated in leptin receptor-deficient mice and treated with a total of 350,000 adipose-derived MSC per wound organized in multiple separate spheroids. Interestingly, for a 12 day time-frame, MSC spheroids resulted in significantly greater rate of wound closure compared to wounds treated with MSC suspension. This outcome may be attributed to higher expression of ECM genes (*tenascin C*, *Collagen VIα3*, and *fibronectin*) and higher secretion of soluble factors (HGF, MMP-2, and MMP-14) in MSC spheroid compared to MSC suspension cultures *in vitro* (Amos et al., 2009). Zhang et al. (2012) intravenously infused 1×10^6 gingiva-derived MSC spheroids or MSC suspension to a 5-fluorouracil-induced oral mycositis mouse model. On day 7, results indicated that MSC spheroids can reverse body weight loss and promote the regeneration of damaged epithelial lining of the mucositic mouse tongues. Interestingly, authors reported that MSC spheroids are capable of increased homing/engrafting to mucositic tongues due to their enhanced CXCR4 expression and may potentially trans-differentiate into epithelial cells via mesenchymal–epithelial transition *in vivo* (Zhang et al., 2012). These data indicate the potential use of MSC spheroids to alleviate the oral mucositis side-effect post-chemotherapy in cancer patients. In another rat skin wound healing model, 1×10^5 adipose-derived MSC spheroids or MSC suspension were applied to 15 mm × 15 mm wounds and covered with hyaluronan gel/chitosan sponge to maintain a moist environment. On day 8, results showed that the MSC spheroid group showed faster wound closure and significantly higher ratio of angiogenesis compared with the MSC suspension group. *In vivo* tracking of fluorescently labeled MSCs

[2]http://clinicaltrials.gov

showed close localization of MSC spheroids to microvessels, suggesting enhanced angiogenesis through paracrine effects. Moreover, MSC spheroid increased engrafting and angiogenesis effects may be attributed to the high expression of cytokine genes (*FGF-1*, *VEGF*, and *CCL2*) and migration-related genes (*CXCR4* and *MMP-1*) (Hsu and Hsieh, 2015). Collectively, in all cases, MSC spheroids provide better therapeutic efficacy compared with traditional MSC suspension in wound healing.

BONE/OSTEOCHONDRAL DEFECTS AND SYNOVITIS

Studies showed that bone/osteochondral defects and knee synovitis can be treated by MSC spheroids. In a delicate study, Sekiya's group generated a full-thickness (5 mm × 5 mm wide, 1.5 mm deep) osteochondral defect rabbit model, and defects were treated with different doses of synovium-derived MSC spheroids (containing 2.5×10^5–20×10^6 MSC/defect) (Suzuki et al., 2012). Post-implantation MSC spheroids could attach to the osteochondral defects by surface tension, whereas at 12 weeks, MSC spheroids containing 2.5×10^6 MSC showed the highest safranin-O-positive area ratio and resulted in regenerated cartilage with thickness similar to the neighboring healthy cartilage. Interestingly, authors reported that MSC spheroids with high cell densities result in failed defect repair and fibrous tissue formation possibly due to cell death and nutrient deprivation effects (Suzuki et al., 2012). In a calvarial bone defect (8 mm wide) rat model, Suenaga et al. treated the rat defects using three different conditions, 3.0×10^7 BM-MSC spheroids, β-TCP granules, or BM-MSC spheroids coated with β-TCP granules. Eight weeks post-implantation, MSC spheroids resulted in full-thickness bone formation with evident vascularization. In contrast, the other two groups had only minimal or non-uniform bone formation at the implanted sites, indicating that β-TCP restricts the bone regenerative capacity of MSC spheroids (Suenaga et al., 2015). Recently, Yanagihara et al. (2018) treated 4 mm wide femoral bone defects in rats with 2.4×10^6 Runx2-transfected MSC spheroids or Runx2-transfected MSC suspension embedded in collagen scaffolds. On day 35, MSC spheroids showed faster bone regeneration compared with MSC suspension and non-transfected MSC, whereas enhanced MSC spheroid migration to the defect sites was correlated with higher expression levels of migration-related genes *CXCR4* and *Integrinα2* (Yanagihara et al., 2018). Recently, in a mono-iodoacetate acute synovial/IFP inflammation rat model, Kouroupis et al. intraarticularly injected 5.0×10^5 infrapatellar fat pad MSC (IFP-MSC) spheroids. Twenty-five days post-infusion, IFP-MSC spheroids effectively degraded Substance P and resolved inflammation and fibrosis of synovial membrane and fat pad tissues in the rat knee. Interestingly, IFP-MSC intraarticular injection not only results in anti-inflammatory and anti-fibrotic effects but also showed strong anabolic/cartilage protective effects. Specifically, in the IFP-MSC spheroid cohort, cartilage integrity was preserved intact up to 28 days (Kouroupis et al., 2021). To conclude, MSC spheroids exert anti-inflammatory/anti-fibrotic effects and are effective for promoting both bone and osteochondral defect regeneration.

MYOCARDIAL INFARCTION

Intramyocardial transplantation of MSC spheroids in rat (Wang C.-C. et al., 2009; Lee et al., 2012; Liu et al., 2013) and porcine (Emmert et al., 2013b) myocardial infarction models resulted in greater heart function improvement compared with MSC suspensions. In an acute myocardial infarction rat model, Wang C.-C. et al. (2009) performed intramyocardial injection of 5.0×10^5 BM-derived MSC spheroids or MSC suspension and evaluated the echocardiography and catheterization measurements 4, 8, and 12 weeks post-operatively. The results showed superior heart function and stimulation of significant increase in vascular density for the MSC spheroid group (Wang C.-C. et al., 2009). In a delicate study, *in vivo* tracking of Dil-labeled UC-derived MSC spheroids showed that they can be differentiated into endothelial and cardiomyocyte cells at 4 weeks post-intramyocardial injection in a rat myocardial infarction model. At 7 weeks, the therapeutic efficacy of UC-derived MSC spheroids is superior to MSC suspension in post-infarction left ventricular remodeling (Lee et al., 2012). Importantly, Liu et al. (2013) showed that adipose-derived MSC spheroids generated on chitosan membranes show a 20-fold increase in cardiac marker gene expression (*Gata4*, *Nkx2-5*, *Myh6*, and *Tnnt2*) compared with MSC suspension cultures. In a similar approach, intramyocardial injection of 1×10^7 adipose-derived MSC spheroids in a rat myocardial infarction model showed better functional recovery compared with MSC suspensions after 12 weeks (Liu et al., 2013). Interestingly, a previous study indicated that intramyocardial injection of MSC spheroids consisting of adipose-derived MSC/human umbilical vein endothelial cells results in low arrhythmogenic potential but no further beneficial effects compared to the untreated group in a rat myocardial infarction model (Kolettis et al., 2018). In a larger animal model study, adipose-derived MSC were first labeled with micron-sized iron oxide particles, and then 2×10^7 MSC spheroids or MSC suspension were intra-myocardial injected in the porcine-infarcted myocardium. Moreover, the MSC spheroid engrafted successfully in 88.8% of animals keeping intact their micro architecture *in vivo*, whereas no arrhythmogenic, embolic, or neurological events occurred in the treated groups for up to 5 weeks follow-up (Emmert et al., 2013b). Therefore, preclinical studies established the feasibility, safety, and beneficial effects of intra-myocardial injected MSC spheroids in infarcted myocardium.

NEOVASCULARIZATION AND ISCHEMIA

In conjunction with the beneficial trophic effects of MSC spheroids toward infarcted myocardium, their applicability has been also investigated for neovascularization *in vivo*. In a mouse hind limb ischemia model, 1.0×10^7 cord-blood MSC

spheroid intramuscular injection significantly increased the number of microvessels and αSMA-positive vessels, resulting in decreased fibrosis in the ischemic region, and attenuated limb loss and necrosis. In comparison, the MSC spheroid group showed a limb salvage rate of 75%, whereas the MSC suspension group resulted in limb salvage rate of only 12.5% (Bhang et al., 2012). Additionally, Lee et al. (2016) showed that intramuscular injected adipose-derived MSC spheroids showed better proliferation than MSC suspension in the ischemic region, an effect that can be attributed to an increased expression of the proliferation marker PCNA. Therefore, MSC spheroids promote vascularization through secretion of angiogenic cytokines, preservation of ECM, and regulation of apoptotic signals.

LIVER AND KIDNEY DISEASE

The potential of MSC spheroids has been also investigated in liver regeneration and kidney injury models. For liver regeneration, two animal models have been tested for hepatectomy and CCl4-induced acute liver failure. In a pioneering study, Liu and Chang (2006) injected intraperitoneally 3×10^7 BM-MSC or hepatocytes in alginate–polylysine–alginate spheroids or suspension formats to treat 90% of hepatectomized rats. Up to day 14, in the BM-MSC spheroid, hepatocyte spheroid, and hepatocyte suspension groups, most rats survived (83–100%) and showed increased liver wet weight. Interestingly, these beneficial effects could be attributed to the increased expression in MSC spheroids of hepatocyte markers cytokeratin 8, cytokeratin 18, albumin, and α-fetoprotein (Liu and Chang, 2006). In an improved approach, 3×10^7 BM-MSC spheroids or MSC suspension were intrasplenically injected to treat 90% of hepatectomized rats. On day 14, survival rate in MSC spheroid group was prolonged by almost 70% compared with the MSC suspension group via the secretion of hepatotrophic factors such as HGF and IL-6 into the liver. Of note, authors reported that implanted MSC may transdifferentiate into hepatocyte-like cells *in vivo* and therefore may render spleen as an ectopic functional liver support (Liu and Chang, 2009, 2012). This hypothesis has to be further investigated as MSC differentiation toward endodermal fate has not been widely established. In a CCl4-induced acute liver failure mouse model, 1×10^6 UC-MSC spheroids or MSC suspension were infused via the tail vein and, at day 2, resulted in liver injury attenuation. Specifically, MSC spheroids could promote IL-6 and IFN-γ secretion but suppress TNF-α serum levels, and therefore significantly reduce tissue necrosis and increase liver regeneration (Li et al., 2015). In a recent study, adipose-derived MSC spheroids have been used to treat an ischemia–reperfusion (I/R)-induced acute kidney injury rat model. Moreover, 2×10^6 MSC spheroids or MSC suspension were directly injected to the kidney cortex, and renal function was investigated for a 14-day follow-up. Results indicated that MSC spheroids are more beneficial to the kidney by reduction of tissue damage, increased vascularization, and amelioration of renal function compared with MSC suspensions. In detail, the MSC spheroid group showed increased levels of VEGF, HGF, and TSG-6 cytokines, and decreased levels of creatinine and blood urea nitrogen in the serum (Xu et al., 2016). Therefore, in both liver and kidney injury animal models, MSC spheroid paracrine actions result in improved therapeutic effects characterized by reduced tissue necrosis, increased tissue regeneration, and improved organ function.

FUTURE CLINICAL PERSPECTIVES

To date, only a limited number of comparative preclinical studies have been performed between MSC spheroids and MSC suspension after 2D culture, whereas no clinical trials exist to evaluate the efficacy of MSC spheroids in clinical settings. As a result, there are no specific criteria to define when MSC spheroids would be preferable over MSC suspension to treat various clinical indications. However, it has become increasingly clear that current conventional and extensive 2D MSC culturing methods, similar to the ones used in public and commercial stem cell biobanks, even though they can ensure the generation of clinically relevant cell numbers for *in vivo* applications, cannot guarantee the preservation of MSC qualitative characteristics and their related high functionality. To circumvent these limitations, the incorporation of 3D MSC culturing approach into cell-based therapy would significantly impact the field, as more reproducible clinical outcomes may be achieved without requiring extensive *ex vivo* MSC manipulation and MSC stimulatory regimes (reviewed in Kouroupis et al., 2018). Specifically, current data indicate that MSC spheroid cultures with or without the usage of biomaterials not only preserve MSC phenotypic and molecular profiles but also significantly reinforce MSC functionality related to their immunomodulatory, anti-fibrotic, angiogenic, and trophic properties. In addition, as initial MSC homing and survival are crucial factors affecting the therapeutic outcome, 3D spheroid formation closely recapitulates the *in vivo* MSC niche, protect MSC viability, and works as a "vehicle" for their effective homing to the affected tissues upon implantation *in vivo*. On this basis, the adaptation of high-throughput regulatory-compliant and reproducible methods for MSC spheroid production would allow their use in clinical settings and contribute to an improved MSC-based product for safer and more effective therapeutic applications.

AUTHOR CONTRIBUTIONS

Both authors have made substantial contributions to the drafting of the article or revising it critically and to the final approval of the version to be submitted.

ACKNOWLEDGMENTS

We are in gratitude to the Soffer Family Foundation and the DRI Foundation for their generous funding support.

REFERENCES

Agarwal, S. K., and Brenner, M. B. (2006). Role of adhesion molecules in synovial inflammation. *Curr. Opin. Rheumatol.* 18, 268–276. doi: 10.1097/01.bor.0000218948.42730.39

Aggarwal, S., and Pittenger, M. F. (2005). Human mesenchymal stem cells modulate allogeneic immune cell responses. *Blood* 105, 1815–1822.

Alimperti, S., and Andreadis, S. T. (2015). CDH2 and CDH11 act as regulators of stem cell fate decisions. *Stem Cell Res.* 14, 270–282. doi: 10.1016/j.scr.2015.02.002

Alvarez-Pérez, J., Ballesteros, P., and Cerdán, S. (2005). Microscopic images of intraspheroidal pH by 1H magnetic resonance chemical shift imaging of pH sensitive indicators. *Magma* 18, 293–301. doi: 10.1007/s10334-005-0013-z

Amos, P. J., Kapur, S. K., Stapor, P. C., Shang, H., Bekiranov, S., Khurgel, M., et al. (2009). Human adipose-derived stromal cells accelerate diabetic wound healing: impact of cell formulation and delivery. *Tissue Eng. Part A* 16, 1595–1606. doi: 10.1089/ten.tea.2009.0616

Ayan, B., Heo, D. N., Zhang, Z., Dey, M., Povilianskas, A., Drapaca, C., et al. (2020). Aspiration-assisted bioprinting for precise positioning of biologics. *Sci. Adv.* 6:eaaw5111. doi: 10.1126/sciadv.aaw5111

Baraniak, P. R., Cooke, M. T., Saeed, R., Kinney, M. A., Fridley, K. M., and McDevitt, T. C. (2012). Stiffening of human mesenchymal stem cell spheroid microenvironments induced by incorporation of gelatin microparticles. *J. Mech. Behav. Biomed. Mater.* 11, 63–71. doi: 10.1016/j.jmbbm.2012.02.018

Bartosh, T. J., Ylöstalo, J. H., Bazhanov, N., Kuhlman, J., and Prockop, D. J. (2013). Dynamic compaction of human mesenchymal stem/precursor cells into spheres self-activates caspase-dependent IL1 signaling to enhance secretion of modulators of inflammation and immunity (PGE2, TSG6, and STC1). *Stem Cells* 31, 2443–2456. doi: 10.1002/stem.1499

Bartosh, T. J., Ylostalo, J. H., Mohammadipoor, A., Bazhanov, N., Coble, K., Claypool, K., et al. (2010). Aggregation of human mesenchymal stromal cells (MSCs) into 3D spheroids enhances their antiinflammatory properties. *Proc. Natl. Acad. Sci. U.S.A.* 107, 13724–13729. doi: 10.1073/pnas.1008117107

Bernardo, M. E., and Fibbe, W. E. (2013). Mesenchymal stromal cells: sensors and switchers of inflammation. *Cell Stem Cell* 13, 392–402. doi: 10.1016/j.stem.2013.09.006

Bhang, S. H., Cho, S.-W., La, W.-G., Lee, T.-J., Yang, H. S., Sun, A.-Y., et al. (2011). Angiogenesis in ischemic tissue produced by spheroid grafting of human adipose-derived stromal cells. *Biomaterials* 32, 2734–2747. doi: 10.1016/j.biomaterials.2010.12.035

Bhang, S. H., Lee, S., Shin, J.-Y., Lee, T.-J., and Kim, B.-S. (2012). Transplantation of cord blood mesenchymal stem cells as spheroids enhances vascularization. *Tissue Eng. Part A* 18, 2138–2147. doi: 10.1089/ten.tea.2011.0640

Blakely, A. M., Manning, K. L., Tripathi, A., and Morgan, J. R. (2015). Bio-pick, place, and perfuse: a new instrument for three-dimensional tissue engineering. *Tissue Eng. Part C Methods* 21, 737–746. doi: 10.1089/ten.TEC.2014.0439

Bulanova, E. A., Koudan, E. V., Degosserie, J., Heymans, C., Pereira, F. D., Parfenov, V. A., et al. (2017). Bioprinting of a functional vascularized mouse thyroid gland construct. *Biofabrication* 9:034105. doi: 10.1088/1758-5090/aa7fdd

Caplan, A. I. (2017). mesenchymal stem cells: time to change the name! *Stem Cells Transl. Med.* 6, 1445–1451. doi: 10.1002/sctm.17-0051

Caplan, A. I., and Correa, D. (2011). The MSC: an injury drugstore. *Cell Stem Cell* 9, 11–15.

Cechin, S., Alvarez-Cubela, S., Giraldo, J. A., Molano, R. D., Villate, S., Ricordi, C., et al. (2014). Influence of in vitro and in vivo oxygen modulation on β cell differentiation from human embryonic stem cells. *Stem Cells Transl. Med.* 3, 277–289. doi: 10.5966/sctm.2013-0160

Centeno, C. J., Busse, D., Kisiday, J., Keohan, C., Freeman, M., and Karli, D. (2008). Regeneration of meniscus cartilage in a knee treated with percutaneously implanted autologous mesenchymal stem cells. *Med. Hypotheses* 71, 900–908. doi: 10.1016/j.mehy.2008.06.042

Chang, S. K., Noss, E. H., Chen, M., Gu, Z., Townsend, K., Grenha, R., et al. (2011). Cadherin-11 regulates fibroblast inflammation. *Proc. Natl.Acad. Sci. U.S.A.* 108:8402. doi: 10.1073/pnas.1019437108

Colle, J., Blondeel, P., Bruyne, A., Bochar, S., Tytgat, L., Vercruysse, C., et al. (2020). Bioprinting predifferentiated adipose-derived mesenchymal stem cell spheroids with methacrylated gelatin ink for adipose tissue engineering. *J. Mater. Sci.* 31:36. doi: 10.1007/s10856-020-06374-w

Cui, X., Hartanto, Y., and Zhang, H. (2017). Advances in multicellular spheroids formation. *J. R. Soc. Interface* 14:20160877. doi: 10.1098/rsif.2016.0877

Curcio, E., Salerno, S., Barbieri, G., De Bartolo, L., Drioli, E., and Bader, A. (2007). Mass transfer and metabolic reactions in hepatocyte spheroids cultured in rotating wall gas-permeable membrane system. *Biomaterials* 28, 5487–5497. doi: 10.1016/j.biomaterials.2007.08.033

da Silva Meirelles, L., Fontes, A. M., Covas, D. T., and Caplan, A. I. (2009). Mechanisms involved in the therapeutic properties of mesenchymal stem cells. *Cytokine Growth Factor Rev.* 20, 419–427. doi: 10.1016/j.cytogfr.2009.10.002

De Bari, C., Dell'Accio, F., Tylzanowski, P., and Luyten, F. P. (2001). Multipotent mesenchymal stem cells from adult human synovial membrane. *Arthritis Rheumatism* 44, 1928–1942.

de Bournonville, S., Lambrechts, T., Vanhulst, J., Luyten, F. P., Papantoniou, I., and Geris, L. (2019). Towards self-regulated bioprocessing: a compact benchtop bioreactor system for monitored and controlled 3D cell and tissue culture. *Biotechnol. J.* 14:1800545. doi: 10.1002/biot.201800545

De Moor, L., Fernandez, S., Vercruysse, C., Tytgat, L., Asadian, M., De Geyter, N., et al. (2020). Hybrid bioprinting of chondrogenically induced human mesenchymal stem cell spheroids. *Front. Bioeng. Biotechnol.* 8:484. doi: 10.3389/fbioe.2020.00484

Deynoux, M., Sunter, N., Ducrocq, E., Dakik, H., Guibon, R., Burlaud-Gaillard, J., et al. (2020). A comparative study of the capacity of mesenchymal stromal cell lines to form spheroids. *PLoS One* 15:e0225485. doi: 10.1371/journal.pone.0225485

Doucet, C., Ernou, I., Zhang, Y., Llense, J.-R., Begot, L., Holy, X., et al. (2005). Platelet lysates promote mesenchymal stem cell expansion: a safety substitute for animal serum in cell-based therapy applications. *J. Cell. Physiol.* 205, 228–236. doi: 10.1002/jcp.20391

Dragoo, J. L., Samimi, B., Zhu, M.-L., Hame, S. L., Thomas, B. L., Lieberman, J. R., et al. (2003). Tissue-engineered cartilage and bone using stem cells from human infrapatellar fat pads. *J. Bone Joint Surg. Br.* 85, 740–747.

Emmert, M. Y., Wolint, P., Wickboldt, N., Gemayel, G., Weber, B., Brokopp, C. E., et al. (2013a). Human stem cell-based three-dimensional microtissues for advanced cardiac cell therapies. *Biomaterials* 34, 6339–6354. doi: 10.1016/j.biomaterials.2013.04.034

Emmert, M. Y., Wolint, P., Winklhofer, S., Stolzmann, P., Cesarovic, N., Fleischmann, T., et al. (2013b). Transcatheter based electromechanical mapping guided intramyocardial transplantation and in vivo tracking of human stem cell based three dimensional microtissues in the porcine heart. *Biomaterials* 34, 2428–2441. doi: 10.1016/j.biomaterials.2012.12.021

Foty, R. A., and Steinberg, M. S. (2005). The differential adhesion hypothesis: a direct evaluation. *Dev. Biol.* 278, 255–263. doi: 10.1016/j.ydbio.2004.11.012

Foty, R. (2011). A simple hanging drop cell culture protocol for generation of 3D spheroids. *J. Vis. Exp.* 51, 2720. doi: 10.3791/2720

Fraker, C. A., Alvarez, S., Papadopoulos, P., Giraldo, J., Gu, W., Ricordi, C., et al. (2007). Enhanced oxygenation promotes beta-cell differentiation in vitro. *Stem Cells* 25, 3155–3164. doi: 10.1634/stemcells.2007-0445

Fraker, C. A., Cechin, S., Álvarez-Cubela, S., Echeverri, F., Bernal, A., Poo, R., et al. (2013). A physiological pattern of oxygenation using perfluorocarbon-based culture devices maximizes pancreatic islet viability and enhances β-Cell function. *Cell Transplantation* 22, 1723–1733. doi: 10.3727/096368912X657873

Friedenstein, A. J., Chailakhyan, R. K., Latsinik, N. V., Panasyuk, A. F., and Keiliss-Borok, I. V. (1974). Stromal cells responsible for transferring the microenvironment of the hemopoietic tissues. Cloning in vitro and retransplantation in vivo. *Transplantation* 17, 331–340.

Frith, J. E., Thomson, B., and Genever, P. G. (2010). Dynamic three-dimensional culture methods enhance mesenchymal stem cell properties and increase therapeutic potential. *Tissue Eng. Part C Methods* 16, 735–749. doi: 10.1089/ten.TEC.2009.0432

Guilak, F., Estes, B. T., Diekman, B. O., Moutos, F. T., and Gimble, J. M. (2010). 2010 nicolas andry award: multipotent adult stem cells from adipose tissue for musculoskeletal tissue engineering. *Clin. Orthopaedics Relat. Res.* 468, 2530–2540. doi: 10.1007/s11999-010-1410-9

Gutzweiler, L., Kartmann, S., Troendle, K., Benning, L., Finkenzeller, G., Zengerle, R., et al. (2017). Large scale production and controlled deposition of single HUVEC spheroids for bioprinting applications. *Biofabrication* 9:025027. doi: 10.1088/1758-5090/aa7218

Hass, R., Kasper, C., Böhm, S., and Jacobs, R. (2011). Different populations and sources of human mesenchymal stem cells (MSC): a comparison of adult and neonatal tissue-derived MSC. *Cell Commun. Signal.* 9:12. doi: 10.1186/1478-811X-9-12

Hsu, S.-H., and Hsieh, P.-S. (2015). Self-assembled adult adipose-derived stem cell spheroids combined with biomaterials promote wound healing in a rat skin repair model. *Wound Repair Regen.* 23, 57–64. doi: 10.1111/wrr.12239

Hsu, S. H., and Huang, G. S. (2013). Substrate-dependent Wnt signaling in MSC differentiation within biomaterial-derived 3D spheroids. *Biomaterials* 34, 4725–4738. doi: 10.1016/j.biomaterials.2013.03.031

Huang, G. S., Dai, L. G., Yen, B. L., and Hsu, S. H. (2011). Spheroid formation of mesenchymal stem cells on chitosan and chitosan-hyaluronan membranes. *Biomaterials* 32, 6929–6945. doi: 10.1016/j.biomaterials.2011.05.092

Ip, B. C., Cui, F., Tripathi, A., and Morgan, J. R. (2016). The bio-gripper: a fluid-driven micro-manipulator of living tissue constructs for additive bio-manufacturing. *Biofabrication* 8:025015. doi: 10.1088/1758-5090/8/2/025015

Jakab, K., Norotte, C., Damon, B., Marga, F., Neagu, A., Besch-Williford, C. L., et al. (2008). Tissue engineering by self-assembly of cells printed into topologically defined structures. *Tissue Eng. Part A* 14, 413–421. doi: 10.1089/tea.2007.0173

Jones, E., Crawford, A., English, A., Henshaw, K., Mundy, J., Corscadden, D., et al. (2008). Synovial fluid mesenchymal stem cells in health and early osteoarthritis: detection and functional evaluation at the single-cell level. *Arthritis Rheumatism* 58, 1731–1740.

Jung, S., Sen, A., Rosenberg, L., and Behie, L. A. (2010). Identification of growth and attachment factors for the serum-free isolation and expansion of human mesenchymal stromal cells. *Cytotherapy* 12, 637–657.

Karnieli, O., Friedner, O. M., Allickson, J. G., Zhang, N., Jung, S., Fiorentini, D., et al. (2017). A consensus introduction to serum replacements and serum-free media for cellular therapies. *Cytotherapy* 19, 155–169. doi: 10.1016/j.jcyt.2016.11.011

Koç, O. N., Day, J., Nieder, M., Gerson, S. L., Lazarus, H. M., and Krivit, W. (2002). Allogeneic mesenchymal stem cell infusion for treatment of metachromatic leukodystrophy (MLD) and Hurler syndrome (MPS-IH). *Bone Marrow Transplant* 30, 215–222. doi: 10.1038/sj.bmt.1703650

Kolettis, T. M., Bagli, E., Barka, E., Kouroupis, D., Kontonika, M., Vilaeti, A. D., et al. (2018). Medium-term electrophysiologic effects of a cellularized scaffold implanted in rats after myocardial infarction. *Cureus* 10:e2959. doi: 10.7759/cureus.2959

Kouroupis, D., Bowles, A. C., Best, T. M., Kaplan, L. D., and Correa, D. (2020a). CD10/Neprilysin enrichment in infrapatellar fat pad–derived mesenchymal stem cells under regulatory-compliant conditions: implications for efficient synovitis and fat pad fibrosis reversal. *Am. J. Sports Med.* 48, 2013–2027. doi: 10.1177/0363546520917699

Kouroupis, D., Bowles, A. C., Greif, D. N., Leñero, C., Best, T. M., Kaplan, L. D., et al. (2020b). Regulatory-compliant conditions during cell product manufacturing enhance in vitro immunomodulatory properties of infrapatellar fat pad-derived mesenchymal stem/stromal cells. *Cytotherapy* 22, 677–689. doi: 10.1016/j.jcyt.2020.06.007

Kouroupis, D., Sanjurjo-Rodriguez, C., Jones, E., and Correa, D. (2018). Mesenchymal stem cell functionalization for enhanced therapeutic applications. *Tissue Eng. Part B* 25, 55–77. doi: 10.1089/ten.teb.2018.0118

Kouroupis, D., Wang, X. N., El-Sherbiny, Y., McGonagle, D., and Jones, E. (2017). "The safety of non-expanded multipotential stromal cell therapies," in *Safety, Ethics and Regulations*, eds P. V. Pham and A. Rosemann (Cham: Springer International Publishing), 91–118.

Kouroupis, D., Willman, M. A., Best, T. M., Kaplan, L. D., and Correa, D. (2021). Infrapatellar fat pad-derived mesenchymal stem cell-based spheroids enhance their therapeutic efficacy to reverse synovitis and fat pad fibrosis. *Stem Cell Res. Ther.* 12:44. doi: 10.1186/s13287-020-02107-6

Krampera, M., Galipeau, J., Shi, Y., Tarte, K., and Sensebe, L. (2013). Immunological characterization of multipotent mesenchymal stromal cells—The international society for cellular therapy (ISCT) working proposal. *Cytotherapy* 15, 1054–1061. doi: 10.1016/j.jcyt.2013.02.010

Le Blanc, K., Frassoni, F., Ball, L., Locatelli, F., Roelofs, H., Lewis, I., et al. (2008). Mesenchymal stem cells for treatment of steroid-resistant, severe, acute graft-versus-host disease: a phase II study. *Lancet* 371, 1579–1586.

Lee, E. J., Park, S. J., Kang, S. K., Kim, G.-H., Kang, H.-J., Lee, S.-W., et al. (2012). Spherical bullet formation via e-cadherin promotes therapeutic potency of mesenchymal stem cells derived from human umbilical cord blood for myocardial infarction. *Mol. Ther.* 20, 1424–1433. doi: 10.1038/mt.2012.58

Lee, J. H., Han, Y.-S., and Lee, S. H. (2016). Long-duration three-dimensional spheroid culture promotes angiogenic activities of adipose-derived mesenchymal stem cells. *Biomol. Ther.* 24, 260–267. doi: 10.4062/biomolther.2015.146

Lewis, E. E. L., Wheadon, H., Lewis, N., Yang, J., Mullin, M., Hursthouse, A., et al. (2016). A quiescent, regeneration-responsive tissue engineered mesenchymal stem cell bone marrow niche model via magnetic levitation. *ACS Nano* 10, 8346–8354. doi: 10.1021/acsnano.6b02841

Li, Y., Guo, G., Li, L., Chen, F., Bao, J., Shi, Y.-J., et al. (2015). Three-dimensional spheroid culture of human umbilical cord mesenchymal stem cells promotes cell yield and stemness maintenance. *Cell Tissue Res.* 360, 297–307. doi: 10.1007/s00441-014-2055-x

Liu, B.-H., Yeh, H.-Y., Lin, Y.-C., Wang, M.-H., Chen, D. C., Lee, B.-H., et al. (2013). Spheroid formation and enhanced cardiomyogenic potential of adipose-derived stem cells grown on chitosan. *BioResearch Open Access* 2, 28–39. doi: 10.1089/biores.2012.0285

Liu, Z. C., and Chang, T. M. S. (2006). Transdifferentiation of bioencapsulated bone marrow cells into hepatocyte-like cells in the 90% hepatectomized rat model. *Liver Transplantation* 12, 566–572. doi: 10.1002/lt.20635

Liu, Z. C., and Chang, T. M. S. (2009). Preliminary study on intrasplenic implantation of artificial cell bioencapsulated stem cells to increase the survival of 90% hepatectomized rats. *Artif. Cells Blood Subst. Biotechnol.* 37, 53–55. doi: 10.1080/10731190802663975

Liu, Z. C., and Chang, T. M. S. (2012). Intrasplenic transplantation of bioencapsulated mesenchymal stem cells improves the recovery rates of 90% partial hepatectomized rats. *Stem Cells Int.* 2012:697094. doi: 10.1155/2012/697094

Lou, Y., Guo, D., Zhang, H., and Song, L. (2016). Effectiveness of mesenchymal stems cells cultured by hanging drop vs. conventional culturing on the repair of hypoxic-ischemic-damaged mouse brains, measured by stemness gene expression. *Open Life Sci.* 11, 519–523.

Ma, D., Zhong, C., Yao, H., Liu, Y., Chen, F., Li, J., et al. (2011). Engineering injectable bone using bone marrow stromal cell aggregates. *Stem Cells Dev.* 20, 989–999. doi: 10.1089/scd.2010.0348

Mackay, A. M., Beck, S. C., Murphy, J. M., Barry, F. P., Chichester, C. O., and Pittenger, M. F. (1998). Chondrogenic differentiation of cultured human mesenchymal stem cells from marrow. *Tissue Eng.* 4, 415–428. doi: 10.1089/ten.1998.4.415

Markou, M., Kouroupis, D., Badounas, F., Katsouras, A., Kyrkou, A., Fotsis, T., et al. (2020). Tissue engineering using vascular organoids from human pluripotent stem cell derived mural cell phenotypes. *Front. Bioeng. Biotechnol.* 8:278. doi: 10.3389/fbioe.2020.00278

Mekhileri, N. V., Lim, K. S., Brown, G. C. J., Mutreja, I., Schon, B. S., Hooper, G. J., et al. (2018). Automated 3D bioassembly of micro-tissues for biofabrication of hybrid tissue engineered constructs. *Biofabrication* 10:024103. doi: 10.1088/1758-5090/aa9ef1

Menard, C., Pacelli, L., Bassi, G., Dulong, J., Bifari, F., Bezier, I., et al. (2013). Clinical-grade mesenchymal stromal cells produced under various good manufacturing practice processes differ in their immunomodulatory properties: standardization of immune quality controls. *Stem Cells Dev.* 22, 1789–1801. doi: 10.1089/scd.2012.0594

Mendicino, M., Bailey, Alexander, M., Wonnacott, K., Puri, R. K., Bauer, et al. (2014). MSC-based product characterization for clinical trials: an FDA perspective. *Cell Stem Cell* 14, 141–145. doi: 10.1016/j.stem.2014.01.013

Meng, R., Xu, H.-Y., Di, S.-M., Shi, D.-Y., Qian, A.-R., Wang, J.-F., et al. (2011). Human mesenchymal stem cells are sensitive to abnormal gravity and exhibit classic apoptotic features. *Acta Bioch. Biophys. Sin.* 43, 133–142. doi: 10.1093/abbs/gmq121

Messina, A., Morelli, S., Forgacs, G., Barbieri, G., Drioli, E., and De Bartolo, L. (2017). Self-assembly of tissue spheroids on polymeric membranes. *J. Tissue Eng. Regen. Med.* 11, 2090–2103. doi: 10.1002/term.2105

Meyers, V. E., Zayzafoon, M., Douglas, J. T., and McDonald, J. M. (2005). RhoA and cytoskeletal disruption mediate reduced osteoblastogenesis and enhanced

adipogenesis of human mesenchymal stem cells in modeled microgravity. *J. Bone Min. Res.* 20, 1858–1866. doi: 10.1359/JBMR.050611

Meyers, V. E., Zayzafoon, M., Gonda, S. R., Gathings, W. E., and McDonald, J. M. (2004). Modeled microgravity disrupts collagen I/integrin signaling during osteoblastic differentiation of human mesenchymal stem cells. *J. Cell. Biochem.* 93, 697–707. doi: 10.1002/jcb.20229

Mironov, V., Visconti, R. P., Kasyanov, V., Forgacs, G., Drake, C. J., and Markwald, R. R. (2009). Organ printing: tissue spheroids as building blocks. *Biomaterials* 30, 2164–2174. doi: 10.1016/j.biomaterials.2008.12.084

Moldovan, N. I., Hibino, N., and Nakayama, K. (2017). Principles of the kenzan method for robotic cell spheroid-based three-dimensional bioprinting. *Tissue Eng. Part B Rev.* 23, 237–244. doi: 10.1089/ten.TEB.2016.0322

Moretti, P., Hatlapatka, T., Marten, D., Lavrentieva, A., Majore, I., Hass, R., et al. (2010). Mesenchymal stromal cells derived from human umbilical cord tissues: primitive cells with potential for clinical and tissue engineering applications. *Adv. Biochem. Eng. Biotechnol.* 123, 29–54. doi: 10.1007/10_2009_15

Mueller-Klieser, W. (1984). Method for the determination of oxygen consumption rates and diffusion coefficients in multicellular spheroids. *Biophys. J.* 46, 343–348. doi: 10.1016/s0006-3495(84)84030-8

Murphy, K. C., Fang, S. Y., and Leach, J. K. (2014). Human mesenchymal stem cell spheroids in fibrin hydrogels exhibit improved cell survival and potential for bone healing. *Cell Tissue Res.* 357, 91–99. doi: 10.1007/s00441-014-1830-z

Murphy, K. C., Hung, B. P., Browne-Bourne, S., Zhou, D., Yeung, J., Genetos, D. C., et al. (2017). Measurement of oxygen tension within mesenchymal stem cell spheroids. *J. R. Soc. Interface* 14:20160851. doi: 10.1098/rsif.2016.0851

Nikolova, M. P., and Chavali, M. S. (2019). Recent advances in biomaterials for 3D scaffolds: a review. *Bioact. Mater.* 4, 271–292. doi: 10.1016/j.bioactmat.2019.10.005

Petrenko, Y., Syková, E., and Kubinová, Š (2017). The therapeutic potential of three-dimensional multipotent mesenchymal stromal cell spheroids. *Stem Cell Res. Ther.* 8:94. doi: 10.1186/s13287-017-0558-6

Pittenger, M. F., Discher, D. E., Péault, B. M., Phinney, D. G., Hare, J. M., and Caplan, A. I. (2019). Mesenchymal stem cell perspective: cell biology to clinical progress. *npj Regen. Med.* 4:22. doi: 10.1038/s41536-019-0083-6

Potapova, I. A., Brink, P. R., Cohen, I. S., and Doronin, S. V. (2008). Culturing of human mesenchymal stem cells as three-dimensional aggregates induces functional expression of CXCR4 that regulates adhesion to endothelial cells. *J. Biol. Chem.* 283, 13100–13107. doi: 10.1074/jbc.M800184200

Potapova, I. A., Gaudette, G. R., Brink, P. R., Robinson, R. B., Rosen, M. R., Cohen, I. S., et al. (2007). Mesenchymal stem cells support migration, extracellular matrix invasion, proliferation, and survival of endothelial cells in vitro. *Stem Cells* 25, 1761–1768.

Redondo-Castro, E., Cunningham, C. J., Miller, J., Brown, H., Allan, S. M., and Pinteaux, E. (2018a). Changes in the secretome of tri-dimensional spheroid-cultured human mesenchymal stem cells in vitro by interleukin-1 priming. *Stem Cell Res. Ther.* 9:11. doi: 10.1186/s13287-017-0753-5

Redondo-Castro, E., Cunningham, C. J., Miller, J., Cain, S. A., Allan, S. M., and Pinteaux, E. (2018b). Generation of Human mesenchymal stem cell 3D spheroids using low-binding plates. *Bio Protoc.* 8:e2968. doi: 10.21769/BioProtoc.2968

Ringden, O., Uzunel, M., Rasmusson, I., Remberger, M., Sundberg, B., Lonnies, H., et al. (2006). Mesenchymal stem cells for treatment of therapy-resistant graft-versus-host disease. *Transplantation* 81, 1390–1397.

Sart, S., Tsai, A. C., Li, Y., and Ma, T. (2014). Three-dimensional aggregates of mesenchymal stem cells: cellular mechanisms, biological properties, and applications. *Tissue Eng. Part B Rev.* 20, 365–380. doi: 10.1089/ten.TEB.2013.0537

Seda Tığlı, R., Karakeçili, A., and Gümüşderelioğlu, M. (2007). In vitro characterization of chitosan scaffolds: influence of composition and deacetylation degree. *J. Mater. Sci.*18, 1665–1674. doi: 10.1007/s10856-007-3066-x

Sheyn, D., Pelled, G., Netanely, D., Domany, E., and Gazit, D. (2010). The effect of simulated microgravity on human mesenchymal stem cells cultured in an osteogenic differentiation system: a bioinformatics study. *Tissue Eng Part A* 16, 3403–3412. doi: 10.1089/ten.tea.2009.0834

Singer, N. G., and Caplan, A. I. (2011). Mesenchymal stem cells: mechanisms of inflammation. *Annu. Rev. Pathol.* 6, 457–478. doi: 10.1146/annurev-pathol-011110-130230

Sorrell, J. M., Baber, M. A., and Caplan, A. I. (2009). Influence of adult mesenchymal stem cells on in vitro vascular formation. *Tissue Eng Part A* 15, 1751–1761. doi: 10.1089/ten.tea.2008.0254

Suenaga, H., Furukawa, K. S., Suzuki, Y., Takato, T., and Ushida, T. (2015). Bone regeneration in calvarial defects in a rat model by implantation of human bone marrow-derived mesenchymal stromal cell spheroids. *J. Mater. Sci. Mater. Med.* 26:254. doi: 10.1007/s10856-015-5591-3

Suzuki, S., Muneta, T., Tsuji, K., Ichinose, S., Makino, H., Umezawa, A., et al. (2012). Properties and usefulness of aggregates of synovial mesenchymal stem cells as a source for cartilage regeneration. *Arthritis Res. Ther.* 14:R136.

Theisen, C. S., Wahl, J. K. III, Johnson, K. R., and Wheelock, M. J. (2007). NHERF links the N-cadherin/catenin complex to the platelet-derived growth factor receptor to modulate the actin cytoskeleton and regulate cell motility. *Mol. Biol. Cell* 18, 1220–1232. doi: 10.1091/mbc.e06-10-0960

Toma, C., Pittenger Mark, F., Cahill Kevin, S., Byrne Barry, J., and Kessler Paul, D. (2002). Human mesenchymal stem cells differentiate to a cardiomyocyte phenotype in the adult murine heart. *Circulation* 105, 93–98. doi: 10.1161/hc0102.101442

Toma, C., Wagner, W. R., Bowry, S., Schwartz, A., and Villanueva, F. (2009). Fate of culture-expanded mesenchymal stem cells in the microvasculature: in vivo observations of cell kinetics. *Circ. Res.* 104, 398–402. doi: 10.1161/CIRCRESAHA.108.187724

Uccelli, A., and Rosbo, N. K. (2015). The immunomodulatory function of mesenchymal stem cells: mode of action and pathways. *Ann. N. Y. Acad. Sci.* 1351, 114–126. doi: 10.1111/nyas.12815

Vorwald, C. E., Ho, S. S., Whitehead, J., and Leach, J. K. (2018). High-throughput formation of mesenchymal stem cell spheroids and entrapment in alginate hydrogels. *Methods Mol. Biol.* 1758, 139–149. doi: 10.1007/978-1-4939-7741-3_11

Wang, C.-C., Chen, C.-H., Hwang, S.-M., Lin, W.-W., Huang, C.-H., Lee, W.-Y., et al. (2009). Spherically symmetric mesenchymal stromal cell bodies inherent with endogenous extracellular matrices for cellular cardiomyoplasty. *Stem Cells* 27, 724–732. doi: 10.1634/stemcells.2008-0944

Wang, W., Itaka, K., Ohba, S., Nishiyama, N., Chung, U.-I., Yamasaki, Y., et al. (2009). 3D spheroid culture system on micropatterned substrates for improved differentiation efficiency of multipotent mesenchymal stem cells. *Biomaterials* 30, 2705–2715. doi: 10.1016/j.biomaterials.2009.01.030

Waterman, R. S., Tomchuck, S. L., Henkle, S. L., and Betancourt, A. M. (2010). A new mesenchymal stem cell (MSC) paradigm: polarization into a pro-inflammatory MSC1 or an immunosuppressive MSC2 phenotype. *PLoS One* 5:e10088. doi: 10.1371/journal.pone.0010088

Weiss, M., and Troyer, D. (2006). Stem cells in the umbilical cord. *Stem Cell Rev. Rep.* 2, 155–162.

Xu, L., Meng, F., Ni, M., Lee, Y., and Li, G. (2013). N-cadherin regulates osteogenesis and migration of bone marrow-derived mesenchymal stem cells. *Mol. Biol. Rep.* 40, 2533–2539. doi: 10.1007/s11033-012-2334-0

Xu, Y., Shi, T., Xu, A., and Zhang, L. (2016). 3D spheroid culture enhances survival and therapeutic capacities of MSCs injected into ischemic kidney. *J. Cell. Mol.Med.* 20, 1203–1213. doi: 10.1111/jcmm.12651

Yanagihara, K., Uchida, S., Ohba, S., Kataoka, K., and Itaka, K. (2018). Treatment of bone defects by transplantation of genetically modified mesenchymal stem cell spheroids. *Mol. Ther. Methods Clin. Dev.* 9, 358–366. doi: 10.1016/j.omtm.2018.04.006

Yang, C. M., Huang, Y. J., and Hsu, S. H. (2015). Enhanced autophagy of adipose-derived stem cells grown on chitosan substrates. *Biores. Open Access* 4, 89–96. doi: 10.1089/biores.2014.0032

Yeh, H.-Y., Liu, B.-H., and Hsu, S.-H. (2012). The calcium-dependent regulation of spheroid formation and cardiomyogenic differentiation for MSCs on chitosan membranes. *Biomaterials* 33, 8943–8954. doi: 10.1016/j.biomaterials.2012.08.069

Yeh, H.-Y., Liu, B.-H., Sieber, M., and Hsu, S.-H. (2014). Substrate-dependent gene regulation of self-assembled human MSC spheroids on chitosan membranes. *BMC Genomics* 15:10. doi: 10.1186/1471-2164-15-10

Ylöstalo, J. H., Bartosh, T. J., Coble, K., and Prockop, D. J. (2012). Human mesenchymal stem/stromal cells (hMSCs) cultured as spheroids are self-activated to produce prostaglandin E2 (PGE2) that directs stimulated macrophages into an anti-inflammatory phenotype. *Stem Cells* 30, 2283–2296. doi: 10.1002/stem.1191

Ylostalo, J. H., Bartosh, T. J., Tiblow, A., and Prockop, D. J. (2014). Unique characteristics of human mesenchymal stromal/progenitor cells pre-activated in 3-dimensional cultures under different conditions. *Cytotherapy* 16, 1486–1500. doi: 10.1016/j.jcyt.2014.07.010

Ylostalo, J. H., Bazhanov, N., Mohammadipoor, A., and Bartosh, T. J. (2017). Production and administration of therapeutic mesenchymal stem/stromal cell (MSC) spheroids primed in 3-D cultures under xeno-free conditions. *J. Vis. Exp.* 121, 55126. doi: 10.3791/55126

Yu, B., Yu, D., Cao, L., Zhao, X., Long, T., Liu, G., et al. (2011). Simulated microgravity using a rotary cell culture system promotes chondrogenesis of human adipose-derived mesenchymal stem cells via the p38 MAPK pathway. *Biochem. Biophys. Res. Commun.* 414, 412–418. doi: 10.1016/j.bbrc.2011.09.103

Zhang, K., Yan, S., Li, G., Cui, L., and Yin, J. (2015). In-situ birth of MSCs multicellular spheroids in poly(l-glutamic acid)/chitosan scaffold for hyaline-like cartilage regeneration. *Biomaterials* 71, 24–34. doi: 10.1016/j.biomaterials.2015.08.037

Zhang, Q., Nguyen, A. L., Shi, S., Hill, C., Wilder-Smith, P., Krasieva, T. B., et al. (2012). Three-dimensional spheroid culture of human gingiva-derived mesenchymal stem cells enhances mitigation of chemotherapy-induced oral mucositis. *Stem Cells Dev.* 21, 937–947. doi: 10.1089/scd.2011.0252

Zimmermann, J. A., and McDevitt, T. C. (2014). Pre-conditioning mesenchymal stromal cell spheroids for immunomodulatory paracrine factor secretion. *Cytotherapy* 16, 331–345. doi: 10.1016/j.jcyt.2013.09.004

Zuk, P. A., Zhu, M., Ashjian, P., De Ugarte, D. A., Huang, J. I., Mizuno, H., et al. (2002). Human adipose tissue is a source of multipotent stem cells. *Mol. Biol. Cell* 13, 4279–4295.

Conflict of Interest: The authors declare that the research was conducted in the absence of any commercial or financial relationships that could be construed as a potential conflict of interest.

frontiers in Bioengineering and Biotechnology

REVIEW
published: 30 March 2021
doi: 10.3389/fbioe.2021.634403

The Importance of Proper Oxygenation in 3D Culture

Hubert M. Tse[1], Graeme Gardner[2], Juan Dominguez-Bendala[2,3] and Christopher A. Fraker[2]**

[1] Department of Microbiology, The University of Alabama at Birmingham, Birmingham, AL, United States, [2] Department of Surgery, Diabetes Research Institute, Leonard M. Miller School of Medicine, University of Miami, Coral Gables, FL, United States, [3] Department of Cell Biology and Anatomy, University of Miami Miller School of Medicine, Miami, FL, United States

Cell culture typically employs inexpensive, disposable plasticware, and standard humidified CO_2/room air incubators (5% CO_2, ~20% oxygen). These methods have historically proven adequate for the maintenance of viability, function, and proliferation of many cell types, but with broad variation in culture practices. With technological advances it is becoming increasingly clear that cell culture is not a "one size fits all" procedure. Recently, there is a shift toward comprehension of the individual physiological niches of cultured cells. As scale-up production of single cell and 3D aggregates for therapeutic applications has expanded, researchers have focused on understanding the role of many environmental metabolites/forces on cell function and viability. Oxygen, due to its role in cell processes and the requirement for adequate supply to maintain critical energy generation, is one such metabolite gaining increased focus. With the advent of improved sensing technologies and computational predictive modeling, it is becoming evident that parameters such as cell seeding density, culture media height, cellular oxygen consumption rate, and aggregate dimensions should be considered for experimental reproducibility. In this review, we will examine the role of oxygen in 3D cell culture with particular emphasis on primary islets of Langerhans and stem cell-derived insulin-producing SC-β cells, both known for their high metabolic demands. We will implement finite element modeling (FEM) to simulate historical and current culture methods in referenced manuscripts and innovations focusing on oxygen distribution. Our group and others have shown that oxygen plays a key role in proliferation, differentiation, and function of these 3D aggregates. Their culture in plastic consistently results in core regions of hypoxia/anoxia exacerbated by increased media height, aggregate dimensions, and oxygen consumption rates. Static gas permeable systems ameliorate this problem. The use of rotational culture and other dynamic culture systems also have advantages in terms of oxygen supply but come with the caveat that these endocrine aggregates are also exquisitely sensitive to mechanical perturbation. As recent work demonstrates, there is a strong rationale for the use of alternate *in vitro* systems to maintain physio-normal environments for cell growth and function for better phenotypic approximation of *in vivo* counterparts.

Keywords: 3D culture, spheroids, oxygenation, gas-permeable, hypoxia, hyperoxia (oxygen)

OPEN ACCESS

Edited by:
Cornelia Kasper, University of Natural Resources and Life Sciences, Vienna, Austria

Reviewed by:
Vanessa L. S. LaPointe, Maastricht University, Netherlands
Elisabeth Ferreira, University of Arkansas for Medical Sciences, United States

***Correspondence:**
Christopher A. Fraker
cfraker@med.miami.edu
Graeme Gardner
gxg780@med.miami.edu

Specialty section:
This article was submitted to Preclinical Cell and Gene Therapy, a section of the journal Frontiers in Bioengineering and Biotechnology

Received: *27 November 2020*
Accepted: *09 March 2021*
Published: *30 March 2021*

Citation:
Tse HM, Gardner G, Dominguez-Bendala J and Fraker CA (2021) The Importance of Proper Oxygenation in 3D Culture. Front. Bioeng. Biotechnol. 9:634403. doi: 10.3389/fbioe.2021.634403

INTRODUCTION

Biomedical research of 3D cell culture has been ongoing for decades, increasing dramatically with the recent boom in stem cell research and associated cellular therapies (Moscona A., 1961; Knisely et al., 1969; Bruland et al., 1985; Li et al., 1992; De Moor et al., 2018; Gargotti et al., 2018; Jokinen et al., 2020; Qadir et al., 2020). Early seminal research focused on tumor spheroids and the generation of *in vitro* models to test therapies against the malignant cells (Inch et al., 1970; Bruland et al., 1985; Vescio et al., 1987). These early works spawned expansive research into basic biological mechanisms such as proliferation, differentiation, cell death, and nutrient/metabolite requirements in culture (Moscona A.A., 1961; Knisely et al., 1969; Carlsson et al., 1979; Gille and Joenje, 1992; Matta et al., 1994; Singhvi et al., 1994; Bader et al., 1996; Gassmann et al., 1996; Groebe, 1996).

Resoundingly, the majority of early research found dramatic improvements with 3D culture compared with 2D culture of the same cells. Simultaneous molecular and functional analysis of 2D and 3D cultures led to the discovery that 3D cultures tend to more accurately recapitulate the *in vivo* environment in cell shape/structure and environment. This, in turn, influences gene/protein expression and cell function. As a result, 3D cultures traditionally behave more like their *in vivo* counterparts. Despite dramatic improvements in expression and function, a substantial gap exists between 3D aggregates/spheroids and the *in vivo* organoids they are meant to model. We posit that one potential explanation for these observed differences is the variability in employed culture methods, particularly related to tissue oxygenation. Through years of foundational research and technological advances, the limitations of tissue oxygenation in culture methods have been described and the critical importance of variables such as cell seeding density, oxygen consumption rate (OCR), growth rate, and media height have been described (Carlsson et al., 1979; Mueller-Klieser and Sutherland, 1982; Heacock and Sutherland, 1986; Mueller-Klieser et al., 1986; Freyer et al., 1991; Gassmann et al., 1996; Groebe and Mueller-Klieser, 1996; Papas et al., 2005; Grayson et al., 2006; Fehrer et al., 2007). Due to the urgency with which all living cells require oxygen for the maintenance of metabolic processes, much focus has shifted to addressing insufficiencies in cell culture either through the design of culture systems based on convective flow and improved oxygen transfer through culture surfaces or by tissue engineering approaches to improve vasculogenesis.

For years, static culture has been performed in gas impermeable systems where steep oxygen and nutrient gradients form, shifting cells/aggregates down alternate pathways of metabolism, growth, and differentiation. Recent work from many groups, including our own, demonstrates that proper oxygenation can dramatically alter the viability and function of cell cultures, particularly of 3D tissues, resulting in an even more physio-normal approximation of their *in vivo* counterparts (Carlsson et al., 1979; Tuncay et al., 1994; Saini and Wick, 2004; Wang et al., 2005; Fraker et al., 2007, 2009, 2013; Powers et al., 2008, 2010; Simon and Keith, 2008; Anada et al., 2012; Cechin et al., 2014). This article will examine the role of oxygen in the growing area of 3D culture for therapeutic cell-based applications as it pertains to both primary endocrine cell aggregates (islets of Langerhans) and endocrine stem cell aggregates (SC-β). The utility of finite element modeling (FEM) as a way of optimizing culture settings to target physiologically relevant tissue oxygen concentration/partial pressures (pO_2 in millimeters of mercury, relative to atmospheric pressure, 760 mmHg) will be highlighted. Particularly, we will examine alternate culture methods utilized historically, prior to the advent of efficient computational modeling, and will examine by retrospective FEM the oxygen profiles in these systems to determine the role of tissue oxygenation in some of the experimental outcomes. FEM can also dramatically reduce experimental waste in terms of materials and labor hours making it an efficient method for designing and validating experiments.

Importantly, tissue oxygenation in both 2D and 3D culture in various devices has been well-studied but the majority of these studies have been focused on conventional oxygen concentrations (95% RA) or extremely hypoxic conditions <4% O_2 and primarily in gas impermeable plastic systems (Knisely et al., 1969; Mueller-Klieser and Sutherland, 1982, 1984; Mueller-Klieser, 1984; Mueller-Klieser et al., 1986; Acker et al., 1987; Deshpande and Heinzle, 2009; Murphy et al., 2017). The conclusions of many such studies in 3D culture demonstrate the steep gradient formation and tissue volume anoxia that is expected in plastic systems. The advent of membrane-based culture systems and methods for improving oxygen delivery to the cell culture surface has created a paradigm shift where historical studies are being repeated under more physiological oxygenation with pronounced differences in cellular viability and function.

CELLULAR OXYGEN DEMAND

Mammalian development occurs at a partial pressure of oxygen (pO_2) governed by mass transfer prior to tissue vascularization (Simon and Keith, 2008). Mass transfer limitations dictate that $\sim$ 0.5–1 mm^3 is the maximal volume that can be adequately oxygenated by simple diffusive permeability, dependent on the tissue specific OCR and the local niche pO_2 (Colen et al., 1999; McGrath et al., 2003). Therefore, much tissue development occurs at a pO_2 approximating anoxia and this is the time period when much of the characteristic tissue proliferation is observed. With the advent of blood flow, pO_2 increases to tissue specific ranges from 3.8 to 100 mmHg with little variation across much larger, perfused regions.

Cellular OCR in the literature ranges between <1 and 350×10^{-18} mol/s. This is in line with the oxygen requirements needed for the metabolism of 2,500 kcal per day which requires approximately 22 mols of oxygen or 2.5×10^{-4} mol/s. Assuming the commonly accepted number of cells in the adult human body of 37.2 trillion, this equates to an average 6.72×10^{-18} mol/cell s^{-1} with variation due to metabolic demand and cell function. Based on an average human cell diameter of 20 μm, this translates to an average rate of 1.6×10^{-3} mol/m^3 of tissue s^{-1} (Wagner et al., 2011).

Historically, both 2D and 3D cell culture protocols have utilized gas-impermeable plastics kept within humidified incubators containing 95% room air (RA) and 5% carbon dioxide (CO_2). Accounting for vapor pressure differences, the standard incubator oxygen partial pressure is approximately 142 mmHg. However, there is much variability in utilized methods related to cell seeding density and media height, further exacerbated by the range of OCR associated with mammalian cells. Particularly, different culture platform geometries necessitate variations in media height to prevent evaporation and provide adequate nutrients. These variations, exhibited in **Table 1**, can be detrimental to cultured cells, especially those with higher OCR.

2D vs. 3D CULTURE: ENDOCRINE CELLS AND CLUSTERS AS AN EXAMPLE

The above variables can affect both 2D monolayer cultures and, more so, 3D aggregates resulting in prolonged exposure to elevated oxygen levels that can serve as a substrate for the formation of toxic free radical species on one extreme and pronounced hypoxia/anoxia, necrosis and impaired function on the other extreme (Kazzaz et al., 1999; Martens et al., 2005). Particularly, the high OCR and 3D geometry of endocrine aggregates (islets of Langerhans, stem cell-derived beta cells) restrict them to a low seeding density and culture medium height of ∼1.3 mm. These cells and clusters have reported OCR most often ranging from 1 to 5.0 × 10^{-2} mol/m^3 s^{-1}, more than an order of magnitude higher than the cellular average. This is not surprising given the critical role they play in the production and storage of multiple hormones and the tight regulation of glucose homeostasis (Papas et al., 2000; Murray et al., 2005; Pi et al., 2007; Buchwald, 2009, 2011; Fraker et al., 2013; Suszynski et al., 2014b; Qadir et al., 2020).

Figure 1 is finite element modeling (FEM) of 2D monolayer cultures showing the pO_2 at the core region across a parametric sweep of OCR relevant to endocrine cells and clusters examining the effect of culture media height on tissue pO_2.

From the model, 2D monolayer culture with 100% confluence is not prone to anoxia. In fact, at oxygen consumption rates at the lower end of the presented range, the pO_2 experienced by the cells is "supra-physiological." This could explain reports with culture at reduced environmental pO_2 that results in improved proliferation and viability, as the lower external pO_2 better represents the physiological niche of the cells (Fraker et al., 2007; Powers et al., 2008, 2010; Millman et al., 2009; Cechin et al., 2014). Using an oxygen consumption rate of 3.0 × 10^{-2} mol/m^3 s^{-1} as a reference value, simply changing the media height by ∼1 mm shifts the core tissue pO_2 nearly 30 mmHg (27 mmHg at 1.11 mm height to 0.9 mmHg at 2.28 mm height). As diffusion distances in vascularized tissues are typically not more than 5–10 μm, there are limited gradients that form *in vivo* related to not only oxygen but also most metabolites and waste products. The extent to which the gradients in culture affects cell function and viability, on the other hand, is not fully known.

In 3D cultures, core anoxia is common due to increased diffusion distances. This is evident in islets and islet-like clusters with sizes typically ranging from 50 to 400 μm. Islets above 100 μm cultured on plasticware experience increasing anoxia and loss of secretory capacity dependent primarily on oxygen consumption rate and media height and less so, related to seeding density. With a typical oxygen consumption range of 1.0–5.0 × 10^{-2} mol/m^3 s^{-1}, islets are limited to a seeding density that is well-established in the literature of about 3% of the culture surface area and a media depth not more than 1.1–1.3 mm (Papas et al., 2005; Avgoustiniatos et al., 2008; Kitzmann et al., 2014). As islet/endocrine spheroid viability and function are exquisitely dependent on tissue pO_2, deviations from the culture recommendations can result in pronounced islet/endocrine cluster loss during culture. In fact, it has been demonstrated in the literature that apoptosis in cultured islets directly correlates with expression of HIF-1a (Moritz et al., 2002). This results in increased costs related to islet culture as a typical human islet preparation of approximately 250,000 islet equivalents (islet size

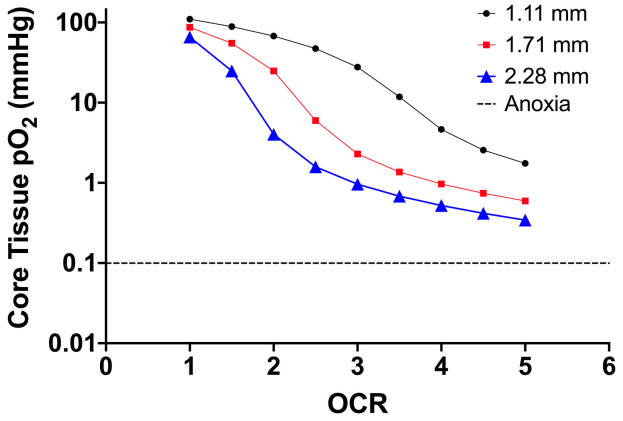

FIGURE 1 | Core tissue oxygen profile of 2D monolayer (20 μm cell diameter) as a factor of culture media height (three different line plots) and increasing OCR (along the *x*-axis). The decrease in core pO_2 corresponds to an increase in OCR along the *x*-axis and the downward shift in core pO_2 is a result of increased media height. The OCR are representative of the published range of most primary endocrine somatic cells and cell lines. The dashed line shows the accepted theoretical cutoff for tissue anoxia and eventual necrotic death in endocrine aggregates.

TABLE 1 | Inherent variations in oxygen diffusion distances (culture medium height) due to the dimensions of typically utilized plastic cell culture systems.

Culture system	Culture surface area (cm^2)	Typical culture medium volume range (mL)	Culture medium height range (mm)
96-well	0.32	0.1–0.2	3.12–6.25
24-well	1.9	0.5–1	2.63–5.26
6-well	9.6	1–3	1.04–3.13
T-75 flask	75	8–15	1.07–2
T-175 flask	175	35–53	2–3.03

1D oxygen diffusion from the air/liquid interface varies from 1.04 to 6.25 mm depending on dimensions and culture medium volume.

scale correction to mean diameter of 150 μm; IEQ) requires 10–12 T175 flasks. Early work by the group of and Colton, Papas, Avgoustiniatos, and Dionne utilized computational modeling to investigate the oxygenation limitations in conventional culture methods for islets of Langerhans (Dionne et al., 1989, 1991, 1993, 1996; Papas et al., 2005). Through their detailed study of OCR in endocrine cells and spheroids, they identified the K_m value associated with islet OCR (0.4 mmHg), and pO_2 values associated with anoxia (∼0.1 mmHg and below) and impaired insulin secretion (∼2.5 mmHg and below). They continued this important work with further in-depth study of (a) the use of OCR as a metric of islet potency, (b) limitations in encapsulation devices and *in vivo* cellular replacement therapies in Type 1 Diabetes Mellitus (T1D), and (c) the development of gas permeable culture systems to address oxygen limitations (Avgoustiniatos et al., 2008; Kitzmann et al., 2014; Suszynski et al., 2014a, 2016; Papas et al., 2016; Cao et al., 2020). In one seminal paper by the group, FEM was performed assuming the standard IEQ diameter of 150 μm cultured in a square array and varying the culture density and culture medium volume to maintain the 1,000 IEQ/mL culture standard. Three different oxygen consumption rates were evaluated. In addition to plastic, culture was also simulated on 275 μm silicone membranes. They observed precipitous increases in anoxia on plastic culture platforms relative to OCR and the combined effect of culture density/medium depth (Papas et al., 2005).

The equivalent scaling originated from hand-counts of numerous islet preparations (rodent, dog, non-human primate, porcine, and human) demonstrating that the size bin with the largest tissue volume percentage was ∼150 μm. Our group confirmed this in studies comparing automated counters with hand counting protocols (Buchwald et al., 2009). **Table 2** shows representative tissue volume distributions across size bins from 184 human islet preparation hand-counts.

The rationale behind the IEQ standardization is clear from the ∼37% of the tissue volume represented by the bins centered around 150 μm. However, over 60% of the tissue volume is above 150 μm which leads to underestimation in anoxic volume in the tissue preparations. To better represent this, our group generated FEM models to represent anoxia in the full islet preparation volume. After solving, anoxic volume percentages were calculated for each size range and then total anoxic tissue volume percentage was determined by the following equation:

$$\%A_{total} = \sum_{50-100}^{>400} \%A_{size} \times \%V_{size}$$

where, $\%A_{total}$ is total volume percentage of anoxic tissue, $\%A_{size}$ is the percentage of anoxic tissue volume determined by FEM for each islet size bin (**Table 2**) and $\%V_{size}$ is the mean volume percentage of tissue for each islet size bin (**Table 2**).

Figure 2 summarizes the effects of the oxygen consumption rate range, three conventional medium height variations (20, 30, 50 mL in a T-175 flask; 1.11, 1.71, and 2.28 mm, respectively) and three seeding densities (20, 30, and 50,000 IEQ in a T-175 flask; 2.76%, 3.67%, and 5.05%, respectively) on islet/islet-like cluster anoxia on standard plastic culture devices.

The models confirm the observed and previously modeled deficiencies of islet/endocrine spheroid culture on plastic systems. Tissue anoxia is observed in IEQ > 100 μm heavily dependent on OCR and culture medium height and less so on seeding density, albeit still a factor.

Despite well-documented culture suggestions and supportive FEM studies from multiple groups, there are still broad deviations in the literature in both islet/endocrine spheroid seeding density and culture medium height that could explain reported variations in pre/post-transplant function and viability. There is a clear need for culture standardization and cost-effective methods for improving culture oxygenation. Recent work has focused on addressing these challenges for the scale-up and implementation of clinical cell-based therapies.

METHODS TO IMPROVE OXYGENATION IN 3D CULTURE: ENDOCRINE CLUSTERS AS AN EXAMPLE

Early islet research groups including those of Colton, Kevin Lafferty and islet isolation pioneer, Paul Lacy, understood the importance of oxygen limitations in culture from early modeling and observed loss of function and viability (Bowen et al., 1980; Dionne et al., 1989, 1991). They explored various methods to improve oxygenation ranging from increasing incubator oxygen concentration to levels as high as 95%, low temperature culture, perfusion systems, and gyroscopic/rotational culture (Scharp et al., 1978; Ono et al., 1979; Lacy et al., 1982). All of these methods ameliorated tissue hypoxia/anoxia but had associated challenges and beneficial unexpected findings.

Increasing External Oxygen Concentration

In studies first by the group of Lafferty and then by Lacy et al. (1982) culture in elevated incubator pO_2 resulted in a stark depletion of tissue-resident immune cells present in islets. These cells surveil and relay information about islet well-being to immune response elements. Additionally, the extended culture resulted in aggregation of individual IEQ into "mega-islets."

TABLE 2 | Tissue volume percentages from 184 human islet preparations broken into IEQ counting size bins.

Size bin	50–100	100–150	150–200	200–250	250–300	300–350	350–400	>400
Mean	7.34%	15.23%	21.1%	16.27%	14.47%	12.40%	9.1%	4.07%
SEM	0.50%	0.70%	0.70%	0.70%	0.90%	0.90%	0.90%	0.70%

The bins centered around 150 μm account for nearly 37% of the total preparation volume, the rationale behind the 150 μm IEQ size.

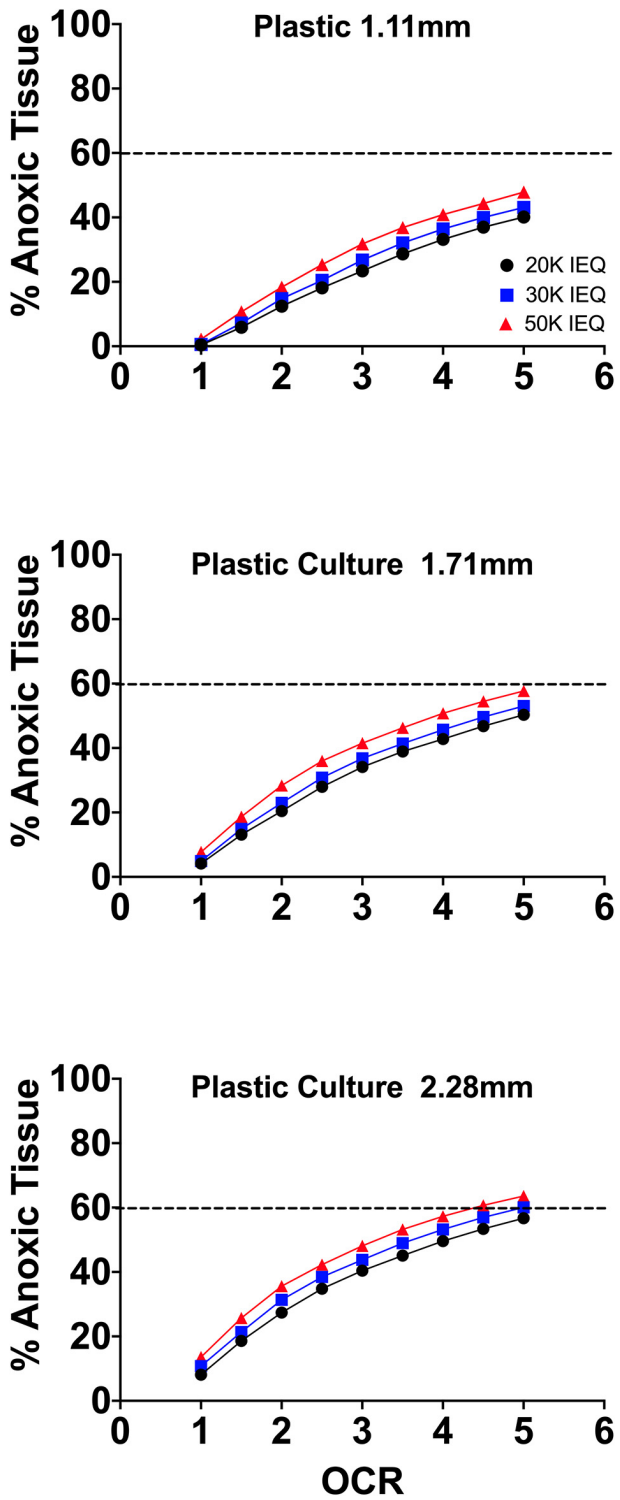

FIGURE 2 | FEM results of islet spheroids in standard culture (95% RA/5% CO_2; plastic surface; 37°C) with varied seeding density and culture medium height across the range of reported islet oxygen consumption rate. Tissue anoxia is observed, primarily in IEQ sizes >100 μm, even at low oxygen consumption rates and is significantly affected by culture medium height (~Δ20% min to max) and increased OCR (~Δ50% min to max) and less so by seeding density (~Δ7% min to max).

The depletion of the tissue-resident immune cells in elevated oxygen resulted in significantly prolonged islet engraftment in allogeneic and concordant xenogeneic transplant settings (Bowen et al., 1980).

In one paper by Bowen et al. (1980), they cultured 50 IEQ in 35 mm dishes with 2 mL of culture medium, initially, moving to 0.75 mL after the first of three culture medium changes in the 4–7 days culture period. Incubator gas concentration was 95% O_2 and 5% CO_2. After the first change of culture medium, they also began to observe aggregation of the IEQ into one large "mega-islet." Interestingly, IEQ that failed to aggregate did not survive the culture at elevated oxygen concentrations suggesting that the aggregation may result in a "mega-islet" pO_2 that better approximates standard culture or *in vivo* levels.

In another paper by Lacy et al. (1982), they modified the 2-stage protocol of Lafferty by first culturing 50 IEQ/well in U-bottom 96-well plates with 200 μL of culture medium. This significantly increased the culture medium height from ~2 mm in the Lafferty protocol to ~6.2 mm for the first stage of the culture progressing to culture on a 35 mm dish with 0.75 mL of culture medium, as in the Lafferty protocol.

In **Figure 3**, using the culture parameters described in the papers of Lafferty and Lacy, we performed FEM of the estimated anoxia during 2-stage mega-islet culture in order to better understand the effects of culture oxygenation on the experimental observations.

The increased pO_2 sustains the larger tissue dimensions at a level of hypoxia/anoxia approximating the culture of IEQ of standard size range and seeding density. There is no apparent oxygenation benefit but the elevated pO_2 allows for IEQ aggregation and reduction of tissue-resident immune

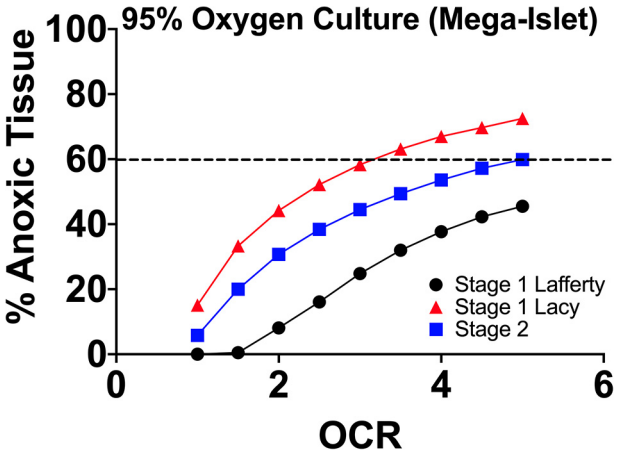

FIGURE 3 | FEM anoxia results of two stage mega-islet cultures (95% O_2/5% CO_2; plastic surface; 37°C) from the group of Lafferty and Lacy, respectively. Prior to aggregation (Stage 1), the tissue anoxia is lower at all oxygen consumption rates but with aggregation, anoxia become significantly higher throughout the tissue given the increase in tissue geometry. The elevated pO_2 maintains non-anoxic tissue at levels approximating culture of IEQs of standard size range (50–400 μm) and seeding density. At the same time, the supra-physiological pO_2 depletes the tissue resident immune cells.

cells. The thought of both groups was that increased oxygen was responsible for the loss of tissue-resident cells, but the presence, indicated by FEM, of similar anoxic tissue volumes to standard 95% RA/5% CO_2 cultures suggests that hypoxia/anoxia may also play a role. In both research efforts, when these mega-islets were utilized in sub-renal capsule transplants in chemically induced diabetic recipients, they improved allogeneic/concordant xenogeneic graft longevity without concurrent immunosuppression. This suggests that potentially (1) the tissue-resident cells play a critical role in graft rejection signaling recipient immune responses and (2) extended culture reduces antigen shedding and thereby, proinflammatory immune responses.

Our group also implemented increased oxygen levels in standard islet culture examining islet function and viability. FEM of this approach is shown in **Figure 4**. The modeled reduction in tissue anoxia was 30–50% compared to conventional 20% O_2. This did not translate to significant *in vitro* functional improvements. This could be the result of supra-physiological concentrations in smaller islets (100, 150 μm) resulting in increased oxidant concentration and potentially, free-radical mediated damage to secretory capacity. These high oxygen levels were not experienced by seeded IEQ in the prior mega-islet experiments due either to increased media depth or closer IEQ seeding proximity. Clearly, there is a balance of proper oxygenation where both too much and too little are detrimental, and the multiple variables involved further complicate efforts to adequately maintain endocrine clusters.

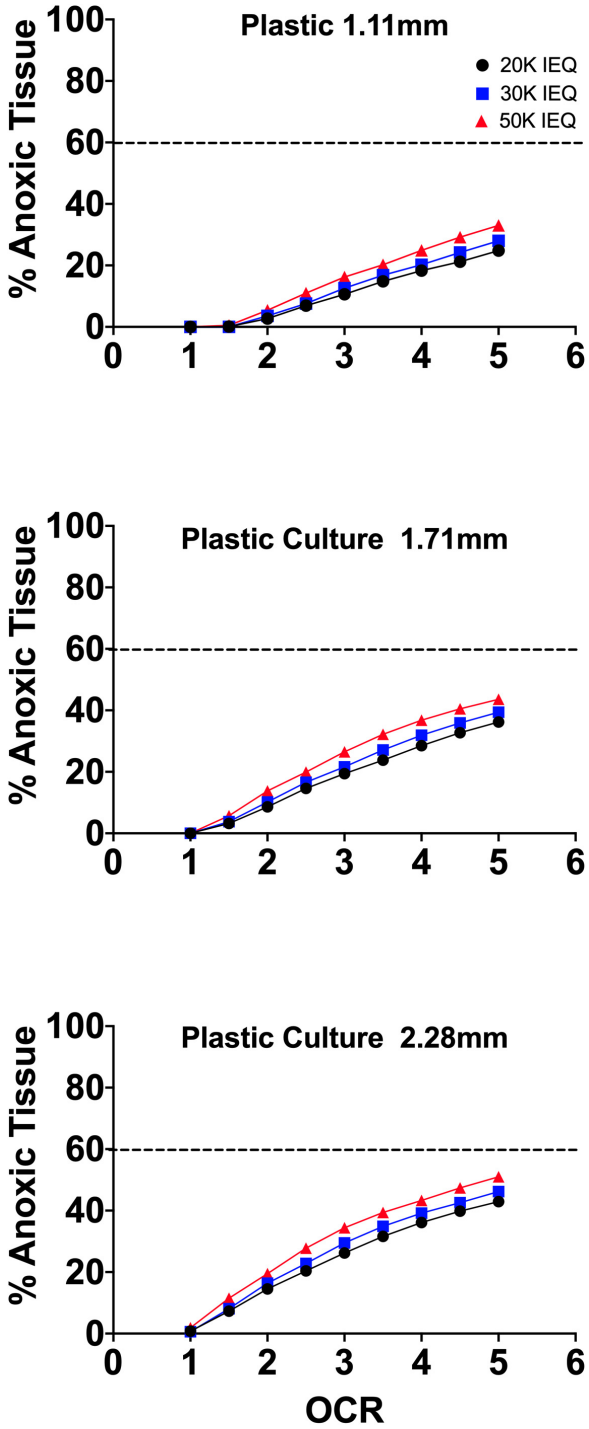

FIGURE 4 | FEM of standard islet culture on plastic with an external oxygen concentration of 35%. The modeled anoxia was ~50–70% relative to culture at 20% O_2.

Culture on Liquid Permeable Transwell Devices

Another approach that has been increasingly implemented in the culture of 3D aggregates, including islets and endocrine precursors/pancreatic progenitors is the use of transwell devices. These come ready to use in most plate well geometries. 3D aggregates are suspended on a liquid permeable membrane raised off of the basal plastic surface of the culture well ~1 mm. Simply elevating the culture above the gas impermeable surface and allowing for mass transfer on both the basal and apical surface of the tissue improves the oxygen profiles. The apical surface is covered by a minimal height of culture medium reducing oxygen mass transfer distances but requiring frequent changes to prevent tissue drying due to evaporative loss (Bigas et al., 1995; Uroic et al., 2010).

As can be seen in FEM (**Figure 5**), the elevation of the tissue above the gas impermeable plastic and closer proximity to the liquid/gas interface causes a significant reduction in tissue hypoxia. Limited device geometries, however, evaporative losses/tissue dehydration at the apical surface and improved culture alternatives have made this approach recently less utilized.

Low Temperature Culture

Another early and continued approach to prevent post-isolation IEQ loss and anoxia is low temperature culture (20–25°C). Started in the late 1970s by the research groups of Lacy, Talmage and others, low temperature culture was observed to reduce antigenicity and immune response, improve function and viability and prevent anoxia and culture losses (Chase et al., 1979; Ono et al., 1979). The benefit of the low temperature culture comes from the reduction in oxygen consumption and metabolic activity of the endocrine clusters, which follow an Arrhenius

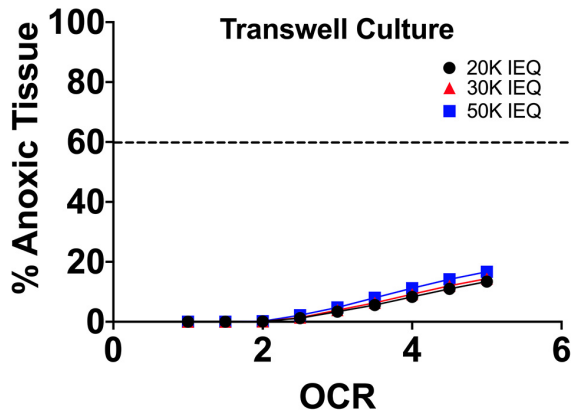

FIGURE 5 | FEM of islet culture on transwell surfaces. The reduction of culture medium height due to closer proximity of the islets to the liquid/gas interface and the imposed distance from the gas impermeable basal surface (plastic) results in significant drops in tissue hypoxia/anoxia at all oxygen consumption rates.

behavior. These reaction rates display an exponential relationship to temperature described by the equation:

$$Rate = Rate_0 e^{\frac{-E_A}{RT}}$$

where, $Rate_0$ is a pre-exponential reaction factor, E_A is the activation energy for the metabolic reaction, R, the universal gas constant (8.314 mol·kJ^{-1} K^{-1}) and T, the temperature in degrees Kelvin. For reactions such as oxygen diffusion in the system, this also results in an exponential decrease in diffusivity. This drop is countered by an increase in dissolved oxygen content (solubility) resulting in a minimal change in oxygen transfer, overall. The exponential drop in oxygen consumption rate (60–70%), however, has a pronounced effect on the tissue oxygen distribution and this significantly reduces the volume of tissue affected by hypoxia/anoxia. This can be seen in the FEM analysis in **Figure 6**.

Overall, tissue anoxia was reduced by 20–35% in low temperature culture relative to standard culture settings and dependent on seeding density and culture medium height. It is not surprising that this reduction in tissue loss would translate to improved function and viability upon return to physiological temperature and would result in reduced antigen shedding and recipient immune response, as was observed when transplanted.

Bioreactors, Gyrotational Culture and Convective-Flow Culture Systems

It is clear from the FEM of various static culture settings that oxygen consumption rate, plating density and tissue diameter are critical variables that are often disregarded in culture design. Additionally, pO_2 gradients range from surface to core values that are non-physiological and this can adversely affect tissue function and viability. This is more prevalent in 3D cell aggregates and presents a substantial obstacle to scale-up and implementation for therapeutic cell replacement applications. Given that most historical research has been performed using plastic culture

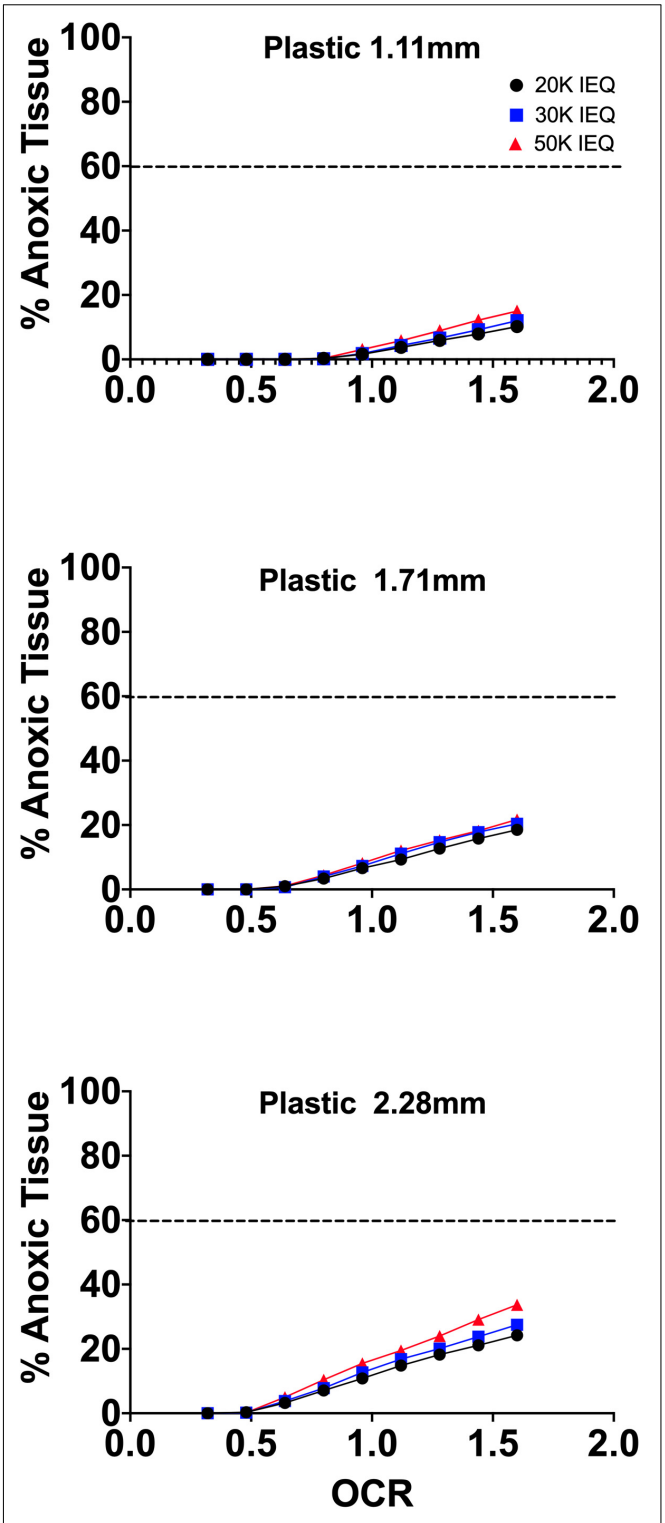

FIGURE 6 | FEM of low temperature islet culture on conventional plastic culture systems. The reduction of temperature significantly reduces tissue anoxia due to the relative Arrhenius drop in oxygen consumption rate (68%) indicated along the *x*-axis (0.32 × standard islet OCR values, 1.0–5.0 × 10^{-2} mol/m^3 s^{-1}). Tissue anoxia was 20–35% less in low temperature culture relative to standard culture settings and dependent on seeding density and culture medium height.

systems and using immortalized cell lines, oxygen limitations have been frequently overlooked. Recently, as culture is moving toward physiologically relevant 3D aggregates, the limitations of oxygenation in plasticware have become apparent and there is a growing body of engineering work in the development of alternative culture systems for enhanced oxygenation.

Initially used in scale-up production of fermentation processes and the production/synthesis of medicinal substances from biological reactions (e.g., insulin production from recombinant DNA), bioreactors have been further engineered for a multitude of applications. Newer systems have varied device geometries and real-time controllers for atmospheric gas concentrations, fluidics, and temperature. The advantage of these systems is that they have the potential to eliminate pO_2 gradients within the culture medium either by continued supply of fresh medium or through constant mixing in contact with the liquid/air interface.

In the context of islets and endocrine aggregates/SC-β, flow systems have long been in use. Early work in the laboratory of Paul Lacy utilized gyrotational culture devices to preserve isolated islets in collaborations with NASA and McDonnell Douglas examining the effects of rotation and microgravity on islet isolation, function, and viability (Buitrago et al., 1977; Scharp et al., 1978; Britt et al., 1981). These devices employed rotation along multiple axes to prevent islet settling onto basal, gas-impermeable culture surfaces and to continuously bathe the islets in well-mixed culture medium. These and further studies in microgravity culture systems with isolated islets demonstrated reduced immunogenicity and improved viability and function over long-term culture periods (Rutzky et al., 2001, 2002; Tobin et al., 2001; Luca et al., 2006).

Spinner flasks aid in the formation of 3D aggregates from single cells by maintaining rotational flow driven by magnetic stirrers. Many systems come with ports for easy gas exchange and media sampling/replacement. Dependent on cell density, rotational speed and time of culture, uniform clusters of a desired spherical geometry can be readily formed. These systems have been utilized in the generation of 3D islet-like spheroids from immortalized beta-cell insulinoma lines (MIN-6) exhibiting improved viability, proliferation and insulin secretion (Lock et al., 2011).

As SC-β production has scaled for pre-clinical and clinical work, high-throughput and large volume culture has dictated the transition from inefficient static culture systems to flow systems, primarily spinner flasks/bioreactors. The groups of Doug Melton and Semma Therapeutics along with former lab members, such as Jeffrey Millman, have established differentiation culture protocols implementing rotational devices to successfully generate reproducible large-scale batches of SC-β (Hrvatin et al., 2014; Pagliuca et al., 2014; Millman et al., 2016; Vegas et al., 2016; Peterson et al., 2020; Helman and Melton, 2021). Of note, until the recent paper by the group of Yoshihara et al. (2020) these aggregates relied on steps of *in vivo* terminal differentiation and a delayed function greater than the 5 days reported in the recent paper (Yoshihara et al., 2020). This delayed response has been attributed by Davis and Melton to a lack of anaplerotic cycling resulting in inefficient glucose responsiveness. This was reversed by exposing the SC-β to metabolites from late glycolysis and intermediate stages of the citric acid cycle (Davis et al., 2020). The SC-β generated by Yoshihara et al. (2020) displayed increased oxidative metabolism with oxygen consumption rates similar to healthy primary islets indicating, perhaps, that the early *in vivo* function was due to proper anaplerotic cycling not observed in the work of Davis and Melton. It should be noted that the entire differentiation procedure of the Evans group was performed on gas-impermeable plastic systems with a basal methylcellulose layer while the Davis and Melton paper utilized planar followed by suspension rotational culture, per their standard protocols.

Culture bags on mechanical rockers can also be used for 3D aggregates, but typically of pre-formed aggregates. In this case, the cells are bathed in culture media that is gently agitated in a rocking motion across the cells (Singh, 1999; Tsai et al., 2017). Their utilization with islets and endocrine spheroids has been limited, however (Schmied et al., 2000). As with spinner flasks, the more advanced systems come with controllers for gas concentration, temperature, fluidics, and contain ports for easy addition and sampling of culture media. Additionally, more advanced spinner flask and rocker systems come with a variety of sensors measuring not only dissolved gas concentration, but also glucose consumption, lactate production and pH of the culture medium.

As would be expected, these systems are ideal for oxygenation throughout the culture environment external to cell clusters/tissue maintaining a uniform tissue surface pO_2. This system completely prevents anoxia in the relevant size range of islets (50–400 μm) across the range of typical oxygen consumption rates (1.0–5.0 $mol/m^3\ s^{-1}$). In fact, even at tissue geometries approaching 750–1000 μm, anoxia is less than experienced by islets of standard size range (50–450 μm) in standard plastic culture.

While ideal for preventing hypoxia/anoxia, bioreactor systems are often cumbersome, require additional equipment, such as magnetic stir plates and interfaces for sensors and gas lines and can increase reagent utilization. Importantly, bioreactors and their associated convective-flow devices can increase the chance for contamination due to needed manipulation and additional component interfaces. The systems have also been shown to generate undesirable shear forces and bubbles that can have adverse effects on cells/tissues. The critical scalar factor related to adverse effects of shear is energy dissipation rate (EDR) expressed in units of W/m^3. In a paper by Shenkman et al. (2009) shear forces on islets of Langerhans in flow culture systems appeared to have minimal effect on viability and function as measured by Caspase activity and oxygen consumption rate (Shenkman et al., 2009). This was observed up to a volumetric flow rate of 50 mL/min translating to an EDR of 9,600 W/m^3. As reference, a spinner flask at a maximal rotation of 200 rpm has an EDR of about 1,500 W/m^3 while bubble rupture or passage through a 200 μL pipette tip in 0.2 s have an EDR of approximately 1×10^5 W/m^3. This paper did not examine secretory function, however, which could be more informative in understanding the subtleties of shear effects as most papers in the field examine endpoints like flow induced necrosis or lysis and not functional effects.

More recent publications utilizing microfluidic systems have demonstrated that shear forces with EDR well below the levels of

spinner flasks impair calcium channel mediated insulin secretion in surface cells of islets (Sankar et al., 2011; Silva et al., 2013). The lack of definitive understanding of the effects of fluidic shear on islet/endocrine spheroid function and viability could explain some of the unexpected outcomes in large-scale SC-β culture protocols, such as delays in terminal differentiation and function. Given the near-clinical stage of this cellular replacement research, there is a need for further detailed study into the range of effects of shear forces on endocrine spheroid viability and function.

Microfluidic Culture Platforms

A recent trend in islet/SC-β culture is the use of microfluidic or lab-on-a-chip culture systems. These platforms assimilate multiple functions into a single unit utilizing flow-based culture. They typically have geometries on the order of square millimeters to centimeters and due to reduced reagent consumption, they can dramatically shrink experimental costs. They are also typically designed with an array of sensors for longitudinal monitoring of temperature, fluid flow/pressure, gas concentration and other pertinent parameters to a specific cell type. They can be used to monitor cellular feedback, for imaging analysis and for biochemical assays, like glucose-stimulated insulin release with islets. The fluidic inputs allow for the introduction of an unlimited array of compounds making the platform useful for pharmaceutical studies and the development of differentiation/culture protocols. Importantly, these platforms allow for the study of compartmentalized cells and tissues to better understand the physiological interactions of, for example, vascular or immune cells with other specific somatic tissues, like islets.

In the context of islet/SC-β research, lab-on-a-chip platforms have been used in select studies examining the prevention of endothelial cell loss in islets post-isolation, dynamic imaging studies, insulin/glucagon/somatostatin secretion studies, differentiation of human embryonic stem cells into SC-β and endocrine spheroid microencapsulation (Sankar et al., 2011; Silva et al., 2013; McMillan et al., 2016; Nourmohammadzadeh et al., 2016; Lenguito et al., 2017; Sharma et al., 2017; Lee G. et al., 2018; Jun et al., 2019). These novel systems are remarkable for small-scale discovery research but one stark omission in most studies has been a comparison to conventional culture methods to see if these systems improve endocrine spheroid viability or function. Additionally, scale-up of these fluidic systems to manage whole islet preparations or batches of SC-β would likely be costly and difficult relative to existing large-scale systems unless merited by significant metabolic improvement in the endocrine spheroids.

GAS-PERMEABLE CULTURE PLATFORMS: PREVENTING ANOXIA IN ENDOCRINE SPHEROID STATIC CULTURE

A simple and cost-effective solution to providing adequate oxygen in the culture of endocrine and other 3D spheroids while eliminating any effects of shear forces is the use of polydimethylsiloxane culture systems (PDMS). Utilized previously in cell culture, primarily as a hydrophobic and non-adherent substrate, PDMS has recently gained favor due to its improved permeability to gasses, including oxygen and carbon dioxide relevant to cell culture (Harris, 1984; Rosdy et al., 1991; Singhvi et al., 1994; Wang and Deen, 2003). Our group and others have implemented gas permeable static culture systems using PDMS as the basal culture surface for the culture of primary islets of Langerhans and endocrine spheroids derived from stem cells (Papas et al., 2005; Fraker et al., 2007, 2013; Avgoustiniatos et al., 2008; Cechin et al., 2014; Kitzmann et al., 2014). PDMS has reported oxygen permeabilities 100–500 times that of polystyrene (Papas et al., 2005; Zhang, 2006). It is also an inert and biocompatible material that is FDA approved for numerous *in vivo* applications and devices making it ideal for *in vitro* cell culture use.

Early PDMS culture work related to islets was done by the group of Papas, Avgoustiniatos, and Colton. They utilized FEM to interrogate oxygen limitations in conventional islet culture methods for islets of Langerhans (Papas et al., 2005). Their results, confirmed by OCR as a measure of islet viability post-culture, demonstrated that culture on silicone rubber devices completely abrogated islet anoxia at culture densities up to ∼4,400 IEQ/cm^2, nearly 25 times the standard culture density. One hundred cm^2 prototypes from Wilson Wolf Manufacturing were implemented with a membrane thickness of 275 μm filled with 500 mL of culture medium. It should be noted that these studies were performed at an incubator pO_2 corresponding to a fully humidified 95% RA/5% CO_2 system (142 mmHg) and that the models assumed an IEQ diameter of 150 μm and did not examine the size range distribution of IEQ. This early prototype was the basis for the G-Rex^{TM} technology now broadly implemented in therapeutic immune and stem cell expansion (Bajgain et al., 2014).

One added benefit of the gas permeable basal surface is that the majority of the oxygen is delivered in close proximity to the cells and this eliminates reliance on oxygen diffusion from the apical liquid/air interface. This dependence on diffusion in plastic culture systems limits the amount of culture medium and therefore, the nutrient supply, that can be added without limiting oxygen supply. In PDMS systems, nutrient supply is not limited by this height restriction. While the devices have a higher per unit cost, culture using the PDMS systems is more efficient and cost-effective by reducing the number of needed flasks, the amount of culture medium and labor involved with maintaining cell cultures.

Our group developed a perfluorosilane-impregnated PDMS 275 μm membrane with a honeycomb support structure designed to maximize surface area for gas transport with support sufficient to prevent membrane damage. Given the high affinity of perfluoro-compounds for oxygen, the inclusion of perfluorosilane further improved oxygen mass transfer. **Figure 7** shows FEM of the anoxic tissue volume percentage of endocrine clusters of representative size range and OCR cultured on the perfluorosilane/PDMS constructs. FEM was performed, as

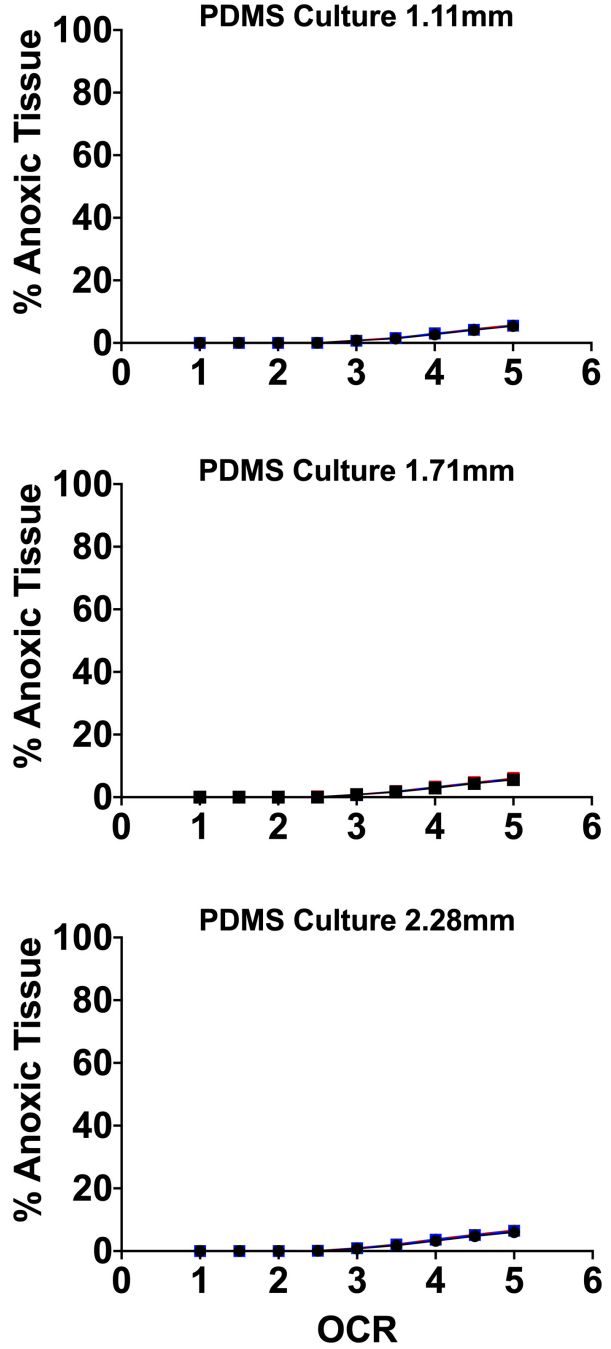

FIGURE 7 | Anoxic tissue volume percentages of endocrine spheroids (representative size range and OCR) cultured on perfluorosilane/PDMS constructs. Anoxia is eliminated in all but the largest aggregate size at the highest oxygen consumption rates. FEM was performed using three seeding densities (2.76–5.05%) and three culture medium heights (1.11, 1.71, and 2.28 mm).

above, using three different seeding densities and three relevant culture medium heights.

Of note, culture on these platforms all but eliminates anoxia in all spheroid geometries except at elevated OCR. In agreement with the earlier findings of Avgoustiniatos et al. (2008), there is virtually no effect from either seeding density or culture medium height at these settings typically utilized in culture on plastic, where both variables have a significant effect.

Recent advances using PDMS surfaces in the culture of endocrine spheroids include the development of printed microwells for controlled seeding of aggregates in a 96 and 384 well format. These devices have the added benefit of providing oxygen from an increased surface area surrounding the 3D clusters in the wells. These concave wells have been successfully used in the formation of pancreatic clusters from purified beta cells (Lee S.H. et al., 2018).

Gas-Permeable Platforms Improve Culture and Terminal Differentiation of Murine Pancreatic Buds

Studies performed in the laboratory of Clark Colton using culture of mouse embryonic stem cells on plastic examined the effect of external oxygen concentrations from 0 to 285 mmHg on proliferative capacity and differentiation either +/− the differentiation inhibiting factor, LIF. They observed that oxygen had minimal effect on undifferentiated cell growth and phenotype (+LIF) and posited that it was likely to have a more pronounced effect on cells undergoing differentiation, as we observed (Powers et al., 2008).

In another paper by the same group, they studied the effect of low oxygen culture on murine ES cells, again demonstrating the reduction of spontaneous differentiation but also the loss of pluripotent gene expression. Importantly, they noted that the oxygen level in the gas phase is often quite different from the oxygen level in the microenvironment of the cells and this is neglected in the vast majority of the literature, until recently, making interpretation of results difficult. This can be seen in the FEM models presented above for 2D and 3D culture. They emphasize the importance of tools like FEM to better understand culture conditions (Millman et al., 2009).

Our group examined the role of oxygen in pancreatic development using pancreatic buds from mouse embryoid bodies (Fraker et al., 2007). In our comparison of pancreatic buds cultured on plastic, both at standard (20%) and elevated concentration (35%) to buds cultured on the perfluoro/PDMS composites, the data supported our models. There was both improved proliferation and differentiation in the buds cultured on the perfluoro/PDMS, as well as absence of tissue hypoxia, in contrast with our immunohistochemical observations in samples cultured at either 20% and 35% incubator oxygen concentration. Gene and protein expression of important pancreatic/endocrine/β-cell developmental markers were significantly elevated in the buds cultured on the perfluoro/PDMS constructs as opposed to both normoxic (20%) and hyperoxic (35%) culture on plastic. Most notably, when compared to the *in vivo* endpoint of terminal differentiation in the pancreatic buds, e16.5, gene and protein expression of key pancreatic markers was non-significantly different between the perfluoro/PDMS

culture and the *in vivo* counterparts, further confirming the importance of oxygenation in the final stages of pancreatic development, as hypothesized. Also, in examining the expression of pancreatic exocrine markers in this setting, oxygenation promoted endocrine over exocrine differentiation. It should be noted that the size of the buds cultured in higher oxygen levels reached 1 mm and there was no evidence of tissue hypoxia by immune staining indicating that their oxygen consumption rate was likely lower than that of conventional islets of Langerhans.

Too Much or Too Little: The Goldilocks Paradox of Oxygen Supply

The supply of oxygen to cultured cells/tissues is a delicate balance between anoxia/hypoxia (too little) and oxidant/radical formation from culture medium substrates (too much). While conventional culture occurs at pO_2 of ∼142 mmHg, vascularized cells in the human body do not typically experience a pO_2 greater than 100 mmHg and are supplied with sufficient oxygen to avoid sustained hypoxia due to short vascular diffusion distances. With 3D islets/endocrine spheroids, it becomes immediately clear from the above FEM why culture of these aggregates is difficult. Their high metabolic rate and large geometries make it difficult to maintain adequate oxygen supply and impossible to do so without non-physiological pO_2 gradients across the path of oxygen transfer (surface to core). *In vivo,* islets are thought to experience a nearly uniform tissue pO_2 of approximately 20–40 mmHg. Therefore, even culture at standard incubator pO_2 results in apical endocrine spheroid surface exposure to supra-physiological levels and basal surface/core anoxia except in the smallest endocrine spheroid dimensions (50–100 μm). In gas permeable culture platforms in standard incubator settings (142 mmHg), the tissue exposure to supra-physiological levels is even greater.

There is evidence in the literature that islets are uniquely susceptible to free-radical/oxidant damage due to glucose sensing suppression of superoxide dismutase and therefore prolonged exposure to elevated pO_2 could be sub-optimal (Gille and Joenje, 1992; Kazzaz et al., 1999; Martens et al., 2005; Pi et al., 2007; Maddalena et al., 2017). For all these reasons, optimizing endocrine spheroid culture requires devices that allow for the maintenance of tissue specific oxygen profiles where core pO_2 is (1) above the anoxic and functional cutoff noted by Avgoustiniatos and others and (2) below arterial concentrations of ∼100 mmHg (Papas et al., 2005; Buchwald, 2009, 2011). To that end, our group and others have examined the effect of physiologically relevant culture pO_2 on endocrine spheroid function and viability utilizing gas permeable platforms demonstrating that culturing at more physiologically relevant pO_2 improves *in vitro* and *in vivo* islet function and viability (Fraker et al., 2013). Culture incubator pO_2 was set guided by FEM to target a maximum tissue volume maintained within a physiological range of 5–95 mmHg, minimizing "hyperoxia" and anoxia. **Figure 8** details the FEM and the subsequent anoxic tissue volume percentage. The models used three seeding densities and culture medium heights, as in prior models, above.

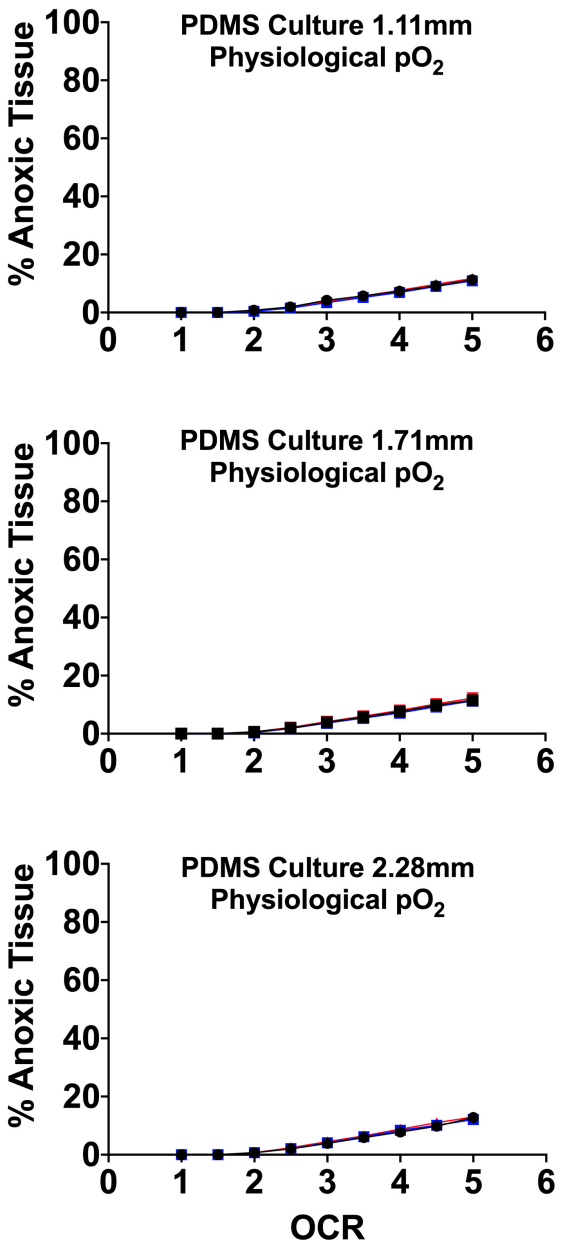

FIGURE 8 | Anoxic tissue volume percentages of endocrine spheroids (representative size range and OCR) cultured on perfluorosilane/PDMS constructs in the presence of physiological pO_2 (95 mmHg). Anoxia is minimal in all but the largest aggregate size at the highest oxygen consumption rates. FEM was performed using three seeding densities (2.76–5.05%) and three culture medium heights (1.11, 1.71, and 2.28 mm).

Gas-Permeable Platforms Improve Human Embryonic Stem (hES) Cell Specification Into Endocrine Fates

As shown in an increasing number of studies, oxygen in culture is recognized as a factor driving both stem cell proliferation and terminal differentiation into endocrine clusters. In 3D aggregates where oxygen gradients are prevalent, lower pO_2 is associated

with proliferative capacity and higher pO_2 drives terminal differentiation through Notch and HIF-1. As shown from the FEM models, above, it is not feasible to successfully modulate oxygen supply to 3D tissues in plastic culture systems, so gas permeable platforms present a useful tool for the tight control of pO_2 experienced by culture spheroids.

A paper by Powers et al. (2010) from 2010 described the historical disconnect between ambient incubator pO_2, pO_{2gas}, and the pO_2 experienced by cells in culture, pO_{2cell}, using FEM and mouse embryonic stem cell differentiation into cardiomyocytes on plastic and PDMS culture surfaces to demonstrate how critical cellular oxygen supply is to desired outcome. They used monolayer cultures on polystyrene and functionalized PDMS surfaces implementing FEM to target specific ranges of pO_{2cell} to determine the effect of standard (142 mmHg), physiological (37 mmHg), and hypoxic (7 mmHg) culture on function and viability. Only on PDMS membranes, where pO_{2cell} is equivalent to pO_{2gas} due to the proximity of the gas supply at the basal surface, were functional cardiomyocytes observed. As reported in other cell culture studies on PDMS, including our own, they frequently observed spontaneous aggregation of single cells into larger spheroids. They noted that this resulted in the formation of pO_2 gradients that had minimal effect on the tissue anoxia of the PDMS group but would have resulted in ∼80% anoxia in spheroids cultured on polystyrene at the highest pO_2 of 142 mmHg. Unfortunately, the only functional assessment was the observation of spontaneous contraction of the cells, which was observed only on PDMS and polystyrene with a PDMS membrane. The largest number of spontaneously contracting cells were observed on the PDMS surface at a pO_{2gas} of 36 mmHg. This demonstrates the importance of physio-normal pO_2 (36 vs. 142 mmHg) in terminal differentiation.

During our work with an early group in the SC-β field, BetaLogics, we postulated that the use of gas permeable culture systems to tailor core tissue pO_2 to that of the physiological niche of pancreatic endocrine tissue (∼20–40 mmHg core tissue pO_2; 80–100 mmHg incubator pO_2) would significantly improve terminal differentiation of hES spheroid progenitor clusters into endocrine fates (Cechin et al., 2014). As these clusters were typically in the size range of IEQ (50–400 μm), the culture on PDMS was designed to maintain maximal tissue volume percentage within a physiological range (∼2.7–100 mmHg). Introducing the PDMS culture systems at the last stage of standard differentiation protocols, after they were formed into spheroids, resulted in significantly improved differentiation into insulin and other endocrine hormone positive cells. Analysis by qRT-PCR showed significantly elevated pancreatic gene expression in hES clusters cultured in gas permeable systems relative to controls. *In vitro* production of insulin in response to glucose, improved engraftment and reversal of diabetes *in vivo*, were also observed. Notably, culture in these systems at physiological pO_2 resulted in dramatically improved segregation of α and β cells, eliminating the challenge of single cell bi-hormonal expression that had plagued other protocols up to that point. This data again confirmed the role of oxygen in endocrine development and function. Given the low oxygen levels (relative to standard oxygen pO_2) present in the *in vivo* niches of most cell types, it is not surprising that mechanisms such as proliferation, terminal differentiation, and pleiotropic function are increasingly being tied to bioenergetic shifts dependent on oxygen.

CONCLUSION AND FUTURE DIRECTIONS

As 3D culture increasingly becomes a preferred mode of physio-mimetic culture, historical culture methods on plastics need to be re-evaluated. Particularly related to tissue oxygenation, the steep gradients that develop from apical to basal surface, both in the culture milieu and in the 3D organoids, lead to hypoxic and anoxic regions, inefficient nutrient metabolism and potentially, shifts in viability, function and gene expression that may deviate in comparison to the same tissue *in vivo*. There is a critical need and a recent surge in device/method research to improve metabolite/nutrient delivery and waste removal in 3D cell cultures. With the emergent data coming from this area of research, it is clear that other variables besides oxygen, such as mechanical forces, growth factors and supportive matrices also play an important role in the culture of organoid systems but metabolic gas exchange has been one of the most challenging obstacles in 3D cell/spheroid research. Given the growing number of therapeutic applications for 3D spheroids, there is a critical need to revisit expansion and differentiation protocols in order to optimize them for their desired end product and application. Much like personalized medicine, individual cell/tissue types have different metabolic and physiological characteristics that are difficult to recapitulate in general culture practices. Like oxygen in the data presented in this work and others, tailoring environmental factors to address the physiological demands of the cultured spheroids can result in a much better *in vitro* model/approximation of the *in vivo* organoid counterpart.

Related to the clinical application of endocrine spheroids, there is much ongoing work to improve/maintain function and viability prior to transplant in an attempt to minimize immune response and accelerate engraftment. Strategies focused on revascularization and co-cultures with supportive mesenchymal stem cells (MSCs) and endothelial precursors (ECs) are making great strides in minimizing post-transplant loss and time to reversal of hyperglycemia. In terms of culture, there is still work to be done to fully understand the role of oxygen in differentiation and function/viability, *in vitro*. Building on past work, minimizing tissue anoxia has a clear effect on transplant immunogenicity and function. With that in mind, combinatorial approaches that slow cellular metabolism (OCR) and maintain tight control of pO_{2cell} could move endocrine spheroid research one-step closer to clinical impact. This could be achieved, as an example, by the use of low temperature culture on gas permeable systems.

Clearly, oxygen is only one of many culture metabolites that plays a role in the viability and function of 2D and 3D cultures. It could be argued that it is the most important given that it has an immediate effect on cell metabolism and the lack of

oxygen can rapidly progress to cellular dysfunction and death. A lack of oxygen in cell systems also results in a build-up of toxic waste products that while largely unnoticeable in the larger culture milieu, might have a pronounced detrimental effect in the cell microenvironment. For example, a shift to anaerobic metabolism and glycolysis increases production of acidic byproducts to compensate for loss of the efficiency of energy production using aerobic respiration. This, in turn, can affect both cellular and environmental pH leading to damage beyond the immediate apoptosis/necrosis caused by anoxia. While not the only participant in the viability of cultured cell/tissue biology, oxygen has an undeniably important role in culture approximation of *in vivo* cell/tissue counterparts.

AUTHOR CONTRIBUTIONS

CF and GG contributed to the conception of the manuscript. CF, GG, HT, and JD-B reviewed the manuscript and wrote the original draft. GG, HT, and JD-B contributed to the manuscript revision and editing. All authors read and approved the submitted version.

FUNDING

Research reported in this manuscript was supported by funding from the National Institute of Diabetes and Digestive and Kidney Diseases of the National Institutes of Health under award number R01DK116875 and the Diabetes Research Institute Foundation. The content is solely the responsibility of the authors and does not necessarily represent the official views of the National Institutes of Health.

ACKNOWLEDGMENTS

The authors would like to acknowledge the ongoing support of the Diabetes Research Institute Foundation and donors who generously fund the cure-motivated research of the DRI.

REFERENCES

Acker, H., Carlsson, J., Mueller-Klieser, W., and Sutherland, R. M. (1987). Comparative pO2 measurements in cell spheroids cultured with different techniques. *Br. J. Cancer* 56, 325–327. doi: 10.1038/bjc.1987.197

Anada, T., Fukuda, J., Sai, Y., and Suzuki, O. (2012). An oxygen-permeable spheroid culture system for the prevention of central hypoxia and necrosis of spheroids. *Biomaterials* 33, 8430–8441. doi: 10.1016/j.biomaterials.2012.08.040

Avgoustiniatos, E. S., Hering, B. J., Rozak, P. R., Wilson, J. R., Tempelman, L. A., Balamurugan, A. N., et al. (2008). Commercially available gas-permeable cell culture bags may not prevent anoxia in cultured or shipped islets. *Transplant. Proc.* 40, 395–400. doi: 10.1016/j.transproceed.2008.01.059

Bader, A., Knop, E., Kern, A., Boker, K., Fruhauf, N., Crome, O., et al. (1996). 3-D coculture of hepatic sinusoidal cells with primary hepatocytes-design of an organotypical model. *Exp. Cell Res.* 226, 223–233. doi: 10.1006/excr.1996.0222

Bajgain, P., Mucharla, R., Wilson, J., Welch, D., Anurathapan, U., Liang, B., et al. (2014). Optimizing the production of suspension cells using the G-Rex "M" series. *Mol. Ther. Methods Clin. Dev.* 1:14015. doi: 10.1038/mtm.2014.15

Bigas, A., Martin, D. I., and Bernstein, I. D. (1995). Generation of hematopoietic colony-forming cells from embryonic stem cells: synergy between a soluble factor from NIH-3T3 cells and hematopoietic growth factors. *Blood* 85, 3127–3133. doi: 10.1182/blood.v85.11.3127.bloodjournal85113127

Bowen, K. M., Andrus, L., and Lafferty, K. J. (1980). Successful allotransplantation of mouse pancreatic islets to nonimmunosuppressed recipients. *Diabetes* 29(Suppl. 1), 98–104. doi: 10.2337/diab.29.1.s98

Britt, L. D., Stojeba, P. C., Scharp, C. R., Greider, M. H., and Scharp, D. W. (1981). Neonatal pig pseudo-islets. A product of selective aggregation. *Diabetes* 30, 580–583. doi: 10.2337/diab.30.7.580

Bruland, O., Fodstad, O., and Pihl, A. (1985). The use of multicellular spheroids in establishing human sarcoma cell lines in vitro. *Int. J. Cancer* 35, 793–798. doi: 10.1002/ijc.2910350616

Buchwald, P. (2009). FEM-based oxygen consumption. *Theor. Biol. Med. Model.* 6:5.

Buchwald, P. (2011). A local glucose-and oxygen concentration-based insulin secretion model for pancreatic islets. *Theor. Biol. Med. Model.* 8:20.

Buchwald, P., Wang, X., Khan, A., Bernal, A., Fraker, C., Inverardi, L., et al. (2009). Quantitative assessment of islet cell products: estimating the accuracy of the existing protocol and accounting for islet size distribution. *Cell Transplant.* 18, 1223–1235. doi: 10.3727/096368909x476968

Buitrago, A., Gylfe, E., Henriksson, C., and Pertoft, H. (1977). Rapid isolation of pancreatic islets from collagenase digested pancreas by sedimentation through Percol at unit gravity. *Biochem. Biophys. Res. Commun.* 79, 823–828. doi: 10.1016/0006-291x(77)91185-8

Cao, R., Avgoustiniatos, E., Papas, K., de Vos, P., and Lakey, J. R. T. (2020). Mathematical predictions of oxygen availability in micro- and macro-encapsulated human and porcine pancreatic islets. *J. Biomed. Mater. Res. B Appl. Biomater.* 108, 343–352. doi: 10.1002/jbm.b.34393

Carlsson, J., Stalnacke, C. G., Acker, H., Haji-Karim, M., Nilsson, S., and Larsson, B. (1979). The influence of oxygen on viability and proliferation in cellular spheroids. *Int. J. Radiat. Oncol. Biol. Phys.* 5, 2011–2020. doi: 10.1016/0360-3016(79)90953-2

Cechin, S., Alvarez-Cubela, S., Giraldo, J. A., Molano, R. D., Villate, S., Ricordi, C., et al. (2014). Influence of in vitro and in vivo oxygen modulation on beta cell differentiation from human embryonic stem cells. *Stem Cells Transl. Med.* 3, 277–289. doi: 10.5966/sctm.2013-0160

Chase, H. P., Ocrant, I., and Talmage, D. W. (1979). The effects of different conditions of organ culture on the survival of the mouse pancreas. *Diabetes* 28, 990–993. doi: 10.2337/diabetes.28.11.990

Colen, K. L., Crisera, C. A., Rose, M. I., Connelly, P. R., Longaker, M. T., and Gittes, G. K. (1999). Vascular development in the mouse embryonic pancreas and lung. *J. Pediatr. Surg.* 34, 781–785. doi: 10.1016/s0022-3468(99)90373-1

Davis, J. C., Alves, T. C., Helman, A., Chen, J. C., Kenty, J. H., Cardone, R. L., et al. (2020). Glucose response by stem cell-derived beta cells in vitro is inhibited by a bottleneck in glycolysis. *Cell Rep.* 31:107623. doi: 10.1016/j.celrep.2020.107623

De Moor, L., Merovci, I., Baetens, S., Verstraeten, J., Kowalska, P., Krysko, D. V., et al. (2018). High-throughput fabrication of vascularized spheroids for bioprinting. *Biofabrication* 10:035009. doi: 10.1088/1758-5090/aac7e6

Deshpande, R. R., and Heinzle, E. (2009). Online monitoring of oxygen in spinner flasks. *Biotechnol. Lett.* 31, 665–669. doi: 10.1007/s10529-009-9919-2

Dionne, K. E., Cain, B. M., Li, R. H., Bell, W. J., Doherty, E. J., Rein, D. H., et al. (1996). Transport characterization of membranes for immunoisolation. *Biomaterials* 17, 257–266. doi: 10.1016/0142-9612(96)85563-3

Dionne, K. E., Colton, C. K., and Yarmush, M. L. (1989). Effect of oxygen on isolated pancreatic tissue. *ASAIO Trans.* 35, 739–741. doi: 10.1097/00002216-198907000-00185

Dionne, K. E., Colton, C. K., and Yarmush, M. L. (1991). A microperifusion system with environmental control for studying insulin secretion by pancreatic tissue. *Biotechnol. Prog.* 7, 359–368. doi: 10.1021/bp00010a011

Dionne, K. E., Colton, C. K., and Yarmush, M. L. (1993). Effect of hypoxia on insulin secretion by isolated rat and canine islets of Langerhans. *Diabetes* 42, 12–21. doi: 10.2337/diab.42.1.12

Fehrer, C., Brunauer, R., Laschober, G., Unterluggauer, H., Reitinger, S., Kloss, F., et al. (2007). Reduced oxygen tension attenuates differentiation capacity

of human mesenchymal stem cells and prolongs their lifespan. *Aging Cell* 6, 745–757. doi: 10.1111/j.1474-9726.2007.00336.x

Fraker, C. A., Alvarez, S., Papadopoulos, P., Giraldo, J., Gu, W., Ricordi, C., et al. (2007). Enhanced oxygenation promotes beta-cell differentiation in vitro. *Stem Cells* 25, 3155–3164. doi: 10.1634/stemcells.2007-0445

Fraker, C. A., Cechin, S., Alvarez-Cubela, S., Echeverri, F., Bernal, A., Poo, R., et al. (2013). A physiological pattern of oxygenation using perfluorocarbon-based culture devices maximizes pancreatic islet viability and enhances beta-cell function. *Cell Transplant.* 22, 1723–1733. doi: 10.3727/096368912x657873

Fraker, C. A., Ricordi, C., Inverardi, L., and Dominguez-Bendala, J. (2009). Oxygen: a master regulator of pancreatic development? *Biol. Cell* 101, 431–440. doi: 10.1042/bc20080178

Freyer, J. P., Schor, P. L., Jarrett, K. A., Neeman, M., and Sillerud, L. O. (1991). Cellular energetics measured by phosphorous nuclear magnetic resonance spectroscopy are not correlated with chronic nutrient deficiency in multicellular tumor spheroids. *Cancer Res.* 51, 3831–3837.

Gargotti, M., Lopez-Gonzalez, U., Byrne, H. J., and Casey, A. (2018). Comparative studies of cellular viability levels on 2D and 3D in vitro culture matrices. *Cytotechnology* 70, 261–273. doi: 10.1007/s10616-017-0139-7

Gassmann, M., Fandrey, J., Bichet, S., Wartenberg, M., Marti, H. H., Bauer, C., et al. (1996). Oxygen supply and oxygen-dependent gene expression in differentiating embryonic stem cells. *Proc. Natl. Acad. Sci. U.S.A.* 93, 2867–2872. doi: 10.1073/pnas.93.7.2867

Gille, J. J., and Joenje, H. (1992). Cell culture models for oxidative stress: superoxide and hydrogen peroxide versus normobaric hyperoxia. *Mutat. Res.* 275, 405–414. doi: 10.1016/0921-8734(92)90043-o

Grayson, W. L., Zhao, F., Izadpanah, R., Bunnell, B., and Ma, T. (2006). Effects of hypoxia on human mesenchymal stem cell expansion and plasticity in 3D constructs. *J. Cell. Physiol.* 207, 331–339. doi: 10.1002/jcp.20571

Groebe, K. (1996). Practical applications of models of oxygen supply, diffusion, and consumption: past, perspectives, and problems. *Adv. Exp. Med. Biol.* 388, 161–175. doi: 10.1007/978-1-4613-0333-6_20

Groebe, K., and Mueller-Klieser, W. (1996). On the relation between size of necrosis and diameter of tumor spheroids. *Int. J. Radiat. Oncol. Biol. Phys.* 34, 395–401. doi: 10.1016/0360-3016(95)02065-9

Harris, A. K. Jr. (1984). Tissue culture cells on deformable substrata: biomechanical implications. *J. Biomech. Eng.* 106, 19–24. doi: 10.1115/1.3138449

Heacock, C. S., and Sutherland, R. M. (1986). Induction characteristics of oxygen regulated proteins. *Int. J. Radiat. Oncol. Biol. Phys.* 12, 1287–1290. doi: 10.1016/0360-3016(86)90155-0

Helman, A., and Melton, D. A. (2021). A stem cell approach to cure type 1 diabetes. *Cold Spring Harb. Perspect. Biol.* 13:a035741. doi: 10.1101/cshperspect.a035741

Hrvatin, S., O'Donnell, C. W., Deng, F., Millman, J. R., Pagliuca, F. W., DiIorio, P., et al. (2014). Differentiated human stem cells resemble fetal, not adult, beta cells. *Proc. Natl. Acad. Sci. U.S.A.* 111, 3038–3043. doi: 10.1073/pnas.1400709111

Inch, W. R., McCredie, J. A., and Sutherland, R. M. (1970). Growth of nodular carcinomas in rodents compared with multi-cell spheroids in tissue culture. *Growth* 34, 271–282.

Jokinen, M., Pittois, K., van den Akker, S., Gutschoven, I., Assmuth, T., Metz, T., Lehtila, H., et al. (2020). Multiphase matrix of silica, culture medium and air for 3D mammalian cell culture. *Cytotechnology* 72, 271–282. doi: 10.1007/s10616-020-00376-w

Jun, Y., Lee, J., Choi, S., Yang, J. H., Sander, M., Chung, S., et al. (2019). In vivo-mimicking microfluidic perfusion culture of pancreatic islet spheroids. *Sci. Adv.* 5:eaax4520. doi: 10.1126/sciadv.aax4520

Kazzaz, J. A., Horowitz, S., Li, Y., and Mantell, L. L. (1999). Hyperoxia in cell culture. A non-apoptotic programmed cell death. *Ann. N. Y. Acad. Sci.* 887, 164–170. doi: 10.1111/j.1749-6632.1999.tb07930.x

Kitzmann, J. P., Pepper, A. R., Gala-Lopez, B., Pawlick, R., Kin, T., O'Gorman, D., et al. (2014). Human islet viability and function is maintained during high-density shipment in silicone rubber membrane vessels. *Transplant. Proc.* 46, 1989–1991. doi: 10.1016/j.transproceed.2014.06.002

Knisely, M. H., Reneau, D. D. Jr., and Bruley, D. F. (1969). The development and use of equations for predicting the limits of the rates of oxygen supply to the cells of living tissues and organs. A contribution to the biophysics of health and disease. *Angiology* 20(Suppl.), 1–56. doi: 10.1177/000319769020011s01

Lacy, P. E., Finke, E. H., Janney, C. G., and Davie, J. M. (1982). Prolongation of islet xenograft survival by in vitro culture of rat megaislets in 95% O2. *Transplantation* 33, 588–592. doi: 10.1097/00007890-198206000-00004

Lee, G., Jun, Y., Jang, H., Yoon, J., Lee, J., Hong, M., et al. (2018). Enhanced oxygen permeability in membrane-bottomed concave microwells for the formation of pancreatic islet spheroids. *Acta Biomater.* 65, 185–196. doi: 10.1016/j.actbio.2017.10.045

Lee, S. H., Hong, S., Song, J., Cho, B., Han, E. J., Kondapavulur, S., et al. (2018). Microphysiological analysis platform of pancreatic islet beta-cell spheroids. *Adv. Healthc. Mater.* 7:1701111. doi: 10.1002/adhm.201701111

Lenguito, G., Chaimov, D., Weitz, J. R., Rodriguez-Diaz, R., Rawal, S. A., Tamayo-Garcia, A., et al. (2017). Resealable, optically accessible, PDMS-free fluidic platform for ex vivo interrogation of pancreatic islets. *Lab Chip* 17, 772–781. doi: 10.1039/c6lc01504b

Li, A. P., Colburn, S. M., and Beck, D. J. (1992). A simplified method for the culturing of primary adult rat and human hepatocytes as multicellular spheroids. *In Vitro Cell. Dev. Biol.* 28A, 673–677. doi: 10.1007/bf02631045

Lock, L. T., Laychock, S. G., and Tzanakakis, E. S. (2011). Pseudoislets in stirred-suspension culture exhibit enhanced cell survival, propagation and insulin secretion. *J. Biotechnol.* 151, 278–286. doi: 10.1016/j.jbiotec.2010.12.015

Luca, G., Calvitti, M., Nastruzzi, C., Macchiarulo, G., Becchetti, E., Neri, L. M., et al. (2006). Effects of simulated microgravity on the morphology and function of neonatal porcine cell clusters cultured with and without Sertoli cells. *Cell Transplant.* 15, 55–65. doi: 10.3727/000000006783982223

Maddalena, L. A., Selim, S. M., Fonseca, J., Messner, H., McGowan, S., and Stuart, J. A. (2017). Hydrogen peroxide production is affected by oxygen levels in mammalian cell culture. *Biochem. Biophys. Res. Commun.* 493, 246–251. doi: 10.1016/j.bbrc.2017.09.037

Martens, G., Cai, Y., Hinke, S., Stange, G., Van de Casteele, M., and Pipeleers, D. (2005). Nutrient sensing in pancreatic beta cells suppresses mitochondrial superoxide generation and its contribution to apoptosis. *Biochem. Soc. Trans.* 33(Pt 1), 300–301. doi: 10.1042/bst0330300

Matta, S. G., Wobken, J. D., Williams, F. G., and Bauer, G. E. (1994). Pancreatic islet cell reaggregation systems: efficiency of cell reassociation and endocrine cell topography of rat islet-like aggregates. *Pancreas* 9, 439–449. doi: 10.1097/00006676-199407000-00005

McGrath, K. E., Koniski, A. D., Malik, J., and Palis, J. (2003). Circulation is established in a stepwise pattern in the mammalian embryo. *Blood* 101, 1669–1676. doi: 10.1182/blood-2002-08-2531

McMillan, K. S., Boyd, M., and Zagnoni, M. (2016). Transitioning from multi-phase to single-phase microfluidics for long-term culture and treatment of multicellular spheroids. *Lab Chip* 16, 3548–3557. doi: 10.1039/c6lc00884d

Millman, J. R., Tan, J. H., and Colton, C. K. (2009). The effects of low oxygen on self-renewal and differentiation of embryonic stem cells. *Curr. Opin. Organ. Transplant.* 14, 694–700. doi: 10.1097/mot.0b013e3283329d53

Millman, J. R., Xie, C., Van Dervort, A., Gurtler, M., Pagliuca, F. W., and Melton, D. A. (2016). Generation of stem cell-derived beta-cells from patients with type 1 diabetes. *Nat. Commun.* 7:11463.

Moritz, W., Meier, F., Stroka, D. M., Giuliani, M., Kugelmeier, P., Nett, P. C., et al. (2002). Apoptosis in hypoxic human pancreatic islets correlates with HIF-1alpha expression. *FASEB J.* 16, 745–747. doi: 10.1096/fj.01-0403fje

Moscona, A. (1961). Rotation-mediated histogenetic aggregation of dissociated cells. A quantifiable approach to cell interactions in vitro. *Exp. Cell Res.* 22, 455–475. doi: 10.1016/0014-4827(61)90122-7

Moscona, A. A. (1961). How cells associate. *Sci. Am.* 205, 142–162. doi: 10.1038/scientificamerican0961-142

Mueller-Klieser, W. (1984). Microelectrode measurement of oxygen tension distributions in multicellular spheroids cultured in spinner flasks. *Recent Results Cancer Res.* 95, 134–149. doi: 10.1007/978-3-642-82340-4_8

Mueller-Klieser, W., Freyer, J. P., and Sutherland, R. M. (1986). Influence of glucose and oxygen supply conditions on the oxygenation of multicellular spheroids. *Br. J. Cancer* 53, 345–353. doi: 10.1038/bjc.1986.58

Mueller-Klieser, W. F., and Sutherland, R. M. (1982). Oxygen tensions in multicell spheroids of two cell lines. *Br. J. Cancer* 45, 256–264. doi: 10.1038/bjc.1982.41

Mueller-Klieser, W. F., and Sutherland, R. M. (1984). Oxygen consumption and oxygen diffusion properties of multicellular spheroids from two different cell lines. *Adv. Exp. Med. Biol.* 180, 311–321. doi: 10.1007/978-1-4684-4895-5_30

Murphy, K. C., Hung, B. P., Browne-Bourne, S., Zhou, D., Yeung, J., Genetos, D. C., et al. (2017). Measurement of oxygen tension within mesenchymal stem cell spheroids. *J. R. Soc. Interface* 14:20160851. doi: 10.1098/rsif.2016.0851

Murray, H. E., Paget, M. B., and Downing, R. (2005). Preservation of glucose responsiveness in human islets maintained in a rotational cell culture system. *Mol. Cell. Endocrinol.* 238, 39–49.

Nourmohammadzadeh, M., Xing, Y., Lee, J. W., Bochenek, M. A., Mendoza-Elias, J. E., McGarrigle, J. J., et al. (2016). A microfluidic. *Lab Chip* 16, 1466–1472.

Ono, J., Lacy, P. E., Michael, H. E., and Greider, M. H. (1979). Studies of the functional and morphologic status of islets maintained at 24 C for four weeks in vitro. *Am. J. Pathol.* 97, 489–503.

Pagliuca, F. W., Millman, J. R., Gurtler, M., Segel, M., Van Dervort, A., Ryu, J. H., et al. (2014). Generation of functional human pancreatic beta cells in vitro. *Cell* 159, 428–439.

Papas, K. K., Avgoustiniatos, E. S., and Suszynski, T. M. (2016). Effect of oxygen supply on the size of implantable islet-containing encapsulation devices. *Panminerva Med.* 58, 72–77.

Papas, K. K., Avgoustiniatos, E. S., Tempelman, L. A., Weir, G. C., Colton, C. K., Pisania, A., et al. (2005). High-density culture of human islets on top of silicone rubber membranes. *Transplant. Proc.* 37, 3412–3414.

Papas, K. K., Long, R. C. Jr., Constantinidis, I., and Sambanis, A. (2000). Effects of short-term hypoxia on a transformed cell-based bioartificial pancreatic construct. *Cell Transplant.* 9, 415–422.

Peterson, Q. P., Veres, A., Chen, L., Slama, M. Q., Kenty, J. H. R., Hassoun, S., et al. (2020). A method for the generation of human stem cell-derived alpha cells. *Nat. Commun.* 11:2241.

Pi, J., Bai, Y., Zhang, Q., Wong, V., Floering, L. M., Daniel, K., et al. (2007). Reactive oxygen species as a signal in glucose-stimulated insulin secretion. *Diabetes* 56, 1783–1791.

Powers, D. E., Millman, J. R., Bonner-Weir, S., Rappel, M. J., and Colton, C. K. (2010). Accurate control of oxygen level in cells during culture on silicone rubber membranes with application to stem cell differentiation. *Biotechnol. Prog.* 26, 805–818.

Powers, D. E., Millman, J. R., Huang, R. B., and Colton, C. K. (2008). Effects of oxygen on mouse embryonic stem cell growth, phenotype retention, and cellular energetics. *Biotechnol. Bioeng.* 101, 241–254.

Qadir, M. M. F., Alvarez-Cubela, S., Weitz, J., Panzer, J. K., Klein, D., Moreno-Hernandez, Y., et al. (2020). Dominguez-Bendala, long-term culture of human pancreatic slices as a model to study real-time islet regeneration. *Nat. Commun.* 11:3265.

Rosdy, M., Grisoni, B., and Clauss, L. C. (1991). Proliferation of normal human keratinocytes on silicone substrates. *Biomaterials* 12, 511–517.

Rutzky, L., Kloc, M., Bilinski, S., Phan, T., Zhang, H., Stepkowski, S. M., et al. (2001). Microgravity culture conditions decrease immunogenicity but maintain excellent morphology of pancreatic islets. *Transplant. Proc.* 33:388.

Rutzky, L. P., Bilinski, S., Kloc, M., Phan, T., Zhang, H., Katz, S. M., et al. (2002). Microgravity culture condition reduces immunogenicity and improves function of pancreatic islets1. *Transplantation* 74, 13–21.

Saini, S., and Wick, T. M. (2004). Effect of low oxygen tension on tissue-engineered cartilage construct development in the concentric cylinder bioreactor. *Tissue Eng.* 10, 825–832.

Sankar, K. S., Green, B. J., Crocker, A. R., Verity, J. E., Altamentova, S. M., and Rocheleau, J. V. (2011). Culturing pancreatic islets in microfluidic flow enhances morphology of the associated endothelial cells. *PLoS One* 6:e24904. doi: 10.1371/journal.pone.0024904

Scharp, D. W., Merrell, R. C., Feldman, S. D., Downing, R., Lacy, P. E., and Ballinger, W. F. (1978). The use of gyrotation culture for the preservation of isolated islets. *Surg. Forum* 29, 100–102.

Schmied, B. M., Ulrich, A., Matsuzaki, H., Ding, X., Ricordi, C., Moyer, M. P., et al. (2000). Maintenance of human islets in long-term culture. *Differentiation* 66, 173–180.

Sharma, V., Hunckler, M., Ramasubramanian, M. K., Opara, E. C., and Katuri, K. C. (2017). Microfluidic approach to cell microencapsulation. *Methods Mol. Biol.* 1479, 71–76.

Shenkman, R. M., Godoy-Silva, R., Papas, K. K., and Chalmers, J. J. (2009). Effects of energy dissipation rate on islets of Langerhans: implications for isolation and transplantation. *Biotechnol. Bioeng.* 103, 413–423.

Silva, P. N., Green, B. J., Altamentova, S. M., and Rocheleau, J. V. (2013). A microfluidic device designed to induce media flow throughout pancreatic islets while limiting shear-induced damage. *Lab Chip* 13, 4374–4384.

Simon, M. C., and Keith, B. (2008). The role of oxygen availability in embryonic development and stem cell function. *Nat. Rev. Mol. Cell Biol.* 9, 285–296.

Singh, V. (1999). Disposable bioreactor for cell culture using wave-induced agitation. *Cytotechnology* 30, 149–158.

Singhvi, R., Kumar, A., Lopez, G. P., Stephanopoulos, G. N., Wang, D. I., Whitesides, G. M., et al. (1994). Engineering cell shape and function. *Science* 264, 696–698.

Suszynski, T. M., Avgoustiniatos, E. S., and Papas, K. K. (2014a). Intraportal islet oxygenation. *J. Diabetes Sci. Technol.* 8, 575–580.

Suszynski, T. M., Avgoustiniatos, E. S., and Papas, K. K. (2016). Oxygenation of the intraportally transplanted pancreatic islet. *J. Diabetes Res.* 2016:7625947.

Suszynski, T. M., Wilhelm, J. J., Radosevich, D. M., Balamurugan, A. N., Sutherland, D. E., Beilman, G. J., et al. (2014b). Islet size index as a predictor of outcomes in clinical islet autotransplantation. *Transplantation* 97, 1286–1291.

Tobin, B. W., Leeper-Woodford, S. K., Hashemi, B. B., Smith, S. M., and Sams, C. F. (2001). Altered TNF-alpha, glucose, insulin, and amino acids in islets of Langerhans cultured in a microgravity model system. *Am. J. Physiol. Endocrinol. Metab.* 280, E92–E102.

Tsai, A. C., Liu, Y., Yuan, X., Chella, R., and Ma, T. (2017). Aggregation kinetics of human mesenchymal stem cells under wave motion. *Biotechnol. J.* 12:1600448.

Tuncay, O. C., Ho, D., and Barker, M. K. (1994). Oxygen tension regulates osteoblast function. *Am. J. Orthod. Dentofacial Orthop.* 105, 457–463.

Uroic, D. S., Baudouin, G., Ferguson, L. A., Docherty, H. M., Vallier, L., and Docherty, K. (2010). A factor(s) secreted from MIN-6 beta-cells stimulates differentiation of definitive endoderm enriched embryonic stem cells towards a pancreatic lineage. *Mol. Cell. Endocrinol.* 328, 80–86.

Vegas, A. J., Veiseh, O., Gurtler, M., Millman, J. R., Pagliuca, F. W., Bader, A. R., et al. (2016). Long-term glycemic control using polymer-encapsulated human stem cell-derived beta cells in immune-competent mice. *Nat. Med.* 22, 306–311.

Vescio, R. A., Redfern, C. H., Nelson, T. J., Ugoretz, S., Stern, P. H., and Hoffman, R. M. (1987). In vivo-like drug responses of human tumors growing in three-dimensional gel-supported primary culture. *Proc. Natl. Acad. Sci. U.S.A.* 84, 5029–5033.

Wagner, B. A., Venkataraman, S., and Buettner, G. R. (2011). The rate of oxygen utilization by cells. *Free Radic. Biol. Med.* 51, 700–712.

Wang, C., and Deen, W. M. (2003). Nitric oxide delivery system for cell culture studies. *Ann. Biomed. Eng.* 31, 65–79.

Wang, D. W., Fermor, B., Gimble, J. M., Awad, H. A., and Guilak, F. (2005). Influence of oxygen on the proliferation and metabolism of adipose derived adult stem cells. *J. Cell. Physiol.* 204, 184–191.

Yoshihara, E., O'Connor, C., Gasser, E., Wei, Z., Oh, T. G., Tseng, T. W., et al. (2020). Immune-evasive human islet-like organoids ameliorate diabetes. *Nature* 586, 606–611.

Zhang, H. (2006). "The permeability characteristics of silicone rubber," in *Proceedings of the Society for the Advancement of Material and Process Engineering Fall Technical Conference*, Dallas, TX.

Conflict of Interest: CF and JD-B have intellectual property/potential financial interests related to the gas permeable culture devices (Oxygen Sandwich) described in the manuscript.

The remaining authors declare that the research was conducted in the absence of any commercial or financial relationships that could be construed as a potential conflict of interest.

frontiers in Bioengineering and Biotechnology

ORIGINAL RESEARCH
published: 24 May 2021
doi: 10.3389/fbioe.2021.624890

Microcarrier Screening and Evaluation for Dynamic Expansion of Human Periosteum-Derived Progenitor Cells in a Xenogeneic Free Medium

Kathleen Van Beylen[1,2], *Ioannis Papantoniou*[2,3,4] *and Jean-Marie Aerts*[1,2]*

[1] M3-BIORES: Measure, Model, and Manage Bioresponses, Division Animal and Human Health Engineering, Department of Biosystems, KU Leuven, Leuven, Belgium, [2] Prometheus, Division of Skeletal Tissue Engineering, KU Leuven, Leuven, Belgium, [3] Skeletal Biology and Engineering Research Centre, Leuven, Belgium, [4] Foundation for Research and Technology – Hellas (FORTH), Institute of Chemical Engineering Sciences, Patras, Greece

An increasing need toward a more efficient expansion of adherent progenitor cell types arises with the advancements of cell therapy. The use of a dynamic expansion instead of a static planar expansion could be one way to tackle the challenges of expanding adherent cells at a large scale. Microcarriers are often reported as a biomaterial for culturing cells in suspension. However, the type of microcarrier has an effect on the cell expansion. In order to find an efficient expansion process for a specific adherent progenitor cell type, it is important to investigate the effect of the type of microcarrier on the cell expansion. Human periosteum-derived progenitor cells are extensively used in skeletal tissue engineering for the regeneration of bone defects. Therefore, we evaluated the use of different microcarriers on human periosteum-derived progenitor cells. In order to assess the potency, identity and viability of these cells after being cultured in the spinner flasks, this study performed several *in vitro* and *in vivo* analyses. The novelty of this work lies in the combination of screening different microcarriers for human periosteum-derived progenitor cells with *in vivo* assessments of the cells' potency using the microcarrier that was selected as the most promising one. The results showed that expanding human periosteum-derived progenitor cells in spinner flasks using xeno-free medium and Star-Plus microcarriers, does not affect the potency, identity or viability of the cells. The potency of the cells was assured with an *in vivo* evaluation, where bone formation was achieved. In summary, this expansion method has the potential to be used for large scale cell expansion with clinical relevance.

Keywords: human periosteum-derived progenitor cells, microcarrier, star-plus, human platelet lysate, spinner flask cell culture

OPEN ACCESS

Edited by:
Dominik Egger,
University of Natural Resources and Life Sciences Vienna, Austria

Reviewed by:
Carlos A. V. Rodrigues,
Universidade de Lisboa, Portugal
Peter Czermak,
University of Applied Sciences Mittelhessen, Germany
Sebastien Sart,
Institut Pasteur, France

***Correspondence:**
Jean-Marie Aerts
jean-marie.aerts@kuleuven.be

Specialty section:
This article was submitted to Bioprocess Engineering, a section of the journal Frontiers in Bioengineering and Biotechnology

Received: *01 November 2020*
Accepted: *27 April 2021*
Published: *24 May 2021*

Citation:
Van Beylen K, Papantoniou I and Aerts J-M (2021) Microcarrier Screening and Evaluation for Dynamic Expansion of Human Periosteum-Derived Progenitor Cells in a Xenogeneic Free Medium. Front. Bioeng. Biotechnol. 9:624890. doi: 10.3389/fbioe.2021.624890

INTRODUCTION

The rising amount of research toward cell therapies is translated in the increasing amount of registered clinical trials on ClinicalTrials.gov of which currently 1409 trials use adult mesenchymal stem/stromal cells (MSC) as a therapeutic cell source. Therapies using these cells target a wide range of diseases including bone disorders, cartilage damage or inflammatory diseases (Durand and Charbord, 2015). This work focusses on specific adult mesenchymal progenitor cells derived

from the human periosteum due to their benefits in skeletal tissue engineering. This periosteum is a thin vascular membrane around most bones, situated between the cortical bone and the covering soft tissue and consists of an outer fibrous layer and an inner cambium layer containing adult mesenchymal progenitor cells (Allen et al., 2004). These human periosteum-derived cells (hPDCs) have similar characteristics as adult mesenchymal stromal cells (MSCs). Both cell types, MSCs and hPDCs, possess self-renewal capacity, express a specific set of MSC markers and are capable of differentiating into a variety of cell types, such as chondrocytes, osteoblasts and adipocytes, as well as myoblasts. The benefits of hPDCs are on the one hand the relatively easy accessibility and on the other hand their high bone regenerative potential (de Bari et al., 2006). They even have a higher growth and differentiation potential than bone marrow stromal/stem cells (BMSCs) (Duchamp de Lageneste et al., 2018). More specifically, hPDCs are valuable in skeletal tissue engineering for the regeneration of defects in long bones, as the periosteum is the main source of the cells involved in the callus formation during facture healing (Nilsson Hall et al., 2020). Treating critical size long bone defects using skeletal tissue engineering has the potential to repair large bone defects as well as joint surface defects. These critical defects were otherwise too large for the body to heal by itself and when left untreated, it could even result in the loss of a limb. Current treatments consist of bone void fillers, which can be natural, synthetic or a combination. However, the outcomes of these commercial bone void fillers remain unpredictable (Slevin et al., 2016).

In order to provide such cell therapies, there is a need to scale-up the expansion of cells since only a small fraction of the required amount of cells can be harvested from a single donor. A therapeutic dose of MSCs requires between 10^7 and 10^9 cells (Jung et al., 2012), while only 10^4 to 10^5 MSCs can be harvested from a single biopsy depending on the source of acquisition (Beitzel et al., 2013). Interesting strategies for large-scale expansion of MSC's are investigated in the review of García-Fernández et al. (2020). Their article describes the importance of choosing the right bioprocess design, such as the culture medium formulation and addresses the different scale-up strategies (García-Fernández et al., 2020). Depending on the type of stem cell used during the therapy, different cell culture vessels are preferred (dos Santos et al., 2013). This work focussed on human periosteum-derived cells (hPDCs), which are an adherent progenitor cell type similar to MSCs. Adherent cells require a surface to attach to, which is typically the bottom of a flask, but could also be hollow fibers or small microcarriers in suspension. Since scale-up is essential to fulfill the demand for MSCs or other cell types used in regenerative medicine products (Olsen et al., 2018), it is important to select the most efficient production process toward large scale productions. MSCs and hPDCs have been expanded in multistack (Lambrechts et al., 2016b) and hollow fiber bioreactors (Jones et al., 2013; Nold et al., 2013; Rojewski et al., 2013; Hanley et al., 2014; Lambrechts et al., 2016a). However, certain challenges mostly related to sub-optimal cell harvest efficiency or lack of process flexibility have established suspension culture as an efficient and flexible set-up for adult progenitor cell expansion. Therefore, dynamic systems with microcarriers were investigated instead of the traditional planar culture systems thanks to the increased surface area to volume ratio.

The selection of an appropriate microcarrier for each cell type is crucial, since it influences the seeding efficiency, proliferation rate and harvest efficiency (Schnitzler et al., 2016). An overview of the most common used microcarriers in cell expansion is given in **Table 1**. Commercial microcarriers differ in core material, coating material, ionic surface charge, porosity, swelling upon hydration and size resulting in different seeding, proliferating or harvesting efficiency for a specific cell type. Important research into the full 3D morphologic characterization of microcarriers using a combination of microfocus X-ray computed tomography (microCT) and contrast-enhanced microCT (CE-CT) is recently reported by our group (de Bournonville et al., 2021).

A clear comparison of the expansion of MSC's using the different microcarriers Cytodex-1, Star-Plus, Plastic, Plastic-Plus and HillexII is given in Loubière et al. (2019). Here, Star-Plus and Plastic-Plus are chosen as the best microcarriers for the cell culture of MSC's derived from umbilical cord based on the criteria of cell attachment, expansion and detachment (Loubière et al., 2019). Health authorities are in favor of avoiding the use of animal components due to safety reasons and animal welfare (Cimino et al., 2017). Hence, the use of human platelet lysate (hPL) as a xeno-free alternative for fetal bovine serum (FBS) supplement has been suggested and evaluated in many studies (Xia et al., 2011; Gottipamula et al., 2012; Oikonomopoulos et al., 2015; Heathman et al., 2016). hPL is a xeno-free medium, containing platelet derived growth factor (PDGF), transforming growth factor beta 1 (TGF-b1), insulin like growth factor (IGF-1), and basic fibroblast growth factor (bFGF) (Gottipamula et al., 2012; Oikonomopoulos et al., 2015; Heathman et al., 2016). The abundance of these growth factors in combination with an environment more closely related to the physiological human body might explain the consistently higher proliferation and culture expansion rate of MSC in hPL media in comparison to FBS (Lohmann et al., 2012). In this study, we investigated the influence of commercial microcarrier types for the expansion of hPDCs in an hPL supplemented medium composition. We strived to verify expansion and harvest efficiency, while simultaneously evaluating the bone forming capacity of the dynamically expanded cells.

The goal of this work was to select the appropriate microcarrier for scalable expansion of hPDCs in a xeno-free medium. In order to do this, different commercial microcarriers were screened based on standard characteristics of seeding, proliferation and harvesting efficiency. Most microcarrier research uses *in vitro* techniques to assess the quality of the cells after expansion. However, this is not a guarantee for *in vivo* success (Nilsson Hall et al., 2020), especially when evaluating progenitor cells derived from different sources. Therefore, this work also evaluated the functionality of the dynamically expanded hPDCs grown on Star-Plus microcarriers by subcutaneous implantations in nude mice.

TABLE 1 | Manufacturing information of commercially available microcarriers, screened in this study.

Abbr.	Microcarrier	Manufacturer	Matrix	Coating	Hydration	Diameter (μm)	Surface area (cm^2/g dry weight)
Animal protein							
Coll	Collagen	Sartorius	Cross-linked polystyrene	Porcine collagen		125–212	360
F3	FACT III	Sartorius	Cross-linked polystyrene	Porcine collagen cationic charge		125–212	360
CultiS	CultiSpher-S	Percell Biolytica AB	Macro porous cross-linked gelatin		Yes	130–380	
Xeno-free							
H2	Hillex II	Sartorius	Modified (cationic amine) polystyrene			160–200	515
Pl	Plastic	Sartorius	Cross-linked polystyrene			125–212	360
Pl+	Plastic-Plus	Sartorius	Cross-linked polystyrene	Cationic charge		125–212	360
St+	Star-Plus	Sartorius	Cross-linked polystyrene	Net positive charge		125–212	360
C1	Cytodex-1	GE Healthcare	Cross-linked dextran	positive charged DEAE groups	Yes	140–200	4400
C0	Untreated	Corning	Polystyrene			125–212	360
SY II	Synthemax II dissolvable	Corning	Cross-linked PGA polymer chains	Corning synthemax II	Yes	200–300	5000

MATERIALS AND METHODS

Experimental Set-Up

Three different types of experiments were performed for the microcarrier screening of ten different commercial microcarriers, shown in **Table 1**. The three experiments are briefly described hereafter and in more detail in the following sections. A scheme of all three experiments is represented in **Figure 1**.

The first experiment consisted of a broad static screening in well plates using eight microcarriers (Plastic, Plastic-Plus, Star-Plus, FactIII, HillexII, Collagen; Cytodex-1, and Corning untreated). A cell pool was seeded for each of the microcarriers in six individual wells of a 24-well plate for the evaluation of seeding efficiency and proliferation rate. 24 h after seeding, three wells were sacrificed for measuring the DNA content of the cells attached to the beads and the DNA of the cells in the supernatant. After 6 days of cell culture, the three other wells of each type of microcarrier were sacrificed to measure the total content of DNA on the cells attached to the microcarriers.

The second experiment selected three microcarriers (Plastic-Plus, Star-Plus, Cytodex-1) from the static screening and added Cultispher-S and Synthemax II dissolvable to perform a dynamic microcarrier screening experiment. The same cell pool as previous screening experiment was used in combination with the five microcarriers in a dynamic expansion. Each microcarrier type was cultured in duplicates in spinner flaks of 100 mL for 8 days. The DNA and metabolites were sampled daily at the same time, before medium replacement.

The third and final experiment evaluated the dynamic expansion of cells from two different donors using one specific microcarrier, Star-Plus. The cells of these two donors were cultured in triplicate spinner flasks resulting in a total of six spinner flasks for the duration of 8 days. After the dynamic culture, the quality of the cells was extensively evaluated.

Static Microcarrier Screening Experiment

Human Periosteum-Derived Progenitor Cells

Human periosteum-derived progenitor cells (hPDCs), used throughout this study, were obtained from periosteal biopsies acquired in the university hospital of KU Leuven at Pellenberg, Belgium (Eyckmans et al., 2010). All patients filled-in the informed consent form of the clinical study, which was approved by the KU Leuven medical ethics committee. The screening experiments were performed with pooled cells from five female donors between the age of 10 and 17. After isolation, the cells were cultured for multiple passages at a seeding density of 5500 cells/cm^2 in high glucose Dulbecco's Modified Eagle's Medium (DMEM) containing 1% sodium pyruvate, supplemented with 1% antibiotic-antimyotic (AA) and 10% serum. The serum added at biopsy for the screening experiments was fetal bovine serum (FBS). After several passages, the cells were frozen in liquid nitrogen until the start of the experiment.

The experiment started with thawing cells and expanding them for two passages in tissue flasks at a seeding density of 5500 cells/cm^2. The decision of taking pooled cells cultured in FBS from biopsy for both microcarrier screening experiments was a practical choice, due to availability of cells. However, hPL was preferred and therefore the cells, which were prior to being frozen cultured in FBS, were deprived from FBS and changed to hPL. During the first passage after thawing at the start of the experiment, the cells were subjected to a serum starvation protocol. This protocol started by culturing the cells in 10% FBS. At confluency, the cells were washed with PBS and the media was replaced with 0.1% FBS. After 24 h of serum deprivation, the cells were harvested and subcultured in 7.5% hPL for at least one passage before the start of an experiment to give the cells time to adapt to the different serum. The choice of using 7.5% of hPL in the media at the start of each experiment was based on previous experiments,

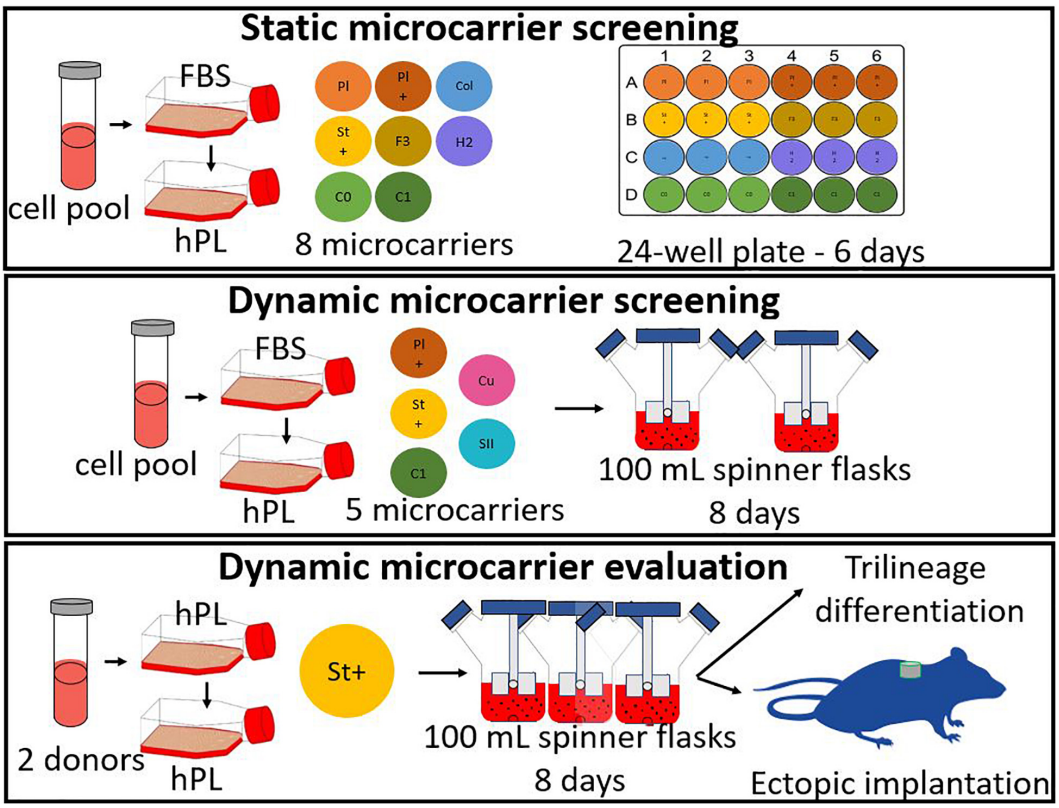

FIGURE 1 | General scheme of the experiments, starting with a static microcarrier screening of 8 microcarriers and followed by a dynamic microcarrier screening of 5 microcarriers. The final experiment evaluated the hPDCs, which were dynamically expanded on the chosen microcarrier Star-Plus, *in vitro* as well as *in vivo*.

indicating that it is economically the best ratio for clinical grade hPL, which is also suggested in literature (Xia et al., 2011; Gupta et al., 2019).

Preparation Culture Vessels and Microcarriers

The vessels used for the static microcarrier screening were CoStar ultra-low attachment 24-well plates (Corning). Each of the eight types of commercial microcarriers (Plastic, Plastic-Plus, Star-Plus, FactIII, HillexII, Collagen; Cytodex-1 and Corning untreated) were seeded in six wells. All microcarriers were weighed to achieve a ratio of 6 cm^2/mL, which is equal to 6 cm^2 for each well. After weighing, if required according to manufacturing instructions, the microcarriers were hydrated in MiliQ water or PBS, and sterilized through autoclaving. The water or PBS from the microcarriers was replaced with complete DMEM, consisting of DMEM+AA+7.5% hPL, and incubated in the wells in 1 mL, 24 h prior to use.

Seeding Protocol

Cells were seeded at a density of 5500 cells/cm^2, resulting in 33,000 cells per well. The pooled cells were added to the well plates while manually stirring the microcarrier suspension, to ensure a homogeneous dispersion. After seeding, the well plates were kept static in the incubators. Besides the six wells seeded with cells for each microcarrier, three additional control wells were seeded with cells but without microcarriers.

Harvesting Protocol

Tissue flasks and well plates were harvested according to the standard protocol of washing with PBS and incubating with TrypLE for 10 min. Followed by removing the cells from the bottom or microcarriers by force, either tapping the sides of the flask or pipetting the medium in the well up and down. The cell suspension was transferred to a falcon tube and medium was added to neutralize the enzymes. To separate the cells from the microcarriers, a 60μm filter was used on top of the falcon tube. The cell suspension was centrifuged at 1300 rpm for 10 min or 160G (Hettich Universal 320/320R centrifuge).

Cell Quantification

Cell counts were performed using 0.25% trypan blue and a Bürker hemacytometer. DNA samples were collected by sacrificing three whole wells, once after 24 h and a second time at the end of the culture period of 6 days. The DNA samples were collected in Eppendorf's and washed twice with PBS by centrifuging the samples for 5 min and removing the supernatant. After removing the excess PBS, RTL buffer with 1% β-mercaptoethanol was added. This mixture was vortexed for 15 s and stored in −80°C. The DNA content in the sample was measured by following the manufactures protocol of the qubit fluorometer where Quant-iT^{TM} dsDNA HS reagent, Quant-iT^{TM} dsDNA HS buffer and Quant-iT^{TM} standard were used.

To measure the seeding efficiency, the DNA of the supernatant as well as the DNA on the microcarriers was measured separately. The seeding efficiency was calculated by dividing the DNA on day 1 attached to the microcarriers by the total amount of DNA found in the well on day 1, as presented in equation 1. The fold increase of the expansion was calculated by dividing the DNA on day 6 by the DNA on day 1, as represented in equation 2.

$$\frac{DNA_{beads}(day1)}{DNA_{beads}(day1) + DNA_{supernatant}(day1)} \quad (1)$$

$$\frac{DNA_{beads}(day1)}{DNA_{beads}(day6)} \quad (2)$$

Live-Dead Cell Viability Assay on Microcarriers

A 0.5 mL homogenous sample of microcarriers was taken on day 6 of the well plate culture period. This sample was placed in a suspension well plate and stained with calcein AM an ethidium homodimer-1(Invitrogen). Live cells have intracellular esterase activity that convert cell-permeant calcein AM to fluorescent calcein. Dead cells have damaged membranes, to which ethidium can enter and bind to nucleic acids. After staining, the samples were visualized using an inverted fluorescence microscope (IX83, Olympus). The live cells appear as green, while dead cells appear as red during imaging.

Actin and Nucleus Staining

A whole 1 mL well containing cells on microcarriers was used for actin and nucleus visualization. The medium was removed from the settled microcarriers and washed with 0.5 mL PBS. After removal of the PBS, the cells were fixated using 0.5 mL of 4% paraformaldehyde (PFA powder diluted in PBS), which was pipetted up and down. The cells with microcarriers were incubated in this fixation solution for 1 h at room temperature, while occasionally stirred. After the incubation period, the PFA was removed and the samples were washed with 0.5 mL PBS. This PBS was then removed and replaced by 0.5 mL of 0.1 M Glycine. After an incubation period of 15 min at room temperature, the samples were washed with PBS and stored in PBS at 4°C until staining.

1 mL staining solution was prepared with 1 μL 4′,6-Diamidino-2-Phenylindole (DAPI, 2.5 mg/mL stock solution, Invitrogen), 4 μL Alexa Fluor 488 Phalloidin (Phalloidin, 200 U/mL stock solution, Life technologies), 20 μL Triton X_{100} and 975μL PBS. The PBS from the fixated samples was removed and 0.5 mL staining solution was mixed in the sample by pipetting up and down. The samples were covered with aluminum foil and incubated at room temperature on a shaker platform for 1 h. After the staining incubation period, the samples are washed with PBS twice and kept in 0.2 mL PBS. The samples were visualized using an inverted fluorescence microscope (IX83, Olympus) or a confocal laser scanning microscope (LSM 880, Zeiss). DAPI stains the nuclei and appears as blue on the imaging, while Phalloidin will stain actin as green.

Dynamic Microcarrier Screening Experiment

Human Periosteum-Derived Progenitor Cells

The same hPDCs pool of five young female donors as previous static screening experiment was used during this dynamic screening experiment.

Preparation Culture Vessels and Microcarriers

The vessels used for the dynamic expansion were 100 mL spinner flasks (Bellco Glass Cat. Number 1965-00100) with a diameter of 65 mm, a height of 135 mm, a center neck of 70 mm and two side arms of 32 mm. Before use, the spinner flasks were coated with Sigmacote (Sigma-Aldrich) by pipetting up and down 25mL sigmacote over all inner surfaces of the spinner flasks. After a night of air drying in the hood, the coating was verified by visual inspection of perfectly formed water droplets on the coated surface. The coated spinner flasks were then sterilized through autoclaving.

All five microcarriers (Cytodex-1, Star-Plus, Plastic-Plus, Cultispher-S, SynthemaxII dissolvable) were weighed to achieve a ratio of 6 cm^2/mL, which is equal to 480 cm^2 for each spinner flask with a working volume of 80 mL. After weighing, if required according to manufacturing instructions, the microcarriers were hydrated in MiliQ water or PBS, and sterilized through autoclaving. The water or PBS from the microcarriers was replaced with pure human platelet lysate (hPL) and placed inside the spinner flasks and in the incubator set at 37°C, 5% CO_2, and 95% relative humidity. 2 h before the inoculation, the pure hPL was replaced by complete medium (DMEM-C), consisting of DMEM+AA+7.5% hPL (Loubière et al., 2019).

Seeding Protocol

Cells were seeded at a density of 5500 cells/cm^2, resulting in 2.64×10^6 cells per spinner flask. The pooled cells were seeded while the spinner flasks were positioned on the magnetic plate at a stirring speed of 30 rpm with 20 mL of DMEM-C to ensure a homogeneous seeding. 5 min after seeding, the stirring speed was set to 0 rpm for 2 h after which 20 mL of DMEM-C was added. This 5 min ON and 2 h OFF protocol was repeated during 8 h. After these initial 8 h, the stirring speed was set at 30 rpm during the next 16 h (overnight). 24 h after seeding, the volume was topped-up from 40 to 80 mL and the stirring speed was increased from 30 to 50 rpm.

Harvesting Protocol

After 8 days of the expansion process, the cells were harvested inside the spinner flasks (Nienow et al., 2014; Rodrigues et al., 2019). The decision to end the culture period after 8 days was based on average hPDC cell growth data cultured in hPL and in tissue flask, unrelated to the type of microcarrier in order to compare all cell culture experiments over the same culture period. The stirring was stopped to let the microcarriers settle inside the spinner flasks, followed by removing as much medium as possible. The microcarriers were washed with PBS until most of the medium was washed out. As much PBS as possible was removed before adding TrypLE and incubating it for 15 min at a stirring speed of 50 rpm, using the manufacturing protocol.

To separate the cells from the microcarriers, the suspension was filtered with a steriflip (60 μm). The filter was washed with medium, to get as much cells, which were stuck between the microcarriers, through the filter and to balance the enzymatic reaction of TrypLE. To remove the TrypLE and medium mixture, the cell suspension was centrifuged at 1300 rpm for 10 min.

Cell Quantification

Cell counts were performed using 0.25% trypan blue and a Bürker hemacytometer. The metabolites were sampled daily at the same time, before medium replacement. The glucose, lactate and lactate dehydrogenase (LDH) in the sampled medium were measured using the Cedex Bio Analyser (Roche).

The DNA samples were collected and measured according to the previously described methods. In order to translate the DNA value to cell numbers, an additional experiment was performed to achieve a standard curve with nine values of known cell numbers ranging from 0 to 55000 cells/mL. The DNA of each cell sample was measured according to the method described above, resulting in a relation between known cell number and measured DNA content as described in equation 3 (**Supplementary Figure 1**, $R^2 = 0.998$). A similar validation on the same cell type has been done in a previous study by Chen et al. (2012).

$$DNA\left(\frac{ng}{mL}\right) = 0.01^{*}\frac{Cells}{mL} + 0.1166 \quad (3)$$

Dynamic Microcarrier Evaluation Experiment

The final experiment evaluated the dynamic expansion of cells from two different donors using one specific microcarrier, Star-Plus. The cells of these two donors were cultured in triplicate spinner flasks resulting in a total of six spinner flasks for the duration of 8 days.

Human Periosteum-Derived Progenitor Cells

The dynamic evaluation experiment was not performed on a cell pool, but on two different male donors, where donor 1 was 22 years old at the time of biopsy and donor 2 was 37 years old. The serum added at biopsy also differs from previous experiments. For the static and dynamic screening experiment, the added serum was fetal bovine serum (FBS), while for the dynamic evaluation, it was human platelet lysate (hPL). Therefore, there was no need for a starvation protocol in this experiment.

Preparation Culture Vessels and Microcarriers

The six spinner flasks and the Star-Plus microcarriers used for the expansion of the two donors in triplicates were prepared as described above.

Seeding Protocol

Spinner flask 1, 2, and 3 were seeded with cells from donor 1 and spinner flasks 4, 5 and 6 with cells from donor 2. The cells were seeded at a density of 5500 cells/cm^2 in 80 mL medium as described above.

Harvesting Protocol

The cells were harvested inside the spinner flasks, similar to the previous described method. The differences between the harvesting of the screening experiment were the increased stirring speed and incubation time. Instead of incubating for 15 min at a stirring speed of 50 rpm, the cells were incubated for 20 min at a stirring speed of 150 rpm. The stirring speed was increased for the last 5 s to 200 rpm to mimic the tapping on the side of standard tissue flaks, which breaks up all cell agglomerates and detaches the cells from the microcarriers. A suspension sample is visually inspected under a bright field microscope to ensure the detachment of the cells. The same separation method was used as previously described to separate the cells from the microcarriers.

Cell Quantification

Cell counts were performed using 0.25% trypan blue and a Bürker hemacytometer. The glucose, lactate, ammonium and pyruvate concentrations in the sampled medium were measured using the Cedex Bio Analyser. The DNA samples were collected and measured as described above.

Live-Dead Cell Viability Assay on Microcarriers

A 0.5 mL homogenous sample of microcarriers was taken on day 1, day 4, and day 6 of the spinner flask culture, while stirring the spinner flasks, to use for live-dead visualization as previously described.

FACS Analysis

Cells from both spinner flasks, after a cell culture period of 8 days, and from confluent tissue flasks were harvested to assess the presence of typical MSC immunophenotypic cluster of differentiation (CD) markers as well as the lack of hematopoietic markers. Flow cytometry was therefore performed using the human antibodies CD73-APC, CD-90-FITC, CD105-PE, CD-14-PerCP, CD20- PerCP, CD34- PerCP and CD45-PerCP (Miltenyi Biotec). Dead cell exclusion was performed using a viability dye (Zombie Aqua, BioLegend). An initial antibody titration to avoid nonspecific antibody biding was achieved following the protocol of Hulspas (2010). The BD Canto II was used for the flow cytometry analysis together with the software BD FACSDiva.

The full compensation setup contained control samples, Fluorescence Minus One (FMO) samples, negative control, dead cell exclusion and the condition samples. The control samples were performed using compensation beads (UltraComp eBeads Affymetrix eBioscience), which were only stained for one of the antibody colors: FITC, PE, APC, or PerCP control. All other samples used half a million cells from tissue flasks each. The FMO samples were stained with all antibodies, except for one. The negative control contained cells without any antibody, and the dead cell exclusion sample was stained only with the viability dye. The cells for the dead cell exclusion contained 50% live and 50% dead cells, achieved by placing the cells 5 min on ice and 5 min in a 60°C water bath. The interested condition samples, either with cells from tissue flasks or spinner flasks, were stained with all antibodies. RNA extraction, cDNA synthesis, and quantitative PCR

The DNA of 1 million cells was sampled at day 0 (before seeding) and day 8 (after harvesting). The DNA sample was centrifuged, the medium was removed and 600μL of RTL

buffer with 1% β-mercaptoethanol was added. This mixture was vortexed and stored in −80°C. The RNeasy Mini kit (qiagen) was used to extract the RNA, followed by using the NanoDrop ND-2000 to quantify the amount of RNA. Synthesizing the cDNA was performed using PrimeScript RT reagent kit, Perfect Real Time (TaKaRa). The final concentration of 5 ng/μL was stored at −20°C until further analysis. QPCR was performed using a 9μL of the mastermix of RNA free water, reverse primer, forward primer and Fast SYBR green (Thermo Fisher Scientific) and 1μL cDNA of the sample. All samples were processed using a rotor gene in duplicates as well as the control sample with RNA free water for each primer. The settings used were a hold of 2 min at 45°C, a second hold of 95°C for 30 s and cycles at 95°C for 3 s and 60°C for 20 s. The results were analyzed using relative quantification ($2^{-\Delta\Delta Ct}$) where the fold change of a specific gene of each sample minus the endogenous control was compared to that specific gene on day 0 of the same donor minus the endogenous control.

In vitro Trilineage Differentiation

Human periosteum-derived progenitor cells can potentially differentiate *in vitro* into chondrocytes, adipocytes and osteoblasts. This differentiation was induced with specific differentiation media, while control samples only receive basal medium.

Chondrogenic differentiation started with seeding 400,000 cells in 20μL DMEM-C with 7,5% hPL in 24-well plates, after 2 h 0.5 mL medium was added. After 24 h, the medium was replaced by chondrogenic differentiation medium containing basal medium, consisting of low glucose DMEM supplemented (Life Technologies) with 1% antibiotic-antimycotic, and a mix of 1X ITS+ Premix (Corning), 100 nM dexamethasone (Sigma), 20 μM Y-27632 inhibitor (Axon medchem), 1 mM ascorbic acid-phosphate (Sigma), 40 μg/mL proline (Sigma), 10 ng/mL TGF β1 (peprotech), 100 ng/mL GDF5 (peprotech), 100 ng/mL BMP2 (peprotech), 0.1 ng/mL BMP6 (peprotech) and 0.2 ng/mL FGF2 (peprotech). This medium was replaced every 2 or 3 days during a culture period of 21 days. At the end of the culture period, the trilineage differentiation was evaluated using alcian blue staining.

For Adipogenic differentiation, a density of 10 000 cells/cm^2 was seeded in a 24-well plate in 0.5 mL DMEM-C. After 24 h, the medium was replaced by adipogenic differentiation medium, where the basal medium consisted of αMEM (Life technologies) supplemented with 1% antibiotic-antimycotic and 10% hPL. The adipogenic differentiation medium also contained 1μM dexamethasone, 10 μg/ml human insulin (Sigma), 100 μM indomethacin (Sigma) and 25 μM 3-Isobutyl-1-methylcanthine (IBMX) (Sigma). This medium was replaced every 2 or 3 days during a culture period of 14 days. The evaluation after the differentiation period was performed using oil red o staining.

Osteogenic differentiation was performed with a seeding density of 4500 cells/cm2 in a 24 well plate and 0.5 mL DMEM-C. After 48 h, the medium was replaced with osteogenic differentiation medium, which contained basal medium with 100 nM dexamethasone, 50 μg/ml ascorbic acid-phosphate and 10 mM β-glycerolphosphate (Sigma). The basal medium was DMEM-C supplemented with 10% hPL. The culture period was 21 days and the medium was replaced every 2 or 3 days. The osteogenic differentiation was evaluated using alizarin red staining.

In vivo Ectopic Implantation and Analysis

After 8 days of cell culture expansion, $1{\cdot}10^6$ cells of each spinner flask after harvesting was seeded on NuOss scaffolds in a volume of 30μL separately. In total, six scaffolds were seeded and left overnight in 12-well plates in DMEM-C for the cells to adhere before implantation the day after. The implantation was performed ectopically on the back of 8 weeks old nude mice (Jackson Laboratory). After 8 weeks, the scaffolds were explanted and fixated overnight in 4% PFA before being switched to PBS.

Nano Computed Tomography Scans

To evaluate the amount of mineralized tissue, the scaffolds were scanned after explantation, on a Phoenix NanoTom M (GE Measurement and control) system using the following scanning parameters: x-ray voltage of 60 kV, current of 170 μA, tube mode 0, filter 0.2 mm Al, target diamond/tungsten. The acquisition parameters used were: fast scans of 15 min with exposure time of 500 ms, averaging of 1, skip 0, detector calibration 2 points, an average voxel size of 2.72 μm and 1800 images.

Histology

Following the nanoCT scans, the scaffolds were decalcified 10 times with at least 24 h in between using EDTA, paraffin embedded, sectioned (5μm) and stained for histologic analysis. The first staining was hematoxylin and eosin (H&E) to visualize the general structure and location of cells in between the left-over scaffolds. The other staining used was Masson's trichrome, which visualized the connective tissue from the cells.

Statistical Analysis

Results are presented as mean ± standard deviation. All statistical analysis were performed with a 95% confidence level for a one or two-sample *t*-test using Matlab version 2018b. The one-sample *t*-test was used when comparing gene expression data to day zero, the null hypothesis. This null hypothesis states that the data has a normal distribution with mean equal to zero and an unknown variance. A two-sample *t*-test is used with a null hypothesis of the two data sets being independent random samples from normal distributions with equal means and equal but unknown variances. In this work, this was used to verify if the data of a specific cell characteristic is significantly different between two donors.

RESULTS AND DISCUSSION

Both microcarrier screening experiments explored together a total of ten different commercial microcarriers, shown in **Table 1**, based on the following criteria: (a) the seeding efficiency, (b) the proliferation efficiency, (c) the harvest efficiency, (d) the quality

of the cells after expansion, and (e) if the microcarrier is made of xenogeneic free material.

Static Microcarrier Screening Experiment

Each of the eight types of commercial microcarriers (Plastic, Plastic-Plus, Star-Plus, FactIII, HillexII, Collagen; Cytodex-1, and Corning untreated) was evaluated in a 24-well plate for seeding efficiency and proliferation rate. Although the objective is to use a xeno-free microcarrier, this selection does include animal protein containing microcarriers to evaluate the difference in performance between the desired xeno-free microcarriers and the animal protein containing microcarriers.

Using light microscopy, it was visible that the control wells without microcarriers contained agglomerates of cells after 3 days without the cells being attached to the bottom of the wells. This indicates that the ultra-low attachment coating of the well was sufficient to avoid competition with the microcarriers. Live-dead staining on the microcarriers showed that the cells attach to one or more microcarriers, leading to the formation of clumps as visualized in **Figure 2**, starting with a static microcarrier screening of 8 microcarriers and followed by a dynamic microcarrier screening of 5 microcarriers. The final experiment evaluated the hPDCs, which were dynamically expanded on the chosen microcarrier Star-Plus, in vitro as well as *in vivo*.

Figure 2 these live-dead stainings (starting with a static microcarrier screening of 8 microcarriers and followed by a dynamic microcarrier screening of 5 microcarriers. The final experiment evaluated the hPDCs, which were dynamically expanded on the chosen microcarrier Star-Plus, in vitro as well as in vivo. **Figure 2** first and third row) are also merged with bright field imaging resulting in simultaneous live-dead as well as bright field imaging of the cells on the microcarriers (starting with a static microcarrier screening of 8 microcarriers and followed by a dynamic microcarrier screening of 5 microcarriers. The final experiment evaluated the hPDCs, which were dynamically expanded on the chosen microcarrier Star-Plus, in vitro as well as in vivo, **Figure 2** second and fourth row). Additional DAPI stained samples of these eight microcarriers as well as the microcarriers Synthemax II dissolvable and Cultispher-S are shown in **Figure 3**.

In order to decide which microcarrier is best suited for a certain cell type, the interaction between the microcarrier and the cells could be studied. An important aspect in this regard is whether the cells spread homogenously over the microcarrier, or if they clump together and not use all the available surface area efficiently. Depending on the cell type, the morphological characteristics of the microcarriers could also increase the available surface area. For example, the Cultispher-S microcarriers are macro-porous and cells smaller than 10 μm could use the surface area inside the pores to adhere to de Bournonville et al. (2021). Another factor influencing the available surface area is the swelling factor of the microcarriers that require hydration, such as Cultispher-S, Cytodex-1 and Synthemax II dissolvable. Furthermore, the interaction between the cell and microcarrier will be influenced by the surface characteristics of the microcarrier, such as the coating material or ionic charge, which can be positively charged (Hillex II, Star-Plus, Plastic-Plus and FACT III, Cytodex-1), negatively charged (Synthemax II dissolvable) or neutral (Corning Untreated, Collagen, Cultispher-S and Plastic).

Future work could analyze the cell spreading objectively based on the amount of cells per microcarrier and the distance between the cells on each microcarrier, using 3D image analysis of a large dataset. However, initial observations in this work on cell spreading indicate that Hillex II performs worse than all other microcarriers based on the heterogenous distribution and the large clumping of cells and microcarriers. Counting the amount of nuclei on each microcarrier in the DAPI stained samples in **Figure 3**, results in a standard deviation of cells per microcarrier, which is biggest for Hillex II and smallest for microcarriers Cultispher-S, Star-Plus, and Plastic-Plus. Therefore it seems that these microcarriers allow a more homogenous spreading of the hPDCs, which is favorable in choosing the best microcarrier.

From six wells of each condition, three whole wells were sacrificed on day 1 to measure all DNA present on the microcarriers as well as in the supernatant. The comparison between the DNA on the microcarriers and the DNA in the supernatant of day 1 gives an indication of the seeding efficiency as presented in **Figure 4A**. The other three wells were sacrificed after a cell culture period of 6 days to measure all DNA on the microcarriers. The DNA on the microcarriers of day 6 is compared to the DNA of day 1 to measure the proliferation of the cells on each type of microcarrier, which is shown in **Figure 4B**, where both DNA measures are converted to cell densities based on the relation explained by equation 3.

Statistical analysis of the seeding efficiencies with a significance level of 95% indicates several significant difference between microcarriers. The Plastic microcarrier has a significant lower seeding efficiency compared to HillexII, Cytodex-1, Corning untreated and collagen coated. In addition, HillexII has a significantly higher seeding efficiency compared to the collagen coated ones. Due to the high variations between the DNA on day 6 of the same microcarrier, there were no significant differences in the fold increase between the different microcarriers.

The three best performing microcarriers based on the average seeding efficiency are HillexII, Cytodex-1 and Plastic-Plus. For the average proliferation, the best performing microcarriers are Cytodex-1, Corning untreated and Star-Plus. Cytodex-1 is therefore the best overall performing microcarrier based on seeding efficiency and proliferation rate, which is in line with other work. A similar preference for Cytodex-1 compared to Hillex II, Plastic, Collagen and Plastic-Plus, was found by Schop et al. (2010) who focused on seeding efficiency as a selection criteria for the expansion of human bone marrow derived MSCs. Our study achieved a seeding efficiency in static culture of 89% (**Figure 4**) compared to a seeding efficiency of 57% by Schop et al. (2010), 80% by Frauenschuh et al. (2007), and 85% by Malda et al. (2003) (Malda et al., 2003; Frauenschuh et al., 2007; Schop et al., 2010).

This static screening is only an indication of how the cells perform on the microcarriers and is not representative for a dynamic cell culture expansion. Therefore this work used the most promising microcarriers based of this screening combined

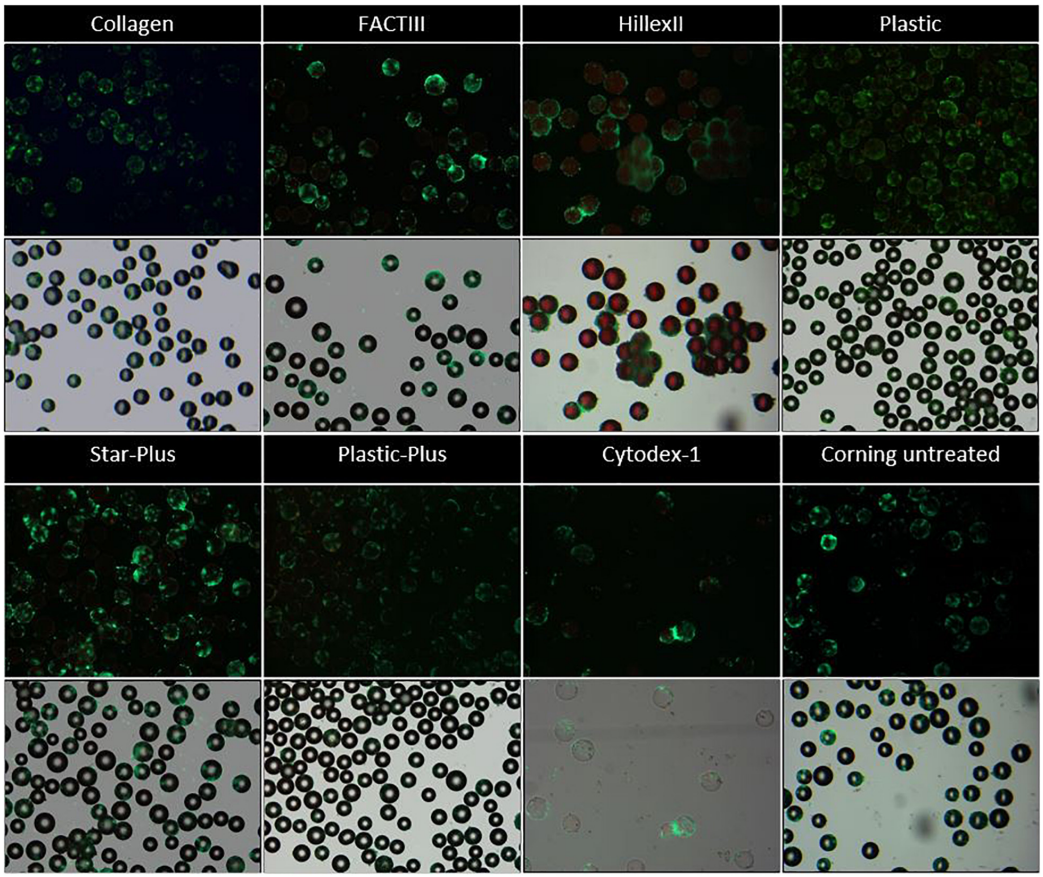

FIGURE 2 | Live dead imaging of the microcarriers Collagen, FACTIII, HillexII, Plastic, Star-Plus, Plastic-Plus, Cytodex-1, and Corning untreated. The figures in row 1 and 3 represent the live-dead stainings, where live cells are stained green and dead cells are stained red. The figures in row 2 and 4 represent the merged images of bright field images combined with the live dead stainings to visualize the cells with respect to the microcarriers.

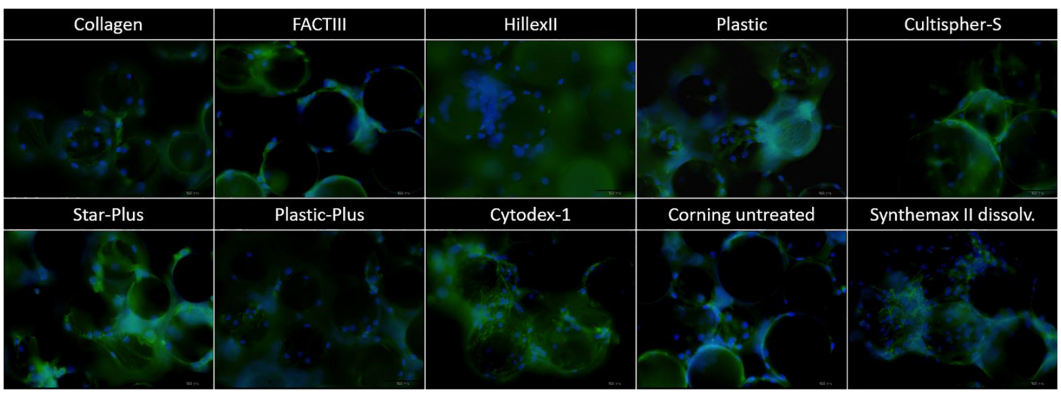

FIGURE 3 | DAPI imaging of the microcarriers Collagen, FACTIII, HillexII, Plastic, Cultispher-S, Star-Plus, Plastic-Plus, Cytodex-1, Corning untreated, and Synthemax II dissolvable. The nucleus is stained blue, the actine is stained green and each picture has a width of 550 μm.

with information in literature to make a selection of microcarriers to be assessed in a dynamic environment.

HillexII was not selected due to the high amount of clumping, the heterogenous spreading of the cells and the fact that it absorbs phenol red from the DMEM-C media and is heavier than other microcarriers. Being heavier would mean that the speed of the impeller in a dynamic environment needs to be increased to assure suspension, which is not favorable for the cells due to shear stress (Betrachtungen, 1968). Gupta et al. (2018) described the effect of an initial culture period at a higher speed 60 rpm

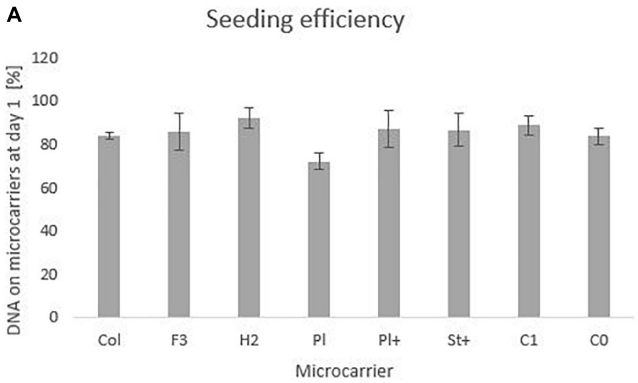

Microcarrier	Seeding efficiency (%)
H2	92.29 ± 4.77
C1	89.01 ± 4.49
Pl+	87.38 ± 8.48
St+	86.90 ± 7.78
F3	86.12 ± 8.62
Col	84.15 ± 1.69
C0	84.13 ± 3.81
Pl	72.26 ± 3.93

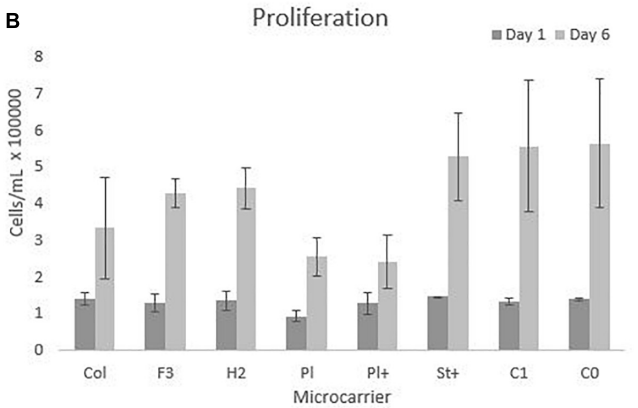

Microcarrier	Fold increase
C1	4.24 ± 1.64
C0	4.06 ± 1.28
St+	3.59 ± 0.78
F3	3.35 ± 0.48
H2	3.33 ± 0.61
Pl	2.77 ± 0.64
Col	2.34 ± 0.68
Pl+	2.00 ± 0.90

FIGURE 4 | Static screening experiments of the microcarriers Collagen, FACTIII, HillexII, Plastic, Plastic-Plus, Star-Plus, Cytodex-1, Corning untreated. **(A)** The seeding efficiency is presented as the amount of DNA attached to the microcarriers after 24 h compared to the time of seeding. **(B)** The proliferation capacity of the cells is visualized as the amount of cells on day 1 compared to day 6. These cell counts are based on DNA calculations converted to cell counts.

compared to 30 rpm, which resulted in a high accumulation of LDH. Therefore they hypothesized the relation of increase culture speed with cell death in the spinner flask system (Gupta et al., 2018). Plastic was also excluded for the following experiments due to the significant lower seeding efficiency compared to other microcarriers. FactII and Collagen did not perform significantly better than the xeno-free microcarriers, therefore we could exclude these animal protein containing microcarriers. The last microcarrier that was excluded for following experiments was Corning untreated, since preliminary results indicated difficulties in harvesting the cells. In addition, there was no specific coating attached to the microcarriers to facilitate the cells to attach to the microcarriers compared to Star-Plus and Plastic-Plus.

The final selection from these eight microcarriers that was assessed in a dynamic expansion are Cytodex-1, Star-Plus and Plastic-Plus.

Dynamic Microcarrier Screening Experiment

The microcarrier screening experiment in a dynamic expansion used the three chosen microcarriers from the first static screening experiment (Star-Plus, Plastic-Plus, and Cytodex-1) and added two interesting extra microcarriers (CultiSpher-S and Synthemax II dissolvable), which are both dissolvable. These were not yet included in the first screening experiment due to availability. However, since they have such an interesting characteristic of being dissolvable, they would have been included in the dynamic screening experiment regardless of their static performance.

These five microcarriers were all cultured in spinner flaks of 80 mL working volume in duplicates for 8 days. Although duplicates are not statistically valid data, there is still interesting information we can deduct from the metabolic results of the dynamic screening of the five microcarriers (Star-Plus, Plastic-Plus, Cytodex-1, CultiSpher-S and Synthemax II dissolvable), which are represented in **Figure 5** and **Table 3**. What is immediately noticeable is the lack of cell growth in the second spinner flask with Cytodex-1 microcarriers. There was no lactate production, there was almost no glucose consumption and the LDH values spiked in the first metabolite sample after 24 h of cell culture. Therefore we will exclude the second spinner flask of Cytodex-1 in further discussions. Overall, the lowest glucose concentration was 13.12 mM and the highest lactate concentration was 17.35 mM indicating that there was no glucose limitation or lactate inhibition.

The metabolic readouts collected in this experiment are used as a 'surrogate marker' for cell proliferation. The first indication

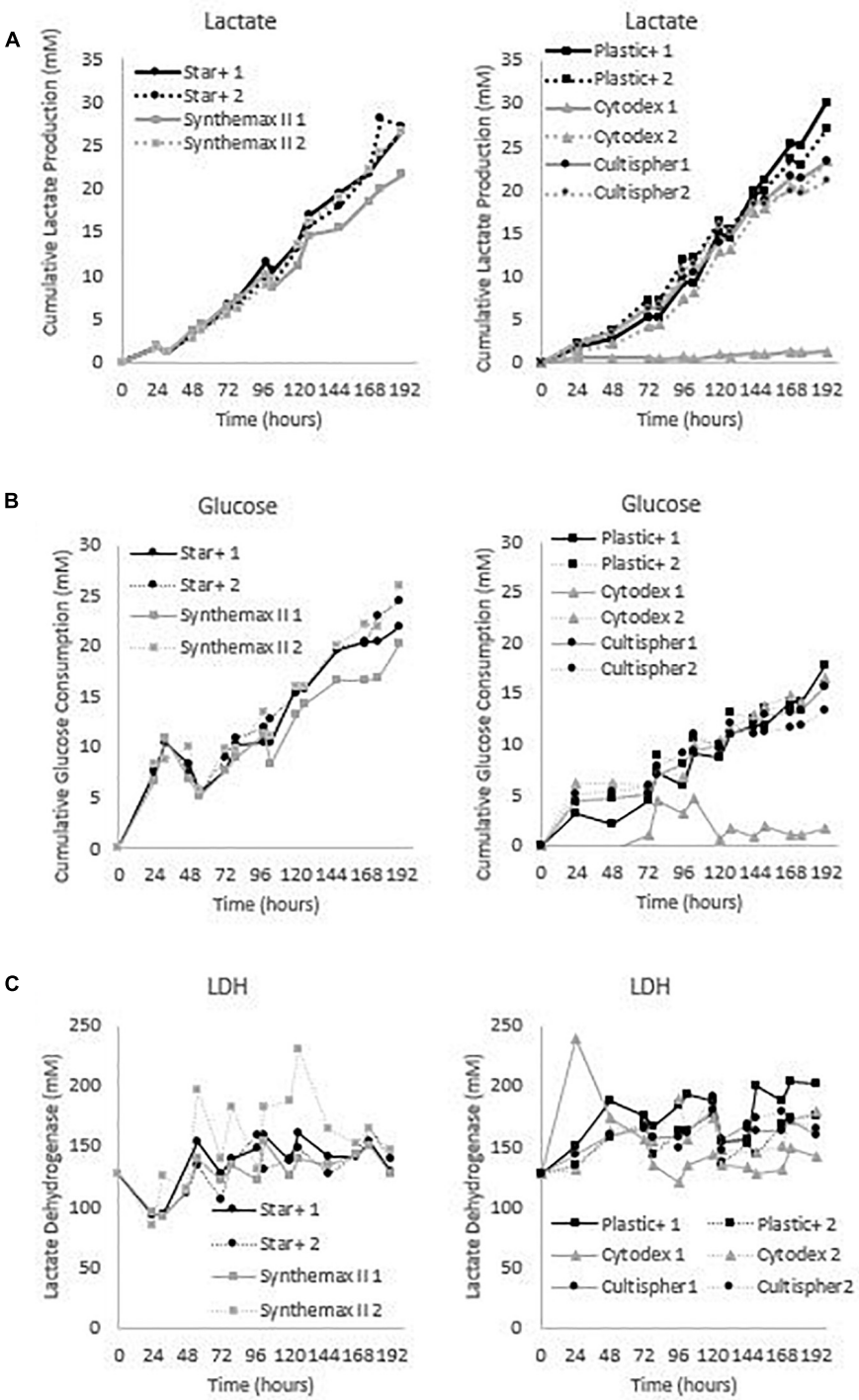

FIGURE 5 | Metabolic profiles for the dynamic screening experiments of the microcarriers Star-Plus, SynthemaxII dissolvable, Plastic-Plus, Cytodex1, and Cultispher-S. The experiments were performed in duplicates for each of the microcarriers. **(A)** Cumulative lactate measurements, **(B)** cumulative glucose measurements and **(C)** Lactate Dehydrogenase (LDH) measurements.

of cell growth is a low minimum glucose concentration or high glucose consumption, since an increase in cells would require an increase in nutrient consumption. A second and similar cell growth indication is based on lactate, where an increase in cells would result in an increase of waste products (Schop et al., 2009). And finally, high LDH concentration are used to indicate cell death (Lobner, 2000). Based on these assumptions, both spinner flaks with Star-Plus microcarriers

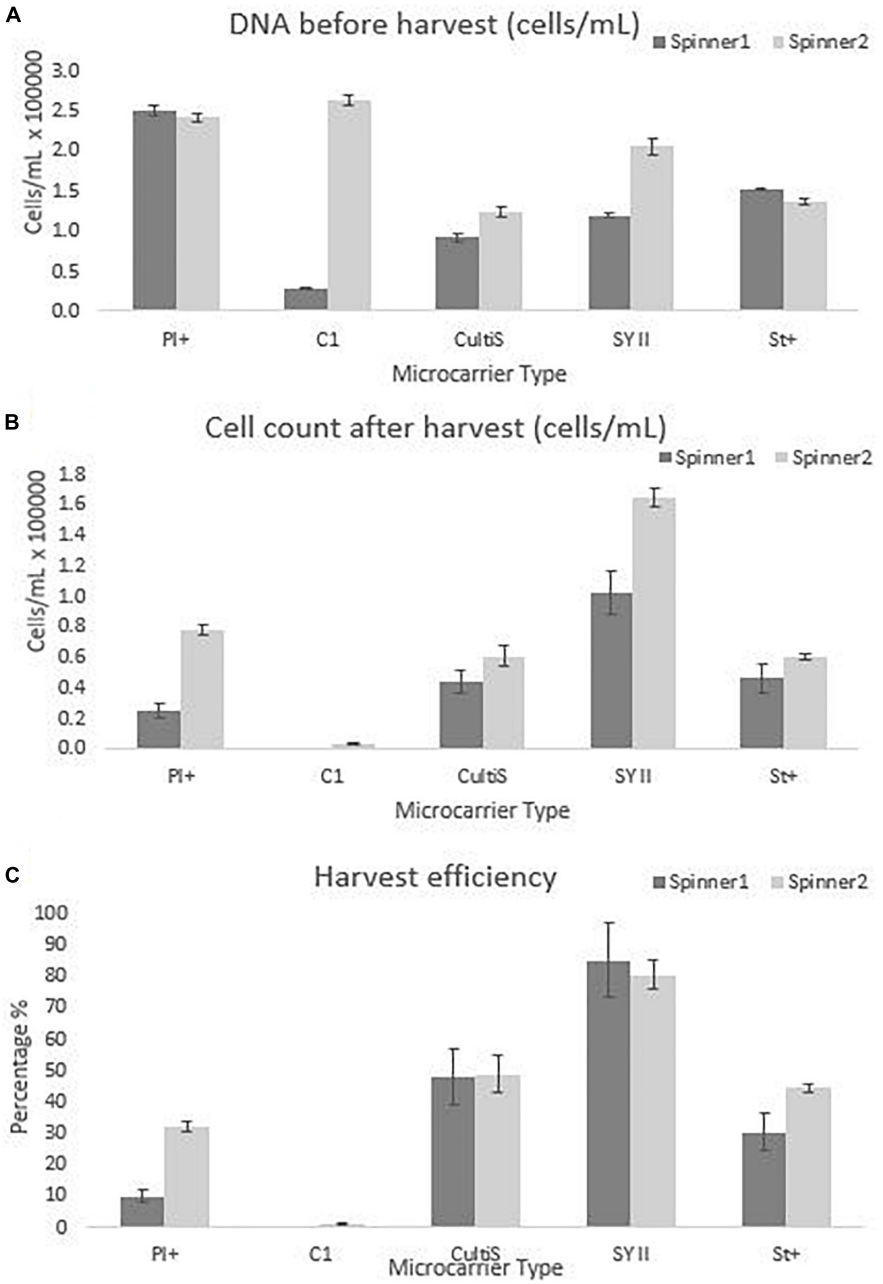

FIGURE 6 | Cell quantity observations for the dynamic screening experiments of the microcarriers Star-Plus, SynthemaxII dissolvable, Plastic-Plus, Cytodex1, and Cultispher-S. The experiments were performed in duplicates for each of the microcarriers. **(A)** The DNA amount of the cells attached to the microcarriers on day 8 before harvest was measured and converted to a cell quantity. **(B)** The cells after harvest were measured for each spinner flask and **(C)** the harvest efficiency was calculated based on the comparison of the cells before harvest with the cells after harvest.

have the best metabolic profiles in relation to cell growth. They combine a high glucose consumption, intermediate lactate production and low LDH values. On the other hand, both Cultispher-S spinner flasks indicate a low amount of cell proliferation based on the lowest glucose consumption, rather low lactate production and rather high LDH concentrations. Cytodex-1 is similar to Cultispher-S but performs slightly better based on the metabolite indications. Both Plastic-Plus and SynthemaxII have contradicting metabolic profiles. Plastic-Plus (1) and SynthemaxII (2) have high values for glucose consumption and lactate production but also a high LDH value, which might indicate a high cell growth combined with a high cell death. For Plastic-Plus (2) and SynthemaxII (1), the glucose consumption and lactate production are lower as well as the LDH values indicating a slower cell growth with lower cell death.

The cell quantity of the experiment was only measured at seeding and at harvesting since intermediate sampling of only 250μL was not representative for the whole spinner flask due to heterogenous sampling. In an effort to measure the cell growth during cell culture, daily DNA samples were taken but there was too much clumping, especially for Cultispher-S, to be representative for the whole spinner flask. Increasing the sample volume would make the sample more representative, but it would also influence the cell growth number. An alternative would be to harvest whole spinner flasks every day. However, the metabolites data described above gives an indication of cell growth or cell death through the cell culture period.

The cell number estimate before harvest was performed by sampling 4 mL of the cell culture and measuring the DNA content. This DNA content was translated to cell number using equation 3, the result is visualized in **Figure 6** and **Table 2**. However, the harvesting protocol used to obtain these results was the one suggested by the manufacturer. These experiments were performed before investigating more optimal harvesting protocols, since optimizing the harvesting of all possible microcarriers was not in the scope of this project. Once a microcarrier was chosen, it was valuable to investigate the harvesting protocol of that specific microcarrier. Ideally this screening experiment could be repeated in case the harvesting protocol of all microcarriers is optimized. Using the manufacturing protocol means that the cells were harvested using a low stirring speed of 50 rpm for 15 min instead of the optimized protocol used in final dynamic microcarrier evaluation experiment, where the stirring speed is increasing toward 150 rpm with an additional 5 s at 200 rpm.

The dynamic microcarrier screening experiment in this work shows proliferation results for hPDCs seeded at 33000 cells/mL and cultured for 8 days to reach a fold increase before harvesting of 8.0 for Cytodex-1, 7.5 ± 0.2 for Plastic-Plus, 4.9 ± 1.8 for Synthemax II dissolvable, 4.4 ± 0.4 for Star-Plus and 3.3 ± 0.7 for Cultispher-S (**Table 2**). Data from Gupta et al. (2018), also working on the expansion of hPDC in spinner flasks, presented a fold increase of 3.2 ± 0.64 after 12 days of hPDCs expansion on Cultispher-S in Fetal Bovine Serum (FBS) based medium (Gupta et al., 2018). However, it is important to be able to harvest the cells from the microcarriers to be used in cell therapies. Since the harvesting in the dynamic microcarrier screening experiment was performed using the manufacturer's protocol without optimization, this was rather low. The final fold increase of the cells after harvesting was therefore almost zero for Cytodex-1, 1.5 ± 1.1 for Plastic-Plus and CultiSpher-S, 1.6 0.3 ± for Star-Plus and 4.0 ± 1.4 for Synthemax II dissolvable (**Table 2**).

From the results of both static and dynamic screening, we selected Star-Plus as an interesting xeno-free microcarrier for the expansion of hPDC to be evaluated in the third experiment. Synthemax II dissolvable was initially the preferred microcarrier for the follow-up experiment due to the simplicity of harvesting, but the microcarrier was discontinued and could not be re-ordered at that time. Similar preferences for Synthemax II dissolvable were reported by Rodrigues et al. (2019), who investigated the expansion of human induced pluripotent stem cells (hiPSCs) on microcarriers. Synthemax II dissolvable resulted in a fold expansion of 4.0 ± 0.8 after 5 days of cell culture (Rodrigues et al., 2019). The reason for not selecting Cytodex-1, was due to the extreme low harvest efficiency, which was also reported in previous research. For example, Kehoe et al. (2012) published harvest efficiency data of 12% for Cytodex-1, whereas we only recovered 1%. Loubière et al. (2019) presents similar findings for the expansion of umbilical cord derived wharton's jelly MSCs, where cells remain attached to Cytodex-1 and Star-Plus and Plastic-Plus are the preferred microcarriers. Plastic-Plus is also preferred in the work of Petry et al. (2016) where fold expansions of 16.4 and 13.8 are achieved after 7 and 6 days of culturing human Umbilical Cord MSCs (Petry et al., 2016). However, they did not compare with Star-Plus, probably because Star-Plus is the newest microcarrier of the SoloHill microcarriers (Sartorius), released at the end of 2015.

TABLE 2 | Fold increase data for hPDCs expanded during dynamic screening experiment of 8 days.

Microcarrier	Fold increase before harvest	Fold increase after harvest
Plastic-Plus	7.5 ± 0.2	1.5 ± 1.1
Cytodex-1 (spinner flask 2)	8.0	0.09
Cultispher-S	3.3 ± 0.7	1.6 ± 0.4
Synthemax II dissolvable	4.9 ± 1.8	4.0 ± 1.4
Star-Plus	4.4 ± 0.4	1.6 ± 0.3

TABLE 3 | Metabolites data for hPDCs expanded during dynamic screening experiment of 8 days.

Microcarrier	Spinner flask nr	Minimum Glucose (mM)	Maximum Lactate (mM)	Maximum LDH (U/L)
Plastic-Plus	1	15.48	17.35	202.9
	2	16.98	14.4	177.05
Cytodex-1	1	19.37	1.81	239.29
	2	16.39	13.87	190.32
Cultispher-S	1	17.34	13.79	180.49
	2	17.03	13.44	190.56
Synthemax II dissolvable	1	16.15	12.21	153.02
	2	13.12	14.93	229.55
Star-Plus	1	13.53	14.26	161.57
	2	14.43	14.63	165.24

Quality Assessment After Star-Plus Expansion

After the initial screening experiments, this work investigated the potential of Star-Plus microcarriers for the expansion of hPDCs. Six different spinner flasks were used, where two donors were expanded in triplicates for 8 days. The quality of the cells after cell expansion on Star-Plus microcarriers was assessed. Donor 1 was 22 years old during biopsy, while donor 2 was 37 years old. Based on literature, we suspect that this age difference could cause differences between the donors regarding their *in vitro* and *in vivo* potential (De Bari et al., 2001). After 8 days of cell culture, the cells were harvested using an improved harvesting

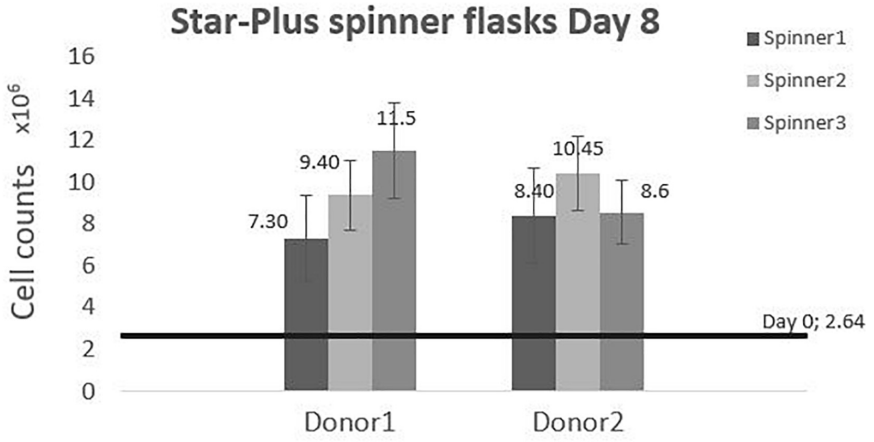

FIGURE 7 | Cell counts of the dynamic Star-Plus evaluation for each of the triplicate spinners of each donor.

method compared to the screening experiments, where the manufacturer's protocol was followed. This improved protocol was based on the work of Nienow et al. (2014), where the cells were incubated for more than 15 min in an enzymatic detachment solution while being stirred at 150 rpm instead of the suggested 40 rpm of the manufacturer, with an additional 5 s at 200 rpm. Their work increased the harvest efficiency of Plastic microcarriers from less than 5 % to higher than 95% (Nienow et al., 2014). In our work, the harvesting efficiency for Star-Plus increased from 37% in the dynamic screening experiment up to 97% in dynamic evaluation experiment. This method was also used in the microcarrier screening work of Rafiq et al. (2016).

The cells harvested after 8 days of cell culture in spinner flasks are visualized in **Figure 7**. The average final cell number, cell density and fold increase after harvesting is shown in **Table 4**. This fold increase of 3.56 for donor 1 is similar to the 2D control of the tissue flask expansion previous to the start of the spinner flask expansion. When extrapolation the cell counts after a 5 day expansion in the tissue flask to 8 days, the fold increase would be 3.22. Due to the high variations in cells harvested from donor 1, there is no statistical difference between the two donors. This variation could be caused by the order of harvesting, where donor 1, spinner flask 1 was harvested first, followed by spinner flask 2 and 3, after which donor 2 was harvested in the same sequence. Increasing knowledge about harvesting the cells throughout the process could result in increased numbers of cells harvested according to the sequence of the three spinner flasks. Besides cell counts, the following evaluations indicate a visible difference between donor 1 and 2. However, cells from both donors expanded on Star-Plus retain their chondrogenic potential, *in vitro* as well as *in vivo*.

TABLE 4 | Cell quantity after harvesting the cells cultured for 8 days in 6 different spinner flasks.

	Donor 1	Donor 2
Cell counts	9.40E+06 ± 2.10E+06	9.13E+06 ± 1.14E+06
Cell density	19 583 ± 4 375	19 028 ± 2 381
Fold increase	3.56 ± 0.80	3.46 ± 0.43

Two donors each cultured in triplicates, starting at 2.46·× 10^6 cells and 5500 cells·cm^{-2}.

TABLE 5 | Bone percentages analyzed from CT scans of cells implanted on NuOss scaffolds after 8 days of expansion on spinner flasks compared to cells only expanded in tissue flasks.

	Spinner flask bone volume (%)	Tissue flask bone volume (%)
Donor 1	9.80 ± 3.34	8.96 ± 0.72
Donor 2	3.85 ± 0.76	2.80 ± 1.77

All cumulative metabolite concentrations were significantly different on day 8 between donor 1 and donor 2, using a two-sample *t*-test with 95% confidence level. The metabolic activity of the cells is visualized in **Figure 8**. According to the findings of Schop et al. (2009), growth inhibition for human MSC's occurs at 35.4mM for lactate concentrations and 2.4 mM for ammonia (Schop et al., 2009). The medium in the spinner flasks of donor 1 reached a maximum lactate level of 25.39 mM at day 7, while the spinner flasks of donor 2 reached a maximum lactate level of 11.84 mM at day 7. Highest ammonium levels for donor 1 were reached on day 5 with a value of 1.75 mM, whereas the culture medium reached a maximum of 1.61 mM at day 7. Due to the high glucose concentration of 25 mM in the medium, the concentration never dropped below 10 mM during the whole cell culture expansion. In addition, the pyruvate concentration starting at 0.95 mM never drops below 0.20 mM. Therefore we can assume there were no inhibitory effects due to glucose or pyruvate depletion or due to a high accumulation of lactate or ammonia.

The live-dead staining of the cells on day 1, 4, and 6 of the cells on microcarriers are shown in **Figure 9**. On day 4, the amount of cells per microcarrier from donor 2 were visibly lower than the density of cells per microcarrier from donor 1.

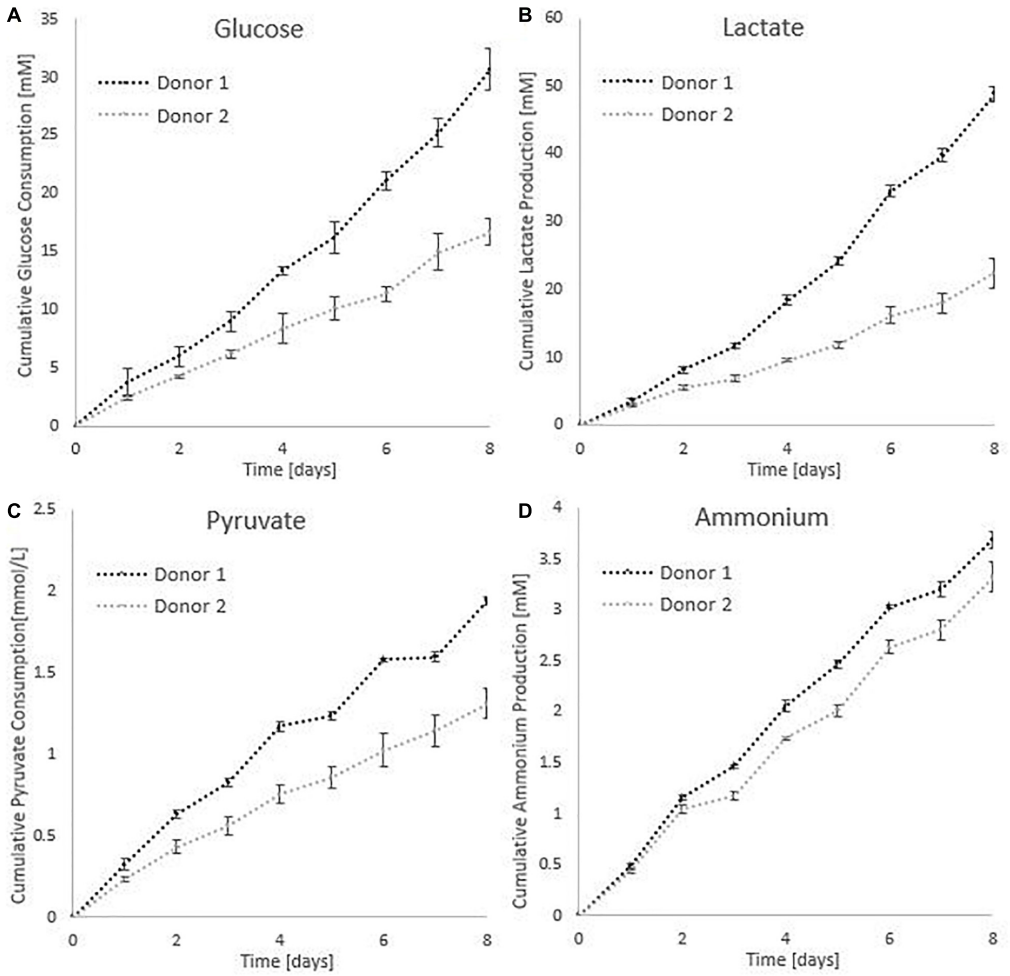

FIGURE 8 | Metabolic profiles for the dynamic Star-Plus evaluation for an average of the triplicate spinners for each of the donors. **(A)** Cumulative glucose measurements, **(B)** cumulative lactate measurements, **(C)** pyruvate measurements, and **(D)** ammonium measurements.

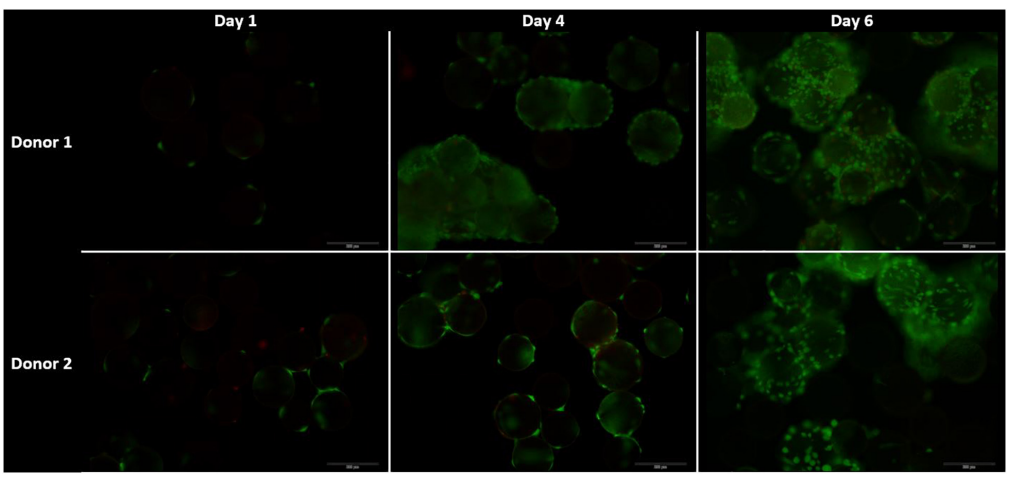

FIGURE 9 | Live dead stainings for the dynamic Star-Plus evaluation on day 1, 4, and 8 for both donor 1 and donor 2. Live cells are stained green by calcein and dead cells are stained red by ethidium.

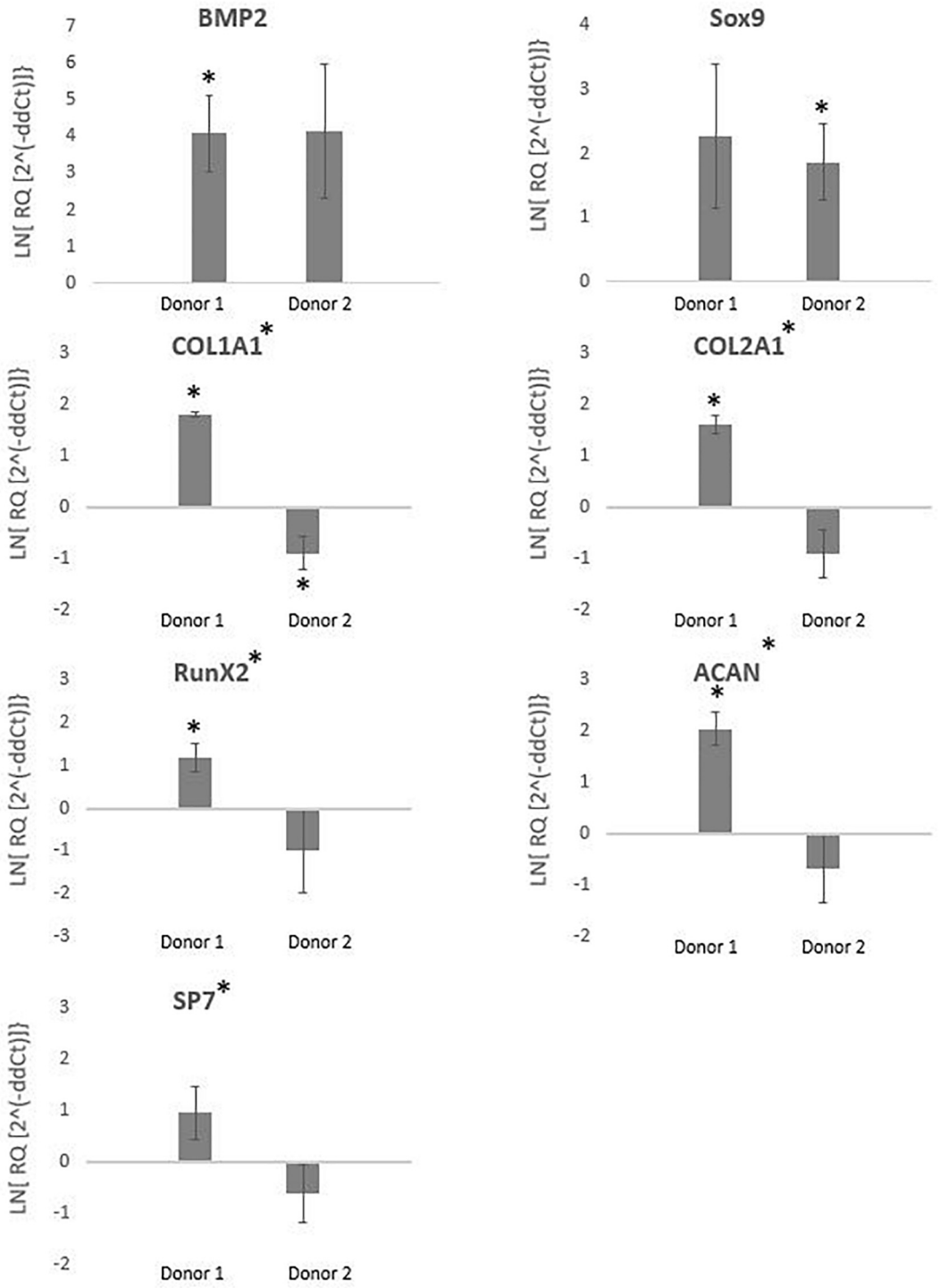

FIGURE 10 | The graphs represent the average gene expressions from hPDCs cultured on Star-Plus in triplicate spinner flasks for two different donors after 8 days compared to day 0. The analyzed genes were bone morphogenetic protein 2 (BMP2), collagen I (COL1A1), RUNX family transcription factor 2 (Runx2), osterix (SP7), 573 sex determining region box 9 (Sox9), collagen 2 (COL2A1), and aggrecan (ACAN). The test uses a significance level of 95%, where (*) placed besides the gene name indicates a significant difference between donor 1 and 2 and (*) placed at the value of a donor indicates the significant difference between that donor on day 8 compared to day 0.

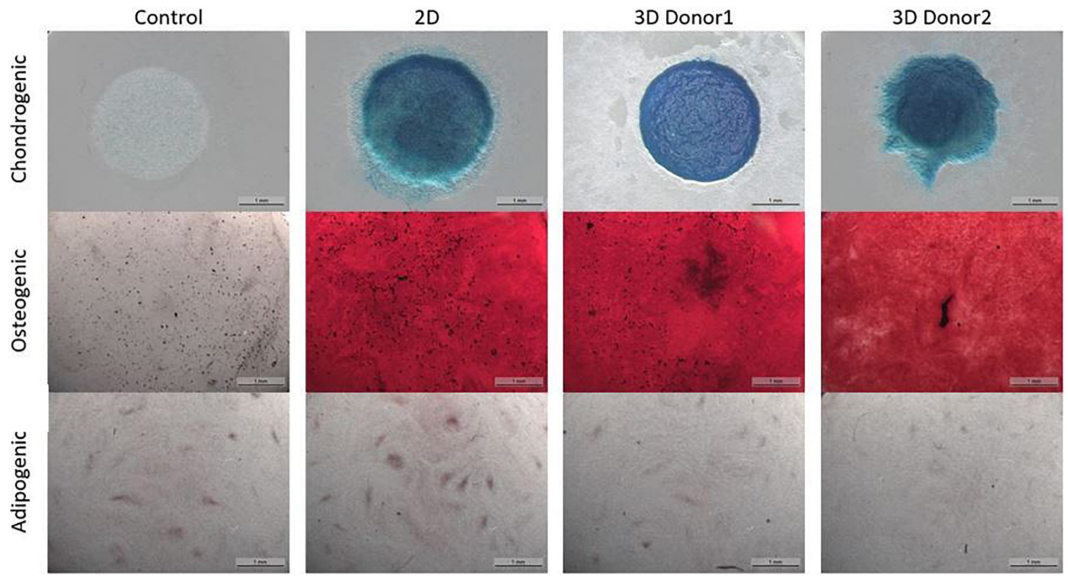

FIGURE 11 | Trilineage differentiation of the dynamic Star-Plus evaluation for a control sample without differentiation medium, a 2D sample from cells cultured in tissue flasks and 3D samples from cells of two different donors cultured in spinner flasks on Star-Plus microcarriers.

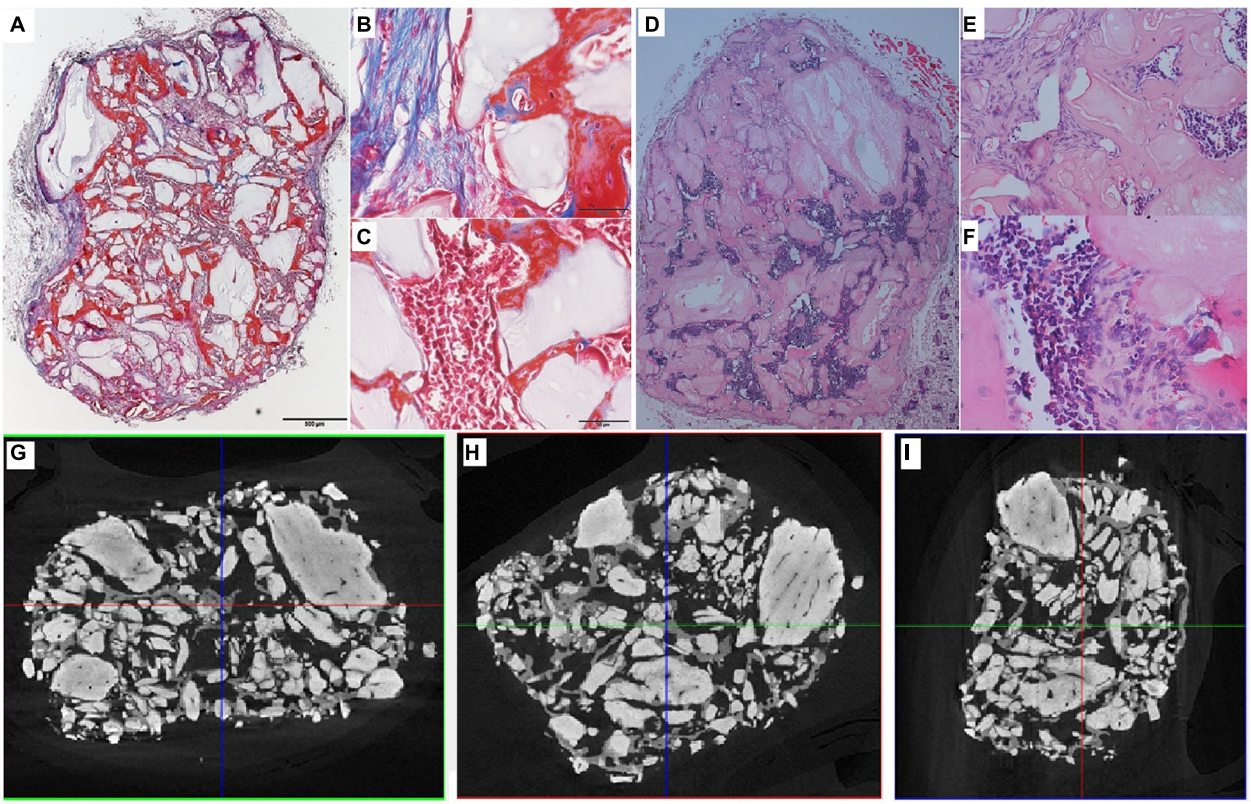

FIGURE 12 | Visualization of explant donor1 spinner flask1 results. **(A–C)** Masson's Trichrome staining. **(D–F)** H&E staining. **(G–I)** nanoCT scans 2D sections in all 3 planes.

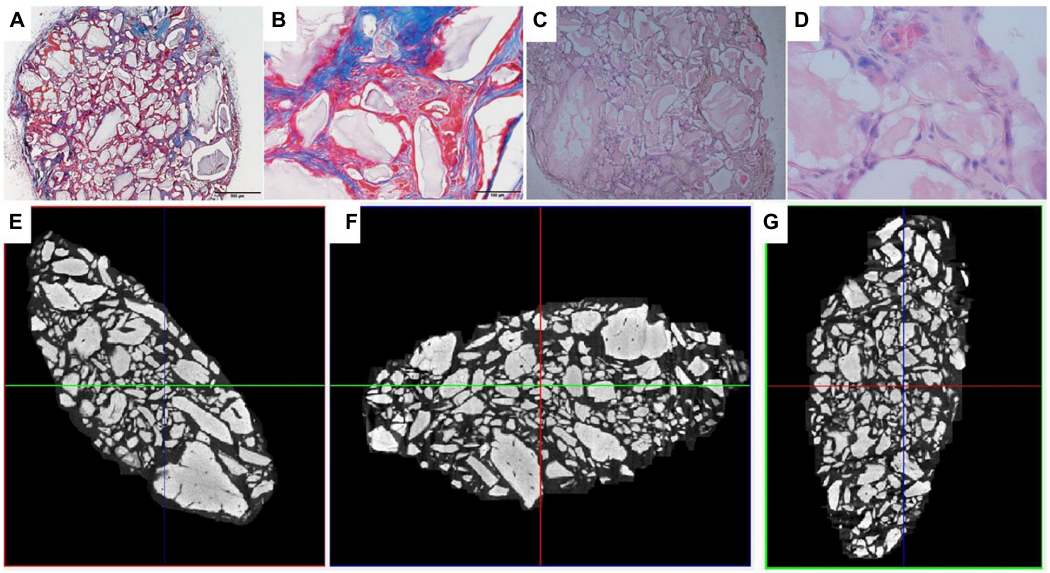

FIGURE 13 | Visualization of explant donor 2 spinner flask1 results. **(A,B)** Masson's Trichrome staining. **(C,D)** H&E staining. **(E–G)** nanoCT scans 2D sections in all 3 planes.

In addition, agglomeration is visible early on in the cell culture expansion, which could limit the cell growth. One method to decrease the agglomeration size is to add more microcarriers to increase the surface area (Ferrari et al., 2012). Another method is to increase the impeller speed in order to reduce the agglomerate size (Jossen et al., 2018). However, increasing the speed of the impeller should be properly investigated, because it could cause unwanted shear stress on the cells (Hewitt et al., 2011).

The International Society for Cellular Therapy (ISCT) proposes as a minimal criteria for MSCs that the markers CD73, CD90, and CD105 should be higher than 95% and the hematopoietic markers (CD14, CD20, CD34, and CD45) should be lower than 2% (Dominici et al., 2006). The FACS results for the cells cultured in spinner flaks compared to tissue flasks are represented in the **Supplementary Figure 2**, where the average expression of CD73 and CD90 are both higher than 95% and the hematopoietic markers are lower than 2%, while the expression of CD105 is reduced to an average of 90%. However, the reduced expression of CD105 has been observed in other literature using dynamic 3D cultures and is reported to be reversible when replating on 2D plastic tissue culture. The causes suggested in literature for the decrease are a too long detachment period, high concentrations of harvesting agent or high agitation rates (Brown et al., 2007; Potapova et al., 2008; Frith et al., 2010; dos Santos et al., 2011). Similar results for both a decrease in CD90 and CD105 were observed by Gupta et al. (2018, 2019) after the expansion of hPDCs on Cultispher-S in spinner flasks, which were described as non-significant. To conclude from these results, the hPDCs immunophenotypic markers were not permanently altered due to the spinner flask culture period and the following *in vivo* experiments will give a better inside in the impact of spinner flasks on the potency of the cells.The gene expressions visualized in **Figure 10** are averaged over the three spinner flasks for each donor. These gene expressions on day 8 of the cell culture are compared to day 0 for bone morphogenetic protein 2 (BMP2), collagen I (COL1A1), RUNX family transcription factor 2 (Runx2), osterix (SP7), sex determining region box 9 (Sox9), collagen 2 (COL2A1), and aggrecan (ACAN). The significant difference between each donor with the control on day 0 or the difference between the donors is calculated using the means and standard deviations of the biological triplicates and indicated by the symbol (*). In case a donor is significantly different from 0, the symbol is presented above the graph of

TABLE 6 | Bone percentages after ectopic implantation of hPDCs on scaffolds in mice for 8 weeks. Data gathered from literature.

Reference	Vessel type	Scaffold	Bioreactor bone volume (%)	Tissue flask bone volume (%)
Lambrechts et al., 2016b	Multiplate	Nuoss	11.6 ± 3.1	12.8 ± 3.3
Lambrechts et al., 2016a	Hollow Fiber	Nuoss	10.3 ± 3.7	11.0 ± 3.8
Kerckhofs et al., 2016	Tissue flask	Chronos		13.13 ± 3.82
Roberts et al., 2011	Tissue flask	Nuoss		13.03 ± 3.57
Roberts et al., 2011	Tissue flask	Bio-Oss		5.13 ± 2.49
Roberts et al., 2011	Tissue flask	Collagraft		1.88 ± 1.35
Roberts et al., 2011	Tissue flask	Vitoss		3.21 ± 2.04

that donor and in case the donors are significantly different from each other, the symbol is indicated besides the graph title from that gene. These results indicate that none of all the genes are simultaneously significantly different for both donors in the same direction. What is visible, is that for Col1a1 both donors are significantly different from the control on day 0, but for donor 1 this is a significant increase, while for donor 2 this is a significant decrease. The effect on gene expression of using Star-Plus in the expansion of the hPDCs is inconsistent between the two donors, which suggests that the influence is more related to donor variability than the expansion on microcarriers.

Sox9, a transcription factor indicative of chondroprogenitor cells, is upregulated for donor 2 and the potent bone inducer BMP2 for donor 1, indicative for genes related to differentiation via the osteogenic lineage (Ikeda et al., 2005; Ji et al., 2017). Although both Sox9 and BMP2 show a distinct upregulated trend, the fold change in both cases is rather low. The down regulation of collagen related cells in the case of donor 2 might suggest that cells are still in a proliferative state and have not yet reached confluency, which would allow secretion of collagen-based extracellular matrix (Tucker et al., 2020). This discrepancy in potency between donors is an integral challenge of the autologous cell therapy field but the qualitative match between *in vitro* measured quality attributes and subtle *in vivo* differences provides hope that markers for evaluating this difference could be develop in the future.

The chondrogenic, osteogenic and adipogenic differentiation after 2 weeks or 3 weeks of differentiation for the cells culture during 8 days in spinner flasks are visualized in **Figure 11**. The trilineage differentiation after expansion in spinner flasks of both donors compared to the control of a 2D expansion on tissue flasks, confirm that the cells retain their initial bone and cartilage forming potency.

Analysis of the CT scans from the scaffolds, seeded with cells after 8 days of spinner flask expansion and after 8 weeks of implantation in nude mice are shown in **Table 5**. The same table also represents the control scaffolds, which were implanted with cells cultured statically in 2D tissue flasks. These results show that no matter what culture system is used, there is a significant difference between donor 1 and 2 when looking at the bone formation. What is also important to notice is that there is no significant difference in bone formation between the two culture systems. This suggests that the cells cultured in spinner flasks with Star-Plus microcarriers achieve similar bone volume formation as the cells cultured in the standard used tissue flasks. In addition, donor 1 has a significant higher bone formation compared to donor 2, both after the 2D as well as 3D expansion. For donor 1, a more developed bone domain has been developed within the CaP scaffolds with a clear presence of bone marrow compartment, suggesting a more rapid process of bone tissue formation. This same trend is visible in the hematoxylin-eosin (H&E) as well as Masson's trichrome stainings, which are presented together with the CT scans in **Figure 12** for donor 1 and **Figure 13** for donor 2.

Besides these *in vitro* methods, which are mainly used in other research on microcarriers, this work also uses *in vivo* bone forming experiments to assess the potency of the cells. The same conclusion for *in vivo* as the *in vitro* methods can be made, namely that both cell batches after the spinner flask expansion of the two different donors have no significant difference in bone formation compared to their 2D control.

Such *in vivo* bone forming experiments are used in other research, also to assess the quality of cells after a cell expansion process under specific conditions (Weiss et al., 2012). The work of Gupta et al. (2019) used this type of experiments to validate the positive effect of hPL on the *in vivo* bone forming potential of hPDCs expanded on Cultispher-S microcarriers in spinner flaks (Gupta et al., 2019). Indications of bone volume percentages achieved of other studies using hPDCs are shown in **Table 6**. Studies where bone volume percentage of a specific culture system is compared to the standard tissue flask system are interesting to compare with. Although the results of the multiplate bioreactor and the hollow fiber are slightly higher than the results of this work, they are not significantly different from their tissue flask control. This indicates that the variation between the systems is due to donor variability and not the cell culture system. The other bone percentage results from literature show that the cell-carrier combination of hPDC and NuOss is superior compared to Bio-Oss, Collagraft and Vitoss.

These results demonstrated that using spinner flasks with Star-Plus microcarriers has no significant difference in cell potency compared to tissue flask cultures. Besides comparing the results of this work with the standard used tissue flasks, other cell culture systems are also interesting to compare to. hPDCs have also been evaluated in a multiplate bioreactor (Xpansion, Pall life sciences) (Lambrechts et al., 2016b) and a hollow fiber bioreactor (Quantum, Terumo) (Lambrechts et al., 2016a), which both conclude that the cells retain their bone forming potency. The main differences and tradeoffs in cell culture systems are the price of the culture system, whether the system is re-usable or disposable, the efficiency of the downstream processes and how well the system can be automated to reduce variations and increase process efficiency.

CONCLUSION

In conclusion, this work demonstrates that Star-Plus is a suitable microcarrier for the expansion of hPDCs in suspension culture. During this expansion process a xeno-free medium was used in 100 mL spinner flasks on different donors. Both *in vitro* assessment, but more importantly also *in vivo* assessments of the expanded hPDCs were carried out. The results of this work showed no significant difference in bone forming potential between the dynamic expansion and the standard tissue flask expansion. Therefore, this work presents a scalable production process of hPDCs using Star-Plus microcarriers in spinner flasks, where the cells maintain their bone forming potential *in vivo*. In this work we demonstrate that expansion efficiency, while safeguarding potency and cell functionality, can be obtained in a clinically relevant context.

DATA AVAILABILITY STATEMENT

The raw data supporting the conclusions of this article will be made available by the authors, without undue reservation.

ETHICS STATEMENT

The animal study was reviewed and approved by KU Leuven Animal Ethics Committee.

AUTHOR CONTRIBUTIONS

KV and IP: conceptualization and investigation. KV: experimental work, formal analysis, data curation, writing–original draft preparation, and visualization. IP and J-MA: resources, supervision, and funding acquisition. KV, IP, and J-MA: writing–review and editing. J-MA: project administration. All authors have read and agreed to the published version of the manuscript.

FUNDING

This research was funded by KU Leuven, grant number C24/17/077.

ACKNOWLEDGMENTS

We would like to thank Kathleen Bosmans for her assistance with the *in vivo* implantation and Filipa Inês de Carvalho Guimarães for her assistance with the initial microcarrier screening experiments.

SUPPLEMENTARY MATERIAL

The Supplementary Material for this article can be found online at: https://www.frontiersin.org/articles/10.3389/fbioe.2021.624890/full#supplementary-material

REFERENCES

Durand, C., and Charbord, P. (2015). *Stem cell biology and regenerative medicine*. Aalborg: River Publishers.

Allen, M. R., Hock, J. M., and Burr, D. B. (2004). Periosteum: Biology, regulation, and response to osteoporosis therapies. *Bone* 35, 1003–1012. doi: 10.1016/j.bone.2004.07.014

de Bari, C., Dell'Accio, F., Vanlauwe, J., Eyckmans, J., Khan, I. M., Archer, C. W., et al. (2006). Mesenchymal multipotency of adult human periosteal cells demonstrated by single-cell lineage analysis. *Arthritis Rheum.* 54, 1209–1221. doi: 10.1002/art.21753

Duchamp de Lageneste, O., Julien, A., Abou-Khalil, R., Frangi, G., Carvalho, C., Cagnard, N., et al. (2018). Periosteum contains skeletal stem cells with high bone regenerative potential controlled by Periostin. *Nat. Commun.* 9, 773.

Nilsson Hall, G., Mendes, L. F., Gklava, C., Geris, L., Luyten, F. P., and Papantoniou, I. (2020). Developmentally Engineered Callus Organoid Bioassemblies Exhibit Predictive In Vivo Long Bone Healing. *Adv. Sci.* 7, 1902295. doi: 10.1002/advs.201902295

Slevin, O., Ayeni, O. R., Hinterwimmer, S., Tischer, T., Feucht, M. J., and Hirschmann, M. T. (2016). The role of bone void fillers in medial opening wedge high tibial osteotomy: a systematic review. *Knee Surgery, Sport. Traumatol. Arthrosc.* 24, 3584–3598. doi: 10.1007/s00167-016-4297-5

Jung, S., Panchalingam, K. M., Wuerth, R. D., Rosenberg, L., and Behie, L. A. (2012). Large-scale production of human mesenchymal stem cells for clinical applications. *Biotechnol. Appl. Biochem.* 59, 106–120. doi: 10.1002/bab.1006

Beitzel, K., McCarthy, M. B., Cote, M. P., Durant, T. J., Chowaniec, D. M., Solovyova, O., et al. (2013). Comparison of mesenchymal stem cells (osteoprogenitors) harvested from proximal humerus and distal femur during arthroscopic surgery. *Arthroscopy.* 29, 301–308. doi: 10.1016/j.arthro.2012.08.021

García-Fernández, C., ópez-Fernández, A. L., Borrós, S., Lecina, M., and Vives, J. (2020). Strategies for large-scale expansion of clinical-grade human multipotent mesenchymal stromal cells. *Biochem. Eng. J* 159, 107601. doi: 10.1016/j.bej.2020.107601

dos Santos, F. F., Andrade, P. Z., Da Silva, C. L., and Cabral, J. M. S. (2013). Bioreactor design for clinical-grade expansion of stem cells. *Biotechnol. J.* 8, 644–654. doi: 10.1002/biot.201200373

Olsen, T. R., Ng, K. S., Lock, L. T., Ahsan, T., and Rowley, J. A. (2018). Peak MSC—Are We There Yet? *Front. Med.* 5:178.

Lambrechts, T., Papantoniou, I., Viazzi, S., Bovy, T., Schrooten, J., Luyten, F. P., et al. (2016b). Evaluation of a monitored multiplate bioreactor for large-scale expansion of human periosteum derived stem cells for bone tissue engineering applications. *Biochem. Eng. J.* 108, 58–68. doi: 10.1016/j.bej.2015.07.015

Lambrechts, T., Papantoniou, I., Rice, B., Schrooten, J., Luyten, F. P., and Aerts, J. M. (2016a). Large-scale progenitor cell expansion for multiple donors in a monitored hollow fibre bioreactor. *Cytotherapy* 18, 1219–1233. doi: 10.1016/j.jcyt.2016.05.013

Rojewski, M. T., Fekete, N., Baila, S., Nguyen, K., Fürst, D., Antwiler, D., et al. (2013). GMP-compliant isolation and expansion of bone marrow-derived MSCs in the closed, automated device quantum cell expansion system. *Cell Transplant.* 22, 1981–2000. doi: 10.3727/096368912x657990

Jones, M., Varella-Garcia, M., Skokan, M., Bryce, S., Schowinsky, J., Peters, R., et al. (2013). Genetic stability of bone marrow-derived human mesenchymal stromal cells in the Quantum System. *Cytotherapy* 15, 1323–1339. doi: 10.1016/j.jcyt.2013.05.024

Hanley, P. J., Mei, Z., Durett, A. G., Cabreira-Hansen Mda, G., Klis, M., Li, W., et al. (2014). Efficient manufacturing of therapeutic mesenchymal stromal cells with the use of the Quantum Cell Expansion System. *Cytotherapy* 16, 1048–1058. doi: 10.1016/j.jcyt.2014.01.417

Nold, P., Brendel, C., Neubauer, A., Bein, G., and Hackstein, H. (2013). Good manufacturing practice-compliant animal-free expansion of human bone marrow derived mesenchymal stroma cells in a closed hollow-fiber-based bioreactor. *Biochem. Biophys. Res. Commun.* 430, 325–330. doi: 10.1016/j.bbrc.2012.11.001

Schnitzler, A. C., Verma, A., Kehoe, D. E., Jing, D., Murrell, J. R., Der, K. A., et al. (2016). Bioprocessing of human mesenchymal stem/stromal cells for therapeutic use: Current technologies and challenges. *Biochem. Eng. J.* 108, 3–13. doi: 10.1016/j.bej.2015.08.014

de Bournonville, S., Geris, L., and Kerckhofs, G. (2021). Micro computed tomography with and without contrast enhancement for the characterization of microcarriers in dry and wet state. *Sci. Rep.* 11, 2819.

Loubière, C., Sion, C., De Isla, N., Reppel, L., Guedon, E., Chevalot, I., et al. (2019). Impact of the type of microcarrier and agitation modes on the expansion performances of mesenchymal stem cells derived from umbilical cord. *Biotechnol. Prog.* 35, e2887.

Cimino, M., Gonçalves, R. M., Barrias, C. C., and Martins, M. C. L. (2017). Xeno-free strategies for safe human mesenchymal stem/stromal cell expansion: Supplements and coatings. *Stem Cells Int.* 6597815, 2017.

Xia, W., Li, H., Wang, Z., Xu, R., Fu, Y., Zhang, X., et al. (2011). Human platelet lysate supports ex vivo expansion and enhances osteogenic differentiation of human bone marrow-derived mesenchymal stem cells. *Cell Biol. Int.* 35, 639–643. doi: 10.1042/cbi20100361

Heathman, T. R. J., Stolzing, A., Fabian, C., Rafiq, Q. A., Coopman, K., Nienow, A. W., et al. (2016). Scalability and process transfer of mesenchymal stromal cell production from monolayer to microcarrier culture using human platelet lysate. *Cytotherapy* 18, 523–535. doi: 10.1016/j.jcyt.2016.01.007

Oikonomopoulos, A., van, Deen WK, Manansala, A. R., Lacey, P. N., Tomakili, T. A., Ziman, A., et al. (2015). Optimization of human mesenchymal stem cell manufacturing: The effects of animal/xeno-free media. *Sci. Rep.* 5, 16570.

Gottipamula, S., Sharma, A., Krishnamurthy, S., Sen Majumdar, A., and Seetharam, R. N. (2012). Human platelet lysate is an alternative to fetal bovine serum for large-scale expansion of bone marrow-derived mesenchymal stromal cells. *Biotechnol. Lett.* 34, 1367–1374. doi: 10.1007/s10529-012-0893-8

Lohmann, M., Walenda, G., Hemeda, H., Joussen, S., Drescher, W., Jockenhoevel, S., et al. (2012). Donor age of human platelet lysate affects proliferation and differentiation of mesenchymal stem cells. *PLoS One* 7:e37839. doi: 10.1371/journal.pone.0037839

Eyckmans, J., Roberts, S. J., Schrooten, J., and Luyten, F. P. (2010). A clinically relevant model of osteoinduction: A process requiring calcium phosphate and BMP/Wnt signalling. *J. Cell. Mol. Med.* 14, 1845–1856. doi: 10.1111/j.1582-4934.2009.00807.x

Gupta, P., Hall, G. N., Geris, L., Luyten, F. P., and Papantoniou, I. (2019). Human Platelet Lysate Improves Bone Forming Potential of Human Progenitor Cells Expanded in Microcarrier-Based Dynamic Culture. *Stem Cells Transl. Med.* 8, 810–821. doi: 10.1002/sctm.18-0216

Rodrigues, A. L., Rodrigues, C. A. V., Gomes, A. R., Vieira, S. F., Badenes, S. M., Diogo, M. M., et al. (2019). Dissolvable Microcarriers Allow Scalable Expansion And Harvesting Of Human Induced Pluripotent Stem Cells Under Xeno-Free Conditions. *Biotechnol. J.* 14, e1800461.

Nienow, A. W., Rafiq, Q. A., Coopman, K., and Hewitt, C. J. (2014). A potentially scalable method for the harvesting of hMSCs from microcarriers. *Biochem. Eng. J.* 85, 79–88. doi: 10.1016/j.bej.2014.02.005

Chen, Y., Sonnaert, M., Roberts, S. J., Luyten, F. P., and Schrooten, J. (2012). Validation of a PicoGreen-Based DNA Quantification Integrated in an RNA Extraction Method for Two-Dimensional and Three-Dimensional Cell Cultures. *Tissue Eng. Part C Methods* 18, 444–452. doi: 10.1089/ten.tec.2011.0304

Hulspas, R. (2010). Titration of fluorochrome-conjugated antibodies for labeling cell surface markers on live cells. *Curr. Protoc. Cytom* (Suppl. 54), 1–9. *vol,

Schop, D., van Dijkhuizen-Radersma, R., Borgart, E., Janssen, F. W., Rozemuller, H., Prins, H. J., et al. (2010). Expansion of human mesenchymal stromal cells on microcarriers: growth and metabolism. *J. Tissue Eng. Regen. Med.* 4, 131–140. doi: 10.1002/term.224

Frauenschuh, S., Reichmann, E., Ibold, Y., Goetz, P. M., Sittinger, M., and Ringe, J. (2007). A microcarrier-based cultivation system for expansion of primary mesenchymal stem cells. *Biotechnol. Prog.* 23, 187–193. doi: 10.1021/bp060155w

Malda, J., Kreijveld, E., Temenoff, J. S., Van Blitterswijk, C. A., and Riesle, J. (2003). Expansion of human nasal chondrocytes on macroporous microcarriers enhances redifferentiation. *Biomaterials* 24, 5153–5161. doi: 10.1016/s0142-9612(03)00428-9

Betrachtungen, T. (1968). Suspending of solid particles in liquid by agitators. *Chem. Eng. Sci.* 9, 244–253. doi: 10.1016/0009-2509(58)85031-9

Gupta, P., Geris, L., Luyten, F. P., and Papantoniou, I. (2018). An Integrated Bioprocess for the Expansion and Chondrogenic Priming of Human Periosteum-Derived Progenitor Cells in Suspension Bioreactors. *Biotechnol. J.* 13, 1700087. doi: 10.1002/biot.201700087

Schop, D., Janssen, F. W., van, Rijn LD, Fernandes, H., Bloem, R. M., de Bruijn, J. D., et al. (2009). Growth, Metabolism, and Growth Inhibitors of Mesenchymal Stem Cells. *Tissue Eng Part A* 15, 1877–1886.

Lobner, D. (2000). Comparison of the LDH and MTT assays for quantifying cell death: Validity for neuronal apoptosis? *J. Neurosci. Methods* 96, 147–152. doi: 10.1016/s0165-0270(99)00193-4

Kehoe, D., Schnitzler, A., Simler, J., Dileo, A., and Ball, A. (2012). Scale-up of human mesenchymal stem cells on microcarriers in suspension in a single-use bioreactor. *BioPharm Int.* 25, 28–39.

Petry, F., Smith, J. R., Leber, J., Salzig, D., Czermak, P., and Weiss, M. L. (2016). Manufacturing of human umbilical cord mesenchymal stromal cells on microcarriers in a dynamic system for clinical use. *Stem Cells Int* 4834616, 2016.

De Bari, C., Dell'Accio, F., and Luyten, F. P. (2001). Human periosteum-derived cells maintain phenotypic stability and chondrogenic potential throughout expansion regardless of donor age. *Arthritis Rheum.* 44, 85–95. doi: 10.1002/1529-0131(200101)44:1<85::aid-anr12>3.0.co;2-6

Rafiq, Q. A., Coopman, K., Nienow, A. W., and Hewitt, C. J. (2016). Systematic microcarrier screening and agitated culture conditions improves human mesenchymal stem cell yield in bioreactors. *Biotechnol. J.* 11, 473–486. doi: 10.1002/biot.201400862

Ferrari, C., Balandras, F., Guedon, E., and Olmos, E. I (2012). Chevalot, and A. Marc, Limiting cell aggregation during mesenchymal stem cell expansion on microcarriers. *Biotechnol. Prog.* 28, 780–787. doi: 10.1002/btpr.1527

Jossen, V., van den Bos, C., Eibl, R., and Eibl, D. (2018). Manufacturing human mesenchymal stem cells at clinical scale: process and regulatory challenges. *Appl. Microbiol. Biotechnol.* 102, 3981–3994. doi: 10.1007/s00253-018-8912-x

Hewitt, C. J., Lee, K., Nienow, A. W., Thomas, R. J., Smith, M., and Thomas, C. R. (2011). Expansion of human mesenchymal stem cells on microcarriers. *Biotechnol. Lett.* 33, 2325–2335. doi: 10.1007/s10529-011-0695-4

Dominici, M., Le Blanc, K., Mueller, I., Slaper-Cortenbach, I., Marini, F., Krause, D., et al. (2006). Minimal criteria for defining multipotent mesenchymal stromal cells. The International Society for Cellular Therapy position statement. *Cytotherapy* 8, 315–317. doi: 10.1080/14653240600855905

dos Santos, F., Andrade, P. Z., Abecasis, M. M., Gimble, J. M., Chase, L. G., Campbell, A. M., et al. (2011). Toward a Clinical-Grade Expansion of Mesenchymal Stem Cells from Human Sources: A Microcarrier-Based Culture System Under Xeno-Free Conditions. *Tissue Eng. Part C Methods* 17, 1201–1210. doi: 10.1089/ten.tec.2011.0255

Potapova, I. A., Brink, P. R., Cohen, I. S., and Doronin, S. V. (2008). Culturing of human mesenchymal stem cells as three-dimensional aggregates induces functional expression of CXCR4 that regulates adhesion to endothelial cells. *J. Biol. Chem.* 283, 13100–13107. doi: 10.1074/jbc.m800184200

Frith, J. E., Thomson, B., and Genever, P. G. (2010). Dynamic three-dimensional culture methods enhance mesenchymal stem cell properties and increase therapeutic potential. *Tissue Eng. - Part C Methods* 16, 735–749. doi: 10.1089/ten.tec.2009.0432

Brown, M. A., Wallace, C. S., Anamelechi, C. C., Clermont, E., Reichert, W. M., and Truskey, G. A. (2007). The use of mild trypsinization conditions in the detachment of endothelial cells to promote subsequent endothelialization on synthetic surfaces. *Biomaterials* 28, 3928–3935. doi: 10.1016/j.biomaterials.2007.05.009

Ikeda, T., Kawaguchi, H., Kamekura, S., Ogata, N., Mori, Y., Nakamura, K., et al. (2005). Distinct roles of Sox5, Sox6, and Sox9 in different stages of chondrogenic differentiation. *J. Bone Miner. Metab.* 23, 337–340. doi: 10.1007/s00774-005-0610-y

Ji, W., Bolander, J., Chai, Y. C., Katagiri, H., Marechal, M., and Luyten, F. P. (2017). *Bone Morphogenetic Proteins: Systems Biology Regulators*. Cham: Springer.

Tucker, D., Still, K., Blom, A., and Hollander, A. P. (2020). Over-Confluence of expanded bone marrow mesenchymal stem cells ameliorates their chondrogenic capacity in 3D cartilage tissue engineering. *bioRxiv*. doi: 10.1101/2020.01.08.897645

Weiss, H. E., Roberts, S. J., Schrooten, J., and Luyten, F. P. (2012). A Semi-Autonomous Model of Endochondral Ossification for Developmental Tissue Engineering. *Tissue Eng. Part A* 18, 1334–1343. doi: 10.1089/ten.tea.2011.0602

Kerckhofs, G., Chai, Y. C., Luyten, F. P., and Geris, L. (2016). Combining microCT-based characterization with empirical modelling as a robust screening approach for the design of optimized CaP-containing scaffolds for progenitor cell-mediated bone formation. *Acta Biomater.* 35, 330–340. doi: 10.1016/j.actbio.2016.02.037

Roberts, S. J., Geris, L., Kerckhofs, G., Desmet, E., Schrooten, J., and Luyten, F. P. (2011). The combined bone forming capacity of human periosteal derived cells and calcium phosphates. *Biomaterials* 32, 4393–4405. doi: 10.1016/j.biomaterials.2011.02.047

Conflict of Interest: The authors declare that the research was conducted in the absence of any commercial or financial relationships that could be construed as a potential conflict of interest.

frontiers in Bioengineering and Biotechnology

ORIGINAL RESEARCH
published: 26 May 2021
doi: 10.3389/fbioe.2021.619930

A Chemically Defined, Xeno- and Blood-Free Culture Medium Sustains Increased Production of Small Extracellular Vesicles From Mesenchymal Stem Cells

Aliosha I. Figueroa-Valdés[1,2,3†], Catalina de la Fuente[1,2,3†], Yessia Hidalgo[1,2,3], Ana María Vega-Letter[1,2,3], Rafael Tapia-Limonchi[1], Maroun Khoury[1,2,3,4] and Francisca Alcayaga-Miranda[1,2,3,4*]*

[1] Cells for Cells, Santiago, Chile, [2] Consorcio Regenero, Chilean Consortium for Regenerative Medicine, Santiago, Chile, [3] Laboratory of Nano-Regenerative Medicine, Centro de Investigación e Innovación Biomédica (CiiB), Universidad de los Andes, Santiago, Chile, [4] School of Medicine, Faculty of Medicine, Universidad de los Andes, Santiago, Chile

OPEN ACCESS

Edited by:
Dominik Egger,
University of Natural Resources and Life Sciences, Vienna, Austria

Reviewed by:
Federica Collino,
University of Padua, Italy
Verena Börger,
Essen University Hospital, Germany

***Correspondence:**
Francisca Alcayaga-Miranda
falcayaga@uandes.cl
Maroun Khoury
mkhoury@uandes.cl

[†] These authors have contributed equally to this work

Specialty section:
This article was submitted to Preclinical Cell and Gene Therapy, a section of the journal Frontiers in Bioengineering and Biotechnology

Received: 21 October 2020
Accepted: 14 April 2021
Published: 26 May 2021

Citation:
Figueroa-Valdés AI, de la Fuente C, Hidalgo Y, Vega-Letter AM, Tapia-Limonchi R, Khoury M and Alcayaga-Miranda F (2021) A Chemically Defined, Xeno- and Blood-Free Culture Medium Sustains Increased Production of Small Extracellular Vesicles From Mesenchymal Stem Cells. Front. Bioeng. Biotechnol. 9:619930. doi: 10.3389/fbioe.2021.619930

Cell therapy is witnessing a notable shift toward cell-free treatments based on paracrine factors, in particular, towards small extracellular vesicles (sEV), that mimic the functional effect of the parental cells. While numerous sEV-based applications are currently in advanced preclinical stages, their promised translation depends on overcoming the manufacturing hurdles posed by the large-scale production of purified sEV. Unquestionably, the culture medium used with the parental cells plays a key role in the sEV's secretion rate and content. An essential requisite is the use of a serum-, xeno-, and blood-free medium to meet the regulatory entity requirements of clinical-grade sEV's production. Here, we evaluated Oxium^{TM}EXO, a regulatory complying medium, with respect to production capacity and conservation of the EV's characteristics and functionality and the parental cell's phenotype and viability. A comparative study was established with standard DMEM and a commercially available culture medium developed specifically for sEV production. Under similar conditions, Oxium^{TM}EXO displayed a three-fold increase of sEV secretion, with an enrichment of particles ranging between 51 and 200 nm. These results were obtained through direct quantification from the conditioned medium to avoid the isolation method's interference and variability and were compared to the two culture media under evaluation. The higher yield obtained was consistent with several harvest time points (2, 4, and 6 days) and different cell sources, including umbilical cord-, menstrual blood-derived mesenchymal stromal cells and fibroblasts. Additionally, the stem cell phenotype and viability of the parental cell remained unchanged. Furthermore, Oxium^{TM}EXO-sEV showed a similar expression pattern of the vesicular markers CD63, CD9, and CD81, with respect to sEV derived from the other conditions. The *in vitro* internalization assays in different target cell types and the pharmacokinetic profile of intraperitoneally administered sEV *in vivo* indicated that the higher EV production rate did not affect the uptake kinetics or the systemic biodistribution in healthy mice. In conclusion, the

Oxium^{TM}EXO medium sustains an efficient and robust production of large quantities of sEV, conserving the classic functional properties of internalization into acceptor target cells and biodistribution *in vivo*, supplying the amount and quality of EVs for the development of cell-free therapies.

Keywords: small extracellular vesicle, exosome, culture medium, xeno-free cell culture, blood-free cell culture, serum-free cell culture, chemically defined, mesenchymal stem (stromal) cells

INTRODUCTION

The therapeutic effects of mesenchymal stem/stromal cells (MSCs) are predominantly based on their secretome, consisting of bioactive secretion of factors and, notably, extracellular vesicles (EV) (Camussi et al., 2013; Pegtel and Gould, 2019; Witwer et al., 2019). Currently, about 1,175 MSC-related clinical trials are listed in the NIH clinical trial database (search carried out in September 2020)[1]. A few dozen cell-based therapies have obtained market authorization in several countries (Cuende et al., 2018), and at least another dozen of approved MSC-based therapies are expected to reach the market by the year 2030 (Olsen et al., 2018). We have recently demonstrated (Kurte et al., 2020) that MSC's high immunoplasticity depends on the exposure duration with the inflammatory milieu, leading into either an enhanced or an impairment therapeutic activity, a matter of great concern for their clinical use. Both the translational advances and the limitation of the use of MSC in some clinical applications have pushed the field toward exploring their therapeutic potential without the need for cell transplantation.

Small extracellular vesicles (sEV) are non-self-replicative lipid-based vesicles secreted by virtually all types of cells under both physiological and pathological conditions (Kalluri and LeBleu, 2020). Unlike cell-based therapy, the use of sEV therapeutics is free of safety concerns related to uncontrolled cell division and immune rejection (Alcayaga-Miranda et al., 2016; Baharlooi et al., 2020). sEV are characterized by bodies smaller than 200 nm in diameter with tetraspanins CD63, CD81, and CD9 present in their membrane (Théry et al., 2018; Witwer et al., 2019). The innovative cell-free strategy based on the application of EV provides the functional effect of the parental stem cell without the negative influence of the pathological environment on their secretion profile. Their role in regenerative medicine is based on the fact that they could "mediate most of beneficial regenerative effects of MSCs without possible side effects of using MSCs themselves" (Sagaradze et al., 2018), showing similar or even superior therapeutic capacity than the treatment with their parental MSCs (Willis et al., 2017). Considering the burst of interest in their biological effects, the use of sEV as cell-free therapy is widely under investigation with promissory preclinical results (Lener et al., 2015; Alcayaga-Miranda et al., 2016; Rosenberger et al., 2019). Moreover, the choice of using sEV over liposomes and other artificial nanoparticles such as nanocarriers has been backed by their higher stability (Askenase, 2020). Currently, only a handful of sEV-based therapeutics have evolved to a state that is mature enough for clinical evaluation (Zipkin, 2019). When products retain uncertainties regarding early steps of development and manufacturing validation, such as reagent use and procedures, their clinical application is faced by regulatory hurdles and reluctant sponsors, hindering their translational pathway (Mastrolia et al., 2019).

The cell culture industry, considered as the main pillar of the biopharmaceutical market, is witnessing a drift away from fetal bovine serum (FBS)-based formulations, favoring the development of chemically defined media, especially for clinical-grade cultures (Kalorama Information, 2018). According to regulatory agencies, manufacturers of human biological medicinal products must favor the use of non-ruminant material in order to avoid the risky use of potentially infectious materials (United States Food and Drug Administration, 2020). Their guidelines propose the use of human platelet lysate (hPL) as an alternative to FBS (European Medicines Agency, 2013; Guiotto et al., 2020). Therefore, new media formulations containing xeno- and blood-free components are required to circumvent the regulatory restrictions, ensuring at the same time the performance consistency in cell culture media. Amidst the cells with therapeutic potential, MSCs are considered as "a critical raw material for regenerative medicine products, including cell-based therapies, engineered tissues, or combinations products" (Olsen et al., 2018).

Since FBS or hPL are supplements rich in their own sEV, the production of both research and clinical-grade sEV must be carried out in exogenous sEV-free medium in order to avoid the contamination of the produced and the exogenous sEV. The use of a serum-depleted medium or medium without FBS (often called "serum starvation") provides an undesired stress environment, which is suboptimal for cell growth and viability, and therefore an undesirable reduction in the secretory rate of sEV to the supernatant (Lehrich et al., 2018; Haraszti et al., 2019). Furthermore, the generated oxidative-stress products can be shuttled within the sEV cargo, leading to important concerns for functional changes and adverse effects. In order to reduce time and resources needed to produce a therapeutic dose, new compliant media are required as the central part of the GMP-compliant manufacturing strategy for increased and reproducible sEV production. A defined and consistent protocol devoid from contaminant and oxidative stress agents will fulfill the quality-control requirements necessary for batch releases, regulation fulfillment, and the taking of sEV's advantages, such as low toxicity, biocompatibility, biological permeability/distribution, ease of handling and storage, and the possibility of loading them in order to use them as drug-delivery vehicles (Roura and Bayes-Genis, 2019; Zipkin, 2019).

Abbreviations: sEV, Small Extracellular Vesicles; DMEM, Dulbecco's Modified Eagle Medium; UC-MSCs, Umbilical Cord-derived Mesenchymal Stromal Cells; NTA, Nanoparticle Tracking Analysis; OA, Osteoarthrosis.

[1]www.clinicaltrials.gov

Here, we report the use of a new serum-, xeno-, and blood-free medium (Oxium^{TM}EXO), tested for the production of extracellular vesicles from umbilical cord-derived human MSCs (UC-MSCs), menstrual blood-derived human MSCs (Mens-MSCs), and fibroblasts. UC-MSCs were chosen because previous work in our laboratory showed that these cells exhibit higher clonogenic, proliferative, and migration potential than bone marrow-derived MSCs (BM-MSCs) and enhanced the secretion of chondrogenic factors (González et al., 2015; Bartolucci et al., 2017). The latter led to probe and demonstrate their safety and efficacy as cell therapy for knee osteoarthritis treatment (Park et al., 2017; Matas et al., 2019). In a similar way, our laboratory and others had demonstrated several therapeutic effects of Mens-MSCs, including antitumor properties (Alcayaga-Miranda et al., 2016; Chen et al., 2019; Rosenberger et al., 2019), and their superiority with respect to several functional aspects in comparison with BM-MSCs (Alcayaga-Miranda et al., 2015a), making them interesting candidates for research in cell-based or cell-free cancer treatments, research that is still ongoing today in our lab. Finally, fibroblasts were used as a non-MSC cell lineage control. Compared to standard (DMEM) and commercially available medium, the cell culture in Oxium^{TM}EXO showed a superior performance in terms of sEV-production numbers while maintaining MSCs and sEV characteristics *in vitro* and *in vivo*. Oxium^{TM}EXO can represent an alternative to produce sEV from tissue-derived human MSCs, applicable from the bench to a large-scale platform, while maintaining cell phenotype and multipotency potential of the sEV cell source.

MATERIALS AND METHODS

Ethics Statement

Menstrual blood and umbilical cord were collected from healthy donors, and osteoarthritis (OA) cartilage was obtained from patients undergoing hip surgery. All tissue samples were collected after written informed consent following institutional guidelines and ethical committee approval. All animal studies were performed at the Cells for Cells Animal Facility in accordance with protocols revised and approved by the Institutional Animal Care and Use Committee of Universidad de los Andes.

Cell Culture, MSC Characterization, and hPL Preparation

Mesenchymal stromal cells (MSCs) were isolated, characterized, cultured, and expanded as we previously described (Alcayaga-Miranda et al., 2015a,b; Bartolucci et al., 2017; Matas et al., 2019) and cryopreserved at low passage (<5) until use. Briefly, cells were cultured in a maintenance medium composed of Dulbecco's modified Eagle's medium (DMEM), high glucose, supplemented with 1% penicillin/streptomycin solution (10,000 U/mL and 10,000 μg/mL, respectively), 1% L-glutamine (200 mM) (all from Gibco, Paisley, United Kingdom), and 5% human platelet lysate (hPL).

All MSCs were characterized according to the guidelines of the International Society for Cell and Gene Therapy (ISCT) (Dominici et al., 2006). The trilineage differentiation capacity of UC-MSCs cultured for 6 days in DMEM, Oxium^{TM}EXO, or commercial medium was evaluated using the StemPro^{TM} differentiation kits (Gibco, Life Technologies, New York, NY, United States) in accordance with the manufacturer's instructions with some modifications. In brief, to induce osteogenic differentiation, cells were grown at 5×10^4 cells/cm^2 with StemPro^{TM} Osteogenesis Differentiation Kit (Cat. #A1007201). After 14 days, calcium deposits were detected by Alizarin Red staining (Sigma-Aldrich, Merck, St. Louis, MO, United States, Cat. #A3757). To induce adipogenic differentiation, cells were incubated with StemPro^{TM} Adipogenesis differentiation kit (Cat. #A1007001) medium at 1×10^4 cells/cm^2. After 14 days, cell differentiation into adipocytes was confirmed by Oil Red O staining of lipidic vacuoles (Sigma-Aldrich, Merck, St. Louis, MO, United States, Cat. #O0625). For chondrogenic differentiation, cells were incubated at 1.7×10^5 cells/μL in 10 μL of culture medium for 1 h to favor micromass formation. Then, cells were cultured in StemPro^{TM} Chondrogenesis differentiation kit (Cat. #A1007101) differentiation medium according to the manufacturer's instructions for 21 days, assessing chondrogenic differentiation with Safranin O staining (Sigma-Aldrich, Merck, St. Louis, MO, United States, Cat. #S2255). Immunophenotyping of MSCs was performed by staining with monoclonal antibodies against CD105 (Cat. #560819), CD90 (Cat. #555596), CD73 (Cat. #561258), HLA-DR-DP-DQ (Cat. #555558), CD34 (Cat. #555824), CD19 (Cat. #644491), CD14 (Cat. #555398), and CD45 (Cat. #5554829) (all from BD Pharmingen, San Diego, CA, United States) using standard protocol. The staining was performed for 20 min at 4°C in darkness, and the dead cells were discarded using Live/Dead fixable yellow stain (Life Technologies, Carlsbad, CA, United States, Cat. #L34968). The analysis was performed by flow cytometry using a FACSCanto^{TM} II cytometer (BD Biosciences, San Jose, CA, United States). The data acquired were analyzed using the FlowJo software V10 (Tree Star, Ashland, OR, United States). The analysis was performed on a minimum of three different cell cultures with cells at passage 5.

To prepare hPL, human-donor platelets (n = 20) were obtained from a blood bank using the platelet apheresis method. hPL was prepared in accordance with a previously described method with some modifications (Burnouf et al., 2016). Briefly, 20-donor pooled groups of platelets were thawed at 37°C for 3 h and then frozen at −80°C overnight. The thaw-and-freeze steps were repeated two times. To remove membrane fragments, the lysate was centrifuged at 13,000 g at 4°C for 20 min and the supernatant was filtered through a 40-μm cell strainer (Falcon, Corning, Tewksbury, MA, United States, Cat. #352340). For the depletion of fibrinogen, 10% w/v sterile $CaCl_2$ (Laboratorio Sanderson, Santiago, Chile, Sanitary Registration #F13540/14) was added to a final concentration of 10 mM. The solution was incubated at 37°C for 2 h to allow the formation of fibrinogen clot, then vortexed for the disruption of the clot and centrifuged at 13,000 g for 15 min at 4°C. The supernatant was filtered in a 40-μm cell strainer, mixed, and aliquoted to freeze at −80°C until use.

Chondrocytes were isolated, characterized, cultured, and expanded as previously described (Rackwitz et al., 2014). Human MSCs and human chondrocytes were donated by Cells for Cells

(Las Condes, Santiago, Chile)[2]. Normal human dermal fibroblasts were purchased from Lonza (Walkersville, MD, United States, Cat. #CC-2511), and the metastatic human breast cancer MD-MB-231 cell line was obtained from the American Type Culture Collection (Manassas, VA, United States, Cat. #HTB-26™) and cultured according to the manufacturer's protocol. All cells were maintained in a humidified incubator (37°C; 5% CO_2) and regularly tested for mycoplasma contamination using a PCR detection kit (Applied Biological Materials Inc., Richmond, BC, Canada, Cat. #G238) according to manufacturer's instructions.

Apoptosis Assay

The cellular apoptosis was evaluated following the protocol as previously described by our group (Rosenberger et al., 2019). Briefly, 6,250 cells/cm^2 were seeded in 100 mm plates (Falcon, Franklin Lakes, NJ, United States, Cat. #353003) in maintenance medium. After 48 h, the culture medium was removed, and the cells were washed three times with phosphate-buffered saline (PBS 1×) before starting the culture in the different induction medium: (a) DMEM high glucose + 1% L-glutamine; (b) Oxium™EXO (Consorcio Regenero S.A., Las Condes, Santiago, Chile; patent No. PCT/CL2019/100175, Tapia-Limonchi et al., 2019); or (c) commercial medium (RoosterBio Inc., Frederick, MD, United States, Cat. #M2001). After 6 days, cell supernatants were mixed with the trypsinized cells in order to include detached dead cells in the analysis. Then, cells were stained with Annexin V-APC (BioLegend, San Diego, CA, United States, Cat. #640920) and 7-aminoactinomycin D (7-AAD) (BioLegend, San Diego, CA, United States, Cat. #420403) in Annexin V binding buffer (BioLegend, San Diego, CA, United States, Cat. #422201). The analysis was performed by flow cytometry using a FACSCanto™ II cytometer (BD Biosciences, San Jose, CA, United States). The data acquired were analyzed using the FlowJo software V10 (Tree Star, Ashland, OR, United States).

Small Extracellular Vesicle Production, Isolation, Characterization, and Staining

Small extracellular vesicles were produced and purified as previously described by our group with some modifications (Alcayaga-Miranda et al., 2016; Lopez-Verrilli et al., 2016; Rosenberger et al., 2019). Briefly, UC-MSC cells in passage 5 were seeded and expanded in a maintenance medium on three 10-layer Nunc™ EasyFill™ Cell Factory™ systems (Thermo Fisher Scientific, Waltham, MA, United States, Cat. #140400) with a density of 6,250 cells/cm^2. After cells reached ∼70% confluence, the maintenance medium was discarded and cells were washed three times with PBS 1× before addition of the induction media for sEV production: (a) DMEM high glucose + 1% L-Glutamine; (b) Oxium™EXO (patent No. PCT/CL2019/100175); or (c) commercial medium (RoosterBio Inc., Frederick, MD, United States, Cat. #M2001). After 6 days, supernatants were collected and divided into two (in order to achieve two independent sEV's isolations per medium), subjected to serial centrifugations of 600 and 2,000 *g* for 10 min at 4°C and sequential filtration with 0.45- and 0.22-μm pore-size PVDF membranes, to later be subjected to ultracentrifugation (Thermo Electron LED GmbH, Langenselbold, Germany, model Sorvall WX+) at 100,000 *g* for 70 min at 4°C in a swinging bucket rotor (Thermo Fisher Scientific, Waltham, MA, United States, Model TH-641). The pellet obtained was resuspended in approximately 100 μl of PBS 1× and stored at −80°C until use. A diagram of the protocol for cell cultures for sEV production and isolation is shown in **Supplementary Figure 1**.

Nanoparticle tracking analysis (NTA) was performed on a NanoSight NS300 system (Malvern Instruments Limited, Worcestershire, United Kingdom) to determine particle concentration and size distribution following the manufacturer's instructions. Briefly, sEV fractions were processed in duplicate and diluted with PBS 1× over a range of concentration to obtain between 10 and 100 particles per image. sEV samples were mixed before the analysis. Five videos of 60 s each per sample were captured (camera level = 8), processed (detection threshold = 3), and analyzed to give the mean and mode of the particle's size, together with a total particle concentration. Further analyses of the collected data allowed the determination of particle concentration according to different size ranges of interest: 0–50 nm; 51–200 nm; 201–300 nm, and those over 301 nm.

Small extracellular vesicles characterization was performed following the International Society for Extracellular Vesicles guidelines (Théry et al., 2018). The evaluation of surface markers of isolated sEV was done as described previously with some modifications (Suárez et al., 2017; Mendt et al., 2018). Briefly, 1.4 × 10^9 particles resuspended in PBS 1× (400 μL) were incubated with Aldehyde/Sulfate Latex beads (1 μL) (Molecular Probes, Eugene, OR, United States, Cat. #A37304) in a rotatory mixer for 10 min at room temperature (RT). After the addition of PBS 1× (final volume of 800 μL), samples were incubated overnight in a rotatory mixer at 4°C. Four hundred microliters of 1 M glycine (0.33 M final concentration; United States Biological, Salem, MA, United States, Cat. #G8160) was added to the samples and incubated through continuous mixing for 1 h at RT. The samples were centrifuged at 8,000 *g* for 2 min at 4°C, and the pellet was resuspended in 100 μL 10% w/v Bovine Serum Albumin (BSA; Winkler Ltda., Santiago, Chile, Cat. #BM-0150) prepared in PBS 1× and incubated with continuous mixing for 45 min at RT. Then, the pellet was resuspended in 10 μL of 2% BSA solution containing separately the primary antibodies (0.5 μL) mouse α-human CD63 (Cat. #556019), CD81 (Cat. #555675), and CD9 (Cat. #555370) (all from BD Pharmingen San Diego, CA, United States) or containing the isotype control (5 μL) mouse IgG_1 (BD Biosciences, San Jose, CA, United States, Cat. #349040); the incubations were performed under continuous mixing for 30 min at RT. The immunolabeled particle-coupled beads were washed once with PBS 1× and incubated with 25 μL of 10% BSA solution for 30 min at RT, to carry out a second wash step with PBS 1×. The pellet was resuspended in 10 μL solution containing 2% BSA and 0.5 μL of secondary antibody α-mouse IgG_1 Alexa Fluor 488 (BioLegend, San Diego, CA, United States, Cat. #406626) and incubated for 30 min at RT. Finally, the sample was washed three times with PBS 1× and the pellet was resuspended in 100 μL of PBS 1× for the acquisition on the cytometer.

[2]www.c4c.cl

The samples were analyzed on the cytometer FACSCanto™ II cytometer (BD Biosciences, San Jose, CA, United States) and were recorded with at least 1×10^5 events of beads. The data were analyzed using FlowJo software V10 (Tree Star, Ashland, OR, United States).

For western blot analyses, whole UC-MSC (obtained after 6 days of culture in DMEM, Oxium™EXO or commercial medium) and isolated sEV lysates were obtained with RIPA 1× buffer containing 1% w/v of protease inhibitor cocktail (Roche Diagnostics, Mannheim, Germany, Cat. #118735800001). Total protein concentrations were determined with Pierce BCA Protein Assay Kit (Thermo Scientific, Rockford, IL, United States, Cat. #23225), and 2.5 μg of each cell lysate or its corresponding sEV-lysate sample was mixed with Laemmli buffer 5×, heated for 5 min at 95°C, separated on 4–20% gels by SDS-PAGE, and transferred to PVDF membranes (GE Healthcare Limited, Chicago, IL, United States, Cat. #RPN303F). Membranes were blocked for 1 h at RT in Odyssey® Blocking Buffer (LI-COR Biosciences, Lincoln, NE, United States, Cat. #927-400000). Primary antibodies used were Syntenin-1 (1:1000; Novus Biologicals, Centennial, CO, United States, Cat. #NBP2-76873), Flotillin-1 (1:2000; Abcam Inc., Cambridge, MA, United States, Cat. #ab133497), Calnexin (1:2,000; Abcam Inc., Cambridge, MA, United States Cat. #ab22595), and TOMM20 (1:1,000; Novus Biologicals, Centennial, CO, United States, Cat. #NBP2-67501). For fluorescence detection of proteins, Invitrogen™ Goat anti-Rabbit (H + L) Highly Cross-Adsorbed secondary antibody, Alexa Fluor Plus 800, was used (1:25,000; Thermo Fisher Scientific, Waltham, MA, United States, Cat. #A32735). Protein signals were captured using a LI-COR Odyssey® imaging system (LI-COR Biosciences, Lincoln, NE, United States). For probing of other proteins on the same membrane, the membranes were washed three times for 10 min before re-incubation of the next primary antibody.

To verify the sEV structure, isolated sEV samples were visualized using transmission electron microscopy (TEM) as previously described (Zavala et al., 2020). Briefly, solutions of 2×10^9 particles in 12 μL final volume (completed with filtered PBS 1×) for each sample were prepared and deposited on formvar/carbon-coated copper meshes (Electron Microscopy Sciences, Hatfield, PA, United States, Cat. #FCF300-CU) for 1 min, followed by negative staining with 15 μL of 2% w/v uranyl acetate solution for 1 min and dried at RT for 15 min. Imaging was performed at the Advanced Microscopy Facility UMA UC on a Tecnai 12 BioTwin transmission electron microscope (operated at 80 kV; FEI Company, Eindhoven, Netherlands) with iTEM software (Olympus Soft Imaging Solutions GmbH, Münster, Germany). Representative images of each sample were taken at 6,000× and 20,500× magnifications.

Staining of sEV for *in vitro* and *in vivo* tracking was performed with the lipophilic near-infrared fluorescent cyanine dye DiR (Biotium, Fremont, CA, United States, Cat. #60017) as previously described by our group (Rosenberger et al., 2019). Briefly, purified sEV were incubated in the dark for 1 h at 37°C with DiR at a concentration of 71 μM and then washed using MW 3000 size-exclusion exosome spin columns (Invitrogen, Carlsbad, CA, United States, Cat. #4484449) according to the manufacturer's instructions. After the spin column, the stained particles were analyzed to determine the concentration through NTA as described above. Note that the same volume of incubation was used in the case of PBS + dye controls.

Secretion Rate of Cell Culture–Derived sEV

Cells were seeded at a density of 6,250 cells/cm^2 in a six-well plate in a maintenance medium (1 mL/well). Once ∼70% confluence was reached, the culture medium was discarded, and the cells were washed three times with PBS 1× before addition of the induction medium (DMEM or Oxium™EXO or commercial) for sEV secretion. At different time points (2, 4, and 6 days), the supernatant (1 mL) was collected and evaluated directly through NTA to quantify the particles and to determine the mean and mode of particle size, as described above. The particle yield was calculated by dividing the number of particles by the number of seeded cells following the Minimal Information for Studies of Extracellular Vesicles (MISEV) guidelines (Théry et al., 2018).

Cellular Uptake of sEV

The evaluation of the uptake of isolated sEV generated in the different induction media was carried out as previously described by our group (Alcayaga-Miranda et al., 2016; Rosenberger et al., 2019). In brief, cells were seeded at a density of 10,000 cells/well in a 24-well format. After 24 h, cells were incubated with DiR-stained sEV (3.8×10^3 part/cell) for 6 h at 37°C. As negative controls of the internalization, the experiment was performed at 4°C, and one well at each temperature was incubated with PBS + DiR solution without sEV. To quantitatively measure the exosome uptake, the cells were trypsinized, washed with PBS 1×, and analyzed for DiR signal on the cytometer FACSCanto™ II cytometer (BD Biosciences, San Jose, CA, United States). The data was analyzed using FlowJo software V10 (Tree Star, Ashland, OR, United States).

In vivo Biodistribution Study

C57Bl/6j mice were purchased from Jackson Laboratories (Bar Harbor, ME, United States, Cat. #000664) and maintained at the Cells for Cells animal facility in accordance with protocols revised and approved by the Institutional Animal Care under American Association for Laboratory Animal Science (AALS) training and certification programs. To evaluate *in vivo* the biodistribution pattern of sEV produced in the different culture media, mice (20-week-old male/female) were intraperitoneally (IP) injected with a 100-μL PBS 1× solution containing $\sim 1 \times 10^8$ particles of freshly purified DiR-stained sEV and non-stained sEV (auto-fluorescence control) (n = 3 per group). Six hours postinjection, sEV's fluorescence intensities were assessed using a LI-COR Odyssey imaging system (LI-COR Biosciences, Lincoln, NE, United States) for the entire animal and excised organs, according to the manufacturer's instructions. As control of the sEV staining procedure, DiR was diluted in 100 μL PBS 1× (at a concentration of 71 μM) and then washed using size-exclusion exosome spin columns.

Statistical Analysis

Results were expressed as the mean ± SEM values. For *in vitro* data, two-way ANOVA followed by Tukey's posttest was used for analysis of multiple-comparison groups and two-tailed Student's unpaired *t*-test to compare two groups. For *in vivo* data, non-parametric tests were used dependently of each case (Kruskal–Wallis or Mann–Whitney). Statistical significance was shown as $^{*}p < 0.05$; $^{**}p < 0.01$; $^{***}p < 0.001$; $^{****}p < 0.0001$. Error bars represent the standard error of the mean (SEM). The number of data used for the statistical analyses is indicated in the figure legends and corresponds to independent experiments.

RESULTS

Proliferation, Cell Surface Markers, and Multipotentiality of UC-MSCs Grown in Oxium^{TM}EXO

In order to determine whether xeno-free media for sEV production alter the UC-MSC characteristics, we evaluated their proliferation rate, the expression of cell surface markers, and the tri-differentiation capacity. As displayed in **Figure 1A**, following 2, 4, or 6 days of culture, we found that at day 4 there is a change in the cell's morphology only seen in Oxium^{TM}EXO, forming a network which continues at least until day 6. Interestingly, from day 4 there is a significant increase in the proliferation of the cells maintained in Oxium^{TM}EXO (**Figure 1B**), reaching at day 6 a mean of 1.36×10^5 live cells, three-fold more in comparison to DMEM (4.13×10^4 live cells) and the commercial medium (4.12×10^4 live cells).

An important aspect of MSCs' compatible culture condition is the maintenance of their stem features. Through the expression analyses of typical MSC surface antigens such as CD73, CD90, and CD105, the absence of CD14, CD19, CD34, CD45, and HLA-DR (as a MSC culture-purity assessment), plus a multi-lineage differentiation potential assay to osteoblasts, adipocytes, and chondrocytes, we were able to determine the stemness of UC-MSCs after being cultured for 6 days in the different media tested for sEV production. According to flow cytometry analyses, all UC-MSCs showed MSC-proper profiles for the expression of CD73 (>95%) and CD90 (>95%). Meanwhile, CD105 expression was moderately low in all conditions (>50%). As expected, cells grown in the different media showed a very low expression of CD14, CD19, CD34, CD45, and HLA-DR (<2%) (**Figure 1C**). Next, through a gold standard mesenchymal lineage differentiation protocol, UC-MSCs cultured for sEV production for 6 days in DMEM, Oxium^{TM}EXO and a commercial medium retained the ability to differentiate into osteoblasts, adipocytes, and chondroblasts as seen by the morphology and positive staining by Alizarin Red for calcium deposits, by Oil Red O staining for lipid vacuoles and by Safranin O staining for matrix proteoglycans, respectively (**Figure 1D**). Negative controls for each type of differentiation are shown in **Supplementary Figure 2**. The present data commensurate the use of Oxium^{TM}EXO as a compatible medium for sustaining MSCs' growth while maintaining their stem cell characteristics *ex vivo*.

UC-MSCs Cultured in Oxium^{TM}EXO Exhibit a Greater Viability Level Following sEV Production Cycle

To verify the viability status of the sEV-producing cells, a flow cytometry analysis of Annexin V and 7-AAD staining was performed (**Figure 1E**). The cells cultured for 6 days in Oxium^{TM}EXO show significantly higher viability (74 ± 13%) and presented less apoptotic and cell death levels (22 ± 14%) in comparison with cells cultured in DMEM (viability = 58 ± 15%; apoptotic and death = 32 ± 17%) or in the commercial medium (viability = 67 ± 10%; apoptotic and death = 28 ± 11%).

Oxium^{TM}EXO Sustains Higher Amounts of Secreted Particles

The key of this study is to set a comparative study, assessing the cell's sEV secretion rate using different available media. The secreted particles were analyzed directly in the conditioned medium at day 2 (**Figure 2A**), day 4 (**Figure 2B**), and day 6 (**Figure 2C**) post-induction using the Nanoparticle Tracking Analysis (NTA). As displayed in **Figures 2A–D**, Oxium^{TM}EXO induces a greater secretion of particles to the conditioned medium with respect to DMEM and the commercial medium at the different time points evaluated. Specifically, as shown in **Figure 2D**, at day 2 the cells cultured in Oxium^{TM}EXO produced 60% more particles ($1.36 \times 10^9 \pm 3.49 \times 10^8$) than in the commercial medium ($8.48 \times 10^8 \pm 7.95 \times 10^7$), but there was no difference in comparison to DMEM ($1.14 \times 10^9 \pm 2.47 \times 10^8$); at day 4 post-induction, there was a higher particle concentration, over three-fold, in the Oxium^{TM}EXO conditioned medium ($4.60 \times 10^9 \pm 6.80 \times 10^8$), which is different from that obtained in DMEM ($1.40 \times 10^9 \pm 4.31 \times 10^8$), and in the commercial medium ($1.30 \times 10^9 \pm 1.66 \times 10^8$); finally, at day 6, the particle concentration continued to increase to almost four-fold in Oxium^{TM}EXO ($5.96 \times 10^9 \pm 7.11 \times 10^8$), while no significant particle concentration differences between DMEM ($1.51 \times 10^9 \pm 3.25 \times 10^8$) and commercial conditioned medium ($1.54 \times 10^9 \pm 2.45 \times 10^8$) were observed at this point.

Since the expected size range for sEV varies between 50 and 200 nm, we analyzed further the number of particles that fall under this range (Théry et al., 2018). As seen in **Figure 2E**, as early as day 2, Oxium^{TM}EXO promotes the secretion of particles within the 51–200-nm size range (69 ± 4.6%), enrichment that is maintained through days 4 (72 ± 5.1%) and 6 (74 ± 2.8%) post-induction. In terms of particle concentration, Oxium^{TM}EXO induces a higher concentration of particles within the 51–200-nm size range at day 4 ($3.82 \times 10^9 \pm 9.05 \times 10^8$) and day 6 ($4.95 \times 10^9 \pm 5.33 \times 10^8$) in comparison to DMEM (day 4 = $1.09 \times 10^9 \pm 6.47 \times 10^8$; day 6 = $1.22 \times 10^9 \pm 5.01 \times 10^8$) and commercial medium (day 4 = $9.61 \times 10^8 \pm 4.10 \times 10^8$; day 6 = $1.15 \times 10^9 \pm 5.19 \times 10^8$), as it is shown in **Figure 2F**. In line with the latter results, the yield of particles per cell was higher in Oxium^{TM}EXO (day 2 = 22,765 ± 5,825; day 4 = 76,673 ± 11,344; day 6 = 99,403 ± 11,850) compared to

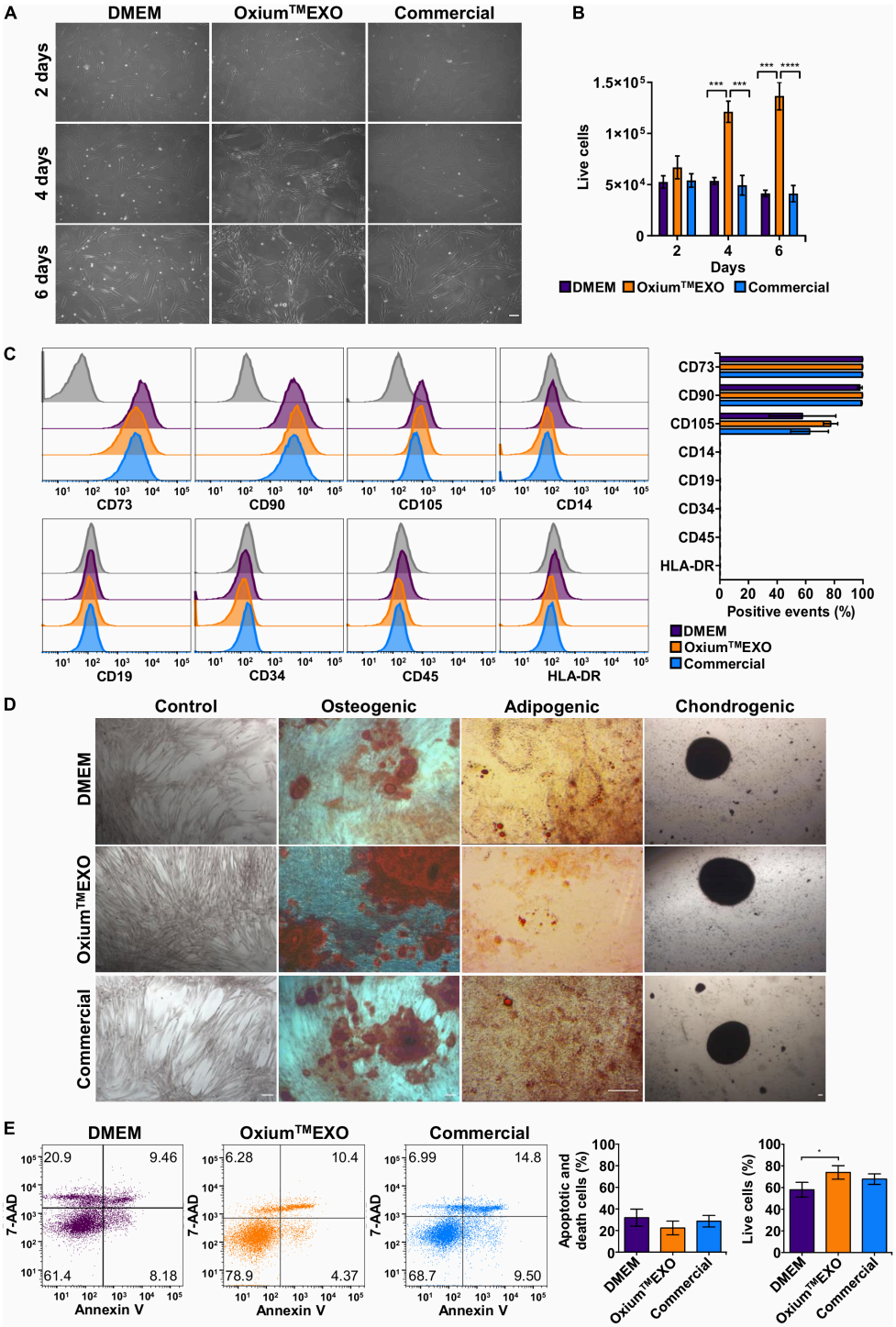

FIGURE 1 | Characterization of UC-MSCs cultured in DMEM, Oxium^{TM}EXO, and commercial medium for sEV production. Umbilical cord-derived mesenchymal stromal cells (UC-MSCs) were evaluated at 2, 4, or 6 days post-induction of sEV secretion with DMEM, Oxium^{TM}EXO, and commercial medium. **(A)** Microscope images showing cell morphology at the different days post-induction, acquired with an Olympus CKX41 microscope using 10× magnification (scale bar 100 μm). **(B)** After 2, 4, and 6 days post-induction, live cells were counted with the Neubauer chamber. $^{**}P < 0.01$, $^{****}P < 0.0001$, two-way ANOVA, followed by Tukey's comparison test. **(C)** Flow cytometry analysis of MSCs' classical surface and purity-control antigens at 6 days post-induction. Histograms of fluorescence intensity for each marker assayed are shown; gray histograms correspond to unstained cell control for each marker. Quantification of positive events for each marker is shown in terms of percentage of total events. **(D)** Multilineage differentiation capacity of UC-MSCs previously cultured for 6 days in the different induction media. Representative images are shown. **(E)** Detection of apoptosis and cell death according to Annexin V/7-AAD staining and its quantification 6 days post-induction. A representative dot plot is shown for each condition. The graphs show mean ± SEM, $n = 6$. $^{*}P < 0.05$, One tailed t-student.

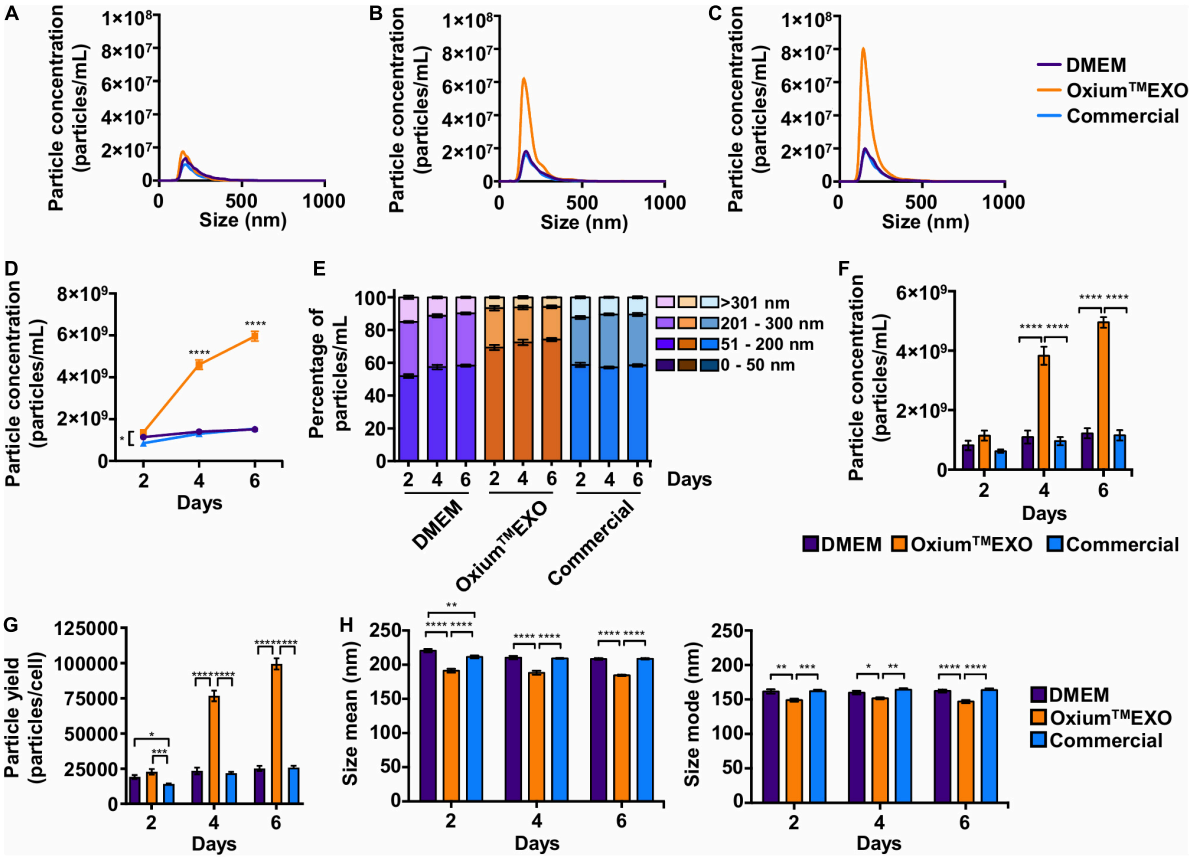

FIGURE 2 | Comparative particle secretion assessment in UC-MSCs cultured in DMEM, Oxium^{TM}EXO, and commercial medium for sEV production. Conditioned media were collected at 2, 4, and 6 days post-induction and analyzed by NTA to assess the particle secretion capacity of cells cultured in DMEM, Oxium^{TM}EXO, and commercial medium. The graphs show the particles' concentrations according to their size after **(A)** 2 days, **(B)** 4 days, and **(C)** 6 days post-induction. **(D)** Total particles' concentration found after 2, 4, and 6 days post-induction with the different media. **(E)** Percentage distribution of particles' concentrations according to their size: 0–50 nm, 51–200 nm, 201–300 nm, and >301 nm. **(F)** Concentrations of particles in the size range of 51–200 nm. $^{****}P < 0.0001$, two-way ANOVA, followed by Tukey's comparison test. **(G)** Number of particles produced by cells in the different media at 2, 4, and 6 days, respectively. **(H)** Particle size's mean and mode obtained in the different media at 2, 4, and 6 days, respectively. $^{**}P < 0.01$, $^{****}P < 0.0001$, two-way ANOVA, followed by Tukey's comparison test. **(A–C)** Graphs show the mean of particle concentrations of five independent-recorded NTA videos. **(D–H)** Graphs show mean ± SEM, $n = 3$.

DMEM (day 2 = 19,077 ± 4,124; day 4 = 23,432 ± 7,189; day 6 = 25,203 ± 5,419) and commercial medium (day 2 = 14,137 ± 1,325; day 4 = 21,702 ± 2,781; day 6 = 25,766 ± 4,085), **Figure 2G**. Interestingly, the overall particles produced in Oxium^{TM}EXO showed a smaller size, as seen in both size mean and size mode (**Figure 2H**). Importantly, these Oxium^{TM}EXO advantages are also observed in other types of cells, such as menstrual blood-derived MSCs (Mens-MSCs; **Supplementary Figures 3**, **5**) and fibroblasts (**Supplementary Figures 4**, **5**), as well as in other UC-MSC donors (**Supplementary Figure 5**), reinforcing the performance of Oxium^{TM}EXO.

Oxium^{TM}EXO-Derived Particles Exhibited Standard sEV Characteristics

With the purpose of characterizing and comparing the quality of sEV produced in the three different culture conditions, we isolated sEV by differential centrifugation, with an additional filtration step of the supernatant prior to ultracentrifugation. This protocol was selected as it represents one of the most widely followed procedures for EV isolation (Théry et al., 2006; Momen-Heravi et al., 2013). The mentioned method allowed the isolation of particles from all three conditioned media, obtaining total particle concentrations in the same order of magnitude of 11 (**Supplementary Table 1**). The NTA analysis revealed a low concentration of particles obtained from Oxium^{TM}EXO ($2.96 \times 10^{11} \pm 1.32 \times 10^{11}$) in comparison to DMEM ($4.69 \times 10^{11} \pm 4.84 \times 10^{10}$), but higher in comparison to the commercial medium ($2.73 \times 10^{11} \pm 5.63 \times 10^{9}$) (**Figure 3A**), while the size's mean and mode were similar among the particles obtained in the three media (**Figure 3B**). It should be noted that the sizes of the particles secreted in Oxium^{TM}EXO were more homogeneous than the sizes of those isolated from DMEM or commercial conditioned medium, according to the size's modes and standard deviation obtained from the NTA video's analyses (**Figure 3C**), showing particle size modes ranging from 131.0 to 204.1 nm for DMEM, 136.2 to 179.1 nm for Oxium^{TM}EXO, and

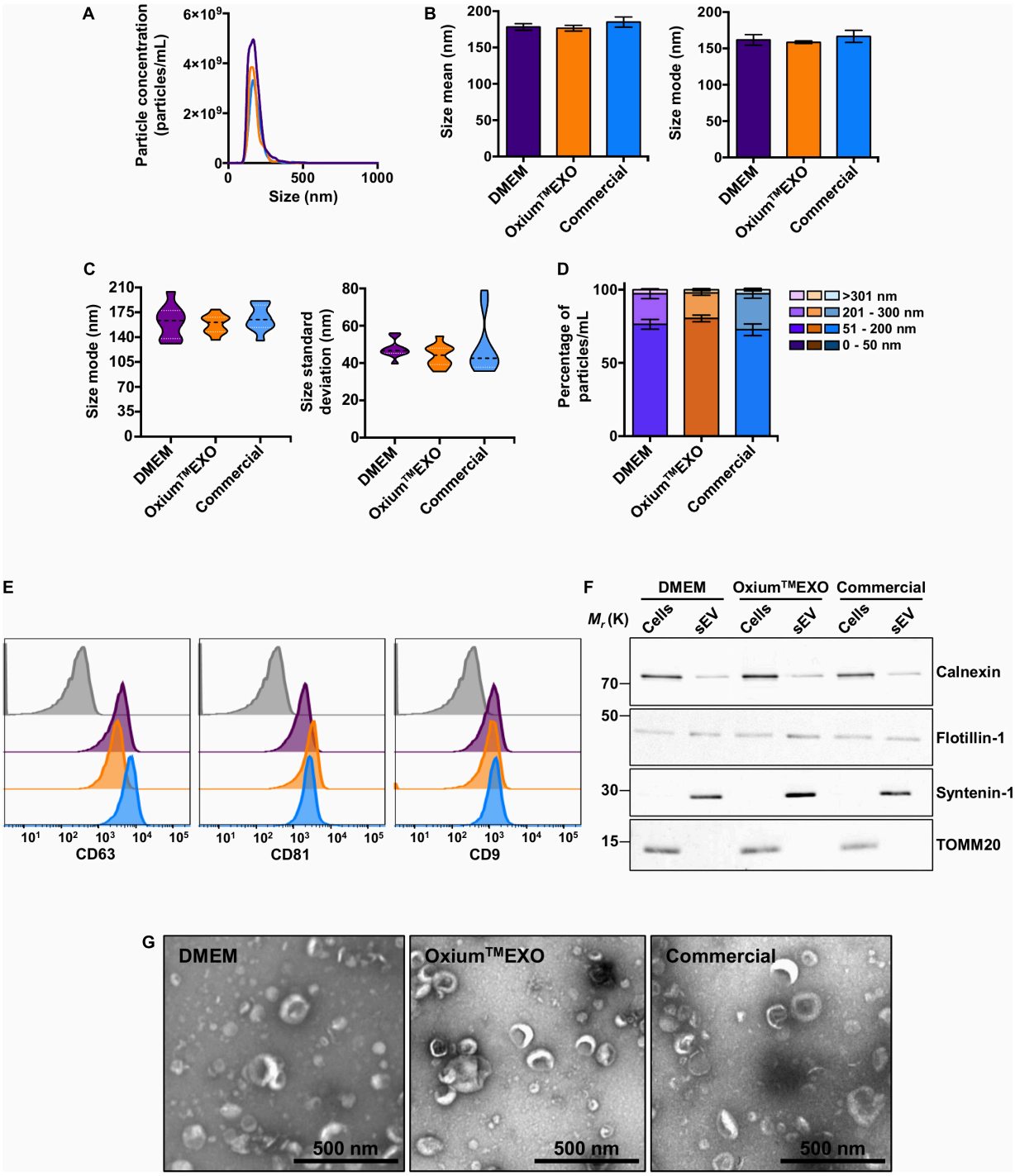

FIGURE 3 | Characterization of isolated UC-MSC-derived sEV produced in DMEM, Oxium^{TM}EXO, and commercial medium. The sEV isolated from the different conditioned media were evaluated in terms of particle concentration, size, classical surface/interior markers, and morphology. **(A)** Histogram showing the particles' concentrations according to their size. Violet line = DMEM-derived sEV; orange line = Oxium^{TM}EXO-derived sEV; light blue line = commercial medium-derived sEV. The mean concentration obtained through NTA of five videos for each type of sEV is shown. **(B)** Size's mean and mode obtained for each type of sEV. **(C)** Size's mode **(left panel)** and standard deviation data **(right panel)** dispersion. **(D)** Percentage distribution of isolated particles' concentrations according to their size: 0–50 nm, 51–200 nm, 201–300 nm, and >301 nm. **(E)** Representative histograms of median fluorescence intensity (MFI) obtained by flow cytometry of classical sEV surface markers. Gray = isotype control; violet = DMEM; orange = Oxium^{TM}EXO, light blue = commercial medium. **(F)** Western blot, illustrating the presence of the sEV's membrane-associated protein Flotillin-1 and the sEV's luminal-scaffold protein Syntenin-1 (involved in sEV's biogenesis). Note that in the isolated sEV there is minimal or no detectable contamination by Calnexin (endoplasmic reticulum) or TOMM20 (mitochondria), respectively. **(G)** Transmission electron microscopy (TEM) by uranyl acetate negative staining of isolated sEV from ultracentrifuge. The graphs show mean ± SEM. $n = 2$.

135.2 to 191.1 nm for the commercial medium. In contrast to the enrichment of particles in the size range of 51–200 nm observed previously in the analyses performed over those particles present in the non-purified conditioned media, once having applied the isolation method we were not able to distinguish a significant enrichment of particles in the size range of 50–200 nm in the processed Oxium^{TM}EXO conditioned medium (**Figure 3D**). Since the chosen isolation method depends on the operator, we believe that a large-scale, fully automated sEV isolation technique could take full advantage of the Oxium^{TM}EXO's high-quantity and homogeneous-size sEV production, while avoiding particle loss and heterogeneity.

Taking into consideration the International Society for Extracellular Vesicles (ISEV) criteria for EV characterization (Théry et al., 2018), a bead-based flow cytometry analysis of the classical CD63, CD81, and CD9 sEV-surface proteins was performed on the isolated particles. As expected, DMEM-, Oxium^{TM}EXO-, and commercial conditioned medium-derived particles presented all of the three sEV typical surface markers CD63 (>90%), CD81 (>90%), and CD9 (>40%) (**Figure 3E**). Moreover, these particles contained other established sEV markers, such as Flotillin-1 and Syntenin-1 (**Figure 3F**). Finally, isolated samples contained cup-shaped vesicles of size and morphology consistent with sEV (**Figure 3G** and **Supplementary Figure 6**), confirming the EV and exosome nature of the three types of sEV isolated in this work.

Oxium^{TM}EXO-Derived sEV Are Internalized by Target Cells

To investigate the cellular uptake level of sEV produced under different media, sEV were stained with DiR, a lipophilic dye that fluoresces intensely when inserted into a lipid membrane. Taking into account the promissory use of sEV as therapeutic agents or as drug-delivery vehicles to treat different pathologies but mainly in cancer and osteoarthritis, the MDA-MB-231 cancer cell line and chondrocytes were selected to be incubated with DiR-stained sEV. The stained sEV isolated from DMEM, Oxium^{TM}EXO, and commercial conditioned medium were found in all cells, forasmuch as the flow cytometry analyses showed that over 95% of the MDA-MB-231-cultured cells were positive for DiR, implying the cell uptake and internalization of the sEV (**Figure 4A**, solid lines). As previously described (Rosenberger et al., 2019), a negative control of sEV internalization was done at 4°C, showing no DiR-positive cells neither for DMEM nor for Oxium^{TM}EXO or commercial DiR-stained sEV (**Figure 4A**, dotted lines). The same experimental setup was done using chondrocytes isolated from patients with osteoarthrosis, showing similar results (**Supplementary Figure 7**). Overall, this result shows that Oxium^{TM}EXO-produced sEV maintain their internalization potential by target cells.

Oxium^{TM}EXO-Produced sEV Maintain Their Biodistribution Profile *in vivo*

To assess the sEV biodistribution for determining the main target organs, mice were injected intraperitoneally (IP) with DiR-stained sEV derived from DMEM, Oxium^{TM}EXO, or commercial conditioned medium. Once euthanized at 6 h postinjection, the brain, heart, lungs, liver, kidneys, spleen, and pancreas were collected and imaged *ex vivo* (**Figures 4B,C**). To subtract the possible background noise due to autofluorescence, non-DiR-labeled sEV were administered as a negative control. In addition, to discard the possibility of unspecific staining due to free dye, 100 μl of 1 × PBS was subjected to the DiR-labeling procedure and injected into mice. For both negative controls, no tissue fluorescence was detected, which suggests a reliable signal from tracking DiR-stained sEV and not merely free dye accumulation in the organ's tissues. Overall, our results show clearly that sEV, independent of their culture condition, display a similar biodistribution pattern. They are able to enter the mouse bloodstream and accumulate after 6 h of IP administration mainly in the liver, spleen, and pancreas, which is in good agreement to previously human sEV biodistribution assays performed in mice (Wiklander et al., 2015).

DISCUSSION

The potential clinical applications of sEV in regenerative medicine and tissue engineering have gained worldwide interest, which is evident from the number of clinical trials under development. As has been previously reported (Zhao et al., 2020), there are 190 and 56 studies registered in the United States National Institutes of Health clinical trials database[1] involving exosomes or extracellular vesicles, respectively. Undoubtedly, to meet the clinical expectations of sEV-based therapies, it is essential to resolve the current limitations of low production efficiency and batch inconsistency of clinical-grade sEV. Along these lines, the use of the adequate culture medium for the generation of sEV can stimulate their secretion, hence improving the production process efficiency. Additionally, for clinical-grade production of sEV, it is essential that the culture medium used is xeno- and blood-free of components to comply the regulatory framework, which seeks to avoid the risk of transmission of infectious agents or the elicitation of an immune response in the patient who will receive a sEV-based therapy (United States Food and Drug Administration, 2020).

The results presented here show that the Oxium^{TM}EXO medium can support the growth of MSCs to a greater degree than that observed in DMEM or in a commercially available medium that was developed specifically for the collection of sEV. Previous reports showed that xeno-free media can alter the proliferative capacity of human MSCs (Gerby et al., 2017), impacting in their secretory and immunomodulatory properties (Yoshida et al., 2018), or even maintain the MSC characteristics but only when grown imbedded in an extracellular matrix (Rakian et al., 2015). In this work, we assayed for basic cellular functional studies as Oxium^{TM}EXO was primarily developed to produce sEV and not as a cell expansion culture medium. Certainly, it has been stated that the metabolic change from FBS-supplemented medium to a xeno-free culture medium impacts the molecular composition including protein, lipid, and miRNA profile changes of purified sEV. This can be explained by the lack of FBS (Li et al., 2015; Haraszti et al., 2019) or

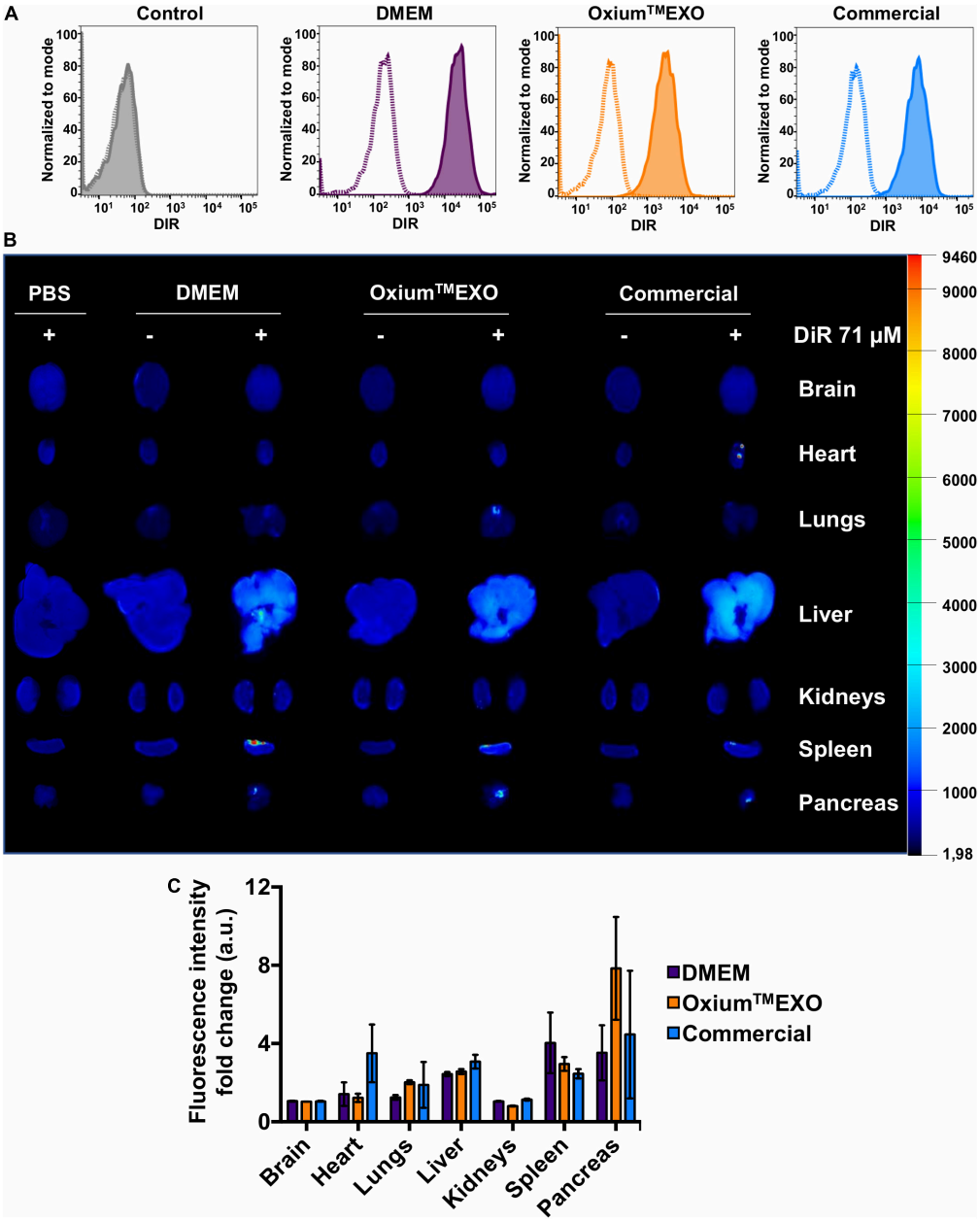

FIGURE 4 | Cellular internalization and *in vivo* biodistribution profile of isolated sEV produced in DMEM, Oxium™EXO, and commercial medium. **(A)** Flow cytometry analysis of MDA-MB-231 cancer cells incubated for 6 h with DiR-stained isolated sEV. Dotted lines = incubation performed at 4°C; solid lines = incubation performed at 37°C; gray histogram = no sEV-incubation control (PBS + DiR); violet histogram = DMEM-derived sEV uptake; orange histogram = Oxium™EXO-derived sEV uptake; light blue histogram = commercial medium-derived sEV uptake. **(B)** Six hours post-injection distribution of DiR-stained isolated-sEV administrated intraperitoneally in mice. **(C)** Fluorescence intensity-fold change observed for each analyzed organ. The fluorescence intensity of DiR-stained sEV-treated mouse organs was normalized with the fluorescence intensity of those organs coming from mice treated with the respective unstained sEV. The graph shows mean ± SEM. *n* = 3 mice for each condition.

by contaminants present in the supplements of the xeno-free medium, altering, for example, the RNA-seq outcomes (Auber et al., 2019). Furthermore, the use of the FBS-depleted medium has also shown altered cellular programs, mainly reducing cell growth and viability (Eitan et al., 2015; Liao et al., 2017; Witwer et al., 2019). Taking into consideration the aforementioned observations, validation studies are required when changing between the cell expansion and sEV production media. The significance and impact of the presumable changes will ultimately depend on the application of interest and in accordance with the expected or desired composition and functionality of the sEV (Witwer et al., 2019). The lower expression observed of CD105 could be attributed to the lack of serum or platelet lysate in the media, which is consistent with previous results

(Mark et al., 2013). Notably, the CD105 data dispersion among the replicates was lower in those cells cultured in Oxium^{TM}EXO. Also, since sEV are composed of complex macromolecular structures that may induce pleiotropic activities, each specific sEV-based application requires its own functional and potency assays. For instance, some applications are looking for MSC-derived sEV with anti-angiogenic activity, while other sources of MSCs can deliver sEV with pro-angiogenic effects (Alcayaga-Miranda et al., 2016). sEV derived from DMEM, Oxium^{TM}EXO, or the commercial medium might not be "one fit for all," and to avoid data misinterpretation, further tests are required for each of the intended application. The key objective of this comparative study is to determine the advantage of using Oxium^{TM}EXO on enhancing the secretion rate of sEV, without modifying its structural, biochemical, and classical properties. This positive impact was determined mainly by the internalization capacity of Oxium^{TM}EXO-produced sEV in variable target cells *in vitro* and by the biodistribution profile *in vivo*.

In the current study, the secretion rate of sEV to the supernatant using DMEM, Oxium^{TM}EXO, and a commercial medium revealed significant differences in terms of particle accumulation through cell culture days. Oxium^{TM}EXO allowed a higher accumulation of particles within the 51- to 200-nm size range, and at least a four-fold increase was measured in comparison to the benchmarked medium. While some authors have suggested that the xeno-free medium positively modulates the secretion rate of sEV (Palamà et al., 2020), achieving a two-fold increase, the comparison was performed by growing the cells in the FBS-free or xeno-free medium, and then sEV production was accomplished by medium changes and maintaining the cells for 72 h in the α-MEM medium until supernatant collection. The supposed FBS-free medium was in fact supplemented with a sEV-depleted FBS, which is still susceptible to be contaminated with FBS-derived sEV, as previously have been demonstrated (Shelke et al., 2014; Lehrich et al., 2018). In the present study, the cells were grown first for 48 h in the hPL-supplemented DMEM and then put through a supplement starvation period of 2, 4, and 6 days before supernatant collection for particle analyses or sEV isolation, achieving with Oxium^{TM}EXO the mentioned four-fold increase.

The ultracentrifugation method used here has been reported to have limitations related to upscaling and reproducibility between laboratories, mainly due to the type of rotor (tilting or fixed angle) and its specific parameters (like rotation radius or sedimentation path length) (Livshts et al., 2015). Differences have even been reported at the same laboratory level. Mendt et al. (2018) performed several GMP-compliant sEV isolates for clinical use by ultracentrifugation, obtaining a range of 9.8–15.6 billion exosomes per bioreactor cycle. We believe that the use of other types of sEV isolation techniques, such as ultrafiltration or tangential flow filtration, is recommended to evaluate with greater precision and reproducibility the effect that Oxium^{TM}EXO has robustly demonstrated in different cell types prior to isolation. Both ultrafiltration and tangential flow filtration have shown higher sEV isolation efficiency of up to four orders of magnitude over the ultracentrifugation method, maintaining the sEV size and morphology while improving sEV sample purity (Watson et al., 2018; Shu et al., 2020; Tian et al., 2020). These size-based, more automated, and less user-dependent isolation techniques minimize sEV losses, maximize sEV throughput, and allow processing of larger amounts of the conditioned medium.

Also, the sEV may exert their therapeutic or delivery-desired function through the interaction with the acceptor target cells. Herein, isolated and stained sEV from DMEM, Oxium^{TM}EXO, and commercially available conditioned media were able to be taken up by human cancer and cartilage cells at 37°C, in accordance with what has been established by the EV community (Russell et al., 2019). Furthermore, these sEV distributed systemically in a healthy mouse model, reaching the liver, spleen, and pancreas, in agreement with previous work in the field (Wiklander et al., 2015; Russell et al., 2019), with no differences at the distribution level among the three types of sEV tested. Taking together, our results imply that the surface markers, cell uptake, and biodistribution pattern of the sEV are not affected by the type of medium used for their production, leaving the quantity of secreted sEV to the supernatant as the essential criterion for favoring the use of one medium over the another, along with the final user's desired sEV functional potency test.

Finally, clinical translation cannot be achieved without considering investor expectations with regard to the product therapeutic potential, conceivable market authorization, and viability. For this reason, economic factors have been also influencing the field and most importantly the accessibility and affordability of these advanced therapies. Hence, a selection of reagents and procedures that may be applied from preclinical to clinical developments aiming to maintain cell consistency and ultimately reduce manufacturing costs is much needed.

DATA AVAILABILITY STATEMENT

The original contributions presented in the study are included in the article/**Supplementary Material**, further inquiries can be directed to the corresponding authors.

ETHICS STATEMENT

The studies involving human participants were reviewed and approved by the Ethics Committee, Universidad de los Andes, Santiago, Chile. The patients/participants provided their written informed consent to participate in this study. The animal study was reviewed and approved by Institutional Animal Care and Use Committee, Universidad de los Andes, Santiago, Chile.

AUTHOR CONTRIBUTIONS

FA-M and MK conceived and designed the study. AF-V, CF, YH, and AV-L were responsible for data acquisition and analysis. AF-V, CF, YH, AV-L, FA-M, and MK participated in the manuscript writing and editing. RT-L participated in the Oxium^{TM}EXO

formulation and manuscript editing. All authors contributed to the article and approved the submitted version.

FUNDING

This work was funded in part by the Chilean National Agency for Research and Development (ANID), through FONDECYT Regular project #1190411 to FA-M, and by Consorcio Regenero, Chile.

ACKNOWLEDGMENTS

The authors specially thank Dr. Jimena Cuenca and her group (Faculty of Medicine, Universidad de los Andes, Santiago, Chile) for their kind donation of the hPL and Daniel Meza for his collaboration in the preparation of Oxium^{TM}EXO medium. The authors sincerely thank all the members of the laboratory for their important contributions to the scientific discussion of this work, especially Nicolás Georges and Hugo Tobar. The authors acknowledge the technical expertise and assistance of Javiera Ponce and Camila Sánchez in the animal experiments.

SUPPLEMENTARY MATERIAL

The Supplementary Material for this article can be found online at: https://www.frontiersin.org/articles/10.3389/fbioe.2021.619930/full#supplementary-material

REFERENCES

Alcayaga-Miranda, F., Cuenca, J., Luz-Crawford, P., Aguila-Díaz, C., Fernandez, A., Figueroa, F. E., et al. (2015a). Characterization of menstrual stem cells: angiogenic effect, migration and hematopoietic stem cell support in comparison with bone marrow mesenchymal stem cells. *Stem Cell Res. Ther.* 6, 1–14. doi: 10.1186/s13287-015-0013-5

Alcayaga-Miranda, F., Cuenca, J., Martin, A., Contreras, L., Figueroa, F. E., and Khoury, M. (2015b). Combination therapy of menstrual derived mesenchymal stem cells and antibiotics ameliorates survival in sepsis. *Stem Cell Res. Ther.* 6:199. doi: 10.1186/s13287-015-0192-0

Alcayaga-Miranda, F., González, P. L., Lopez-Verrilli, A., Varas-Godoy, M., Aguila-Díaz, C., Contreras, L., et al. (2016). Prostate tumor-induced angiogenesis is blocked by exosomes derived from menstrual stem cells through the inhibition of reactive oxygen species. *Oncotarget* 7, 44462–44477. doi: 10.18632/oncotarget.9852

Askenase, P. W. (2020). Artificial nanoparticles are not as good as the real thing. *Nature* 582:S5. doi: 10.1038/d41586-020-01764-0

Auber, M., Fröhlich, D., Drechsel, O., Karaulanov, E., and Krämer-Albers, E. M. (2019). Serum-Free media supplements carry MiRNAs that co-purify with extracellular vesicles. *J. Extracell. Vesicles* 8:1656042. doi: 10.1080/20013078.2019.1656042

Baharlooi, H., Azimi, M., Salehi, Z., and Izad, M. (2020). Mesenchymal stem cell-derived exosomes: a promising therapeutic ace card to address autoimmune diseases. *Int. J. Stem Cells* 13, 13–23. doi: 10.15283/ijsc19108

Bartolucci, J., Verdugo, F. J., González, P. L., Larrea, R. E., Abarzua, E., Goset, C., et al. (2017). Safety and efficacy of the intravenous infusion of umbilical cord mesenchymal stem cells in patients with heart failure: a phase 1/2 randomized controlled trial (RIMECARD trial [randomized clinical trial of intravenous infusion umbilical cord mesenchymal Stem Cells on Cardiopathy]). *Circ. Res.* 121, 1192–1204. doi: 10.1161/CIRCRESAHA.117.310712

Burnouf, T., Strunk, D., Koh, M. B. C., and Schallmoser, K. (2016). Human platelet lysate: replacing fetal bovine serum as a gold standard for human cell propagation? *Biomaterials* 76, 371–387. doi: 10.1016/j.biomaterials.2015.10.065

Camussi, G., Deregibus, M. C., and Cantaluppi, V. (2013). Role of stem-cell-derived microvesicles in the paracrine action of stem cells. *Biochem. Soc. Trans.* 41, 283–287. doi: 10.1042/BST20120192

Chen, L., Qu, J., and Xiang, C. (2019). The multi-functional roles of menstrual blood-derived stem cells in regenerative medicine. *Stem Cell Res. Ther.* 10, 1–10. doi: 10.1186/s13287-018-1105-9

Cuende, N., Rasko, J. E. J., Koh, M. B. C., Dominici, M., and Ikonomou, L. (2018). Cell, tissue and gene products with marketing authorization in 2018 worldwide. *Cytotherapy* 20, 1401–1413. doi: 10.1016/j.jcyt.2018.09.010

Dominici, M., Le Blanc, K., Mueller, I., Slaper-Cortenbach, I., Marini, F. C., Krause, D. S., et al. (2006). Minimal criteria for defining multipotent mesenchymal stromal cells. the international society for cellular therapy position statement. *Cytotherapy* 8, 315–317. doi: 10.1080/14653240600855905

Eitan, E., Zhang, S., Witwer, K. W., and Mattson, M. P. (2015). Extracellular vesicle-depleted fetal bovine and human sera have reduced capacity to support cell growth. *J. Extracell. Vesicles* 4, 1–10. doi: 10.3402/jev.v4.26373

European Medicines Agency (2013). *Guideline on the Use of Bovine Serum in the Manufacture of Human Biological Medicinal Products*. EMA/CHMP/B (30 May 2013). Amsterdam: European Medicines Agency, 1–8.

Gerby, S., Attebi, E., Vlaski, M., and Ivanovic, Z. (2017). A new clinical-scale serum-free xeno-free medium efficient in Ex vivo amplification of mesenchymal stromal cells does not support mesenchymal stem cells. *Transfusion* 57, 433–439. doi: 10.1111/trf.13902

González, P. L., Carvajal, C., Cuenca, J., Alcayaga-Miranda, F., Figueroa, F. E., Bartolucci, J., et al. (2015). Chorion mesenchymal stem cells show superior differentiation, immunosuppresive and angiogenic potentials in comparison with haploidentical maternal placental cells. *Stem Cells Transl. Med.* 4, 1109–1121. doi: 10.5966/sctm.2015-0022

Guiotto, M., Raffoul, W., Hart, A. M., Riehle, M. O., and di Summa, P. G. (2020). Human platelet lysate to substitute fetal bovine serum in HMSC expansion for translational applications: a systematic review. *J. Transl. Med.* 18:351. doi: 10.1186/s12967-020-02489-4

Haraszti, R. A., Miller, R., Dubuke, M. L., Rockwell, H. E., Coles, A. H., Sapp, E., et al. (2019). Serum deprivation of mesenchymal stem cells improves exosome activity and alters lipid and protein composition. *IScience* 16, 230–241. doi: 10.1016/j.isci.2019.05.029

Kalluri, R., and LeBleu, V. S. (2020). The biology, function, and biomedical applications of exosomes. *Science* 367:eaau6977. doi: 10.1126/science.aau6977

Kalorama Information (2018). *Global Cell Culture Markets (Media, Sera, Reagents)*. Washington, DC: Kalorama Information.

Kurte, M., Vega-Letter, A. M., Luz-Crawford, P., Djouad, F., Noël, D., Khoury, M., et al. (2020). Time-Dependent LPS exposure commands MSC immunoplasticity through TLR4 activation leading to opposite therapeutic outcome in EAE. *Stem Cell Res. Ther.* 11:416. doi: 10.1186/s13287-020-01840-2

Lehrich, B. M., Liang, Y., Khosravi, P., Federoff, H. J., and Fiandaca, M. S. (2018). Fetal bovine serum-derived extracellular vesicles persist within vesicle-depleted culture media. *Int. J. Mol. Sci.* 19:3538. doi: 10.3390/ijms19113538

Lener, T., Gimona, M., Aigner, L., Börger, V., Buzas, E., Camussi, G., et al. (2015). Applying extracellular vesicles based therapeutics in clinical trials – an ISEV position paper. *J. Extracell. Vesicles* 4:30087. doi: 10.3402/jev.v4.30087

Li, J., Lee, Y., Johansson, H. J., Mäger, I., Vader, P., Nordin, J. Z., et al. (2015). Serum-Free culture alters the quantity and protein composition of neuroblastoma-derived extracellular vesicles. *J. Extracell. Vesicles* 4:26883. doi: 10.3402/jev.v4.26883

Liao, Z., Muth, D. C., Eitan, E., Travers, M., Learman, L. N., Lehrmann, E., et al. (2017). Serum extracellular vesicle depletion processes affect release and infectivity of HIV-1 in culture. *Sci. Rep.* 7:2558. doi: 10.1038/s41598-017-02908-5

Livshts, M. A., Khomyakova, E., Evtushenko, E. G., Lazarev, V. N., Kulemin, N. A., Semina, S. E., et al. (2015). Isolation of exosomes by differential centrifugation:

theoretical analysis of a commonly used protocol. *Sci. Rep.* 5:17319. doi: 10.1038/srep17319

Lopez-Verrilli, M. A., Caviedes, A., Cabrera, A., Sandoval, S., Wyneken, U., and Khoury, M. (2016). Mesenchymal stem cell-derived exosomes from different sources selectively promote neuritic outgrowth. *Neuroscience* 320, 129–139. doi: 10.1016/j.neuroscience.2016.01.061

Mark, P., Kleinsorge, M., Gaebel, R., Lux, C. A., Toelk, A., Pittermann, E., et al. (2013). Human mesenchymal stem cells display reduced expression of CD105 after culture in serum-free medium. *Stem Cells Int.* 2013:698076. doi: 10.1155/2013/698076

Mastrolia, I., Foppiani, E. M., Murgia, A., Candini, O., Samarelli, A. V., Grisendi, G., et al. (2019). Challenges in clinical development of mesenchymal stromal/stem cells: concise review. *Stem Cells Transl. Med.* 8, 1135–1148. doi: 10.1002/sctm.19-0044

Matas, J., Orrego, M., Amenabar, D., Infante, C., Tapia-Limonchi, R., Cadiz, M. I., et al. (2019). Umbilical cord-derived mesenchymal stromal cells (MSCs) for knee osteoarthritis: repeated MSC dosing is superior to a single MSC dose and to hyaluronic acid in a controlled randomized phase I/II trial. *Stem Cells Transl. Med.* 8, 215–224. doi: 10.1002/sctm.18-0053

Mendt, M., Kamerkar, S., Sugimoto, H., McAndrews, K. M., Wu, C. C., Gagea, M., et al. (2018). Generation and testing of clinical-grade exosomes for pancreatic cancer. *JCI Insight* 3:e99263. doi: 10.1172/jci.insight.99263

Momen-Heravi, F., Balaj, L., Alian, S., Mantel, P. Y., Halleck, A. E., Trachtenberg, A. J., et al. (2013). Current methods for the isolation of extracellular vesicles. *Biol. Chem.* 394, 1253–1262. doi: 10.1515/hsz-2013-0141

Olsen, T. R., Ng, K. S., Lock, L. T., Ahsan, T., and Rowley, J. A. (2018). Peak MSC-Are we there yet? *Front. Med.* 5:178. doi: 10.3389/fmed.2018.00178

Palamà, M. E. F., Shaw, G. M., Carluccio, S., Reverberi, D., Sercia, L., Persano, L., et al. (2020). The secretome derived from mesenchymal stromal cells cultured in a xeno-free medium promotes human cartilage recovery in vitro. *Front. Bioeng. Biotechnol.* 8:90. doi: 10.3389/fbioe.2020.00090

Park, Y.-B., Ha, C.-W., Lee, C.-H., Yoon, Y. C., and Park, Y.-G. (2017). Cartilage regeneration in osteoarthritic patients by a composite of allogeneic umbilical cord blood-derived mesenchymal stem cells and hyaluronate hydrogel: results from a clinical trial for safety and proof-of-concept with 7 years of extended follow-up. *Stem Cells Transl. Med.* 6, 613–621. doi: 10.5966/sctm.2016-0157

Pegtel, D. M., and Gould, S. J. (2019). Exosomes. *Ann. Rev. Biochem.* 88, 487–514. doi: 10.1146/annurev-biochem-013118-111902

Rackwitz, L., Djouad, F., Janjanin, S., Nöth, U., and Tuan, R. S. (2014). Functional cartilage repair capacity of de-differentiated, chondrocyte- and mesenchymal stem cell-laden hydrogels in vitro. *Osteoarthritis Cartilage* 22, 1148–1157. doi: 10.1016/j.joca.2014.05.019

Rakian, R., Block, T. J., Johnson, S. M., Marinkovic, M., Wu, J., Dai, Q., et al. (2015). Native extracellular matrix preserves mesenchymal stem cell 'Stemness' and differentiation potential under serum-free culture conditions. *Stem Cell Res. Ther.* 6:235. doi: 10.1186/s13287-015-0235-6

Rosenberger, L., Ezquer, M., Lillo-Vera, F., Pedraza, P. L., Ortúzar, M. I., González, P. L., et al. (2019). Stem cell exosomes inhibit angiogenesis and tumor growth of oral squamous cell carcinoma. *Sci. Rep.* 9:663. doi: 10.1038/s41598-018-36855-6

Roura, S., and Bayes-Genis, A. (2019). Toward standardization of mesenchymal stromal cell-derived extracellular vesicles for therapeutic use: a call for action. *Proteomics* 19:e1800397. doi: 10.1002/pmic.201800397

Russell, A. E., Sneider, A., Witwer, K. W., Bergese, P., Bhattacharyya, S. N., Cocks, A., et al. (2019). Biological membranes in EV biogenesis, stability, uptake, and cargo transfer: an ISEV position paper arising from the ISEV membranes and EVs workshop. *J. Extracell. Vesicles* 8:1684862. doi: 10.1080/20013078.2019.1684862

Sagaradze, G. D., Nimiritsky, P. P., Akopyan, Z. A., Makarevich, P. I., and Efimenko, A. Y. (2018). "Cell-Free therapeutics' from components secreted by mesenchymal stromal cells as a novel class of biopharmaceuticals," in *Biopharmaceuticals*, eds M.-K. Yeh and Y.-C. Chen (London: InTech). doi: 10.5772/intechopen.78605

Shelke, G. V., Lässer, C., Gho, Y. S., and Lötvall, J. (2014). Importance of exosome depletion protocols to eliminate functional and RNA-Containing extracellular vesicles from fetal bovine serum. *J. Extracell. Vesicles* 3:24783. doi: 10.3402/jev.v3.24783

Shu, S. L., Yang, Y., Allen, C. L., Hurley, E., Tung, K. H., Minderman, H., et al. (2020). Purity and yield of melanoma exosomes are dependent on isolation method. *J. Extracell. Vesicles* 9:1692401. doi: 10.1080/20013078.2019.1692401

Suárez, H., Gámez-Valero, A., Reyes, R., ópez-Martín, S. L., Rodríguez, M. J., Carrascosa, J. L., et al. (2017). A bead-assisted flow cytometry method for the semi-quantitative analysis of extracellular vesicles. *Sci. Rep.* 7:11271. doi: 10.1038/s41598-017-11249-2

Tapia-Limonchi, R., Khoury, M., and Meza-Rojas, D. (2019). *Composition and Method for the Cultivation, Expansion, Preservation and/or Pre-treatment of Cells*. Available online at: https://patentimages.storage.googleapis.com/31/5d/71/c85c4ecd535d9b/WO2019100175A1.pdf (accessed October 13, 2020).

Théry, C., Amigorena, S., Raposo, G., and Clayton, A. (2006). Isolation and characterization of exosomes from cell culture supernatants and biological fluids. *Curr. Protoc. Cell Biol.* 30, 3.22.1–3.22.29. doi: 10.1002/0471143030.cb0322s30

Théry, C., Witwer, K. W., Aikawa, E., Alcaraz, M. J., Anderson, J. D., Andriantsitohaina, R., et al. (2018). Minimal information for studies of extracellular vesicles 2018 (MISEV2018): a position statement of the international society for extracellular vesicles and update of the MISEV2014 guidelines. *J. Extracell. Vesicles* 7:1535750. doi: 10.1080/20013078.2018.1535750

Tian, Y., Gong, M., Hu, Y., Liu, H., Zhang, W., Zhang, M., et al. (2020). Quality and efficiency assessment of six extracellular vesicle isolation methods by nano-flow cytometry. *J. Extracell. Vesicles* 9:1697028. doi: 10.1080/20013078.2019.1697028

United States Food and Drug Administration. (2020). *Food and Drugs.* 21CFR§1271.210.

Watson, D. C., Yung, B. C., Bergamaschi, C., Chowdhury, B., Bear, J., Stellas, D., et al. (2018). Scalable, CGMP-Compatible purification of extracellular vesicles carrying bioactive human heterodimeric IL-15/lactadherin complexes. *J. Extracell. Vesicles* 7:1442088. doi: 10.1080/20013078.2018.1442088

Wiklander, O. P. B., Nordin, J. Z., O'Loughlin, A., Gustafsson, Y., Corso, G., Mäger, I., et al. (2015). Extracellular vesicle in vivo biodistribution is determined by cell source, route of administration and targeting. *J. Extracell. Vesicles* 4:26316. doi: 10.3402/jev.v4.26316

Willis, G. R., Kourembanas, S., and Mitsialis, S. A. (2017). Toward exosome-based therapeutics: isolation, heterogeneity, and fit-for-purpose potency. *Front. Cardiovasc. Med.* 4:63. doi: 10.3389/fcvm.2017.00063

Witwer, K. W., Van Balkom, B. W. M., Bruno, S., Choo, A., Dominici, M., Gimona, M., et al. (2019). Defining mesenchymal stromal cell (MSC)-derived small extracellular vesicles for therapeutic applications. *J. Extracell. Vesicles* 8:1609206. doi: 10.1080/20013078.2019.1609206

Yoshida, K., Nakashima, A., Doi, S., Ueno, T., Okubo, T., Kawano, K. I., et al. (2018). Serum-Free medium enhances the immunosuppressive and antifibrotic abilities of mesenchymal stem cells utilized in experimental renal fibrosis. *Stem Cells Transl. Med.* 7, 893–905. doi: 10.1002/sctm.17-0284

Zavala, G., Ramos, M. P., Figueroa-Valdés, A. I., Cisternas, P., Wyneken, U., Hernández, M., et al. (2020). Semipermeable cellulose beads allow selective and continuous release of small extracellular vesicles (SEV) from encapsulated cells. *Front. Pharmacol.* 11:679. doi: 10.3389/fphar.2020.00679

Zhao, A. G., Shah, K., Cromer, B., and Sumer, H. (2020). Mesenchymal stem cell-derived extracellular vesicles and their therapeutic potential. *Stem Cells Int.* 2020:8825771. doi: 10.1155/2020/8825771

Zipkin, M. (2019). Exosome redux. *Nat. Biotechnol.* 37, 1395–1400. doi: 10.1038/s41587-019-0326-5

Conflict of Interest: MK is the chief scientific officer of Cells for Cells and Consorcio Regenero. MK and RT-L are co-inventors of the patent for the formulation of Oxium^{TM}EXO. All other authors received stipends from Consorcio Regenero, a public and private funded Chilean Consortium for Regenerative Medicine.

frontiers in Bioengineering and Biotechnology

ORIGINAL RESEARCH
published: 15 July 2021
doi: 10.3389/fbioe.2021.614324

One-Time Optimization of Advanced T Cell Culture Media Using a Machine Learning Pipeline

Paul Grzesik and Sebastian C. Warth*

R&D Cell Culture Systems, CellGenix GmbH, Freiburg, Germany

The growing application of cell and gene therapies in humans leads to a need for cell type-optimized culture media. Design of Experiments (DoE) is a successful and well known tool for the development and optimization of cell culture media for bioprocessing. When optimizing culture media for primary cells used in cell and gene therapy, traditional DoE approaches that depend on interpretable models will not always provide reliable predictions due to high donor variability. Here we present the implementation of a machine learning pipeline into the DoE-based design of cell culture media to optimize T cell cultures in one experimental step (one-time optimization). We applied a definitive screening design from the DoE toolbox to screen 12 major media components, resulting in 25 ($2k + 1$) media formulations. T cells purified from a set of four human donors were cultured for 6 days and cell viability on day 3 and cell expansion on day 6 were recorded as response variables. These data were used as a training set in the machine learning pipeline. In the first step, individual models were created for each donor, evaluated and selected for each response variable, resulting in eight final statistical models ($R^2 > 0.92$, RMSE < 1.5). These statistical models were used to predict T cell viability and expansion for 10^5 random *in silico*-generated media formulations for each donor in a grid search approach. With the aim of identifying similar formulations in all donors, the 40 best performing media formulations of each response variable were pooled from all donors ($n = 320$) and subjected to unsupervised clustering using the k-means algorithm. The median of each media component in each cluster was defined as the cluster media formulation. When these formulations were tested in a new set of donor cells, they not only showed a higher T cell expansion than the reference medium, but also precisely matched the average expansion predicted from the donor models of the training set. In summary, we have shown that the introduction of a machine learning pipeline resulted in a one-time optimized T cell culture medium and is advantageous when working with heterogeneous biological material.

Keywords: T cells, culture media design, machine learning, design of experiment, screening, cell culture, cell and gene therapy, donor variability

OPEN ACCESS

Edited by:
Fergal J O'Brien,
Royal College of Surgeons in Ireland, Ireland

Reviewed by:
Emilio L. Cano,
Rey Juan Carlos University, Spain
Joschka Boedecker,
University of Freiburg, Germany

****Correspondence:***
Paul Grzesik
Pawel_Grzesik@web.de

Specialty section:
This article was submitted to Preclinical Cell and Gene Therapy, a section of the journal Frontiers in Bioengineering and Biotechnology

Received: *05 October 2020*
Accepted: *28 May 2021*
Published: *15 July 2021*

Citation:
Grzesik P and Warth SC (2021) One-Time Optimization of Advanced T Cell Culture Media Using a Machine Learning Pipeline. Front. Bioeng. Biotechnol. 9:614324. doi: 10.3389/fbioe.2021.614324

INTRODUCTION

In autologous cell therapy approaches, cells from a given patient are isolated, may be genetically modified to fulfill a therapeutic purpose and expanded in order to provide a sufficient dose of the cell product (Kazmi et al., 2009; June et al., 2018). In case of T cell therapy, the donor material is isolated from peripheral blood and consists of T cells and multiple other cell types. Even when T

cells are purified by their common surface marker CD3, they differ in each donor in expression of other surface markers as well as in their metabolic and functional capacity (Mahnke et al., 2013; Klein Geltink et al., 2018). In the manufacturing process, these cells are typically activated by ligation of the T cell co-receptors CD3 and CD28 to trigger expansion of T cells and are cultured for several days in culture media supplemented with appropriate cytokines (Trickett and Kwan, 2003; Xu et al., 2014). In this process, an efficient and robust expansion of T cells from any donor regardless of the heterogeneity of cell populations is essential not only to meet the specifications of good manufacturing practice but also because timely manufacturing of the cell product can be critical to patient treatment (Gee, 2018). This can be achieved with an optimized cell culture medium formulation that supports the expansion of each donor's T cells.

Cell culture media are complex mixtures of substances such as nutrients, salts, trace elements, buffers, hormones, carrier proteins, etc. (Yao and Asayama, 2017). For each cell type, the optimal composition and amounts of these components must be determined by suitable experimental setups.

For decades, the Design of Experiments (DoE) has been used for the development of cell culture media (Yao and Asayama, 2017). Sequential strategies, such as screening of several components followed by characterization of the relationships between the variables and finally their optimization, have proven to be particularly successful in bioprocessing (Castro et al., 1992; Kim et al., 1998; Liu et al., 2001). Recently, high-throughput technology in combination with exhaustive experimental designs has enabled rapid optimization of the medium for fed-batch cultures within a short time (Jordan et al., 2013; Rouiller et al., 2013; Bayer et al., 2020). While these strategies can be easily implemented using established cell lines such as Chinese hamster ovarian cells, the design of cell culture media for primary T cells is of greater challenge. The heterogeneous populations of cells purified from different human donors show a high degree of variability in cell expansion and viability, which leads to donor-dependent effect sizes of the screened media components and therefore makes sequential strategies with different donors in succession difficult.

To meet these challenges, we present in this study the extension of traditional experimental design with machine learning to optimize a cell culture medium for T cell expansion in one step. We applied a definitive screening design (Jones and Nachtsheim, 2011) with a minimum number of tested formulations, which allowed screening of a maximum number of different components in a given experimental system. In traditional workflows (**Figure 1A**) scientists focus on inference using interpretable model architectures such as ordinary least squares regression (OLS) to select significant features based on cell biological understanding. In contrast, we used competitive machine learning algorithms such as *elastic net regularized general linear models* (Zou and Hastie, 2005) and *random forest* (Breiman and Schapire, 2001). These complex model architechtures generate highly complex models which are less interpretable than traditional OLS models but have better prediction accuracy (**Figure 1B**). These algorithms were used to build individual high-performance statistical models, to predict cell expansion and viability of random *in silico* generated media formulations. We aimed to identify media compositions that encompass different media requirements of cells from individual donors. For this purpose, we pooled the top 40-predicted media formulations from each donor and used *k*-means clustering to identify clusters across donors with similar compositions. Using the median component level of each cluster we defined a cluster medium formulation that would potentially support expansion of cells from all donors. Finally, we demonstrated the enhanced performance of the selected cluster medium formulations in a confirmation experiment against other test and reference media for T cell expansion on a new test set of four different donors. The evaluation of model performances on the test set showed that our machine learning models were able to predict T cell expansion with higher precision than a single response linear regression model based on pooled data (traditional approach).

MATERIALS AND METHODS

Cell Culture

$CD3^+$ T cells were purified from healthy human donor blood preparations by negative magnetic bead isolation (EasySep™ Human T Cell Isolation Kit, Stemcell Technologies) and cryopreserved. Thawed cells were activated using Dynabeads Human T-Activator CD3/CD28 (Thermo Fisher) at a ratio of 1:1 bead:cell in test media or reference media in the presence of IL-7 (10 ng/ml, CellGenix) and IL-15 (10 ng/ml, CellGenix). Cells were cultured at 37 °C in a humidified incubator at 5% CO_2 in 96-well U bottom plates with two to three repeats per condition. On day 3 cells were splitted and reseeded with cytokine-containing media. To determine cell viability, cells were labeled with 7-Amino-Actinomycin D (7-AAD, BD-Pharmingen) and analyzed by flow cytometry. Cell count was determined using an Attune Nxt Flow Cytometer (Thermo Fisher).

Culture Media

Test media were prepared from a common base medium with the 12 test components added at the appropriate amounts according to the DoE levels. To control for media preparation, a reference medium with defined expansion properties was prepared in parallel. All media were adjusted to pH = 7.2 and osmolality = 300 mOsm/Kg H_2O.

Data Processing and Modeling

All statistical analysis were carried out with the statistical software R v3.6.0 (R Core Team, 2020) and RStudio v1.1.463 (2009–2018 RStudio, Inc.). Data processing and visualization was carried out with package tidyverse v1.2.1. Design of Experiments was carried out with package daewr v1.1-7 and rsm v2.1.0. Modeling and feature selection was carried out with package caret (using the integrated ranger package v4.6-7, glmnet package v2.0.18 and MASS package v7.3-51.4). Cluster analysis was carried out with package cluster v2.1.0 and clustertend v1.4, visualization of multivariate data analysis was carried out with package factoextra v1.0.6.

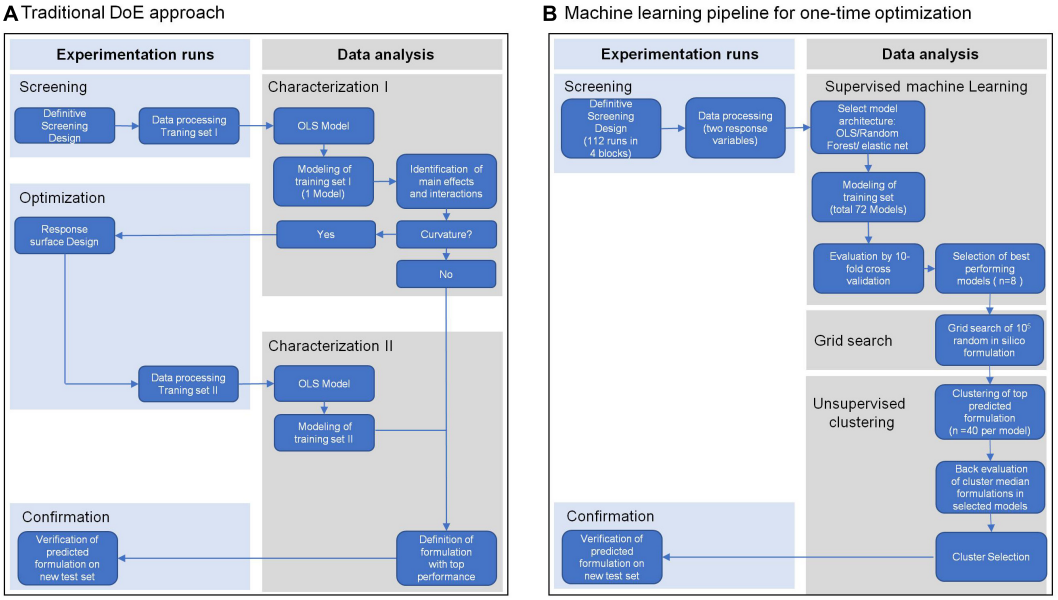

FIGURE 1 | Overview of the traditional Design of Experiment (DoE) approach **(A)** and of a machine learning pipeline **(B)**. Both approaches include a screening step for data collection, in this case from expansion of T cells from four different healthy donors in a definitive screening design. Traditional DoE uses interpretable model architectures across all donors such as ordinary least squares regression (OLS) to select significant features (Characterization I). A second experimental step is applied to screen for optimal parameter levels (Optimization II). In a second modeling step using OLS the optimal parameter levels are determined for an optimal media formulation (Characterization II) that is experimentally confirmed (Confirmation). The machine learning pipeline **(B)** uses competitive machine learning algorithms to generate complex models for every response variable in every donor, which allow high prediction accuracy but are less interpretable (Supervised machine learning). After cross-validation these models are used to select the top 40 media formulations for every donor and every response variable from a random set of 10^5 *in silico* media formulations (Grid search). The top 40 formulations of all donors and responses are clustered by formulation similarity and a cluster formulation was defined by the median component level of all formulations in a cluster (Unsupervised Clustering). Back evaluation of cluster formulations in the donor models for every response allows selection of the media formulation with the best response across all donors and responses, which again is experimentally confirmed (Confirmation).

As statistical tests in sections "Clustering and Selection of in silico Formulations", "Evaluation of Selected Cluster Medium Formulation on a New Set of Donors", and "Evaluation of Model Performance" an ANOVA followed by Tukey *post hoc* test at a significance level <0.05 was performed.

RESULTS

Strategy Outline

We aimed to improve a proprietary base medium formulation for the expansion of primary human T cells. In contrast to a traditional optimization strategy based on sequential screening, characterization and optimization (sco) steps (Anderson, 2019) (**Figure 1A**), we carried out a one-time media optimization using a machine learning pipeline. We reasoned that cell viability at an early stage of cell culture might be influenced by an independent set of components than the T cell expansion at the end of culture, which could additionally contribute to overall expansion. Therefore, we selected T cell viability on day 3 and T cell expansion on day 6 as response variables. To account for the donor variability, we included cells from four human donors into the analysis as independent experimental blocks. This data served as our training set for the modeling steps. Our strategy consisted of following steps (**Figure 1B**) which are described in detail in sections "Data Collection," "Data Modeling," "Prediction of *In Silico* Formulations," "Clustering and Selection of High-Performance *In Silico* Formulations," and "Evaluation of Selected Cluster Medium Formulations on a New Set of Donors."

Data Collection

We selected 12 cell culture media components (c01–c12), which might impact the performance of the base medium formulation in terms of T cell viability on day 3 and T cell expansion on day 6 of cell culture. These components belong to different categories, such as buffer substances, metabolically active components, proteins or trace elements. The diversity of selected components makes it difficult to draw conclusions about potential main effects of single components and synergistic effects of multiple components, so that an experimental design with high resolution was required. We decided on a $2k + 1$ definitive screening design (Jones and Nachtsheim, 2011) in three levels (in scaled notation, -1, 0, and 1) to investigate main effects, curvature and interactions of the screened components with a minimum number of runs. One experimental block resulted in a total of 26 runs, consisting of 25 formulations and the reference medium with known performance (**Supplementary Table 1**). T cells isolated from four different donors were investigated in separate experimental blocks, resulting in four randomized complete blocks and a total

of 104 runs. T cell viability on day 3 and T cell expansion on day 6 were recorded. The data was processed and served as our training set for the model building process.

The screening results of T cell viability on day 3 showed two categories of test media with low (<75% viable cells) and high performance (>75% viable cells) (**Figure 2**, upper panel). In terms of T cell expansion on day 6, each test combination showed a lower performance (median expansion units < 26) than the reference medium (**Figure 2**, lower panel).

Data Modeling

To meet the challenge of the high response variability introduced by using cells from different donors, we first built statistical models with the training set of four donors for each experimental block and each response variable separately. Centered and scaled data were used for this step.

First, we defined three different initial model equations (**Supplementary Table 2**) to account for different possible constellations of main, quadratic and two-way interaction terms of the 12 media components.

Next, we selected three different model algorithms for the statistical modeling: ordinary least squares regression (OLS) with stepwise AIC feature selection, random forest and elastic net regularized general linear models (glmnet) with automated multiple feature selection. To evaluate the model performance on the training set, we performed a tenfold cross-validation and automated hyperparameter tuning during the modeling step. Details of the model hyperparameter tuning of all final models are outlined in **Supplementary Table 5**.

In this way, nine independent statistical models were generated for each donor and each response variable, resulting in 72 final models. The statistical models were ranked by root mean squared error (RMSE) and coefficient of determination (R^2) and one final model with highest R^2 and lowest RSME was selected for each donor and response variable.

Due to a higher robustness toward overfitting of the data (Zou and Hastie, 2005), we selected best performing glmnet and random forest models over linear regression models for predictions of *in silico* formulations. The eight selected models showed high prediction power on the training set, with $R^2 > 0.92$ and RMSE less than 1.5 units (**Table 1**).

Prediction of *in silico* Formulations

Predictions of T cell viability and expansion were carried out via grid search. Component c02 was expensive and sought to be reduced in the final media formulation. Therefore, a constraint of component c02 to medium level was introduced.

We generated 10^5 random formulations over the experimental space of the 12 screened components and used these as input data for prediction of expansion and viability in the previously selected models for each donor. The formulations were ranked and the top 40 performing formulations for T cell viability or expansion from each of the eight models were pooled, resulting in 320 formulations. These formulations were used for the following clustering step.

Clustering and Selection of High-Performance *in silico* Formulations

First, the clustering tendency of the 320 formulations was assessed by means of the hopkings test (0.423), revealing weak structures. Next, the *k*-means algorithm was used for clustering of the centered and scaled data. To find the optimal number of clusters, the average within-cluster distance to the centroid using the "elbow" method was determined (**Figure 3**, upper panel). Here we selected six clusters for further analysis. The cluster integrity was examined based on the silhouette width.

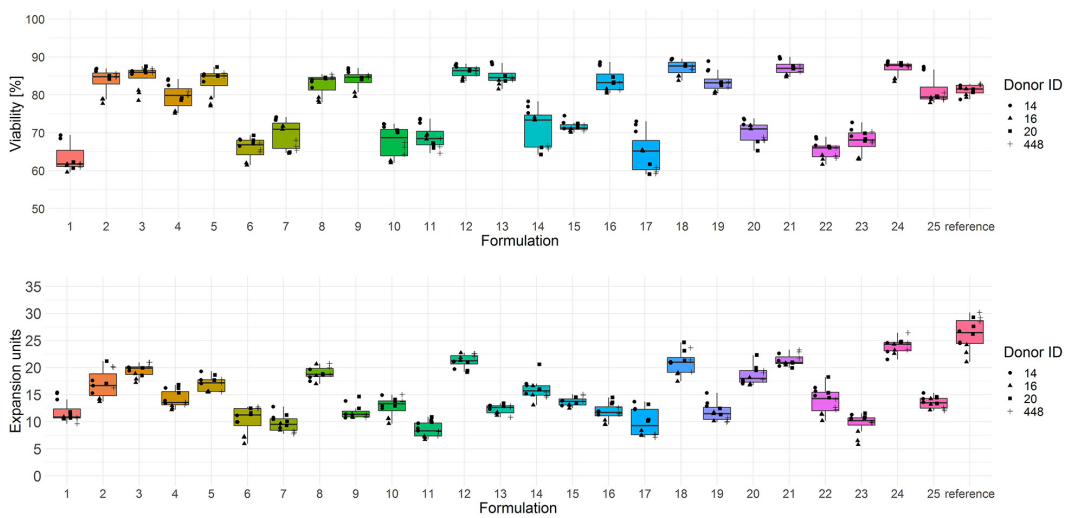

FIGURE 2 | Cryopreserved CD3$^+$ T cells purified from human donors (n = 4) were thawed and activated using anti-CD3/anti-CD28-coupled magnetic beads in test media or reference media in the presence of IL-7 and IL-15 (10 ng/ml, CellGenix) in three technical replicates. On day 3 cells were labeled with 7-AAD and cell viability was determined (*upper panel*). On day 6 cell counts were determined by flow cytometry and expansion was calculated (*lower panel*). Symbols indicate replicate values of individual donors.

TABLE 1 | Final model and its performance on the train set for each response and each donor.

Donor ID	Response	Model ID	Method	Train RMSE	Train R^2
014	Expansion	b1.model7e	Glmnet	1.16	0.93
016	Expansion	b2.model9e	Glmnet	0.97	0.96
020	Expansion	b3.model8e	Glmnet	1.44	0.92
448	Expansion	b4.model9e	Glmnet	1.06	0.96
014	Viability	b1.model4v	Random forest	1.10	0.98
016	Viability	b2.model9v	Glmnet	0.82	0.99
020	Viability	b3.model9v	Glmnet	1.05	0.99
448	Viability	b4.model9v	Glmnet	1.13	0.99

The average silhouette width was scored 0.15, confirming weak structures (**Figure 3**, lower panel). For cluster visualization, dimensionality reduction (principal component) was performed and 6 partially overlapping clusters could be identified by plotting the two highest dimensions on X- and Y-axis, exploring 30% of the variation (**Figure 4**).

While cluster 2 and 6 consisted mainly of formulations of the viability response (92 and 98.44%), formulations in cluster 1 and cluster 4 were mainly from the expansion response (82.69 and 76.12%). Cluster 3 consisted of nearly equal distribution of formulations from viability (53.19%) and expansion response (46.81%), which might explain the overlap on clusters 1 and 4 (**Table 2**). This data revealed that favorable formulation characteristics differ depending on the response variable, resulting in inhomogeneous clusters.

The median of each component of the observations within the six cluster was calculated to obtain a prototypic formulation of each cluster (**Figure 5**). These cluster medium formulations were "back-evaluated" by predicting the expansion and viability in the selected models for each donor. Data were grouped by cluster and summarized by median of expansion and viability. While the predicted values of viability were very similar for all clusters, the predicted expansion varied markedly (**Supplementary Table 3**). We therefore selected the medium formulation of cluster 1 and 4 for further experimental evaluation, as both formulations showed higher predicted median values of T cell expansion than the formulations of cluster 2, 3, and 6, respectively. The in-depth evaluation of the clusters revealed that clusters 1, 4, and 5 contained formulations of all donors for the expansion response which correlated with the higher predicted median expansion across all donors. On the contrary, clusters 2, 3, and 6 contained only formulations of three donors (Cluster 3), two donors (Cluster 2) or only one donor (Cluster 6), which in any case correlated with lower predicted median expansion across all donors (**Supplementary Figure 1A**

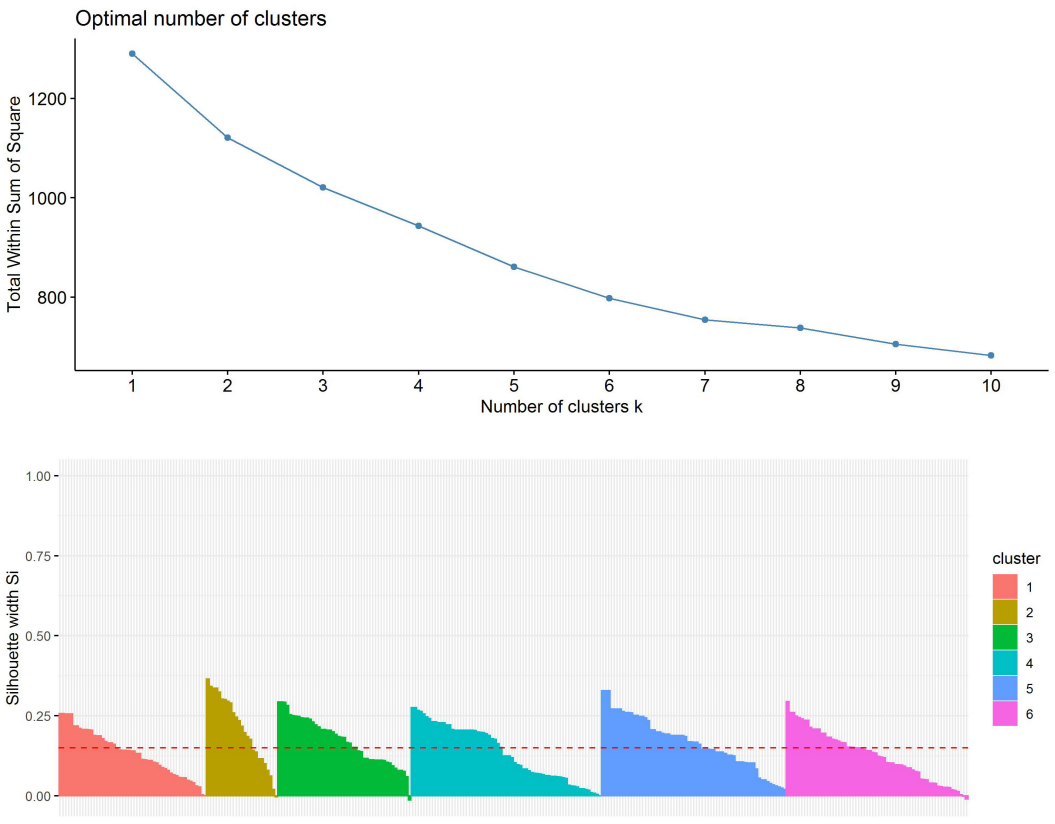

FIGURE 3 | Evaluation of optimal number of clusters by the "elbow" method using the total within Sum of Squares (**upper panel**). Evaluation of cluster integrity by calculation of Silhouette width of each cluster (**lower panel**).

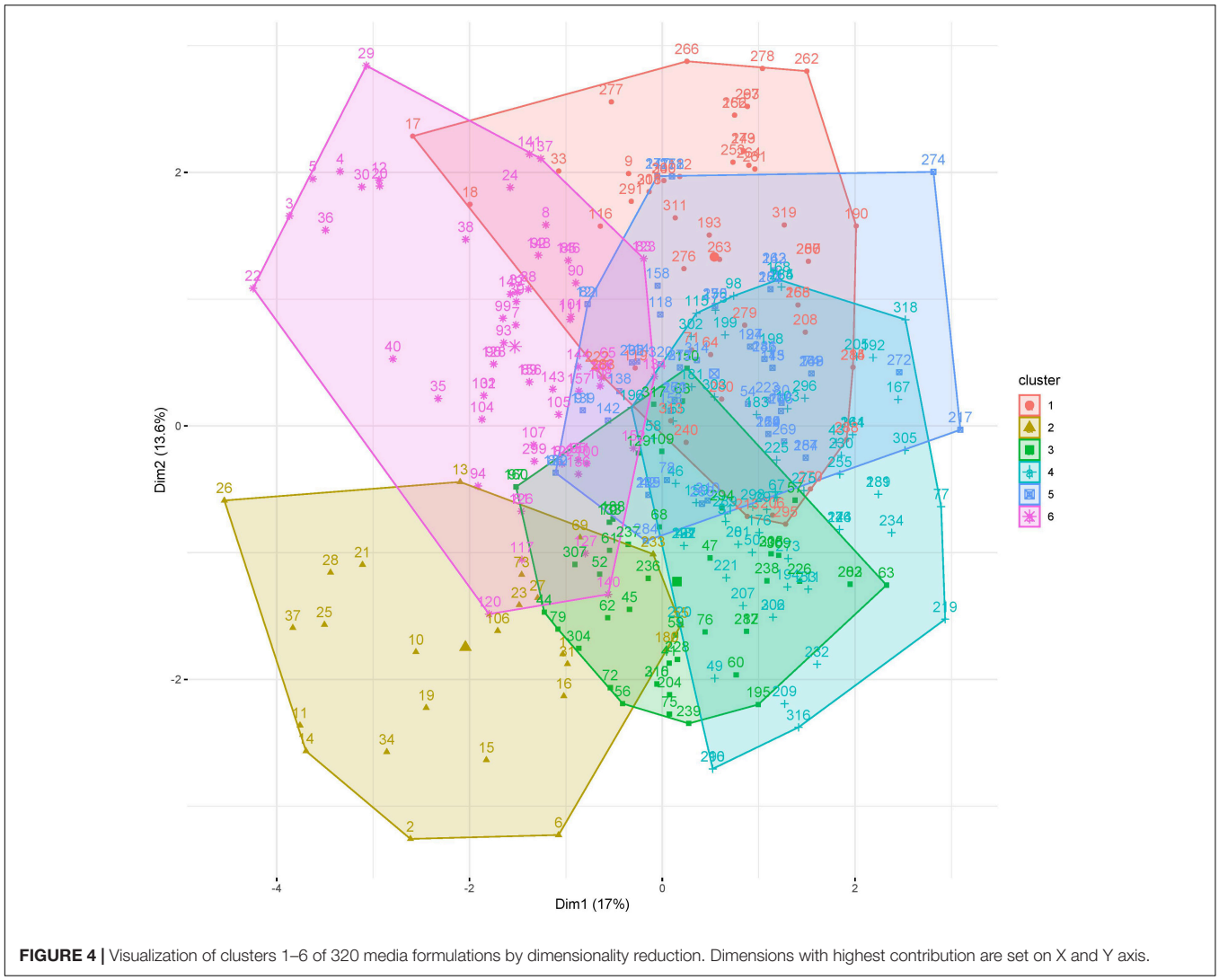

FIGURE 4 | Visualization of clusters 1–6 of 320 media formulations by dimensionality reduction. Dimensions with highest contribution are set on X and Y axis.

TABLE 2 | Number and proportion of media formulations within the clusters.

Cluster number	Response	Formulations (*n*)	Percentage (%)
1	Expansion	43	82.69
	Viability	9	17.31
2	Expansion	2	8.00
	Viability	23	92.00
3	Expansion	22	46.81
	Viability	25	53.19
4	Expansion	51	76.12
	Viability	16	23.88
5	Expansion	41	63.08
	Viability	24	36.92
6	Expansion	1	1.56
	Viability	63	98.44

and **Supplementary Table 3**). In addition, cluster medium formulation 1 and 4 differed significantly in their characteristics by relative concentrations of component c05 and c08. A weak difference could be identified for components c04, c07, and c010 (**Figure 5**).

Evaluation of Selected Cluster Medium Formulations on a New Set of Donors

Cluster medium formulations 1 and 4 were used in a confirmation experiment against six test media obtained by a traditional optimization strategy using a single response *ordinary least squares* regression model that is based on pooled expansion data from the definitive screening design. For the linear regression model, the training data of T cell expansion at day 6 were pooled and a single linear regression model was built to obtain a medium formulation that is characterized by enhanced robustness against donor variability. As expected, the final model performance was lower when compared to the individual models obtained from the machine learning approach (R^2 = 0.85, RMSE = 1.79). Six media formulations from the single response linear regression model that differed in the

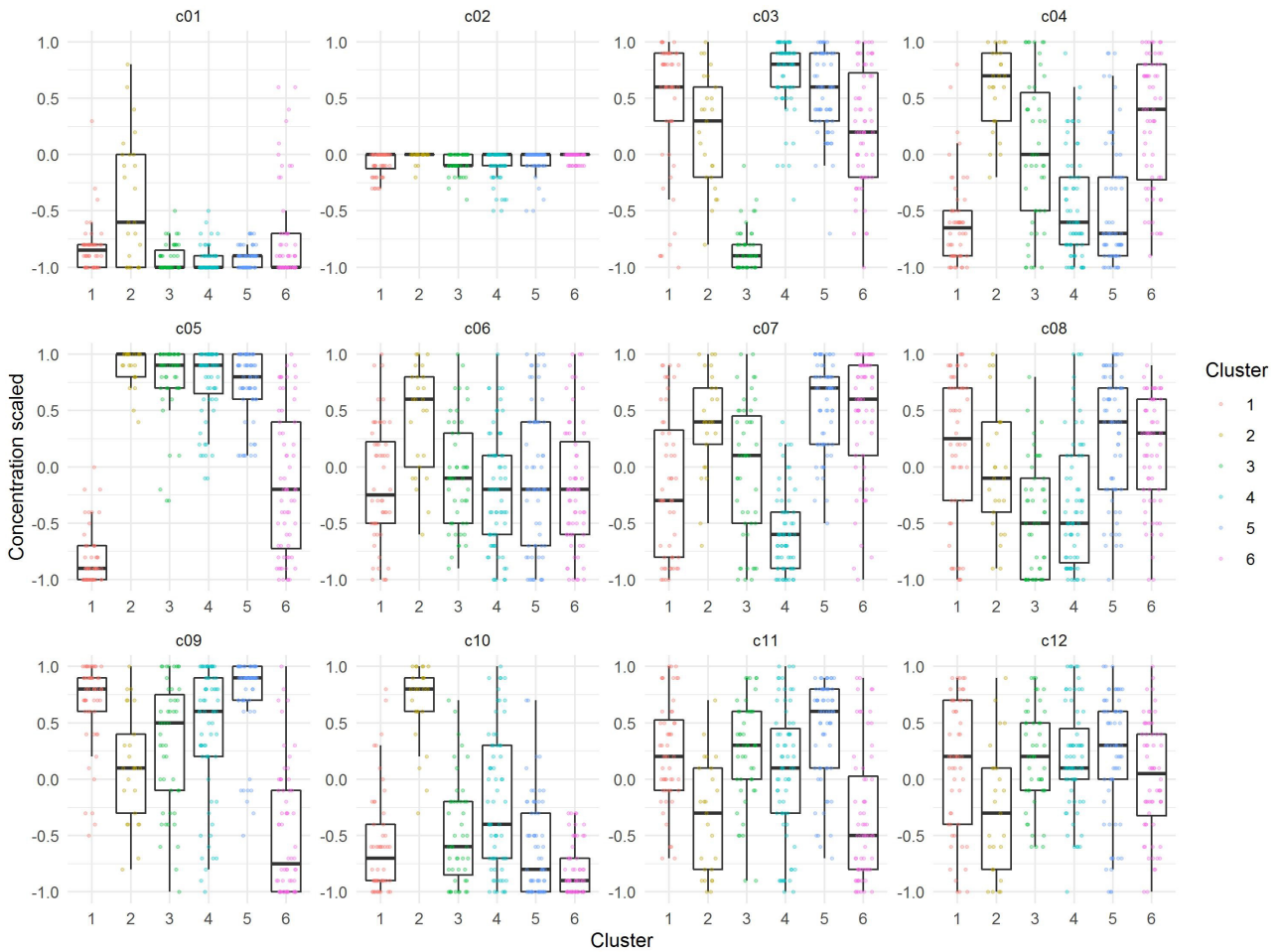

FIGURE 5 | Visualization of relative concentrations of each component in the identified Cluster medium formulations. Dots are representing each individual formulation, while boxes represent the median and spread of the data.

concentration of the screened components were selected and used for the confirmation experiment (**Supplementary Table 4**).

To evaluate the performance of the identified media formulation, T cells from a test set of four new donors were expanded in a randomized complete block design, resulting in a total of 36 confirmation runs.

Both cluster medium formulations showed significantly higher T cell expansion (median > 30 expansion units) compared to all test media from the single response linear regression model as well as to the reference medium (**Figure 6**, lower panel and **Tables 3A,B**). T cell viability after culture in cluster medium formulation 1 was significant lower on day 3 in comparison to cluster medium formulation 4 or the reference medium, yet viability was in a very narrow range across all media (>75%) (**Figure 6**, upper panel).

Evaluation of Model Performance

To reveal the performance of the statistical models, we compared the experimental values for T cell viability and expansion of the test set with the predicted counterparts from the final statistical models of the training set. Using the individual models, the prediction of the T cell expansion averaged over all donors was highly accurate. For cluster medium formulation 1, 30.54 expansion units with an IQR of 2.16 were predicted compared to the experimental value of 30.53 with an IQR of 4.31 expansion units. For cluster medium formulation 4, 31.65 expansion units with an IQR of 4.87 were predicted compared to 30.36 with an IQR of 3.94 experimental expansion units (**Table 3A**).

The model performance for the viability response on day 3 was less accurate. While the predicted values for both cluster medium formulations were estimated at 85% viability with an IQR of 4.31 and 3.94, the viability in the confirmation experiment was 78.55% with an IQR of 2.67% for Cluster 1 and 80.85% with an IQR of 1.62% for Cluster 4 (**Table 3A**). The prediction of T cell expansion with the single response regression model for expansion at day 6 was not that accurate compared to the individual models. Four of the six test media formulations showed a significant deviation of the predictions from their experimental values (**Table 3B**).

To evaluate the benefit of the clustering step, we performed an *in silico* experiment, where only the component-wise median of the best performing formulations from all donor-specific

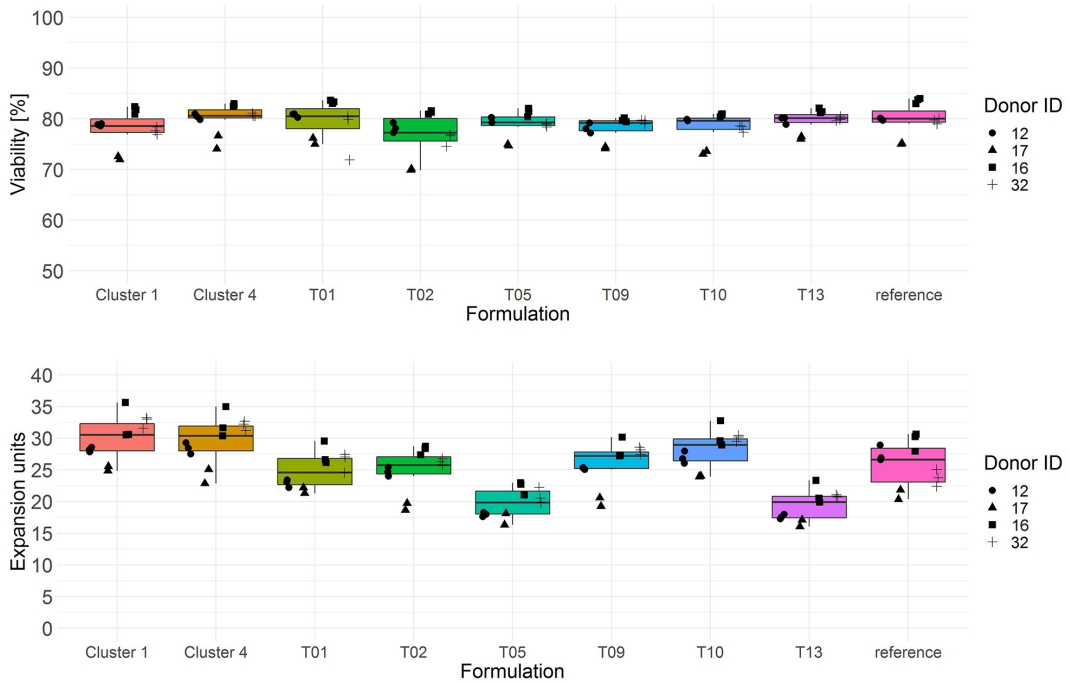

FIGURE 6 | Cryopreserved CD3$^+$ T cells purified from human donors (n = 4) were thawed and activated using anti-CD3/anti-CD28-coupled magnetic beads in test media or reference media in the presence of IL-7 and IL-15 (10 ng/ml, CellGenix) in three technical replicates. On day 3 cells were labeled with 7-AAD and cell viability was determined **(upper panel)**. On day 6 cell counts were determined by flow cytometry. T cell expansion is expressed in expansion units **(lower panel)**. Symbols indicate replicate values of individual donors.

TABLE 3 | Comparison of predicted vs. experimental values of the test set for the individual models (median of n = 4 models) **(A)** and the single regression model of pooled data **(B)**.

(A)

Response	Formulation ID	Predicted values (median)	IQR	Experimental values (median)	IQR
Expansion	Cluster 1	30.54	2.16	30.53	4.31
	Cluster 4	31.65	4.87	30.36	3.94
Viability	Cluster 1	85.23	4.31	78.55	2.67
	Cluster 4	85.86	3.94	80.58	1.62

(B)

Response	Formulation ID	Predicted values	Experimental values (median)	IQR
Expansion	T01	20.30	24.60	4.17
	T02	19.99	25.74	2.72
	T05	19.87	19.86	3.60
	T09	19.76	27.22	2.59
	T10	19.74	28.95	3.47
	T13	19.63	19.90	3.38

regression models were simulated. This simple ensembling method generated a medium formulation with a predicted expansion of 27.65 units with an IQR of 0.36 and a viability of 83.28% with an IQR of 1.55% averaged over all donors. While the result was very similar in terms of the viability response, the predicted expansion was lower compared to cluster medium formulations 1 and 4, respectively. Taken together our new one-time media optimization approach was able to predict a culture media formulation based on a training set of human donors, that significantly improved expansion of T cells from a new set of human donors in a confirmation experiment.

DISCUSSION

The biggest challenge in the development of cell culture media for cell therapies is the high variability of biological material obtained from different human donors. This fact complicates a conventional DoE-based sequential optimization strategy consisting of screening, characterization and optimization blocks due to donor-dependent effect sizes of the screened components.

In this work we present the implementation of a machine learning pipeline into DoE-based development of cell culture media, resulting in a one-time media optimization strategy that combines component screening with component level optimization in one experiment by using statistical models that focus on prediction rather than on inference.

The use of competitive modeling algorithms such as random forest or elastic net and cross-validation to assess model performance enabled us to extract extensive statistical information to build individual models for every donor of the training set with improved predictive power. In comparison,

predictions made by an interpretable single response regression model based on pooled data of all donors were less accurate due to variability introduced by donor-dependent effect sizes of the screened components.

Instead of aggregating donor data for modeling, which is commonly preferred in a sco strategy when operating with high variance of the data, we pooled high performance predictions from each donor model and used unsupervised clustering to identify formulations with similar characteristics. The formulations in each clusters contained *in silico* formulations from all input models suggesting that a prototypic cluster medium formulation could be beneficial for each donor and would subsequently yield a cell culture medium with high robustness for all donors. This clustering step turned out to be more efficient than a more basal ensembling method that was not supported by unsupervised machine learning. Of note, the small sample size of $n = 4$ donors resulted in weak overlapping cluster structures and a certain risk of under-representation of the population, which could decrease the robustness of the final medium. We evaluated the cluster composition according to the proportion of different donor formulations and selected cluster 1 and 4, which represented all four donors, for the confirmation experiment. Using the median value of each component within the cluster, we were able to confirm a robust expansion reaction for the selected cluster medium formulations in all four donors of the test set.

For the selected cluster media formulations, the predictions for T cell expansion made with the individual donor models precisely matched with the median expansion response observed experimentally for a test set of new donors. Having reliable models that allow predictions of experimental outcomes opens further perspectives for media optimization and characterization. For example, inspection of the mathematical model terms may uncover the contributions of individual media components. One may further modify the formulation by eliminating undesired factors from the formulation *in silico* and re-evaluate manual adjustments of the formulation in the original model. Here, again, component effects that only apply to specific donors can be monitored by back evaluation in the different donor models.

Notably, the predictions for the viability response were less precise than for the expansion response. The spread of the viability over the four donors of the test data set was higher than in the training data set and was likely not in the response space covered by our initial models. This highlights the requirement to use donors in the training data set that reflect the distribution of all observed responses in the donor population as good as possible to improve the predictive power of the models.

Although the viability on day three was not improved in Cluster1 formulation, compared to cluster 4 formulation, both formulations achieved similar T cell expansion on day 6. This suggests that moderate differences in cell viability at the beginning of the culture do not necessarily affect the degree of cell expansion observed later in the culture. Apart from that, a culture medium that confers high cell viability early in culture is always favorable in shorter protocols that rely more on cell viability and substitute exponential expansion of cells by increased starting cell numbers or *in vivo* expansion of cells.

In summary, we have shown that the extension of the traditional DoE-based strategy with a machine learning pipeline allows the generation of statistical models with excellent predictive power for T cell expansion. This new approach might be a competitive alternative to a more traditional strategy in which model interpretation is highly desired in the optimization process. Our pipeline facilitates the discovery of high-performance cell culture media formulations in a one-time optimization approach that achieved high media performance across donors from one training data set without the need for sequential experiments. This applies to primary culture media development as well as to other applications, where responses of individual donors to a specific input vary due to biologic variance, for example in biotechnological process development for T cell therapies with the need to optimize seeding cell density, incubation times, media feed or perfusion regimens, gene transfection procedures etc. The described experimentation strategy can lead to a major reduction of the experimental effort and can shorten development times substantially and thereby help to optimize robust autologous cell products for viable therapies for every particular patient.

DATA AVAILABILITY STATEMENT

The original contributions presented in the study are included in the article/**Supplementary Material**, further inquiries can be directed to the corresponding author.

AUTHOR CONTRIBUTIONS

PG study conception and design of the experiments, development and coding of the machine learning pipeline, data analysis and interpretation, and drafting of the manuscript. SW study conception, design of experiments, acquisition and interpretation of data, and drafting of the manuscript. Both authors approved the submitted version.

ACKNOWLEDGMENTS

We thank Benedikt Steinle, Juna Leppert, and Cagatay Yilmaz for their support in conducting the cell culture experiments. We are grateful to Ursula Schultz and Till Puschmann for critical reading of the manuscript.

SUPPLEMENTARY MATERIAL

The Supplementary Material for this article can be found online at: https://www.frontiersin.org/articles/10.3389/fbioe.2021.614324/full#supplementary-material

REFERENCES

Anderson, M. J. (2019). *Know the SCOR for Multifactor Strategy of Experimentation: Screening, Characterization, Optimization and Ruggedness Testing*. Minneapolis: Stat-Ease, Inc, 56–61.

Bayer, B., von Stosch, M., Striedner, G., and Duerkop, M. (2020). Comparison of Modeling Methods for DoE-Based Holistic Upstream Process Characterization. *Biotechnol. J.* 15:e1900551. doi: 10.1002/biot.201900551

Breiman, L., and Schapire, E. (2001). *Random forests. Machine. Learning*. Available Online at: http://citeseerx.ist.psu.edu/viewdoc/summary?doi=10.1.1.125.5395 (accessed May 12, 2021).

Castro, P. M. L., Hayter, P. M., Ison, A. P., and Bull, A. T. (1992). Application of a statistical design to the optimization of culture medium for recombinant interferon-gamma production by Chinese hamster ovary cells. *Appl. Microbiol. Biotechnol.* 38, 84–90. doi: 10.1007/BF00169424

Gee, A. P. (2018). GMP CAR-T cell production. *Best Pract. Res. Clin. Haematol.* 31, 126–134. doi: 10.1016/j.beha.2018.01.002

Jones, B., and Nachtsheim, C. J. (2011). A Class of Three-Level Designs for Definitive Screening in the Presence of Second-Order Effects. *J. Qual. Technol* 43, 1–15. doi: 10.2514/6.2000-4890

Jordan, M., Voisard, D., Berthoud, A., Tercier, L., Kleuser, B., Baer, G., et al. (2013). Cell culture medium improvement by rigorous shuffling of components using media blending. *Cytotechnology* 65, 31–40. doi: 10.1007/s10616-012-9462-1

June, C. H., O'Connor, R. S., Kawalekar, O. U., Ghassemi, S., and Milone, M. C. (2018). CAR T cell immunotherapy for human cancer. *Science* 359, 1361–1365. doi: 10.1126/science.aar6711

Kazmi, B., Inglefield, C. J., and Lewis, M. P. (2009). Autologous cell therapy: current treatments and future prospects. *Wounds* 21, 234–242.

Kim, E. J., Kim, N. S., and Lee, G. M. (1998). Development of a serum-free medium for the production of humanized antibody from Chinese hamster ovary cells using a statistical design. *In Vitro Cell. Dev. Biol. Anim.* 34, 757–761. doi: 10.1007/s11626-998-0029-6

Klein Geltink, R. I., Kyle, R. L., and Pearce, E. L. (2018). Unraveling the Complex Interplay Between T Cell Metabolism and Function. *Annu. Rev. Immunol.* 36, 461–488. doi: 10.1146/annurev-immunol-042617-053019

Liu, C. H., Chu, I. M., and Hwang, S. M. (2001). Factorial designs combined with the steepest ascent method to optimize serum-free media for CHO cells. *Enzyme Microb. Technol.* 28, 314–321. doi: 10.1016/S0141-0229(00)00346-X

Mahnke, Y. D., Brodie, T. M., Sallusto, F., Roederer, M., and Lugli, E. (2013). The who's who of T-cell differentiation: human memory T-cell subsets. *Eur. J. Immunol.* 43, 2797–2809. doi: 10.1002/eji.201343751

Rouiller, Y., Périlleux, A., Collet, N., Jordan, M., Stettler, M., and Broly, H. (2013). A high-throughput media design approach for high performance mammalian fed-batch cultures. *MAbs* 5, 501–511. doi: 10.4161/mabs.23942

R Core Team (2020). *R: A Language and Environment for Statistical Computing*. Vienna: R Foundation for Statistical Computing.

Trickett, A., and Kwan, Y. L. (2003). T cell stimulation and expansion using anti-CD3/CD28 beads. *J. Immunol. Methods* 275, 251–255. doi: 10.1016/S0022-1759(03)00010-3

Xu, Y., Zhang, M., Ramos, C. A., Durett, A., Liu, E., Dakhova, O., et al. (2014). Closely related T-memory stem cells correlate with in vivo expansion of CAR.CD19-T cells and are preserved by IL-7 and IL-15. *Blood* 123, 3750–3759. doi: 10.1182/blood-2014-01-552174

Yao, T., and Asayama, Y. (2017). Animal-cell culture media: history, characteristics, and current issues. *Reprod. Med. Biol.* 16, 99–117. doi: 10.1002/rmb2.12024

Zou, H., and Hastie, T. (2005). Regularization and variable selection via the elastic net. *J. R. Statist. Soc. B.* 67, 301–320. doi: 10.1111/j.1467-9868.2005.00503.x

Conflict of Interest: The authors declare that the research was conducted in the absence of any commercial or financial relationships that could be construed as a potential conflict of interest.

Advantages of publishing in Frontiers

OPEN ACCESS
Articles are free to read for greatest visibility and readership

FAST PUBLICATION
Around 90 days from submission to decision

HIGH QUALITY PEER-REVIEW
Rigorous, collaborative, and constructive peer-review

TRANSPARENT PEER-REVIEW
Editors and reviewers acknowledged by name on published articles

Frontiers
Avenue du Tribunal-Fédéral 34
1005 Lausanne | Switzerland

Visit us: www.frontiersin.org
Contact us: frontiersin.org/about/contact

REPRODUCIBILITY OF RESEARCH
Support open data and methods to enhance research reproducibility

DIGITAL PUBLISHING
Articles designed for optimal readership across devices

FOLLOW US
@frontiersin

IMPACT METRICS
Advanced article metrics track visibility across digital media

EXTENSIVE PROMOTION
Marketing and promotion of impactful research

LOOP RESEARCH NETWORK
Our network increases your article's readership